100 | Springer Proceedings in Physics

K. Dickmann
C. Fotakis
J. F. Asmus
(Eds.)

Lasers in the Conservation of Artworks

LACONA V Proceedings, Osnabrueck, Germany, September 15–18, 2003

Springer

SPRINGER PROCEEDINGS IN PHYSICS 100

SPRINGER PROCEEDINGS IN PHYSICS

79 **Nonlinear Dynamics and Pattern Formation in Semiconductors and Devices**
Editor: F.-J. Niedernostheide

80 **Computer Simulation Studies in Condensed-Matter Physics VIII**
Editors: D.P. Landau, K.K. Mon, and H.-B. Schüttler

81 **Materials and Measurements in Molecular Electronics**
Editors: K. Kajimura and S. Kuroda

82 **Computer Simulation Studies in Condensed-Matter Physics IX**
Editors: D.P. Landau, K.K. Mon, and H.-B. Schüttler

83 **Computer Simulation Studies in Condensed-Matter Physics X**
Editors: D.P. Landau, K.K. Mon, and H.-B. Schüttler

84 **Computer Simulation Studies in Condensed-Matter Physics XI**
Editors: D.P. Landau and H.-B. Schüttler

85 **Computer Simulation Studies in Condensed-Matter Physics XII**
Editors: D.P. Landau, S.P. Lewis, and H.-B. Schüttler

86 **Computer Simulation Studies in Condensed-Matter Physics XIII**
Editors: D.P. Landau, S.P. Lewis, and H.-B. Schüttler

87 **Proceedings of the 25th International Conference on the Physics of Semiconductors**
Editors: N. Miura and T. Ando

88 **Starburst Galaxies**
Near and Far
Editors: L. Tacconi and D. Lutz

89 **Computer Simulation Studies in Condensed-Matter Physics XIV**
Editors: D.P. Landau, S.P. Lewis, and H.-B. Schüttler

90 **Computer Simulation Studies in Condensed-Matter Physics XV**
Editors: D.P. Landau, S.P. Lewis, and H.-B. Schüttler

91 **The Dense Interstellar Medium in Galaxies**
Editors: S. Pfalzner, C. Kramer, C. Straubmeier, and A. Heithausen

92 **Beyond the Standard Model 2003**
Editor: H.V. Klapdor-Kleingrothaus

93 **ISSMGE**
Experimental Studies
Editor: T. Schanz

94 **ISSMGE**
Numerical and Theoretical Approaches
Editor: T. Schanz

95 **Computer Simulation Studies in Condensed-Matter Physics XVI**
Editors: D.P. Landau, S.P. Lewis, and H.-B. Schüttler

96 **Electromagnetics in a Complex World**
Editors: I.M. Pinto, V. Galdi, and L.B. Felsen

97 **Fields, Networks, Computational Methods and Systems in Modern Electrodynamics**
A Tribute to Leopold B. Felsen
Editors: P. Russer and M. Mongiardo

98 **Particle Physics and the Universe**
Proceedings of the 9th Adriatic Meeting, Sept. 2003, Dubrovnik
Editors: J. Trampetić and J. Wess

99 **Cosmic Explosions**
On the 10th Anniversary of SN1993J
(IAU Colloquium 192)
Editors: J. M. Marcaide and K. W. Weiler

100 **Lasers in the Conservation of Artworks**
LACONA V Proceedings,
Osnabrück, Germany, Sept. 15–18, 2003
Editors: K. Dickmann, C. Fotakis, and J.F. Asmus

101 **Progress in Turbulence**
Editors: J. Peinke, A. Kittel, S. Barth, and M. Oberlack

102 **Adaptive Optics for Industry and Medicine**
Proceedings
of the 4th International Workshop
Editor: U. Wittrock

Volumes 50–78 are listed at the end of the book.

K. Dickmann C. Fotakis J.F. Asmus
(Eds.)

Lasers in the Conservation of Artworks

LACONA V Proceedings,
Osnabrück, Germany, Sept. 15–18, 2003

With 298 Figures and 54 Tables

Springer

Professor Dr. Klaus Dickmann
Lasercenter FH Münster, Stegerwaldstr. 39, 48565 Steinfurt, Germany
E-mail: laserlab@fh-muenster.de

Professor Dr. Costas Fotakis
FO.R.T.H./I.E.S.L., P.O. Box 1527, Vassilika Vouton, 71110 Heraklion, Crete/Greece
E-mail: fotakis@iesl.forth.gr

Professor Dr. John F. Asmus
University of California, Institute for Pure and Applied Physical Sciences
San Diego, 9500 Gilman Drive, La Jolla, CA 92093-0360, USA
E-mail: jfasmus@ucsd.edu

ISSN 0930-8989

ISBN 3-540-22996-5 Springer Berlin Heidelberg New York

Library of Congress Control Number: 2004116520

Typesetting by the authors/editors
Cover concept: eStudio Calamar Steinen
Cover production: *design & production* GmbH, Heidelberg

Printed on acid-free paper SPIN: 10952498 57/3141/ad 5 4 3 2 1 0

Preface

The 5th International Conference LACONA V (Lasers in the Conservation of Artworks) was held in Osnabrück (Germany) in September 2003.

LACONA's aim is to provide an opportunity for scientists from universities and research laboratories to meet and especially for restorers, art historians and laser manufacturers to present and discuss new results concerning the application of laser technology in the restoration of artworks. This conference also offers opportunities to initiate cooperative projects between professionaly from the various fields of science and its application.

In 1995 this idea was realized for the first time by Professor Costas Fotakis from Foundation for Research and Technology Hellas Institute (FO.R.T.H.) in Crete, Greece, where 100 international attendees took part in LACONA I. Since then the field of "Lasers in the Conservation of Artworks" has gained considerably in importance. As a consequence a large number of nationally (e.g. DBU, Germany) and internationally funded (e.g. EU) research projects have been carried out. Furthermore international working groups were established (e.g. COST G7). There has also been a substantial increase in publications concerning laser application in restoration since LACONA I. It has turned out that a close cooperation between scientists and restorers seems to be of utmost importance for the future of laser applications in artwork restoration. Based on the success of LACONA I, other LACONAs were organized: 1997 in Liverpool, 1999 in Florence and 2001 in Paris.

LACONA V took place at the modern "Center for Environment Communication (ZUK) of the German Federal Environment Foundation (DBU)" from September 15–18, 2003. There were more than 80 presentations (50 oral, 30 posters) given by attendees coming from all over the world. While there was a distinct decrease in presentations compared to previous LACONAs for specific topics (e.g. laser cleaning of stone) the number of contributions in other fields such as analyses and diagnostics strongly increased. This is also true for online-monitoring during laser cleaning.

I am grateful to the members of the Scientific Committee as well as to the Editorial Committee for their advice and support in reviewing all papers. I also acknowledge the sponsorship by the "German Federal Environment Foundation (DBU)" and the administrative support of the "Center for Environment Communication (ZUK)".

I would like to give my thanks to Dr. John F. Asmus, the pioneer in laser cleaning, and to Professor Costas Fotakis, founder of LACONA, for the many stimulating discussions and their assistance to LACONA V.

Steinfurt, August 2004 *Klaus Dickmann*

Contents

Part II Laser Cleaning of Metal

Part III Laser Cleaning Miscellaneous

Part V Side Effects

Part VI Pigments, Conservation Layers

List of Chairs and Committees

Chair

Klaus Dickmann
Lasercenter FH Münster (LFM), University of Applied Sciences,
Steinfurt, Germany

Co-Chair

Costas Fotakis
Foundation for Research and Technology Hellas (FO.R.T.H),
Institute of Electronic Structures and Laser (IESL),
Heraklion, Greece

John F. Asmus
Institute for Pure and Applied Physical Sciences,
University of California, San Diego, USA

Scientific Committee

Margaret Abraham
Los Angeles County Museum of Art, USA

John F. Asmus
Institute for Pure and Applied Physical Sciences,
University of California, San Diego, USA

Giorgio Bonsanti
Facoltà di Scienze della Formazione, Torino, Italy

Martin Cooper
National Museum and Galleries on Merseyside, Liverpool, UK

Klaus Dickmann
Lasercenter FH Münster (LFM), University of Applied Sciences,
Steinfurt, Germany

Editorial Committee

Philippe Bromblet
CICRP, Marseille, France

Martin Cooper
National Museum and Galleries on Merseyside, Liverpool, UK

Costas Fotakis
Foundation for Research and Technology Hellas (FO.R.T.H),
Institute of Electronic Structures and Laser (IESL),
Heraklion, Greece

Klaus Hinsch
Carl-von-Ossietzky-University Oldenburg, Germany

Wolfgang Kautek
Federal Institute for Materials Research and Testing,
Berlin, Germany

Jana Kolar
National and University Library of Slovenia, Ljubljana, Slovenia

Johann Nimmrichter
BDA Restaurierungswerkstätten, Vienna, Austria

Roxana Radvan
INOE-CERTO, Bucharest-Magurele, Romania

Hannelore Römich
Fraunhofer-Institut für Silicatforschung,
Wertheim-Bronnbach, Germany

Renzo Salimbeni
Istituto di Fisica Applicata "N. Carrara",
Sesto Fiorentino, Italy

Hans Scholten
Art Innovation b.v., Hengelo, Netherlands

Manfred Schreiner
Academy of Fine Arts, Vienna, Austria

Robert Sobott
Labor für Baudenkmalpflege, Naumburg (Saale), Germany

Véronique Vergès–Belmin
Laboratoire de Recherche des Monuments Historiques,
Champs sur Marne, France

Gert von Bally
Westfälische Wilhelms-Universität, Laboratory of Biophysics,
Münster, Germany

Kenneth Watkins
University of Liverpool, Department of Engineering,
Liverpool, UK

Vassilis Zafiropulos
Foundation for Research and Technology Hellas (FO.R.T.H),
Institute of Electronic Structures and Laser (IESL),
Heraklion, Greece

Local Organising Committee

Markus Große Ophoff
Center for Environment Communication (ZUK), Germany

Nicole Frommeyer
Center for Environment Communication (ZUK), Germany

Klaus Dickmann
Lasercenter FH Münster (LFM), University of Applied Sciences,
Steinfurt, Germany

Elke Engelhardt
Lasercenter FH Münster (LFM), University of Applied Sciences,
Steinfurt, Germany

List of Contributors

Art in the Service of Science

J.F. Asmus

Institute for Pure and Applied Physical Sciences, University of California
San Diego, 9500 Gilman Dr., La Jolla, 92093–0360, USA
jfasmus@ucsd.edu

Abstract. In fields such as studio art, art conservation, archaeology, anthropology, music, and architecture it is often understood that many of the advances emerge from the introduction of new developments from science and technology. Scientific research is often justified on the basis of its past as well as potential future fallout into other endeavors as diverse as medicine, manufacturing, and the humanities. The diffusion of scientific innovation into the practice of art conservation has been punctuated by the introduction of a series of diverse technologies. Trace element and isotopic analyses, infrared imaging, ultraviolet fluorescence inspection, advanced coatings and adhesives, scanning electron microscopy, and photon/electron microprobes are notable examples. For the past thirty years various laser technologies have demonstrated utility in the practice of art conservation, as well. These include photon cleaning and divestment, holographic display and nondestructive analysis, surface characterization through laser fluorescence, radiation scattering and absorption, as well as laser-induced ultrasound. At the dawn of laser technology's introduction into the art conservation field (1972–74) the Center for Art/Science Studies (CASS) was established at the University of California, San Diego (UCSD) with the hope of accelerating and broadening the diffusion of scientific developments into art conservation practice. Surprisingly, one of the first events in the CASS/UCSD transpired when a Visual Arts Department student employed a primitive laser statue cleaner to "correct" a silk-screen print. In the course of maintaining her laser this art student discovered a dramatically improved method for aligning the complex optical beam train by utilizing her artistic training. A few months later another CASS/UCSD student in the Photographic Arts Program (while modifying a ruby laser to experiment with theater-lighting special effects) discovered an improved laser beam-profile diagnostic technique. These two, seemingly trite, examples of scientific serendipity "in reverse" are not isolated anomalies. History is replete with instances of art coming to the aid of science and technology. Examples include Samuel Morse's drawing upon his skill as a painter in support of his electrical engineering research, the collaboration of Michele Besso and Albert Einstein in the formulation of Special Relativity, Picasso's vision of wave-function collapse in Quantum Electrodynamics, and Jay DeFeo's depiction of Big Bangs and Black Holes while cosmologists were focusing on Fred Hoyle's steady-state continuum theory of the universe.

1 Introduction

The Center for Art/Science Studies (CASS) was established at the University of California, San Diego (UCSD) in 1974 in order to foster formal interactions between students and faculty in the arts with students and faculty in the sciences. The majority of these cross-disciplinary activities involved members of the Schools of Visual Arts, Theater, Oceanography, Physics, Medicine, Chemistry, Space Sciences, and Applied Mechanics. In its early years CASS developed into a program of "Science in the Service Art". Technologies such as isotopic analyses, holography, laser illumination and surface modification, digital-computer image processing, ultrasonic imaging, and magnetic resonance imaging (MRI) were applied to art in the areas of display, history, interpretation, performance, restoration, conservation, and creative expression. For the most part the stimulus for developing such connections came from a search for ways of applying current scientific innovation to the arts. However, it was a surprising revelation to eventually realize that the artists were contributing to the sciences, as well. This reversal of "common sense" has roots going back to the earliest civilizations and includes notable recent artistic contributions to general relativity, quantum electrodynamics, and cosmology [1]. (At the present time the art/science roll of CASS is being carried on by its successor, the Center for Research in Computing for the Arts, CRCA).

Science has been applied to diverse activities in the arts for generations [2]. The earliest instances probably involved the selection of tools and materials for painting and sculpture. Lighting, acoustics, and special effects may have received attention quite early in the performance arts of the stage. In the mid-twentieth-century radiocarbon dating, infrared and ultraviolet inspection, trace-element quantification, and the introduction synthetic materials became ubiquitous in the practice, conservation, and/or authentication of art.

It was realized after a number of years that a reverse technology transfer had also been taking place on a routine basis within the CASS Program. This phenomenon of serendipity, wherein art and artists contributed to science, had been transpiring with regularity, but had gone on virtually unnoticed for a decade. The contributions by artists in the program included new ways of aligning lasers, improved laser-beam diagnostics, low-cost raster-scanning systems, commercial applications for photonic cleaning, novel construction materials for lasers, and improved sample preparation for SEM and XRF analyses. It was as if the diverse talents of students and staff were functioning in unison in the manner of the mind of a Leonardo da Vinci [3]. An investigation of this phenomenon led to the realization that this flow from art to science has been taking place throughout history. In fact there are countless examples of art and artists anticipating major scientific advances by years and sometimes by decades and even centuries. Well known examples range from the wave aspect of light to the space-time continuum. For

example Pollock was painting fractals well in advance of the mathematical formulation by Mandlebrot. Further, DeFeo was painting the "Big Bang", super novae, and the "Big Crunch" even before cosmologists had invented these terms. The art-science connection penetrates still deeper in mystery upon realization of the role that the arts performed in the creative processes of many of the greatest of the recent scientists such as Albert Einstein ("an extraordinary genius"), Marie Curie, Werner Heisenberg, J. Robert Openheimer ("an ordinary genius: dreamy, artistic, emotional"), Linus Pauling, and Richard Feynman ("no ordinary genius"). (Feynman's daughter, Joan, maintains that her father visualized the world in four dimensions and that different terms in mathematical equations appeared to him in different colors) [4].

2 Art in the Service of Science

In many instances members of the CASS Program inspected a conservation specimen repeatedly in the SEM between laser-divestment or laser-consolidation irradiations. A kinematic specimen mount and a micrometer stage aided in returning to the same field of view after each of the repeated laser irradiation cycles. Sometimes this procedure proved to be difficult and tedious. One of the art students was studying the silk screen process and was inspired to attach a bit of silk to the SEM specimen. This silk grid (Fig. 1) not only eased the specimen relocation process, but also was compatible with the SEM coating (gold/palladium) and withstood repeated laser shots.

Upon entering the CASS Program art students were routinely instructed in the operation, alignment, and maintenance of lasers. A key aspect of this instruction was learning to align the axis of a laser rod with that defined by the other elements of the beam train. For years this had been performed with a HeNe alignment beam and a target card with a pinhole. One day it was discovered that an art student had replaced the pinhole with a fragment of silk fabric from the silk-screening class. Instead of a point spot, the silk behaved as a two-dimensional diffraction grating and yielded an array of spots (Fig. 2). The student had discovered that adjusting the laser rod position so as to symmetrize the diffraction pattern yielded a perfect alignment in a fraction of the time required with the pinhole technique.

The preceding two examples of the artist in the service of the scientist may seem quaint. However, they (and numerous other similar events in the CASS program involving PVC lasers and novel "zapping" paper) illuminate and parallel a profound phenomenon in the tension between the artistic perception and the process of scientific discovery.

On an epic scale Shlain [2] has demonstrated quite convincingly that a great many innovative artists such as Leonardo, Magritte, Dali, Picasso, and Matisse anticipated the great discoveries of physics and cosmology long before the scientific community recognized these. The works of the above

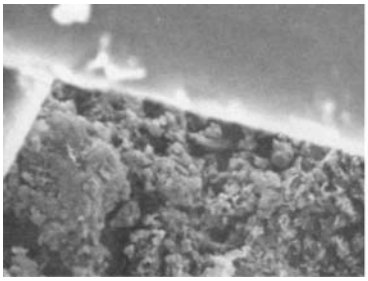

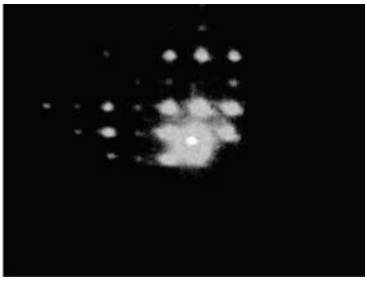

Figs. 1 and 2. Silk threads for SEM position location (*left*) and Silk alignment beam vignetted by off-axis laser rod (*right*)

as well as many other great artists are laced with both hints and major themes that portray the concepts and features of planetary motion, gravity, relativity, and quantum mechanics years, decades, and even generations prior to the actual scientific discoveries. A modern example of this phenomenon is illustrated by Figs. 3 (a Jackson Pollock drip painting) and 4 (a fractal image). Recent mathematical analyses have revealed that some of the Pollock paintings conform to the mathematics of fractals (over the surface-tension-dictated scale of his patterns). In the tradition of the connections cited above Pollock was painting fractals (1948) decades before the discovery of fractal mathematics by the Nobel Laureate, Benoit Mandelbrot (1976).

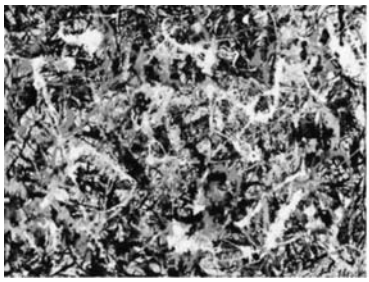

Figs. 3 and 4. "Drip painting" by Jackson Pollock and a computer-generated fractal image

CASS participation in the restoration and study of Jay DeFeo's painting, "The Rose" (The Whitney Museum of American Art), uncovered a series of her 50-year-old paintings portraying many of the modern concepts of astrophysical cosmology. Her "Rose" (originally the "Death Rose") is seen as the "Big Crunch" or a "Black Hole" by many observers. (Thomas Hoving, former director of the Metropolitan Museum of New York, associates it with Genesis [5].) Her "Jewel" has been adopted by cosmologists to portray the "Big Bang", the "Primal Bang" or a "Hyper Nova". Many are struck with

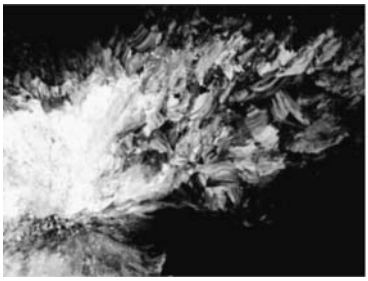

Figs. 5 and 6. The "Annunciation" painting by DeFeo (*left*) and a Hubble telescope image from space (*right*)

the similarity of her "Annunciation" (Fig. 5) with recent Hubble Telescope images of cosmic explosions (Fig. 6).

Shlain demonstrated in "Art and Physics" [2] that throughout history there are countless examples of an eerie precognition or clairvoyance in cutting-edge art of subsequent breakthroughs in physics. Most notable are Leonardo's studies of shadows (1501) that anticipated the discovery of the clues to planetary motion by Copernicus (1543), Giotto's concept of the linear time line (1276–1337) before d'Oresme introduced graphical plots (1360), and Katsushika Hokusai's 36 views of Fuji in a space-time continuum (1823–29) that preceded Minkowski's four-dimensional formulation by almost a century.

Shlain concludes that there are deep connections between the creative processes in the arts and sciences. It follows that such creative congruencies and premonitions may be found within individual scientist artists, as well. The innovative mind of a Leonardo da Vinci may not have been and entirely unique phenomenon. Several of the greatest scientists of the 20th Century illustrate this point.

3 Scientist Artists

References to the arts in the lives of 20th Century scientists are ubiquitous in many of their biographies. For instance, according to Otto Hahn [6], "In Haigerloch, Heisenberg sometimes slipped away from the scientists in the cave at the base of the cliff and made his way to the 18th Century Baroque church at its top. There he would play Bach fugues on the organ (April 1945)." In "Madam Curie" [7] there are references to piano, voice, and original poetry. Niels Bohr was known for his fascination with Cubism... "that an object could be several things, could change... allowed contradictory views to coexist in the same natural frame" [8].

It is widely perceived that the most colorful, flamboyant, enigmatic, and intelligent of the 20th Century physicists was Richard Feynman. His classroom lectures were dazzling in their clarity, originality, and insight. In

Figs. 7 and 8. Nobel Laureate Richard Feynman as teacher, performer, musician, and stage actor (Fig. 7, *left*), and on the *right* (Fig. 8) are examples of his graphical art including the world's largest artwork (*upper left*, in the Mojave Desert, as seen from an earth-orbiting satellite), the smallest artwork (*upper right*, as seen in an electron microscope), and two of his sketches (*bottom*)

addition he was an accomplished party entertainer, professional musician, and stage actor (Fig. 7). He claimed to have executed the largest artwork (visible from an orbiting satellite) and the smallest artwork (requiring an electron microscope) as well as excellent sketches and cartoons (Fig. 8).

Both Picasso and Feynman chose to portray quantum-electrodynamical processes in a graphical form (Fig. 9).

The fact that Albert Einstein played the violin is thought by many to be merely one of his eccentricities; much like his refusal to wear socks. According to his lifelong friend and collaborator, Michele Besso, "He often told me that one of the most important things in his life was music. Whenever he felt that he had come to the end of the road or into a difficult situation in his work he would take refuge in music and that would usually resolve all his difficulties".

Figs. 9 and 10. Picasso painting interpreted as wave function of "vibrating vacuum energy" collapsing into a face and the corresponding Feynman diagram (*left*), and Albert Einstein the artist with violin (*upper left*), as puppeteer (*right*), and family artist (*lower left*) on the right

The enduring friendship and mutual respect between Einstein and Besso began when they met at a concert. Einstein sums up his attitude toward Besso in his 1905 paper, "On the Electrodynamics of Moving Bodies", (which is devoid of any references, whatsoever) with the acknowledgement "In conclusion I wish to say that in working at the problem here dealt with I have had the assistance of my friend and colleague, M. Besso, and that I am indebted to him for several valuable suggestions". Besso noted that Einstein's "intuitive approach was almost like painting a picture. It was an experience that taught me the difference between knowledge and understanding". Thus, it appears that Einstein may have been the artist (Fig. 10) of the pair and the much more successful Federal Institute student, Besso, contributed the rigor. Perhaps, it is summed up best by the quotes:

"Art is the queen of all sciences, communicating knowledge
to all generations..."
Leonardo da Vinci
"Imagination is more important than knowledge."
Albert Einstein

4 The Bohemian Index

The observation put forth above that some prominent scientists have an artistic temperament and orientation is well known. However, some of the implications of this phenomenon have only recently been studied with rigor. In "The Rise of the Creative Class" [10] Richard Florida presents research data establishing that it takes a special set of circumstances to give birth to a "Silicon Valley". Conventional wisdom has long held that for a technological megalopolis to expand and flourish there must be a local deeply-embedded intellectual/research environment as often found in conjunction with major universities.

In studying both successful and failed "Silicon Valleys" Florida's research (described in "The Rise of the Creative Class") developed the concept of the "Bohemian Index" as a measure of a community's openness, diversity, tolerance, and artistic rebellion and daring. These factors promote the emergence of creative habitats and ecosystems. Such conditions draw creative individuals. Some of these will establish creative commercial ventures. If this takes place in the proximity of a technological region of excellence (universities and/or research laboratories), still more creative individuals will be drawn to the community, and this pool of talent becomes a magnet that attracts still other creative organizations. This recipe leads then to the emergence of the archetypal "Silicon Valley".

Florida contrasts his own university's (Carnegie Mellon in Pittsburgh) stillborn efforts to create a technological megalopolis with the seemingly unlimited commercial successes represented by the San Francisco Bay area (with

the cultures of Haight-Ashbury and Berkeley), by Seattle (with the Fremont culture), and by Austin (with "Austin City Limits"). Even within the LACONA community there is at least one similar development. Most of the earliest art conservation research with lasers (1972–75) was either in or under the guidance of the museums of London [11]. Thirty years later one finds the majority of the conservation, academic, and industrial work in this field in the United Kingdom has shifted to the region in and around Liverpool: the home of "The Beatles".

Acknowledgements

Conversations with L. Shlain, C. Pedretti, and V. Besso were most helpful in developing this paper.

References

1. J. Asmus, Science in the service of art (and vice versa), SPIE Proceedings (2003) in press
2. L. Shlain, *Art & Physics: Parallel Visions in Space, Time & Light*, Morrow, New York, 1991
3. C. Perdetti, *Leonardo, A* Study *in Chronology and Style*, University of California Press, Berkeley, 1973
4. D. Goodstein and J. Goodstein, *Feynman's Lost Lecture*, Norton, New York, 1996
5. T. Hoving, *Greatest Works of Art in Western Civilization*, Artisan, New York, 1997
6. T. Powers, *Heisenberg's War*, Knopf, 1993
7. E. Curie, *Madame Curie*, Doubleday, New York, 1938
8. K. Cole, *Sympathetic Vibrations*, Bantam, New York, 1984
9. I. Walther, *Picasso*, Taschen, Cologne, 2000
10. R. Florida, *The Rise of the Creative Class*, Basic Books, New York, 2002
11. J. Asmus, M. Seracini, and M. Zetler in *Lithoclastia*, Vol. 1, No. 1, 1976

Part I

Laser Cleaning of Paper

Laser Cleaning Investigations of Paper Models and Original Objects with Nd:YAG and KrF Laser Systems

H. Scholten[1], D. Schipper[1], F.J. Ligterink[2], J.L. Pedersoli Jr.[2], P. Rudolph[3], W. Kautek[3], J.B.G.A. Havermans[4], H.A. Aziz[4], B. van Beek[5], M. Kraan[5], P. van Dalen[6], V. Quillet[7], S. Corr[8], and H.Y. Hua-Ströfer[9]

[1] Art Innovation, Hengelo, The Netherlands
h.scholten@art-innovation.nl
[2] Netherlands Institute for Cultural Heritage, Amsterdam, The Netherlands
[3] Federal Institute for Materials Research and Testing, Berlin, Germany
[4] Netherlands Organisation for Applied Scientific Research, Delft, The Netherlands
[5] KOP-Papierrestauratie, Arnhem, The Netherlands
[6] Art-Conservation b.v., Vlaardingen, The Netherlands
[7] Atelier Quillet, Loix en Ré, France
[8] Paper conservation Susan Corr, Corrandulla (Co. Galway), Ireland
[9] Hai Yen Institute for Conservation of Works of Art, Mannheim, Germany

Abstract. Conventional cleaning methods (mechanical, wet) are not always sufficient for the restoration of brittle papers, fissures and sensitive inscriptions. Partial cleaning of paper in the vicinity of sensitive media, such as water-colour, is particularly difficult because of the lack of precision using conventional techniques. In these cases, where high spatial accuracy and localized treatments is necessary, laser cleaning might promise to be an additional tool for conservators.

1 Introduction

The variety of combinations of different types of foreign matter (dirt) on paper objects can present complex cleaning problems in paper conservation. Current cleaning methods using conventional means (solvents, mechanical) are not always sufficient to solve problems such as local cleaning in the vicinity of sensitive media. Lasers may offer a valuable tool for solving problematic cases. This cooperative research project entitled "Paper Restoration using Laser Technology" (PARELA, EVK4-CT-2000-30002), funded by the European Commission, has the objective of developing a laser system suitable for the accurate, efficient and safe cleaning of paper objects. Major results of the project will be presented here with emphasis on the practical application of laser cleaning in paper conservation.

A range of cleaning problems that are cumbersome or impossible to treat using conventional methods has been selected by paper conservators participating in the project, including the following types of foreign matter

commonly found on paper objects: surface dust; adhesives (natural and synthetic); pressure-sensitive tapes; inks and stamps; "sticky fingers" (skin surface lipid, possibly combined with dust); stains from foxing, fungi and oil.

Two parallel lines of research have been pursued: (1) critical assessment of the results of laser treatment of a representative group of real paper objects displaying the selected problems; and (2) evaluation of the immediate and long-term chemical and physical alterations of the paper substrate caused by laser treatment, using paper/dirt model systems. The experience gained is used to build a dedicated laser cleaning station for paper objects. Central issues are the spatial resolution of the laser guiding system, which is critical for precision work in the presence of sensitive media, and the detection system for monitoring the progress of the treatment in real time.

2 Experimental Methods

2.1 Laser Systems

So far three different laser systems have been used within the project. One is a diode-pumped Q-switched Nd:YAG pulsed laser (pulse duration <10 ns; repetition rate <1 KHz) operating at 1064 and 532 nm, designed and set up by the Federal Institute for Materials Research and Testing (BAM), Berlin, Germany [1, 2]. The laser beam is scanned onto the area to be cleaned using an array of moveable mirrors. The maximum scanning area is of 14 cm × 14 cm, and the focus beam diameter is of the order of ∼100 µm. A video camera situated next to the optical head captures the image of the surface to be cleaned, which is digitised and displayed on a computer screen where the area(s) to be lasered can be selected via software and where the progress of the treatment can be monitored and documented. The station is provided with halogen and ultraviolet illumination for diagnosis, and an exhausting system to remove volatile/vaporised residues. The support stage is 70 cm × 100 cm, and the objects are typically mounted under weights to keep them flat. Fibre beam delivery is available as an option for manual cleaning. When closed, the housing of the laser workstation makes it a Laser Class 1 Option, i.e., eye protection is not needed.

The second laser system, also located at the BAM Institute, which was used in the project is another Nd:YAG laser operated at 355 nm. Here positioning is done with a separate x-y stage, so that the sample moves and the laser beam is stationary.

The third laser system belongs to Art Innovation (A.I.) b.v., Hengelo, The Netherlands. It consists of a Lambda Physik Compex 205 excimer laser operating at 248 nm; pulse duration ∼20 ns, repetition rate range 1–50 Hz; pulse energy range 0–600 mJ/pulse; maximum average power 30 W. The laser beam, which is X: Gaussian, Y: top hat, and which has a working spot size of X: 0.2–10 mm and Y: 1–35 mm, is delivered by a motorised articulated arm,

and the focussing optics consist of a cylindrical telescope yielding a collimated beam in X. Additional features are a HeNe aiming beam, on-line monitoring and analysis by Laser-Induced Breakdown Spectroscopy, auto focus system, and high resolution viewing camera [4].

3 Materials and Methods

3.1 Determination of Short and Long Term Behaviour of Laser Treated Papers

Three well characterised paper types, (sulphite wood pulp, cotton linters, and a mechanical wood pulp, were chosen for the evaluation of the immediate and long-term chemical and physical alterations of the paper substrate caused by laser treatment. These papers were laser treated at the BAM Institute at three different wavelengths (355 nm, 532 nm and 1064 nm just below the (direct observable) alteration threshold. In order to simulate long-term effects, the laser treated papers were next subjected to an accelerated ageing procedure at TNO by storing the papers for 12 days at 90°C and 50% R.H. (relative humidity). The sensitivity of colorimetry, infrared spectroscopy, and chemoluminescence was tested on the laser-treated and artificially aged samples at ICN. Mechanical strength tests were performed at TNO.

3.2 Model Systems for Laser Removal of Ink and Adhesives

In addition to the evaluation of laser treatment on the pure paper substrate, two paper sample systems were developed in the project to simulate two common types of conservation problems found on paper. A paper model was devised to represent conservation problems encountered with tapes and adhesives and a model system was developed for inks and stamps. The test papers were made on the 3 different test papers (linters, acid mechanical and sulphite).

For the ink and stamp model a bleeded area of ink was made to simulate staining and water damage. The aim was to remove the bleeded spot from the paper. A second model was made to represent undesired stamps and writing or graffiti. For this model either blue ballpoint ink or ecoline ink was drawn over a rectangular ecoline ink stamp in a cross shape fashion. The aim is to remove the ballpoint ink or ink stamp without removing the ecoline stamp underneath.

For the adhesive tape model on paper three different pressure sensitive tapes (Scotch tape 840 S, Sello tape L and masking tape) were applied to A4 sized sheets of the above-mentioned types of paper. To simulate a realistic situation in which adhesives are used for repairs, a tear was made in one end of the paper. A length of adhesive tape was then applied over the tear. A second length of adhesive was applied to an undamaged part of the sheet to simulate the use of adhesive tape as reinforcement (backing).

3.3 Laser Cleaning Trials on Original Objects

Finally, a selection was made of a group of original objects representing the range of cleaning problems as found on naturally aged paper objects. The originals include: adhesive layer (probably animal glue) covering a printed text on a rag paper; adhesive from a pressure-sensitive tape on a mechanical pulp paper [3]; fungi stains covering a writing ink text on a blue-dyed 20th century paper; felt tip pen on a modern alkaline office paper; water-based stamp (methyl violet) on a mechanical pulp paper; oil-based stamp (probably carbon black) on a late 19th century paper; surface dust on a rag paper. Besides the variations in the compositions of both foreign matter and substrates, the distribution of the former on and in the paper varies significantly from object to object, and in most cases the foreign matter is non-uniformly distributed.

3.4 Comparison of Laser versus Conventional Cleaning of Ink and Tape Models

In order to evaluate the laser cleaning results in an objective manner, the conservators in the project were separately asked to treat a full set of test systems with conventional cleaning methods according to their best possible practices and techniques. A special grading system was developed by the conservators in order to assess the conventional cleaning methods and compare the results with the laser cleaned objects.

The targeted areas were marked and documented before and after laser and conventional treatment by photography and by multispectral imaging.

3.5 Laser Cleaning Procedure

The actual laser cleaning experiments were carried out at BAM and AI. Selection of laser treatment parameters was based on past experience with comparable materials and pre-testing on the objects to be treated. The progress of treatment was assessed visually and with multi-spectral imaging by examining the object after each sequence of pulses.

Selection of laser treatment parameters was carried out by visual examination of a test matrix created by systematically lasering little squares on the layer to be removed, with varying energy density and step distance overlap. A (visually) optimal cleaning result within the test matrix is defined by a minimal colour difference between the dirt-containing area and the surrounding paper, in combination with a minimal discolouration and/or structural change of the paper.

The laser cleaning procedure was systematically evaluated according to the following aspects: suitability of the laser guiding system; suitability of the detection system; cleaning efficiency; occurrence of undesired side effects.

4 Results

A number of laser cleaning effects on paper have been observed during the preliminary evaluation of project results. The most commonly observed side effects of laser cleaning on paper are:

1. "***Fluffing***" of the paper surface induced by the forceful expulsion of particles located between the fibrous structure of the paper, causing the fibres to stand up.
2. "***Thinning***" of the paper thickness by excessive removal of material (ablation).
3. "***Charring***" or "***Carbonization***" of the paper or pigments often caused by high levels of laser radiation.
4. "***Yellowing***" or discoloration of the paper surface or pigments.

Preliminary results of the laser cleaning process on paper clearly show that laser treatments using a wavelength of 532 nm has no or very limited effect on the mechanical properties of paper, which is a relief to curators and conservators.

The measurement of colorimetric changes during and after laser treatment proves to be the most sensitive and informative tool to monitor the laser cleaning process. Therefore, imaging colorimetry will be further developed to form an on-line monitoring method in the final design of the laser cleaning station.

5 Prototype for Selective Laser Cleaning

Based on the research performed in this project, a special station was be built within the PaReLa project using a Nd:YAG laser system operating at 532 nm, to demonstrate the benefits of laser treatment of paper. The commonly encountered complexity of composition and relative distribution of the dirt/substrate combinations on paper objects requires a high spatial positioning accuracy of the laser beam and automatic decision algorithm(s) to discriminate between dirt and paper and between dirt and media, as well as to control the number of pulses per spot.

In this prototype the required high spatial positioning was achieved by combining imaging techniques with the high accuracy scanning mirror system of the laser system, see Fig. 1.

During this procedure, first a digital image is taken from the object. Then the user can, through digital image processing with a computer, select those areas that need to be cleaned. In cases where there is printed text on the object the text can be isolated and the laser can scan around it. The accuracy of this technique is near pixel level. Finally, a black and white image is created, where the white indicates where the laser should not hit the surface, and the black indicates the area that needs to be treated as indicated in Fig. 2.

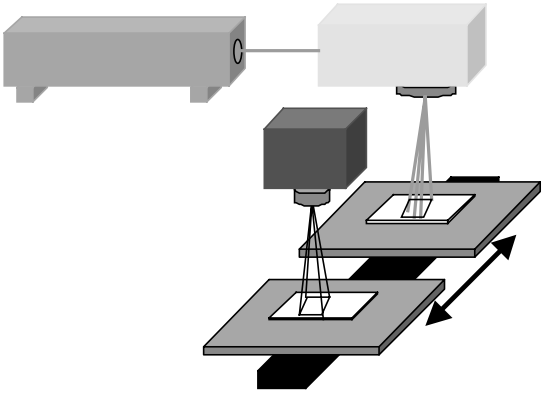

Fig. 1. Diagram of laser cleaning station set-up, consisting of the Nd: YAG laser, the scanning head and the digital camera

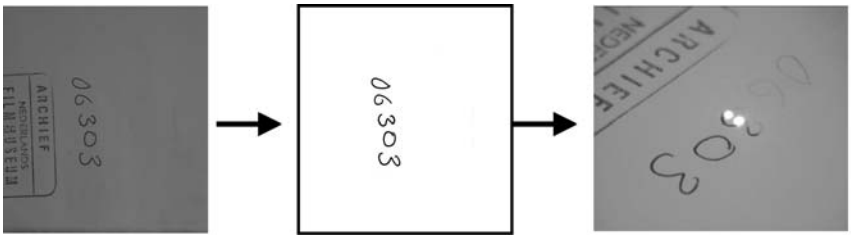

Fig. 2. Selective cleaning procedure involving three steps: (**1**) digital image taken from object, (**2**) isolate area to be cleaned (*black*) and (**3**) the selective laser treatment

Criteria such as contrast/colour differences are monitored in different regions of the electromagnetic spectrum (UV, VIS, IR) to ensure that the laser cleaning process is performed within safe boundaries as defined by conservators.

In the specific case where the removal of homogenously distributed adhesive was required from art objects, satisfactory cleaning results were obtained with the existing UV laser station at Art Innovation. Removal of adhesive left by pressure sensitive tape could be performed with sufficient accuracy and speed to be economically interesting to conservators.

5.1 Selective Cleaning Demonstration

The selective removal of chalk inside the crown on the paper documents is a good example of the accurate cleaning possible with the prototype laser cleaning station. In Fig. 3 before and after laser treatment images are shown of the removal of chalk in and around a coat of arms. In Fig. 4 a magnified

Fig. 3. Selective removal of chalk from paper (*left*) before cleaning the object, (*middle*) digital isolated black and white image and (*right*) the object after laser treatment

Fig. 4. Detail view of the before (*left*) and after image (*right*), showing the removal of chalk inside the crown, demonstrating the accuracy of the cleaning

section of Fig. 3 is show, where the chalk has been removed from within the coat of arms, to indicate the accuracy of the system.

6 Conclusions

As a cleaning strategy, the selective laser ablation of dirt located between paper does not yield satisfying results. Laser treatment seems to be most successful in cases where the material to be removed is located on the surface or has penetrated only slightly between the fibres. On basis of the laser cleaning trials, it can be concluded that the green laser (532 nm) has the highest cleaning efficiency and the least (visual and chemical) side effects for the removal of inks, stamps and surface dirt from originals.

The UV laser (248 nm) has proven to be the most effective tool in the removal of homogenous layers of adhesive from original objects [5].

Acknowledgements

Financial support was provided by the European CRAFT project "Paper Restoration using Laser Technology (PaReLa)", EVK4-CT-2000-30002.

References

1. P. Rudolph, F. J. Ligterink, J. L. P. Jr., M. v. Bommel, J. Bos, H. A. Aziz, J.B.G.A. Havermans, H. Scholten, D. Schipper, and W. Kautek, *Characterisation of Laser-Treated Paper.* Applied Physics A, 2003
2. P. Rudolph, et al. *Laser-Induced Alteration of Contaminated papers.*, COLA 2003, Applied Physics A, 2003
3. L. Spencer, T. Fourrier, J. Anderson, A. E. Hill: Canvas glue removal using a 248 nm Excimer Laser, ICOM, vol. 1, 1999, pp 336–340
4. J. H. Scholten and D. A. Schipper, *Advanced workstation for controlled laser cleaning of paintings*, Proceedings of SPIE Vol. 4402, 2001, pp 121–129
5. J. H. Scholten and P. van Dalen *Laser cleaning of pressure sensitive tapes on paper*; practical application, research and risk assessment, CR laser special, 2003, pp 41–51

Anti-Fungal Laser Treatment of Paper: A Model Study with a Laser Wavelength of 532 nm

E. Pilch[1], S. Pentzien[2], H. Mädebach[2], and W. Kautek[2]

[1] Austrian State Archives, Vienna, Nottendorfer Gasse 2, 1030 Vienna, Austria
[2] Federal Institute for Materials Research and Testing Laboratory for Thin Film Technology, Unter den Eichen 87, 12205 Berlin, Germany
wolfgang.kautek@bam.de

Abstract. Biodeterioration of organic cultural heritage materials is a common problem. Particularly the removal of discoloration caused by fungal pigments is yet an unsolved problem in paper conservation. In the present study, cellulose (cotton and linters) and 16th century paper (rag), were incubated with several fungi types, such as *Cladosporium, Epicoccum, Alternaria, Chaetomium, Aspergillus, Trichophyton,* and *Penicillium* on agar for three weeks. Then they were immersed in 70% Ethanol for removal of hyphae and mycelia and deactivation of the remaining conidia. These specimens were laser-treated in a computer-controlled laser cleaning system with a high pulse energy diode pumped Q-switched Nd:YAG laser operating at 532 nm and a pulse duration of 8 ns. Colour differences were determined spectrophotometrically. Best cleaning results were observed with fungi such as *Penicillium* and *Alternaria*. Dry laser cleaning generally turned out to be superb over wet bleaching approaches.

1 Introduction

Biodeterioration of organic cultural heritage materials is a common problem [1, 2]. Cellulose is probably the most abundant material of biological origin on the earth and is a prime source of energy for many fungi. While the conventional sanitizing techniques for removal of fungal material from paper using chemical or physical means have proved sufficient in many cases [2], the removal of discoloration caused by fungal pigments is yet a problem in paper conservation.

There are very rare reports on the removal of fungi from paper by lasers [3, 4]. A far-UV krypton fluoride (KrF) excimer laser was able to remove *Aspergillus niger* mould from filter paper while viable spores and mould fragments were released into the atmosphere [5]. Actually UVB radiation of a 308 nm XeCl excimer laser can be used for the treatment of skin mycosis fungoides [6]. That means that UV laser radiation can deteriorate fungi.

However, irradiation of cellulose with even a near-UV excimer laser at 308 nm resulted in photo-oxidative degradation of the paper substrate, accompanied by an increase in oxidized groups content (carbonyl or carboxyl)

and a severe decrease in degree of polymerisation [7, 8]. That means that successes of anti-fungal laser treatments with UV lasers are accompanied by photochemical paper deterioration.

There are several types of fungal damage on paper, such as (1) surface damage caused by obstruction of any image by the growth of colonies, and embedded fruit bodies. (2) Discoloration may be caused by pigments either produced in fruiting bodies, or located in mycelium, or secreted into the paper substrate. (3) Structural deterioration of the paper may be due to the enzymatic digestion of cellulose. Many species of moulds are involved in cellulose decomposition, but none are more widespread than species of the ascomycete genus Chaetomium.

Conventional anti-fungal treatment consists of (1) mechanical removal of fungal bodies (brush, suction devices, scalpel), of (2) disinfection by fungicides (ethanol 70%, fungicide, bleaching), and removing of discolorations of the object (solvents, bleaching) [3].

In this context, sanitizing by ethanol (70%) with 0,2% PHB-esters was done, though it does not act very sporicidal [9]. This process was followed by laser irradiation at a visible wavelength of 532 nm known to be the least aggressive to the paper matrix [7, 8].

2 Experimental

Fungi common on decaying plant materials have been chosen for this study because they are potential decomposers of cellulose, i.e. paper. (1) *Cladosporium* forms dark *greenish to black* colonies, which are black in reverse. (2) *Epicoccum* is easily recognized by its nearly spherical spores (conidia) on clustered conidiophores (sporodochia). The colonies are usually some shade of *red, orange, or yellow*. (3) *Alternaria* shows *dark brown* spores borne in simple or branched chains from the tips of simple dark conidiophores. (4) *Chaetomium*, a particularly strong cellulose decomposer, is characterized by densely hairy, egg-shaped fruiting bodies (perithecia) containing asci, which in turn enclose *brown* spores (ascospores). (5) *Aspergillus* is recognized by its distinct conidiophores terminated by a swollen vesicle bearing flask-shaped phialides. The spores come in *several* colours. It is sometimes pathogenic to man. (6) *Trichophyton* has *colourless* spores (conidia). It usually occurs as a skin parasite (dermatophyte) on man and animals but occasionally also in soil, leather, feathers, etc. (7) *Penicillium* is recognized by its dense brush-like spore-bearing structures. The spores (conidia) are nearly always *green*. *Penicillium* is a large and difficult genus encountered almost everywhere, and usually the most abundant genus of fungi in soils. Some species produce toxins and may render food inedible or even dangerous. On the other hand cheeses such as Roquefort, Brie, Camembert, Stilton, etc. are ripened with species of *Penicillium* and are quite safe to eat. The drug penicillin is produced by *Penicillium chrysogenum*, a commonly occurring mould in most homes [10].

Pure cultures of these species were subcultured in Petri dishes containing malt agar with the so-called slide culture technique. A block of sterile agar was cut out of a Petri dish and was placed upon a sterile slide resting on a bent glass tube within a sterile Petri dish. A few spores of a fungus were inoculated at the edges of the sterile agar block and topped with a cover glass for incubation on either cotton filter paper or handmade rag paper from around 1600. A disc of moist filter paper in the dish maintained humidity for the culture. After incubation at room temperature for three weeks, the paper samples were taken out of the dishes and immersed in 70% ethanol with PHB-ester for removal of hyphae and mycelia and deactivation of the remaining conidia. After drying, coloured stains remained as contaminant. To reduce shrinks and folds, samples were slightly moistured (1 hour) using a Gore-Tex laminate and then flattened for easier handling during laser cleaning. Chemical bleaching was done in a 0.5% $KMnO_4$ solution for 30 s, which was terminated by submersion in 1% potassium metabisulfite.

The laser treatment of these paper samples contaminated with the above described fungi remnants were undertaken with the wavelength 532 nm at the Federal Institute for Materials Research and Testing, Berlin. A computerized prototype laser cleaning system, based on a high pulse energy diode pumped Q-switched Nd:YAG laser operating with a pulse duration of approximately 8 ns, a repetition rate <1 kHz, and a maximum energy 2.5 mJ was employed. The set-up consisted of a scanning optical system (254 mm focal length) which delivered a spot size of approximately 100 µm and maximum energy densities (fluences) in the range of up to $F(532\,\mathrm{nm}) = 10\,\mathrm{Jcm}^{-2}$. An integrated exhaust system served to remove fungal tissues.

The multi-spectral imaging system (MuSIS 2007, Art Innovation, Hengelo, The Netherlands) operated in a spectral range from 320 nm up to 1550 nm. Several imaging modes were employed: visible reflection, infrared reflection, visible fluorescence, and ultraviolet reflection.

Semiquantitative colour measurements (spectral reflectance) were carried out with the same system. The illumination conditions were the same as in the imaging mode (qualitatively similar spectral characteristics as standard illuminant D_{65} with UV and VIS components) and were kept constant. CIE-$L^*a^*b^*$ colour coordinates were therefore formally used for the evaluation. Data allow relative, not absolute, comparisons under the described conditions in respect to lightness changes ΔL, saturation and hue changes given by the chromaticity coordinates Δa^* and Δb^*. The vector between two data sets in the colour sphere is the colour difference ΔE that is very useful for semiquantitative assessments of colour changes:

$$\Delta E = \sqrt{L^{*2} + a^{*2} + b^{*2}} \tag{1}$$

Lightness changes ΔL quantified by this relative technique could be correlated with the cleaning status. The overall colour difference ΔE includes also the colour changes for which the human eye is particularly sensitive.

3 Results and Discussion

Mechanical removal by rubber and scalpel of all fungi remnants after the alcohol treatment showed practically no success in almost all cases. The discoloration could not be reduced, only paper fibres were removed in an uncontrolled way.

Chemical bleaching by $KMnO_4$ after the alcoholic treatment led to acceptable improvements of the sample appearance in the cases of *Trichophyton*, *Epicoccum* and *Penicillium*. Limited success was observed with *Cladosporium*, *Chaetomium*, *Alternaria*, and *Aspergillus*.

Laser irradiation after the ethanol leaching resulted in drastic improvements of the specimens' appearance to the naked eye in respect to discoloration with all fungi types except *Cladosporium* and *Aspergillus*. The almost black remnants of *Cladosporium* present deeply in the bulk of the paper matrix could not be removed, and resulted in a dark brown appearance. The colourless *Aspergillus* deteriorated the paper fibre and the printing ink extensively. Therefore laser-induced alterations became relatively irrelevant. *Alternaria* caused substantial problems with mechanical and chemical treatments but yielded good results by Laser treatment. This grows in surface-near regions and therefore can be removed without paper ablation. In contrast, *Chaetomium* grows deeply in the paper matrix with its hair-like aspendices. Therefore, conventional approaches were completely unsuccessful, whereas the laser could yield an acceptable cleaning affect (Figs. 1a, 2a). *Epicoccum* exhibits leaching remnants deeply distributed in the paper matrix with various colours. Bleaching resulted in relatively good in-depth discoloration. The

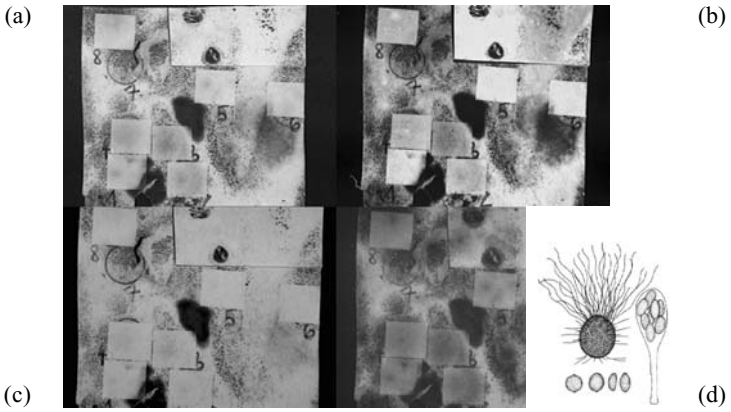

Fig. 1. *Chaetomium* on cotton paper (Whatman filter paper). Multispectral Imaging. (**a**) VIS reflectivit (**b**) fluorescence (**c**) IR reflectivity (**d**) UV reflectivity. Fluence 0.8–2.3 Jcm^{-2}. $KMnO_4$-bleached sample in *upper right* corner of each image. Insert [10]: drawing of egg-shaped fruiting *chaetomium* bodies (perithecia) containing asci, which in turn enclose 4-8 brown spores (ascospores)

Fig. 2. *Chaetomium* on handmade rag paper (∼1600 A.C.). Multispectral Imaging. (**a**) VIS reflectivity (**b**) fluorescence (**c**) IR reflectivity (**d**) UV reflectivity. Fluence 0.5–1.3 Jcm^{-2}. $KMnO_4$-bleached sample in *lower right* corner of each image

laser could remove coulored material near the surface, and deep contaminant regions were left over causing a brownish colour. *Penicillium* material was converted into almost black material by the alcohol treatment. It could well be removed by mechanical and bleaching processing. The type 7 however, grew deeper in the paper and therefore was resistant to mechanical removal. The laser was very successful, at least in the surface-near regions (Figs. 3a, 4a). *Cladosporium* grows deeply in the fibre material forming dark leaching products that could not be affected by neither mechanical nor chemical treatment. The laser yielded a limited success near the surface.

Multispectral imaging allowed documenting laser-cleaning results in comparison to cut paper sections, which have undergone bleaching in permanganate instead. Laser cleaning examples of *Chaetomium* and *Penicillium* on cotton paper and rag are represented in Figs. 1 and 2, and 3 and 4, respectively. These two fungi show that remnants after the removal of hyphae and mycelia and the deactivation of the remaining conidia by ethanol could be removed by the laser at least in surface-near regions. The ablation threshold fluences determined by microscopic inspection were at least $F_{\mathrm{th}} \sim 1.4\,\mathrm{Jcm}^{-2}$ for the pure cotton paper, and at least $F_{\mathrm{th}} \sim 1.0\,\mathrm{Jcm}^{-2}$ for the rag paper. The applied laser fluences ranged below the ablation thresholds and above. In the latter case, the laser was used as a "contactless scalpel".

An appreciable deep cleaning action is documented by the IR reflectivity images (c). The laser turned out to be more efficient than the aggressive bleaching process (a, d). The fluorescence images (d) may be used to identify

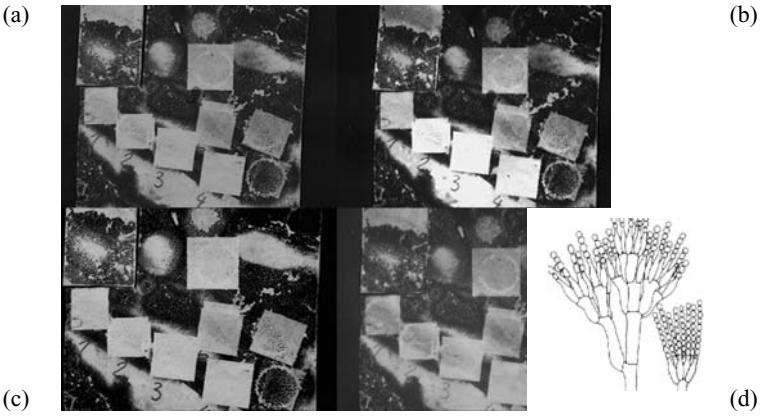

Fig. 3. *Penicillium* on cotton paper (Whatman filter paper). Multispectral Imaging. (**a**) VIS reflectivity (**b**) fluorescence (**c**) IR reflectivity (**d**) UV reflectivity. Fluence 0.1–1.8 Jcm^{-2}. $KMnO_4$-bleached sample in *upper left* corner of each image. Insert [10]: drawing of dense brush-like spore-bearing structures of *Penicillium*

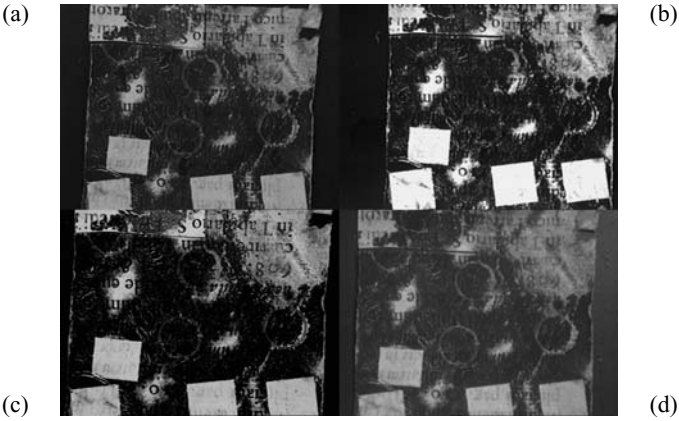

Fig. 4. *Penicillium* on handmade rag paper ($\sim$ 1600 A.C.). Multispectral Imaging. (**a**) VIS reflectivity (**b**) fluorescence (**c**) IR reflectivity (**d**) UV reflectivity. Fluence 0.3–1.8 Jcm^{-2}. $KMnO_4$-bleached sample in *upper left* corner of each image

possible irreversible material changes. The *Aspergillus* type examined showed efficiency in deteriorating printing ink on the rag paper. It was practically colourless, so that the laser interaction was comparatively inefficient.

The spectral imaging system was further used for semiquantitative colour change measurements according to the *CIE*-$L^*a^*b^*$ formalism. This allowed an even more detailed analysis.

This approach was used to identify irreversible changes of the paper types caused by the chemical treatment, alcohol vs. $KMnO_4$ (Table 1). Both

Table 1. Influence of fungicide and bleaching liquid treatment on pure paper. Colorimetric data (CIE-$L^*a^*b^*$ colour coordinates), colour difference ΔE, brightness ΔL (Averaged over 7 measurements). Treated status vs. original sample

Paper Type	Colorimetry		Ethanol vs. Orig.	$KMnO_4$ vs. Orig.
Rag	VIS reflectance	ΔL	−1.4	−3.4
		ΔE	6.1	7.1
	Fluorescence	ΔL	−12.2	−20.1
Cotton	VIS reflectance	ΔL	+7.0	+4.7
		ΔE	8.4	5.7
	Fluorescence	ΔL	−36.3	−36.3

treatments cause conceivable colour changes expressed by $\Delta E \sim 5 - 9$. The cotton darkened it both cases ($\Delta L > 0$) whereas the old rag underwent a slight cleaning. The change of the entire fluorescence spectrum could be expressed by a ΔL evaluation. Interestingly, the pure cotton type showed a drastic increase of fluorescence in both chemically very different liquid treatments suggesting irreversible chemical alterations. This was found to a weaker extent with the old rag.

Tables 2 and 3 sum up the lightness change (ΔL) results of all investigated fungi except *Aspergillus*, which was exempted because of its lack of colour.

Table 2. Influence of laser/alcohol treatment and bleaching on rag paper contaminated with fungi. Brightness ΔL (CIE-$L^*a^*b^*$ colour coordinates), treated vs. pure or infected sample. Laser parameters, $F/R/N$: fluence F[Jcm^{-2}]; scan rate R [pulse per mm]; number of scans N

	Fungus on Rag	Laser Parameters $F/R/N$	ΔL Laser vs. pure "Success"	ΔL Laser vs. Fungus "Efficiency"	ΔL $KMnO_4$ vs. Fungus "Efficiency"
1	*Cladosporium*	0.8/20/3	4	−65	−29
2	*Epicoccum*	0.8/20/5	16	−27	−38
3	*Alternaria*	0.8/40/2	10	−55	−39
4	*Chaetomium*	0.8/40/2	36	−29	−6
6	*Trichophyton*	0.8/20/2	13	−19	−23
7	*Penicillium*	0.8/20/3	−5	−71	−16
8	*Penicillium*	0.8/20/2	1	−70	−38

The comparison of ΔL of the infected areas after and before the laser interaction ("Laser vs. fungus") and after and before the $KMnO_4$ bleaching ("$KMnO_4$ vs. Fungus") is a measure for the "efficiency" of the cleaning process. A high negative ΔL indicates a strong relative cleaning effect. Clearly,

Table 3. Influence of laser/alcohol treatment and bleaching on cotton paper contaminated with fungi. Brightness ΔL (CIE-$L^*a^*b^*$ colour coordinates), treated vs. pure or infected sample. Laser parameters, $F/R/N$: fluence F [Jcm^{-2}]; scan rate R [pulse per mm]; number of scans N

	Fungus on Cotton	Laser Parameters $F/R/N$	ΔL Laser vs. Pure "Success"	ΔL Laser vs. Fungus "Efficiency"	ΔL $KMnO_4$ vs. Fungus "Efficiency"
1	*Cladosporium*	1.3/40/1	19	−50	−13
2	*Epicoccum*	1.3/20/1	27	−23	−21
3	*Alternaria*	0.8/40/1	−2	−68	−58
4	*Chaetomium*	1.3/20/2	1	−36	−73
6	*Trichophyton*	1.3/20/2	8	−59	−42
7	*Penicillium*	1.8/20/5	−1	−66	−16
8	*Penicillium*	1.3/20/1	14	−48	−13

the laser showed the higher efficiency versus the chemical bleaching. The laser exhibits the most negative ΔL values when used on *Cladosporium*, *Alternaria* and *Penicillium*, which species show the dark material remnants. On *Epicoccum*, *Chaetomium* and *Trychophyton* the laser is less efficient but still comparable to the chemical bleaching process.

A further criterion for the laser cleaning result is the comparison of ΔL of the infected areas after laser irradiation with pure and uninfected samples ("Laser vs. pure"). The best result would be the resemblance of the cleaned surface with the original pure surface ("Success"), i.e. $\Delta L \sim 0$. In this respect, the substrates exhibit different behaviours. On cotton (Table 3), the best success was observed again with the dark types *Alternaria* and *Penicillium*, but not *Cladosporium*. Even *Chaetomium* and *Trichophyton* could be removed so that ΔL almost resembled that of the pure cotton paper. On rag (Table 2), the darkest species *Penicillium* shows the best cleaning success followed by *Cladosporium* and *Alternaria* in analogy to the "efficiency" described above.

4 Conclusions

Laser cleaning experiments were done at 532 nm after sanitizing fungi-overgrown cotton and rag paper by ethanol. Chemical bleaching by $KMnO_4$ was compared. Remnants after the removal of hyphae and mycelia and the deactivation of the remaining conidia by ethanol could be removed by the laser at least in surface-near regions.

Spectral imaging served to register the visible reflection, infrared reflection, visible fluorescence, and ultraviolet reflection in a spectral range from 320 nm up to 1550 nm. Semiquantitative colour change measurements according to the *CIE-$L^*a^*b^*$* formalism allowed to identify irreversible changes of

the paper types caused by the chemical treatment, alcohol vs. $KMnO_4$. Both paper types showed an increase of fluorescence in both liquid treatments suggesting irreversible chemical alterations.

The comparison ofΔL of the infected areas after and before the laser interaction and after and before the $KMnO_4$ bleaching was a measure for the "efficiency" of the cleaning processes. The laser turned out more efficient than the chemical treatment, particularly on *Penicillium*, *Alternaria,* and *Cladosporium*, which species show the dark material remnants. A further criterion was the comparison of the brightness ΔL of the infected areas after laser irradiation with pure uninfected samples ("Success"). Again laser cleaning of *Alternaria* and the *Penicillium* types showed the best success.

Acknowledgements

The EUREKA project "Laser Cleaning of Paper and Parchment (LACLEPA)" $\sum$! 1681 served as an umbrella for this research. One of the authors (W.K.) acknowledges partial financial support by the EU TMR project No. FMRX-CT98-0188. We thank D. Müller-Hess, Vienna, for valuable discussions.

References

1. B. Zyska, Intern. Biodeter. Biodegrad., Vol. 40, 43–51, 1997
2. M. Nittérus, Restaurator, Vol. 21, 25–40, 2000
3. H. Szczepanowska, C. Lovett Jr., J. Amer. Inst. for Conservation, Vol. 31, 147–160 1992
4. H. M. Szczepanowska, W. R. Moomaw, J. Amer. Inst. for Conservation, Vol. 33, 25–32, 1994
5. T. R. Friberg, V. Zafiropulos, M. Kalaitzaki, R. Kowalski, J. Petrakis, C. Fotakis, Lasers in Medical Sci., Vol. 12, 55–59, 1997
6. R. Soda, A. P. Vidolin, M. Esposito, M. S. Chimenti, A. Di Stefani, L. Bianchi, Experim. Dermatology, Vol. 11, 279–279, 2002
7. J. Kolar, M. Strlic, S. Pentzien, W. Kautek, Appl. Phys. A, Vol. 71, 87–90, 2000
8. J. Kolar, M. Strlic, D. Müller-Hess, A. Gruber, K. Troschke, S. Pentzien, W. Kautek, J. Cultural Heritage, Vol. 1, S221–S224, 2000
9. M. Nittérus, Restaurator, Vol. 21, 101–115, 2000
10. D. Malloch, Department of Botany, University of Toronto, 1997

Observation of the Post-Processing Effects due to Laser Cleaning of Paper

K. Ochocińska-Komar[1], A. Kamińska[2], M. Martin[3], and G. Śliwiński[1]

[1] Polish Academy of Sciences, IF-FM, Gdańsk, Poland
corrina@imp.gda.pl
[2] National Museum, Gdańsk, Poland
[3] Instituto de Quimica Fisica Rocasolano, CSIC, Madrid, Spain

Abstract. Samples of artificially contaminated model papers were cleaned by the use of pulsed Nd:YAG laser at 1064 nm and 532 nm and the ArF excimer laser 193 nm. The post-processing effects were analysed basing on comparison of DRIFT spectra and colorimetric data obtained before and after accelerated ageing. In the DRIFT spectra measured after the laser surface cleaning at 1064 nm, the largest long-term changes were observed for the gelatin-sized paper. This paper revealed higher oxidization than the non-sized one after irradiation at 193 nm, too. Presence of gelatin resulted also in yellowing and darkening of the laser treated paper after prolonged ageing.

1 Introduction

The laser cleaning of historical documents on paper and parchment represents a relatively new conservation technique and is intensively studied recently. Compared to the well established methods, i.e. dry or wet which are characterized by the use of mechanical action and are often supported by an application of solvents and chemicals, the pulsed laser radiation acts selectively and is controllable. It allows for a well localized removal of surface contamination with a minimal damage to the substrate fibers. However, a safe application of that tool requires an adequate selection of the laser interaction parameters. Also questions addressing the post-processing effects such as the yellowing, discoloration and changes of the chemical composition of the substrate material should be clarified [1, 2].

In this paper the results of experimental study of the long term effects due to laser irradiation of the cotton paper are reported. The paper samples are made in conformance with the paper production methods used in the past and are characterized by the properties and composition close to these of the historical paper. Samples are treated by the Nd:YAG and ArF lasers at wavelengths of 532, 1064 and 193 nm and at fluencies below damage threshold (0.3–0.9 J/cm^2). The accelerated ageing is applied for checking of the post-processing, long term effects due to laser treatment. The DRIFT and colorimetric measurements are performed for sample characterization and the results are discussed.

2 Experimental

Samples of a high purity, hand-made, non-bleached cotton paper (A) and also of the same material, gelatin-sized (B) were investigated. These paper samples were selected because of properties and chemical composition close to those of the historical hand-made paper.

The model samples were artificially contaminated with graphite powder and surface-cleaned by the Nd:YAG laser at 1064 nm or 532 nm (20 Hz, pulsewidth 6 ns), and for both irradiation wavelengths the same fluence around 0.6 J/cm^2 was applied. The ageing was performed at 90°C and relative humidity of 65% for the periods of 5 and 10 days which was equivalent to ageing under natural storage conditions for 25 and 50 years, respectively.

For DRIFT measurements the FTIR spectrometer (IFS66, BRUKER) equipped with the diffuse reflectance unit was used and the spectra were recorded for all samples before and after processing, and after artificial ageing, too.

Samples of the same paper, but not surface-covered by graphite were treated by the 193 nm ArF excimer laser. After irradiation at fluencies of 0.3; 0.6 and 0.9 J/cm^2 the DRIFT spectra were recorded. Also the colorimetric measurements were performed in conformance with the CIE Lab system by using the DMS apparatus (Autronic) with an illuminant D65.

3 Results and Discussion

The data obtained from division of the spectra for laser-treated samples by the spectra of untreated and uncovered by graphite ones are shown in Figs. 1 and 2.

The spectrum of the laser-cleaned (532 nm) sample A revealed changes larger than that of sample B, although the band positions were nearly the same for both of them. A number of bands characteristics for the paper samples was observed: the broad OH band (3600-3200 cm^{-1}); bands of CH, CH_2 and CH_3 groups (∼2890 cm^{-1}) and also some bands from the fingerprint region. These bands corresponded to the stretching and bending modes of cellulose elements COC, CO and CH_2 at 1180/1130/1090/890 cm^{-1} and 1430 cm^1, respectively. The increase of band intensities was due to formation of the inter- and intra-molecular bonds directly after irradiation [2]. For both samples cleaned at 532 nm the relative changes in intensities decreased after prolonged ageing. This indicated on recover of the primary chemical composition of the paper.

For samples cleaned at 1064 nm the spectral changes observed via band intensities increased due to ageing. The intensity growth of the C=O band (1650 cm^{-1}) was due to oxidization effect which accompanied the ageing of cellulosic paper. This was most distinct for the gelatin-sized sample B in agreement with literature [2, 3]. The graphite-free samples which were treated

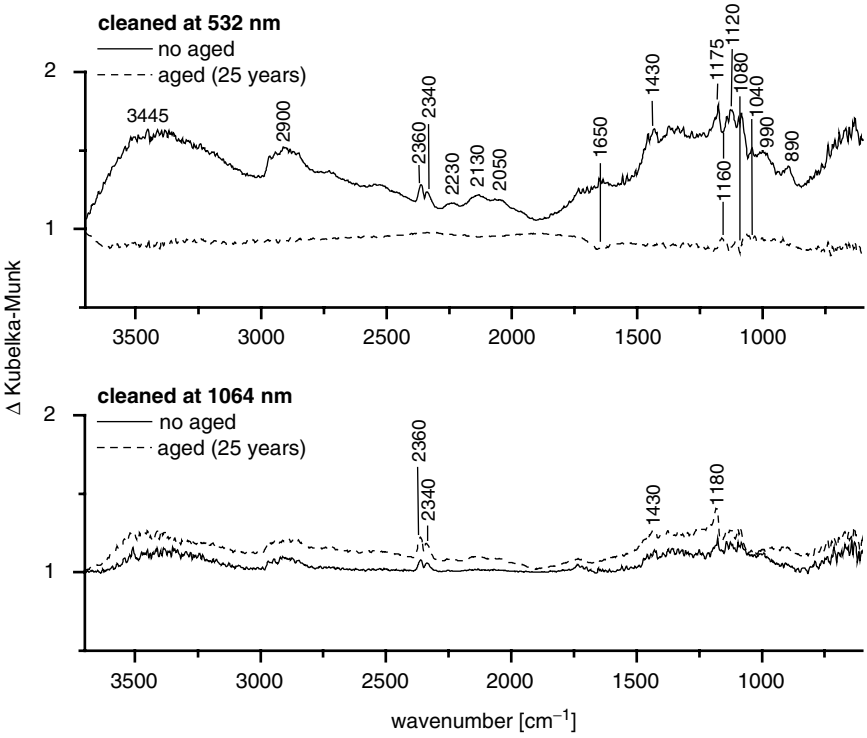

Fig. 1. DRIFT spectra of sample A after laser irradiation

by the 193 nm ArF laser revealed growth of the band intensities with increasing fluency of the laser applied for cleaning. The largest differences between the laser-treated and untreated samples were observed in the fingerprint region – see Fig. 3. Even the smallest ($0.3\,\mathrm{J/cm^2}$) irradiation fluency resulted in marked intensity differences of the cellulose bands for sample B whereas sample A remained almost intact after irradiation under the same conditions. Also, the sample B appeared more oxidized than sample A which was concluded from the band intensity increase at $1640\,\mathrm{cm^{-1}}$ after laser treatment.

The colorimetric results in the form of time dependences of the standard parameters **L*** (lightness) and **y** (yellowness) calculated from CIE values XYZ; $y = Y - Z$, were summarized in Figs. 4 and 5. The data were obtained as averages of measurements at 5 various locations of non-overlapping spots. In the long term changes of L* after laser irradiation of samples A and B no distinct differences were observed compared to the non-treated samples.

However, except of sample A treated at 532 nm in general smaller values of L for the treated samples after ageing were observed. The sample B irradiated at 532 nm showed the largest decrease of lightness after prolonged ageing. The change of yellowing of sample A proceeded similarly for the

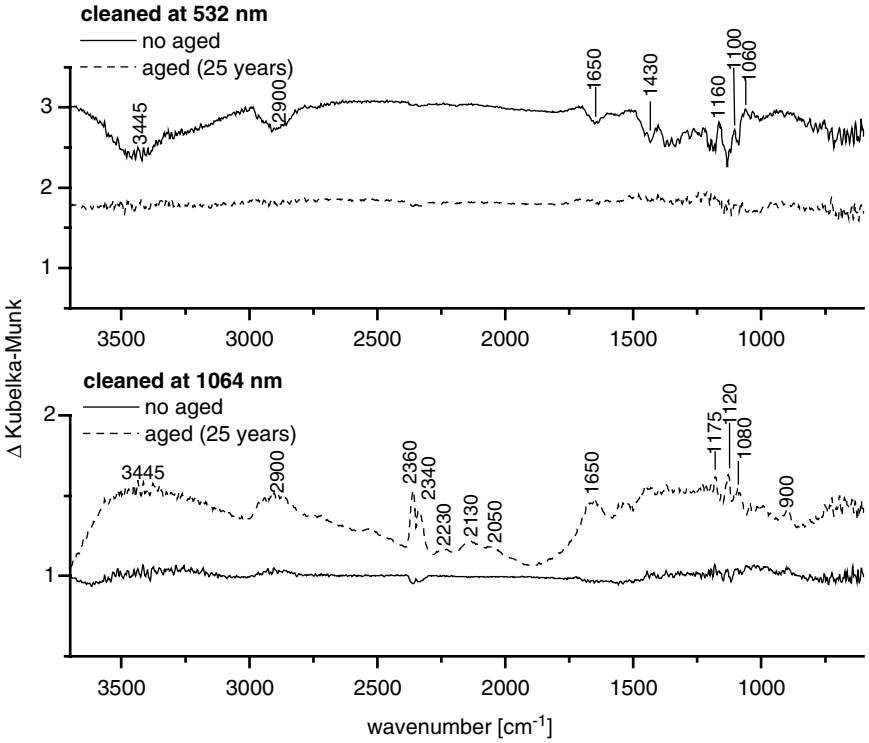

Fig. 2. DRIFT spectra of sample B after laser irradiation

laser-irradiated and non-irradiated samples. In contrary, for sample B irradiated at both wavelengths a dramatic increase of yellowing was observed after ageing. The yellowness of that sample irradiated by the 532 nm and 1064 nm laser increased by a factor of three and more than two, respectively.

4 Conclusions

The post-processing effect due to laser irradiation at different wavelengths of the cotton-based, model paper samples of properties and composition similar to the historical paper was investigated by means of the DRIFT and colorimetric techniques. The experimental results indicated that the presence of gelatin in the paper substrate influence significantly the laser irradiation effects observed on the long time scale. In the DRIFT spectra measured after the laser surface cleaning at 1064 nm, the largest long-term changes were observed for the gelatin-sized paper. This paper revealed higher oxidization than the non-sized one after irradiation at 193 nm, too. The presence of gelatin resulted also in yellowing and darkening of the laser treated paper after prolonged ageing.

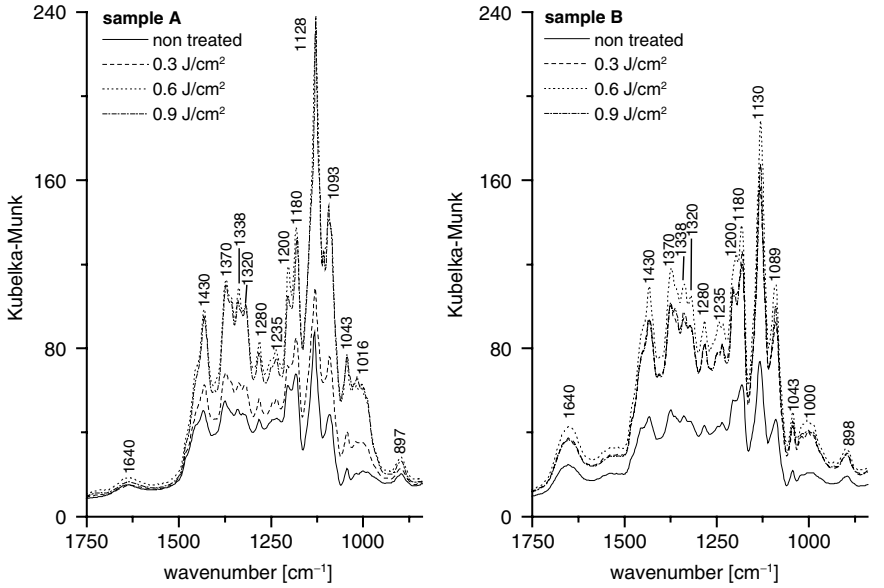

Fig. 3. The fingerprint region in the DRIFT spectra of samples treated by the 193 nm ArF laser

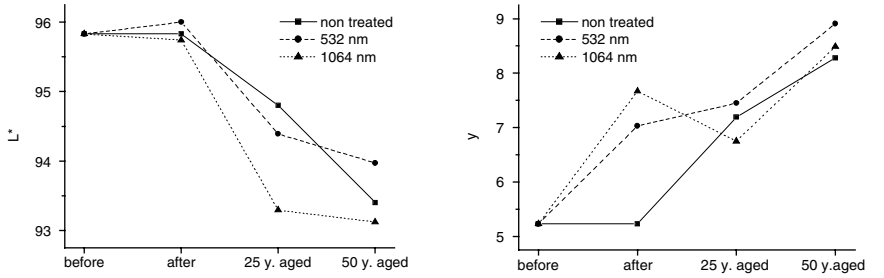

Fig. 4. The sample A; long term changes of lightness and yellowness due to laser irradiation at 532 and 1064 nm

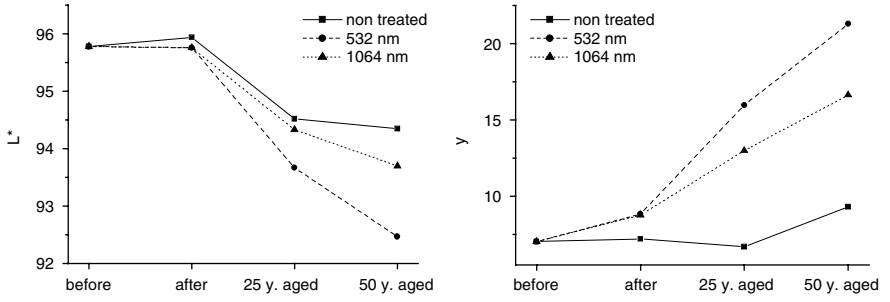

Fig. 5. The sample B; long term ligthness and yellowing due to laser irradiation at 532 and 1064 nm

Acknowledgements

This work was supported by the State Committee for Scientific Research (KBN) via projects: KBN 2 H01E 033 25 and SPUBM/COST and also by the bilateral agreement between Polish Academy of Sciences (PAN) and Spanish Council for Scientific Research (CSIC).

References

1. K. Ochocińska, A. Kamińska, and G. Śliwiński, in *Journal of Cultural Heritage*, Vol. 4, 188, 2003
2. J. Kolar, M. Strlic, S. Pentzien, and W. Kautek, in *Applied Physics A,* Vol. 71, 87, 2000
3. M. Ali, A. M. Emsley, H. Herman, R. J. Heywood, in *Polymer,* Vol. 42, 2893, 2001

The Post-Processing Effects due to Pulsed Laser Ablation of Paper

A. Kaminska[1], M. Sawczak[2], M. Cieplnski[3], and G. Sliwinski[2]

[1] National Museum in Gdansk, 80-822 Gdansk, Poland, ul.Torunska 1
alkamin@hot.pl
[2] Institute of Fluid-Flow Machinery Pol. Acad. of Sci., 80-952 Gdansk ul. Fiszera 14, Poland
[3] Pulp and Paper Research Institute, 90-950 Lodz, Poland, ul. M.Sklodowskiej-Curie 19/27

Abstract. For contemporary samples the effect of pulsed laser ablation applied at wavelengths selected from the range UV – near IR of 266, 355, 532 and 1064 nm were investigated. All the samples were made by the same method and of the same material, i.e. mixture of pure cotton cellulose and wood-pulp. Results of the colorimetric measurements indicate the most effective surface cleaning at 532 nm for the artificially soiled samples. An artificial aging resulted in neglectable changes in lightness and yellowness of the laser cleaned laboratory soiled samples but influenced the changes in non soiled samples. Marked changes were noticed due to 266 nm, 355 nm and 1064 nm irradiation and were ascribed to the photochemical damage of the cellulose fibres and to enhanced absorption of the laser radiation by the soil particles.

1 Introduction

The cleaning and conservation of historical documents on paper represent a difficult task for restorers due to the delicate substrate material. Until recently, for cleaning of the paper surface the mechanical methods and tools such as erasers or scalpels, and also chemical ones with the use of water and other solvents were used. The irreversible changes of the substrate structure and chemical composition, and also surface damage resulted often due to these procedures and were extensively discussed [1, 2].

Recently, the use of laser radiation for cleaning and restoration of historical documents was proposed. This technique allows avoiding the effects encountered when using the traditional, mechanical and chemical procedures to remove surface impurities. Moreover, the laser assures a non-contact and solvent-free, well localised action, and also computer control of the process [3–6].

It is known, that even if physical changes to the structure of the cellulose fibres are not observed immediately after the paper restoration, they can appear due to aging. These time dependent changes are difficult to notice by the naked eye. However, they can be effectively investigated by using artificial aging together with measurement of the absolute color changes.

This was confirmed by several spectrocolorimetric studies and allowed for better understanding of the chemical and structural processes involved [7–9].

The laser radiation used for ablative cleaning of the paper surface may have various effects on the structure of the cellulose fibres, depending on the laser interaction parameters such as the wavelength, fluence, pulse length and the total energy deposited. There are two types of interaction effects, depending on the wavelength and the paper substrate: the photo-chemical reactions caused by UV radiation which lead to photo-oxidation, and thermo-chemical ones due to IR radiation which are responsible for heating and the thermal decomposition of the cellulose. In both cases the destruction of the cellulose bonds occurs [10–13].

Both the photo-oxidation and the h-chemical reactions lead to similar processes that accompany natural aging. The oxidation and photo-oxidation reactions lead to cellulose pigment bonds and cellulose-chromophores, which are responsible for the paper yellowing being a clear sign of aging. Cellulose chromophores develop from hydroxyl, aldehyde and ketone groups. During natural aging the appearance of aldehyde groups around 2–3 atoms of carbon hydroxyl groups represent the main reason for the changes in colour [14].

In this work, the surface cleaning by means of laser ablation is performed on a modern, paper made from mixture of cellulose and wood pulp with and without additional gelatine glue. For the reference samples, and laser-processed ones, artificial aging is applied. Measurements of colorimetric parameters such as yellowing, absolute changes of colour and lightness were performed.

2 Experiment

The artificial and original paper samples were selected in order to collect a set of substrate materials representative so for the high quality XIX century historical documents made from wood pulp and cellulose mixture sized with gelatine as well as for application in restoration and conservation works [15]. In the experiment the following samples were investigated:

A. mixture of wood pulp and pure cotton cellulose (40% and 60%)
B. as A, gelatine-sized in the ratio of 3% vs. total sample mass (Gelatine glue, Kremer, Poland)
C. as B, laboratory soiled (contamination amount 20% of the mass of clean sample)

Samples A, B, and C were prepared and supplied by the Pulp and Paper Research Institute in Lodz. The artificial soiling under laboratory conditions was obtained by means of charcoal powder (CHEMIA, Warszawa).

For the ablative laser cleaning a pulsed Nd:YAG laser (Quantel) characterized by a pulse duration of 6 ns (FWHM), pulse repetition of 20 Hz and a nearly gaussian intensity distribution was applied. The laser was operated at

wavelengths of 1064 nm, and alternatively also at 532 nm 355 nm and 266 nm when the SHG, THG and FHG modules were used, respectively. The spot diameter in the laser interaction region was changed in the range of the wavelengths from 1.7 mm to 4.5 mm and the fluencies were selected and controlled by means of the beam expander together with a focusing lens (f = 200 mm) and joulemeter (Gentec). Values of fluence were varied between 0.3–0.9 J/cm^2 in order to operate in the range between the ablation and damage thresholds of a given material. In this way so the occurrence of the minimal cleaning effects as well as preservation against the substrate damage was assured. The respective threshold values were obtained prior to the sample cleaning experiments.

The accelerated aging was applied to the laser-processed and also reference samples in a closed climatic chamber at a temperature of 353 K and at 65% RH (rel. humidity) for a period of 10 days, which was equivalent to the aging of paper under natural conditions for 50 years, respectively.

In order to analyze the absolute colour changes due to laser processing the spectrophotometer (L&W Elrepho) operating with illuminant CIE C and the CIE standard colorimetric observer Z° in conformance with the CIELAB Colour System was applied. The entrance port diameter of the integrating sphere was equal to 8 mm, and the measurements were made at a temperature of 297 K (23°C) and RH of 50%. The data representative for a given surface area was obtained as averages of the series of 4 individual measurements made at various spot locations without overlapping. For data conversion into the **Lab** colour space a standard numerical code was used, with **L** – for lightness, **Δa** for red or green colour changes and **Δb** for the yellow or blue changes. Moreover, two descriptive parameters were calculated: the colour enhancement **C** and the yellowing **Yell/DIN** according to DIN 6167).

3 Results and Discussion

Data obtained from the colorimetric measurements were compared for the three groups of samples A, B, C.

3.1 Sample A

The laser irradiation at various wavelengths of 1064 nm, 532 nm, 355 nm and 266 nm caused a little change of the colorimetric parameters. After 10-day aging of these samples the parameter L dropped for about two units for the samples treated with 532 nm and 1064 and for those treated with 266 nm and 355 nm for about 4 and 5 units.

The R_{457} parameter, which describes the whiteness of the paper, became smaller for the samples treated with 266 nm, 355 nm, 532 nm and 1064 nm. After 10 days of aging it dropped from about 7 till 18 units for the sample surface treated with 266 nm.

The green-red changes in colour, which are described by the parameter, were very similar for all the samples. The samples become more reddish but the changes were very negligible (about 1 unit for all the samples).

The yellow-blue changes in colour described by the b parameter were similar for all the four samples: the values of samples treated with 532 nm, 355 nm and 1064 nm grew, which means that the surface becomes more yellow however the biggest change was recorded for the surface of the sample treated with 266 nm (about 7 units). The sample treated with 532 and 1064 nm became yellow for about 3 units, which was the smallest change. Results of measurements of the parameters b are shown in Fig. 1.

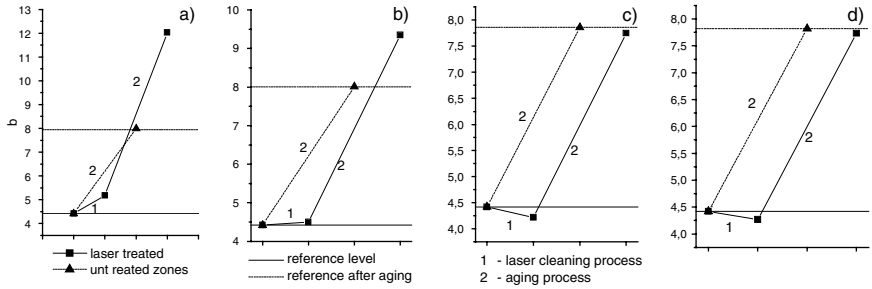

Fig. 1. The yellow-blue changes in colour (b) recorded on the cellulose and wood pulp paper surface after laser treatment with: (**a**) 266 nm (**b**) 355 nm (**c**) 532 nm (**d**) 1064 nm

The yellowing due to laser interaction was the most noticeable for the surface of the sample treated with the irradiation of 266 nm. It rose for about 12 units and for about 9 units for the sample treated with 355 nm. Compared to the rest of the treated samples it was the biggest change. For the sample treated with the irradiation of 532 nm and 1064 nm the change was about 7 units. For the samples treated with 1064 nm and 532 nm the yellowing process proceeded much the same as in the case of reference zones.

3.2 Sample B

The samples of the same paper, but sized on the surface with gelatine glue, became darker after the laser irradiation and after 10 days of artificial aging the change became deeper of about 1 unit for all the samples. The L parameter went down generally about 1 unit for the entire irradiated surface. The difference of parameter R_{457} between the untreated zones and treated ones was about one unit.

The green – red changes indicated by the parameter a were not even for the samples. The surface irradiated with 266 nm and 1064 nm became greener. The change was minimal for the samples irradiated with 532 nm

(below 1 unit) and about 1 unit for sample irradiated with 266 nm. Samples irradiated with 355 nm and 532 nm became redder in appearance and for the sample irradiated with 1064 nm the change were significant: about 10 units.

The parameter b, which indicates the yellow-blue changes in colour moved toward the yellow for the surface, irradiated with UV laser. The biggest change was observed for 266 nm. Irradiation with 532 and 1064 nm laser resulted in change the b parameter towards a blue colour. The biggest change (about 2 units) occurs for the surface irradiated with 1064 nm (Fig. 2).

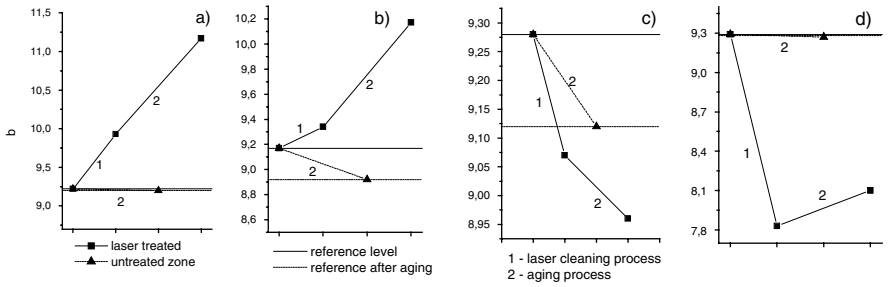

Fig. 2. The yellow-blue changes in colour (b) recorded on the cellulose and wood pulp paper surface sized with gelatine glue after laser treatment with: (**a**) 266 nm (**b**) 355 nm (**c**) 532 nm (**d**) 1064 nm

The most noticeable change after 10 days of artificial aging was observed for the samples treated with 266 nm and 355 nm radiation. The yellowing on the surface of the samples grew for the samples and achieved greater value after 10 days of artificial aging. Samples treated with 532 nm and 1064 nm after the laser treatment become less yellow but after 10 days of artificial aging of the sample treated with 1064 nm the Yellowness parameter rose for about 1 unit comparing to the reference level of untreated zone.

3.3 Sample C

For the same kind of paper, i.e. laboratory soiled with a layer of charcoal powder dust, the significant changes were recorded after laser irradiation. L parameter increased for all the irradiated samples for about 20 units and the biggest difference was recorded for the surface irradiated with 266 nm and 1064 nm from 62.37 to 81.24 and 81.20. After 10 days of artificial aging there were not many changes in the L parameters, only the surface of the sample irradiated by 355 nm radiation went lighter for about two units. The R_{457} parameter became higher for all the samples. The differences were similar for all the samples and the biggest one was recorded for the sample treated with radiation 266 nm – 17 units.

The b parameter, which indicates the yellow-blue changes moved towards a yellow colour for all the samples. The most significant change was recorded for the samples irradiated with 532 nm (about 6 units) and 1064 nm (about 8 units). Results of measurements of the parameter b are shown in Fig. 3.

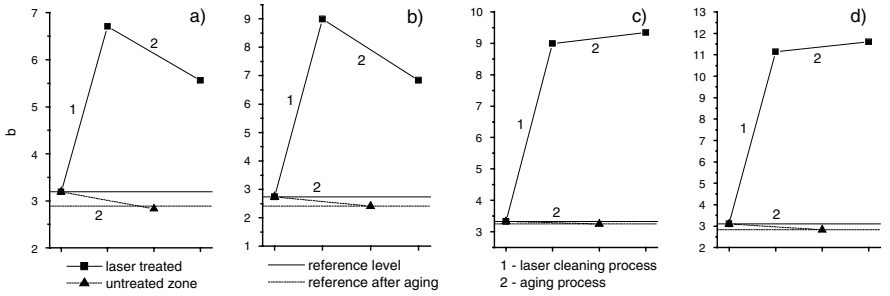

Fig. 3. The yellow-blue changes in colour (b) recorded on the cellulose and wood pulp paper surface sized with gelatine glue and laboratory soiled after laser treatment with: (**a**) 266 nm (**b**) 355 nm (**c**) 532 nm (**d**) 1064 nm

The general level of yellowing on the surface of the samples grew for all the samples. The most noticeable change was observed for the samples treated with 1064 nm radiation: 18 units and 532 nm about 11 units. The sample irradiated with 266 nm changed only for 3 units.

4 Conclusions

Samples produced contemporarily from pure cellulose and wood pulp generally become lighter in appearance after the laser treatment, especially when it comes to the laboratory soiled paper. The paper samples made from pure cellulose and wood pulp became the most yellowed under the influence of 266 nm and 355 nm radiation. The results above shows, that ultraviolet radiation accelerates the aging process in cellulose. Samples of paper artificially soiled with the charcoal powder dust were effectively cleaned at all laser wavelengths applied. In the case of the 1064 nm radiation the largest surface yellowing was measured compared to 266 nm, 355 nm and 532 nm. This was ascribed to the thermal component prevailing in processes due to material ablation induced at the longest wavelength applied. For samples produced contemporarily with the gelatine glue additive the increased yellowing of the paper surface after laser cleaning with 266 nm and 355 nm was revealed, for the sample of since this additive increased the range of absorption of the paper. In conclusion, it was found that the UV radiation at 266 nm and 355 nm had the least beneficial effect on the paper. This is due to the photochemical damage of the cellulose fibres. The near IR at 1064 nm enhanced absorption

of the laser radiation by the soil particles when it comes to the laboratory soiled samples. This indicates that laser cleaning of the hand-made paper by means of pulsed laser radiation at 532 nm represents the best solution and is in agreement with the literature [15, 16].

References

1. R. Moroz and E. A. Roever, Restaurator 14, 1996, 172
2. P. Sterlini, Paper Conservation News 76, 1995, 3
3. K. Ochocińska, A. Kamińska, and G. Śliwiński, Journal of Cultural Haritage 4, 2003, 188
4. K. Ochocińska, M. Sawczak, M. Martin, J. Bredal-Jörgensen, A. Kamińska, and G. Śliwiński, in print in Radiation Physics and Chemistry
5. A. Kamińska, M. Sawczak, G. Śliwiński, in print, Proc.SPIE XII ISQE, Varna, 2002
6. J. Caverhill, I. Latimer, and B. Singer, The Conservator, No. 20, 1996, p 65
7. D. D. Soares Oliviero, Rosa M. Miranda, Costa Jose L.C., Appl. Optics Vol.38, No. 30, 1999, p 6307
8. D. Müller-Hess, K. Troschke, J. Kolar, M. Strlic, W. Kautek, and S. Pentzien, Restauroforum 8, 2001, p 604
9. W. Surewicz, "Podstawy technologii mas wlóknistych", Wydawnictwo NT, Warszawa, 1971, pp 34–54
10. J. Kolar, M. Strlic, S. Pentzien, and W. Kautek, Applied Physics A. 71, 2000, pp 87–90
11. E. Berger "Istoria rozwitia techniki maslinajziwopisi", Moskwa, 1961, pp 311–313
12. Z. K. Annis and B. M. Reagan, Studies in conservation 24, 79, 1989, pp 171–178
13. E. Sobiczewska, ZKPIS, UMK Toruń, 1994, pp 6–7
14. J. Dąbrowski and J. Siniarska–Czplińska, Rękodzieło papiernicze" Wydawnictwo Czasopism i Książek Technicznych, Sigma NOT Sp. z o.o., W-wa (1991)
15. J. Kolar, M. Strlic, and M. Marimcek, Applied Physics A 75, 2002, pp 1–4
16. W. Kautek, S. Pentzien, D. Müller-Hess, K. Troschke, and R. Teule, Procc.SPIE Vol. 4402, 2001, p 139.

Laser Cleaning of Pressure Sensitive Tapes on Paper

J.H. Scholten[1], P. van Dalen[2], S. Corr[3], P. Rudolph[4], J.B.G.A. Havermans[5], H.A. Aziz[5], and F.J. Ligterink[6]

[1] Art Innovation b.v., Hengelo, The Netherlands
h.scholten@art-innovation.nl
[2] Art Conservation b.v., Vlaardingen, The Netherlands
[3] Paper conservation Susan Corr, Corrandulla (Co. Galway), Ireland
[4] Federal Institute for Materials Research and Testing, Berlin, Germany
[5] Netherlands Organisation for Applied Scientific Research, Delft, The Netherlands
[6] Netherlands Institute for Cultural Heritage, Amsterdam, The Netherlands

Abstract. Cleaning of paper objects can be very complex due to various combinations of contaminants. Conventional chemical and mechanical cleaning methods suffer from the common phenomenon that the foreign matter is diluted into the substrate rather than removed. In these cases, and where high spatial accuracy and localized treatments is necessary, laser cleaning promises to be an additional tool for conservators.

1 Introduction

Conservation of paper objects commonly deals with severe damage of variable origin. Frequently, these damages are divided into sub-categories such as *foxing* (coloured stains are formed on the paper), *use* (the tax form with coffee stains and written notes in textbooks) and *old repairs* such as the use of self adhesive tapes.

At present, conservation of these types of damage, if feasible, is very time consuming. Current cleaning techniques are often based on the use of organic solvents, liquid nitrogen, water, or a scalpel-blade knife. As scientific research in the conservation field progresses, the drawbacks of these conventional methods become more and more obvious. The use of a scalpel-blade (mechanical cleaning) can cause fiber damage, while chemical cleaning is difficult to perform locally, often dilutes the foreign matter into the paper substrate and produces emission of highly volatile organic compounds, which can be harmful to the conservator.

There is a need for new conservation technologies aiming at safe paper cleaning. However, the viability of these methods has to be verified, considering both the efficiency and long-term effects. The research presented in this paper was carried out within the cooperative research project entitled "Paper Restoration using Laser Technology" (PARELA, EVK4-CT-2000-30002), funded by the European Commission. The emphasis of this paper lies on the

practical application of laser cleaning to remove the adhesives left by pressure sensitive tapes.

2 Conservation Considerations of Pressure Sensitive Tapes

Much has already been written on the types of pressure sensitive tapes that have been used in the past and of those that are currently available, including amongst others, sellotape, scotch tape, masking tape and archival tape. All are proprietary brands which differ in both the carrier material and the chemical composition of the adhesive layer but, pertinently, they all eventually lose their adhesive properties, turn yellow, ultimately harden and consequently embrittle the paper fibre, albeit at different rates. This is why it is imperative for the conservator to remove these tapes.

Because of ease of application their use has been widespread and indiscriminate, they have been used for both repair and attachment, as much on culturally valuable material as on day-to-day objects of no significance. Their removal is therefore a regular procedure in the work of a conservator.

3 Assessment of Traditional Methods

From its application, a tape passes through several distinguishable stages in its deterioration. Initially, the adhesive layer is dry and very sticky, adhering strongly to the paper substrate whilst remaining closely bonded to its own carrier material. The tape is first removed using a scalpel and directed warm air, the residual adhesive is then removed from the surface of the paper using a rubber square [3, 4].

The next stage is usually characterised by a general softening of the adhesive layer that becomes tacky. As a result, the carrier may move or slip slightly on the adhesive layer. The adhesive is still clear although probably turning a little yellow, and it may have begun to penetrate the paper fibre. Again it may be possible to remove the carrier by easing it off with a scalpel and even to "ball" the adhesive layer with an eraser to facilitate removal. Sometimes, however, an appropriate solvent has to be introduced.

The final stage in a continuous oxidative action on the adhesive layer results in a product that is quite different in colour, form and function from the original. The adhesive generally crystallises, becoming hard and brittle, it will usually turn dark brown and where it has been absorbed into the paper fibre it is likely that it will have cross linked with it. This discolours the paper and may cause it to appear translucent. All adhesive properties are gone and the carrier, if in place, is retained out of memory of a former function.

If the hardened adhesive has remained on the surface, it is sometimes possible to prise it off with a scalpel, risking loss of paper fibre. Usually the

adhesive has penetrated in to the structure of the paper to some degree and a solvent is required.

Solvents are an important tool in the conservator's repertoire, and, used carefully, can achieve great results. But, there are accompanying risks. All solvents are toxic to the conservator to some degree, some solvents of themselves can leave an oily residue in the paper, solvents can soften the binding agent in ink and paint media and solvents can reduce the natural moisture content of the paper fibre at molecular level. Therefore, the method of solvent application requires consideration sensitive to the media and the paper.

Local treatment methods include poultice, exposure to solvent fumes and treatment on the vacuum table. The disadvantages of local treatment include the risk that the solvent may carry dissolved material further into the paper fibre leaving a residue at the interface between the treated and untreated areas. This can result in tide marking that appears in later years.

Total immersion of the paper in a suitable solvent allows for even dispersion of the adhesive into the solvent solution. However, the adhesive will most likely migrate throughout the complete object. In addition, the paper fibre can be saturated with solvent, which can remain for long periods of time before complete evaporation, increasing the risk of inducing chemical changes in the inks.

4 Selected Objects and Treatment Method

By using carefully chosen originals, it is possible to test which type of laser treatment is most effective at a certain degradation stage [1, 5], according to the classification of the three-stage deterioration process of rubber based adhesives by Feller [2], being:

I. oxidative induction stage
II. oxidation stage
III. crosslinked stage.

The Film museum Amsterdam submitted the following non-valuable original posters. According to the conservators, these specific posters properly represent the conservation problems encountered with pressure sensitive tape:

- poster Filmweek (6303D)
- poster Operetteliefde (2586D)
- poster Nikdo (06.22.5047)

The material used for these posters is wood pulp. Masking tape has been applied to reinforce the edges of the posters against wear and tear. The adhesive of the tape tends to migrate to the verso side of the paper during natural ageing. Due to the migration, the paper has discoloured. Furthermore the adhesive eventually hardens causing the paper to become brittle and finally the tape carrier will fall off. Before laser treatment, poster 2586D

and 06.22.5047 were judged to be in degradation stage I. On poster 6303 D a certain area was chosen where the adhesive had hardened and migrated through to the other side of the poster according to degradation stage II and III.

Effective conventional cleaning and laser cleaning requires prior removal of the tape carrier to gain access to the adhesive layer. The carrier on both posters was removed using the hot-air tool. Most of the adhesive was left behind on poster 2586D and as expected the substance was very sticky. On some samples a part of the tape carrier has been retained to assess future post-ageing of the samples.

5 Laser Cleaning Procedure Using UV Laser

The UV laser system developed by Art Innovation is originally designed for cleaning of paintings [6]. It consists of a Lambda Physik Compex 205 excimer laser operating at 248 nm; pulse duration ∼20 ns, repetition rate range 1–50 Hz; pulse energy range 0–600 mJ/pulse; maximum average power 30 W. The laser beam, has an adjustable working spot size of X: 0.1–10 mm and Y: 1–35 mm, and is delivered by a motorised articulated arm. Additional features are a HeNe aiming beam, on-line monitoring and analysis by Laser-Induced Breakdown Spectroscopy, auto focus system, and high resolution viewing camera.

On poster 6303 D, areas with hardened (cross-linked) and sticky adhesive layers were chosen for treatment. Laser parameters such as pulse energy, spotwidth, overlap, number of pulses per spot and number of scans were optimised in an iterative manner [7].

Poster 2586D was used to check that the optimal parameters found on poster 6303D were still valid when applied to a different original object and not just a "lucky shot". With a pulse energy of approximately 220 mJ, a spotwidth of 1 mm, an overlap of 80% percent between consecutive spots, 2 laser pulses per position and a large number of scans (>15) similar, reproducible results to poster 6303D were obtained.

A larger area on poster 06.22.5047 was cleaned using these optimal cleaning parameters. After mechanical removal of the carrier, the distribution of the adhesive is not even or homogenous but irregular. Due to the large spot-size of the UV laser complete removal of adhesive would cause thinning of areas where the paper was not covered by adhesive. Therefore, the sticky adhesive layer on poster 06.22.5047 Nikdo was spread and flattened by a spatula to form a homogenous layer before treatment with the UV laser.

After treatment, visual evaluation by conservators showed that the surface was satisfactorily cleaned. However, the surface still felt slightly sticky to touch, indicating fragments of adhesive still remained. These fragments can be observed more clearly in fluorescence and ultraviolet reflection. No visual changes could be observed on the verso side of the poster.

6 Conclusions

An additional assessment had to be made after ageing of the posters to evaluate if the laser treatment has induced effects that only become apparent after certain time has passed. Following the laser treatment additional aging was performed by storing the papers for 12 days @ 90°C and 50% R.H. (relative humidity). Although it might be observed that the chosen temperature of 90°C induces effects not seen during natural ageing and therefore might be considered to be too high, the purpose of post-ageing in this specific case is to visualize and enhance possible negative effects of UV laser cleaning and conventional cleaning.

After ageing, the front sides of all posters exhibit a strong brown discoloration along the edges, matching the position of the masking tape on the recto. The reason for this discoloration is migration of the adhesive through the paper due to the ageing process; the migrated and hardened adhesive now corresponds to degradation stage III, see Fig. 1.

Visual assessment clearly shows that areas that have been laser treated display considerably less discoloration on both sides of the posters. Obviously, the removal of the adhesive due to the laser treatment prevents migration of

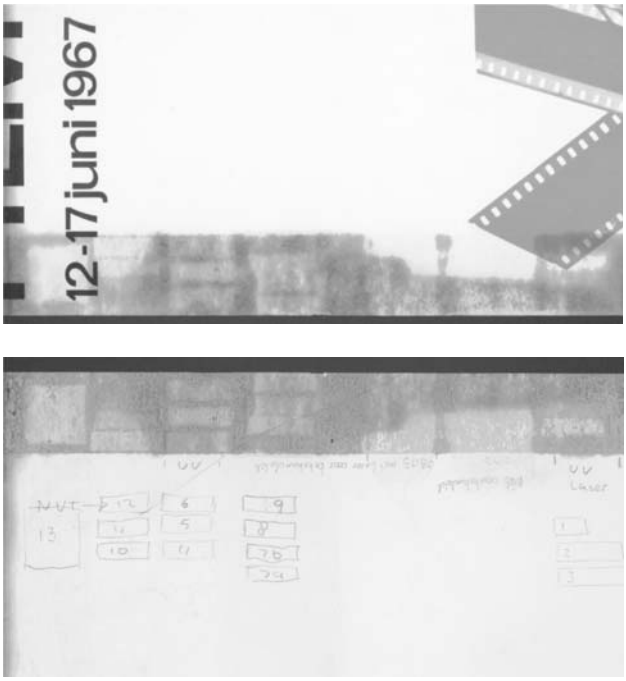

Fig. 1. Front (*top*) and back (*bottom*) of poster 6303D after ageing, notice the tide lines left by the use of solvent

adhesive and discoloration of the paper. More important however is the fact that the intense ultraviolet laser radiation to which the treated areas have been subjected has not induced any additional discoloration.

Another remarkable effect that becomes visible after the aggressive ageing procedure is "bleeding" of the plasticizers along the edges of the masking tape carrier, as can be most clearly seen in Fig. 2. The reverse sides of the posters show a light brown discoloration, which is caused by residual, adhesive.

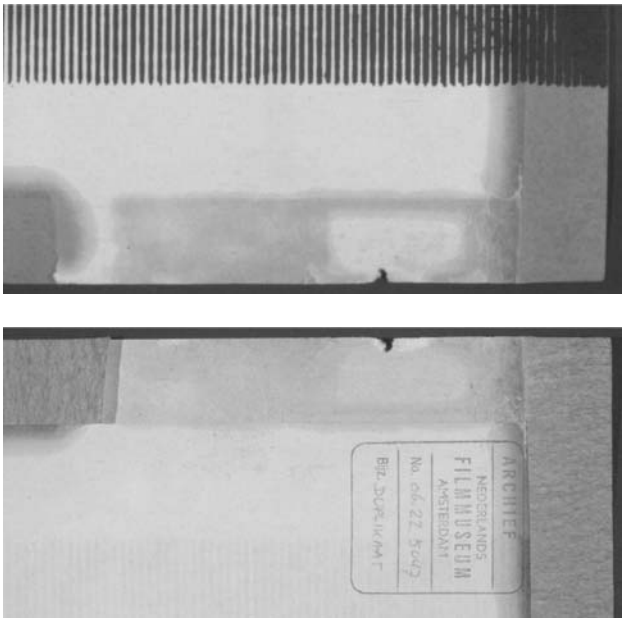

Fig. 2. Front (*top*) and back (*bottom*) of poster 06.22.5047 after ageing

Acknowledgements

Financial support was provided by the European CRAFT project "Paper Restoration using Laser Technology (PaReLa)", EVK4-CT-2000-30002.

References

1. P. Rudolph, F. J. Ligterink, J. L. P. Jr., M.v. Bommel, J. Bos, H. A. Aziz, J.B.G.A. Havermans, H. Scholten, D. Schipper, and W. Kautek, *Characterisation of Laser-Treated Paper.* Applied Physics A, 2003
2. R. L. Feller and D. B. Encke, Stages of Deterioration: The Examples of Rubber Cement and Transparent Mending Tape, *Science and Technology in the Service of Conservation*: Preprints, IIC, Washington D.C., 1982

3. M. Smith, N. M. M. Jones, S. L. Page, and M. L. Dirda, Pressure Sensitive Tape and Techniques for its Removal from Paper. *Journal of the AIC*, vol. 23, No. 2, Spring 1984
4. E. O'Loughlin and L. S. Stiber, a closer look at Pressure-Sensitive Adhesive Tapes: update on Conservation Strategies. Manchester Papers, 1992, pp 280–286
5. L. Spencer, T. Fourrier, J. Anderson, and A. E. Hill, Canvas glue removal using a 248 nm Excimer Laser, ICOM, vol.1, 1999, pp 336–340
6. J. H. Scholten and D. A. Schipper, Advanced workstation for controlled laser cleaning of paintings, Proceedings of SPIE Vol. 4402, 2001, pp 121–129
7. J. H. Scholten and P. van Dalen, Laser cleaning of pressure sensitive tapes on paper; practical application, research and risk assessment, CR laser special, 2003, pp 41–51

Chemistry of Parchment-Laser Interaction

L. Puchinger[1], S. Pentzien[2], R. Koter[2], and W. Kautek[2]

[1] Vienna University of Technology
Institute of Chemical Engineering, Getreidemarkt 9/173, 1060 Vienna, Austria
lpuching@mail.zserv.tuwien.ac.at
[2] Federal Institute for Materials Research and Testing Laboratory for Thin Film Technology, Unter den Eichen 87, 12205 Berlin, Germany
wolfgang.kautek@bam.de

Abstract. Laser-induced chemical modifications of various types of contemporary and ancient parchments have been studied. Such research in physico-chemical diagnostics is the prerequisite of computer-aided laser destructionless processing based on off-line and on-line diagnostics. The photometric determination of the water-soluble degradation products of collagen proved to be a sensitive method to detect laser-induced alterations of parchment even below the ablation threshold fluence. It is indicative for changes on the molecular level. The shrinking temperature measurement by the micro-hot-table technique turned out to be sensitive only to laser treatment that caused photochemical reactions (i.e. UV, 308 nm). At the visible (532 nm) and the infrared wavelengths (1064 nm), photochemical alterations are absent, solely thermally induced crosslinking of the collagen fibres is observed. Scanning electron microscopy proved only sensitive to phase changes like melting accompanying ablation above the threshold fluence.

1 Introduction

Restorers have begun to use pulsed lasers [1–3]. The contactless laser cleaning of biogenetic surfaces such as parchment (Fig. 1) has been studied however

Fig. 1. Contaminated ancient psalterium parchment (15th century, Southern Germany; private W. Kautek)

only in recent years [4–9]. Laser cleaning of parchment to some extent parallels dermatological laser applications that are regarded as a multi billion-dollar market [10, 11]. There, selective photothermolysis of pigmented subsurface structures, such as melanin particles, enlarged blood vessels, and tattoo ink particles, or char-free vaporization of skin takes place. Then the skin's natural physiological mechanisms break down and remove the laser-altered remnants. In parchment cleaning, however, natural resorption of laser-altered remnants is absent, and contaminants have to be removed completely without any irreversible morphological and chemical conversions of the substrate.

Modern analytical chemistry offers valuable tools to investigate laser-induced degradation, i.e. morphological and chemical changes, of such a biogenetic fibre material. On-line laser-induced plasma spectroscopy (LIPS) and on-line laserinduced fluorescence (LIF) during laser cleaning of model systems consisting of multilayer composites of carbon containing contaminants, pigments and parchment have been reported [4–6]. Since LIPS relies on the destruction of a substrate, it provides limited applicability in the in-situ monitoring of non-destructive laser cleaning of parchment and paper. However, a substantial list of mainly inorganic pigments shows strong LIF emission intensity, and provide good spectroscopic separation from the LIF emission of the parchment substrate [4–6]. Further, colour metrics and Diffuse Reflectance Infrared Fourier Transform Spectroscopy (DRIFT) are powerful techniques to verify any laser-induced chemical alterations both of the pigment-binder coatings and the parchment [7, 8].

In the present study, a multi-method approach was undertaken with scanning electron microscopy, the photometric determination of the water-soluble degradation products of collagen, and the shrinking temperature measurement by the micro-hot-table technique.

2 Experimental

The parchment samples described in this paper are based on animal hide, goat and calf origin (Gerberei Ludwig Edlauer, Enns, Austria, and Carl Wildbrett, Bobingen, Germany). Ancient specimens were selected and provided by the Biblioteca Apostolica Vaticana [12].

Parchment is commonly manufactured from the dermis layer of animal skin after strong alkaline removal of the epidermis and the subcutaneous tissue layers. It mainly consists of collagen fibres. Their molecular subunits are polypeptide chains with various amino acid side chains R_x:(-NH-CHR_x-CO-)$_n$. The major constituent is the hydroxyproline amino acid polypeptide protein. The structure of collagen consists of three individual protein strands in the a-helix conformation. These are rigidly held by strong hydrogen bonding interaction between the hydroxyl of the hydroxy-proline and the amino hydrogens of adjacent glycine units. In parchment manufacture, two-dimensional reorientation of the collagen fibres takes place in a stretching

and drying process controlled by $CaSO_4$, CaO, and $CaCO_3$ additives. Often a plasticising rehydration end-treatment is applied using egg white and linseed oil.

Laser treatments were undertaken by three different laser wavelengths (308 nm, 532 nm, 1064 nm) at the Federal Institute for Materials Research and Testing, Berlin. An excimer type (Lambda Physik, model EMG 150) filled with XeCl gas was used for a wavelength of 308 nm. The pulse duration was 17 ns and the repetition rate ranged between 1 and 2 Hz. The wavelengths of 1064 nm and 532 nm were delivered by a computerized prototype laser cleaning system, based on a high pulse energy diode pumped Q-switched Nd:YAG laser operating with a pulse duration of approximately 8 ns, and a maximum energy of 5 mJ (1064 nm) and of 2.5 mJ (532 nm), respectively. The set-up consisted of a scanning optical system (254 mm focal length) which delivered a spot size of approximately 100 µm. The repetition rate was 500 Hz.

The sample preparation for the photometric determination of the water-soluble degradation products of collagen in laser-treated parchment required 10–25 mg of parchment, which was ultrasonically treated in 1 ml H_2O for 1 (1/2) hours. After filtration of the insoluble components, the solution was mixed with 2 ml 6N HCl in a 15 ml-Sovirel tube. After the end of CO_2 evolution, an 18-hour acidic treatment at 110°C followed. The hydrolysed solution was then mixed with 7 ml citrateacetate buffer (pH 6), neutralized with 4N NaOH, and diluted with 25 ml distilled water. 1 ml of the extract was mixed with 2 ml propanol and 1 ml chloramine-T solution in a 20 ml-test-tube and left for 20 min. Upon addition of a 1 ml aldehyd-perchloric acid mixture it was heated in a water bath at 60°C for 20 min. After cooling, photometry of the hydroxyproline colour complex was done in a 1 cm-cuvette at 550 nm versus a standard of distilled water. The calibration was performed with a collagen standard.

The measurement of shrinkage temperature in the so-called micro-hot-table technique demands small samples of parchment fibres (∼0.3 mg) [13], which were heated in water on a microscope slide positioned on a microscope hot table (Nikon Eclipse L200). During heating the fibres started shrinking at the shrinking temperature (T_s), which depends on the stability of the collagen.

3 Results and Discussion

The quantity of water-soluble degradation products of collagen is affected by laser radiation already below the ablation threshold fluence, F_{th}, at which material removal is detected under microscopic inspection (Table 1). The solubility of the modern parchment increased with 308 nm at low fluences (0.3 Jcm^{-2}) possibly due to photochemical degradation (Table 2). The ancient specimen already showed increased solubility at even lower fluence (0.1 Jcm^{-2}), but exhibited a decreased value at 0.3 Jcm^{-2}, where the modern

Table 1. Ablation threshold fluences

	Ablation Threshold Fluence/Jcm^{-2}		
Parchment	308 nm	532 nm	1064 nm
Modern (Goat 57)	0.7	3.0	3.0
Ancient (Vatican 4)	0.5	0.8	0.8

Table 2. Photometric determination of the water-soluble degradation products of collagen in laser-treated parchment. Dashed lines indicate positions of ablation thresholds (Table 1)

		Solubility/µg mg^{-1}		
Parchment	Fluence/Jcm^{-2}	308 nm	532 nm	1064 nm
Modern	0.0	13.97	13.97	13.97
(Goat 57)	0.3	17.31		
	0.8	-----	13.62	
	1.0			11.47

	4.0			11.82
Ancient	0.0	15.86	15.86	15.86
(Vatican 4)	0.1	18.99		
	0.2		12.54	
	0.3	12.50		
	0.5	-----		7.94
	0.8		10.53	
			----------	

sample still showed molecular degradation. Obviously, the decrease of soluble products indicates crosslinking or other analogous phase changes.

At the visible (532 nm) and the infrared wavelengths (1064 nm), the photochemical phenomena were absent, and the only result was a decrease of the solubility due to thermally induced crosslinking of the collagen fibres. Both photochemical (308 nm) and photothermal (532 nm, 1064 nm) alterations occurred already at fluences below the respective ablation thresholds as indicated in Table 2 by horizontal dashed lines.

Scanning electron microscopy (SEM) detected massive phase changes like melting and boiling that accompanied the ablation (vaporization) of the material above F_{th}. However, no changes were observed at $\mathrm{F} < F_{\mathrm{th}}$, where the water-soluble degradation products of collagen already were affected by the laser treatment and exhibited changes on the molecular level.

The hydrothermal stability by the micro-hot-table technique relies on heating collagen above the helix-coil transition temperature, which causes a collapse of the rod-like three-stranded collagen unit into random coils, which

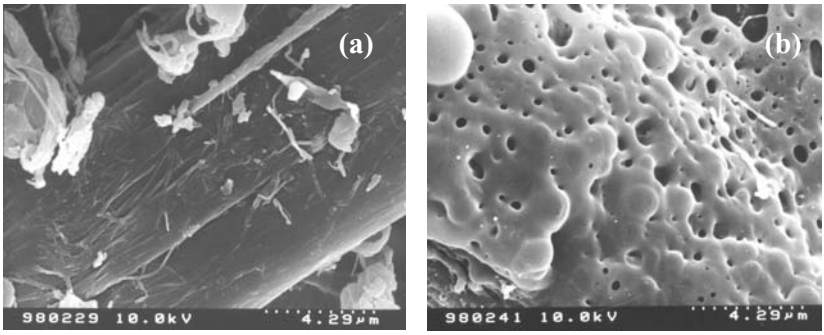

Fig. 2. Scanning electron micrographs of laser treated calf parchment (Carl Wildbrett, Bobingen, Germany). 308 nm, 17 ns, spot dimension 0.17 mm × 5.50 mm, scanning speed 0.05 mm/s, ablation threshold $F_{\mathrm{th}} \sim 0.7\,\mathrm{Jcm}^{-2}$. (**a**) $F = 0.0\,\mathrm{Jcm}^{-2}$, (**b**) $F = 3.6\,\mathrm{Jcm}^{-2}$

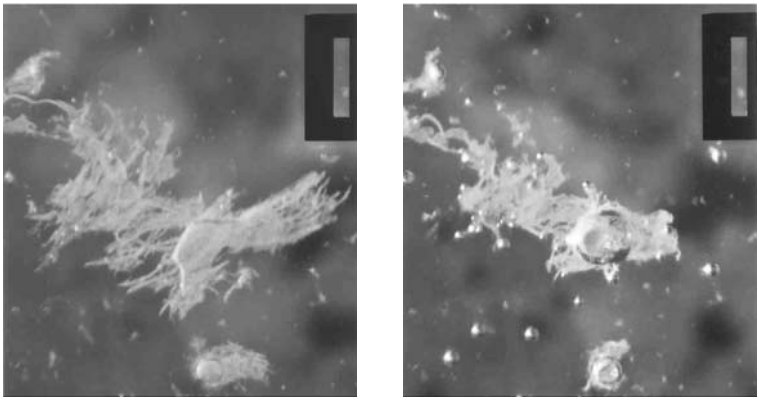

Fig. 3. Hydrothermal stability after UV-laser treatment (308 nm) by the microhot-table technique. Micrographs of ancient parchment flakes (Vatican 4) after laser irradiation ($0.5\,\mathrm{Jcm}^{-2}$). *Left*: 23°C; *right*: 60°C. Lower row high contrast presentation

then constitute gelatine [14]. When collagen hide fibres are heated in water they will deform and this deformation was seen as shrinkage of the fibres (Fig. 3). The hydrothermal stability of the fibres decreased in proportion to the state of deterioration.

This technique proved sensitive to laser irradiation that caused photochemical reactions as e.g. collagen polymer degradation (Table 3; comp. Table 2, 308 nm). The shrinking temperature, T_s, was only decreased under UV laser treatment, also at $F < F_{\mathrm{th}}$. Wavelengths which caused mainly thermal reactions (e.g. crosslinking, melting etc.) did not affect T_s. even though some laser fluences were chosen above the ablation thresholds.

Table 3. Hydrothermal stability of parchment by the micro-hot-table technique

Laser Wavelength	Shrinking Temperature, T_s[°C]/{Fluence [J/cm^2]}			
	Untreated	308 nm	532 nm	1064 nm
Modern (Goat)	60	45 $\{0.3 < F_{th}\}$	59 $\{2.0 < F_{th}\}$	60 $\{1.0 < F_{th}\}$
Ancient (Vatican 4)	48	39 $\{0.5 \sim F_{th}\}$	50 $\{0.2 < F_{th}\}$	49 $\{1.0 \sim F_{th}\}$

The photochemical deterioration at 308 nm observed by the increase of soluble products (Table 2) and the decrease of T_s (Table 3) may be related the oxidation of collagen. Both oxidative and acidic deterioration is reflected in the measurements of the increase of soluble products and the shrinkage temperature. These methods are therefore valuable indicators for the total degree of deterioration of a parchment sample. Recently, shrinkage temperatures determined by micro-thermomechanical analysis was correlated with the amino acid residue composition of parchment, in particular proline and hydroxyproline [15].

Oxidative breakdown processes of parchment base on heat and light [16]. Parchment starts degrading at tripeptides in clusters of charged amino acids following the pattern: (1) loss of mainly the basic amino acids Lysine, Arginine, Hydroxylysine, and the imino acids Proline and Hydroxyproline, (2) gain of acidic amino acids, (3) formation of small amounts of breakdown products. Autoxidation of parchment occurs only in the presence of light [17]. Accordingly, one can conclude from our findings (Tables 2, 3) that hydroxyl radicals are generated by UV laser irradiation. These may attack carbon atoms in peptide side chains (indicated with an asterix) as shown in an example of lysine R-C*H_2-NH_2 $\rightarrow$ +[•OH] $\rightarrow$ R-CHO + NH_3 $\rightarrow$ +[O_2, H_2O] $\rightarrow$ R-COOH with R as the rest of the Lysine side chain, -$(CH_2)_3$-, including the peptide main chain. Polar groups, particularly carboxylic acid functions (besides some conjugated double bonds) are then formed.

4 Conclusions

Photometric determination of the water-soluble degradation products of collagen is a sensitive method to detect laser-induced alterations of parchment. These occur already below the ablation threshold fluence and are indicative for changes on the molecular level.

UV laser light (308 nm) causes photochemical degradation i.e. molecular degradation at moderate fluencies far below the ablation threshold. At higher fluences, less for ancient aged parchment, photothermal alteration takes over the behaviour.

At the visible (532 nm) and the infrared wavelengths (1064 nm), the photochemical phenomena are practically absent. Solely thermally induced crosslinking of the collagen fibres is increasingly observed with increasing fluence.

The hydrothermal stability and shrinking temperature measurements by the micro-hot-table technique rendered itself sensitive only to laser irradiation that caused photochemical reactions (i.e. UV, 308 nm). Wavelengths which caused mainly thermal reactions (e.g. crosslinking, melting etc.) did not affect T_s even though some laser fluences were chosen above the ablation thresholds.

Scanning electron microscopy (SEM) is only sensitive to massive phase changes like melting and boiling accompanying ablation (vaporization) above the threshold fluence.

The photochemical deterioration at 308 nm observed by the increase of soluble products and the decrease of the shrinking temperature may be related to oxidative breakdown processes, which occur only in the presence of light.

Acknowledgements

One of the authors (W. K.) acknowledges the auspices of the EUREKA programme in the context of the EUROCARE project "Laser Cleaning of Paper and Parchment (LACLEPA)", No. EU 1681, and partial financial support by the EU TMR project "Modelling and Diagnostic of Pulsed Laser-Solid Interaction: Applications to Laser Cleaning", No. FMRX-CT98-0188.

References

1. W. Kautek and E. König (Eds.), *Lasers in the Conservation of Artworks I*, Restauratorenblätter (Special Issue), Verlag Mayer & Comp., Wien, 1997
2. *Lasertechnik in der Restaurierung*, Restauro **104**(6) (Special Thematic Issue), 1998
3. M. Cooper, *Laser Cleaning in Conservation*, Butterworth-Heinemann, 1998
4. W. Kautek, S. Pentzien, P. Rudolph, J. Krüger, and E. König, Appl. Surf. Sci. 127-129, 746, 1998
5. P. Rudolph, S. Pentzien, J. Krüger, W. Kautek, and E. König, Restauro **104**(6), 396, 1998
6. W. Kautek, S. Pentzien, J. Krüger, and E. König, in *Lasers in the Conservation of Artworks I*, Restauratorenblätter (Special Issue), Edited by W. Kautek and E. König, Mayer & Comp., Wien, 69, 1997
7. W. Kautek, S. Pentzien, P. Rudolph, J. Krüger, C. Maywald-Pitellos, H. Bansa, H. Grösswang, and E. König, in *Optics and Lasers in Biomedicine and Culture*, Edited by C. Fotakis, T. Papazoglou, and C. Kalpouzos, Optics within Life Science Series, Springer-Verlag, Heidelberg, 100, 2000
8. W. Kautek, S. Pentzien, P. Rudolph, J. Krüger,C. Maywald-Pitellos, H. Bansa, H. Grösswang, and E. König, J. Cultural Heritage **1**, S233, 2000

9. W. Kautek, S. Pentzien, D. Müller-Hess, K. Troschke, R. Teule, in *Laser Techniques and Systems in Art Conservation*, SPIE **4402**, 130, 2001
10. J. G. Manni, Biophotonics International, May/June, 40, 1998
11. H. Hogan, Biophotonics International, November, 62, 2000
12. P. Canart, ancient parchments chosen and provided by the Biblioteca Apostolica Vaticana
13. R. Larsen, M. Vest, and K. Nielsen J. Soc. Leather Technol. Chemistry **77**, 151, 1993
14. A. N. Fraga and R. J. J. Williams, Polymer **26**, 113, 1985
15. M. Odlyha, N. S. Cohen, G. M. Foster, A. Aliev, E. Verdonck, and D. Grandy, J. Therm. Anal. Calorim. **71**, 939, 2003
16. F. O'Flaherty, W. T. Roddy, and R. Lollar, *The Chemistry and Technology of Leather*, Vol. 4, Reinhold Publishing Corporation, New York, 1965
17. René de la Rie E., Studies in Conservation **33**, 53, 1988

Part II

Laser Cleaning of Metal

Femtosecond Laser Cleaning of Metallic Cultural Heritage and Antique Artworks

T. Burmester[1], M. Meier[2], H. Haferkamp[1], S. Barcikowski[1], J. Bunte[1], and A. Ostendorf[1]

[1] Laser Zentrum Hannover e.V., Hollerithallee 8, 30419 Hannover, Germany
bk@lzh.de

[2] Niedersächsisches Landesamt für Denkmalpflege (Lower Saxony department of preservation of ancient monuments), Scharnhorststr. 1; 30175 Hannover, Germany

Abstract. Numereous metallic artworks show environmental damages. Often corrosion products and other contaminations can not be removed sufficiently by conventional techniques such as chemical cleaning agents. Within the framework of an 18-month project, LZH is carrying out investigations with the aim to develop a new cleaning method for antique metallic artworks with a temperature-sensitive surface using femtosecond (fs) laser technology to avoid damage or discoloring of the original surface. In the presented work the removal of corrosion products or pigment coatings from original objects made of copper, bronze and silver using a Titan-Saphir femtosecond laser is being investigated. This laser cleaning technology will be qualified at the end of the project by an exemplary restoration of a part of a bronze sculpture createtd by Adrian de Vries in 1648. In the frame of the project, the influence of the laser fluence and of the repetition rate on the specific removal efficiency of the various corrosion products is analysed. Specific fluence thresholds have been found for the removal of different types of corrosion products and pigment coatings. A sequential removal by non-thermal ablation of discrete corrosion layers or products has been achieved by varying the laser fluence.

1 Introduction

Copper and bronze materials suffer from various corrosion processes caused by atmospherical influence mainly such as O_2, water and air pollutants (SO_2, soot, gypsum, silica). Most of the outdoor placed objects show different corrosion states and damage phenomena at various regions of the object surface mostly depending on the distinguishable range of influence of water and wind [1].

The goal of restoration measures is to generate a homogenous and esthetical view and to inhibit further corrosion processes which may lead to irreversible damages or changes of the morphology of the original surface. Hence, the porous corrosion layers which contain humidity and also gases (basic copper sulfates and -chlorides as well as dust containing components)

promote corrosion processes and have to be removed. Near to the metallic surface, copper- and tin oxides can be found which build a strong and non porous layer. These oxide layers passivate the surface and avoid further corrosion, so they should be left on the surface [2].

The absorption and interaction of the laser irradiation with the metal target depends not only on the laser wavelength but can also interact with a plasma cloud which is build of hot gases of ions [4, 5]. The plasma cloud absorbs a part of the laser irradiation and also induces a heat transfer to the target surface which can lead to melting, discoloring or damaging processes [6]. Those negative effects on restoration applications of metallic objects and also the melting of the metallic phase can be avoided by using femtosecond laser irradiation when the laser fluence is below the threshold of plasma formation [7–9].

2 Experimental Methods and Materials

The investigations have been carried out by using a femtosecond laser system (center wavelength: 780 nm; pulse duration: 140–1500 fs; laser output-power: 1.5 W; repetition rate: 5 kHz) (see Fig. 1). A 2-D-Scanner device was used to guide the laser beam and realize different feed strategies. A 3-D motordrive Nano-positioning unit has been used to handle the objects and to move them to their exact placement. The original materials were taken from a current restoration measure and have been provided by the Lower Saxony Department of Preservation of Ancient Monuments (NLD) and the North German Center of Material Science of Heritage (ZMK) as well as by the restorer Wolfgang Conrad and Haber & Brandner GmbH.

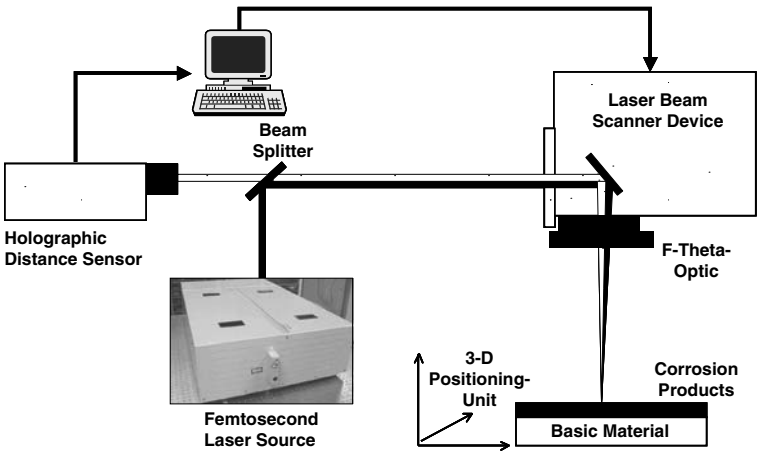

Fig. 1. Experimental Set-up

3 Results and Discussion

During the last 12 month systematic investigations/studies on the removal of corrosion layers of original copper and bronze artworks using a fs-laser source were carried out by the authors. An important observation was that the threshold fluences for plasma formation can significantly raise when the object surface is humidified before laser treatment. Using this method all relevant corrosion layers can be removed even when a laser fluence higher than the threshold fluence for plasma formation (of the dry surface) is needed. Hence, any damaging or discoloring of the oxide layers or metal surface could be sufficiently avoided.

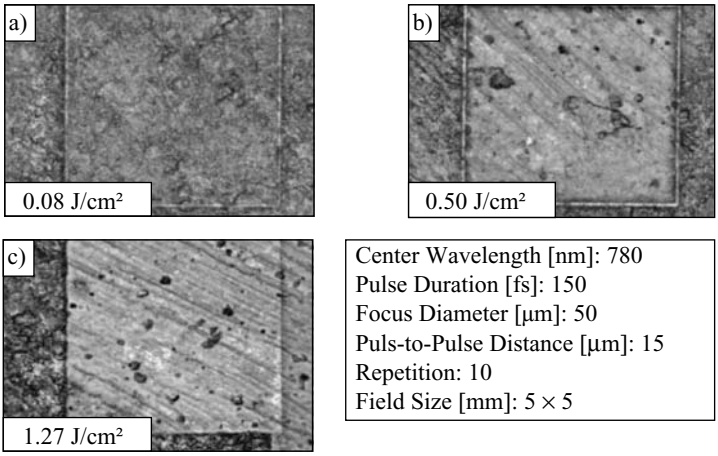

Fig. 2. Light microscopy images of a fs-laser treated bronze object ("Plümicke"-memorial plaque, ca. 1962) showing threshold fluences for the removal of different corrosion products

Figure 2 shows some sucsessful results of the selective removal of corrosion layers of a bronze object. Using a laser fluence between 0.08–0.5 J/cm^2 the green layer of basic Copper-Sulfates is removed (Fig. 2a). The thin blue layer of basic Copper Carbonates was removed using a laser fluence between 0.5–1.27 J/cm^2 (Fig. 2b), while a laser fluence >1.27 J/cm^2 leads to a removal of the oxide layers (Fig. 2c). The presented results of the cleaning experiments show that a high selective removal of differnet corrosion layers is possible with a femtosecond-laser source using different laser fluences.

To remove corrosion products even from a high porous surface (see Bronchantit and Antlerit spots in Fig. 2b and 2c) a modified process control is needed to be integrated. Within the next month, the Laser Zentrum Hannover will carry out investigations to develop a suitable automatic process control using a holographic distance sensor together with an adaptive focusing optic.

Figure 3 gives several examples of cleaning results from another outdoor bronze sculpture, which shows a high amount of different corrosion products and thus, a very inhomogeneous outlook. In this case, part of the basic bronze material is seriously damaged or corroded. The upper layers containing organic components and soot can sucsessfully be removed using low laser fluences of 0.07–0.12 J/cm^2 (Fig. 3a). Most of the surface areas show a strong layer of a mixture of Cuprit and basic Copper Carbonats which have a red or violett appearance. White layers containing Tin Oxide can sufficiently be removed using a laser fluence between 0.34–0.49 J/cm^2 (see Fig. 3c). The layers of Cuprit and basic Copper Carbonates can be removed using a laser fluence between 0.49–0.86 J/cm^2 (see Fig. 3d and 3e), which leads to a different visual surface appearance depending on the respective chemical composition of these corrosion products lying under- neath. Using high laser fluences (>0.86 J/cm^2) also leads to an inhomogeneous surface appearance with different amounts of Copper Oxides as well as exposed bronze material.

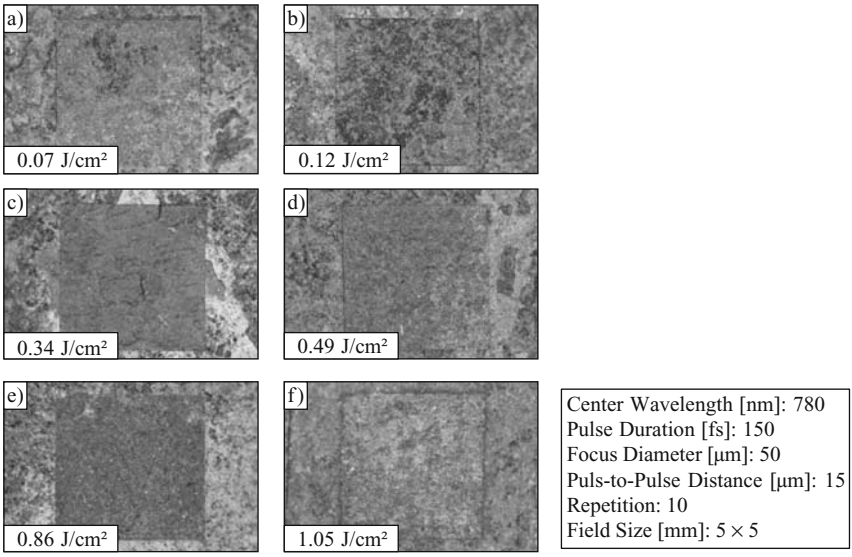

Fig. 3. Light microscopy images of an fs-laser treated bronze object ("Der Schauende"-created by Prof. Herbert Volwahsen in 1936) showing threshold fluences for the removal of different corrosion products

The Laser Zentrum Hannover carried out several systematic investigations on the removal of corrosion products from copper materials using femtosecond laser soures. Most of these materials have a less complex structure of the corrosion layers in comparison to most of the outdoor bronze objects.

Figure 4 shows some examples of the cleaning results of outdoor corroded copper plates. Organic components and soot can sufficiently be removed using

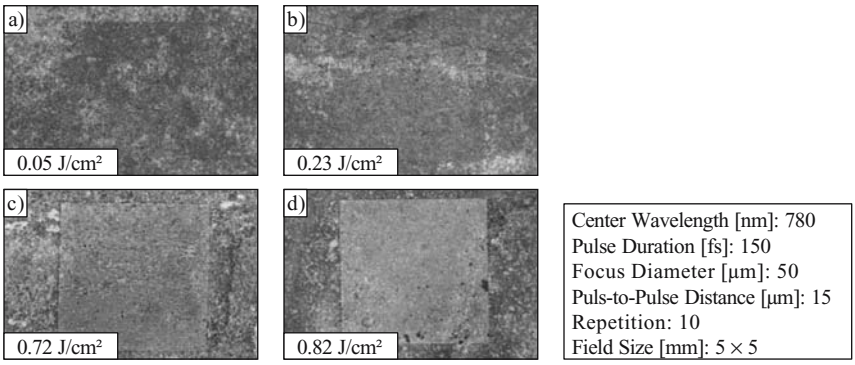

Fig. 4. Light microscopy images of an fs-laser treated copper roof plate (Church in Graz, Austria) showing threshold fluences for the removal of different corrosion products

a laser fluence of 0.05–0.23 J/cm^2 (see Fig. 4a) without damaging or discoloring the layers underneath. The green corrosion layers containing different basic copper Sulfates can be successfully removed using a laser fluence of 0.23–0.72 J/cm^2 (see Fig. 4b). Using laser fluences between 0.72–0.82 J/cm^2 Copper Oxides like Cuprite will be removed obtaining a bright orange colored copper surface.

The cleaning or restoration of outdoor copper materials using femtosecond laser sources proved to be a promising method with a high efficiency and without damaging the layers which are to be preserved.

Figure 5 shows some confocal microscopy images of the bronze surface topography using different laser fluences. Image (a) and (b) show the result of the removal of an inhomogenous dust layer with a laser threshold of 0.05 J/cm^2, while the removal of Copper Sulfates starts at laser fluences >0.11 J/cm^2. Exceeding the laser fluence to a value >0.58 J/cm^2, the oxide layer will be removed (Fig. 5c). The result of a laser treatment without humidification is given in (Fig. 5d) using a laser fluence which is higher than the treshold value of the plasma formation. This topography shows the result of melting processes which were induced by the plasma cloud where each laser pulse generated a crater leading to a rough and discolored surface.

Even though economic aspects were not the aim of the presented study, the estimation of ablation ratios and required time for cleaning of a given surface area may lead to a comparision with conventional techniques. The ablation rates for the removal of the different corrosion products and layers were acquired using confocal microscopy. Consequently, the required time of fs-laser processing for selective removal of different corrosion products on tin bronze and copper bronze objects are given in Table 1. The surface specific ablation rate mainly depends on the thickness of the respective corrosion layer. In general, the required time to remove corrosion products from copper

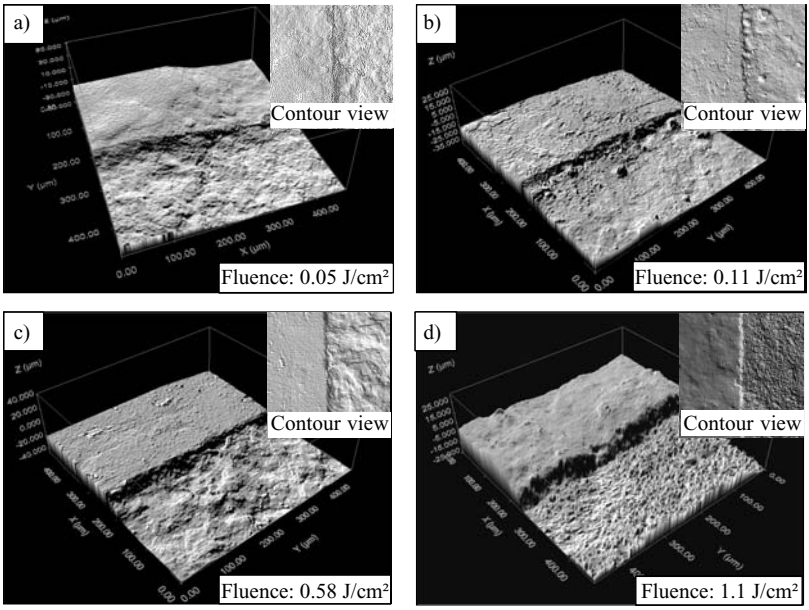

Fig. 5. Confocal microscopy pictures of a fs-laser treated outdoor bronze object ("Friedrich III statue") showing the surface topography at different laser fluences (pulse duration: 150 fs, focus diameter: 50 µm, pulse-to-pulse distance: 15 µm, repetition: 10)

outdoor objects was higher than for bronze materials. To give a synopsis to future application of this technology, an estimation of the theoretical required time of ablation for a letter-size and square meter surface area is given in Table 1. The required period is in the range of 60–110 hours for a letter size area and 140–250 days (7 h) for a square meter.

Even if manual cleaning, cleaning using Nd:YAG lasers and fs-laser cleaning show completely different tool-material interaction and specific limitations which are inherent to each technology, a comparison of the required time may lead to a discussion of the future use in practice. The required time and handling for devices during fs-laser ablation is in the same order of magnitude than during manual restoration, but much lower than during Nd:YAG laser ablation.

The mobility of such a laser source is still limited, which is a disadvantage compared to Nd:YAG lasers. Therefore, fs-laser source development has to make progress regarding pulse duration stability, compactness and robustness of the system as well as increasing the maximum pulse energy (at high repetition of several 10 kHz) if it shall compete with conventional techniques in practical use. Furthermore, robust beam guidance and handling devices including beam guidance and adaptive optics are needed to allow a wider range of applications inc luding outdoor use. Of course, during this further

Table 1. Required time of fs-laser processing for selective removal of different corrosion products on tin-bronze and copper bronze objects

	Corrosion Products and Layers	Surface Specific Ablation Time [min/cm^2]	Theoretical Required Time of Ablation Including 5 Minutes Adjustment Time per cm^2 Surface Area	
			Per Area of a A4-Page (630 cm^2) [h]	Per Square Meter [Days à 7 h]
Tin-Bronze Objects	Organic Compounds and Soot	1.5–1.8	68	155
	Tin Oxide	2.2–3.1	76	171
	Basic Copper Sulfates (Bronchantie Antlerite)	2.5–4.5	79	179
	Basic Copper Carbonates (Malachit)	2.2–5.7	76	171
	Tenorite	5.5–10.2	110	250
Copper Objects	Organic Compounds and Soot	0.8–1.4	104	236
	Basic Copper Sulfates (Bronchantie Antlerite)	1.2–3.5	61	138
	Basic Copper Carbonates (Malachit)	0.9–1.8	65	148
	Tenorite	4.2–8.5	62	140
	Cuprite	3.2–7.8	97	219

development of tabletop systems towards mobile systems, fs-specific safety aspects have also to be considered [10].

4 Conclusions

Numereous metallic artworks can not be cleaned sufficiently by conventional techniques or with chemical cleaning agents. This concerns especially temperature sensitive metallic materials like bronze and copper. The development of a new restoration method or technique is demanded to avoid damaging or discoloring of the original surface. In the presented work the removal of corrosion products from original objects made of copper and bronze using a Titan-Saphir femtosecond laser has been investigated. The results of the presented investigations show that a selective and sequential removal of different corrosion products or layers can be sufficiently obtained using different laser fluences in between the achieved threshold values even in cases of a complex

structure of the composition of the corrosion layers. However, the corrosions inside of caverns or from a high porous surface are still limiting the quality of the restoration result. Therefore, the focal position has to be controlled using an online distance control unit.

5 Outlook

In the frame of future work the Laser Zentrum Hannover will finish the investigations to develop an automatic process control using a distance sensor combined with an adaptive focussing optic to adjust the proper laser fluence to obtain the demanded restoration results. After integrating this process control device to the experimental set-up, this new laser cleaning technology will be tested by pilot applocation on part of a bronze sculpture createtd by Adrian de Vries in 1648 (see Fig. 6).

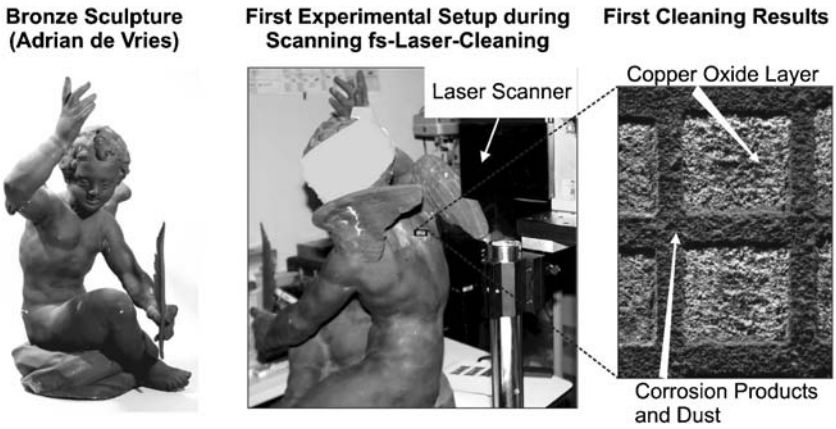

Fig. 6. Foto of a bronze sculpture created by Arian de Vries in 1648

Acknowlegdements

Part of the presented work was supported by the Deutsche Bundesstiftung Umwelt (DBU). The authors would like to thank the DBU for its support and also the restorer Wolfgang Conrad and Haber & Brandner GmbH for providing the original copper and bronze objects.

References

1. B. Stöckle and A. Krätschmer, “Die atmosphärische Korrosion von Kupfer und Bronze”. In M. Mach, “Metallrestaurierung”, Arbeitshefte des Bayerischen Landesamtes für Denkmalpflege, Bd. 94, München 1998

2. M. Mach, "Bildatlas typischer Oberflächenphänomene von frei bewitterten Bronzen", In Bronze- und Galvanoplastik, Hrsg. Landesamt für Denkmalpflege Sachsen, Arbeitsheft 5, pp 152–155, 2001
3. K. G. Watkins, "A review of materials interaction during laser cleaning in art restoration", In Lasers in the Conservation of Artworks I, Heraklion Crete Grece, Verlag Mayer & Comp. Wien, pp 7–15, 1997
4. V. I. Bergel'son, A. P. Golub, T. V. Loseva, I. V. Newchinov, T. I. Orlova, and S. P. Popov, "Appearance of a layer absorbing laser radiation near surface of a metal target" Sov. J. Quant. Electronic, Vol. 4, p 704 ff, 1974
5. M. Bass, M. A. Nasser, and R. T. Swimm, "Impulse coupling to aluminium resulting from Nd:Glass laser irradiation induced metal removal", J. Appl. Phys., Vol. 61, pp 1137–1139, 1987
6. J. C. Bushnell and D. J. McCloskey, "Thermoelastic Stress Production in Solids", J. Applied Physics, Vol. 39, p 5541, 1968
7. S. Nolte, C. Momma, and G. Kamlage, "Polarization Effects in Ultrashort-Pulse Laser Drilling", In: Applied Phyics A: Materials Science & Processing, Vol. A 68, pp 563–567, 1999
8. F. Korte, J. Serbin, J. Koch, A. Egbert, C. Fallnich, A. Ostendorf, and B. N. Chichkov, "Towards Nanostructuring with femtosecond laser pulses", Applied Physics, A 77, pp 229–235, 2003
9. H. Haferkamp, S. Paschko, F. von Alvensleben et al., "Laser Material Processing Techniques for Shape Memory Alloys", In: MICRO.tec2000, Conference Proceedings, Vol. 2. VDE World Microtechnologies Congress, 25.–7. September 2000, Hannover. Berlin, Offenbach: VDE Verlag, pp 13–17, 2000
10. J. Bunte, S. Barcikowski, T. Puester, T. Burmester, M. Brose, and T. Ludwig: Secondary Hazards: 9.2 Particle and X-Ray Emission. Chapter 9.2 In: Femtosecond Technology for Technical and Medical Applications (Pulb.: Dausinger, Lichtner, Lubatschowski), Springer Series "Topics in Applied Physics Topics in Applied Physics", in press (ISBN 3 540 20114 9)

Archaeological Ironwork: Removal of Corrosion Layers by Nd:YAG-Laser

K. Dickmann[1], J. Hildenhagen[1], J. Studer[1], and E. Müsch[2]

[1] Lasercenter Fachhochschule Münster (LFM), FB Physikalische Technik, University of Applied Sciences, Stegerwaldstr. 39, 48565 Steinfurt, Germany
hildenh@fh-muenster.de
[2] Westf. Museum für Archäologie, Amt für Bodendenkmalpflege, An den Speichern 12, 48157 Münster, Germany

Abstract. Often archaeological ironwork is covered by a thick corrosion layer. In many cases the corrosion crust exceeds the volume of the original ironwork several times. In order to expose the original topography, containing several information about the former manufacturing process, recently the laser gained increasing interest. Investigations were carried out by a novel Nd:YAG-Laser with frequency multiplying (1064 nm, 532 nm, 355 nm, 266 nm). It has turned out that the combination of conventional cleaning methods (for coarse removal of corrosion crusts) with Nd:YAG-Laser technique (for fine removal) opens new possibilities in restoration of strongly corroded archaeological iron work.

1 Introduction

Corrosion of iron in the ground is a complex electrochemical process whereby the ground water with dissoluted salt acts as the electrolyte. Thus depending on the iron quality, state of the ground and various ambient conditions in general ironwork from excavations is covered by thick corrosion layers. The corrosion process simplified may be explained as follows (Fig. 1): mainly Fe II compounds are oxidized and hydrolized partially to Fe III-compounds. This process results into an inner layer of magnetite [Fe_3O_4] and an outer crust of goethite [α-Fe(III)OOH]. Furthermore, grounds containing high content of specific anions can also cause other corrosion products (e.g. phosphate, carbonate, sulphate and sulfite). Within this compound, the original iron surface is defined as the transition from magnetite to goethite (Fig. 1, left). The interior contains the metallic core so far the ironwork is not mineralised completely. Continuous corrosion leads to increasing growth of the magnetite layer towards the centre while the goethite layer growths towards outside. Figure 1 (right) shows a typical "corrosion lump" with strong corrosion effects.

For our investigations we employed ironwork (fittings, knifes, clip of fibula) originating from Anreppen/Germany (Roman Camp; silica sand ground) and Rozedehausen/Germany (settlement from Middle Ages; loam ground).

In order to release the original iron surface containing valuable information about the former manufacturing process, various methods to remove the

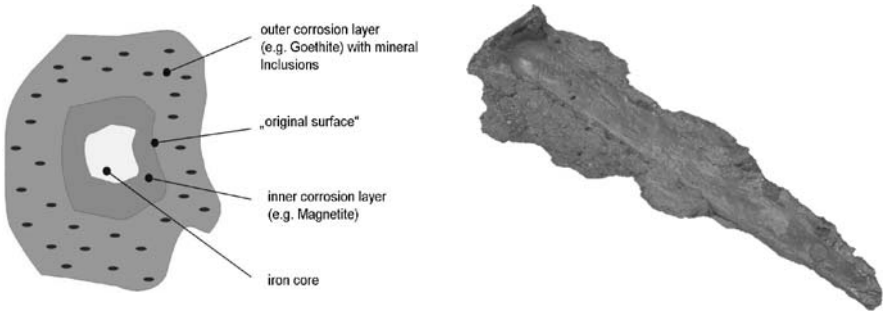

Fig. 1. Formation of corrosion crusts; *left*: typical cross-section of corroded iron work and definition of "original surface", *right*: Archaeological iron nail from Roman Camp/Germany with strong corrosion crusts partially removed

corrosion layer are utilised. Nowadays mechanical cleaning is carried out by scalpels or scrapers, ultrasonic chisels, disc grinders and micro sandblasting with various abrasive materials. An alternative processing method is heating up the corroded ironwork ($\leq$350°C) in a plasma chamber or oven inside an inert or reduced atmosphere [1]. As a result the corrosion crust becomes crumbly due to microcracks.

An inherent disadvantage of all cleaning methods mentioned above is their risk of damaging the original ironwork surface.

In various papers [2–4] laser cleaning of corroded bronze, lead, silver and aluminium is reported. However (so far as known) laser cleaning of corroded archaeological iron in first attempts was only studied by [5].

2 Laser Equipment and Archaeological Iron Samples

For experimental studies a Q-switched Nd:YAG-Laser ($t_d \approx 8$ ns) was used with optional frequency multiplying (ω/1064 nm; 2ω/532 nm; 3ω/355 nm; 4ω/266 nm). The maximum pulse energy was 1500 mJ@ω, 800 mJ@2ω, 450 mJ @3ω and 260 mJ@4ω, respectively. Our samples originate from the excavations of Anreppen/Germany (Roman Camp) and Rozedehausen/Germany (settlement from Middle Ages). The roman ironwork was found in fine-grained white silica sand with various ground conditions due to variations in humidity and fertilizing influence. The medieval ironworks from Rozedehausen was found in a loam ground. All samples were made available by the Museum for Archaeology in Muenster.

3 Experimental Results

It was investigated that there are different fluence thresholds for the removal of the corrosion crust, modification (e.g. blackening) of the original

iron surface and (undesired) removal of the original iron matter. All fluence thresholds show a distinct downward tendency with decreasing wavelength. It has turned out that the threshold for removal of corrosion crust was lowest in most cases (Fig. 2).

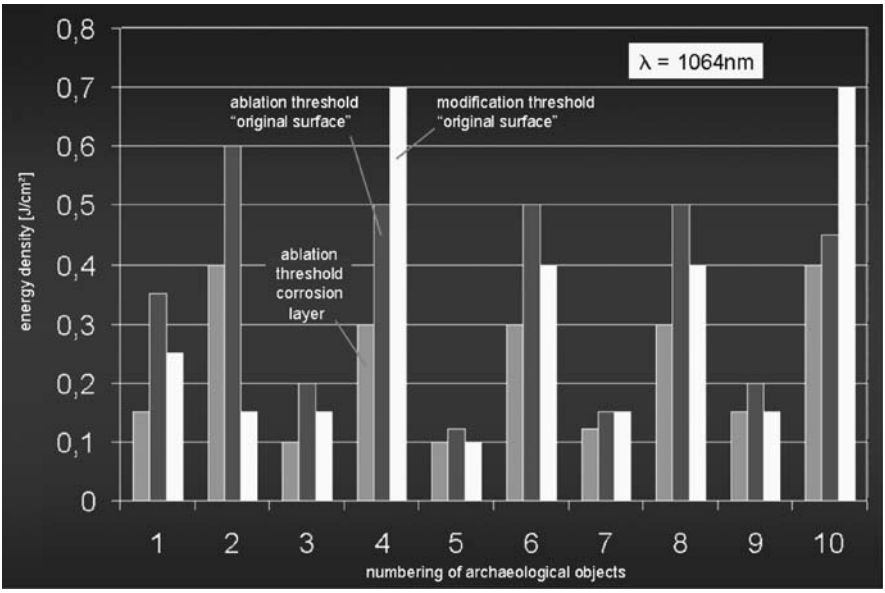

Fig. 2. Different fluence thresholds for various corroded iron works

In all cases the removal process was accompanied by a blackening of the interaction area as depicted in Fig. 3.

Beside blackening effect, for some ironworks being excavated from silica sand ground, we also observed a remaining part of silica grains on the surface after the cleaning process. Obviously this is due to the fact of highly transparency of Silica at the employed wavelengths. The maximum removal rate was $>10\,\mu g$/pulse@1064 nm, $<10\,\mu g$/pulse@532 nm and $\ll 10\,\mu g$/pulse@355 nm/266 nm at a constant spot size area of $0{,}25\,cm^2$. Thus with regard to practical applications for further studies only 1064 nm and 532 nm were used.

Analytical investigations using pyrometer and SEM reveal a minor thermal load onto the exposed iron surface. However, high resolution imaging by SEM gave obvious indications for tiny molten areas in the range of some micro meters. Using EDX and XPS we detected an increasing content of Fe on the surface after laser cleaning (from 65% to 96%). An explanation might be given by the reduction of various iron oxides, as for example $Fe_2O_3 \rightarrow FeO$ or $FeO \rightarrow Fe$. Also we detected a distinct decrease of carbon which obviously is due to the ablation of organic impurities.

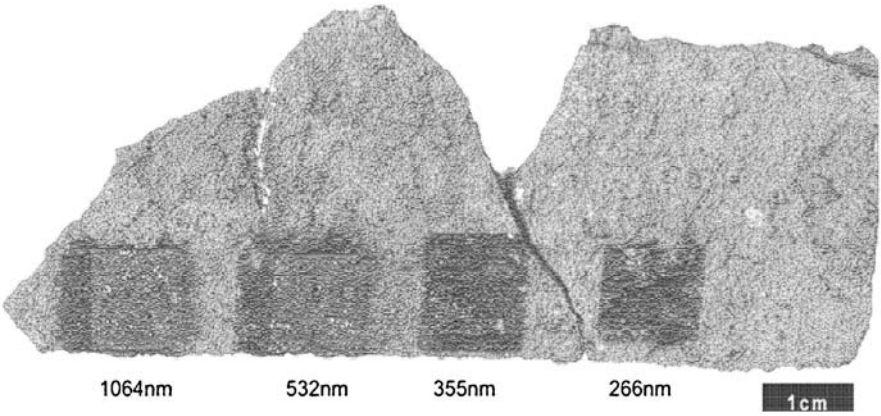

Fig. 3. Blackening on an iron fragment (Roman Camp near Cologne) after treating at different Nd:YAG-Lasers wavelengths

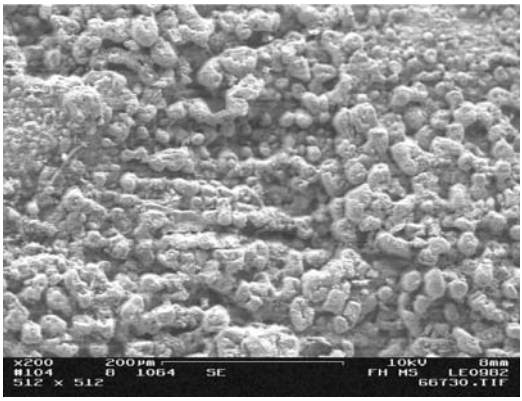

Fig. 4. SEM-top view on a laser cleaned ($\lambda = 1064\,\text{nm}$) iron area: tiny molten areas in the µm-range arise on the surface

4 Transfer of Results to Archaeological Objects

A comparison of a laser cleaned area ($\lambda = 1064\,\text{nm}$) on a corroded iron bar to a sandblasted one is given in Fig. 5. As can be seen that the laser cleaned surface (left) contains more original roughness, while the sandblasted area shows a more smoothened surface due to the abrasive effect of corund micro particles. A similar result was obtained for $\lambda = 532\,\text{nm}$.

As known from laser cleaning of other artworks (e.g. stone [6]), using a thin liquid film on the surface may support the removal process. In our study we used ethanol instead of water and obtained an increase of the removal rate up to 60%. As an interesting side effect it has turned out that the liquid additive also completely removes adhering silica grains from the surface (see Fig. 6).

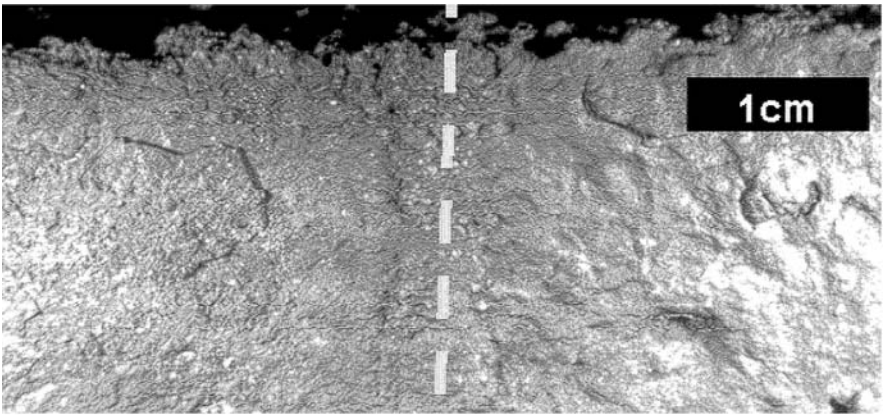

Fig. 5. Iron bar with 2 mm corrosion crust (Rozedehausen/Germany); *left*: Laser cleaned (λ = 1064 nm, H = 2,6 J/cm^2, 7 min), *right*: Microsandblasted (58–88 µm corund grains, 1–3 bar, 30 min)

Fig. 6. Liquid film (ethanol) on the surface also removes silica grains; *left*: laser cleaned (λ = 1064 nm) with ethanol liquid film; *right*: laser cleaned (λ = 1064 nm) without ethanol liquid film

This might be explained by the laser induced vaporization of ethanol causing high pressure onto the single grains.

In cooperation with the Museum for Archaeology/Muenster (Germany) laser cleaning technique was applied to several originals of corroded ironwork. In any case a coarse removal of corrosion crust was provided by rotating grinding tools. Laser radiation @ 1064 nm was used in order to remove the

width=[8cm]

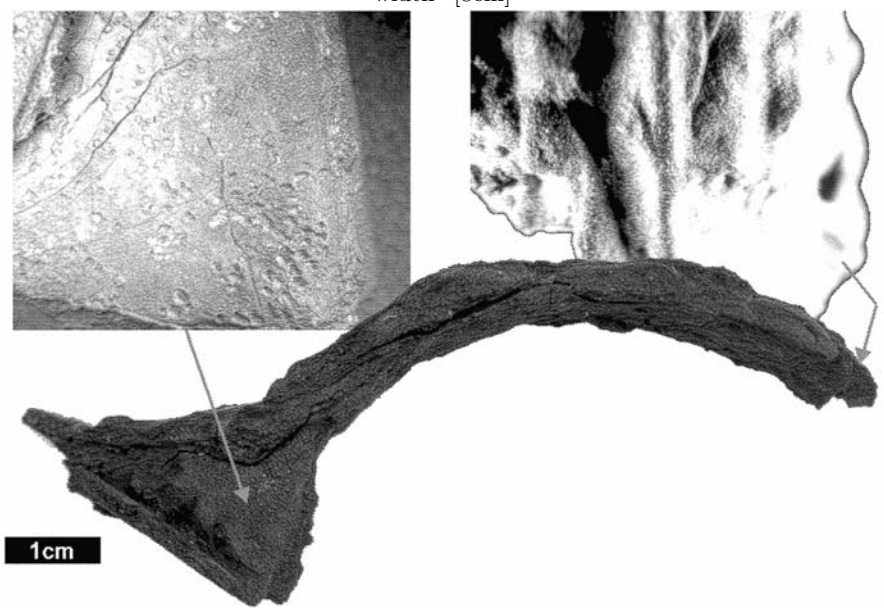

Fig. 7. Clip of a fibula; cleaned with Nd:YAG-Laser ($\lambda = 1064\,\text{nm}$, $\text{H} = 2{,}2\,\text{J/cm}^2$), 1 hour cleaning procedure

Fig. 8. Iron bracket from Roman Camp Anreppen/Germany. Fine cleaning with laser (@ 1064 nm) was 16 minutes while it was 50 minutes for sandblasting (this figure demonstrates the laser cleaned side)

remaining thin corrosion layer. As shown exemplary in Fig. 7 fine details on the original surface of a clip from a fibula (Roman Camp) could be exposed. Delicate ornaments appeared and gave indications to the former treatment process of the clip. The duration for the laser cleaning procedure was 1 hour.

For a comparison of the processing time for laser cleaning in contrast to sand blasting an iron bracket (Roman Camp Anreppen/Germany) with a 2 mm thick corrosion layer was used. Both sides of the bracket were precleaned by a restorer using mechanical coarse removal techniques. Following the restorer used laser radiation (1064 nm, 2,6 J/cm^2, 5 Hz) and sand blasting (corund 70 µm, 1–3 bar) for final cleaning on each side. The state "clean" was defined by the restorers experience. For the iron bracket shown in Fig. 8 the processing time for laser cleaning was 16 minutes while it was 50 minutes for sandblasting. Furthermore it has turned out that the laser cleaned surface is characterized by a more delicate surface in contrast to a more smoothened surface for sandblasting.

Acknowledgements

This project was funded by the "Deutsche Bundesstiftung Umwelt (DBU)", Grant No: 08300.

References

1. E. Müsch, Ein thermisches Verfahren zur Reduktion von archäologischen Eisenobjekten, AFWL Ausgrabungen und Funde in Westfalen-Lippe 9/A, Münster 1997, S. 129–150
2. P. Heinrich, Ein eiserner byzantinischer Ringkettenpanzer, Restauro, Vol. 6, Callwey, München 1998, pp 383–387
3. C. Degrigny, E. Tanguy, R. Le Gall, V. Zafiropulos, and G. Marakis, Laser cleaning of tarnished silver and copper threads on museum textiles, LACONA 4, Journal of Cultural Heritage, Vol. 4, Sup. 1, 2003, pp 152–156
4. W. Conrad, H. Wust, and G. Wiedemann, Freilegung von Grünpatina mit dem Laserstrahl, Restauro, Vol. 6, Callwey, München 1998, pp 422–429
5. Y. S. Koh and I. Sarady, Laser removal of corroded layers from archaeological ironwork, LACONA 4, Journal of Cultural Heritage, Vol. 4, Sup. 1, 2003, pp 129–133
6. S. Klein, T. Stratoudaki, Y. Marakis, V. Zafiropulos, and K. Dickmann, Comparative study of different wavelengths for IR to UV applied to clean sandstone, Appl. Surface Science 157 (2000) pp 1–6

Laser Cleaning of Metal Surface – Laboratory Investigations

P. Mottner[1], G. Wiedemann[2], G. Haber[3], W. Conrad[4], and A. Gervais[5]

[1] Fraunhofer Institute for Silicate Research (ISC), Bronnbach Branch, 97877 Wertheim Bronnbach, Germany;
peter.mottner@isc.fraunhofer.de
[2] Fraunhofer Institute for Material and Beam Technology (IWS), Winterbergstr. 28, 01277 Dresden, Germany
[3] Haber & Brandner GmbH, Lichtenfelserstr. 3, 93057 Regensburg, Germany
[4] Freelance Restorer, Obere Parkstraße 10, 06295 Lutherstadt Eisleben, Germany
[5] North German Centre for Material Knowledge of Cultural Assets, registered association (ZMK), Scharnhorststr. 1, 30175 Hannover, Germany

Abstract. The interaction of various metal alloys with laser energy generated by a Nd:YAG medium (λ = 1064 nm, 532 nm, and 355 nm) has been examined systematically by the variation of laser parameters. With the help of model coupons, alteration/ablation thresholds of uncorroded/corroded surfaces of iron, pure copper and copper alloys were determined, leading to first recommendations for the cleaning of originals. Surface absorption measurements in the UV/VIS/IR wavelength regions completed the interaction studies.

1 Introduction

In the last decades, laser treatments of various material surfaces have been investigated not only for industrial purposes, but also for the cleaning of sensitive artwork surfaces [1]. Experiments have mainly been performed on original objects with special cleaning challenges, leading to conclusions valid only for limited material compositions in combination with special surface phenomena [2]. Especially in the last decade, interests were focused on more sophisticated research concerning the interaction between laser energy and surface layers [2, 3]. Systematic investigations including laser treatments of artificial model samples have been performed successfully on stone [4], paper [3], and stained glass [3, 5]. The work on metals presented here follows this experimental scheme. For metal alloys, systematic research work has been published only very rarely until now, e.g. on bronze, archaeological and gilded objects [2, 3].

Within a 3 years research project in Germany, the interaction of various metal surfaces with different laser sources is being monitored, focusing on the ablation of surface deposits such as corrosion crusts caused by outdoor or indoor weathering, aged preservation coatings, dirt deposits, graffiti, traces of paint, lime or rust. The experiments are mainly dedicated to cleaning challenges represented by pilot objects, consisting of copper, bronze, brass,

iron, tin alloys, and gilded lead. The results will be transferable to other metal monuments with comparable surface phenomena as well. Tests have been performed first on cast model coupons and on substrates originating from cast-off originals. The determination of alteration and ablation thresholds (for surface layers) and alteration thresholds (for underlying substrates worth to be preserved) are in the focus of interest. The results reported here deal particularly with the removal of surface corrosion and represent an intermediate project stage.

The work is supported by the Deutsche Bundesstiftung Umwelt (German Foundation for the Environment) in Osnabrück. The project finished its first year of performance.

2 Experimental Methods

Within the first project stage, as model samples coupons of iron/steel and copper alloys including bronze have been examined. Newly cast samples and moreover, corroded original samples, originating from copper roofs (Denmark, early 20th century, and Germany, 18th ct.), from a 17th ct. German bronze, and from a 19th ct. German wrought iron object had been available and treated. For both – the new cast samples and the originals – alteration and ablation effects had been monitored.

The ablation/alteration thresholds can be described as follows:

Metal Surface / Threshold definition	Uncorroded sample surface	Corroded sample surface or surface covered with dirt, paint or coatings
Alteration threshold	beginning change in colour (partly: change of roughness)	beginning change in colour
Ablation threshold	beginning loss of bulk material	beginning loss of surface layer

In the case of a sample surface covered with corrosion, dirt, paint or coatings a second stage of ablation threshold (2) can be defined, where bulk metal loss occurs. It could be proved experimentally, that the laser parameters for this effect are comparable to the ablation thresholds on related uncorroded samples (see definition above; within examination error limits), as expected. The examination was performed by light (optical) microscopy of the surface.

As laser sources, the available wavelength region from UV to the near IR with special relevance to portable Nd:YAG systems (basic wavelength, second and third harmonics) have been covered. For the experiments, the following laser types and parameters have been chosen for systematical variations:

Laser source:	Nd:YAG (BMI/Thales "Artlight NL102" and BMI/Thales "pulsed multiband OPO")
Wavelength λ (nm):	1064, 532, 355
Fluence H (J/cm^2):	0.17 – 0.3 – 0.8 – 1.0 – 3.0
Absolute pulse number N:	1, 20, 100
Repetition rate/Frequency F (s^{-1}):	no (for N = 1), 2, 10
Pulse length:	6 ns

The scheme of the laser matrix is shown in Fig. 1 (left; separate matrices for different λ), together with its application on an uncorroded steel coupon (right; for $\lambda = 532$ nm). The beginning alteration for this material/laser energy combination is clearly to be seen at H = 0.30 J/cm^2 (in the parameter field N = 100 @ F = 2). The error limits of the experimental fluence output H can be estimated to be ±10%.

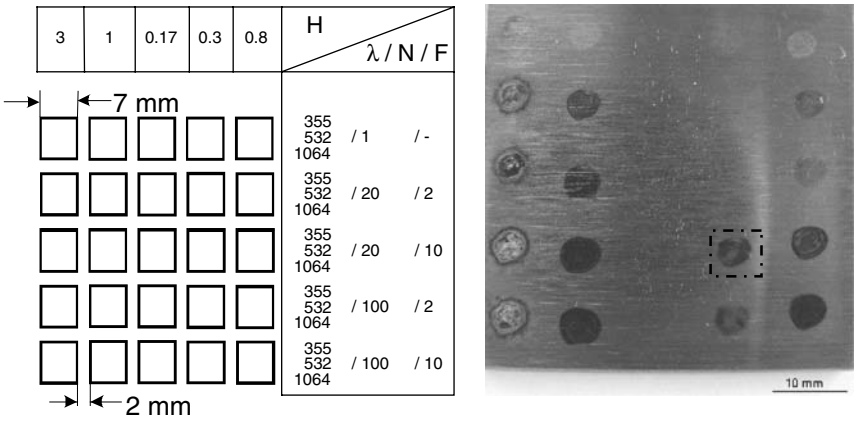

Fig. 1. Scheme of the laser matrix (*left*), matrix application on an uncorroded iron/steel coupon (*right*; $\lambda = 532$ nm; light microscopy; beginning alteration marked with a square)

Application of various laser wavelengths implies absorption measurements of different surface species to choose the most effective equipment for cleaning. Therefore, measurements in the nearUV/VIS/IR region have been carried out on corroded iron and copper surfaces.

3 Results and Discussion

The results of the absorption measurements on iron and copper are presented in Fig. 2 for the near UV/VIS/near IR (left) and for the near IR/IR region (right).

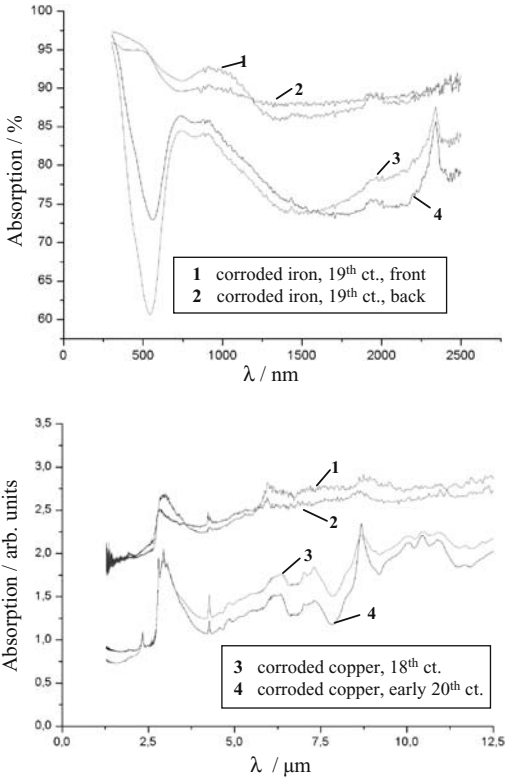

Fig. 2. Absorption spectra of corroded iron and copper surfaces. Near UV/VIS/near IR region (*top*) and near IR/IR region (*bottom*)

The spectra show minimum absorption especially for corroded copper in the wavelength region of $\lambda = 500$–$600\,\mathrm{nm}$. High absorption and maxima are present at values $\lambda < 500\,\mathrm{nm}$ and $\lambda = 800$–$1000\,\mathrm{nm}$. Therefore, the basic wavelength ($\lambda = 1064\,\mathrm{nm}$) and third harmonic ($\lambda = 355\,\mathrm{nm}$) of the Nd/YAG-laser should be well suited for cleaning applications aiming at the reduction of the patina and the second harmonic ($\lambda = 532\,\mathrm{nm}$) for the treatment of superficial surface layers whilst presuming patina preservation. The absorption maxima for all investigated samples at $\lambda \approx 3\,\mu\mathrm{m}$ corresponds with the emission wavelength of the Er:YAG laser, outlining it as a potential cleaning tool for future experiments.

The results of the systematic laser treatment of the model samples (alteration/ablation thresholds) are presented in Table 1.

Examples for the surface phenomena observed at various laser parameters are shown in Figs. 3–5 for copper with an uncorroded (newly prepared) and a patinated surface (early 20th century), monitored on a macroscopical (Fig. 3) and on a microscopical scale (Figs. 4, 5). Significant visual changes of adjacent

Table 1. Alteration/ablation thresholds of model samples (uncorroded/ corroded), treated with a Nd:YAG laser source (basic wavelength, second and third harmonics)

Sample Surface (uncorroded)	Alteration Thresholds (H-N-F)	
	$\lambda = 1064$ nm	$\lambda = 532$ nm
Iron/steel	0.80 J/cm^2 - 20 - 2	0.30 J/cm^2 - 100 - 2
Copper	0.80 J/cm^2 - 20 - 2	0.80 J/cm^2 - 1 - no
Sn-bronze	0.80 J/cm^2 - 20 - 2	0.80 J/cm^2 - 1 - no
Sn/Zn/Pb – bronze	0.80 J/cm^2 -1 - no	0.80 J/cm^2 - 1- no
Brass	0.80 J/cm^2 - 20 - 10	0.80 J/cm^2 - 1 - no

Sample Surface (uncorroded)	Alteration Thresholds (H-N-F)	
	$\lambda = 1064$ nm	$\lambda = 532$ nm
Iron/steel	0.80 J/cm^2 - 100 - 2	1.00 J/cm^2 - 20 - 2
Copper	1.00 J/cm^2 - 20 - 2	1.00 J/cm^2 - 20 - 2
Sn-bronze	3.00 J/cm^2 - 1 - no	0.80 J/cm^2 - 100 - 2
Sn/Zn/Pb – bronze	0.80 J/cm^2 - 20 - 2	0.80 J/cm^2- 20 - 10
Brass	3.00 J/cm^2 - 20 - 2	0.80 J/cm^2- 100 - 2

Sample Surface (corroded)	Surface Corrosion Product	Alternation Thresholds (H-N-F)		
		$\lambda = 1064$ nm	$\lambda = 532$ nm	$\lambda = 355$ nm
Iron (19th ct.)	FeOOH, Fe_2O_3	0.80 J/cm^2 - 20 - 2	0.30 J/cm^2 - 20 - 2	–
Copper (early 20th ct.)	Brochantite (cuprite)	0.30 J/cm^2 - 20 - 2	0.17 J/cm^2 - 20 - 2	0.17 J/cm^2 - 1 - no
Copper (18th ct.)	Cuprite (brochantite)	0.30 J/cm^2 - 20 - 2	0.30 J/cm^2 - 1 - no	0.17 J/cm^2 - 20 - 10
Bronze (17th ct.)	Antlerite, brochantite	0.30 J/cm^2 - 10 - 2	–	–

Sample Surface (corroded)	Surface Corrosion Product	Alternation Thresholds (H-N-F)		
		$\lambda = 1064$ nm	$\lambda = 532$ nm	$\lambda = 355$ nm
Iron (19th ct.)	FeOOH, Fe_2O_3	0.80 J/cm^2 - 20 - 2	0.30 J/cm^2 - 100 - 10	–
Copper (early 20th ct.)	Brochantite (cuprite)	0.80 J/cm^2 - 20 - 2	0.30 J/cm^2 - 100 - 2	0.17 J/cm^2 - 100 - 2
Copper (18th ct.)	Cuprite (brochantite)	0.80 J/cm^2 - 20 - 10	0.30 J/cm^2 - 20 - 10	0.17 J/cm^2 - 20 - 2
Bronze (17th ct.)	Antlerite, brochantite	0.35 J/cm^2 - 10 - 2	0.25 J/cm^2(- 10 - 2)	0.15 J/cm^2(- 10 - 2)

laser-cleaned matrix areas (see laser matrices in Fig. 1 for steel and in Fig. 3 for copper) can directly be correlated with the existence of a threshold value as stated in Table 1. Especially for copper, alteration threshold surface effects are visualised in detail in Figs. 4b and 5b, ablation threshold results in Figs. 4c and 5c.

For the samples studied, the interaction between surface and laser energy is more intense with decreasing laser wavelength (resulting in a lower threshold value). Few exceptions can be stated in case of the ablation threshold values for uncorroded samples (see Table 1), but these parameters are normally far beyond what is foreseen for the treatment of an object. For corroded iron, ablation values for the crust are quite comparable to the alteration

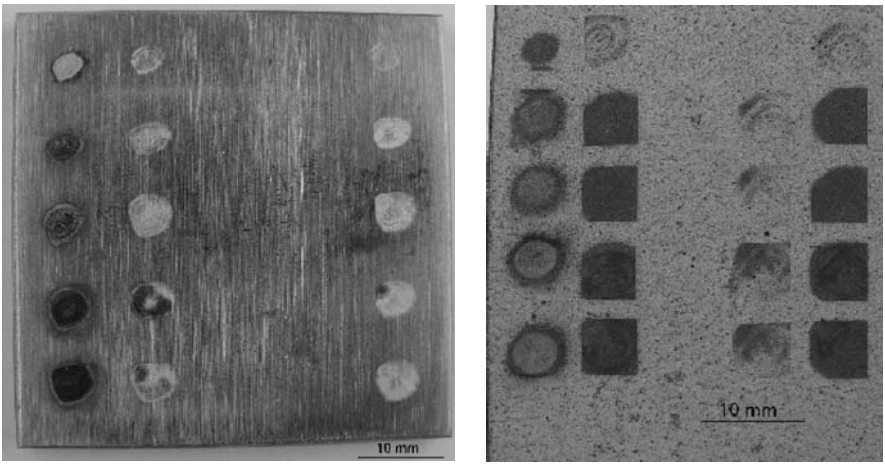

Fig. 3. Light microscopy: Laser matrix on copper with an uncorroded (*left*; $\lambda = 532\,\text{nm}$) and patinated surface (*right*; $\lambda = 1064\,\text{nm}$)

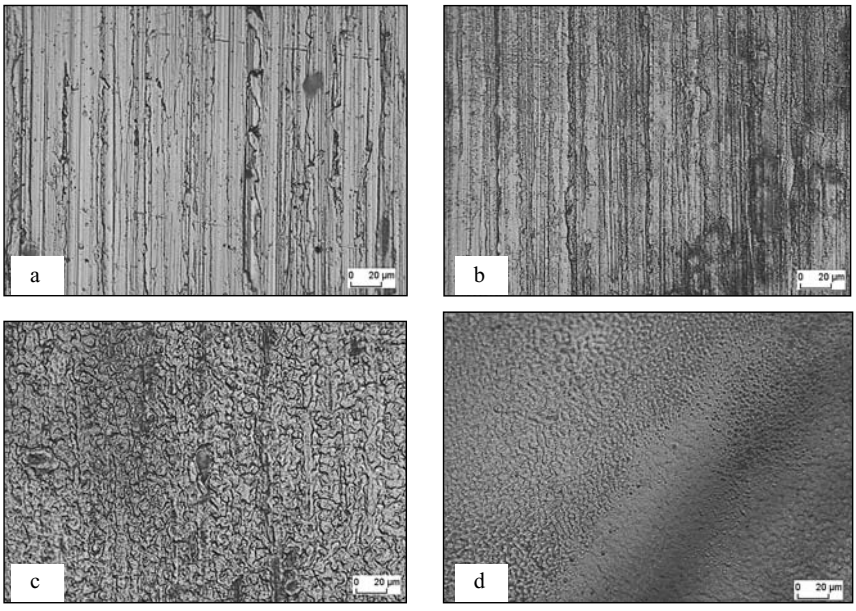

Fig. 4. Light microscopy: Subsequent laser treatment of copper (uncorroded surface); (**a**): untreated surface; (**b**): colour change (*right side*, alt. threshold); (**c**): material loss (abl. threshold); (**d**): final state with material loss (*left side*), melting spots, colour changes (*right side*)

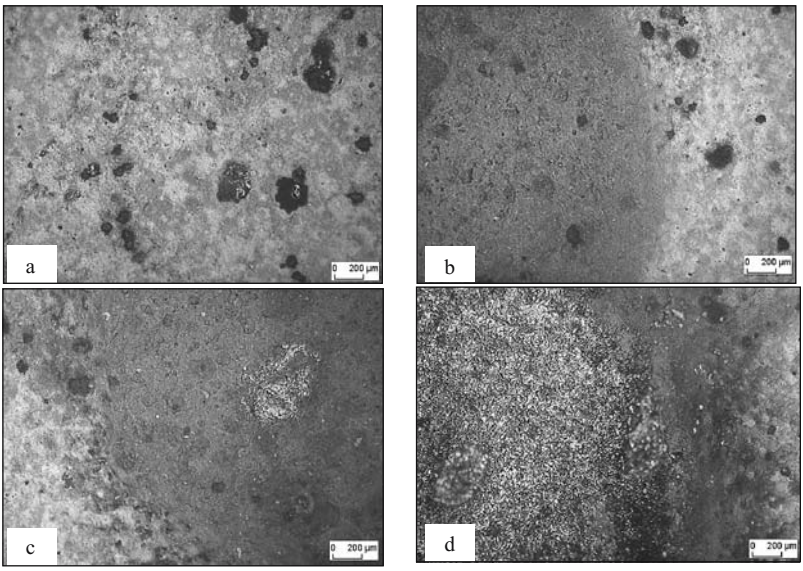

Fig. 5. Light microscopy: Subsequent laser treatment of Copper (patinated surface); (**a**): untreated surface (pits down to the bulk, *black spots*); (**b**): colour change (*left side*, alt. threshold); (**c**): patina loss (*right side*, abl. threshold); (**d**): final state with patina loss, damage and loss of bulk metal (*left side*, abl. threshold (2))

thresholds of the bulk. Therefore, careful reduction of the rust layer is recommended. The cleaning experiments for copper and bronze showed, that ablation can be observed at laser parameter combinations (H-N-F) where no alteration effect of the underlying substrate occurs (exception: equal values for copper, 20th ct., $\lambda = 1064\,\mathrm{nm}$), indicating the possibility of a self limiting cleaning process, if a reduction of the corrosion layer is envisaged. According to the general conservation strategy in the case of copper alloys, alteration and ablation of the patina should in most cases be avoided (in contrast to iron/steel). The related alteration thresholds are low ($0.30\,\mathrm{J/cm^2}$(1064 nm) or lower), requiring careful laser applications, too. A reduced interaction of the patinated copper (or comparable bronze) surfaces with the second harmonic ($\lambda = 532\,\mathrm{nm}$), as indicated by the UV/VIS/IR – absorption measurements, could not be observed. The absorption properties of the surface seem to be superimposed by other effects (plasma generation, shockwave effect, thermal interaction etc).

4 Conclusions

Cleaning applications on iron and bronze monuments, based on the results on model substrates presented above, are under investigation with first

promising results. The removal of iron corrosion layers (rust) and also the reduction of dirt and black (corrosion) crusts on bronze and brass seem possible without any damage of the underlying substrate. Further pilot applications combined with instrumental analysis will follow. Furthermore, laser treated areas will be compared with results obtained by means of established cleaning techniques.

References

1. M. Cooper, Laser cleaning in conservation, Butterworth-Heinemann, London (GB), 1998
2. Conf. proceedings LACONA III, Florence (I), April 1999, J. Cult. Heritage, Supp. 1, 2000
3. Conf. proceedings LACONA IV, Paris (F), September 2001, J. Cult. Heritage, Supp. 1, 2003
4. Laserstrahlreinigung von Naturstein (eds. Siedel, Wiedemann), Fraunhofer IRB Verlag, 2002
5. Reinigung von hist. Glasmalereien mit Lasertechnik (ed. Römich), Fraunhofer IRB Verlag, 2000

1320 nm Range Nd:YAG-Laser in Restoration of Artworks Made of Bronze and Other Metals

S. Batishche[1], A. Kouzmouk[1], H. Tatur[1], T. Gorovets[2], U. Pilipenka[3], and V. Ukhau[3]

[1] Institute of Physics of National Academy of Sciences of Belarus (IP), Minsk, Belarus
batis@bas-net.by
[2] National Art Museum of Belarus (NAM), Minsk, Belarus
kaa@dragon.bas-net.by
[3] Research enterprise "Belmicrosystems" of "Integral" Amalgamation (REBIA), Minsk, Belarus
ukhau@tut.by

Abstract. Investigations on optimization of methods of laser cleaning of metal artworks by pulses of microsecond and nanosecond duration on wavelengths of 1064 nm and 1320 nm of Nd:YAG-Lasers were fulfilled. Comparison of results of cleaning under different conditions was done.

1 Introduction

Since the first successful experiment made by John Asmus [1] on laser cleaning of lead and corroded bronze, a number of successful applications of the new technology have been demonstrated for cleaning artworks made of various metals (aluminium, bronze, copper, steel, brass, silver and some others) with the radiation of various lasers (Q-switched and free-running Nd:YAG-Laser, CO_2 and XeCl lasers, Nd:YAG-Lasers with harmonic generators) delivered to a target through an articulated arm or fiber [2–5].

Under the influence of the ideas developed by Martin Cooper from the National Museums and Galleries on Merseyside (NMGM) in [6], NAM in cooperation with IP and REBIA has successfully used Q-switched and free-running Nd:YAG-Lasers working at 1064 nm, 532 nm and 1064 nm, respectively, for laser cleaning of metal artworks since 1996. Laser cleaning showed high cost efficiency and qualitative advantage in comparison with the conventional widely used mechanical (scalpel, polishing), chemical and electrochemical cleaning techniques [7]. At present, NAM mostly uses a free-running 1064 nm Nd:YAG-Laser cleaning system with fibre transportation due to its high flexibility and usability. This technique has won the recognition in Belarus.

This paper discusses the extension of the operating wavelength into the relatively eye-safe 1320 nm range (representing here a set of Nd:YAG-Laser

lines at 1318, 1338, 1357 and 1440 nm and meaning that laser radiation can be concentrated at one line with high efficiency and reliability [8, 9]).

2 Laser Sources

Radiation of four laser systems was utilized.

1. Long pulse (LP) Nd:YAG-Laser with fiber transportation, wavelength $\lambda = 1064$ nm, pulse energy E = 4.0 J, full pulse duration FD = 100 ÷ 120 μs and half-height duration HHD = 40 ÷ 60 μs, repetition rate f = 1 ÷ 25 Hz;
2. LP Nd:YAG-Laser with fiber transportation, $\lambda = 1320$ nm, E = 2.0 J, FD = 100 ÷ 120 μs and HHD = 40 ÷ 60 μs, f = 1 ÷ 25 Hz;
3. Short pulse (SP) Q-switched Nd:YAG-Laser, $\lambda = 1064$ nm, E = 2.0 J, or $\lambda = 532$ nm, E = 0.8 J, HHD = 15 ns, f = 1 ÷ 7 Hz;
4. SP Q-switched Nd:YAG-Laser, $\lambda = 1320$ nm, E = 1.0 J, HHD = 40 ns, f = 1 ÷ 5 Hz.

3 Laser Cleaning of Metal Art Works

It is known that at the surface of artworks made of bonze or other copper alloys there are present a large number of different complex compounds and minerals, whose structure is difficult to identify [10]. Some of them contain molecules of water, as chalcanthite ($CuSO_4 \cdot 5H_2O$), $CuCl_2 \cdot 2H_2O$, or molecules of $Cu(OH)_2$, as malachite ($CuCO_3 \cdot Cu(OH)_2$), azurite ($2CuCO_3 \cdot Cu(OH)_2$), brochantite ($CuSO_4 \cdot 3Cu(OH)_2$). Cuprite (Cu_2O) melts at 1229 ÷ 1235°C, black copper oxide (CuO) decomposes at 1026°C. The melting temperature of pure copper is 1083°C. The melting temperatures of bronze, brass and other copper alloys are still lower, varying from 857 to 1050°C, which means that thermal removal of Cu_2O or CuO layers from bulk bronze goes with melting the latter, as a rule.

If heated, the compounds change as follows: At 100 ÷ 200°C, inner water is released. At 200 ÷ 300°C, $Cu(OH)_2$ decomposes into CuO and H_2O, $CuCO_3$ breaks down into CuO and CO_2, and $CuSO_4$ dissociates into CuO and SO_3 (Cu_2O appears as well). The gas released fills up micro caverns of the superficial contamination layer. In the case of fast heating, as under the action of high intensity pulsed laser radiation, the gas absorbs laser energy thus increasing the pressure in the caverns. At some moment, the caverns explode removing away a substantial amount of contamination. If heating is not fast enough, the gas can leave the superficial layer through micropores without explosion. In this case a film of CuO or Cu_2O may appear, which can be highly adhesive to the bulk of an artwork. The gas and water released have strong absorption in the range of 1300 ÷ 1500 nm. Therefore, laser cleaning

with a Nd:YAG-Laser operating in the 1320 nm range would require lower energy densities and allow more delicate cleaning of copper artworks.

As the starting point, we have conducted investigations on the thresholds of some key phenomena occurring on the surface under the laser action for metal objects, including some real artworks, made of different copper alloys.

Before experiments, all samples were photographed and the detailed description of their corrosion state was made. The samples were preliminarily cleaned from dust and nonresistant contaminations with a soft brush.

The study of chemical composition of metal and corrosion products before and after cleaning was conducted by methods of local X-ray spectral analysis on the S-360 raster-type electronic microscope with the AN-10000 analyzer, electronic Auger-spectroscopy on the PHI-660 F. Perkin Elmer spectrometer. The state of a surface before and after laser action was explored with the optical microscope INM-100 (Leica) and the high resolution scanning electron microscope S-806 (Hitachi).

Although the course of laser action was distinct for each sample because of differences in the composition of alloys and pollution layers and in the initial state of the surfaces, the generalized features can be given for all wavelengths and pulse durations we used. With increasing pulse energy of laser radiation incident on the polluted surface, the laser action passes in order the following stages: generation of steam fog corresponding to the above mentioned emanation of different gases from the polluted layer, then glowing of the surface, then flame with a plume of pollution, and finally flame with ablation of bulk material. The stages of glowing and flame are accompanied by sound.

Table 1 presents some bulk material ablation thresholds (BMAT) (J/cm^2). The copper and brass plates, massive brass cube had the smooth surfaces with no visible pollution on them and were modeling objects. The brass dish and the fragment of bronze chandelier had layers of brown patina on the surface and were real artworks. The brass dish also had a heterogeneous layer of blue-green color.

Table 1. Bulk material ablation thresholds

Object	LP 1064nm	LP 1320nm	SP 532nm	SP 1064nm	SP 1320nm
Copper plate, 0.6 mm thick	>63.5	>28.5	0.64	1.31	1.2
Brass plate, 0.3 mm thick	18.8	23.8	0.66	1.26	1.3
Massive brass cube	9.48	11.9	0.46	0.74	0.88
Brass dish	2.75	5.63	0.48	0.92	0.92
Fragment of bronze chandelier	15.3	17	0.57	0.68	1.2

As seen from Table 1, BMAT depend on wavelength, pulse duration, composition of alloy and contamination. In all cases for LP regime BMAT

are much higher (more than 10 times) than for SP regime. For LP, BMAT (excluding the copper plate, for which BMAT was not reached under the given experimental conditions) are substantially higher for $\lambda = 1320$ nm. For SP regime this dependence is not so pronounced for 1064 and 1320 nm, but BMAT are undoubtedly lower for $\lambda = 532$ nm than for $\lambda = 1064$ nm.

Table 2 gives the thresholds (mJ/cm^2) of the removal of the green-blue layer from the brass dish. It should be noted that a thin brown layer (possibly Cu_2O) always remained on the surface after laser action in LP regime. However, when laser intensity was lower than BMAT but ensured flame and a plume of pollution, the brown layer had low adhesion to the bulk and could be easily removed with fabric or rubber, especially with additional wetting by water, ethanol, glycerin or their mixtures.

Table 2. Green-blue layer removal thresholds

LP 1064nm	LP 1320nm	SP 532nm	SP 1064nm	SP 1320nm
750	710	102	70	120

As seen from Table 2, the threshold is lower at 1320 nm than at 1064 nm for LP, but higher at 532 nm then at 1064 nm for SP. On the other hand, it is higher at 1320 nm then at 1064 nm for SP, which can be connected with the fact that the laser pulse at 1320 nm is three times longer than the one at 1064 nm. In SP regime, the brown layer formed was thinner and its removal from the object was easier, but the dynamical range of laser cleaning without damaging of the bulk material was narrower than in LP regime.

Figure 1 shows typical results of laser cleaning of the base of the silver-coated bronze candlestick under optimal conditions.

Fig. 1. The base of the candlestick before and after laser cleaning (one side with one laser source)

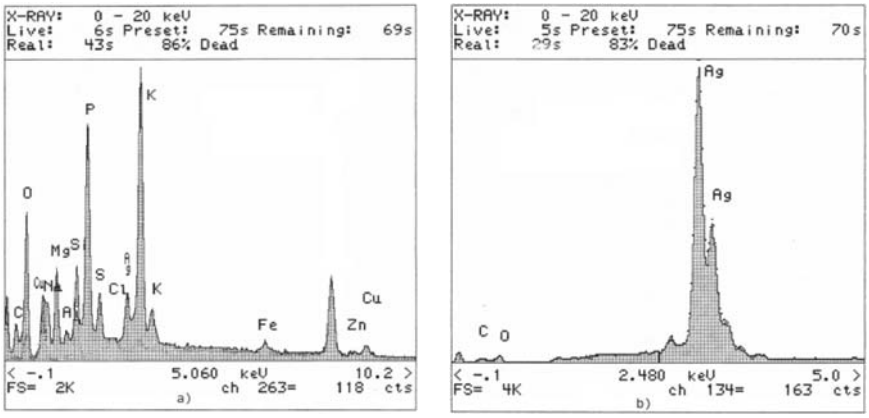

Fig. 2. X-ray patterns of the candlestick base surface before (**a**) and after (**b**) laser cleaning by Q-switched radiation on 1064 nm

The surface of the base was covered by a thin layer of corrosion and pollution of various color and density. The analysis of the chemical composition of the surface before laser processing showed the presence of a large number of chemical elements (C, O, Cu, Na, Mg, Al, Si, S, P, Cl, Ag, K, Fe and others), (Fig. 2a).

As known, the presence of S and Cl in the superficial layer of a metal artwork is most dangerous, so special attention was paid to finding conditions for practically full elimination of S and Cl from the surface.

Cleaning in LP regime at 1064 and 1320 nm resulted in light and dark areas on the surface. The analysis of the chemical composition of the surface showed that the light areas represented practically pure silver (Fig. 2b). In the dark areas, besides silver, there were only some traces of C, O, P, Cu, S, Si, Cl. Cleaning in SP regime at 1064 and 1320 nm resulted in that the whole surface became light, the dark areas were absent. The light areas represented pure silver.

4 Laser Cleaning of Archaeological Metal Samples

In the experiments, a bronze fastener was used (approx. A.D. 50, Fig. 3), which had been found by an expedition of the Institute of History (the National Academy of Sciences, Republic of Belarus) in an archeological dig on the territory of the Republic of Belarus. The object stayed in the soil for a long time, which resulted in its poor state. It was covered by dense depositions of ground and clay with dissemination of sand. The removal of ground was conducted mechanically (with scalpel and brush) under the microscope.

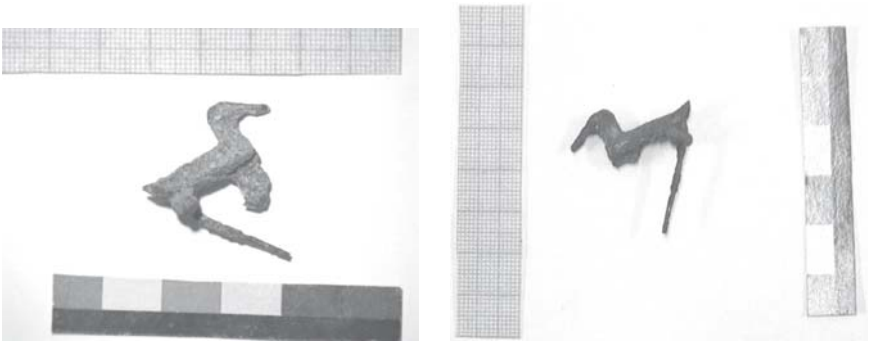

Fig. 3. A bronze fastener before and after laser cleaning

The analysis of the chemical composition of the material showed that the fastener had been made of copper alloy (Cu, Zn, Sn, Fe), containing some other chemical elements: K, P, Cl, S, Fe, Zn, K, Ca.

Laser cleaning was conducted in LP and SP regimes at 1064 nm. Since the corrosion layers were rather thick and dense, their removal was conducted layer by layer under the microscope to prevent destruction of the fastener's base. Deleting all corrosion layers revealed numerous decorative notches on the surface and made the mechanism of the fastener operable.

The investigations of the chemical composition of the surface after laser cleaning showed that the sample was completely cleaned from contamination with the exception of few points where minor amounts of Cl, S, and Ca still remained.

5 Conclusions

The results show that the removal of contamination occurs both in LP and SP regimes at 1064 and 1320 nm. For thick objects when heating is low, the results for LP are practically identical as for SP, with a substantial benefit being an opportunity of fiber transportation of laser energy for long distances (tens of meters). On the surface, a layer of patina always remained in LP mode. The layer of patina could completely disappear in SP mode. It should be stressed that removal of patina, as a rule, occurs with melting bulk bronze material. In the case of thin metal objects, better results are obtained in SP regime (which agrees with S. Siani et al. [11, 12]) especially when coatings of silver or other metals are dealt with. In all cases, the experts found laser cleaning of metal artworks at 1320 nm less damaging. This can be explained by strong absorption in this spectral range of water and other gases released under laser action into the superficial layer. So, a lower superficial layer removal threshold is attained and more delicate cleaning of artworks is possible.

Besides, at 1320 nm in LP mode, a wider energy range of laser cleaning not damaging bulk material is realized.

From the viewpoint of restaurateurs, both 1064 and 1320 nm in LP an SP modes are needed to obtain the best results for metal artworks.

Acknowledgements

The authors deeply appreciate Prof. Costas Fotakis and Dr. Vassilis Zafiropulos from FORTH-IESL and Dr. Martin Cooper from NMGM for their collaboration and attention to the work. The work was financed by the International Scientific Technical Centre in the framework of the project B-373-2.

References

1. J. F. Asmus, in *Light Cleaning: Laser Technology for Surface Preparation in the Arts*, Technol. Conserv. 3 (1978) 14–18
2. Jang Debin, Luo Yi, and Gao Min, in *Proceedings of EEC China workshop on preservation of cultural heritages*, Xian, Shaanxi, China, 1991, 102–109
3. J. Larson, in *From Marble to Chocolate: The Conservation of Modern Sculpture*, Tate Gallery Conference, Archetype Publications, London, 1995, 55–58
4. C. A. Cottam, D. C. Emmony, J. Larson, and S. Newman in *Lasers in the Conservation of Artworks*, (LACONA I), Restauratorenblaetter (Special Issue), Mayer & Comp., Vienna, 1997, 95–98
5. C. A. Cottam, and D. C. Emmony, in *Lasers in the Conservation of Artworks*, (LACONA II), Restauratorenblaetter (Special Issue), Mayer & Comp., Vienna, 1999
6. M. Cooper, in *Laser Cleaning in Conservation: An Introduction*, Butterworth-Heinemann, Oxford, 1998
7. S. A. Batishche, T. V. Gorovets, N. N. Kalashnik, Y. A. Karachun, I. N. Panshina, and N. M. Pogranovsky, in *Proceedings of the 3d Conference on Laser Physics and Spectroscopy*, Grodno, Belarus, 1997, 173–175
8. S. A. Batishche, A. A. Kouzmouk, N. A. Malevich, and G. A. Tatur, in *Instrumentals and Experimental Techniques*, Vol. 42, 666–669, 1999
9. S. A. Batishche, A. A. Kuz'muk, N. A. Malevich, and G. A. Tatur, in *Quantum Electronics*, Vol. 30, 673–674, 2000
10. M. K. Kalish, in *Natural Protective Films on Copper Alloys*, Metallurgia, Moscow, 1971
11. R. Pini, S. Siano, R. Salimberi, M. Pasquinucci, and M. Miccio, in *Lasers in the Conservation of Artworks*, (LACONA III), Journal of Cultural Heritage, Elsevier, Paris, 2000, 129–137
12. S. Siano, M. Miccio, D. Morejon, R. Pini, G. De Marinis, M. Dapiaggi, and G. Artioli, in *Lasers in the Conservation of Artworks*, (LACONA V, Abstract book), Osnabrueck, Germany, 2003, 107–108

Surface Cleaning of Iron Artefacts by Lasers

Y.S. Koh[1] and I. Sárady[2]

[1] Kiruna Center for Conservation of Cultural Property, Arent Grapegatan 20, 981 32 Kiruna, Sweden
yangsook.koh@sfmv.se
[2] Luleå University of Technology, 971 87 Luleå, Sweden
Istvan.Sarady@mb.luth.se

Abstract. In this paper the general method and ethics of the laser cleaning technique for conservation are presented. The results of two experiments are also presented; experiment 1 compares cleaning of rust by an Nd:YAG laser and micro-blasting whilst experiment 2 deals with removing the wax coating from iron samples by a TEA CO_2 laser. The first experiment showed that cleaning with a pulsed laser and higher photon energy obtained a better surface structure than micro blasting. The second experiment showed how differences in energy density affect the same surface.

1 Introduction

For cleaning metal artefacts, conservators often use techniques such as the use of dental tools or micro blasting to assist with the removal of corrosion. With these methods very small fragments of the original artefact are often removed from the surface. These methods are difficult to control which easily results in over-cleaning of the surface which may reduce the visual appeal of a surface and in extreme cases even accelerate further decay. The organic materials used in conservation over the years, such as adhesives and protective coatings also decay and age resulting in the need for re-treatment of the object. For removing of old conservation material before a re-conservation process, solvents are often used. However, solvents can be environmentally harmful and represent a health hazard. In extreme cases chemical residues left on the artefact can cause long-term problems.

Laser cleaning is a modern conservation technique which has been taken from industrial and medical uses of lasers. Laser cleaning uses no chemicals and leaves no residues making it ideal for use in the conservation and restoration of archaeological artefacts and artwork.

Attempts at cleaning of artwork using lasers began in 1970s. The laser technique has become an important tool for the precise removal of surface pollutants without damaging the underlying material [1].

The most common type of laser used in conservation is the Q-switched Nd:YAG laser which provides very short pulses of high energy, near infrared radiation at a wavelength of 1.064 μm. The most important parameter when using Nd:YAG laser for cleaning is the energy density/fluence of the laser

beam which is defined as the energy per unit area, J/cm^2. The energy density/ fluence should be high enough to remove the dirt layers but low enough to ensure that the substrate surface is not damaged. However these principles work best for materials such as polluted stone, parchment, textiles, paintings and stained glass, which show a high contrast between absorption and reflection of the surface contaminants and substrate.

Investigations into using Nd:YAG laser for cleaning metal artefacts have also been carried out [2, 3]. The TEA CO_2 laser, providing short pulses of infrared radiation at a wavelength of 10.6 μm, has also been used for metal artefacts [4, 5].

2 Experiment

Two comparative experiments were performed in this study; cleaning of rust and cleaning of wax on old iron samples. The samples used were iron objects excavated in northern Sweden. These have similar corrosion products to those seen on even older archaeological objects.

Experiment 1 compared the cleaning effects of a Nd:YAG laser with conventional cleaning using micro-blasting.

Experiment 2 investigated the cleaning effects of a TEA CO_2 laser at three different energy densities, achieved by varying the distance between the focal point of the laser and the surface of the artefact.

2.1 Experiment 1

The sample, part of an old iron scythe, was cut into three pieces. The first piece was kept as a reference of the object before treatment.

Before cleaning the surface was covered with red-brown corrosion products of iron (Fig. 1a). Some parts of the surface had flaked off and were unstable. One of the pieces was cleaned by using the Nd:YAG laser whilst the other was cleaned by micro blasting (Table 1). After cleaning both samples were treated by the same conservation procedure. Firstly desalting in deionised

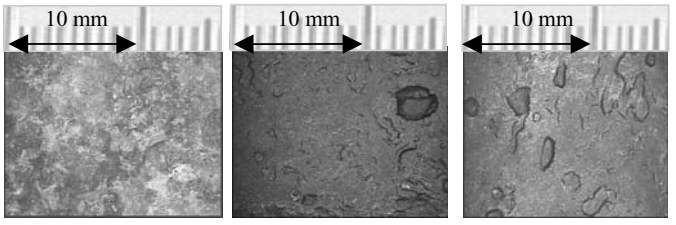

Fig. 1. Surface of the samples before (**a**) and after conservation (**b**, **c**)

Table 1. Cleaning of samples using Nd:YAG laser pulses and micro-blasting

Reference	Laser Cleaned		Micro-Blasted	
No cleaning	Lynton Paragon XL		Micro blast	
	Nd:YAG	frequency doubled	Medium	Aluminium oxide
	Wavelength	532 nm (Green)	Size Ø	0.050–0.075 mm
	Pulse energy	3.5 J/cm^2	Pressure	0.5 MPa
	Frequency	10 HZ		
	Spot form	round		
	Beam transport	articulated arm		
	Focusing	defocused		

water and then removal of rust products resulting from the desalting process using a rotating brush. The samples were then soaked in ethanol, dried in a vacuum chamber and coated with microcrystalline wax.

2.2 Experiment 2

A part of an old iron spade was divided into four small squares, about 2 cm × 2 cm. The samples were prepared by cleaning with a rotating brush and then coated with microcrystalline wax giving the samples a dark smooth waxy surface.

Three of the samples were treated by using the TEA CO_2 laser with one being retained as a reference. The distance between the focal point of the laser and the sample was varied as shownin Table 2 and Fig. 2 to compare the cleaning effect of different energy densities and to find the optimal cleaning distance for similar iron object.

Table 2. Removal of wax from samples taken from a spade using TEA CO_2 laser (Alltec, Allmark 870). Wavelength: 10.6 µm, Frequency: 2 Hz, Spot form: square, Beam transport: 90° deflection

Reference (a)	Cleaned at Distance 33 cm (b)	Cleaned at Distance 32 cm (c)	Cleaned at Distance 31 cm (d)
No irradiation	Spot size: 0.65 × 0.6 cm^2 Energy density: 5.1 J/cm^2	Spot size: 0.5 × 0.42 cm^2 Energy density: 9.5 J/cm^2	Spot size: 0.3 × 0.33 cm^2 Energy density: 20.0 J/cm^2

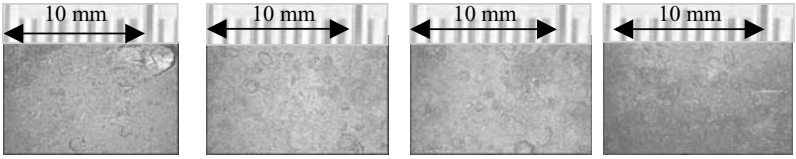

(a) Reference (b) Distance 33cm (c) Distance 32cm (d) Distance 31cm

Fig. 2. Surface of the samples before (**a**) and after TEA CO_2 laser cleaning (**b**, **c**, **d**)

3 Results and Discussion

The corroded iron surface on archaeological artefacts is often unstable and easy to flake off as seen in the reference sample in Fig. 1a. Corrosion products are commonly inhomogeneous and their chemical and physical properties can vary over the same sample. In the first experiment both cleaning methods removed corrosion products from the samples. However, the microscope pictures, Fig. 1, show that the sample cleaned by laser leaves a smoother surface than that cleaned by micro-blasting. Using micro-blasting, more of the surface flaked off in an uncontrolled manner during cleaning, which resulted in the roughness observed. The laser, on the other hand, caused less stress on the unstable surface, which results in a better preservation of the surface structure. However, it was noted that laser cleaning was more time consuming than micro blasting, because a laser spot covered a much smaller area than the jet of abrasive particles from the micro-blasting equipment.

As well as inorganic corrosion products such as rust, surface coatings such as wax often require removal before a re-conservation of metal artefacts. In experiment 2 most of the wax could be removed by 1 or 2 pulses from the TEA CO_2 laser. However, rough surfaces were difficult to clean completely. The laser spots must be overlapped to ensure complete removal of the wax coating.

The surface of the sample which was cleaned at the highest energy density, $20\,J/cm^2$ Fig. 2d, became darker, probably due to oxidation of the material or dehydration of surface rust. For the sample cleaned at the lowest energy density, $5.1\,J/cm^2$ Fig. 2b, some of wax coating remained after cleaning with 1 or 2 pulses. More pulses could cause damage to the surface. Optimum results were obtained with an energy density of around $10\,J/cm^2$ with the optics used Fig. 2c. This allowed cleaning with 1 to 2 overlapping pulses without surface damage.

Cleaning of organic coatings using a TEA CO_2 laser showed promising results in earlier studies [4, 5]. All metals are highly reflective in the far infrared and because of this can be subjected to high laser radiation fluence with no significant surface heating and therefore no surface damage. The TEA CO_2 laser ($10.6\,\mu m$) used in the experiments was thus a logical choice for cleaning metal artefacts which retain a non-corroded metal core since the laser radiation vaporises the surface contaminants and is then reflected from

the underlying metal. However, the interaction between laser radiation and different contaminants may be complex and needs to be investigated on a case-by-case basis prior to extensive cleaning.

The formation of plasma (partially ionised cloud of vapour) above the irradiated metal object can affect the effectiveness of the cleaning. The plasma can cause increased surface damage due to so called plasma heating which results in discolouring/darkening of the surface. This problem was observed in experiment 2 where dark spots were seen on the sample irradiated at the highest energy density 20 J/cm^2 (Fig. 2d). Plasma formation can be prevented by using a shielding gas stream, for example nitrogen, over the sample surface.

Due to the vaporization of the surface contamination, an audible "click" can be heard when the laser impinges on the surface. The character of this sound varies with laser parameters. An experienced operator will "hear" when the cleaning process is most effective. It is also possible to use advanced signal processing to provide closed loop feedback [6].

Absorptivity is also affected by surface roughness; rough surfaces absorbing more strongly than smooth ones. Very rough surfaces, with cavities and other "hidden" areas are difficult to clean since much material is in the shadow of the laser beam. This problem can be partially overcome by using low energy pulses and irradiating from different directions.

To study the pre- and post-irradiated surfaces, Raman spectroscopy was used since it is non-destructive and allows sure indication of the presence or absence and identification of a wide range of organic and inorganic compounds. As would be expected, the cleaned samples from experiment 1, which involved removal of rust and inorganic contaminants, showed similar surface chemistry. In experiment 2, where wax was to be removed, the Raman spectrum of the reference sample showed a clear indication of the wax. On the irradiated samples no spectral lines originating from the wax were seen, confirming that the laser cleaning process was very effective.

4 Conclusions

Laser cleaning is an effective technique for assisting in the conservation of metal artefacts since it provides a high degree of control during cleaning allowing fragile objects or items with much surface detail to be effectively cleaned. This degree of control is essential when preserving items with surface relief, original tool markings and surface patina.

However, the technique must be used with care since process parameters must be set so as to prevent over cleaning. At present process parameters must be set on a case-by-case basis and there remains much to be investigated before lasers will be commonly used in metal conservation. It is therefore important to use good monitoring and controlling techniques and skilled operators with experience of the process to achieve the most satisfactory results.

Acknowledgements

The authors gratefully acknowledge Norrbotten's Research Council, Luleå, Sweden, and the National Heritage Board, Stockholm, Sweden, who sponsored this study.

References

1. M. Cooper, *Laser Cleaning in Conservation: An Introduction*, Butterworth-Heinemann, Oxford, 1998
2. R. Pini, S. Siano, R. Salimbeni, M. Pasquinucci, and M. Miccio, in *Journal of Cultural Heritage*, Vol. 1, 129–137, 2000
3. S. Siano and R. Salimbeni, in *Studies in Conservation,* Vol. 46, 269–281, 2001
4. C. A. Cottam and D. C. Emmony, in *the Conservation of Artworks (LACONA I),* Edited by W. Kautek, E. König, 95–98, 1997
5. Y. S. Koh and I. Sárady, in *Laser Techniques and Systems in Art Conservation*, SPIE Proceedings, Vol. 4402, 46–53, 2001
6. J. M. Lee, K. G. Watkins, and W. M. Steen, in *The International Journal of Advanced Manufacturing Technology,* Vol. 16, 649–655, 2000

Part III

Laser Cleaning Miscellaneous

Experimental and Theoretical Indications on Laser Cleaning

J. Marczak, K. Jach, A. Sarzynski, and R. Ostrowski

Institute of Optoelectronics, Military University of Technology, 2 Kaliskiego Str., 00-908, Warsaw, Poland
jmarczak@wat.edu.pl, kjach@wat.edu.pl, asarzynski@wat.edu.pl

Abstract. The paper presents influence of laser radiation parameters on velocity of encrustation removal from artworks and heritage architectural objects. The influence of laser fluence and pulsewidth on the velocity of graphite removal from aluminium substrate is discussed on the basis of developed numerical model. Selected experimental results of influence of laser wavelength and fluence on velocity of encrustation removal for different heritage objects are given as well as remarks on laser cleaning process are presented.

1 Introduction

For all cleaning methods it is necessary to remove the secondary deposits and dirty layers with no damage of original substrates. The main problem connected with the mechanical or chemical cleaning of artworks is a lack of sufficient control of original surface protection against its erosion.

The increasing interest in laser cleaning of artworks and historical objects results from the great advantages of this technique as compared with the conventional, mechanical and chemical restoration of objects [1–4]. However, it requires the high precision in selection of laser parameters particularly in cleaning of unique artworks. It is particularly important for the materials much more fragile than stone objects. Several experiments connected with this problem have been carried out and described in the literature [4–8].

The presented paper is devoted to the laser cleaning, with a special emphasis on the selection and consideration of physical parameters of a laser source and the encrustation: radiation wavelength, intensity of object irradiation, absorption coefficients of deposits. Chemical and physical properties of the surface impurity layers may change from point to point within the same sample. Absorption coefficient of the layers depends strongly on the environmental conditions like the air humidity and air contaminants (pollution). In spite of this, the theoretical description of laser cleaning is necessary as it allows the explanation of several characteristic features of the processes under investigation. Moreover, sometimes it is very difficult to find (or experimentally determine) empirical functions and coefficients describing the behavior of real encrustation within a wide range of thermodynamic parameters. Particularly difficult is to determine the thermal conductivity or absorption

coefficient as a function of temperature, density, and ionisation degree. That is why we are interested in a qualitative analysis of the processes under investigation. So we use a graphite instead of the impurity and an aluminium base instead of the real substrate in our calculations. Mechanical, optical and thermodynamical characteristics of graphite and aluminium are much better known than characteristics of real impurities and substrates. This numerical model has been described in detail in [9, 10]. Shortly, in the model based on the hydrodynamic equations for continuous medium we have taken into account the absorption of laser radiation, ionisation of the medium, thermal conductivity, shock-waves and elastic medium characteristics. On the other hand, the phase transitions (melting, vaporization) have not been considered. Thereof, the analysis of interaction of laser radiation with the target is, so-called "not-threshold" and the final results are only qualitative.

The paper discusses also the factors influencing on the selection of laser pulse parameters, based on a wide experience in the field of laser cleaning of several important heritage objects [11–13], simulation experiments including removal of candle soots on a glass plate [14, 15] as well as the results of numerical calculations.

The conclusions related to the ablation of superficial layers are also presented.

2 Optical Properties of Deposits

The optical properties of deposits are the one of the basic factors determining the range and type (wavelength) of energy of pulsed laser radiation to be used. Examined constitution and the wider analysis of deposits showed their variable optical properties. For example, the reflected (scattered) radiation intensity depends on the material chemical and physical state. It may be as large as in the case of MgO (which may be regarded as perfect scatterer– scattering coefficient over 97% in a wide optical spectral range), or as small as in the case of soot (which may be regarded as perfect absorber – absorption coefficient of order $10^5\,\mathrm{cm}^{-1}$) (see Fig. 1).

The experiment confirmed, that it as a significant difference in the effective thickness of deposit removal. It is difficult and even sometimes impossible to calculate (numerical modeling) the characteristics of real deposits, because their spatial structures and optical-physical properties are complex and their presence is of random nature. Moreover, optical, mechanical and thermodynamical properties of encrustation and substrate are generally not known as well as they could change from point to point inside the same sample (see Fig. 2 and Table 1). Even, during laser cleaning, wet substrate can change to be dry because of sun shining.

The preliminary results of measurements of chemical composition of deposit elements on sandstone sample are shown in Table 1. The measurements

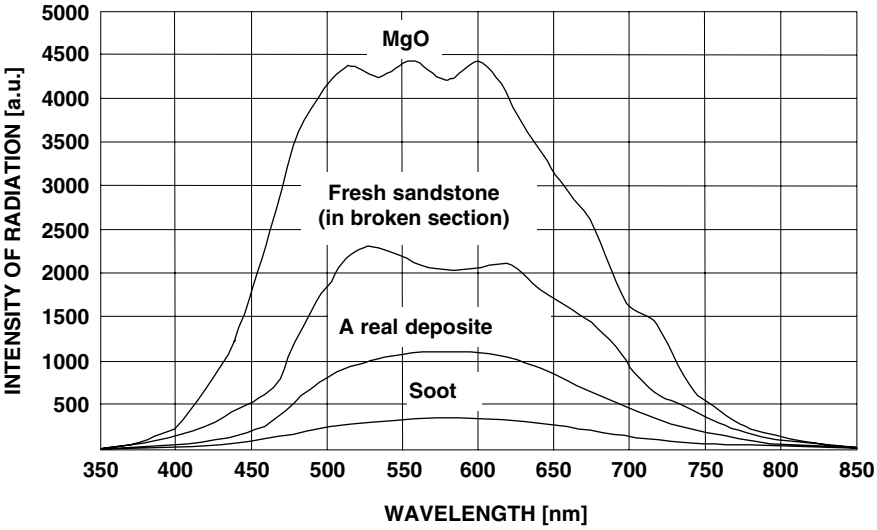

Fig. 1. Comparison of radiation intensity scattered (diffusively reflected) by different materials. Intensity values include spectral efficiency of spectrometer's detector

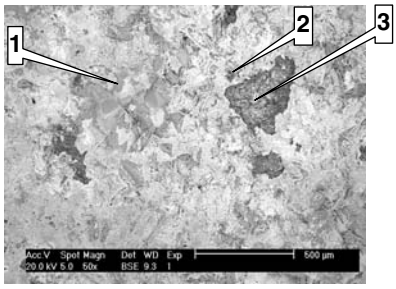

Fig. 2. View of the surface of a sandstone sample from Sigismund's Chapel with depositions. Digits denote EDS SEM analysis points

have been done in the three random points of a sample using EDS SEM method as a reference for this small area (2 mm^2).

3 Influence of Laser Beam Parameters

Interaction of laser radiation with matter depends on the power density. It was experimentally confirmed that deposits and substrate materials illuminated with short laser pulses of high intensity have several common features. Surfaces of these materials undergo ablation process only when the irradiation level q (J/cm^2) exceeds the threshold value q_{thr}. For several materials

Table 1. Chemical composition of a sandstone deposit sample from Sigismund's Chapel

Point 1			Point 2			Point 3		
Element	Wt %	At %	Element	Wt %	At %	Element	Wt %	At %
C	3.74	5.69	C	4.48	6.25	C	2.87	4.36
O	67.68	77.26	O	78.97	82.79	O	68.42	77.90
Mg	2.19	1.65	Mg	13.42	9.26	Na	1.31	1.04
Al	6.30	4.27	Al	0.48	0.30	Mg	2.79	2.09
Si	10.91	7.10	Si	1.33	0.80	Al	7.46	5.03
S	0.27	0.16	S	0.30	0.15	Si	11.07	7.18
Cl	0.77	0.40	Cl	0.56	0.26	S	0.37	0.21
K	2.06	0.96	Ca	0.33	0.14	Cl	0.45	0.23
Ca	4.14	1.88	Ti	0.14	0.05	K	1.02	0.47
Ti	0.22	0.08				Ca	0.78	0.35
Fe	1.52	0.50				Ti	0.34	0.13
Zn	0.19	0.05				Fe	2.91	0.95
						Zn	0.22	0.06
Total	100	100	Total	100	100	Total	100	100

a strong limitation connected with the possible damage of substrate surface and undesired colour modification can occur.

It is strongly suggested to use the threshold and just above the threshold fluence values of laser irradiation for removal of deposits from historical objects. Thus, the thickness of the layer removed by a laser pulse is rather small and the process can be easily controlled to avoid the substrate damage.

One of the most important parameters of laser radiation used for removal of deposits from artworks surfaces is the distribution of energy density in a cross-section of a laser beam. The laser beams used for deposits removal should have uniform distribution of energy density, so called "top hat". Uniformity of energy distribution in a laser beam cross-section depends on many factors, mainly on the optical construction of laser resonator [16, 17]. Gaussian distribution of a laser beam is not recommended. Difference between temperatures in a centre of illumination of a sample for "top hat" type beam and Gaussian beam of equal powers and short laser pulse can reach more than 30%.

On the basis of the developed numerical model describing the interaction of pulsed laser radiation with matter, selected results of numerical calculations have been presented: plasma pressure, temperature, density, velocity of graphite ablation process for aluminum substrate. Numerical calculations were made for power densities in the range of $q = 5 \times 10^5\,\mathrm{W/cm^2}$ to $q = 5 \times 10^9\,\mathrm{W/cm^2}$. Several results of numerical calculations for graphite illuminated with intensive laser radiation are presented (Figs. 3, 4).

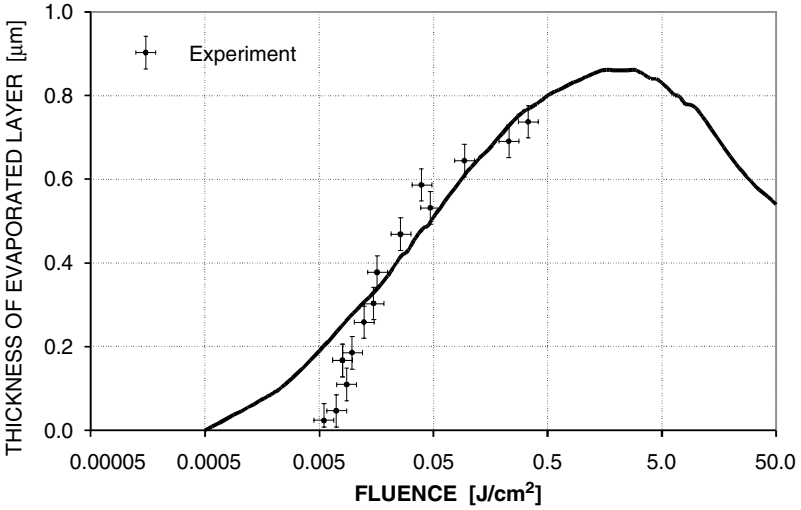

Fig. 3. Influence of the fluence on the thickness of evaporated graphite layers on aluminium substrate: *solid line* – numerical calculations; *crosses* – experimental results. Nd:YAG laser, 1064 nm, triangular shape of laser pulse, pulse duration 5 ns

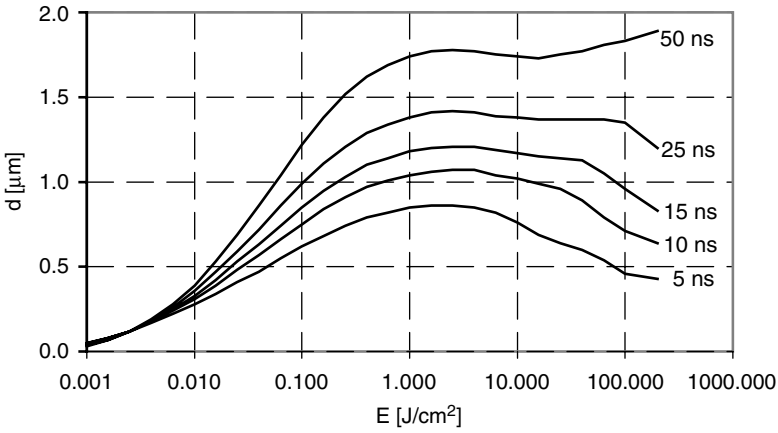

Fig. 4. Calculated thickness of graphite layer evaporated from aluminum substrate by a laser pulse: the numbers denote pulse widths. Triangular shape of laser pulse and homogeneous graphite layer are assumed (initial thickness of graphite layer was 3 μm)

We do not see any particular threshold in numerical results inside the Fig. 3 and Fig. 4. It is caused mainly by the neglecting of melting and vaporization in our numerical model. Various pulse durations and energy densities were assumed. The calculation results (thickness of evaporated graphite layer from aluminum substrate using laser pulses of triangular shape and pulse widths of t = 5, 10, 15, 25, and 50 ns in dependence on pulse radiation density are shown (Fig. 4).

4 Influence of Wavelength

The absorption coefficient of material depends on its temperature and wavelength of radiation. These dependencies are difficult to determine for deposits. Thus, experimental investigations of influence of radiation wavelength on ablation threshold and ablation velocity of superficial layers should be carried out.

Figure 5 shows a diagram of the rate of deposit removal from a sandstone plate versus the level of irradiation (four wavelengths) [14, 15].

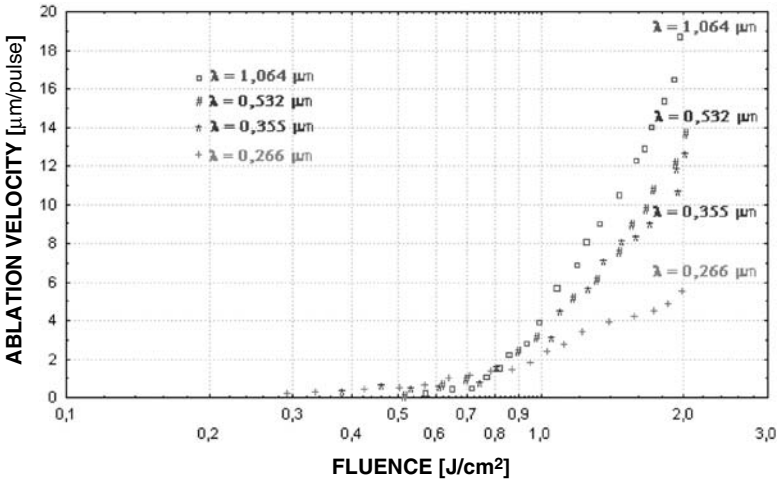

Fig. 5. Results of experiments for laser cleaning. Thickness of impurity layer evaporated from sandstone relief slab by a laser pulse. The Nd:YAG laser (600 mJ, 12 ns) with the second, third and fourth harmonic generation was used (but we used only pulse energies 25 mJ for each harmonic)

After the analysis of deposits removal rate, the highest rate is observed for the wavelength $\lambda = 1.06\,\mu\text{m}$. The highest ablation threshold of 0.7–0.8 J/cm^2, corresponds to this wavelength. The lowest ablation threshold of 0.3 mJ/cm^2 is observed for the wavelength of $\lambda = 0.266\,\mu\text{m}$, but the removing rate is

several times lower than in the case of $\lambda = 1.06\,\mu m$ for the comparable fluence of about $2\,J/cm^2$.

The application of the wavelengths of $\lambda = 0.532\,\mu m$ and $\lambda = 0.355\,\mu m$ results in the comparable removing rates of deposits, when the levels of object irradiation are similar. Moreover, for these wavelengths, the threshold energy densities of deposit removal are almost similar and in practice their values are about 0.5–0.6 J/cm^2.

5 Influence of Graphite Porosity

Deposits very often have a porous structure and as a result they absorb atmospheric gases and soak water.

Pores, first of all having large surfaces and containing gases and water, strongly change various physical characteristics of deposits. In such porous media, the absorption coefficient may become large enough to cause significant absorption of laser radiation resulting in the increase of temperature and significant heating of the medium. Gases and water that are present in pores make medium ionisation easier resulting in the increase of radiation absorption. Water allows deeper penetration of radiation resulting in the heating of the thicker medium layer.

In a laser treatment of materials, a term "regulation" of absorption coefficient of radiation is known, adequately to the treatment aims and laser characteristics. "Regulation of absorption coefficient" is frequently realised by the change of wavelength (wavelength conversion (harmonics) of a laser, e.g., CO_2 instead of Nd:YAG). When metal surfaces are hardened with laser, absorption coefficient can be changed only by wavelength altering. For porous structure, however, direct influence on properties of treated deposits is possible. For example, the initial heating or saturation with water causes significant change in the all properties of porous medium. Finally, absorption coefficient, medium density, its thermal and mechanical properties are changed. Due to the possibility of practical influence on medium properties, the rate and the efficiency of deposits removal can be controlled (Fig. 6).

6 Conclusions

The interaction of laser radiation with a surface of solid body is a complex process. These phenomena depend on chemical and physical properties of surface as well as on parameters of laser beam itself.

Presented theoretical model confirms conclusions drawn for several numerical and experimental results including our work. Experimental results for soot (flame of stearin candle) removal from thin glass plate (average thickness of 21 μm) are consistent for numerical calculations.

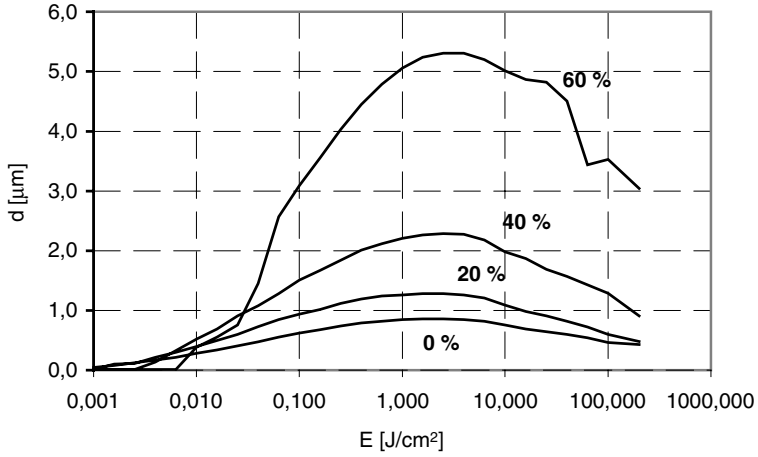

Fig. 6. Thickness of graphite layer evaporated from aluminum substrate by a laser pulse. Results of the numerical calculations for porous medium. Digits denote the percent of total volume of pores

It can be stated, that all results confirm the many common features for totally different media:

- the ablation is observed only above some threshold value of irradiation q_{thr} even for the thin liquid layer modifying the deposit;
- the ablation velocity "d" (µm/pulse), defined as a thickness of removed layer per one laser pulse is connected with the level of material irradiation;
- the ablation velocity of each deposit has its maximum (Figs. 3, 4, 6) which depends on laser pulse-width (Figs. 4, 6). Further increase of radiation intensity (fluence) causes the decrease in a thickness of evaporated layer. It is due to the reflection of incident radiation in so-called critical layer;
- the level of irradiation at the ablation threshold q_{thr} decreases with the increase of absorption coefficient of a medium;
- the degree and the range of material damage around ablation area decreases with the increase of absorption intensity and the decrease of pulse duration.

References

1. A. L. Schawlow, *Lasers*, Science, Vol. 149, pp 13–22 (1965)
2. J. Asmus, *The application of laser radiation to the cleaning of statuary*, Bulletin of the First annual meeting of AIC, 1, s. 39–49 (1973)
3. Lacona I, W. Kautek, E. Konig, C. Fotakis, K. Watkins, and G. Bonsanti (Eds), Lacona I, *Laser in the Conservation of Artworks*, 4-6 October 1995, Heraklion, Crete, Greece; Proceedings of Lacona I, Verlag Mayer & Comp, Vienna (1997)
4. M. Cooper, *Laser in conservation. An Introduction*, Butterorth- Heinemann, (1999)

5. Lacona II, Firenze, R. Salimbeni and Bonsato (Eds), *Laser in the Conservation of Artworks*, (1997)
6. Lacona III, *Laser in the Conservation of Artworks*, Liverpool (1999)
7. Lacona IV *Laser in the Conservation of Artworks*, 11-14 September 2001, Amphitheatre Rohan Louvre, Paris
8. *Laser Techniques and Systems in Art Conservations*, Proceedings of SPIE, Vol. 4402, Munich '2001
9. J. Marczak, *Wykorzystanie promieniowania laserowego w renowacji dziel sztuki i obiektów zabytkowych w architekturze*, Zeszyty Naukowe Instytutu Maszyn Przeplywowych PAN w Gdansku, "Lasery i nowe techniki w konserwacji obiektów zabytkowych '2002", Vol. 524/1483/2002, str. 23–46 (2002) – in Polish
10. J. Marczak, K. Jach, and A. Sarzynski, *Numerical Modelling of Laser – Matter Interaction,* Proceedings of SPIE, Optical Metrology for Arts and Multimedia, Vol. 5146, pp 215–225, Munich 2003
11. H. Hryszko, A. Koss, J. Marczak, and M. Strzelec, *Laser Cleaning of Seventeenth Century Flax gonfalon*, 5th European Commission Conference on Research for Protection, Conservation and Enhancement of Cultural Heritage, Cracow, 14–16 May 2002
12. Andrzej Koss, and Jan Marczak, *Lasers in the renovation of works of art*, Ist European Forum on Renovation Information, Cracow, 14–16 February 2002
13. Jan Marczak et al., *E!2542 RENOVA LASER – Laser renovation of monuments and works of arts*, Proceedings of the 5th EC Conference "Cultural Heritage Research: a Pan-European Challenge", May 16–18, 2002, Cracow, p 243
14. J. Marczak, *Surface Cleaning of Art Work by UV, VIS and IR Pulse Laser Radiation*, Proceedings SPIE, Vol. 4402, Laser Techniques and Systems in Art Conservations, pp 202–209 (2001)
15. J. Marczak, *Badania Porównawcze Usuwania Wtórnych Nawarstwien z Piaskowca za Pomoca Lasera Emitujacego Promieniowanie o Dlugosci Fal od UV do IR*, Przeglad Mechaniczny, Nr 4, str. 9–14 (2002)
16. J. Marczak, *Designs of the Resonators Increasing the Efficiency of Laser Oscillators*, Proc. SPIE - Laser Technology IV, Vol. 2202, pp 110–119, (1993)
17. J. Firak, and J. Marczak, *Optical Mirrors with Variable Reflectance*, Proc. SPIE - Laser Technology IV, Vol. 2202, pp 196–200, (1993)

Er:YAG Laser Applications on Marble and Limestone Sculptures with Polychrome and Patina Surfaces

A. deCruz[1], M.L. Wolbarsht[2], R.A. Palmer[2], S.E. Pierce[2], and E. Adamkiewicz[3]

[1] Duke University Museum of Art, Durham, NC, USA
adecruz@duke.edu
[2] Duke University, Durham, NC, USA
[3] Orlando, FL, USA

Abstract. The Er:YAG laser (2.94 µm) has been used safely and effectively to ablate contaminants from polychrome surfaces of marble and limestone sculptures. The pieces studied were 13th, 14th and 15th century polychromes and a patina surface of a Roman marble sculpture from the 2nd Century AD. The surface encrustations removed included calcite, gypsum, whewellite, soluble salts, atmospheric deposits, organic films, lichen and other fungal growths that cover the sculptures. The laser removal of organic deposits with the Er:YAG laser was especially effective. A microscopic study of the polychrome surfaces before and after removal of the encrustations showed preservation of the polychrome pigments. Infrared absorption and x-ray fluorescence spectral analyses of the ablated materials and of the surfaces before and after laser ablation were used for evaluation of the mechanism of the laser action and for comparison of the results of Er:YAG laser treatment with traditional conservation methods.

1 Introduction

Er:YAG laser exposure at 2.94 µm has previously been shown to effectively remove old varnish and other encrustations without inducing unwanted chemical or physical changes on the painted surfaces of canvas and wood panels [1, 2]. This removal technique is enhanced by dampening the surface with a liquid, such as water, containing hydroxyl (OH) bonds, since the OH stretching absorption band coincides with the laser wavelength [3]. The present study deals with the removal of encrustations from polychrome and patina surfaces of stone sculptures by means of Er:YAG laser ablation. The sculptures are from the Brummer Collection of the Duke University Museum of Art, Durham, North Carolina, U.S.A. and include:

1. A **Roman Marble Entablature** of the 2nd century A.D. with calcite encrustation;
2. A French sandstone **Head of a Man**, of the 13th century encrusted with black and yellow/orange lichen and accumulated atmospheric deposits;

3. An Italian 15th century marble **Madonna and Child** relief, with polychrome remnants that cover 1/3 of the surface; and
4. A French 14th century limestone **Head of an Apostle** with polychrome surface that is blackened from atmospheric deposits, dirt, soot and egg emulsion embedded in the color surface.

2 Methods

Two Er:YAG lasers (emission wavelength, 2.94 µm) were used: a Conservator 2940, and *High Power Erbium CrystaLase,* both manufactured by Mona Laser of Orlando, Fla. The two lasers differ only in their maximum power levels, each emitting a 250 µs "macro-pulse" consisting of a train 1–2 µs micro-pulses about 2–14 µs apart. The radiation of the *Conservator 2940* is delivered into a 1.5 m long, 1 mm bore, hollow glass waveguide, with a pen-like tip. The pulse from the *High Power Erbium CrystaLase* is delivered with an articulated arm, producing a 1–3 mm diameter spot size. The macro-pulse frequency for both lasers is 10 to 15 Hz. In a typical procedure the energy threshold of the material to be removed from the sculpture surface was first established. In removing calcite for example, the area to be ablated was moistened with distilled water, and the *High Power Erbium CrystaLase* energy level was adjusted until efficient removal was achieved. For calcite removal, 94 mJ to 130 mJ/pulse at 10 Hz, with pulse focused at 1 mm diameter was a typical threshold. Auxiliary wetting liquids used with other materials included: distilled water with 2% surfactant (Tween), ethanol, and ammonium hydroxide at 3 and 10%.

Macroscopic and microscopic evaluations were made before and after laser treatment. The ablated materials were collected by intercepting the laser ablation plume from the sculpture surface with calcium fluoride (CaF_2) or barium fluoride (BaF_2) plates. Infrared spectroscopic analysis of the ablated materials was carried out with a Bruker IFS/66v/S Fourier transform infrared (FTIR) spectrometer in conjunction with OPUS-NT software version 3.1. Spectra of the ablated materials were measured by transmission directly on the CaF_2 or BaF_2 plates. FTIR ATR (attenuated total reflection) analysis was carried out on micro fragments excised from the surface with a scalpel before and after laser ablation. ATR spectra were measured with a Thermo Nicolet 360 FTIR spectrometer with Omnic E.S.P.S.I. software. X-ray fluorescence studies were done on both laser-ablated and excised materials, with a Jeol 6400 scanning electron microscope, Gresham energy dispersive 30 m 2ATW x-ray detector and pulse processor by 4pi Analysis Revolution software. The effectiveness of traditional cleaning methods was tested using: distilled water and Orvis neutral soap; a poultice of Fullers earth, distilled water and ammonium hydroxide; a poultice of cellulose fiber (Cocoon, by Wistox Products); an ammonia-based biocide; and/or Solvent Gel Base with DMSO.

As a result of these studies it was determined that laser treatment was the preferred method in the cleaning process (as detailed below).

3 Results and Discussion

Example (1). **Roman Entablature**, 2nd Century AD, (30″ × 12″ × 3″), marble. The surface of the marble relief was moderately well preserved although about 1/3 of the surface was disfigured by a black-to-dark brown hard cementing calcite encrustation. The calcite could not be removed with traditional solvents, poultices, mechanical or abrasive means without adversely affecting the stone surface. On preliminary examination the 1–3 mm-thick encrustation appeared to be gypsum. However, x-ray fluorescence (Fig. 1) did not show the presence of sulfur in the ablated material but did reveal quantities of aluminum and silicon and traces of iron, in addition to the dominant presence of calcium, consistent with calcite and environmental contamination. The traces of iron would contribute to the black color of the encrustation. FTIR transmission measurements (Fig. 2) clearly show that calcium carbonate (in the form of calcite) was the predominant material removed in ablation, together with minor amounts of material containing hydroxyl groups and hydrocarbon bonds. Controlled removal of the calcite was possible without causing abrasion of the marble surface (Fig. 3). A pulse energy of 96 mJ to 126 mJ with a spot size varying in diameter from 1 to 3 mm was used. The surface was dampened with distilled water prior to laser treatment. FTIR ATR spectra of fragments excised from the surface before and after laser ablation, as well as XRF spectra of the same materials, are also consistent with the removal of mostly calcite in the ablation process.

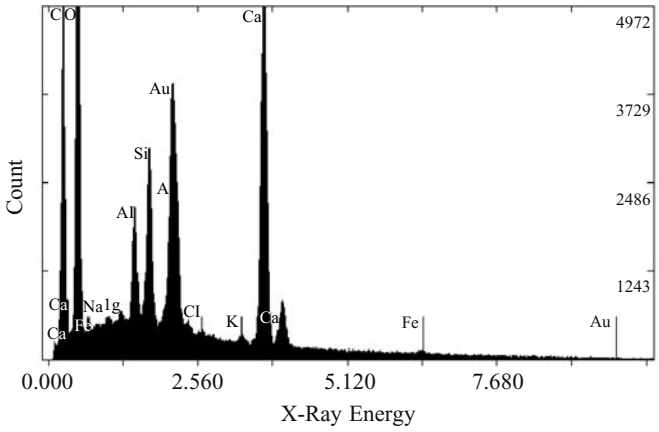

Fig. 1. X-ray fluorescence spectrum of material ablated from the Roman Entablature (with gold conductive layer)

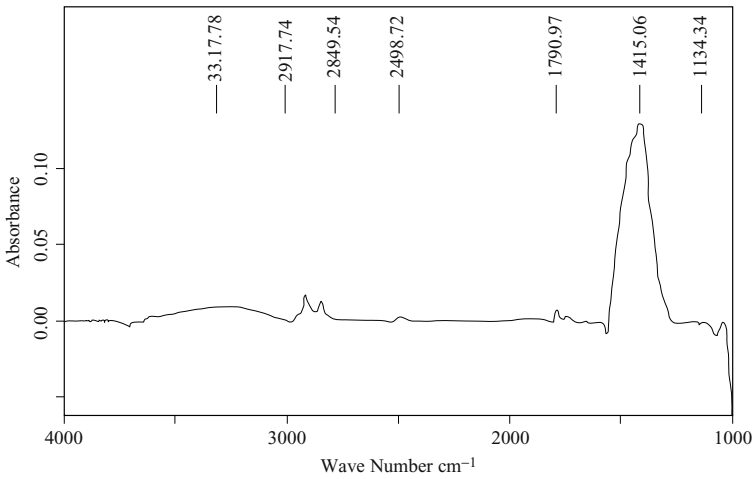

Fig. 2. FTIR spectrum of material ablated from Roman Entablature

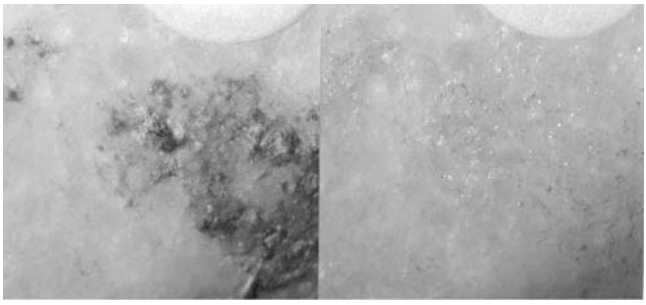

Fig. 3. Roman entablature microphotographs before (*left*) and after (*right*) laser ablation

Example (2). The **Head of a Man**, French 13th century ($15 \times 13'' \times 14''$) encrusted with lichen that has invaded the sandstone surface. The **Head** is a unique example that was selected for exhibition in the Duke University Museum of Art. However, it could not be exhibited in a museum environment with the lichen growth that obscured the details of the sculpture and posed an environmental hazard. Cleaning tests with a biocide were conducted. This ammonia-based solution was applied according to directions, with a spray, full concentrate, manipulated with a natural bristle brush and flooded with distilled water. Some of the lichen was removed; however, a considerable amount of the lichen that was attached to the stone remained. The stone was allowed to dry, and the biocide to penetrate into the stone and effect delayed lichen removal, but after five weeks the lichen was still in place. We

also applied a poultice with biocide, and the effect was again, only a partial removal of lichen. Flooding with water caused the sandstone to soften. This was not a desirable result.

After microscopic and ATR studies to characterize the untreated surface, we applied pulsed laser radiation with the *High Power Erbium CrystaLase*, with various energy levels and found that the lichen began to be ablated at *ca.* 55 mJ with pulse rate of 10Hz. FTIR transmission spectra of the ablated material and FTIR ATR spectra of scalpel-excised surface material were measured to understand better the interaction of the laser radiation with the lichen and stone surface.

The ablated material intercepted on the CaF_2 plate produced a complex FTIR transmission spectrum (Fig. 4). A very strong absorbance is seen at 1659 cm^{-1} with a shoulder at 1541 cm^{-1}. There is also a very strong, broad absorbance at 3288 cm^{-1}. Several peaks are also seen between 1167 and 1030 cm^{-1}. In addition to the C-O peak seen at 1414 cm^{-1}, there is also a shoulder at 1461 cm^{-1}.

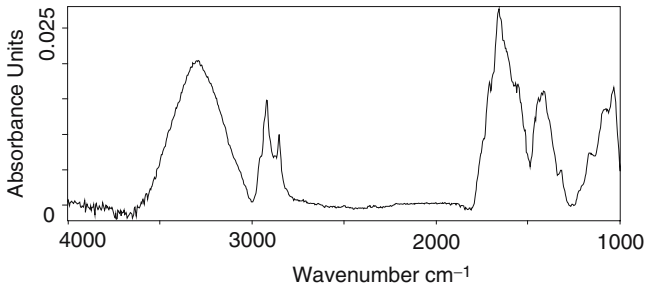

Fig. 4. FTIR spectrum of material ablated from lichen encrusted area on Head of a Man

FTIR ATR spectra of samples removed from the surface with a scalpel showed the extent of the lichen growth (Fig. 5). We attempted to sample the lichen without removing any of the stone. However, the spectra clearly show that this was not successful. The spectrum of the sample taken before ablation shows peaks at 3288, 1659, 1541, 1461, 1414, 1167, 1030 cm^{-1} whereas the spectrum from the cleaned fragment has only one major peak at 1410 cm^{-1} (along with minor peaks at 2875, 2512, 1795, 1395, 848, 872 and 712, all consistent with $CaCO_3$). No bands attributable to organic or biological material were observed after laser ablation.

Burial has allowed the calcareous surface of the **Head of Man** piece to become pervaded by the lichen growths (Fig. 6). The spectrum of the ablated material clearly indicates that biological material was removed from the surface of the stone. For instance, amide bands at 1659 and 1541 cm^{-1} can be seen in the spectrum for the material ablated from a spot of gray lichen on

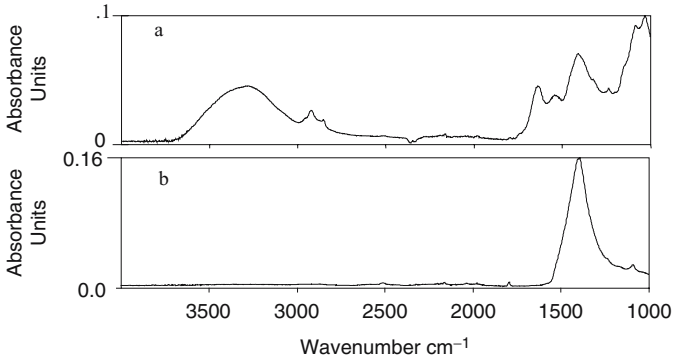

Fig. 5. FTIR ATR spectra of material excised from the surface of the Head of a Man before and after laser ablation

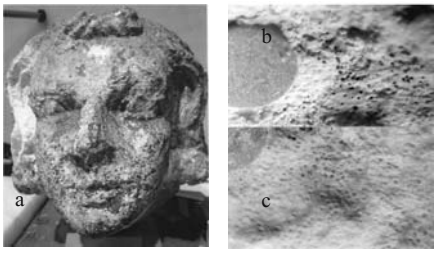

Fig. 6. Head of a Man. (**a**) Cleaned and uncleaned surface and micro-photographs (**b**) before and (**c**) after ablation

the surface and indicate the presence of proteins and/or peptides (Fig. 4). The peak for the NH stretching vibration is seen at 3288 cm^{-1}, and polysaccharide linkages are seen in the three peaks from 1167 to 1030 cm^{-1}. In addition to the C-O peak seen at 1414 cm^{-1}, there are hydrocarbon peaks at 2917, 2850, and 1461 cm^{-1}. In fact, the FTIR ATR spectrum of material excised from the cleaned surface shows that the laser has removed all the lichen and other organic material Fig. 5. Photomicrographs of the surface before and after cleaning Fig. 6 also indicate that the surface has been completely cleaned of lichen.

From these data we can conclude that the Er:YAG laser is able to completely ablate all traces of lichen from the stone surface, but that, as indicated both by the FTIR transmission spectrum of the ablated material and the FTIR ATR spectrum of the material excised from the surface before laser treatment, the lichen-corrupted surface layer of the stone is inseparable from the lichen itself and is also ablated.

Example (3). The **Madonna and Child**, a 15th century marble relief ($20'' \times 19.5'' \times 7''$) with polychrome remnants covering 1/3 of the surface, was tested for traditional cleaning using successively: a poultice with and without

ammonium bicarbonate; distilled water with neutral soap; a prepared gel and a base solvent. The poultice loosened the encrustation on the stone, which was then cleaned with distilled water and neutral soap applied with a brush and rinsed with distilled water. The poultice did not remove the black film that covered the polychrome. However, it did soften the polychrome, which then detached easily from the stone. Wetting the polychrome layer with any liquid caused it to swell, and any abrasion with a medium or soft bristle brush caused physical damage to the polychrome. In contrast, the *Er:YAG Conservator 2940* laser easily removed the black crust with 13 mJ per pulse delivered through a hollow glass wave-guide at 15 Hz. Material was ablated onto CaF_2 or BaF_2 plates either dry or after dampening (effectively staining) the surface with dilute ammonium hydroxide.

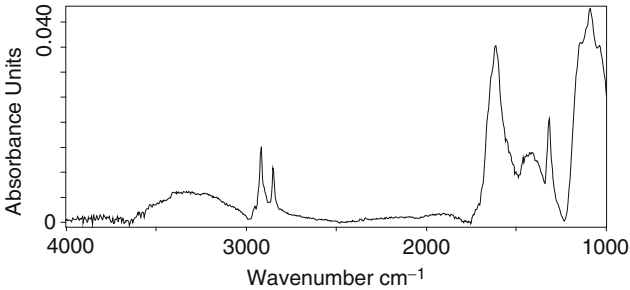

Fig. 7. FTIR spectrum of material ablated from a painted section of the Madonna and Child

The spectrum of material ablated from the dry painted surface (Fig. 7) shows notable peaks at 1616, 1415, 1315, 1149, and 1091 cm^{-1}. Figure 8 shows the FTIR-ATR spectrum of fragments taken before and after laser ablation. Several differences between the spectra are worth noting. Specifically, the

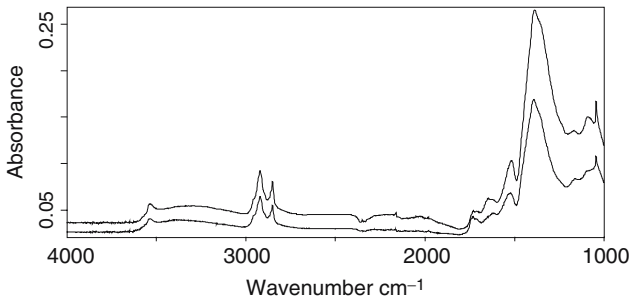

Fig. 8. FTIR ATR spectra taken of a small fragment from the surface of the Madonna and Child before (*top*) and after laser ablation

peak at 1616 cm^{-1} is significantly diminished in the spectrum of the sample taken after cleaning. Also, the peak that was seen at 1090 cm^{-1} in the spectrum of the un-cleaned surface becomes a shoulder centered at 1100 cm^{-1} in the spectrum of the cleaned surface. The peak at 1540 cm^{-1} is much smaller in the spectrum of the surface after ablation. In addition, the peak at 1415 cm^{-1} is also much weaker. In contrast to the IR data, the XRF spectra (Fig. 9) of the amples before and after cleaning show a remarkable difference in the relative amounts of elemental contaminants. Aluminum and silicon both are decreased precipitately in the spectrum of the cleaned surface.

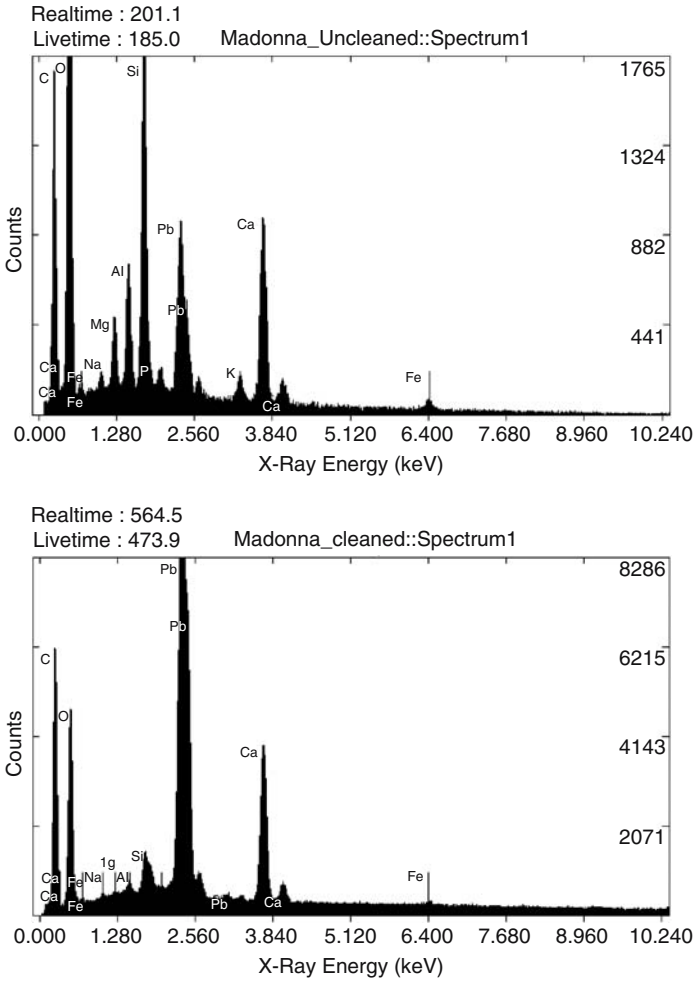

Fig. 9. XRF spectra of fragment from Madonna and Child before (*top*) and after cleaning

The spectrum of the ablated material from the **Madonna and Child** (Fig. 7) indicates that the laser has removed several contaminates. The 1616, 1149, and 1091 cm^{-1} peaks correspond to calcium sulfate dihydrate, gypsum. Gypsum forms on calcareous stone when that stone is in the presence of sulfur and nitrogen oxides and moisture. Also, the 1315 cm^{-1} peak is characteristic of whewellite. Whewellite, calcium oxalate monohydrate, forms as the result of bio-deterioration of stone or from the degradation of pigments. A comparison of the FTIR ATR spectra of material from the surface before and after ablation further indicates that the substrate was not damaged during cleaning (Fig. 8). The absorbance corresponding to the polychrome do not change significantly in the cleaned spectrum as seen in the hydrocarbon peaks, hydroxyl band, and peaks related to carbonyl stretching at 1730, 1648, and 1101 cm^{-1}. (Gypsum being a relatively minor contaminant, the loss of sulfate is hardly noticeable here.) However, the XRF data (Fig. 9) clearly reveal the difference between the un-cleaned and cleaned surfaces. In the spectrum from the un-cleaned sample, aluminum and silicon are the most abundant elements besides calcium, oxygen, and carbon. This is due to the presence of aluminosilicates, which do not produce prominent absorptions in the mid IR. The XRF spectrum of the cleaned surface shows a dominant lead peak while the levels of aluminum and silicon are relatively insignificant, indicating that the contaminating aluminosilicates (essentially dirt) has been removed, leaving the lead white ($PbCO_3$) paint exposed.

Example (4), the French limestone **Head of an Apostle** ($14'' \times 8'' \times 9''$), required the removal of black and tan encrustation embedded in the paint matrix The sample area to be ablated was moistened with 5% ammonium hydroxide, and the *Conservator 2940* laser was set to 13 mJ/pulse and 15 Hz repetition rate, with the pulse focused at 1 mm diameter. Samples were ablated onto CaF_2 and BaF_2 plates. These samples were taken from areas on the neck and the cheek. Figure 10 shows the FTIR transmission spectrum of the ablated material. Hydrocarbon peaks at 2915 and 2848 cm^{-1}, which are seen in many spectra of ablated material, are seen here as well; however, the relative peak heights were much higher in this case. The strongest absorbance is at 1620 cm^{-1} with other weaker peaks at 1317, 1160, and 1091 cm^{-1}.

A comparison of the FTIR ATR spectra from samples taken before and after ablation Fig. 11 shows several changes after laser cleaning. The peak seen at 1541 cm^{-1} in the spectrum of the material from the un-cleaned surface is not seen in the spectrum of the cleaned surface. Also, the hydrocarbon peaks at 2919 and 2857 cm^{-1} are both diminished. A peak at 1236 cm^{-1} is also reduced in the spectrum from surface exposed to laser radiation. The large C-O peak at 1398 cm^{-1} has shifted to 1415 cm^{-1}. This peak is also diminished, allowing the shoulder at 1317 cm^{-1} to become a well-resolved peak.

The data from the **Head of Apostle** demonstrate the Er:YAG laser's ability to selectively remove certain layers. When a trained conservator

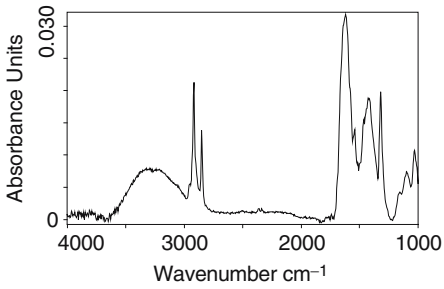

Fig. 10. FTIR transmission spectrum of material ablated from Head of Apostle

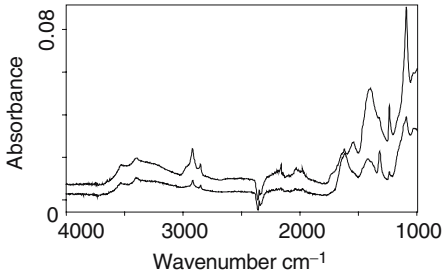

Fig. 11. FTIR ATR spectra of small piece taken from Head of Apostle before (*top*) and after laser ablation

controls the laser, the contaminants can be removed one layer at a time leaving the original color surface unaltered. The relatively strong hydrocarbon peaks in the spectrum of the ablated material (Fig. 10) indicate that the discolored layer has been removed from the surface. These bands, in addition to those at 1651, 1541, 1419, and 1236 cm^{-1}, are consistent with a layer of egg emulsion applied over the color surface. The discoloration of this layer accounts for the degradation of the appearance of the piece. Such layers, embedded in the paint matrix are impossible to remove with solvents. In addition, the peaks at 1620 and 1160 cm^{-1} indicate that gypsum was also removed, and the peaks at 1317 and 1091 cm^{-1} are consistent with whewellite, which can form as the result of pigment degradation. The FTIR ATR spectra also are consistent with the removal of gypsum and egg, as seen in the reduction of peaks at 1620 and 1160 cm^{-1} and 2916, 2849, 1541 and 1236 cm^{-1}. However, the characteristic whewellite peak at 1317 cm^{-1} is not reduced. This may be explained by reasoning that the whewellite is related to the pigment and would not be totally removed without removing pigment as well.

4 Summary

Surface ablation at 2.94 µm using the Er:YAG laser relies on the strong absorption of OH bonds in absorbing surface water and in other liquids adherent to the surface, which results in superficial heating. [4, 6]. When surface moisture is rapidly heated by laser exposure, a phase transition of water to steam occurs. The expansion of the steam, in effectively micro-explosions, breaks up surface encrustations into small particles in a process closely related to the traditional method of steam distillation – but on a micro scale. The ablated material is near the phase transition temperature (100°C for water), which initiates little or no chemical activity. The ablation leaves little heat behind to affect the material of the surface [5]. For example, dampening calcite (Example 1) allowed the thinnest possible surface layer to be ablated. Because the laser energy is almost completely dissipated in changing the water into steam, further heating is prevented, and the ablation is confined at the surface. The effects of laser ablation on organic materials and chloride salt present in lichen (Example 2) efficiently removed the contaminated materials from the stone even where it had invaded the stone surface. In (Example 3), laser ablation was effective in removing sulfate and chloride salt from the delicate paint layer, which is composed of lead-based pigment in an organic medium. No alteration of the paint layer occurred. A discolored layer of egg embedded in the color surface (Example 4) was removed from the color layer without ablating pigment or causing chemical or physical alteration to the paint.

5 Conclusions

The results presented here have demonstrated that the Er:YAG laser at 2.94 µm can efficiently remove both organic and inorganic materials from polychrome and patina stone sculptures without causing chemical or physical changes to the sculpture surface. FTIR spectra of ablated materials and of samples excised from the surface before and after laser ablation, combined with XRF spectroscopy of the same materials, provide convincing evidence of the nature of the ablated materials and of the mechanism of interaction between the laser and the contaminants. XRF is a good complement to FTIR spectroscopy in this case. Together, the two methods provide a more complete picture of the contaminants on the surface of the stone than either would alone.

Acknowledgements

This work has been supported by grants from The Mary Duke Biddle Foundation and The Ottmar Foundation. The authors thank Michael P. Mezzatesta, Director, and Sarah Schroth, Curator, Duke University Museum of Art, for

their knowledge and support in the conservation of the sculptures in the museum's collection. Thanks also to Susanne Hauger and Richard W. Levy for helpful suggestions and to Peter Ingram, for measuring the x-ray fluorescence spectra and for assistance in their interpretation.

References

1. P. Bracco, G. Lanterna, M. Matteini, K. Nakahara, O. Sartiani, A. deCruz, M. L. Wolbarsht, E. Adamkiewitz, and M. P. Colombini, "The Er:YAG laser. An innovative tool for controlled cleaning of old paintings: testing and evaluation," *Proceedings of LACONA IV*, Paris, September 11–14, (2001) 121–124
2. M. P. Colombini, A. Andreotti G. Lanterna, and M. Rizzi, "A novel approach for high selective microsampling of organic painting materials by Er:YAG laser ablation", *Journal of Cultural Heritage*, **3** Elsevier, Paris (2003)
3. A. deCruz, S. Hauger, and M. L. Wolbarsht, "The Role of Lasers in Fine Arts Conservation and Restoration", *Opt. Photon News*, **10** (1999) 36–40
4. A. deCruz, M. L. Wolbarsht, and S. A. Hauger, "Laser removal of contaminants from painted surfaces" *Journal of Cultural Heritage*, supplement 1-2000, Elsevier, Paris 2000.
5. M. Matteini, Giancarlo Lanterna, "Il Laser a Erbio per la pulitura dei dipinti: Verifiche tecniche e analitiche", *Kermes*, Ottobre-Decembre (2001) 55–61
6. M. L. Wolbarsht, A. deCruz, S.A. Hauger "Physics & chemistry of surface ablation by Er:YAG lasers", *Proceedings of LACONA IV*, "Lasers in the conservation of artworks", Paris, September 11–14 (2001) 117–120

Lasers Cleaning of Patrimonial Plasters

E. Tanguy[1], N. Huet[2], and A. Vinçotte[2]

[1] University of Nantes, LPIO, Faculté des Sciences et Techniques, 2, rue de la Houssinière, 44000 Nantes, France
eric.tanguy@physique.univ-nantes.fr
[2] Arc'Antique, 26, rue de la Haute Forêt, 44300 Nantes, France
arc.antique@wanadoo.fr

Abstract. The use of the lasers Q-switched Nd:YAG to remove the dust of the stone monuments especially sculpture gradually replaces the more abrasive technique of sandblasting. This tendency made us consider the lasers as solution for the cleaning of ceramics and the plasters. Indeed in museums, these materials are often covered with dirty mark (dust, grease, etc.) which is difficult to remove without damaging the object. This paper deals with the impact of different types of lasers (Nd:YAG first and third harmonic) irradiation on plaster and with the effects on its morphology and its crystallography. Plaster is an interesting material because of its typical acicular crystals altered at low temperature. That is why synthesis samples were prepared, constrained in temperature then analysed by various processes (SEM, XRD, TGA...). These results were compared with samples cleaned by laser. That enabled us to conclude that plasters cleaned by UV-laser (third harmonic of the Nd:YAG) underwent neither yellowing, nor morphological or crystallographic changes. It has to be opposed to the intense yellowing, and sometimes morphological destruction, which appears with an infrared wavelength (first harmonic of the Nd:YAG).

1 Introduction

Numerous plasters are found in museums (original sculptures, fine copies or simple casts). Plaster ends to get dirty very quickly what is due to its mineralogical and physical characteristics (dielectric constant...). Because of its natural fragility and sensitivity to moisture and physical actions, the removing of greasy dust is ordinary based on peeling methods or rubbing-out. Sometimes these traditional techniques turn out to be ineffective or damaging especially when fineness of details exclude physical operation or when the dust layers are too hard. In those cases, the use of lasers, already employed for stone [1], has then been considered.

2 Choice of the Wavelength

The first tests have shown that after cleaning with an infrared Nd:YAG laser an intense yellowing appeared (Fig. 1a) while the use of the third harmonic of the Nd:YAG laser permits to recover a surface colour close to the initial

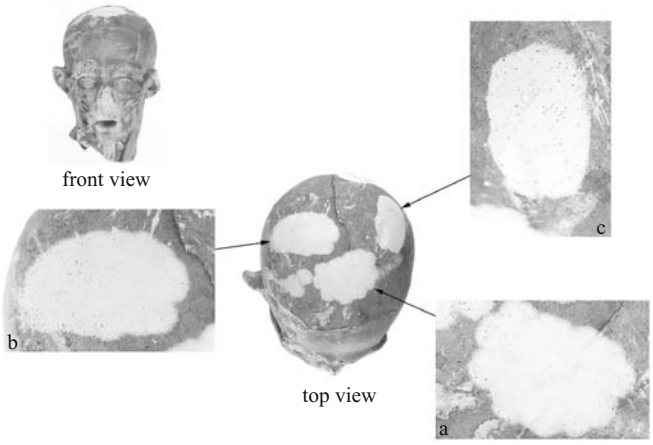

Fig. 1. Plaster écorché cleaned by Nd:YAG, (**a**) 1st harmonic, (**b**) 2nd harmonic, (**c**) 3rd harmonic

one (Fig. 1c). Nevertheless, this method seems to give out a too white surface (Fig. 1c) compared to the traditional methods of cleaning. The yellowing obtained following cleaning by the infra-red Nd:YAG laser [2, 3] is reversible by using the third harmonic of the Nd:YAG laser without apparent damage for the surface. The cleaning of the plaster by the third harmonic of the Nd:YAG laser gave very good results but we must check out that neither morphological nor crystallographic modification will occur. Therefore, we made some measurements on some plaster samples.

3 Preparation of the Samples

The diversity and the complexity of the plaster artworks and the dirty marks which cover them are not taken into account, the results obtained in this study will be only indicative. We chose a plaster of the Molda 3 type, typically used for moulding (impurity rate lower than 1%) and mixed the powder and water without any additive. However, it is common that the sculptors or the moulders complex this formulation (by addition of milk to improve texture, for example). The plaster was versed in metal moulds of approximately $20\,cm^3$. The samples were dried at 50°C, without causing any transformation of phase or fast desiccation [4].

All the analyses presented below are related to the face in contact with the air during drying. The gypsum crystals of this kind of surface are less organized there Fig. 2 than those on the faces in contact with the mould, where the phenomenon of growth is directed. Thus, the possible effects of the laser will be more easily observable and the damage on surface will be maximized.

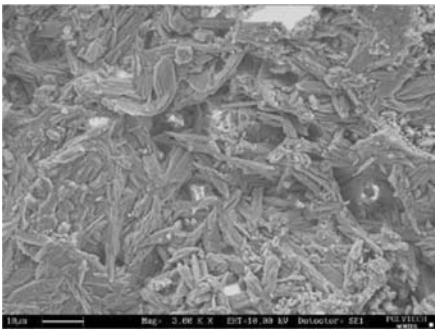

Fig. 2. Crystal morphology of the face in contact with the air

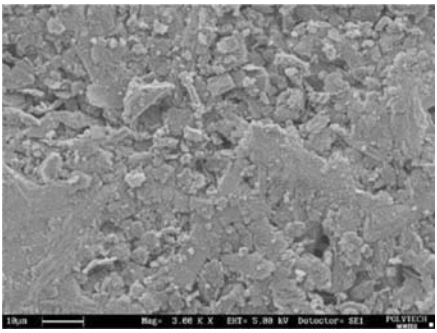

Fig. 3. Deposit of carbon graphit

A natural dust contamination would be too long and insufficiently reproducible. We thus chose a deposit of carbon graphite reduced to powder and applied to the brush (Fig. 3). This powder forms part of porosities and makes it possible to obtain a fine and homogeneous layer.

4 Treatment in Temperature

Laser ablation induced a fast but localized rise in temperature in the medium. However the modifications of phase of the plaster occur for temperatures ranging between 100°C and 1200°C Fig. 4. Plaster is an interesting material because of its typical acicular crystals ($CaSO_4.2H_2O$ β) altered at low temperature (120°C = $CaSO_4.0{,}5H_2O$ β) [4]. In order to detect possible modifications of phases of the plaster cleaned by laser, samples were first thermally treated, at various temperatures, then they were observed with the SEM and, eventually they were reduced to powder and analysed by x-rays diffraction (Fig. 5). These data will be employed as references and will be compared with the results obtained after the laser cleanings. The fine grains

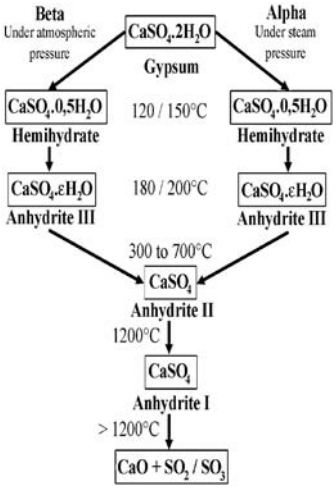

Fig. 4. Dehydration of the gypsum function of the temperature

observed at 300°C (Fig. 5) may be attributed to transformation of the sample to anhydrite.

5 Laser Cleaning

Because of problems of yellowing in the use of the fundamental wavelength of the Nd:YAG laser [2], we studied also the method of cleaning by the third harmonic of the Nd:YAG laser [3]. Each sample was dirtied and cleaned on half of its surface to preserve a part for comparison (Fig. 6). The energy used at the 1064 nm wavelength is 360 mJ (2.88 J/cm^2) and 90 mJ (0.72 J/cm^2) at the 355 nm (10 Hz).

Cleaned surfaces were compared with the samples treated in temperature using SEM and x-rays diffraction as shown in Fig. 7

According to this figure, the plaster cleaned by UV does not undergo any morpho-logical or crystallographic modification. Moreover, this method of cleaning by the third harmonic of the Nd:YAG laser shows clearly that the restored colour is the same one as the original colour. On the other hand, it is interesting to note that the surface cleaned by the fundamental wavelength of the Nd:YAG laser presents a morphological modification of its surface, that is due to a too significant abrasion and maybe the influence of the heat on the phase (Fig. 8).

The ablation thresholds of the dirt was estimated at 0.16 J/cm^2 for the UV and 0.23 J/cm^2 for IR. The alteration threshold of the plaster is around 1.41 J/cm^2 for IR. Following these experiments, tests were carried out on real works so as to validate these first results.

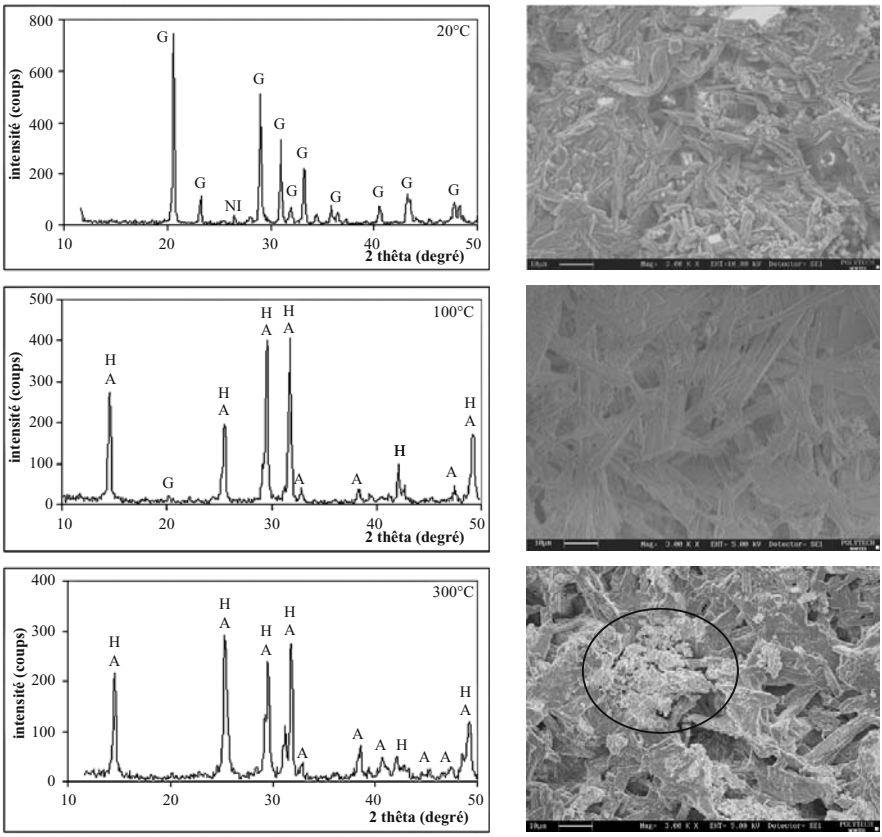

Fig. 5. Modification of the plaster phases versus temperature at 20, 100 and 300°C (DRX – SEM), G: gypsum, H: hemihydrate, A: anhydrite

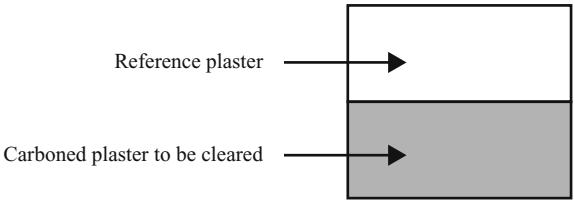

Fig. 6. Sample before cleaning

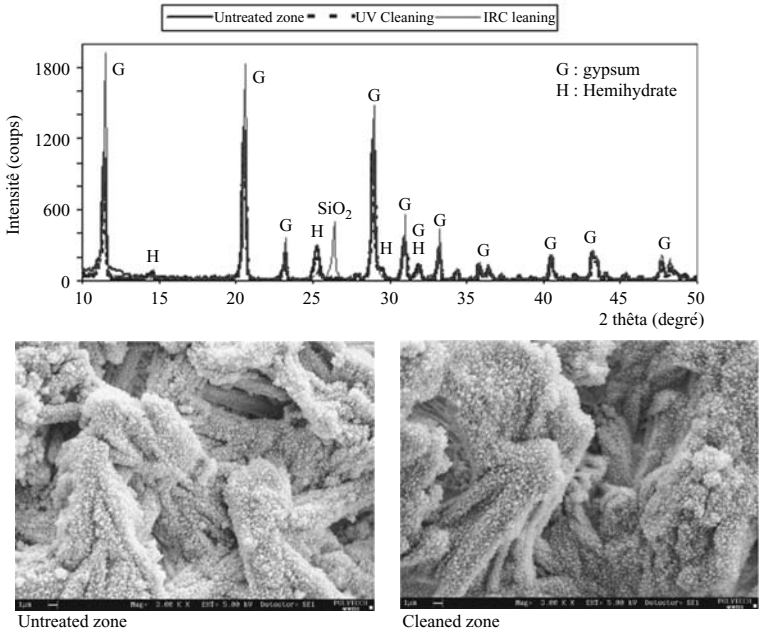

Fig. 7. Sample after and before cleaning with UV wavelength at 0.72 J/cm^2 (DRX – SEM)

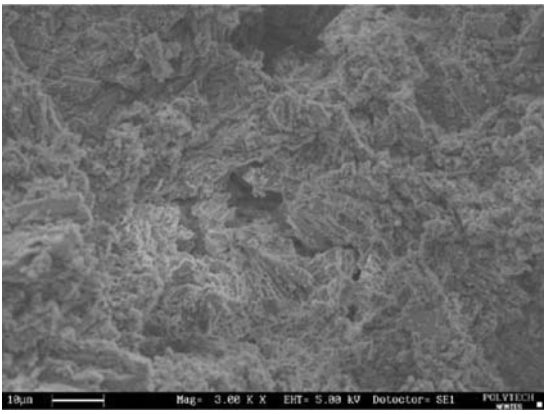

Fig. 8. Sample after cleaning with 1064 nm wavelength: fractionation of the crystals

As it can be seen in Fig. 9, an intense plasma is formed on the surface of the object under the impact of the laser beam.

As can be seen in Fig. 10, we cleaned part of a pieta using UV laser at 0.41 J/cm^2 with satisfactory results. Indeed, surfaces are perfectly cleaned

Fig. 9. plasma formed on the surface

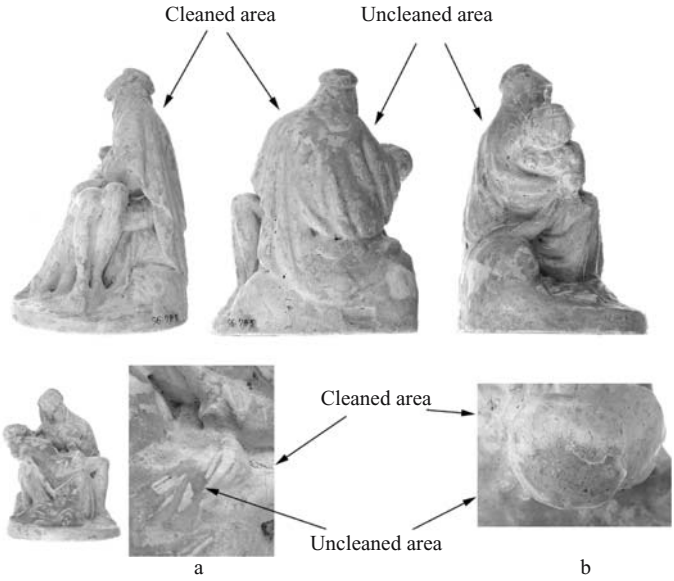

Fig. 10. Pieta partially cleaned by UV laser

and the fine structure of the moulding or the surface quality is still preserved, even the fragile white coating.

6 Conclusion

The cleaning of the plaster using the third harmonic of Nd:YAG laser modifies neither the colour, neither the crystallo-graphic structure nor the phase

of material. This technique appears as an interesting alter-native to the traditional methods of cleaning of the plasters as well for ceramics.

The researches have to be continued on a variety of historical plasters as well as on comparisons with the traditional methods of cleaning and their potential damages on morphological structure of the material.

References

1. M. Cooper, *Laser cleaning in conservation, an introduction*, Butterworth Heinmann Ed., Oxford, 1998
2. V. Zafiropulos and al., Yellowing effect and discoloration of pigments: experimental and theoretical studies, in *Journal of Cultural Heritage*, Vol. 4, pp 249–256, 2003
3. G. Marakis and al., Comparative study on the application of the 1st and the 3rd harmonic of a Q-switched Nd:YAG laser system to clean black encrustation on marble, in *Journal of Cultural Heritage*, Vol. 4, pp 83–91, 2003
4. C. Collot, Connaissance du plâtre, in *ABC mines*, Bull. 19, pp 35–44, Juillet 2001

Overpaint Removal on a Gilded Wooden Bas-Relief Using a Nd:YAG Laser at 1.064 µm

M. Strzelec[1], J. Marczak[1], A. Koss[2], and R. Szambelan[2]

[1] Institute of Optoelectronics, Military University of Technology, 2 Kaliskiego Street, 00-908 Warsaw, Poland
mstrzelec@wat.edu.pl

[2] Inter-Academy Institute for Conservation and Restoration of Works of Art, Academy of Fine Arts, 37 Wybrzeze Kosciuszkowskie, 00-379 Warsaw, Poland
raphael@wp.pl

Abstract. The paper presents the work on laser renovation of wooden bas-relief (lime tree), consisting of three figures: Saint Anna and Mary with Jesus, made by unknown artist at the beginning of XVII century. Almost whole relief surface is covered by gilding placed on a special preparation (bolus alba) with binding media. The painting layers cover only the parts of complexion and hairs of figures. The application of a 1.064 µm, Q-switched, Nd:YAG laser, allowed to unveil, in a short time the intact substrate of the object with well preserved gilding remains.

1 Introduction

Polychromes on wood are amongst the most important artistic European expressions from the XV century onwards [1–5]. The paper presents the work on laser cleaning of wooden bas-relief (lime tree), consisting of three figures: Saint Anna and Mary with Jesus, made by unknown artist at the beginning of XVII century. Almost the whole relief surface is covered by a gilding placed on a special preparation (bolus alba) with binding media. The painting layers cover only the parts of the central area and hairs of figures. The substantial part of relief was coated by a dark layer of secondary painting, which was an old attempt of reconstruction of primary gilt. It was not possible to remove this dark layer with the careful use of different solvents. Moreover, such tests led to uncontrolled extraction of gilding remains, still existing under the covering dark encrustation.

2 Description of the Object

The bas-relief presenting Saint Anna is the property of Diocese Museum in Sandomierz, Poland. Probably, the object is a part of an altar from parish church in Nieznamierowice, Masovian Province (I-st decade of the XVII'th century). The iconographic type of the saint Anna relief is the composition of three figures: Saint Anna, Mary and Jesus (Fig. 1). The relief has a rectangular shape of height – 120 cm, width – 73.5 cm, ended at the top with

Fig. 1. Bas relief of Saint Anna before the restoration

semicircle (diameter slightly smaller than rectangular width). The central figure is naked Jesus – sculpture surrounded by other figures. At the left side we can find Saint Anna and at the right side – Maria. The latter figures are sitting on the bench, which is covered with a cushion. Representing of the Holy Spirit dove is placed above Jesus head and higher we can see the figure of the God the Father. The figures form two iconographic groups: horizontal with Saint Anna and vertical with figures of the Holy Trinity.

The canopy with fancy arranged curtains forms a background of the scene. Below the canopy we can see an angel head with opened wings. The composition illustrates the dual lineage of Christ – iconography of three figures (Saint Anna) and heavenly (Holy Trinity).

The wooden substrate (lime wood) is covered with a priming ground consisting of mixed chalk/glue deposition. The partially destroyed gilding is placed on almost the whole relief surface on a special preparation (bolus alba) with binding media [6]. Painting layers cover only the complexion and hair of figures. Some parts of bas-relief: background, curtains fragments, angel wings, scarf of Saint Anna, book, dove, cushion and floor are covered with dark secondary layer. Detailed inspection detected gold foil below the layer, which can be a darkening old attempt to the former reconstruction of the original gilt. Investigations do not exclude that losses of gold gilding were in the past filled up with silver flakes and covered with varnish, which was a kind of gold imitation. The influence of hydrogen sulfide from the surrounding

Table 1. Gilding layer (stratigraphic analysis from the top of layers)

Sample Number	Place	Dimensions (Thickness)	Visual Description	Identification
13	Courtain (gold part, right side)	C = 0.005 mm B = 0.03–0.05 mm, A = 0.8–2 mm	C – thin gold thread, B – thin mould-orange layer, A – white layer with nonhomogeneus structure including translucent crystals	C – gold foil, B – pulment (ferric compounds), A – priming ground (chalk)
14	Maria's dress	C, B – 0.02 mm, A – 0.3 mm	As above	As above
15	Upper horizontal part of canopy	D, C – 0.005 mm, B – 0.01 mm, A – 0.2–1.5 mm	D – thin dark layer, C – thin gold thread, B – mould-orange layer, A – as above	D – dirty layer, B – pulment (as above), A – as above
16	Ball in the hand of Child	C – 0.005 mm, B – 0.02 mm, A – 0.3 mm.	C – thin gold thread, B – thin mould-orange layer, A – as above	As above

air caused formation of dark sulfides. The stratygraphic analysis of selected parts of object are illustrated in the Table 1 and Fig. 2.

3 Results of Laser Cleaning

The main problem during the conservation of the presented wooden art object was connected with the selection of the appropriate technology of removing the dark layer described above. Initial trails of careful removal using organic solvents was not successful. The layer was resistant to several solvents used, often removing laying below gold remains, which should be saved. Moreover, the infringement of thin layer of primary ground has been observed during mechanical cleaning (Fig. 3).

Much better results have been obtained during preliminary trials of laser cleaning. Utilization of Nd:YAG, Q-switched laser Model RENOVALaser1 [7] with carefully selected fluence allowed to remove the whole dark, secondary layer without destroying the primary ground (Fig. 3). RENOVALaser1 device is equipped with an optical fibre delivery system, which, in this case has been not equipped with optical focusing subassembly. It allowed the precise

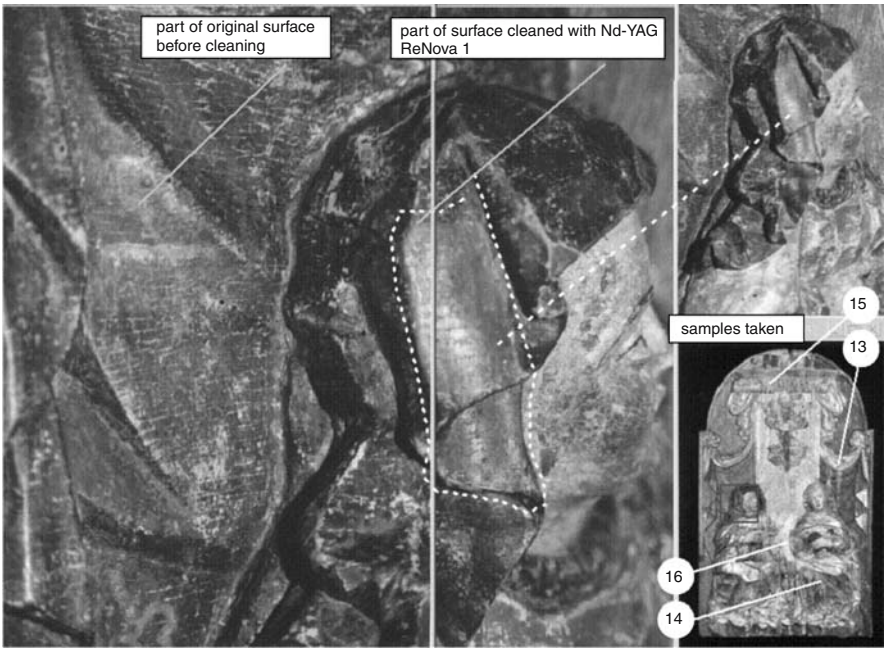

Fig. 2. Illustration of places of samples presented in Table 1

control of fluency depending on the distance of fiber to the object. No influence on "bolus alba" and golding has been observed. As it can be seen from Fig. 3, paint brush traces on primary ground (pulment) were also preserved. In several places, particularly inside hollows, the encrustation was thicker and more firmly joined with substrate. In each case, the controlled increase of laser fluence allowed to obtain the completely clean area. The illustration of the quality of laser renovation is shown in Fig. 4.

4 Conclusions

The use of laser for presented wooden bas-relief was the best and only one solution, characterized also by the smallest interference into the original object structure. The result, that could not be obtained using various solvents is now satisfactory. The additional advantages of laser cleaning are: the lack of hazardous chemicals during the process and the short time of renovation.

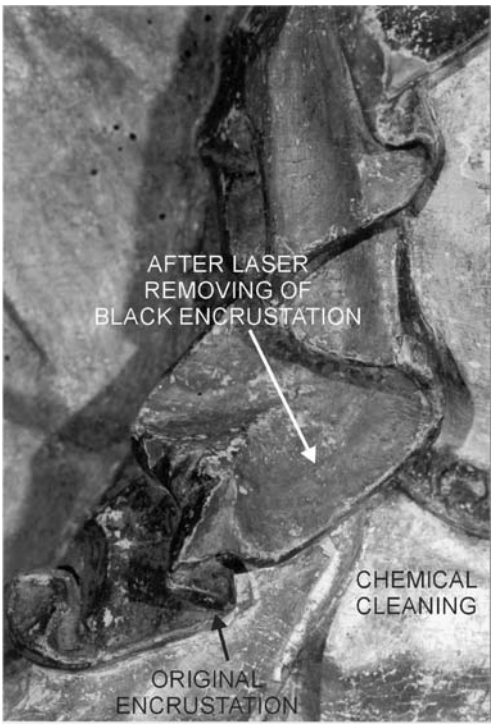

Fig. 3. Photograph shows the results of laser removing of dark encrustation (secondary painting layer) in comparison with parts cleaned with organic solvents

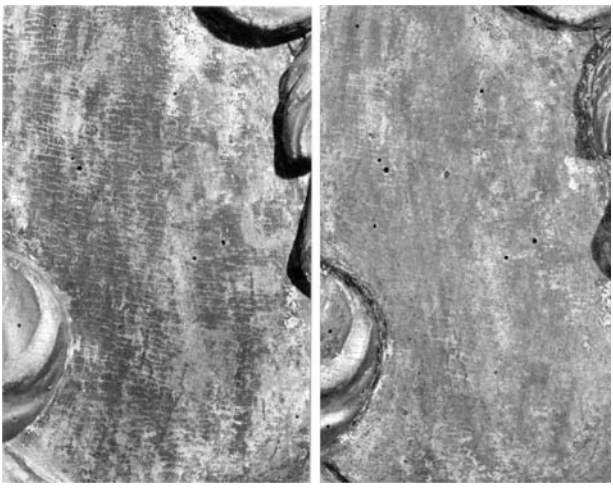

Fig. 4. Fragment of background (in magnification) above the *left* curtain; *left*: before cleaning; *right*: after laser cleaning. Paint brush traces can be seen

References

1. M. Castillejo et al., Journal of Molecular Structure, 550–551, (2000), 191–198
2. G. Calcagno and A. Bristol "Laser beam cleaning of decorated plaster surfaces of the monumental XVIth century staircase of the Grimani Palace in Venice, Italy, Proceedings of LACONA IVth Conference in Paris, 11–14 September 2001, p 229
3. M. Matteini et al., "Laser and chemical cleaning tests for the conservation of the "Porta del Paradiso", ibidem, p 77
4. H. Wust et al., "The potential of laser application for selective cleaning and removal of different layers on wooden artifacts", LACONA V, abstracts, p 45 (in print)
5. K. Melsessanaki et al., "The role of varnish in the stratograpic analysis..." ibidem p 204
6. "Bolus alba" – a kind of pulment (bole) under the gold plates, consisting of natural bolus clay, different glues and additives: oils, wax. The colour of pulment depends on the contamination of metal oxides. It can be yellow, white (bolus alba), brown and black
7. J. Marczak et al., Denkmal 2002 – Einsatz neuer Technologien für die Restaurierung und Diagnose der Kunstwerke, 30. Oktober bis 02. November, Leipzig, Germany

Pulsed Laser Cleaned Natural History Specimens with Reference to the Removal of Conductive Coatings

L. Cornish[1], G. Miller[1], and C. Jones[2]

[1] Department of Palaeontology, The Natural History Museum, Cromwell Road, South Kensington SW7 5DB United Kingdom
lpc@nhm.ac.uk
[2] Department of Mineralogy, The Natural History Museum, Cromwell Road, South Kensington SW7 5DB United Kingdom
cgj@nhm.ac.uk

Abstract. A low power dual-wavelength Q-switched Nd:YAG pulsed laser has been used to clean the surfaces of microfossil specimens from the collections of the Natural History Museum, London. A Q-switched laser is found to be very effective for cleaning surface coatings of fossil material. These coatings are traditionally very difficult to remove. The short pulse length ensures there is no or very little temperature rise in the underlying surface.

1 Introduction

Many specimens for which scanning electron microscopy (SEM) is invaluable are electrical insulators, for example microfossils. To promote the emission of secondary electrons, and to prevent charging of the surface it is usual to coat such specimens with a thin layer of metal. Coatings such as gold (most commonly used), gold palladium, carbon and aluminium are used. These coatings are normally applied by sputtering in a glow discharge, for this technique is omni-directional and tends to give a fine-grained deposit, whilst the apparatus required is comparatively simple and inexpensive since a high vacuum is not required. Problems arise when it is desired to return a specimen to its original uncoated condition, for example to allow successive treatments or because too thick a coating has been accidentally applied. Even samples which have been correctly coated may be rendered unsuitable for subsequent optical and analytical examination, due to the highly reflective nature of the gold film and its interference X-ray emission. Scientific information about the specimens can also be lost as traces of internal structures and colours are obscured by coatings. For these reasons there is frequently a reluctance to allow SEM examination of certain material, e.g. type specimens unless a Variable Pressure SEM is available.

2 Removal of Gold Coatings

Attempts have therefore been made to remove the metal film by suitable reagents, which must obviously not attack the substrate. Gold is recovered from specimens with aqueous sodium cyanide. A major obstacle is the highly toxic nature of cyanides, necessitating rigorous Health and Safety measures and a high degree of supervision and control unwanted in most laboratories. Also specimens have occasionally disintegrated. Mercury amalgamates gold, but does not remove it completely and adds its own background. The second most common coating, gold palladium, looks similar to gold coatings on specimens but cannot be reliably removed using the sodium cyanide method. Specimens in museums and research collections often do not have accurate records of which type of coating has been used, particularly if the coatings were applied before the specimens were donated. Safer and potentially less destructive methods are therefore needed to remove coatings from these types of specimens. Gold coatings have been removed by laser from a small shrew's jaw coated for SEM study [1]. The same technique is employed here on coated micropalaeontological specimens to test the suitability of this method.

3 Experimental Methods

The following micropalaeontological specimens were chosen as a pilot study

- *Annectina biedai* Agglutinating foraminifera. Eocene. From BP Borehole FA 6-2 Fortes Field North Sea. A siliceous microfossil with a rough, grainy surface texture.
- *Elphidium* sp., From recent beach sand Dogs Bay. Ireland. Microcrystalline Calcite.

Each microfossil was adhered onto a single one cm diameter aluminium stub. Specimens were then coated with a 20 micron layer of gold palladium using a sputter coater and photographed in the SEM. Previous work on the shrew jaw material had shown us that a single pulse of infra red wavelength (1064 nm) at a fluence of $0.5\,\mathrm{J/cm^2}$ was enough to successfully remove gold from the fossil surface. The above samples were cleaned at the same wavelength with a reduced fluence of $0.3\,\mathrm{J/cm^2}$as the surfaces were more fragile. Repetition rate was set as low as the machine would allow. Each specimen was cleaned with one laser pulse. Specimens were then re-photographed in the Variable Pressure SEM and the same selected area investigated to check for signs of damage to the specimens.

4 Results and Conclusions

The results are promising and can be seen in Figs. 1–2. The coating has been completely removed and the structure of the microfossil remains intact. Current work includes testing of a larger selection of microfossils with differing composition and structure. Different adhesives are also being evaluated for their response to the laser beam.

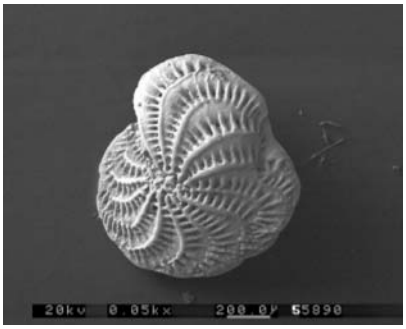

Fig. 1. *Elphidium* sp coated prior to laser cleaning

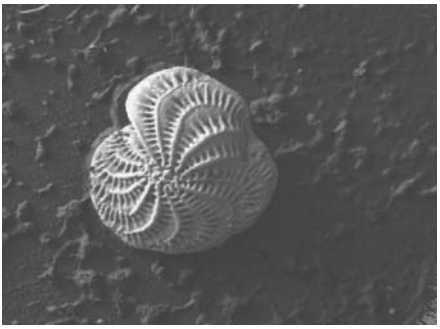

Fig. 2. After laser cleaning

5 The London Consortium of Laser Users

In 1999 a joint research equipment initiative was set up between The Natural History Museum, Imperial College of Science, Technology and Medicine, The Victoria and Albert Museum, The Royal College of Art and the Tate Gallery. A grant was awarded in March 2000 through the Engineering and Physical

Sciences Research Council which enabled the purchase of a Dual wavelength laser cleaning system. The participating institutions share time on the laser and a Laser Users group has been set up locally to share results. The focus of the group is the practical applications of laser cleaning to museum objects combined with studies of damage thresholds during cleaning procedures. Materials tested by the group include marble, terracotta, stone, plastic, metal, glass, paintings and geological material.

Reference

1. L. Cornish and C. Jones, In *Conservation Science 2002*. Edited by J. Townsend, K. Eremin & A. Adriaens, Archetype 101–106

Laser Cleaning Studies of Hard Insoluble Aluminosilicate Crusts on Minoan (LM IIIC) Pottery

S. Chlouveraki[1], P. Pouli[2], K. Melessanaki[2], K. Zervaki[1], and M. Yiannakaki[1]

[1] Institute for Aegean Prehistory – Study Center for East Crete (INSTAP-SCEC), Pachia Ammos, 72 200, Crete, Greece
stefie@instapec.gr

[2] Foundation for Research and Technology-Hellas (FORTH), Institute of Electronic Structure and Laser (IESL), Heraklion, PO Box 1527, 71110, Crete, Greece

Abstract. The main objective of this study is to investigate the feasibility of laser cleaning methodologies for the removal of insoluble aluminosilicate crusts from ceramic surfaces excavated from Late Minoan IIIC sites in eastern Crete. Laser cleaning tests involved the use of various laser systems with different wavelengths (1064 and 355 nm), pulse duration (7 ns and 120 µm), energy density values (0.3 to 1.6 J/cm^2) and cleaning methodologies (e.g. combination of wavelengths, water assisted laser cleaning etc.). The results from the laser-cleaning methodologies employed were evaluated and compared against those obtained from application of mechanical and of chemical means for encrustation removal.

1 Introduction

The recent Greek-American and American Excavations on East Crete have brought to light three sites, Chrysokamino, Halasmenos, and Azoria dating from Late Minoan to Early Archaic periods. A common feature to all these sites is the hard and thick encrustation that covers the ceramics. Cleaning such pottery is the most difficult and time consuming stage of the conservation process, as the encrustations are often thick, strongly adhered to the ceramic surface and harder than the ceramic itself. The conventional methods of cleaning, chemical or mechanical, are usually not very effective or require long time and hard effort. Chemical cleaning, by means of hydrochloric or nitric acid solutions, has in most cases failed. Mechanical cleaning with scalpel under the microscope requires a very long time and careful control in order to preserve technological information such as fine wheel marks and finger prints as well as painted and incised decoration that may exist on the underlying surface. The result is not always the desired one as the removal of the encrustation often results in loss of surface slip or painted decoration that remains attached on mechanically removed flakes. Decorated surfaces bearing thin and fragile layers of paint present a challenge to the conservator. Thus, the

problems associated with conventional cleaning methods are often difficult or impossible to overcome.

2 Experimental Methods

2.1 Characterization of the Encrustations

Encrustations were studied by means of macroscopic and microscopic observation, Laser Induced Breakdown Spectroscopy (LIBS) and X-Ray Diffraction (XRD). According to their macroscopic characteristics they were classified in three categories:

a. thick crusts, loosely attached to the surface
b. thick crusts, strongly attached to the surface
c. thin strong crusts, attached to the surface

XRD and LIBS analysis showed that all three types of crust consist of aluminosilicate minerals cemented in a siliceous matrix. This is insoluble in the chemical cleaning agents used for the conservation of ceramics.

2.2 Cleaning Tests

Considering the increasing amounts of pottery that is excavated and the difficulties in cleaning the edges and the surfaces of pottery, series of cleaning studies were carried out on various fragments of ritual objects such as goddesses with upraised arms, snake tubes and pinax fragments from the recently excavated shrine of Halasmenos [4]. Conventional cleaning tests were carried out at the W.D.E. Coulson Conservation Laboratory of the INSTAP Study Centre for East Crete that hosts the material [5], while laser cleaning tests were performed at FORTH-IESL (Table 1).

Conventional cleaning tests included chemical and mechanical methods or combinations. Various methods such as scalpel, tape and PVA peels and poultices were effective on encrustations crusts of Type a and c while they had very little effect on Type b. Laser cleaning was tested mainly on crusts of Type b for cleaning and on Type a and c for finishing surfaces that had been roughly cleaned with one of the above mentioned methods.

Laser cleaning tests were implemented with a) Q-switched pulses (7 ns) from a Nd:YAG laser, both at its fundamental frequency (1064 nm) and its third harmonic (355 nm), for the tests in Table 1, [BMI 5022 DNS10 series Nd:YAG laser system]. b) Long Nd:YAG pulses (120 μs) at 1064 nm, for the tests of Table 2 [EOS 2000 El.En. laser system].

Laser cleaning tests were performed directly on encrustations and on areas previously cleaned by mechanical means (scalpel), in both dry and wet conditions. The individual action of infrared (Infrared Tests 1-10, 13) and

Table 1. Specifications of cleaning tests with Q-switched Nd:YAG Laser

Q-switched Nd: YAG Laser Cleaning Tests at 1064 nm (IR)							
Test Window	Fluence (Jcm^{-2})	Pulses	Water	On Crust	Scalpel Cleaned	Discoloration	Result
1	1.6	10	-	x	-	-	-
2	1.6	20	-	x	-	-	-
3	1.6	10	-	-	x	x	x
4	1.6	20	-	-	x	xx	xx
4a	1.7	20	x	-	x	-	xx
5	1.6	20	x	x	-	x	-
6	1.6	40	x	x	-	-	x
7	1.6	20		-	x	xx	x
8	1.6	10	x	-	x	-	xx
9	1.6	20	x	x	-	-	–
10	1.6	20					–
	1.6	20					–
13	1.2	10	x	x	-	-	x
	1	10					
Q-switched Nd:YAG Laser Cleaning Tests at 355 nm (UV)							
Test Window	Fluence Jcm^{-2}	Pulses	Water	On Crust	Scalpel Cleaned	Discoloration	Result
11	0.6	20	-	-	x	x	xx
12	0.6	20	x	-	x	-	xx
15	0.4	70 (10 + 10 + 50)	x	x	-	-	x
17	0.4	35 (10 + 10 + 10 + 5)	x	-	x	-	xx
Q-switched Nd:YAG Laser Cleaning Tests at 1064 nm and 355 nm (IR + UV)							
Test Window	Fluence Jcm^{-2}	Pulses	Water	On Crust	Scalpel Cleaned	Discoloration	Result
14	1.2	0.4	20	-	x	-	x
16	1.6	0.4	60 (10p × 6) 10	x	x	-	–

ultraviolet (Ultraviolet Tests 11, 12, 15, 17) radiation has been considered as well as their combination (Infrared + Ultraviolet Test 14) and their complementarity (Ultraviolet to clean and Infrared to finish Test 16) (Table 1, Photo 1).

The above tests were performed on both smooth surfaces such as the interior or exterior surface of the ceramic as well as on the irregular surfaces of the sections along the breaks. The irregular broken surfaces require intensive and thorough cleaning in order to achieve good adhesion during mending,

Table 2. Specifications of cleaning tests with Long pulse Nd:YAG Laser

Q-switched Nd: YAG Laser Cleaning Tests at 1064 nm (IR)							
Test Window	Fluence Jcm^{-2}	Pulses	Water	On Crust	Scalpel Cleaned	Discoloration	Result
A	5	25		x	-	x	-
B	4	20 + w	x	x	-	x	-
C	6.8	(5p + w) × 5	x	x	-	xx	-
C	8.5	(2p + w) × 10	x	x	-	xx	-
D	8.5	(2p + w) × 10	x	x	-	xx	-
D	5	(2p + w) × 5					
E	8.5	(2p + w) × 10	xx	x	-	-	x
F	8.1	(2p + w) × 10	xx	x	-	-	x
G	8.5	(2p + w) × 10 (soak 3min)		x	-	-	xxx
H	5	(2p + w) × 10 (soak 3min)		x	-	-	xxx

while exterior surfaces require high precision cleaning in order to prevent loss of material and to preserve the decoration or technological characteristics of the surface.

3 Results and Discussion

Infrared cleaning at energy density values that lay beyond the ablation threshold for typical aluminosilicate crusts (1 to 1.6 J/cm^2) [3] were quite effective in removing the encrustation. On the other hand, Ultraviolet cleaning at energy density values that lay between 0.4 and 0.9 J/cm^2 [3] was not able to ablate the crust. It was effective however, in finishing surfaces that had already been cleaned with scalpel or tape peals.

Some discoloration occurred in both Ultraviolet and Infrared and especially where long pulses were applied. Test A (Table 2, Fig. 1) resulted in burning and discoloration of the encrustation which led us to apply water in the next steps. In Tests B and C the application of water with a brush, every 5 and 2 pulses, was not enough to prevent discoloration or burning on the crust while in D, where the testing was taken a little further the same problem occurred on the surface of the ceramic as well. Discoloration in Test D, as measured in Munsell Soil Color Charts, altered the color of the surface slip from very pale brown 10YR 7/4, towards light greenish grey GLEY2 10G 5/1. Discoloration was finally prevented by application of drops of water prior to irradiation (Tests E and F) or even more by soaking the area for a few minutes (Tests G and H). Cleaning was much more effective and fast on crusts that had been saturated with water.

In Tests 3, 4, 5, 7 (Table 1, Fig. 1) a slighter discoloration towards GLEY2 10G 7/1 occurred. Slight discoloration, towards GLEY1 N7, also occurred in

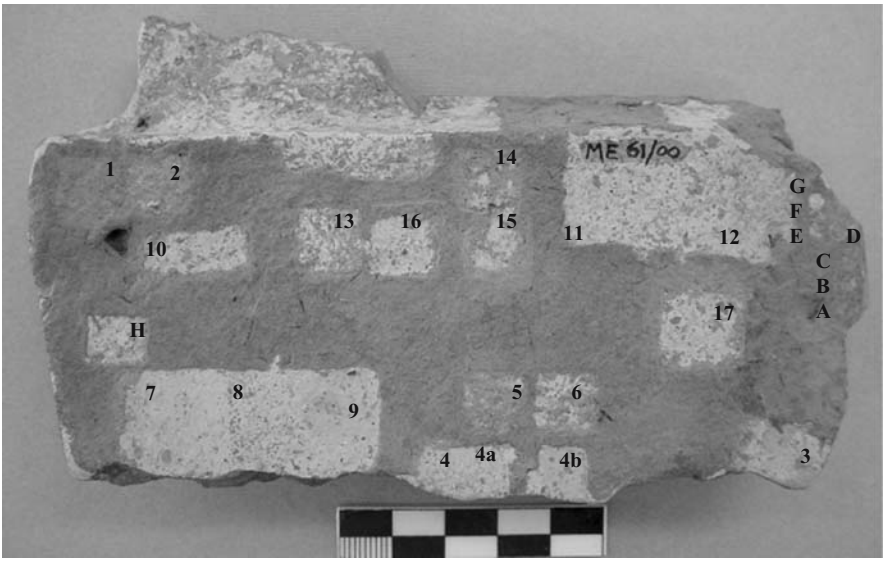

Fig. 1. Laser cleaning tests on the back side of a Pinax fragment from the LM IIIC Shrine of Halasmenos

test 11. We were able to overcome these side effects with the application of a thin film of water on the surface (i.e. 4a, 8, 12, 13, 16, 17). In most instances we were able to achieve the desired result with high precision without removing any of the yellowish slip of the surface. Moreover, the surface finishing tests, where the irradiation was applied on surfaces that had already been roughly cleaned, were especially successful.

4 Conclusions

Amongst the various laser cleaning systems that were used, it was possible to select the most effective ones and to schedule a series of new tests which will allow a further and more thorough analytical study. The most satisfying results were observed when long pulses of Nd:YAG radiation at 1064 nm were applied on surfaces that had been soaked in water for 3 min. Such pulses at energy fluence values that lay between 4 and 8 J/cm^2 and with soaking in water prior to cleaning or with the systematic application of water could remove successfully the thick crust without discoloration and/or non-homogeneities. The tests performed up to now showed that laser cleaning is much more qualitative and fast when combined with mechanical cleaning (elimination of the thickness of the crust with scalpels and/or peals). The desired degree of cleaning of the exterior surfaces varies according to the characteristics of the ceramic such as decoration, surface finish, patina, etc. The results of the

cleaning tests need to be further evaluated by analytical characterisation of both the encrustation and the laser treated surface, with various techniques such as SEM/EDAX, ICP/MS, PIXE. Procedures that require sampling and preparation of cross-sections of the cleaned/uncleaned surfaces, and therefore sampling permission must be obtained before we proceed to the next phase of this study.

References

1. S. Buys and V. Oakley, Conservation and Restoration of Ceramics, Butterworth Heinemann (1993) 84–98
2. Munsell Soil Color Charts, Munsell® Colors, Cretag Magbeth, New Windsor 1998 revised edition
3. P. Pouli, V. Zafiropulos, C. Balas, Y. Doganis, and A. Galanos, Laser cleaning of inorganic encrustation on excavated objects: evaluation of the cleaning result by means of multi-spectral imaging, *Journal of Cultural Heritage*, Vol 4, 338–342, 2003
4. M. Tsipopoulou, A new Late Minoan III shrine at Halasmenos – Ierapetra, in Potnia, edited by R Laffineur, W. D. Niemeier, D. Karageorgis, Université de Liége, University of Texas, 2001, pp 237–242 Papageorgakis
5. K. Zervaki and S. Chlouveraki, Cleaning methods for aluminosilicate encrustations on the ritual ceramic objects of the Late Minoan Shrine of Halasmenos, 9th International Congress on Cretan Studies, Elounda, 1–6 October 2001- (in press)

Laser Removal of Protective Treatments on Limestone

M. Gómez-Heras[1], E. Rebollar[2], M. Alvarez de Buergo[1], M. Oujja[2], R. Fort[1], and M. Castillejo[2]

[1] Institute of Economic Geology, CSIC-UCM, Facultad de Ciencias Geológicas, Universidad Complutense de Madrid, 28040 Madrid, Spain
[2] Institute of Physical Chemistry Rocasolano, CSIC, Serrano 119, 28006 Madrid, Spain
marta.castillejo@iqfr.csic.es

Abstract. This work presents an investigation of the laser removal of polymeric materials acting as consolidants and water-repellents on limestone used on buildings of architectural and artistic value. The removal of the consolidant Paraloid B-72 and the water-repellent product Tegosivin HL-100, applied on samples of *Colmenar*and *Bateig* limestone, was studied as a function of the laser wavelength, by using the four harmonics of a Q-switched Nd:YAG laser (1064, 532, 355 and 266 nm). Elimination of the coatings and subsequent surface modifications were monitored through colorimetry, roughness measurements and scanning electron microscopy (SEM). The fundamental laser radiation was effective in removing the treatments, although thermal alteration processes were induced on the calcite crystals of the limestone. The best results were obtained by irradiation in the near UV at 355 nm.

1 Introduction

Polymeric products are applied on stone materials used on buildings or sculptures of artistic value for consolidation purposes and to protect them from water intake [1, 2]. Elimination of these coatings is sometimes required when their efficiency has decreased, have caused deterioration (change of colour, flaking) or when another incompatible treatment has to be applied [3, 4]. Classical ways to remove protective treatments are based on the use of solvents, poulticing or mechanical methods. Although some treatments, especially those based on acrylic resins, have been considered to be reversible due to their solubility in certain solvents, the available removal techniques suffer from several drawbacks and new efficient removal methods are investigated [2, 5].

Laser techniques have gained acceptance as advanced tools to clean stone surfaces with applications including the removal of black encrustations, biological deposits or other contaminants from different types of stone [6–9]. Optimal laser cleaning operates by ablation of the external unwanted layers without deteriorating the underlying substrate. At the infrared wavelength of the laser radiation delivered by Q-switched Nd:YAG lasers, the ablation threshold fluence of the clean stone is higher than the threshold fluence of

black crusts. For practical cleaning, a fluence in the ablation threshold gap can be used (self-limiting effect). However, at shorter wavelengths in the UV-VIS range delivered by excimer lasers or the harmonics of the Nd:YAG laser, the self-limiting effect is not operative. Therefore, on-line diagnostic techniques, such as laser-induced breakdown spectroscopy (LIBS) or monitoring of the acoustic wave accompanying the ablation process, have to be coupled to the cleaning process for controlling laser damage of the substrate [10, 11].

In this work we investigate the suitability of laser irradiation to remove protective treatments used as consolidants and water-repellents applied on limestone, a material used extensively throughout Europe in the building of monuments. This follows a preliminary study [12] performed in a more limited set of stone samples.

2 Experimental Methods

This study was carried out on prismatic samples of two limestone varieties, *Colmenar* and *Bateig*. Petrophysical properties, measured following NORMAL guidelines and RILEM recommendations [13, 14] are listed in Table 1. *Bateig* limestone features a much higher porosity than *Colmenar*. The samples were impregnated by immersion into solutions of two protective polymeric products Paraloid B-72 and Tegosivin HL-100 described in Table 2. Typical measured thickness of coatings is 1.8 and 0.8 µm for PB-72 and HL-100 respectively. Uncoated reference samples were kept for comparison.

Table 1. Petrophysical properties of two types of limestone

	Colmenar	Bateig
Bulk density (g/cm^3)	2.59	2.13
Porosity accessible to water (%)	3.4	21.9
Water saturation(%)	1.3	10.3
Water absorption after 48 hours (%)	0.8	7.5
Porosity accessible to Hg (%)	3.6	15.9

Table 2. Protective stone treatments

Product/Solvent	Purpose Use	Composition
PB-72/Xylene	Consolidant and adhesive	Copolymer of methyl acrylate and ethyl methacrylate
HL-100/White Spirit	Water-repellent	Low molecular weight modified polysiloxane resin

The samples were irradiated with the fundamental wavelength of a Q-switched Nd:YAG laser (Quantel, Brilliant B, pulse duration 5 ns, 10 Hz) at 1064 nm and its harmonics at 532, 355 and 266 nm. The laser output was directed to the surface of the sample by the help of prisms. At each wavelength, the irradiation fluence was chosen below the corresponding previously determined stone ablation thresholds. Table 3 summarizes the threshold values and the irradiation conditions of the samples. It should be noticed that the ablation thresholds of the two coatings are above those of the bare stone [12].

Table 3. Ablation threshold fluences (J/cm^2) and irradiaton conditions of limestone samples and PB-72 coatings (number of pulses in parenthesis); (a) values from [12]

	266 nm	355 nm	532 nm	1064 nm
Uncoated *Colmenar*	0.4 (a)	0.9 (a)	1.7 (a)	3.0 (a)
Uncoated *Bateig*	–	0.7	–	–
PB-72	0.5 (a)	1.3 (a)	4.3 (a)	>8.3 (a)
Irradiation *Colmenar*	0.2 (1800)	0.4 (1800)	0.9 (1800)	2.3 (1800)
Irradiation *Bateig*	–	0.4 (600)	–	–

Changes induced by laser irradiation on the surface chromatic parameters (in the CIE $L^*a^*b^*$ system [15]) and on the yellowness index [16] were measured with a Minolta CM 2002 spectrocolorimeter. To assess morphological changes of the surface, the parameters R_a, arithmetic mean deviation of the roughness profile, and R_p or mean value of roughness depth, were evaluated by a roughness instrument (Surtest SJ-201, Mitutoyo). Scanning electron microscopy (SEM), performed with a JEOL JSM 6400 instrument on graphite sputtered samples, served to verify the degree of elimination of the treatments and the alterations induced on the stone substrate.

3 Results and Discussion

The removal of the treatments was found to be dependent on the laser irradiation conditions and on the characteristics of the coatings, including thickness. Table 4 lists the changes induced by laser irradiation on chromatic properties of limestone samples. Irradiation of the treated *Colmenar* stone at 1064 nm results in a global colour change, $\Delta E^* = (\Delta L^{*2} + \Delta a^{*2} + \Delta b^{*2})^{1/2}$, in relation to the uncoated stone, slightly higher than 3 units for both treatments. In the case of PB-72, this value is less than the global colour variation induced by application of the treatment ($\Delta E^* = 4.5$), indicating that the chromatic modifications are reverted by irradiating at this wavelength. For both PB-72 and HL-100, the conditions of the 355 nm irradiation are the most effective

Table 4. Changes in Yellowness Index (ΔYI) and global colour variation (ΔE^*) of *Colmenar* limestone. Data for *Bateig* samples are in parentheses. Values are related to uncoated (UC), non-irradiated (NI) stone

	NI		266 nm		355 nm		532 nm		1064 nm	
	ΔYI	ΔE^*	ΔYI	ΔE^*	ΔYI	ΔE^*	ΔYI	ΔE^*	ΔYI	ΔE^*
UC	–	–	−1.1	2.0	−2.9	1.8 (6.5)	−0.2	1.0	−4.6	6.3
PB-72	7.9	4.5	6.0	3.2	3.4	1.5 (8.4)	6.7	4.2	−4.7	3.2
HL-100	0.3	1.0	0.9	1.4	−2.3	1.6 (5.0)	−1.4	1.8	−3.1	3.5

in the recovery of the chromatic properties displayed by the bare *Colmenar* limestone. Irradiation at 355 nm caused more discoloration on coated *Bateig* than on the less porous *Colmenar* samples.

Application of protective products changes slightly the roughness of the surface, as represented in Fig. 1 This figure also shows the changes induced in the roughness by laser irradiation of the bare (uncoated) and treated stone. The modifications of roughness are considerable under irradiation at 1064 nm, whereas irradiation at the conditions of the shorter wavelengths induce lesser changes. Irradiation of samples coated with PB-72 at 532, 355 and 266 nm does not modify significatively the roughness, in comparison with the uncoated original stone, although these changes are slightly higher in the case of samples coated with HL-100.

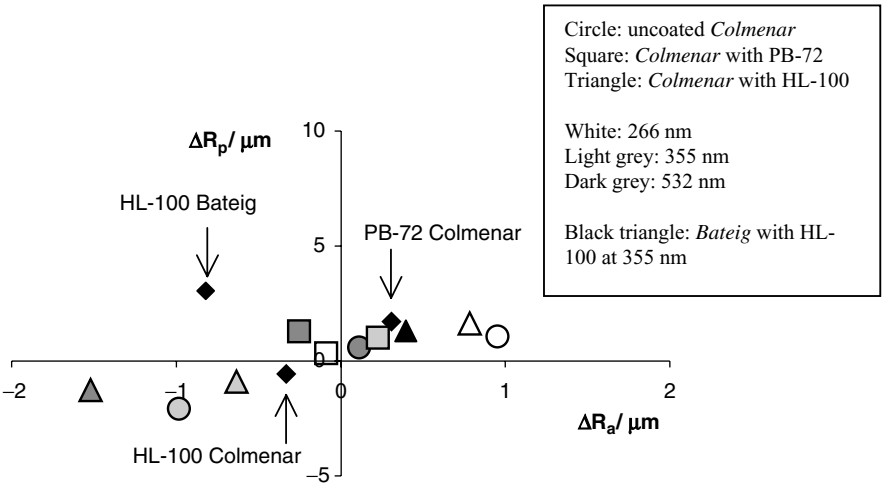

Fig. 1. Changes of R_a and R_p roughness parameters induced by laser irradiation of *Colmenar* and *Bateig* samples. The origin of coordinates represents the values of the uncoated, non-irradiated samples. Values for irradiation at 1064 nm are out of scale

SEM measurements give evidence of the laser removal of the treatments. As an example we show in Fig. 2 images of the surface of *Colmenar* and *Bateig* samples coated with PB-72 and exposed to various laser irradiation conditions. The fundamental radiation at 1064 nm is effective in removing the treatments but thermal alteration processes are induced on the constituent calcite crystals. This is shown in Fig. 2e where the originally sharp edges are softened as a consequence of melting. Irradiation in the UV at 266 and 355 nm is a clean etching process, leading to partial or to complete elimination of the coating. In samples coated with HL-100 similar results are obtained, although a more radical elimination of the protective layer has been observed. This suggests the dominance of ablative photodecomposition mechanisms involving bond breaking of polymer chain bonds [17] operating at these UV wavelengths.

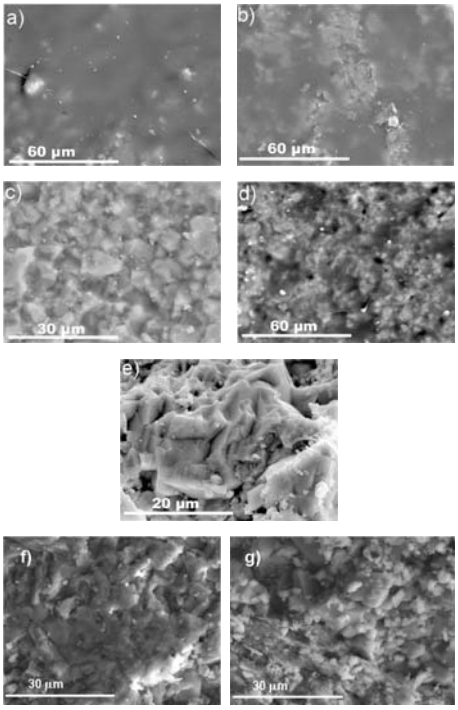

Fig. 2. SEM images of the surface of limestone samples coated with PB-72: (**a**) *Colmenar* non-irradiated, (**b**) to (**e**) *Colmenar* irradiated at 266, 355, 532 and 1064 nm respectively, (**f**) *Bateig* non-irradiated, (**g**) *Bateig* irradiated at 355 nm

4 Conclusions

In conclusion, laser removal of protective polymeric products applied on limestone, does not show a self-limiting effect at any of the four Nd:YAG wavelengths. Therefore, determination of safe conditions for treatment removal, ensuring no damage to the stone substrate, has to be performed through careful assessment of the laser irradiation effects. Laser removal of the coatings strongly depends on the type of product and on the stone variety. Protective coating layers with lower thickness, as those achieved by immersion of the stone into HL-100 solutions, are more effectively removed. On the other hand, we have noticed that laser irradiation causes stronger discoloration in coated *Bateig* than in *Colmenar* samples. The higher porosity of the former may have some influence, but the final reason for this effect is not clear.

We have found that at the intermediate wavelengths of this study, especially at 355 nm, the outer layer of coating is thinned down or even removed when using fluences below the ablation threshold and a high number of pulses. Colorimetric and roughness measurements demonstrate that laser irradiation under these conditions make the coated surface to recover the characteristic colour and roughness parameters of the bare stone, while SEM measurements indicate that thermal alteration of the constituent calcite crystals is the main consequence of damage to the underlying substrate. These results show the potential of the third harmonic of the Nd:YAG laser for the removal of protective stone coatings.

Acknowledgements

Support from Projects BQU2000-1163-C02-01 (*Spanish Ministry of Science and Technology*) and 06/0134/2003 (*Comunidad de Madrid*, CM) is gratefully acknowledged. Thanks are given to *Ministry of Education and Culture* (MGH), CM (MO) and *Spanish Thematic Network on Cultural Heritage* of CSIC (MA, ER) for fellowships. SEM measurements were carried out at *Centro de Microscopía Electrónica Luis Bru* (Universidad Complutense, Madrid).

References

1. H. R. Sasse and R. Snethlage, *Scien. Technol. Cult. Herit.* **5**, 85, 1996
2. M. Alvarez de Buergo and R. Fort, *Prog. Org. Coat.* **43**, 258, 2001
3. A. E. Charola, A. Tucci, and R. J. Koestler, *J. Am. Inst. Conser.* **25**, 83, 1986
4. D. Erhardt, *J. Am. Inst. Conser.* **22**, 100, 1983
5. B. Appelbaum, Criteria for treatment: reversibility, *J. Am. Inst. Conser.* **26**, 65, 1987
6. M. I. Cooper, Laser Cleaning in Conservation: An Introduction, Butterworth-Heinemann, Oxford, 1998
7. G. Lanterna, and M. Matteini, *J. Cult. Herit.* **1**, 529, 2000

8. A. Costela, I. García-Moreno, C. Gómez, O. Caballero, and R. Sastre, *Appl. Surf. Sci.* **207**, 86, 2003
9. S. Scheerer, M. Abraham, and O. Madden, *J. Cult. Herit.* **4**, 223s, 2003
10. I. Gobernado-Mitre, J. Medina, B. Calvo, A. C. Prieto, L. A. Leal, B. Pérez, F. Marcos, and A. M. De Frutos, *Appl. Surf. Sci.* **96–98**, 474, 1996
11. P. Maravelaki-Kalaitzaki, V. Zafiropulos, and C. Fotakis, *Appl. Surf. Sci.* **148,** 92, 1999
12. M. Gómez-Heras, M. Alvarez de Buergo, E. Rebollar, M. Oujja, M. Castillejo, and R. Fort, *Appl. Surf. Sci.* **219**, 290, 2003
13. Assorbimento d'acqua per capillarità -Coefficient di assorbimento capillare, I.C.R.-C.N.R. Doc. NORMAL 11/85, 1986; Permeabilità al vapor d'acqua, I.C.R.-C.N.R. Doc. NORMAL 21/85, 1986
14. RILEM, Commission 25-PEM (Protection et erosion des monuments), *Mater. and Struct.* **75**, 175, 1980
15. CIE, in Publication CIE n&ordm 15.2, Colorimetry, 2nd Edition, Central Bureau of the CIE, Vienna, 1986
16. ASTM E 313-00, "Standard Practice for Calculating Yellowness and Whiteness Indices from Instrumentally Measured Color Coordinates", ASTM International
17. R. Srinivasan, and B. Braren, *Chem. Rev.* **89**, 1303, 1989

Comparison of Cleaning Methods for Stained Glass Windows

H. Römich[1], P. Mottner[1], J. Hildenhagen[2], K. Dickmann[2], G. Hettinger[3], and F. Bornschein[4]

[1] Fraunhofer-Institut für Silicatforschung (ISC), Bronnbach 28, 97877 Wertheim, Germany
hannelore.roemich@isc.fraunhofer.de
[2] Laserzentrum Fachhochschule Münster (LFM), Stegerwaldstraße 39, 48565 Steinfurt, Germany
[3] Dombauverwaltung Köln (DBH), Roncalliplatz 2, 50667 Köln, Germany
[4] Dombauamt Erfurt, Domstufen 1, 99084 Erfurt, Germany

Abstract. Any cleaning process for stained glass windows has to consider the effectiveness of the treatment but also the potential damage for the art object. A variety of mechanical and chemical methods is currently used in restoration practice. The most effective ones are criticized because of their long-term risks. Therefore, an interdisciplinary research project, carried out in Germany and funded by the "Deutsche Bundesstiftung Umwelt (DBU)" had explored the possibilities and limits of lasers for cleaning glass windows. At previous LACONA conferences the Excimer Laser equipment and results from the research project have been presented. This contribution puts the cleaning experiments in a broader context, by comparing lasers with conventional techniques. Scientific and practical aspects will be discussed, focussing on the removal of crust and aged polymers.

1 Introduction

The aim of any cleaning procedure for stained glass windows is to regain their colourful transparency and to reduce further damage by surface deposits. Gypsum and syngenite or various carbonates are formed as corrosion products from the reaction of leached glass components with air pollutants. Due to re-crystallisation over time and the inclusion of dirt, these crusts may become very dense and well adhering to the glass surface. Other disfiguring surface deposits may be built by micro-organisms. In addition, the transparency of glass can be reduced by polymers, originally applied as surface coatings or paint consolidants, which can turn yellow or brown by natural ageing.

Any cleaning procedure for sensitive glasses should remove the deposits only as far as necessary to improve the transparency, without damaging the hydrated glass surface underneath. In the case of corrosion crusts, conservators intend to leave a thin residual layer on the surface, rather than removing the crust down to the bulk glass, which would initiate further degradation.

Special attention is necessary when cleaning painted areas, since the loss of paint would irreversibly damage the artistic integrity of the object.

2 Removal of Corrosion Crusts

For the ablation of powdery corrosion crusts, mainly mechanical methods are used in the workshops in Europe. Bristle brushes are the softest tools, whereas glass fibre brushes, scalpels and airbrasive techniques are bearing the risk to scratch the surface. Any mechanical damage on the surface will enhance further degradation [1].

Figure 1 shows the result of a cleaning test with bristle brushes on a model glass, on which a powdery corrosion crust has been simulated by accelerated ageing in a climate chamber [1]. The degree of cleaning has to be controlled by the operator, preferably under a microscope.

Fig. 1. Model glass with corrosion crust, partially cleaned with brushes (overview, transmitted light)

Within an interdisciplinary project a prototype laser cleaning station was constructed, especially for the treatment of stained glass panels [2–4]. An Excimer laser operating at 248 nm was selected as appropriate laser source. The energy density, the frequency (f) and the number of pulses (n) was modified to explore the ablation rate on model samples. Depending on the colour and the chemical composition of the crust and the glass, energy densities between 0.25 and 2.0 J/cm^2 were used. Since this covers the same range found as alteration threshold for the sensitive substrates, this process is not self-limiting and has to be carefully controlled under the microscope.

Figure 2 shows a model glass with different spots cleaned with laser: at 2.0 J/cm^2 (n = 100 pulses, f = 25 Hz) the crust is completely removed down to the bulk (bright spot on the left), whereas with 0.25 J/cm^2 (n = 100 pulses, f = 4 Hz), almost no cleaning effect is achieved (spot on the right). For this type of sample the most appropriate result was obtained at 1.25 J/cm^2 (n = 100 pulses, f = 10 Hz).

Medieval glass from Erfurt has developed an extremely dense encrustation during the centuries (Figs. 3 and 4). In this case all mechanical cleaning

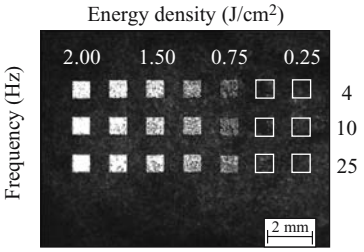

Fig. 2. Model glass with corrosion crust, partially cleaned with Excimer laser (detail, transmitted light)

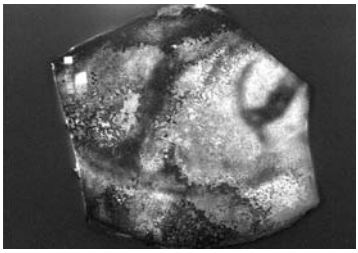

Fig. 3. Original glass from Erfurt cathedral with dense corrosion crust, cleaning experiment in the left corner (overview, transmitted light)

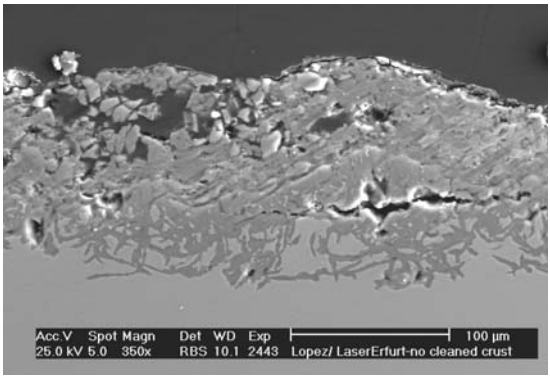

Fig. 4. Original glass from Erfurt, area with no cleaning (SEM of a cross section)

methods failed. Chemical agents, such as EDTA (ethylene diamino-tetra-acetic-acid or the corresponding salt) are highly effective, but may dissolve not only the calcium in the gypsum crust but also in the glass network, thus inducing further degradation. Cleaning pastes with ammonium carbonate as reactive agent are less dangerous and still effective (Fig. 5 [1]).

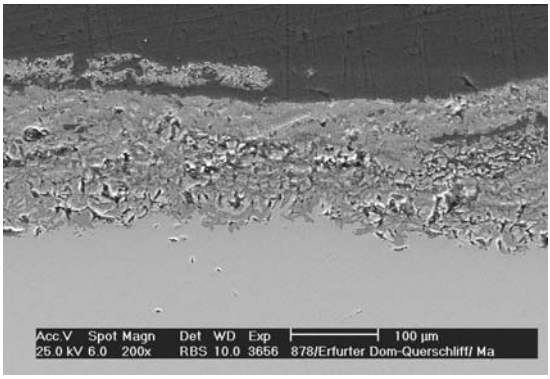

Fig. 5. Original glass from Erfurt cathedral, chemical cleaning (SEM of a cross section)

For this cleaning problem a laser treatment at $0.75\,\mathrm{J/cm^2}$ and 50 pulses has increased the transparency sufficiently, whereas an irradiation at $2.0\,\mathrm{J/cm^2}$ and 200 pulses has already produced irreversible damage (Fig. 6).

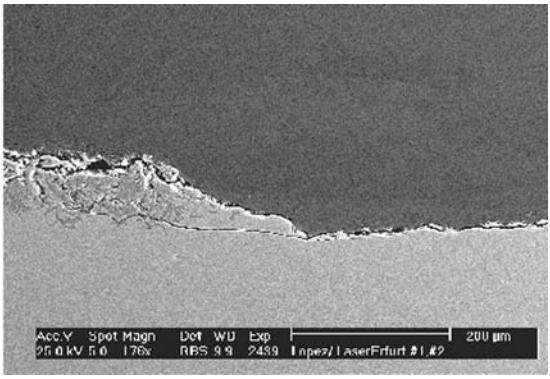

Fig. 6. Original glass from Erfurt cathedral, cleaning with laser: on the left with $0.75\,\mathrm{J/cm^2}$ and 50 pulses; on the right with $2.0\,\mathrm{J/cm^2}$ and 200 pulses (SEM of a cross section)

3 Removal of Aged Polymers

Mechanical methods can be applied only if the polymers are brittle or if they are waxy and thick and can be scraped away. Many polymers can be removed with organic solvents, even after a few years of weathering. Wax represents

one of the most difficult cleaning problems, since it has a low solubility at room temperature.

On model samples artificially aged wax has been successfully removed with the Excimer laser at $0.25\,J/cm^2$ and 100 pulses. On original glasses higher energy densities were necessary, for example around $1.0\,J/cm^2$ for epoxy resins. One of the problems encountered on originals was the laser ablation of dirt on the surface of the coating, since the grains have provoked irregular cleaning [2–4].

4 Risk Assessment

Mechanical methods are effective only for removal of porous deposits from the glass surface. They are easy to handle without costly equipment. More effective mechanical tools have to be controlled carefully by the operator, which requires skill and expertise. Scratches on sensitive glasses may enhance local degradation.

Chemical reagents can be controlled by adjusting the pH-value and by limiting the time of exposure. Nevertheless, the surface has to be kept wet for a few hours and the poultice has to be removed completely to avoid damage later-on. Liquids or pastes can not be limited to small sections within a glass segment.

Lasers may offer an alternative for severel cleaning problems. The main advantage is the limitation of the effect to a small spot. This is of special importance for stained glass, where no large uniform surfaces have to be treated, but only small areas, for which the degree of cleaning has to be adjusted. Since the energy density required for the removal of deposits may cause alterations on the sensitive surface, the process is not self-limited and requires careful control in a microscope or even better, with additional analytical methods (e.g. LIBS).

References

1. H. Römich, E. Jägers, M. Torge, W. Müller and K. Adam, Reinigung – eine Gradwanderung, in A. Wolff (ed.) "Restaurierung und Konservierung historischer Glasmalerei", Verlag Philipp von Zabern, Mainz (2000) 101–128
2. F. Fekrsanati, J. Hildenhagen, K. Dickmann, P. Mottner and U. Drewello, Feasibility studies on applying UV-lasers for the removal of superficial deposits from historic glass, Studies in Conservation 46 (2001) 196–210
3. H. Römich, K. Dickmann, P. Mottner, J. Hildenhagen and E. Müller, Laser cleaning of stained glass windows - final results of a research project, Journal of Cultural Heritage 4 (2003) 112–117
4. H. Römich (ed), *Reinigung von historischen Glasmalereien mit Lasertechnik,* Fraunhofer IRB Verlag, Stuttgart, (2000)

Results of Nd:YAG Laser Renovation of Decorative Ivory Jug

M. Strzelec[1], J. Marczak[1], R. Ostrowski[1], A. Koss[2], and R. Szambelan[2]

[1] Institute of Optoelectronics, Military University of Technology, 2 Kaliskiego Street, 00-908 Warsaw, Poland
mstrzelec@wat.edu.pl

[2] Inter-Academy Institute for Conservation and Restoration of Works of Art, Academy of Fine Arts, 37 Wybrzeze Kosciuszkowskie, 00-379 Warsaw, Poland
raphael@wp.pl

Abstract. The heterogeneity and hygroscopity of ivory excludes the utilization of aqueous solutions in its conservation. The acid, basic solutions and organic solvents are also not recommended. The paper presents the alternative, safe and efficient technique of laser renovation of ivory on the example of decorative jug.

1 Introduction

The characteristic difficulties connected with conventional cleaning of ivory result from its physical and chemical properties, particularly hygroscopity and anisotropy. Ivory consists of dentine surrounded by a cortex, which is a strong cement layer of $3 \div 4$ mm. Dentine contains around 60% of inorganic salts (calcium, magnesium phosphate, calcium carbonate, fluorides) and 40% of organic substances, mainly collagen, which is responsible for ivory elasticity. During the changes of temperature and humidity ivory expands and contracts which can cause its warping, torsional deflection and fracturing. These effects can also be found near contacts with other materials like wood and particularly metals. Moreover, temporal alterations of ivory substrate are connected with the lack of light and air (yellowing) as well as with air pollution (grayish encrustation).

2 Description of the Object

The ivory decorative jug, presented in Fig. 1 was probably made in France at the second half of XIX century by unknown author. Currently it is the property of museum in Oporow, Poland. Apart from characteristic destructions mentioned above, the whole object was covered with a thin layer of grayish inorganic encrustation and organic aliphatic compounds. The thicker clusters of encrustation were found at deeper reliefs or engravings, well bounded with the substrate. Microscopic observations confirmed penetration of encrustation into the ivory. The whole surface of elephant ivory was covered with natural yellow patina.

Fig. 1. Photograph of ivory decorative jug

During the production process, the jug was turned on a lathe and shallowly sculptured. Individual pieces were assembled using threads in the ivory substrate and metal screws. The dimensions of the jug are as follows:

Height − 73 cm,
Standarea − 27 × 27 cm,
Largestdiameter − 15 cm.

The theme of relief is a figural presentation of nymphs parade. Unusual are the impressive dimensions of decorative jug. It shows not only the unique value of material itself, but also a high skill and experience of the artist.

3 Experiment

The laser used in the presented paper was a Q-switched Nd:YAG system ReNOVALaser1 (Fig. 2), with a pulse length of 8 ns (FWHM), output energy 100 mJ, repetition rate of 10 Hz, fundamental wavelength of 1064 nm and a fiber optics beam delivering system. The laser output energy was controlled by pyroelectric detector (Laser Precision Corporation Rj 7620, probe RjP-734). After the optical fibre, without any focusing optics, the laser energy was at the level of 20 mJ, enough for stepped, careful removal of encrustation using fluency controlled by the distance to the object (maximum 2 J/cm^2).

Figure 3 presents a fragment of jug during the cleaning process. Black lines show the cleaned areas (left part of ivory element and several tests at the right side of internal surface of object).

Fig. 2. The Photograph of ReNOVALaser 1 system

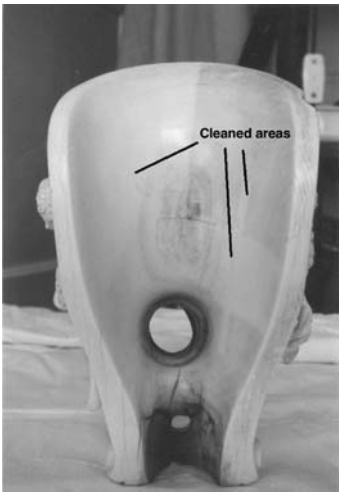

Fig. 3. Illustration of laser cleaning of ivort jug (*back side*)

It was emphasised above, that natural encrustation is non-homogeneous along the whole object surface, don't possesses also the equal thickness, structure and even colour. Similar experiments, but dealing with the artificially made ink stains of ivory, have been presented in [1].

In the presented experiment, a fiber optics spectrophotometer was applied to estimate, in a clear-out and objective way, the level of cleaning of ivory [2]. It was a commercial system produced by Ocean Optics (model 2000). Light emitted by halogen lamp was delivered to the cleaned place of object by means of one optical fiber. Backscattered light was collected by six other fibers surrounding the central one and then transmitted through optical system to diffraction grating of spectrometer. After dispersion, a response of the linear matrix of CCD detectors was displayed on the monitor of computer. Figure 4 shows the experimental arrangement and results of these measurements are shown on Fig. 5.

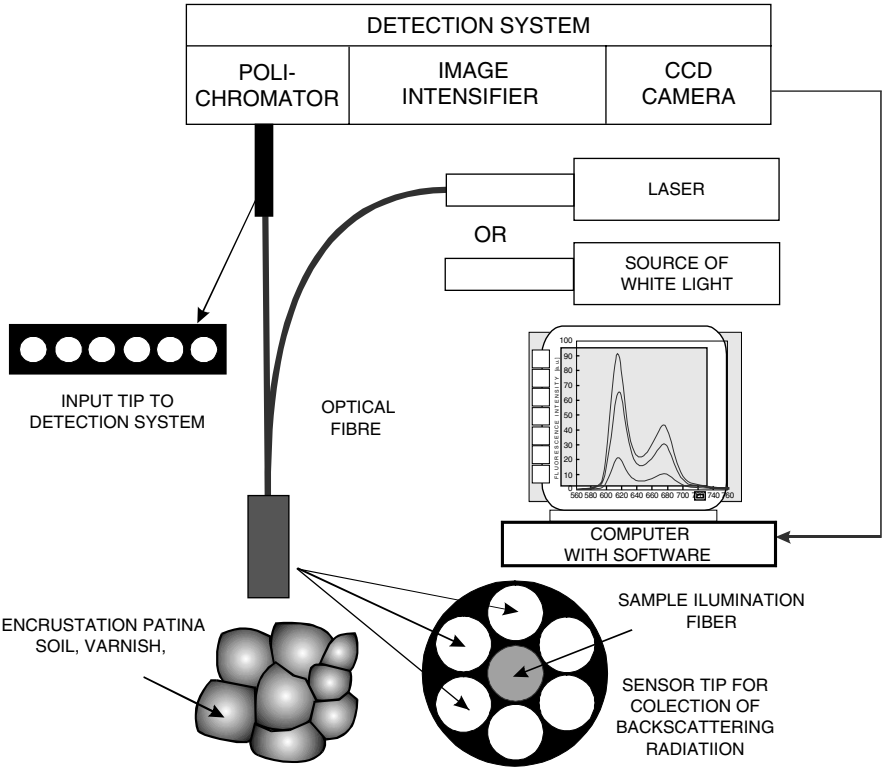

Fig. 4. Scheme of measurement system for determination of wavelength dependent reflection coefficient

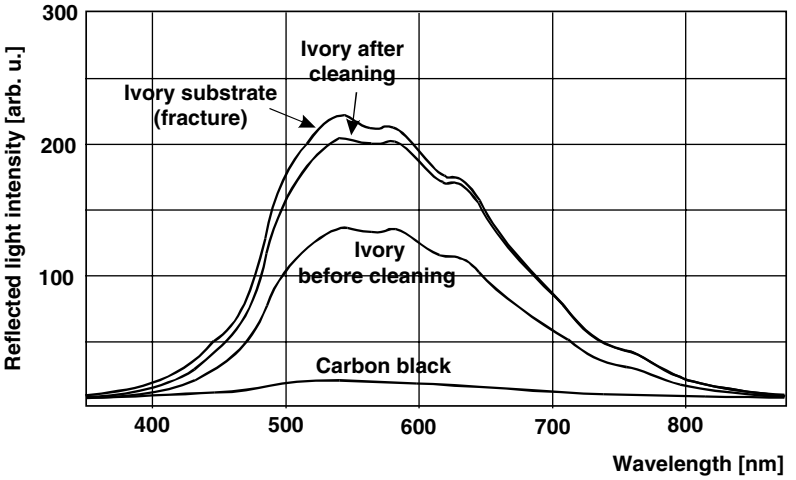

Fig. 5. Results of measurements of light amplitude scattered from the surface of investigated fragment of ivory

The condition of the ivory surface after laser treatment has been tested using a standard microscope (50x magnification). There were no observable destructions of the primary ivory substrate. It is difficult to compare the obtained results with the results of other methods of ivory cleaning. Never mind, it should be stated, that proposed technology is fast, ecological (no solvents) and safe for the object, if we take into consideration the problems connected with the hygroscopity and anisotropy of ivory, signalized in the introduction to the paper. Another advantage is also a lack of contact of cleaning tool (laser beam) with the delicate object surface.

4 Conclusions

It was shown, that ivory objects, very sensitive to conventional restoration processes can be effectively and safely renovated using laser technique. Registration of visible light allowed to determine the level of cleaning. These results can be compared with the results obtained using a new, acoustic experimental method [3].

References

1. O. Madden et al., "Removal of Dye-based Ink Stains fro Ivory: Evaluation of Cleaning Results Based on Wavelength Dependency and Laser Type", LACONA IV Conference, "Lasers in the conservation of artworks", 11–14 September 2001, Paris, Proceedings, p 37

2. J. Marczak, “Surface cleaning of art work by UV, VIS and IR pulse laser radiation”, Proceedings of SPIE, vol. 4402, (2001), pp 202–209
3. J. Kolar, M. Strlic, V. S. Selih, M. Marincek, J. Marczak, R. Ostrowski, and M. Strzelec, “Surface modification during Nd:YAG (1065 nm) pulsed laser cleaning of organic fibrous materials”, LACONA V Conf., “Lasers in the Conservation of Artworks, 15-18 Sept. 2003, Osnabrueck, Germany, paper KJ-22/03

Part IV

Case Studies

The Conservation Intervention on the *Porta della Mandorla*

S. Siano[1], A. Giusti[2], D. Pinna[2], S. Porcinai[2], M. Giamello[3], G. Sabatini[3], and R. Salimbeni[1]

[1] Istituto di Fisica Applicata, Consiglio Nazionale delle Ricerche, Florence Italy
s.siano@ifac.cnr.it
[2] Opificio delle Pietre Dure, Florence, Italy
[3] Istituto di Geochimica Ambientale e Conservazione del Patrimonio Culturale Lapideo

Abstract. We investigated the conservation problems of the *Porta della Mandorla*, a masterpiece of the early Florentine Renaissance. The aim of the work was the statement of practicable cleaning protocols based on laser ablation. To this goal, a thorough petrographic characterisation of the state of conservation was performed, which addressed a set of laser cleaning tests by Q-switching and short free running Nd:YAG lasers. The main optimisation problem was the yellow-orange appearance associated with laser ablation by Q-switching lasers. Following the explanation of such a cleaning result, two practicable solutions based on suitable pulse duration or wavelength selections were successfully demonstrated then different intervention protocols were proposed.

1 Introduction

The *Porta della Mandorla* is one of the two north portals of the Cathedral of Florence. The masterpiece was initiated between 1380–90 and concluded in the 1421. Various sculptors operating in Florence at that time contributed to the work. Among these, Nanni di Banco (∼1384–1421), who was the author of the big relief of the tympanum representing the Assumption of the *Madonna della Cintola*. Besides this certain attribution there are historical and esthetical elements which suggest the involvement of other great names of the Italian Renaissance, such as Iacopo della Quercia, Donatello, and Luca della Robbia.

The portal decorations were crafted by using three lithotypes, which are statuary marble (Carrara), serpentinite (Verde di Prato), and a calcareous marl (Marne del Sugame). The former was employed to sculpture the scene of the tympanum by Nanni di Banco and other relieves, while the latter green and red stones were used to craft the inlaying of the frameworks, archivolt, and jambs.

The only documented cleaning treatment of the past is the one performed round the 1871–2, when the incrustation was removed with a solution achieved by mixing hydroflouric acid residues and sulphuric acid. Up to now, no information were found about further interventions.

Here we investigated the state of conservation of the masterpiece by Nanni di Banco and the one of other marble relieves then the optimisation of laser based cleaning approaches was carried out. Along with a rigorous statement of the possible laser treatments, which gives a relevant contribution to the solution of an important conservation problem, our study also focus on the origin of the well-known yellow appearance associated with QS laser ablation of black crust on stones [1–3] and on the possible laser solutions of such a problem.

2 Methods

The state of conservation of the artwork was investigated through FT-IR, XRD, SEM-EDX, and ultra-thin section analyses performed on a few small samples taken in representative areas. This allowed a thorough description of the conservation problem whose features led us to preliminary select the laser cleaning approach as the most suitable on the basis of previous extensive conservation studies on various marble artworks (see for example [3–5]).

Cleaning tests were carried out by employing four commercial laser systems. Q-switching (QS) Nd:YAG (1064–532 nm), 450–200 mJ, 8 ns, articulated arm (Palladio, Quanta System SpA). The hand piece usually included a 1 m focusing lens and a diffusing optical window to homogenise the beam. Two short free running (SFR) Nd:YAG: 1000 mJ, 50–120 µs, fibre-coupled (EOS 1000, El.En. SpA) and 1000 mJ, 20 µs, fibre-coupled (Smart Clean El.En. SpA), respectively. QS Nd:YAG (1064 nm): 120 mJ, 25 ns, fibre-coupled (Laserblast 50, Quantel). The latter three systems are equipped with a hand piece providing a good spatial homogeneity trough a single lens imaging system.

The aims of the optimisation study were the following. 1) Evaluation of the laser ablation as main cleaning treatment. 2) Understanding the nature of the expected yellow-orange appearance associated with QS Nd:YAG laser ablation [1–3]. 3) Statement of practicable protocols providing careful cleaning and an acceptable chromatic distribution, by avoiding in particular a strong contrast with respect to the whitish eroded areas.

The cleaning results were evaluated from stratigraphic and chromatic point of views through ultra-thin section analysis and standard colorimetry. This latter was performed by a calibrated spectral camera (SpectraScan® PR 704) providing CIE standard parameters. The colour systems here employed were $L^*a^*b^*$ and $L^*C_{ab}h_{ab}$, where L^* is the lightness, a^* the red-green and b^* the blue-yellow coordinates. The chroma C_{ab} and hue angle h_{ab} are respectively defined as: $C_{ab} = (a^{*2} + b^{*2})^{1/2}$ and $h_{ab} = \arctan(b^*/a^*)$.

3 State of Conservation

As can be seen in Fig. 1, the more projecting relieves of the tympanum suffer the erosion by rain washing while undercuts appear heavily encrusted. In these latter areas, which are of main relevance for the laser cleaning treatments, the black crust represents just the outer stratum of a complex stratigraphy involving various layers as shown in the ultra-thin section images of Fig. 2. Actually, beneath the black crust (A) two *scialbatura* layers can be observed (B, C) whose binder is now prevalently gypseous. The outer one is a fine plastering with a prevalently quartzeous inert component, partially sulphated carbonatic binder, and pigments (ochres and black carbon). The third layer (C) is another *scialbatura*, which can be differentiated from the previous one for the lower density of inert material and pigments, as well as for the completely sulphated binder. The layer D is microcrystalline gypsum arose probably from the sulphation of lime milk. The last layer, in proximity of the marble substrate (E) is likely composed by Ca-oxalates, now strongly incoherent and sulphated. This stratification characterisation was also assessed by FT-IR, XRD and SEM-EDX.

Fig. 1. The tympanum of the *Porta della Mandorla*: the Assumption of the *Madonna della Cintola* by Nanni di Banco

The stratigraphy shown in Fig. 2 is the one including the maximum number of layers but different situations were found in the various zones of the portal, such as minor number of layers, different pigmentation hue, and also an area with an orange varnish above the black crust. These features, along with the advanced state of deterioration of the marble substrate in some zones, made the statement of the intervention tasks very difficult because of the various conservative and esthetical concerns associated with the possible cleaning degrees. Despite these aspects are still under discussion,from a conservative standpoint there are no doubts about the necessity to remove the most of the big amount of stratified gypsum laying on the surface of the masterpiece. This implies the removal of the two *scialbatura* layers while

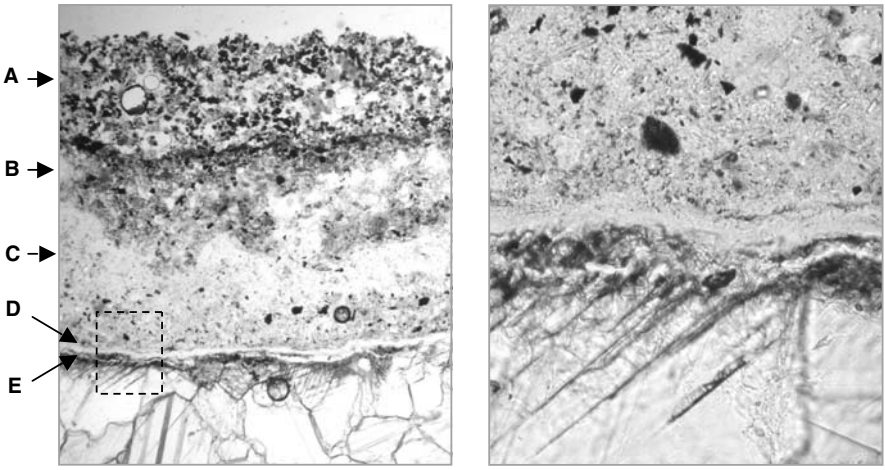

Fig. 2. Representative stratigraphy (transmitted light // nicols): (**A**) black crust (400 µm), (**B**) *scialbatura* layer (300–400 µm), (**C**) *scialbatura* layer (300–400 µm), (**D**) thin gypsum layer (∼25 µm), (**E**) very sulphated Ca-oxalates film

more questionable concerns are related to the layers in close proximity of the marble substrate (D, E, in Fig. 2). Anyway, before starting the cleaning trials on large areas we carried out a historical research in order to date the *scialbatura* applications. A photo by Alinari Brothers taken around 1890 not showing the present surface features allowed us to attribute the thin plasters to the twentieth century.

4 Cleaning Results

Laser cleaning tests were carried out both in situ and on taken samples. The operative fluences for QS lasers were between 0.4–1.5 J/cm^2 with a damage threshold around 2.5–3 J/cm^2, depending on specific substrate features such as the presence of grey veins. SFR laser did not induce relevant side effects up to 10–15 J/cm^2 while the minimum operative fluence was about 2 J/cm^2 on black crust [6] and 5 J/cm^2 on *scialbaturas*. The trials were performed at pulse frequency rates not exceeding 15 Hz in order to avoid cumulative heating effects [7].

Significant phenomenological differences were associated with the laser ablation by QS and SFR laser systems, respectively. In particular, the former provided a relatively high efficiency with respect to the latter. Whereas the long pulses emitted by EOS 1000 (50–120 µm) were not suitable for areas presenting thick *scialbaturas* because of the very low ablation rate and unsatisfactory cleaning result. Actually, in such cases the cleaning needs impracticable irradiation times, the treated areas exhibit a grey-yellow hue, and the

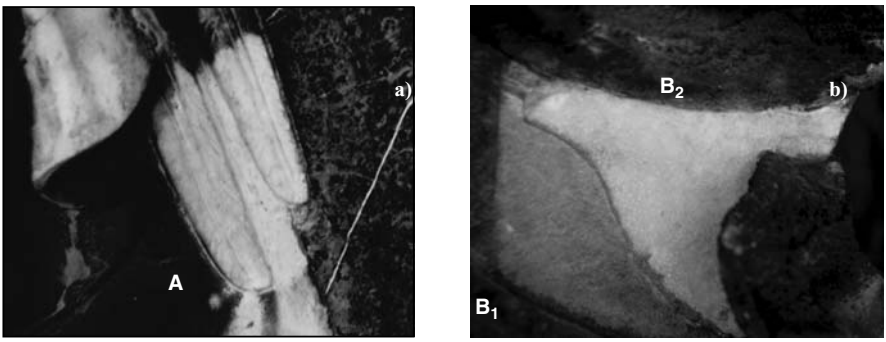

Fig. 3. Cleaning results achieved by QS Nd:YAG laser (Palladio: 1064 mm). (**a**) Thin *scialbatura* removed by 0.5–1 J/cm^2 laser irradiation. (**b**) Thick *scialbaturas* exposed by 1 J/cm^2 (C_1) and deep cleaning by 1.5 J/cm^2 (C_2) laser irradiation

final cleaning degree appear incomplete to the naked eye. Conversely, Smart Clean (20 μs) resulted more effective providing a good cleaning result from a stratigraphic and chromatic point of views, as already reported in previous works [8].

Palladio (1064 nm) provided the highest efficiency allowing to remove thick stratification with a few tens of shots while a few shots were effective for slightly encrusted areas. The exposed surfaces appear usually of a yellow-orange colour with different degrees of chromatic saturation and hue. According with previous investigations [2, 3] this optical effect can be originated by various causes such as for examples iron oxides spread or simply left over the surface by laser ablation process, as well as degraded oily substances and so on. Anyway, no one of these hypotheses was exhaustively investigated in cases of real interest and no laser solutions were practically demonstrated. Thus the so called "yellowing effect" associated with QS laser ablation still represents a significant obstacle to the dissemination of the laser techniques. In our experience SFR laser provide in many cases a solution of the problem but with a significant increase of the treatment time due to the lower ablation efficiency. This disadvantage is acceptable for valuable objects such as important sculptures or in cases where QS lasers are "optically or mechanically too aggressive", but can represent a real limitation for large areas such as historical stone façades. For this general reason and to overcome the present esthetical problems without renouncing to the high efficiency provided by QS lasers in stratified areas with a coherent substrate, we performed diagnostic insights on the yellow-orange appearance including in situ spectral and colour measurements (Fig. 4a) , as well as specific stratigraphic investigations of treated areas on small samples taken from the masterpieces.

Fig. 4. (**a**) In situ spectral and colour measurements. (**b**) Adjacent areas (C_1 and C_2) treated at the same luence ($0.8 J/cm^2$) exhibiting different colours (L^*,a^*,b^*,C_{ab},h_{ab}): (C_1) 74.2, −0.21, 12.8, 12.8, −1.55 (*light yellow*); (C_2) 71.6, −1.15, 7.15, 7.24, −1.41 (*white-gray*)

5 Yellow-Orange Appearance

For the most part of the cleaned areas the observations to the naked eye allowed to rule out the colour was due to oily substances or to selective back scattering associated with surface microstructure [2, 9]. This because the yellow-orange appearance was sometime very localised within the cleaned surface with natural white zones adjacent to the coloured ones. Thus for examples, white grooves in yellow areas were observed in the test site A shown in Fig. 3a while the site C (Fig. 4b) exhibited two distinct areas with yellow and natural white-grey (veined marble) colours, respectively, as quantified by spectral reflectance and colour measurements. These observations suggested to attribute to pigments such as the ochres contained in the *scialbaturas* and secondary iron minerals (oxalates) the most significant contribution to the yellow-orange appearance of cleaned areas. On the other hand it was not clear whether a sputtering effect or incomplete removal was the cause of the chromatic result. From cross section observation of samples cleaned by Laserblast at $0.9 J/cm^2$ and Smart Clean at $6.6 J/cm^2$, we found the zone treated by QS laser presented a residual pigmented layer,which was not visible in zones cleaned by SFR laser. The residual layer associate with QS Nd:YAG lasers (1064 nm) was well visible also in various ultra-thin section such as for example the one shown in Fig. 5a. Surface and stratigraphic observation evidenced the contribution associated with eventual sputtering effects was negligible whereas the most of the yellow-orange appearance was due to a residual microlayer ($\leq 5\,\mu m$) containing ochres and (sometime) oxalate traces above an apparently pseudomorphic sulphation representing the real surface of the artefact.

The incomplete removal can be attributed to the high reflectivity of the iron minerals and to the high diffusivity of the gypsum matrix in the

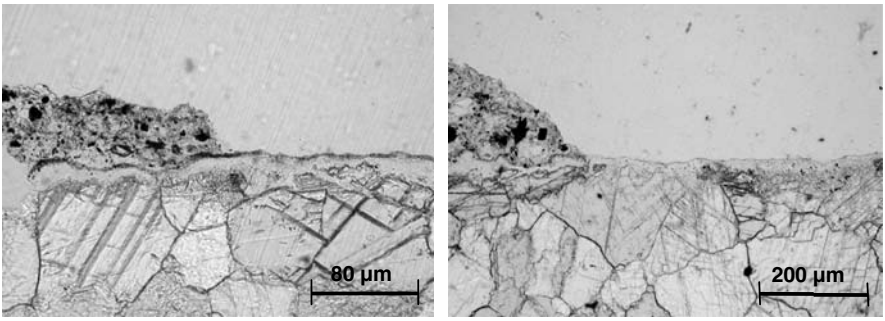

Fig. 5. Cleaning transition achieved by Palladio observed through ultra-thin sections. (**a**) First harmonic (1064 nm), 0.8 J/cm^2. (**b**) First harmonic at 0.8 J/cm^2 then second harmonic (532 nm) at 0.4 J/cm^2: The residual pigmented layer left by first harmonic was removed by second harmonic irradiation

NIR. There are hence two possible solutions based on a local energy density (J/cm^3) increase. 1) High fluence released in times whose associated thermal diffusion length is lower than the thickness of the pigmented layer. 2) Radiation wavelength strongly absorbed by the chromophores at relatively low fluence. In the present case the former solution means lasers with a pulse duration in the order of 1–10 µs, being the thickness of the residual layers we observed between 2–5 µm. The latter solution is practicable whenever no relevant fluence dependent side effects are involved. Whereas the wavelength solution represented by second harmonic (532 nm) can be employed whenever there is a favourable optical discrimination (as for white stones) and no specific intensity dependent side effects are evidenced.

Following the laboratory tests on samples we performed further cleaning trials on the artwork in order to demonstrate on meaningful areas the effectiveness and practicability of double wavelength (Palladio), double pulse duration (any QS laser then Smart Clean), or standalone SFR (Smart Clean) laser treatments. Advantages and drawback associated with the three cleaning protocols were evidenced. The different protocols we stated are now under evaluation in terms of comparative cleaning results, eventual integration with light chemical or mechanical treatments, costs, and other. Anyway, we extensively proved the overcoming of the colour appearance problem by standalone laser treatments.

6 Conclusions

As main issue of the laser cleaning optimisation study described in this work, the conservation intervention on the *Porta della Mandorla* will likely start with an overall laser treatment. At the moment the laser system(s) which will be employed is (are) not yet selected. Anyway, in our opinion the first

treatment step could be conveniently performed by QS Nd:YAG (Palladio) especially in heavily stratified areas where SFR (Smart Clean) would require relatively long treatment times. Whereas, the finishing laser treatment avoiding yellow-orange appearances is a matter of choice (second harmonic or SFR). Further details about laser cleaning of the *Porta della Mandorla* will be reported elsewhere.

Acknowledgements

The authors wish to acknowledge the Department for Productive Activity of the Tuscany Region (PRAI Programme) for the financial support provided to the present investigation through the project Optocantieri.

References

1. P. Bromblet, M. Labouré, and G. Orial, in *Journal of Cultural Heritage* **4**, 17s, 2003
2. V. Vergès-Belmin and C. Dignard, *Journal of Cultural Heritage* **4**, 238s, 2003
3. S. Siano, A. Casciani, A. Giusti, M. Matteini, R. Pini, S. Porcinai, and R. Salimbeni, in *Journal of Cultural Heritage* **4**, 123
4. G. Sabatini, M. Giamello, R. Pini, S.Siano, R. Salimbeni, in *Journal of Cultural Heritage* **1**, S9, 2000
5. S. Siano, R. Pini, R. Salimbeni, M. Giamello, A. Scala, F. Fabiani, and P. Bianchini, in *Proceeding of the 9^{th} International Congress on Deterioration and Conservation of Stone*, Elsevier, Amsterdam 2000, 569
6. S. Siano, R. Pini, and R. Salimbeni, in *ALT 99, International Conference on Advanced Laser Technologies*, Edited by Pustovoy and V.I. Konov, SPIE Vol. 4070, 27, WA USA, 2000
7. S. Siano, F. Fabiani, R. Pini, R. Salimbeni, M. Giamello, and G. Sabatini, in *Journal of Cultural Heritage*, **1**, S47, 2000
8. P. Maravelaki-Kalaitzaki, V. Zafiropulos, P. Pouli, D. Anglos, C. Balas, R. Salimbeni, S. Siano, and R. Pini, in *Journal of Cultural Heritage* **4**, 77s, 2003
9. V. Zafiropulos, C. Balas, A. Manousaki, Y. Marakis, P. Maravelaki-Kalaitzaki, K. Melesanaki, P. Pouli, T. Stratoudaki, S. Klein, J. Hildenhagen, K. Dickmann, B. S. Luk'Yanchuk, C. Mujat, and A. Dogariu, in *Journal of Cultural Heritage* **4**, 249s, 2003

The Capability of the Laser Application for Selective Cleaning and the Removal of Different Layers on Wooden Artworks

G. Wiedemann[1], K. Pueschner[2], H. Wust[1], and A. Kempe[1]

[1] Fraunhofer Institute Material- and Beam Technology Winterbergstrasse 28, 01277 Dresden, Germany
guenter.wiedemann@iws.fraunhofer.de
[2] Hauptstraße 25, 01762 Hartmannsdorf Germany
karsten.pueschner@t-online.de

1 Introduction

The material "wood" plays a very important role in the field of art and cultural heritage and its application reveals an extraordinary variety. It is encountered as

- an early construction material,
- a means of adornment of the interior of representative rooms, pewages, carved altarpieces, wall panels, sculptures, furniture.

With respect to the maintenance of wooden cultural assets the conservatory problems are at least as varied as its applications. Nearly all maintenance and restoration methods include a removal of dirt, protective layers or paint. In this contribution you will find some examples and a few general conclusions with respect to the possibilities and the limits of the laser application.

2 Experience with Unpainted Wooden Surfaces

Already at LACONA III and in [1] we presented results of the laser beam cleaning of the medieval (six hundred years old) panelled chamber. The decision to use the non-contact laser beam cleaning resulted from the demand to avoid further loss of substance of the partly heavily damaged wall panels (Fig. 1). The use of conventional cleaning techniques such as mechanical and wet cleaning applied to the varied layers consisting of dirt, soot, gypsum paint and wallpaper reveal here definitely their limits.

With respect to its art-historical relevance the decision for the laser beam cleaning was preceded by a series of scientific investigations with the aim to demonstrate the non-damage of the cleaning process. These were:

- measurement of the absorption parameters of the layers to be removed,
- measurement of the absorption parameters of the material wood,
- measurement of the thermal parameters of wood,

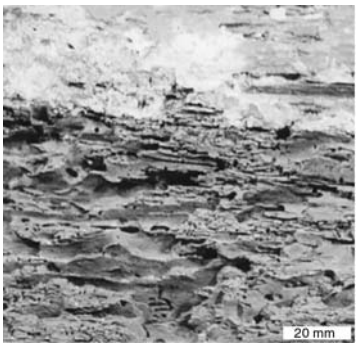

Fig. 1. Part of a heavily damaged wooden panel with multiple coatings

- careful experimental determination of the ablation threshold of every layer,
- careful experimental determination of the damage threshold of the wooden substrate.

Because of their basic importance the absorption parameters of pine and beech wood in comparison to those of chosen paints are shown in Fig. 2. The removal thresholds of different paints in comparison to the damage thresholds of wood are given in Fig. 3.

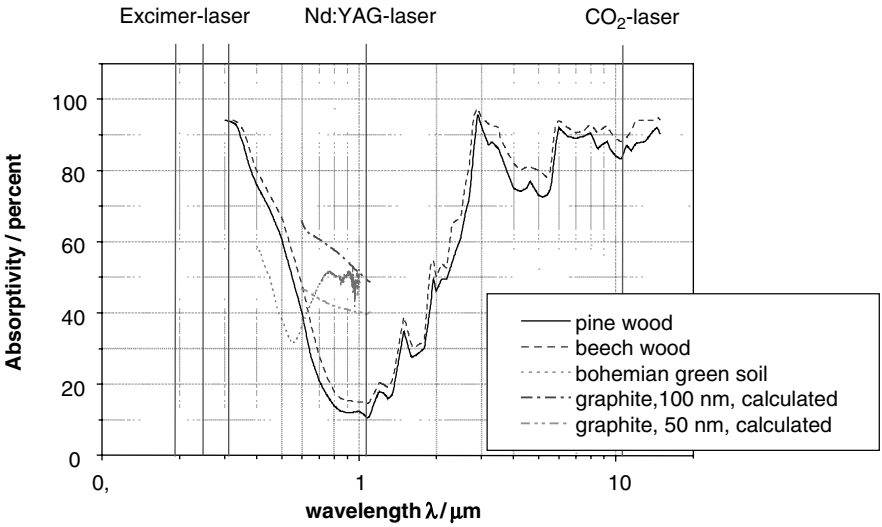

Fig. 2. Absorption of spruce and beech wood vs. wavelength, compared with absorption of typical coatings

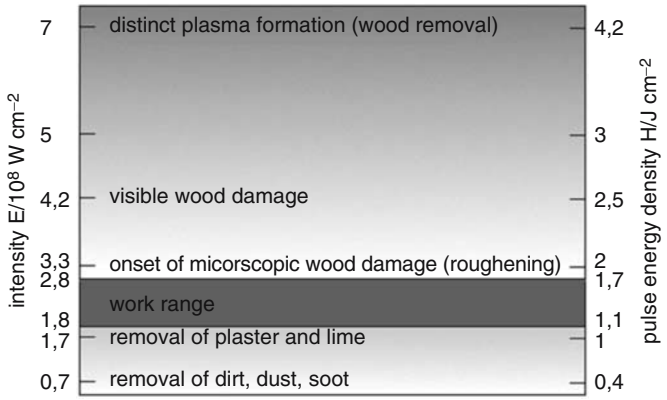

Fig. 3. Threshold values for layer removal and wood damage for the Nd:YAG laser NL 102

Beyond the damage thresholds of further wood species were investigated in dependence of the wavelength of the used short pulsed laser. The criteria was the beginning of microscopic changes at the surface.

The samples were made from new wood, air-dried with a unitary surface treatment. Figure 4 shows exemplarily a wood surface irradiated with different pulse energy densities. On the left side a visual, macroscopic impression, on the right side a section of the same surface in a 14-fold magnification. Since from the visual impression there are no changes visible, microscopically, however, there are remarkable changes visible. Beech wood shows a roughening at $H = 0{,}2\,J/cm^2$. For oak at $H = 0{,}13\,J/cm^2$ colour changes were observed.

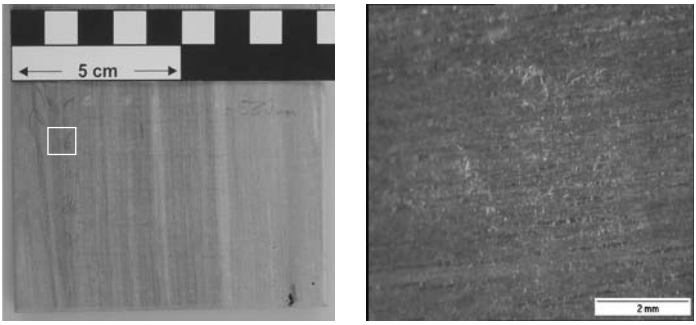

Fig. 4. Criteria for the reaction and damage threshold of air-dried timber: birch wood, $\lambda = 532\,nm$. *left*: survey; *right*: detail of probe 7; roughening at $H = 0{,}2\,J/cm^2$

Figure 5 gives a survey of damage thresholds of investigated wood species in dependence of the wavelength of the laser beam.

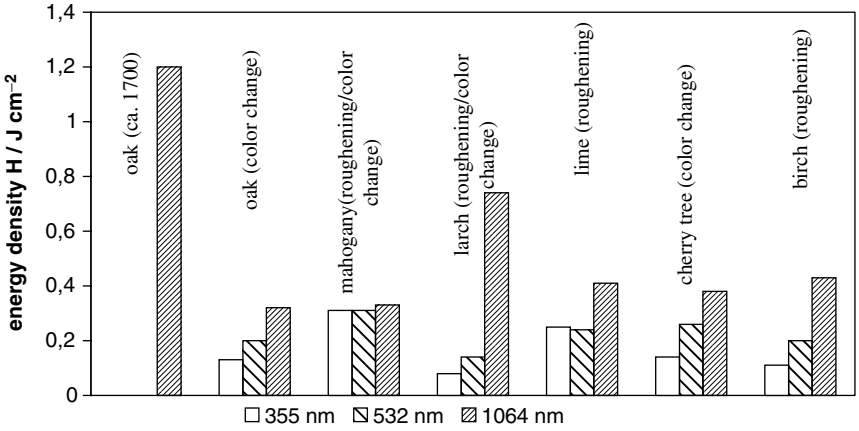

Fig. 5. Reaction threshold of different kinds of wood vs. wavelength of laser

The threshold density for the damage increases with the wavelength. This can be explained with the wavelength-dependent absorption behaviour, as shown in Fig. 2.

The differences in the threshold density between the wood species imply several questions:

- influence of the age of the wood (see oak, Fig. 5),
- influence of the colour,
- influence of the humidity,
- influence of the chemical composition of the woods,
- influence of the inhomogenity, resp. changes of the composition.

Fig. 6. Removal of monochromatic repaint (sitting Madonna around 1250, Laase/Mecklenburg, carved oak), *left* before and *right* after laser cleaning

In the next example for successful laser cleaning the removal of a monochrome repaint of an early-Gothic sitting Madonna (12th century) is demonstrated. Figure 6 shows the sitting Madonna before and after the laser cleaning. In order to achieve a high effciency parts of the thick repaint have ben removed by solvents before the laser cleaning.

In the famous interior decoration company "Deutsche Werkstätten Hellerau", the director's office has got a very decorative wooden wall, consisting of inlays of different wood species. During the period of the former German Democratic Republic a part of this wall were hidden by other wooden parts. During the restoration these overlays were removed, but adhesive and wooden remains were still there. In order to reconstruct the natural, unpainted surface these remains could be removed by a scalpel quite easily and quite quickly. Tests to remove the adhesive and lacquer remains resulted in a disappointing blotted wooden surface. However, the removal by the Nd:YAG laser NL 102 was successful. With relative low energy density a complete removal with a self-limitation at the bright woods of the inlays could be achieved in a relatively short time. At the dark inlay parts of moor oak (the production process is unknown so far) we could not achieve a self-limitation of the removal process but the adhesive and lacquer remains could be completely removed. During a longer radiation the darker wooden parts became brighter. Since the removal at low pulse frequencies on the dark wood could be observed without problems and a further radiation could be stopped before a damage of the original surface emerged, the laser application is a preferable treatment, here too. Figure 7 shows the satisfactory result.

Fig. 7. Panelling with wooden inlay – "Deutsche Werkstätten Hellerau" – results

The laser beam removal (short pulse Nd:YAG laser, λ =1,06 µm, interaction time $t_w \leq 10$ ns) is a very high-quality procedure applicable with the aim of the cleaning or the exposure of natural, unpainted wood including pre-damaged surfaces, just as the laser is applied in the case of natural, unpainted stone surfaces. Nevertheless it is absolutely necessary to investigate

the importance of the influences of the manifold inhomogeneous natural resource wood. Thus the laser cleaning is a very fine alternative to traditional processes.

3 Experience with Painted Wooden Surfaces

In general you can say that problems emerging in the laser beam cleaning and exposure of painted stone surfaces are also all present in the case of painted wooden surfaces. In addition to the importance of the absorptivity and transformation temperatures of the substrate and the layers to be removed, the corresponding parameters of the layers to be retained, too, have to be found.

Apart from the pigments and binders the following aspects have to be considered:

- the penetration of layers,
- the adhesion of paints,
- the pre-treatment of the wooden surface (before the paint is applied).

Up to now there are only a few results in scientific investigations with respect to a laser application. Thus it is very important to get systematic experimental investigations, which take all the previous aspects (absorption behaviour, thermatic constant standard etc.) into consideration. Furthermore it is important that these investigation methods are quick ones. The following example of a removal of transparent varnish layers from the original oak panelling of the Green Vault in Dresden shows this procedure. In connection with the reconstruction of the Royal Palace in Dresden, the original parts of the interior of the Green Vault are presently restored (Fig. 8).

Fig. 8. Royal palace Dresden, Green vault pretiosensaal around 1930

Within the restoration the reconstruction of the original surface design of the unpainted, varnished oak panel was a part of the task. In general the removal of varnish layers is done with the aim to lay bare original surfaces or to remove contaminated or light blooming and blanching varnish layers

before a new varnish is applied. Main focus of this task is the removal of a spirit-soluble pigmented resin varnish (1890) from the aged dried original linseed varnish (Figs. 9, 10). In general there are different methods to remove varnishes:

- solvent or solvent-like methods (solvent gel, resin soap, enzyme gels),
- mechanical removal (scalpel, erasion),
- fine blasting methods,
- cryo methods,
- combination methods.

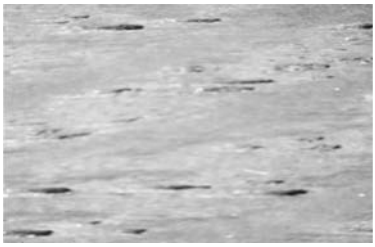

Fig. 9. Original wooden surface with an oil varnish dated to 1723 without repainting

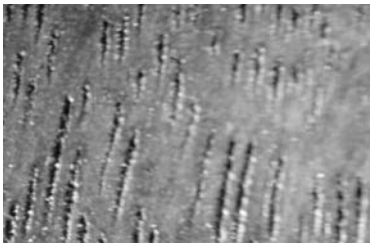

Fig. 10. Surface with dark pigmented varnish dated to 1890 which should be removed again

After some trials it became clear that none of these methods would show satisfactory results. So the removal by solvents was not successful because the very thin original linseed varnish left open pores in the wood surface into which the dissolved resin containing dark pigments would penetrate, and thus cause a darker appearance [4]. Washing out the resin by excessive solvent application would not be appropriate. It might even result in a severe damage of the original oil varnish (Fig. 11)

A. Unger, advisory chemist of the project from the Rathgen-Laboratory advises these methods only in cases of emergencies, because of the problematic

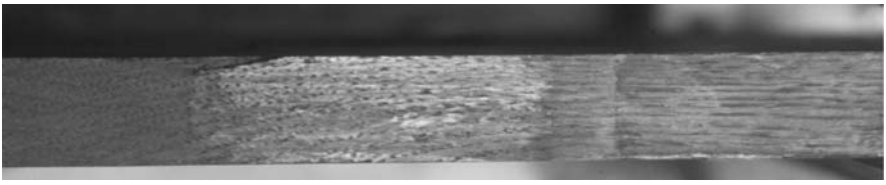

Fig. 11. Exposure sample with Ethanol gel – after drying the exposed area it comes to a light blooming and blanching of the original oil varnish

discussion of wood preservatives (DDT, PCP, lindane in wood and in the varnish). This is the reason why the laser beam ablation has been taken into consideration.

At first we wanted to remove the complete repaint, that means the repaint, applied in 1890 and the original linseed paint. Although a layer separation was desired, it seemed to be impossible. In any case the open-pored picture could be reached and a new oil varnish could have been applied.

At the beginning of the laser application (Nd:YAG-Laser NL 102) we determined the threshold values. At an even very low energy intensity an interaction with the surface of the varnish, to be removed, took place. The removal began at an energy density of 0,17 J/cm^2. An ideal working area was at an energy density of 0,43–0,50 J/cm^2. At the backside of a trial area we determined the threshold intensity of the row oak wood by laser beam influence. With approx. 1,2–1,4 J/cm^2 it is far beyond of that of the varnish removal.

After the removal at the lowest possible energy of the contaminated, dark varnish another layer appeared on the oak wood, which achieved after a subsequent cleaning of the fine dust a new depth effect. This layer has been analysed by a FT-IR spectroscopy and corresponded to the FT-IR spectra of the area, which has been identified as the original varnish beneath the metal fitting.

Thus we had to define the aim of this laser application anew. It meant not only to remove the varnish from the open-pored wooden surface, but we aspired to remove the resin-containing pigmented varnish layer from the oil varnish, which was applied 1723. We had the possibility of a selective removal of the resin varnish from the original oil varnish. This result can be explained by the different absorption behaviour. The threshold values of the two varnishes are different because of the weak pigmentation of the repaint of 1890 (Fig. 12).

The preservation of the original paint was thus possible without any damages or swelling, facts which occurred in the case of the solvent trials. The regeneration of the depth effect was done with vinegar water of 10% (Fig. 13).

In these cases of the varnish removal the laser shows clear advantages. These results in this quality would not have been possible, if other methods had been applied. Even with respect to a cost comparison with other

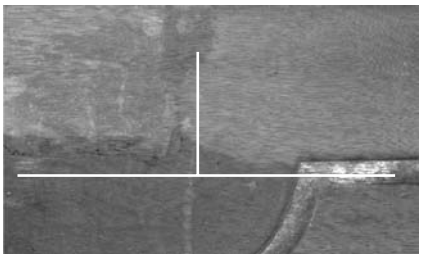

Fig. 12. Comparison of different methods of removing varnish – after treatment with solvent (*above left*), after laser treatment (*above right*), aspect before cleaning (*below*)

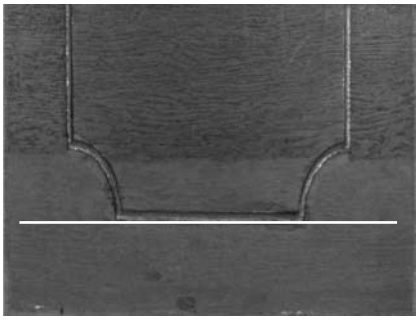

Fig. 13. Inlay of the panel. *Above*: laser treated area after subsequent cleaning with vinegar water (10%), *below*: area after laser cleaning without subsequent cleaning

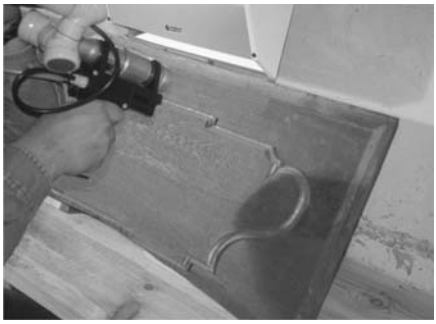

Fig. 14. Laser cleaning of an oak panel in the Emaillezimmer

traditional solvent methods the laser technique has been definitely the better one. The varnish laser removal was successfully finished in 2002 (Fig. 14).

Figure 15 shows the removal of a resin/protein-bonded repaint on a crucifix, which had a delicate protein-bonded lapis lazuli layer (natural

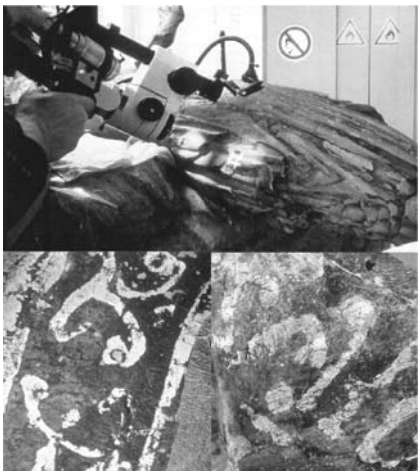

Fig. 15. Removal of a resin/protein-bonded repaint from a delicate protein-bonded lapos lazuli layer with a fone golden pattern, applied on a waxen emulsion (object: polychromatic wooden crucifix, national museums of Berlin, Prussian cultural heritage, sculpture gallery) – *above*: execution of the test – *below left*: laser cleaned – *below right*: mechanical/with solvent cleaned

ultramarine) with a fine golden pattern, applied on a waxen emulsion, in the area of the waistcloth.

First the lower absorption of the white repaint and the lower thermic constancy of the lapis lazuli paint spoke against a laser ablation. Nevertheless the laser experiments were successfully performed because the firstly preferred mechanical removal by a scalpel revealed an extraordinary time exposure. The dense repaint flaked off already before the completed laser removal. From the technical point of view we had to avoid that a further laser pulse would hit the bare lapis lazuli surface. Here we worked at a low pulse energy, which enabled a manual stop of the radiation between two pulses (approx. 2 Hz). Detailed investigations showed that the repaint had been applied on a contaminated original surface, which avoided a firmer connection with the original.

In a representative Renaissance building in Goerlitz (Saxony) you can find a very decorative wooden ceiling of approx. 100 m^2 size. The original paint consists of a glue-bonded whiting base ground.

On this ground there is a glue-bound whiting auripigment fond, which is partly painted florally and figuratively with reddish-brownish ochre. Thereon shellac has been applied as a protective layer. This layer was repainted again with a black casein-bonded paint. The aim of this restoration here is to remove the black paint layer and the shellac and to lay bare the original paint. First trials were performed at a spare part (Fig. 16). Here we succeeded in removing both layers. At a low energy density ($H<0{,}1\ J/cm^2$) the efficiency was quite

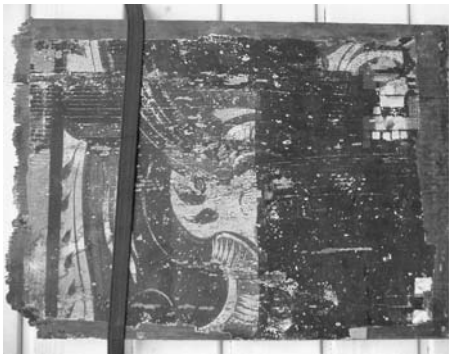

Fig. 16. Laser cleaning of a glue-bonded original painting under shellec and black casein-bonded repainting

high and the ablation process was self-limiting. In comparison to the exposure by traditional methods, the sample areas were more high-contrasted and high-coloured. The cause for this phenomenon (possible modifications of the original material) is presently investigated.

4 Summary

We could demonstrate that the laser ablation for the cleaning or the exposure of wooden artwork is a very promising technique. Using a short pulse lasers with a wavelength of approx. 1064 nm the material "wood" has a higher reaction- and damage threshold than the removal threshold of most of the other layer material. This fact can be explained by the lower absorption at this wavelength.

It is of importance to investigate in the exposure and cleaning of unpainted wooden surfaces, because, as demonstrated in this contribution, the insight into this subject is not sufficient up to now.

Especially with respect to painted wooden surfaces it is, up to now, impossible to give a standardized formula. The here presented procedure: careful tests with an accompanying scientific investigation – will endure further on.

Furthermore detailed and fundamental scientific investigations are necessary for a full understanding.

For the authors it is very important to point out that emerging vapors and particles have to be exhausted directly at the source. First investigations have shown that the exhaustion presents a precondition for a riskless working and thus for a wider application.

References

1. G. Wiedemann, M. Schulz, J. Hauptmann, H.-G. Kusch, S. Müller, M. Panzner, and H. Wust: Laser cleaning applied in the restoration of a medieval wooden panel chamber at Pirna, Journal of Cultural Heritage, 1(2000), pp 247–258
2. G. Wiedemann, H. Wust, A. Kempe et al.: Laserstrahlabtragen dünner Deckschichten – eine alternative Reinigungsmethode für die Restaurierung und Denkmalpflege – Möglichkeiten und Grenzen, Arbeitblätter für Restauratoren, 2(2001), pp 69–102
3. R. Schwarz: Möglichkeiten der Untersuchung und Restaurierung von Parkettfußböden an Beispielen aus dem ne uen Schloss in Bayreuth, Diplomarbeit FH Köln 1996, pp 94–101
4. K. Pueschner: Firnisabnahme an offenporigen Hölzern- Möglichkeiten des Lasers im Vergleich zur Lösemittelabnahme, Restauro, 1(2002), pp 40–45
5. H.-G. Kusch, Th. Heinze, and G. Wiedemann: Hazardous emissions and health risk during laser cleaning of natural stones, Journal of Cultural Heritage, 1(2002)

The Pilot Restoration Yard of the Church of San Frediano in Pisa: Results of a Multidisciplinary Study

C. Baracchini[1], R. Pini[2], F. Fabiani[3], M. Ciafaloni[1], S. Siano[2], R. Salimbeni[2], G. Sabatini[4], M. Giamello[4], M. Franzini[5], M. Lezzerini[5], M. Spampinato[6], F. Gravina[7], and F. Andreazzoli[8]

[1] Soprintendenza Beni Ambientali, Architettonici, Artistici e Storici, Pisa, Italy
[2] Istituto di Fisica Applicata, C.N.R., Firenze, Italy, R.Pini@ifac.cnr.it
[3] RestauroItalia srl, Capezzano Pianore (LU), Italy
[4] Dip. di Scienze Ambientali, Sez. di Geochimica Ambientale, Univ. di Siena, Italy
[5] Dipartimento di Scienze della Terra, Univ. di Pisa, Italy
[6] Private geologist, Pisa, Italy
[7] Dipartimento allo Sviluppo Economico della Regione Toscana, Firenze, Italy
[8] Scuola di Specializzazione in Archeologia, Univ. di Pisa, Italy

Abstract. In the frame of the EC Project "RIS+ Tuscany: Transfer of innovative technologies for Cultural Heritage" we carried out a pilot restoration yard to apply and evaluate laser cleaning procedures in the conservation of stones and decorations on the façade of the church of S. Frediano (XI–XII Cent.) in Pisa. A multidisciplinary scientific committee was established, formed by art historians, architects, physicists, geologists, and conservators. Italian firms involved in conservation services and in laser technology participated in the project. The conservation has been recently completed after two years of work, providing a critical evaluation on the effectiveness and safety of optimized laser cleaning operations, the definition of an integrated conservation protocol which included the laser technique, as well as other conventional cleaning techniques, and the evaluation of time productivity and operative costs of laser operations.

1 Introduction

In recent years, the Tuscany Region Government, and in particular the Department for Economy Development, has been playing a promotional role in the field of research and application of new technologies for Cultural Heritage by supporting research projects, some of them devoted to laser techniques in conservation for diagnostics and restoration. Beside the development of new laser instrumentation originated by the cooperation between industries, research centers and universities, one of the key ideas was to test these new technologies in application trials and in real operative conservation interventions under the supervision of conservation centers and local branches of the Italian Ministry of Cultural Heritage.

Within this frame, we chose to open a pilot restoration yard in the church of San Frediano in Pisa, considering the use of laser cleaning procedures since the planning phase of conservation. This approach required the process of acquiring the data related to the building birth-process, its state of conservation, the nature of the stones used, and the origin, function and age of the surface layers (patinas), in order to arrange a detailed project of intervention. This initiative called the attention of scientists and conservators, organized in a scientific committee, which was very active throughout the duration of the work, and used the restoration yard as laboratory in the open to test the new procedures and to discuss about their applicability. The participation of a conservation firm and of the laser industry sponsoring the activities has also been of significant relevance.

The main aims of this pilot conservation were the following:

- to test and verify the effectiveness of the laser cleaning technique and its integration with the conventional ones.
- to set up an application protocol, based on a careful preliminary investigation on stone and patinas of the façade, in order to improve the effectiveness and reliability of laser cleaning.
- to perform objective evaluations on cost and effectiveness of the laser procedures in comparison with the traditional ones.
- to draw and practically test the guidelines of new indications and recommendations for the correct use of laser cleaning, within the frame of UNI-Normal activity.

2 Preliminary Studies and Conservation Planning

The church of San Frediano (XI–XII Cent.), located in the center of Pisa, is a remarkable monument of the purest pisan-romanesque style. Its façade was built partly of reused marble of Roman origin and partly of other Tuscan stones (see Fig. 1).

Prior to conservation, the following studies were performed:

- Topographic and photogrammetric survey of the façade
- Historical and stratigraphic study to identify the building birth-process
- Study on the state of conservation, supported by a wide campaign of sampling and petrographic analyses
- Study on the more suitable cleaning technique on the various intervention sites.

These studies allowed us to identify a first building-phase (XI–XII Cent.), where calcarenite stone, known with the local name of *Panchina* was used. Subsequently, when the facade was still under construction, different types of marble (Carrara marble, Eastern marble, Monte Pisano marble) were inserted to compose a decorative pattern (including columns, capitals and portals)

Fig. 1. The church of San Frediano in Pisa

inspired by the coeval Cathedral of Pisa. A third phase was recognized in the upper part of the façade, re-built in the XVII century after a devastating fire, using quartzite, gray limestone, sandstone and calcareous breccia. Finally, the central mullioned window, which had been walled also in the XVII century, was reopened during the XIX century, after a partial re-working of the stone.

On the basis of this chronology, a wide campaign of sampling and petrographic analyses was carried out to understand the different layers (up to five) observable on the stone surface. All samples were analyzed by stereomicroscope and in thin (35 m) and ultra-thin (10 m) cross-sections under polarizing transmitted and reflected light. X-ray diffraction analyses were carried out to check and complete the microscopic data.

As for the state of conservation of the façade, petrographic analyses revealed that most of the exposed surface was covered by deposits, patinas and thick "black crusts" produced by sulphation of carbonatic stones. Marble decorations showed decohesion and pulverisation phenomena, leading us to avoid wet cleaning.

The analysis also revealed a complex stratigraphy of the superficial horizon made of several superimposed layers of calcium oxalate films (whewellite and weddellite), showing different colors due to the inclusion of carbon particulate and iron oxides and hydroxides.

Deciding which layer had to be removed and at which level the cleaning should arrive thus became the central problem, as well as selecting and testing an optimized cleaning technique allowing high precision removal and causing the minimal damage.

In most of the samples, two distinct films of calcium oxalate were found: an upper weddellite film (dihydrate Ca-oxalate) with an evident pigment

load made of black carbon and Fe-ochre, and an underlying whewellite film (monohydrate Ca-oxalate) completely lacking any load. Sometimes, another film composed of both whewellite and weddellite was observed between these two layers, containing inclusions of iron oxides and quartz.

The two films were explained as the gradual transformation of two distinct treatments executed in two different historic moments. Thanks to the reconstructed chronology, we hypothesized that the weddellite film with the pigment load responded to a later attempt of rendering the already dirt surface uniform, while the whewellite film appeared to us as the result of a more ancient treatment, aimed at protecting the underlying material.

In the light of this interpretation, the goal of the conservation became the removal of the black crust, of the underlying calcium oxalate weddellite film, and of the calcium oxalate whewellite film with inclusions of iron oxides and quartz. The cleaning action had to be stopped at the level of the whewellite film in direct contact with the stone surface.

To clean such a complicated structure, the use of laser ablation was considered the most appropriate technique since it permitted a higher precision to stop the cleaning at the proper stratigraphic level. Moreover, marble decorations, because of their erosion and decohesion, could take advantage of a highly controlled and non contact cleaning action as the one provided by laser ablation.

3 Conservation Activities

Two laser devices were employed for cleaning operation: Smart Clean and EOS 1000 produced by EL.EN. Both of them belongs to the class of Nd:YAG lasers with intermediate pulse duration (20–50 μs), which have been suitably developed for stone cleaning [1]. They are equipped with optical fiber delivery systems of various lengths (5–20 m) and emit a maximum energy of 2 and 1 Joule/pulse, respectively.

Laser treatment was mostly applied to the marble decorations presenting the worse state of conservation. In consideration of the complexity of the surfaces to be treated, an appropriate cleaning procedure was set up in each specific case.

Supported by previous tests to determine both laser ablation and damage thresholds, laser operation allowed gradual and controlled removal of the alteration to reach the desired cleaning level, as shown in Fig. 3.

Cleaning operations, carried out by Restauroitalia srl under the technical management of Francesca Falchini, were accompanied by further sampling for mineralogical and petrographic analyses in order to evaluate the effectiveness and safety of each cleaning phase. Colorimetric reflectance analyses were also performed on patinas and related to the required degree of cleaning.

However, where the crust was thicker, laser ablation was used in association with other conventional techniques, such as micro sandblasting,

Fig. 2. Detail of a marble capital, partially cleaned by a Nd:YAG laser

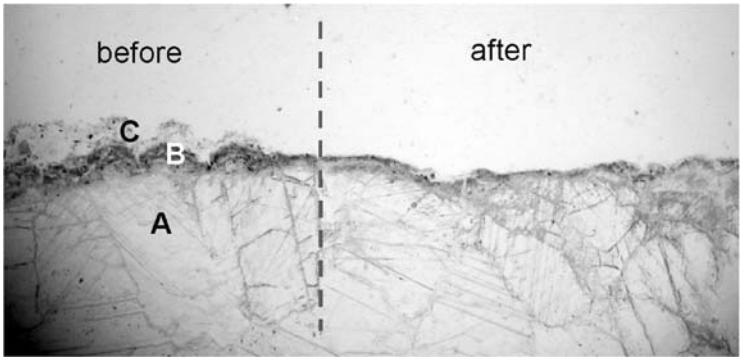

Fig. 3. Ultra-thin section of marble sample collected from a capital. A: marble; B: superimposed films of whewellite and weddellite; C: black crust. Laser cleaning allowed the preservation of the whewellite film, as requested by the cleaning protocol

scalpel cleaning, Ammonium Carbonate patches. The possibility to combine such cleaning methods with laser ablation, and eventually with surface preconsolidation on marble had been tested and analyzed in previous laboratory studies [2].

Laser cleaning was also tested on *Panchina* stone, but the very wide surface to be cleaned and the irregular surface of the stone suggested to complete the intervention with conventional techniques.

The evaluation of laser productivity was also performed. Starting with values of 100–200 hours/m^2, recorded in the early stages of laser applications, last results indicated a significant reduction down to about 40 hours/m^2. The main reason for this improvement was the use of a suitably designed hand piece including an optical system to adjust the laser spot diameter (1–8 mm), which allowed to maximize the area of the treatment by keeping the

laser fluence in the previously determined safety interval. Also, the growing experience of the conservators, along with the advancement of the work, helped to improve this figure.

4 Conclusions

In conclusion, the pilot restoration yard of the façade of San Frediano represents one of the few cases where the use of laser cleaning on extensive stone surfaces was considered since the planning phase of the intervention.

Thanks to the strong cooperation of the different competencies expressed by the scientific committee, it represented a significant opportunity to test and validate laser cleaning techniques. In fact, the yard was used as a laboratory in the open to test new laser devices as well as new application protocols of laser cleaning, alone and in association with other conventional cleaning procedures.

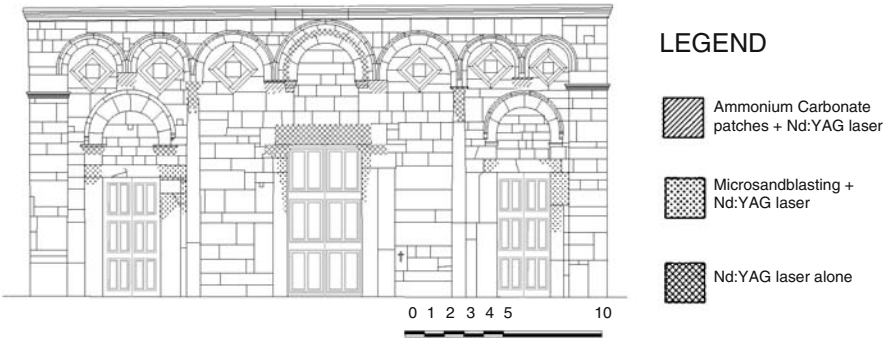

Fig. 4. Scheme of the lower part of the façade showing the sites of laser application

Very good results were obtained from the conservation point of view: application on decorated surfaces with respect of fine details, fully preservation of patinas, successful treatment even of highly altered surfaces. Such results were obtained without causing undesired side effects on stone color and reflectance properties. Regarding cleaning productivity, most of the data have still to be analyzed, but preliminary results indicate that values around some tens of hours/m^2 are achievable with optimized application procedures.

Finally, positive and encouraging results obtained in the restoration yard of San Frediano convinced the Superintendence Board of Pisa to consider further laser cleaning application on façades of other churches in Pisa.

Acknowledgements

Parts of the studies presented here have been carried out in the frame of the "OPTOCANTIERI" Project, supported by the Program of Innovative Actions of Tuscany Region. We would like to thank D. Cartei and S. Catassi, the directors of the yard, and M. Jodice of the University of Florence. We also thank the manufacturer of the lasers we used, El.En. Spa, Calenzano, Italy, and in particular A. Zanini.

References

1. A. Zanini, F. Margheri, S. Modi, and M. Scortecci, "A line of laser systems for applications in the restoration yard and in the restorer studio", in: *Laser Techniques and Systems in Art Conservation*, Edited by R. Salimbeni Ed., SPIE Vol. 4402, pp 108–113, Bellingham, WA, 2001
2. S. Siano, R. Pini, R. Salimbeni, M. Giamello, A. Scala, F. Fabiani, and P. Bianchini, "Integration of laser with conventional techniques in marble restoration", in: *9th International Congress on the Deterioration and Conservation of Stone*, Edited by V. Fassina, Vol. 2, pp 569–576, Elsevier Science B.V., Amsterdam, 2000

A Bronze Age Pre-Historic Dolmen: Laser Cleaning Techniques of Paintings and Graffiti (The Bisceglie Dolmen Case Study)

G. Daurelio

Private senior researcher in Laser Material Processing & Art Restoration, Viale Italia 27/12, I-70027, Palo del Colle, Bari, Italy
g.daurelio@virgilio.it

Abstract. The whole building was included and covered by an elliptical plan tumulus as reported for other similar monuments situated in the same territory of BISCEGLIE and GIOVINAZZO (in South of Italy). The monument was built by a community established in that area to mark their territory. It has a typical funerary character (funeral urn) and it was destined to the collective sepulture in the Middle Bronze Age, as indicated by the ceramic finds, accompanying the rich dead men, copper objects and ornaments, bones and amber recovered inside together with human rests. Degradation Mapping and Laser Cleaning with Photographs, during and after the process in-situ were carried out. Black incrustations and writings (by some different felt pens, marking pens, permanent black and colored ink pigments – fluorescent and no, as well as permanent text liner markings and spayed black paint) were cleaned by using a portable Nd:YAG Laser (λ 1.06 µm – 0.53 µm, in N-Mode and Q-Switch Mode, Laser pulse duration 150 µs or 6 ns – f 1 to 10 Hz – E max. 500 mJ per pulse in 1st harmonic and 200 mJ per pulse in 2nd harmonic). So, according to the different ink types three different laser cleaning techniques were used.

1 Introduction

This complex monument has been discovered at the beginning of this century and studied by M. Gervaso. Only the central gallery, constituted by two large vertical slabs, obtained from calcareous rocks remains of the whole structure. It represents the local geological emergence and ends in a rectangular plan "cell" with walls and covering built with analogous slabs. Because of its dislocations, in the open country far the centre of BISCEGLIE (Bari – Italy) and its long and persisting exposition to atmospheric agents, numerous problems arise for its preservation and protection from the recent acts of vandalism.

2 Laser Source for Monumental Cleaning

A Nd:YAG laser, portable, articulated arm with seven tilting mirrors, pulsed, Normal and Q-Switch Mode, Repitition Rates from 1 to 10 Hz, Pulse Width (6 ns per Q-Switch Mode and 150 µs in N-Mode for λ 1.064 µm and 0.53 µm)

and maximum Energy per pulse (200 mJ per pulse per λ 0.53 µm // 500 mJ per pulse in N-Mode and Q-Switch Mode), Model PALLADIO, QUANTA SYSTEM, Milan, Italy was used.

3 Laser Cleaning Techniques – Preliminary Tests

Before treating the Dolmen it was necessary to test some different techniques on stones, like the DOLMEN monument, on which different spray paints (in diverse colors), permanent text liners and felt pens and marking pens both fluorescent and not ones, were deposited.

1st Technique – This technique is commonly used by many researchers and laser cleaning operators [1–5], by using a beam in air (articulated arm and mirrors) or into a guiding fiberglass. On the first the 2nd harmonic (0.53 µm), by using 1 to 10 Hz frequency range and energy levels from 25 to 200 mJ per pulse was used as well as the beam comes out of the source. For this first experimental tests *no good results* were obtained. So, that the 1st harmonic (λ 1.06 µm) in N-Mode was employed at a fixed frequency value of the 10 Hz and diverse values (from 100 to 500 mJ per pulse) of the energy as a beam not focused one. The result on the all writings and graffiti and paints is no good; sometime a light de-coloration was obtained. All above reported was tested as in *dry mode* as in *wet mode* (by using a continuous layer of de-ionized water on the surfaces to be clean [1, 5]; rather in many cases the presence of the water deteriorates the situation as the phenomenon is typically a thermo-effect and the water subtracts energy to the cleaning process on the targeted surface [1, 3, 5, 6]. Also the 1st harmonic (λ 1.06 µm) and Q-Switch Mode (6 ns pulse width – 1 to 10 Hz and 100 to 500 mJ/pulse) was used as on different text liners and felt pens as on the spray paints. So that the following observations were carried out:

- for ballpoint pens (biro), red, black and blue colors . . . No positive results
- for *pencils* (types H – HB and B) it is interesting to note that already from 300 mJ/pulse some ablation effect begins to see; anyway it is easier to remove the hard graphite rather than the soft graphite. In order it is better to clean the type H rather than HB or B. This is possible as the soft graphite is easily coming – in surface stone.
- For *indelible markers* (in different colors) *No positive results* were obtained even if 10 Hz and 500 mJ/pulse were employed. It is possible to hypothesize that this wavelength is completely reflected by these inks
- For *paint markers* (water-proof/not blurred/mat or brilliant one), light blue, rose and yellow colors, till to 200 mJ/pulse *no effect was visible.* If the energy level is increased till to 500 mJ/pulse *the ablation was not obtained but only the initial color becomes more intense.*
- On the *sprayed paints* (yellow, red, black and blue colors) the following remarks were noted:

- *Red* ... *no positive results* by using 500 mJ/pulse – 10 Hz
- *Blue*, at 500 mJ/pulse – 10 Hz, *a very light effect* can be seen
- *Yellow*, at 500 mJ/pulse – 10 Hz, *a very light effect* can be seen but it is not interesting one
- *Green*, at 500 mJ/pulse – 10 Hz, *a light ablation effect* has carried out but the stone surface remains lightly colored
- *Black*, already at 300 mJ/pulse – 5 Hz, *a light ablation effect* can be seen but an interesting, quickly and *full result* can be obtained at 500 mJ/pulse – 10 Hz

2nd Technique – As the previous results were not positive, an other technique was adopted. This one, called by friends and some colleagues Daurelio Technique number 1, [7–9] was already applied many years ago for the de-painting on the March 1993 [7] and for many other surfaces treatments (cleaning, de-rusting, de-oiling, de-oxidizing, de-greasing, pickling etc. on the metals, alloys and steels) by using an integrated focused beam, carried out by an integrating segmented multifaceted converging optical devices (ZnSe lens or a parabolic mirror) on the July 1996 [8, 9]. In these tests it consists to impose a cylindrical Plano – convex quartz lens before the beam reaches the surface to be cleaned. So it is possible to transform a circular shape beam in a rectangular one. The focal length of the lens was 200 mm. At the same time the use of a shaped beam as focused or defocused one – according to the different defocusing grades requested – and an increased level of safety for the laser operator and casual spectators may be reached. By employing this technique the levels of energy density per pulse at maximum energy value (500 mJ/pulse) could be calculated as in N-Mode as in Q-Switch Mode:

per N-Mode
Spot Area ˜ $2.6 \pm 0.4\,\mathrm{mm}^2$ Energy Density σ_E ˜ $190 \pm 30\,\mathrm{mJ/mm}^2$
Per Q-Switch Mode
Spot Area ˜ $3.8 \pm 0.6\,\mathrm{mm}^2$ Energy Density σ_E ˜ $130 \pm 20\,\mathrm{mJ/mm}^2$

Also for this 2nd technique both the Modes and different working parameters (as focused or not focused beam, repetition rate, energy and energy density) were tested. It is clear that anyway the N-Mode produces only a thermal effect on the inks to remove while the Q-Switch lets to operate by a shock-wave process with some diverse energy and specific energy levels. In fact even if in many cases the N-Mode produced some interesting results (no much more ones), the best ones were obtained by using Q-Switch Mode. So, for the *Paint removal* different lower energy level threshold values were found

Black	100 mJ/pulse
Blue	100 mJ/pulse
Red	300 mJ/pulse
Green and Yellow	100 mJ/pulse (focused beam)

Regarding to the biro inks (red, blue and black) the results are good but 500 mJ/pulse –10 Hz are necessary.

The same one is valid for *pencils graphite* (B – HB and H types). *It is very easy to clean them.* It is true that the graphite could be removed simply used a common pencil rubber but in such cases the optical removing could be useful for operating on deep and chiselled stones and other ones.

On the contrary a different behaviour showed the indelible markers and paint markers.

On the first ones: *No effect was reached* even if a strictly focused beam was used at maximum energy level. *Only a very light de-coloration* was noted.

On the second ones:

- For *paint markers, water based*, orange and green colors, a *complete removal was possible but only by using 500 mJ/pulse – 10 Hz and a focused beam.* Even if it is possible it is necessary much more attention because it is easy to damage the stone surface.
- For *paint markers, not water based*, light blue, rose and yellow colours. The yellow paint is more easily removed (even if with some difficulty) but the other two colours showed the same behaviour, previously shown by using the laser beam without cylindrical lens; that is, the starting colour of the paint marker inks becomes more and more intense.

3rd Technique – This one, called *Daurelio technique number 2*, [10] was tested for the first time on the last 11 of April 1999 and applied on the Dolmen in situ. Only for the *paint markers (not water based)* and for the *indelible marking pens* and *text-liner pens*, as *fluorescent ones or not fluorescent*, this last technique was used. Also this 2nd technique, as dry or wet one, did not give the hoped results, even if different working parameters were tested. It was evident that the problem is the surface absorption of the impinging laser beam from this particular inks, absorbed into the bulk material, the stone, for some tens or hundreds micrometers depth. It is also clear that the ink absorption by the stone depends on many and different conditions of which the density, composition, porosity, compactness and so on. On the typical calcareous stones as the Dolmen many inks are suddenly and fully absorbed as these stones are particularly porous ones and so "drink" the inks.

Applying this last technique the writings, figures and graffiti were covered by a very thin wet layer of a mixture, composed by water and earth (loam), that is, oxides and salts of Iron and Aluminium (a typical red-brown earth) that offer a good and easy absorption of the infrared radiation. A counter-check, executed by using only a water wet surfaces or a continuous water layer on these inks, very hard to remove, did not furnish some positive results. So if some practical and experimental conditions are applied the infrared radiation can be absorbed by the coating layer and suddenly transfer the incoming laser energy (in Q-Switch Mode) to the inks absorbed into the surface stone. A shock-wave effect takes place on the stone surface coated by a loam and the goal was finally reached. It is necessary to pay much more attention to use this technique by a focused beam (as a last resource) as it necessarily also removes a *bit* (tens or hundreds of micrometers) of surface stone (impregnates

of inks or paints). So it is easy to produce an "image", rectangular shape one (specular image of the focused beam), on the stone if the process has not carefully evaluated and tested. On the other hand the possible alternative technique could be the classical chemical solvents that produce much more and more damages (washing away and dripping traces) on the monumental stones and . . . on this Dolmen these irreversible damages are clearly to-day visible, even if produced many years ago, for solving the same problems.

4 Laser Cleaning Techniques for the Dolmen Restoration

On the monument an accurate degradation mapping was carried out as a first stage of the works, so that the different types of writings, paintings were evaluated and some previous laser cleaning tests executed.

Black Incrustations (due to the lighting the fires of wood branches by farmers for warming themselves during the winters), paintings (by sprayed black paint) and writings (by marking pen/felt pen/ball point pen/graphite pencil and text liner marking pen) were noted. The used pens, utilized permanent/fluorescent ink pigments in different colors (light blue – pink – black – green), producing on the calcareous stones diverse and large writings traces. Some previous cleaning works (no by laser), executed by some chemical solvents, even if had no easily removed the paintings and writings, had also produced *"for ever"* some visible damages (washing away and dripping traces) on the monument. Degradation mapping and laser cleaning with photographs, during and after the process in-situ were carried out.

In this art restoration work two different portable laser were tested, according to the needs and the surface absorption of the laser beam wavelengths (1.06 and 10.6 micron) by the traces on the stone. A continuous, pulsed or super-pulsed CO_2 laser beam as well as N-Mode, Q-Switch Mode, 1st and 2nd harmonics (1.06 and 0.53 micron) of a Nd:YAG Laser were employed.

At the end only the Q-Switch Mode (6 ns-f 1 to 10 Hz – E max. 500 mJ per pulse) at 1.06 micron was the suited and wined one.

Black incrustations and sprayed black paintings were easily cleaned and removable by a defocused and Q-Switched Nd:YAG Laser beam. On the opposite side the laser ablation of the different writings resulted very difficult to evaporate, even if a Q-Switched laser beam, defocused of focused one, by employing high values of repetition rate and pulse energy were tested.

The usual thermal and/or shock-wave techniques did not produce some beneficial surface effects. The laser beam appeared to be fully reflected by these inks and pigments, especially in presence of fluorescent and/or permanent inks. It was also proved to dry the writings with de-ionized (and no) water to increase on the surface the optical coupling and absorption between the laser energy and the inks as well as furnishing a very thin layer of

de-ionized water on the "graffiti" during the laser surface processing, but *the results were negative*.

To enhance the laser absorption on the surface a colored and wetted mixture coating (water and earth) has been successfully employed, previously referred as a 3rd laser cleaning technique. In this way it was possible to clean the Dolmen without any visible damage.

5 Conclusions

Three different laser cleaning techniques have been reported and tested before on stone samples and after on the Dolmen in-situ. After the usual degradation mapping phase the different types of writings, graffiti, black incrustations, paintings, text-liners and paint markers were identified on the different parts of the Dolmen surfaces. So, according to the previous results, obtained on the prepared samples, each diverse technique was applied for the different "material" to remove from the surface Dolmen stones. The following results can be reassumed: By using the usual and common technique, that is the use of the laser beam as it comes out from the multi-articulated arm or guiding fiberglass may easily remove only black incrustations and sprayed paints (only the black color one). For all other "graffiti materials" no positive results were noted. The adoption of a rectangular shaped laser beam (2nd technique) lets to remove the materials above cited and also biro inks, pencil graphite and all the spayed colored paints, but no results on the indelible and/or fluorescent and/or paint markers were obtained. For these last ones it was necessary to employ a rectangular shaped laser beam together a coating layer of a mixture of the water and red-brown earth (3rd technique). Only so all the materials with different grades of difficulties could be removed.

References

1. M. Cooper, in *Laser Cleaning in Conservation: An Introduction,* Butterworth Heinemann
2. S. Siano, R. Pini, in *Optics Communications,* 135 (1997) 279–284
3. Ya. B. Zeldovich and Yu. P. Raizer, in *Physics of Shock Waves and High Temperature Hydrodynamic Phenomena,* Vol. 1, Academic Press, 1967
4. S. Siano, f. Margheri, P. Mazzinghi, R. Pini, R. Salimbeni, in *Applied Optics*, Vol. 36, n.27, 7073 to 7079, 1997
5. J. C. Miller, in *Laser Ablation: Principles and Applications*, Springer Verlag, 1994
6. H. S. Carslaw, Conduction on Heat in Solids,. 2nd Edition, Clarendon Press, Oxford 1989, pp 75–84
7. G. Daurelio, G. Chita, V. Santacesaria, R. Lassandro, in *New Techniques for Paint Removal,* Brite European Project, BE 51 07-92, 1992

8. G. Daurelio, G. Chita, *Laser Restoring Tests on Ceramics and Stony Materials,* Monografia Centro Laser, in 5 gionarta Le Scienze della Terra e L?archeometria, Bari, 19–20 Sept. 1998
9. G. Daurelio, G. Chita, M. Cinquepalmi, in *COLA '99 Proceedings, Applied Physics A – Materials Science & Processing,* A 69, 1 to 4, 1999
10. G. Daurelio, F. Radina, O. De Pascale, C. Milone, M. Cinquepalmi, E. Lattarulo, in *LACONA III,* Florence, April 1999

Part V

Side Effects

Evaluating the Effectiveness of Lasers for the Removal of Overpaint from a 20th C Minimalist Painting

C. McGlinchey[1], C. Stringari[2], E. Pratt[2], M. Abraham[3], K. Melessanaki[4], V. Zafiropulos[4], D. Anglos[4], P. Pouli[4], and C. Fotakis[4]

[1] Solomon R. Guggenheim Museum, New York, USA
chris_mcglinchey@moma.org
[2] The Museum Of Modern Art, New York, USA
[3] The Los Angeles County Museum of Art, California
[4] Foundation for Research and Technology-Hellas, Crete

Abstract. Recent results from laser cleaning studies on a painting from Ad Reinhardt's "Black Square" series (1960's) are presented. This painting, which travelled extensively, suffered various damages and at one stage was completely over-painted. Unfortunately, this overpaint is not reversible via traditional conservation methods and in this respect test cleanings have under a variety of more traditional conservation treatments. These subsequent treatments were minimally invasive and employed only small amounts of solvent or aqueous treatments, often through tissue. This has led to tests conducted using lasers as a possible means to remove the overpaint. In addition to visual examination of the cleaned areas and LIBS data, NIR and UV imaging analysis, FTIR and X-ray fluorescence spectroscopy, scanning electron microscopy have been used to characterize the effect of laser treatments on the exposed surface. Practical and technological challenges critical to the development of a laser protocol that achieves the uniform surface appearance that minimalist works of contemporary art demand will be discussed.

1 Introduction

In this work we're reporting on the efficacy of laser divestment of overpaint from a painting created in 1966. The painting in question is a minimalist work of art created by the New York based painter Ad Reinhardt. The painting was deemed unexhibitable and is now in the study collection of the Solomon R Guggenheim Museum. This project is a collaborative research effort that has demonstrated a possible method to reverse the damaged which was possible due to financial support from AXA Fine Art Insurers.

Ad Reinhardt started working on this particular method of painting in the late 1950's and continued until the late 1960s. The visual effect he created was a velvety surface that appeared, at first glance, like a large monochromatic black painting. Only after letting your eyes adjust to the dark could you begin to see the subtle difference in color shifts he constructed by squaring-out fields within the painting. He created many black paintings in this series. Some were as large as 60 inches square but not all were square in proportion

with the proportion of the painted areas also varied. Fortunately, we can compare similar paintings in pristine condition to gain a better sense of what the surface of the study painting looked like originally. What is common to all paintings from this series is that the overall dimension were divided into sub-squares where the black was subtly shifted in hue by the addition of a little red, blue and green pigment. Reinhardt was able to achieve the velvety appearance by draining the medium from tubes of Windsor and Newton Mars black. By removing the excess oil this would insure that the appearance would be matt. The draining procedure began by adding turpentine solvent to mars black oil paint in a jar and letting the oil dissolve up into the turpentine.

The overpaint consists of several layers of acrylic emulsion along with a transparent "sealant" layer between the overpaint and the original. For this series of paintings, Reinhardt produced a lean paint film by utilizing a drained oil process. Mock-ups with a paint layer stratigraphy similar to this complexity were first analyzed at LACMA's laser facility using nanosecond UV (308 nm), visible (532 nm) and IR (1064 nm) lasers. Based on the visual assessment of areas treated, some of the results effectively separated the acrylic emulsion from the lean oil paint film.

Autofluorescence characteristic of the overpaint was seen in the outer surface of cross sections of the study painting. In each square the topmost layers of the overpaint appear to be organic binder- in this case an acrylic emulsion that was identified by FTIR spectroscopy- over acrylic paint. The first layer of overpaint is a transparent organic layer void of pigment that we think was intended to serve a sealant layer to isolate the overpaint from the original. All the materials used in the overpaint were identified as acrylic emulsions by FTIR microscopy. In addition to viewing the cross-sections in visible light and ultraviolet, they were examined by SEM-EDS. So we know the elemental composition of each layer. The elements in each layer of overpaint were identified and the squares had between 8 and 12 layers of overpaint. The fact that the binders are dissimilar and pigments vary from layer to layer as proven by SEM and FTIR could be used to monitor the progress of overpaint removal. Further, one aspect about this painting that might make the application of laser treatment tenable is that this is a minimalist work. Consequently, once parameters are established the same protocol could, in theory, be used to remove large areas of overpaint. On the other hand, variations in film thickness may result in remaining artifacts after laser treatment. In short, we reached the phase where the research indicated that lasers might serve as a viable means to remove the overpaint.

2 Experimental Method for Work with the Nd:YAG

The first series of Laser cleaning tests were carried out at LACMA's laser facility with Meg Abraham. The value in going to Los Angeles was due to the fact that we could test UV, Vis and IR lasers. For a number of reasons,

it was difficult to justify the transportation of the actual study painting to Los Angeles so mock-ups reflecting the construction of the overpainted Reinhardt were created. Carol Stringari constructed the original part of the mock-up, that is, the Reinhardt technique part of the mock-up, nearly 20 years ago when she was researching his technique during the 1983 Reinhardt retrospective. The overpaint was more recent and the materials used for that phase were chosen on the basis of the FTIR results from the overpaint samples of the study painting. Once the overpaint was dry select samples were aged under accelerated conditions to better approximate the age of the actual study painting.

3 Results and Discussion

It was apparent from the findings at LACMA that the IR laser appeared to be the most effective at separating the overpaint from the oil paint. It is interesting to note that, in this instance, the paint did not divest in the form of plasma. Instead, it blistered and separated away from the oil paint and could be easily pulled away with tweezers. We thought one side-benefit to this manner of separation was that since it remained over the original it could protect the original from excess laser pulses. From a polymer thermal analysis perspective, these results suggested that the IR was leveraging the difference in heat capacity between the high organic content in the overpaint and the low organic content in the original. That is, the original being chiefly mars black (Ferro-ferric oxide), with a minimum amount of organic material functioning as binder has a much higher heat capacity than the organic rich overpaint. For the first time during the Reinhardt project we felt that this intractable problem might actually have a solution.

4 Experimental Method for Work with the Excimer

Following these preliminary findings further test cleanings of the painting were carried out at FORTH using an excimer laser (248 nm) and in some instances the lowest layers of overpaint were subsequently treated with an nanosecond IR laser (1064 nm). In all cases, elemental monitoring was conducted by laser induced breakdown spectroscopy (LIBS) prior to treatment and correlated to elemental data previously obtained from SEM data of cross-sections. While the bulk of the material was removed via laser, lower layers of overpaint or remaining residues were removed.

Prior to tests in the lab the group discussed the most feasible use of the facility at FORTH. It was decided to first explore the use of the UV excimer laser and attempt to clear down to the organic layer, what we referred to previously as the “sealant layer”, residing immediately above the overpaint. It was proposed that the Infrared laser might be useful as a follow-up technique

after excimer treatment. Based on our work at LACMA we thought the IR laser might prove useful for "blistering" off the last vestiges of sealant layer.

5 Results and Discussion

As worked progressed with the excimer laser it became apparent that there are two potential technical problems that could compound the treatment. First I'll talk about the ramifications of uneven overpaint layers. Reinhardt's technique retained the texture of the canvas. In contrast, it appears that the overpaint has smoothed out the surface. Consequently, there are thick and thin passages in the overpaint that could result in the original paint being exposed in areas where the overpaint is thin. In the week that we spent in Crete we thought initially this might be a significant problem, and initially advocated the development of masking agents to protect the areas that were being exposed too quickly. As worked progressed it appeared that this problem diminished, but it did not completely even out as we approached the original surface. The small bands on the left of the treated area correspond to areas that received fewer numbers of pulses and thus correspond to higher layers of overpaint.

One potential problem we encountered was the banding pattern that appeared at the edge of an area being treated. The beam profile may need to be cleaned up – if that is possible, or at least factored in the extent of overlap required in adjacent areas. We were able to minimize the problem by adjusting the overlap, yet we were not able to eliminate it. What might help is only treating a spot with a minimum of pulses before moving to an adjoining area. While this results in a more gradual process and minimizes the "hard-edge" that would otherwise be created we don't know how much extra time this would add to treating the entire painting.

We have yet to conclude whether or not there was any benefit to using the IR laser, but what immediately caught our attention was the bluing effect it had on the overpaint. In Fig. 1 you see a section that has been treated by the excimer to remove most of the overpaint but the IR has gone past the excimer treated area and into the top layers of the overpaint. We are not sure exactly what the bluing effect is, but we do know from SEM and XRF results that the top surface in this area contains both ultramarine and cadmium red. Perhaps this is an alteration of cadmium red, or possible a degradation of red dye undetected by the analytical methods used in this project. Though latter is unlikely since it would have likely influenced the UV fluorescence.

Interestingly, we also observed this to a lesser degree on mock-up samples that were light aged in a xenon arc fadeometer. The spectral power distribution reveals that xenon has a high output in the IR region between 800 and 1000 nm. Given the results from the fadeometer where the samples are never deprived of oxygen we don't think that this particular alteration is the type that requires a reducing atmosphere.

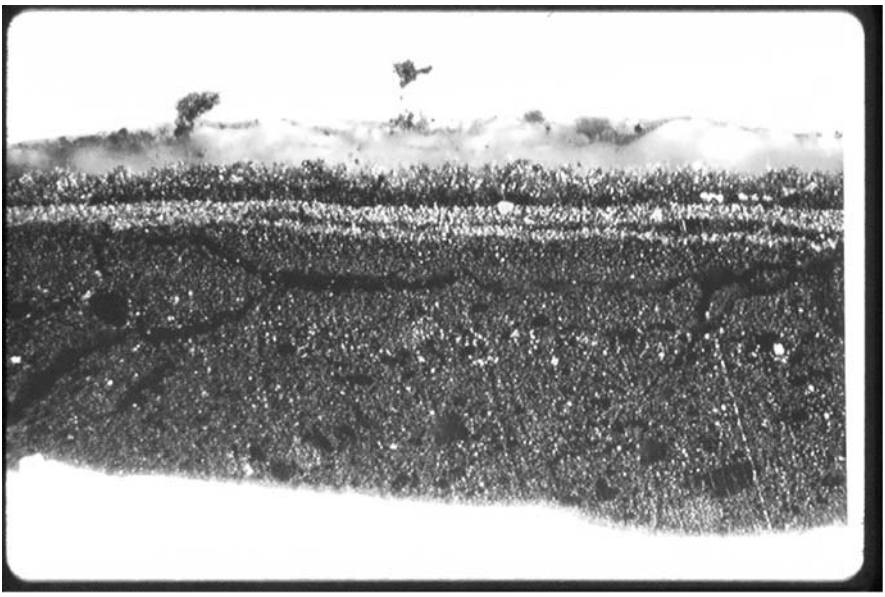

Fig. 1. The elements in each layer of overpaint were identifies in cross section and the squares had between 8 and 12 layers of overpaint

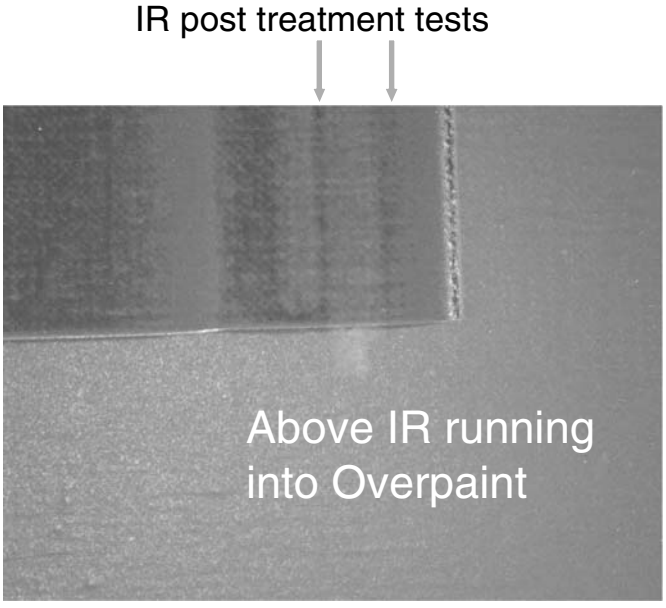

Fig. 2. A section that has been treated by the excimer to remove most of the overpaint but at on point, the IR has gone past the excimer treated area and into the top layers of the overpaint

After treatment the painting was examined at Guggenheim and Carol worked on the laser treated areas with gentle methods that one might consider using on a surface as delicate as a Reinhardt. These treatments consisted of gently rolling a slightly moistened cotton swab over treated surface. This simple treatment did appear to remove the remaining overpaint to expose a surface that looked like the surface of an original Reinhardt. I apologize for the quality of the image, but the extreme right shows the original surface after cleaning.

Based on the findings after cross-sections were examined, it does look as if the area treated has successfully removed the overpaint. We think the cracks you see here are preexisting and not the result of laser treatment. Cracks are not particularly surprising for a painting consisting of such a lean binder and could possibly be one of the contributing factors that lead to its overpainting. Further, element scans show the preponderance of iron, element which corresponds well with the original.

6 Conclusion

To conclude, scholars and contemporaries of Reinhardt have recently looked at the painting and do believe that the treated areas are far closer to his original visual effect. But this does not mean we should take this as our cue to wrap-up the technical investigation. We must continue to proceed with caution. It does look like the laser treatment for this painting is viable for small areas. But technical problems remain and although we have a much better idea on what to anticipate we must also be prepared for the unexpected if we are to carry this treatment out on a larger scale.

With that in mind, we must research the following as we move forward: first, verification that the subtle variations in hue originally created by Reinhardt are preserved during the treatment process and that the preexisting cracking, evident in cross sections, is not exacerbated by the treatment, second, that a protocol be developed that minimizes the potential risk of creating a visual banding effect in the appearance of the original surface as it is revealed, and third, a plan of action needs to be created that will allow the team to stop the process and deal with local variations in both texture and composition.

Acknowledgements

The group working on this project is large, but we could not have progressed as far as we have without the assistance of many others. Special mention needs to be made in the case of the scientists and technitions at FORTH and Odile Madden at LACMA. We would also like to acknowledge the National Center for Preservation Technology and Training, The Kress Foundation and Axis International for their support.

References

1. Lucy Lippard, *Ad Reinhardt*, 1966
2. Meg Abraham, Odile Madden, Thomas Learner, and Carole Havlik *Evaluation of the effects of laser irradiation on modern organic pigments* in LACONA V – this volume
3. R. Teule, H. Scholten, O. F. van den Brink, R. M. A. Heeren, V. Zafiropulos, R. Hesterman, M. Castillejo, M. Martin, U. Ullenius, I. Larsson, F. Guerra-Librero, A. Silva, H. Gouveia, and M. B. Albuquerque. *Controlled UV laser cleaining of painted artworks: a systematic effect study on egg tempera paint samples.* LACONA VI in Journal of Cultural Heritage, Vol. 4 Supplement 1 2003
4. O. Madden, M. Abraham, S. Scheerer, and L. Warren, *The effects of laser irradiation on varnishes polymers and waxes.* in LACONA V – this volume

Evaluation of Laser Cleaning of Parchment Documents with a Q-Switched Nd:YAG Laser at 1064, 532 and 266 nm

M. Vest[1], M. Cooper[2], and R. Larsen[1]

[1] School of Conservation Esplanaden 34, 1263 Copenhagen K., Denmark
mv@kons.dk
[2] The Conservation Centre, National Museums Liverpool, Whitechapel, Liverpool L1 6HZ, England
martin.cooper@liverpoolmuseums.org.uk

Abstract. Laser cleaning experiments with a short-pulsed Q-switched Nd:YAG laser at 1064, 532 and 266 nm were performed on new clean parchment and on artificially dirtied samples. Samples were analysed with optical microscopy, low vacuum scanning electron microscopy, shrinkage temperature measurements and colour measurements. Results show that at 266 nm, laser cleaning seems inappropriate. Laser cleaning at 532 nm showed promising results at around 0.5 J/cm^2 close to the cleaning threshold. Laser cleaning at 1064 nm resulted in a yellowish discoloration and at higher fluence levels surface damage.

1 Introduction

Within the world of conservation laser cleaning of parchment is still only at an experimental stage. Basic research into the effects of laser cleaning, which avoids the problems of physical contact with the parchment or the script, is valuable as traditional methods are either problematic or not completely satisfactory. Traditional cleaning procedures of parchment documents include dry as well as wet cleaning of the surface. Dry cleaning is carried out with different kinds of erasers, and depending on the nature of the object the cleaning process can cause changes in the surface structure. Most wet cleaning methods include the use of water mixed with a solvent and cause less mechanical pressure than the use of erasers. Nevertheless, after drying the surface can suffer from damages such as an increased transparency and changes in smoothness. Another major problem related to water based treatment of parchment is that a fibre structure, which appears intact upon visual observation can be transformed into a gelatinous substance by contact with water. The purpose of this research project is to establish whether a Nd:YAG laser can be safely used to clean historical parchment documents and if so, to establish the optimum parameters for different cases. This paper presents initial results.

2 Experimental Methods

Cleaning experiments were performed on new clean calf parchment (Z.H. de Groot, the Netherlands). The experiments were repeated on new parchment covered with artificially prepared dirt. According to the producer (Particle Technology Ltd., England) standard test dust (ASHRAE 52-76) consists of 23% carbon black, 72% SiO_2 with traces of Fe_2O_3, Al_2O_3, Cr_2O_3, Na and K Oxide and 5% cotton linters staple. The dust was mixed with 1% liquid paraffin and evenly distributed over the surface with a stiff brush. Additional sets of parchment samples were prepared with iron gall ink, applied with a brush, and then standard test dust was applied. The preparation method of iron gall ink was as given by Neevel [1]. Samples were allowed to oxidize for three days before cleaning.

The laser cleaning experiments were carried out using a short-pulsed Q-switched Nd:YAG laser (Phoenix 2+ Laser Cleaning System, Lynton Lasers Ltd, UK) which supplies laser radiation at wavelengths of 1064, 532 and 266 nm in pulses of 5–10 ns duration. At 1064 nm and 532 nm the laser beam was delivered via a jointed articulated arm and through a focusing lens in the handpiece. This was clamped at a fixed position above the sample, which was mounted on a moveable x-y table controlled by a computer. Laser cleaned samples of an approximate size of 20×20 mm were prepared by scanning the sample under the laser beam at a known rate; each area of surface was exposed to approximately 22 pulses, more than sufficient to remove surface dirt. The repetition rate was kept constant at 1.25 Hz and cleaning tests were performed at five average fluence levels (±20%): 0.3 J/cm^2, 0.5 J/cm^2, 1.0 J/cm^2, 1.5 J/cm^2 and 2.0 J/cm^2. At 266 nm the beam was delivered directly from a bench top assembly connected to the laser system by means of the articulated arm. At this wavelength the beam was horizontally delivered and the sample mounted vertically. Samples were kept still during cleaning, the cleaned area corresponded to beam size and received 22 pulses. Repetition rate was 1.25 Hz. Cleaning tests were performed at the fluence levels (±20%): 0.03 J/cm^2, 0.07 J/cm^2, 0.1 J/cm^2, 0.2 J/cm^2, 0.3 J/cm^2, 0.4 J/cm^2, 0.5 J/cm^2, 0.7 J/cm^2 and 1.3 J/cm^2.

The cleaned parchment surfaces were examined by optical microscopy and low vacuum scanning electron microscopy performed with a JSM-5310 LV SEM using non-conducting samples.

Colour changes on the laser cleaned parchment surface were measured with a Minolta CM-+632600d spectrophotometer. Measuring conditions were: d/8, SCE, UV included, backing material was photographic white board. Colour calculation: CIELAB, D65, 10°. Results are given as a mean of three measurements, Ø = 8 mm for the cleaned areas which were of limited size. The mean value for the clean parchment is calculated from 10 measurements taken across the skin which was used for the experiments.

Shrinkage temperature (T_s) measurements were performed on a Mettler FP82 Hot Stage, which is thermostatically controlled through a Mettler FP90

Central Processor. Measurements were performed in duplicate on collagen fibres from the parchment surface; fibres were immersed in water and heated at a rate of 2°C/minute. During heating the sample was observed through a stereo microscope at 40x magnification.

The shrinkage temperature (T_s) reflects the hydrothermal stability of the parchment collagen and is a measure of the degree of deterioration. The shrinkage process of fibres can be divided into sub-intervals with different levels of shrinkage activity. Start of the main shrinkage interval is the shrinkage temperature (T_s), which can be determined with an accuracy of ±2°C. Within each sub-interval the shrinkage activity is the observable shrinkage of fibres and its intensity depends on the degree of deterioration [2, 3].

3 Results and Discussion

Microscopic evaluation of laser cleaning tests at 266 nm showed that fibres were etched away or severely damaged. Fibre damage was observed on both clean and dirtied samples treated at a fluence level of 0.07 J/cm^2 and at all fluence levels above that. At the fluence level 1.3 J/cm^2 the surface was etched away and at lower fluence levels the fibrous surface was altered into a "melted" smooth area. On the treated clean samples a whitening of the surface appeared. Figure 1 shows a clean parchment surface treated at 0.7 J/cm^2 to the left and the surface is severely damaged compared to the untreated area to the right. At Fig. 2a cross section of the same sample shows the laminar structure of parchment and it appears that surface damage at the upper edge of the cross section has a very superficial character of less than 10 µm.

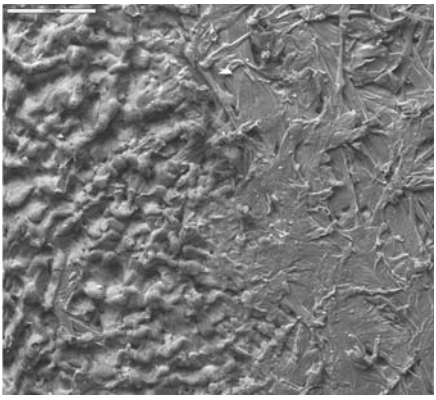

Fig. 1. Electron micrograph of a clean parchment surface treated at 0.7 J/cm^2 at 266 nm (*left*) and an untreated area (*right*)

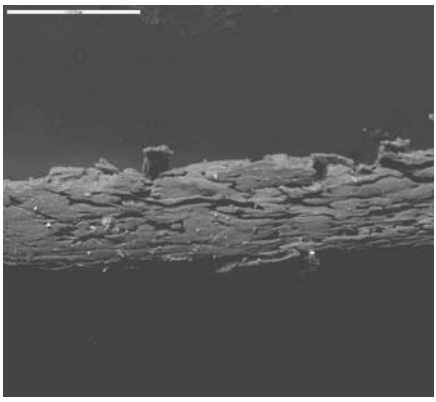

Fig. 2. Electron micrograph of a clean parchment cross section with the laser treated surface uppermost and the surface treated at 0.7 J/cm^2 at 266 nm

Cleaning threshold was around 0.5 J/cm^2 but the surface damage was still severe at that level. Shrinkage temperature measurements showed that the very thin layer of "melted" fibres in the surface were so damaged that they did not possess the ability of shrinkage. A larger bulk of fibres showed a shrinkage temperature level comparable to the untreated reference although the intensity of shrinkage was much lowered compared to the reference sample.

At 532 nm the surface topography was left undamaged up to 1.0 J/cm^2 but at 1.5 J/cm^2 and 2.0 J/cm^2 fibre damage was observed both on the dirtied and clean samples (Figs. 3a and 3b).

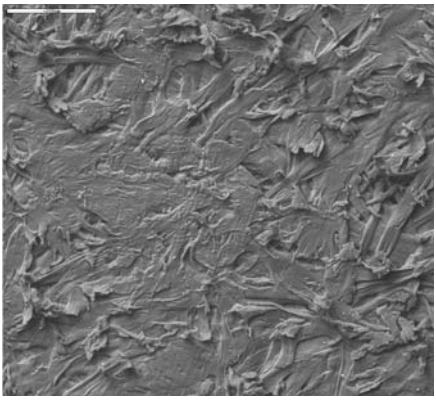

Fig. 3a. Electron micrograph of a clean untreated reference parchment for samples treated at 532 nm

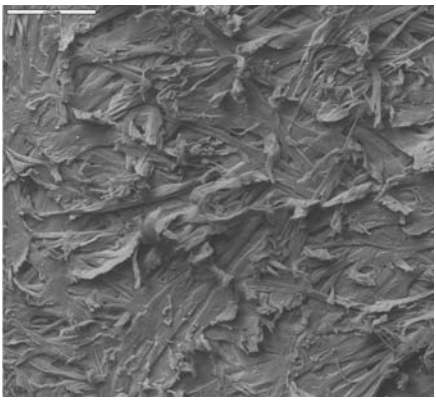

Fig. 3b. Electron micrograph of a clean parchment surface treated at 2.0J/cm^2 at 532 nm

At 1064 nm the surface topography was undamaged up to 1.5 J/cm^2 but at 2.0 J/cm^2 fibre damage was observed both on the dirtied and clean samples (Figs. 4a and 4b).

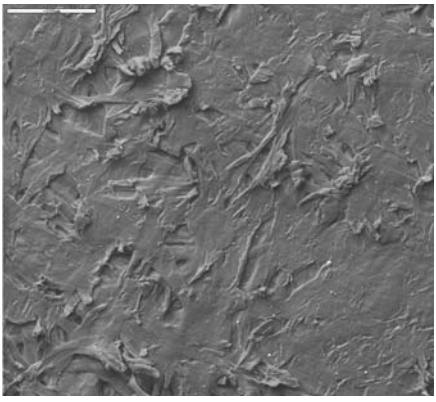

Fig. 4a. Electron micrograph of a clean untreated reference parchment for samples treated at 1064 nm

At 532 and 1064 nm the level of shrinkage temperature was measured on the clean sample sets after laser treatment at five fluence levels. At 532 nm the shrinkage temperature varied between 41.1°C and 46.4°C and at 1064 nm the shrinkage temperature varied between 43.7°C and 48.7°C (Table 1). An untreated reference sample had a shrinkage temperature of 44.5°C. Larsen et al. have measured the shrinkage temperature at ten different locations on new parchment and found it in the range 56.4°C–60.2°C. Triplicate measurements showed an average standard deviation of 1.11 for thirty measurements [2]. In

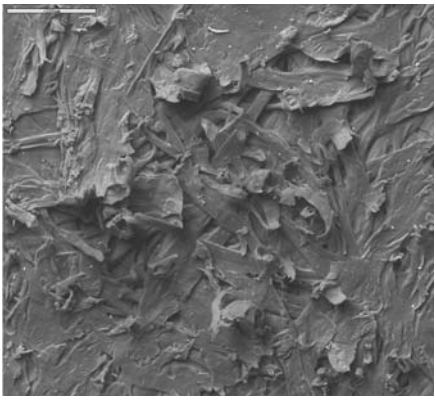

Fig. 4b. Electron micrograph of a clean parchment surface treated at 2.0 J/cm^2 at 1064 nm

Table 1. Shrinkage temperature, T_s (°C) with standard deviation (std) for laser treated clean parchment samples treated at 532 nm and 1065 nm at five fluence levels

	532 nm: T_s (std)	1064 nm T_s (std)
Reference		44.5 (1.2)
0.3 J/cm^2	43.0 (0.6)	48.7 (1.3)
0.5 J/cm^2	46.4 (0.3)	43.7 (1.7)
1.0 J/cm^2	42.0 (2.1)	44.5 (0.7)
1.5 J/cm^2	44.6 (0.6)	47.7 (0.2)
2.0 J/cm^2	41.1 (1.0)	44.3 (0.1)

the present experiment the size of each laser treated sample and the reference sample was 2×2 cm taken from different areas of the skin. Consequently, fibre samples are from different areas, and it is likely that a possible decrease in shrinkage temperature after laser cleaning will be overshadowed by the natural variation across the skin. Therefore, further measurements must be performed on fibre samples taken from the same area before and after laser cleaning. Furthermore, measurements must be performed on the dirtied sample set to investigate the influence of laser cleaning on the hydrothermal stability.

Colour measurements on samples cleaned at 532 nm showed that removal of dirt was accompanied by a slightly darker surface at 0.3 J/cm^2. At the three highest fluence levels, 1.0 J/cm^2, 1.5 J/cm^2 and 2.0 J/cm^2, the surface was bleached. This is reflected in an increase of the L* value compared to the reference as seen in Fig. 5. Cleaning at 0.5 J/cm^2 gave results closest to the untreated clean reference, although the b* value showed a slight increase (Fig. 6).

Colour measurements on samples cleaned at 1064 nm showed that removal of dirt was accompanied by a slightly darker surface at the three lowest fluence

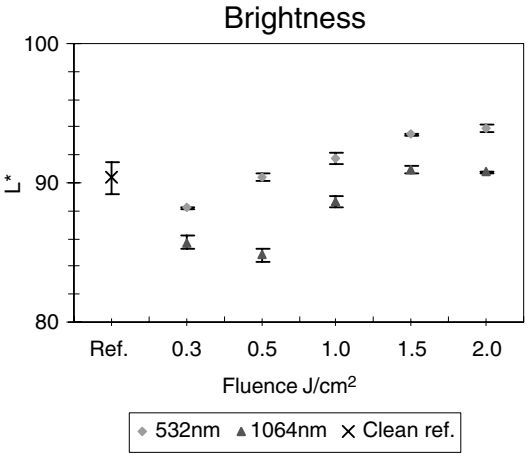

Fig. 5. Colour changes (L* values) for dirtied samples after laser cleaning at 532 nm and 1064 nm at five fluence levels; included is a clean untreated reference. L* value for a dirtied reference is 34.77 (std: 0.83)

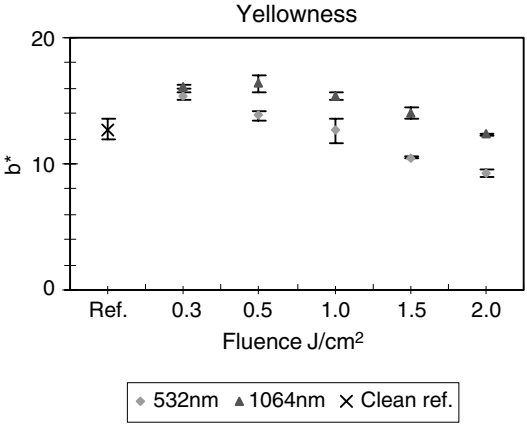

Fig. 6. Colour changes (b* values) for dirtied samples after cleaning at 532 nm and 1064 nm at fice fluence levels; included is a clean untreated reference. b* value for a dirtied reference is 0.46 (std: 0.38)

levels, seen as a decrease in the L* value. At 1.5 J/cm^2 and 2.0 J/cm^2, however, the L* value reached the level of the clean untreated reference (Fig. 5). The b* value showed a marked increase up to a fluence level of 1.5 J/cm^2 compared to the clean untreated reference (Fig. 6). At 2.0 J/cm^2 the b* value was the same as for the clean reference. Clean parchment samples, which were treated at the same fluence levels as dirtied samples showed a slight increase in L* but the b* values were unchanged. This shows that yellowing

of the surface occurs only as a result of removal of dirt as reported for other substrates subjected to laser cleaning at 1064 nm [4].

Severe damage to the layer of iron gall ink was found at all samples treated at 266, 532 and 1064 nm. However, this may be due to the freshly prepared iron gall ink which has different properties compared to historic script which is often more brownish. Furthermore the number of pulses was set higher than would normally be used in a practical cleaning situation. Previous work showed an undamaged historic iron gall ink script after cleaning at 1064 nm, 1.25 Hz, 0.4 J/cm^2 and with very few pulses [5]. Cleaning results on new iron gall ink showed that future studies must focus on samples, which have undergone accelerated ageing or on historic samples.

A summary of the initial results obtained at 532 nm and 1064 nm is given in Table 2.

Table 2. Summary of changes found on dirtied and clean parchment samples treated at 532 nm and 1064 nm at five fluence levels: cleaning effect, damage to surface structure and colour changes

	Wavelength			
	532 nm		1064 nm	
Fluence (J/cm^2)	Dirtied surface	Clean surface	Dirtied surface	Clean surface
0.3	Removal of dirt Slightly yellow	Slightly brighter	Removal of dirt Yellowing	No changes
0.5	Removal of dirt Slightly yellow	Slightly brighter	Removal of dirt Yellowing	No changes
1.0	Removal of dirt Brighter	Slightly brighter	Removal of dirt Yellowing	Slightly brighter
1.5	Removal of dirt Surface damage Brighter	Surface damage Brighter	Removal of dirt Yellowing	Slightly brighter
2.0	Removal of dirt Surface damage Brighter	Surface damage Brighter	Removal of dirt Surface damage	Surface damage Slightly brighter

4 Conclusions

Laser cleaning at 266 nm caused severe damage to the parchment surface and seems to be inappropriate for practical laser cleaning, this is in agreement with previous findings [6]. Cleaning results at 532 nm showed promising results around 0.5 J/cm^2, as first results did not show laser induced changes in the parchment at fluence levels close to the cleaning threshold. At 1064 nm the yellowing of the cleaned surface was found on samples cleaned at fluence levels up to 1.5 J/cm^2. The dirtied sample cleaned at a fluence level of 2.0 J/cm^2 was comparable to the clean reference with respect to colour but fibre damage in the surface was observed.

Acknowledgements

Thanks to Tine Rauff and Katrine Minddal, School of Conservation for measuring shrinkage temperatures. The project was financially supported by Direktør dr. techn. A.N. Neergaards og hustrus Fond, Denmark and Christian og Ottilia Brorsons Rejselegat, Denmark.

References

1. J. G. Neevel, Restaurator **16**, 143–160, 1995
2. R. Larsen, D. V. Poulsen, and M. Vest, in *Microanalysis of Parchment*, Edited by R. Larsen, London, 55–62, 2002
3. R. Larsen, M. Vest, D. V. Poulsen, and U. B. Kejser, in *Environment Leather Project*, Edited by R. Larsen, Copenhagen, 145–159, 1996
4. V. Vergès-Belmin and C. Dignard, Journal of Cultural Heritage **4**, 238s–244s, 2003
5. M. Cooper, S. Sportun, A. Stewart, M. Vest, R. Larsen, and D. V. Poulsen, The Conservator **24**, 71–79, 2000
6. S. Sportun, M. Cooper, A. Stewart, M. Vest, R. Larsen, and D. V. Poulsen, Journal of Cultural Heritage **1**, 225–232, 2000

Cleaning of Soiled White Feathers Using the Nd:YAG Laser and Traditional Methods

C. Dignard[1], W.-F. Lai[2], N. Binnie[1], G. Young[1], M. Abraham[3], and S. Scheerer[4]

[1] Canadian Conservation Institute, 1030 Innes Road, Ottawa, Ontario K1A 0M5 Canada
carole_dignard@pch.gc.ca
nancy_binnie@pch.gc.ca
gregory_young@pch.gc.ca

[2] Central Conservation Section, LCSDHK, 4/F HK Heritage Museum, 1 Man Lam Road, Sha Tin, Hong Kong, China
wflai@lcsd.gov.hk

[3] Los Angeles County Museum of Art, 5905 Wilsire Blvd, Los Angeles, CA 90036, USA
mabraham@LACMA.org

[4] School of Bioscience, University of Wales, P.O. Box 915, Cardiff CF10 3TL, Wales, UK
stefscheerer@yahoo.de

Abstract. Cleaning of soot-soiled white feathers was assessed using the Nd:YAG laser (1064 and 532 nm, with or without added water; 355 nm, no added water) and various traditional (vacuum, solvent and detergent) methods. Physical damage occurred at 355 nm starting at 0.12 J/cm^2. Soiled areas were often yellower after cleaning at most laser parameters tested, but not using traditional methods. The best laser result was using 532 nm at 0.39 J/cm^2. XPS analysis found that the 164 eV binding energy for sulphur, corresponding to the disulphide bond, disappeared upon laser-cleaning soiled areas in dry conditions (no added water) at all wavelengths, suggesting chemical damage or masking by a residue.

1 Introduction

It is known that Nd:YAG laser soil removal from various substrates can result in a yellower surface [1]. This was recently also found for wool, a keratin similar to feather, and linked to chemical damage [2]. Laser studies on coloured or yellowed feathers have found no physical damage nor any discoloration occurring [3–6], however, discoloration can be difficult to detect on coloured substrates. This study assessed Nd:YAG laser cleaning of white, naturally soiled feathers at 1064, 532 and 355 nm, and with or without added water. Physical damage, cleanliness and colour changes were compared to results using various traditional cleaning methods. Surface damage was assessed by X-ray photoelectron spectroscopy.

2 Experimental Methods

White feathers were sampled from 2 pelican specimens dating from the 1950s which were soiled with soot on their exposed surface during a fire in 1990 [7]. The interest in using these feathers soiled from a fire was that they provided true-life examples of what a conservator may need to clean; a disadvantage, however, was that each feather was slightly different in condition and in the quantity of soot which was deposited on it. Where the feathers were not soiled because they were covered by other overlapping feathers, these areas appeared white, although closer inspection showed them to be lightly dusty. The feathers' structure was disturbed from years of unprotected museum exposure, therefore only gross physical damage could be assessed. The number of exposed, soiled feathers available were limited, therefore limiting the number of tests that could be replicated.

Nine traditional cleaning methods were investigated: vacuum cleaning (mini-vacuum cleaner used at a low suction and soft brush); water; 1,1,1 trichloroethane; white spirit; ethanol; 1% Vulpex^{R} (alkaline methylcyclohexyl oleate, an anionic detergent) in ethanol, 1,1,1 trichloroethane or white spirit; 0.5% Triton^{R} XL-80N (alkyloxy-polyethylene-oxypolypropyleneoxy ethanol, a non-ionic surfactant) in water. Wet cleaning was carried out by brushing the solution along the barbs (from rachis to edge) with a soft brush while the feather was laid flat on a blotting paper, soot upwards. The blotter was changed and the treatment was repeated until no more soot transfered onto the blotting paper. One feather was cleaned per method.

A "Coherent" (California) Q-switched Nd:YAG laser (top hat beam profile, 3 ns pulse length) was used, with Edmond Scientific Plano-Concave lenses to diverge the beam. The energy was measured using a Coherent "LaserMate P" energy meter, and the beam size, using unplasticized polyvinylchloride (UPVC) sheet. One to three spots were tested per set of parameters.

The feathers were examined using a Zeiss OpMi-1 microscope. Areas of interest were mounted with carbon tape on aluminium planchets and gold-coated to ensure conductivity, then examined using a Hitachi S-530 scanning electron microscope, with the working distance being 8 mm and the accelerating voltage 20 kV.

Colour was measured using a Minolta CM-2022 spectrophotometer with D65 illumination, 10° Standard Observer and specular reflection excluded. A minimum of 3 measurements was taken at each location (4 mm circular area) and averaged. White paper was placed under each feather to provide a standard background, thus the colour obtained is relative (there is a contribution from the surface below).

X-Ray photoelectron spectroscopy was carried out by Kratos Ultra XPS using monochromated A1 K α X-radiation and charge neutralization since the sample was not conducting. The sample was cut and mounted on an analysis stub with carbon tape. Each element detected was run at high resolution for

peak postion, shape and for quantification. Two areas were analyzed on each sample and the average was taken in atomic percent. The depth of detection was 7.5 nm.

3 Results and Discussion

3.1 Physical Damage

The traditional cleaning methods did not show objectionable damage, only small-scale disruption of the barbules. Aqueous treatments could cause some larger-scale disruption (barbs disinterlocking) but this could usually be restored through preening. However in one case, washing a delicate feather with Triton XL in water resulted in the structure totally opening up, and the original structure could not be restored by preening. For the laser-cleaned feathers, examination using the microscope and SEM revealed no physical damage except in the sooted areas cleaned at 355 nm in the higher fluence range tested: at 0.12 J/cm^2 barbules became frizzled at the centre of the laser spot over an area covering 6–7 barbs, while at 0.16 J/cm^2 the damage was more severe and spread over 9–10 barbs, and was noticeable to the naked eye as a tiny spot of disruption which appeared yellow.

3.2 Cleanliness, Appearance and Colour Measurements

Colorimetric results are shown in Fig. 1. For the laser cleaned spots, instead of before treatment measurements, soot-soiled spots adjacent to those laser cleaned were used for comparison. Because the feathers were originally soiled in a fire and not in an experimentally controlled fashion, each feather before cleaning had a slightly different quantity of soiling on their surface, and therefore a slightly different colour, as can be seen in Fig. 1, but this variation remained within a certain range: the b* value ranged between 5 and 12 units, the a* was always less than 1 unit, and the L* value ranged between 62 and 75 units. Cleaning black soiling from a white substrate was expected to increase the L* range while leaving the chroma (a* and b*) ranges unchanged. This was indeed the case after cleaning using the traditional methods: the feathers appeared white to light grey and had a significantly higher L* value, with no significant chroma change (Δa* and Δb*). The feather cleaned with Triton XL in water appeared the cleanest, while those cleaned with Vulpex in either white spirits or 1,1,1-trichloroethane gave good results but did not appear as white. This is confirmed by their L* values after cleaning, which are the highest (close to 90) for these three solutions. The next best cleaning results were visually found to be with white spirits, ethanol and 1% Vulpex/ethanol, which also is in general agreement with the L* values (close to 85). Vacuum cleaning was ineffective. Both trichloroethane and water alone did not clean very well, the latter due to poor wetting.

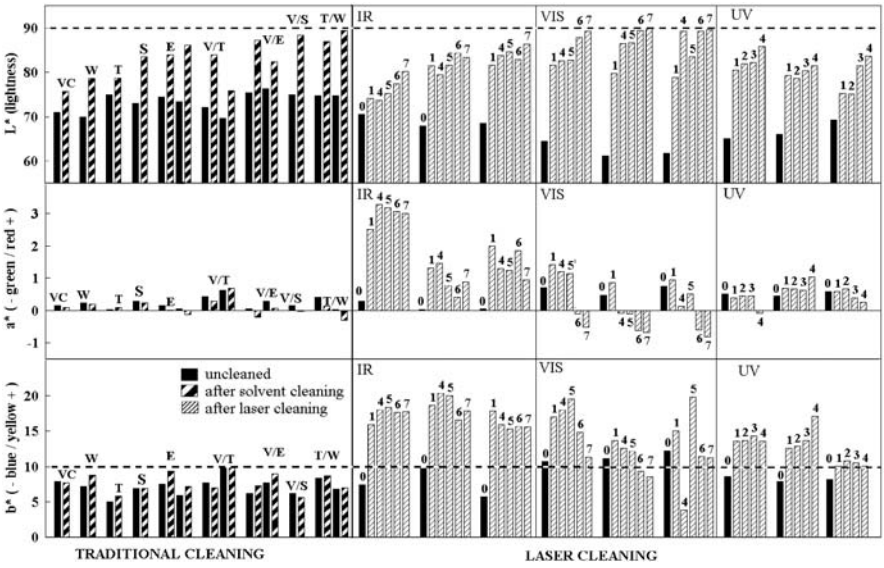

Fig. 1. Chromaticity values on soiled feathers cleaned using traditional methods and the laser at 1064 nm (IR), 532 nm (VIS) and 355 nm (UV). Traditional methods: black bars = before treatment; VC = vacuum cleaning; W = water; T = 1,1,1-trichloroethane; S = white spirit; E = ethanol; V/E = 1% Vulpex in ethanol; V/T = 1% Vulpex in 1,1,1-trichloroethane; V/S = 1% Vulpex in white spirit; T/W = 0.5% Triton XL in water. Laser cleaning at 3 Hz, 100 pulsed: 0 = uncleaned, soot-soiled area adjacent to laser-cleaned areas; 1 = 0.08 J/cm^2; 2 = 0.10 J/cm^2; 3 = 0.12 J/cm^2; 4 = 0.16 J/cm^2; 5 = 0.24 J/cm^2; 6 = 0.31 J/cm^2; 7 = 0.39 J/cm^2

In the case of the soiled laser cleaned samples, at all wavelengths increasing the fluence usually led to a progressive increase in L*, indicating progressive soot removal. Overall the best L* results were obtained using 532 nm: at the two highest fluences tested, L* is comparable to the best levels obtained using traditional methods (L* = 90). However, laser-cleaned surfaces often were discolored: at all wavelengths the b* value is usually higher than the range measured before treatment (5–12 units), sometimes going as high as 20 units. In comparison, the b* range for the traditionally cleaned samples remained identical to the before-cleaning range of 5–12 units. As well, the a* values on the IR samples were high; visually they appeared yellow-orange. Samples cleaned at 355 nm visually appeared cream-coloured, uneven in tone and spotty, perhaps due to defects in the focussing lens. The discoloration was not necessarily progressive: it often happened significantly even at the lowest fluence level and did not progress much further as the fluence was increased. The least discoloration was found with 532 nm at the two highest fluences tested: a* and b* are low and comparable to the ranges measured before treatment, as well as after traditional cleaning. Visually, the spots

cleaned at 532 nm appeared clean and white but with a cream-coloured halo on the perimeter which could not be measured with the colorimeter. It is not known whether cleaning by scanning over a larger area would produce this halo.

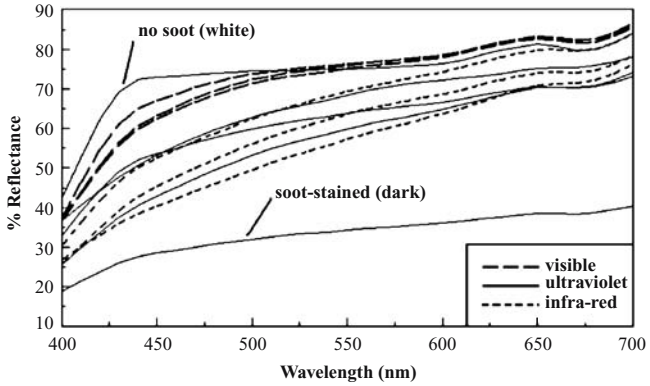

Fig. 2. Reflectance spectra of 3 sets of sooted spots on feathers, cleaned in the visible (532 nm), ultraviolet (355 nm) and infra-red (1064 nm). Fluences: at 532 and 1064 nm: 0.39 J/cm^2; at 355 nm: 0.16 J/cm^2. An unsooted and dusty, and a sooted feather are also shown

Figure 2 gives the reflectance spectra for the triplicate sets of soot-soiled laser cleaned spots at the fluence that gave the best cleaning result. At all wavelengths, the reflectance improved with respect to the uncleaned, soot-soiled sample, especially toward the red end of the spectra, but it never reached the level of the spectra of the non-sooted, lightly dusty areas. The best results were obtained using 532 nm. Nonetheless, for this wavelength the spectra does not follow the same curve as that of the non-sooted, dusty feather: reflectance is lower in the blue end of the spectrum and slightly higher in the red end of the spectrum. This means that the appearance after laser cleaning at this wavelength is different to that of a non-sooted, untreated feather. Using 1064 nm and 355 nm, the spectra consistently remained even lower, especially in the blue end of the spectra but even in the red end as well.

Laser cleaning was also tested at the same parameters on non-sooted but lightly dusty areas, to assess whether the discoloration that was obtained after laser-cleaning the soot-soiled samples was linked to the presence of the soot, or if it was due only to the exposure to laser irradiation. (Note that no totally unsoiled feathers were available.). For all wavelengths, the non-sooted, lightly dusty samples after laser cleaning became cleaner and white with no apparent discoloration. The chroma (a* and b*) values were lower than, or

at the most equal to, the values obtained for the soot-soiled and laser cleaned areas.

Further tests were carried out on soot-soiled samples at 1064 and 532 nm as a preliminary survey to determine whether it was possible to obtain some degree of cleaning with no yellowing using different parameters than those in Fig. 1, and in particular, using lower fluences, water-assisted conditions, and different frequencies and number of pulses. Water-assisted laser cleaning was carried out by applying clean distilled water on the soiled feathers using a cotton swab, immediately prior to laser irradiation. The swab was dipped in the water and gently dabbed onto the surface to transfer a small but visible amount of water to the feather surface. Colour measurements for these sets of tests are shown in Fig. 3 Two sets of the triplicate tests presented in Fig. 1 (0.31 J/cm^2 with not water, one set at 1064 nm, the other at 532 nm) are reproduced here as benchmarks, for comparative purposes, recall that the set at 532 nm were among the best results, with L* close to 90 and very little discoloration. None of the other tests shown in Fig. 3 came close to matching this quality of cleaning, and further tests were not pursued. It should be noted that there were not enough samples to repeat this new round of tests to check reproducibility, nor to carry out the tests with all parameters independantly

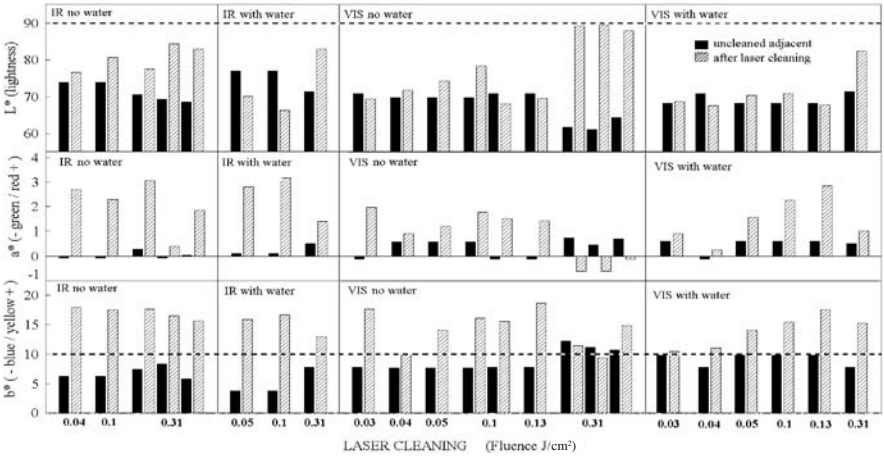

Fig. 3. Chromaticity values of sooted spots laser cleaned with and without water. Adjacent soot-soiled spots (non-laser cleaned) are given as reference. Parameters: 0.03 J/cm^2 = 10 Hz 10,000 pulses (p.); 0.04 J/cm^2 = (IR) 10 Hz 300 p., (VIS) 10 Hz 600 p.; 0.05 J/cm^2 = (IR) 10 Hz 100 p., (VIS no water) 10 Hz 300 p., (VIS with water) 10 Hz 200 p.; 0.10 J/cm2 = (IR) 10 Hz 100 p., (VIS no water) 1st test 10 Hz 100 p., 2nd test 1 p., (VIS with water) 10 Hz 200 p.; 0.13 J/cm^2 = (no water) 1 Hz 2 p., (with water) 10 Hz 50 p.; 0.31 J/cm^2 = (no water) (these results are the same as Tests #6 (IR) and (VIS) shown in Fig. 1); 3 Hz 100 p., (with water) 3 Hz 20 p

controlled, and so firm conclusions should not be drawn. Further tests would be required.

3.3 X-ray Photoelectron Spectroscopy

The XPS results are shown in Fig. 4. It should be noted that the soiled and dry laser-cleaned samples in this figure (the 4th through to the 9th samples shown) correspond to the samples measured colorimetrically in Fig. 1 at the same laser cleaning parameters (they are the first sample of the 3 in the triplicate tests). The duplicate measurements presented in Fig. 4 at 532 nm at 0.24 J/cm^2, are the same as the first two measurements at that fluence level and wavelength, of the triplicate set shown in Fig. 1. The last two tests presented in Fig. 4 at 1064 nm using water assisted conditions correspond to the samples identified with the same parameters in Fig. 3.

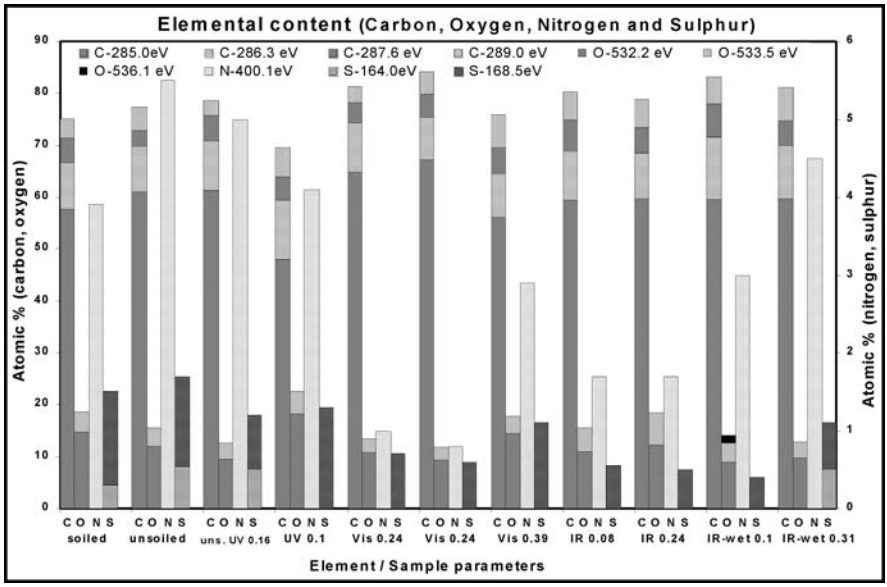

Fig. 4. Content (atomic %) and binding energies (eV) of carbon (C), oxygen (O), nitrogen (N) and sulphur (S) found at the surface of control and laser cleaned feathers. Hydrogen not included in the 100%. Soiled = soot-soiled, no treatment. Unsoiled = no soot, dusty, no treatment. Uns. UV 0.16 = unsoiled, 355 nm, 0.16 J/cm^2. The following tests on soiled areas were laser cleaned at 3 Hz, 100 pulses unless otherwise specified: UV 0.1 = 355 nm, 0.1 J/cm^2; Vis 0.24 = 532 nm, 0.24 J/cm^2; Vis. 0.39 = 532 nm, 0.39 J/cm^2; IR 0.08 = 1064 nm, 0.08 J/cm^2; IR 0.24=1064 nm, 0.24 J/cm^2; IR-wet 0.1 = 1064 nm with water, 0.1 J/cm^2 at 10 Hz, 100 pulses, IR-wet 0.31 = 1064 nm with water, 0.31 J/cm^2 at 3 Hz, 20 pulses

The non-treated feather surface was expected to consist of keratin altered by weathering and ageing [8], dust, soot and oils from preening and handling. The soot-soiled sample contained less carbon but more oxygen than the non-sooted dusty sample; a possible explanation is that some oxygen was bound to the surface of the carbon-rich soot agglomerates, as can be found, along with nitrogen and sulphur, on carbon black [9]. No specific conclusion can be drawn from the variations in elemental composition after the various laser-cleaning tests since it is possible that the soot contained the same four major elements as in the aged keratin, each in unknown proportions: thus theses variations could be due to partial soot removal, masking of the substrate by redeposition of a chemically-altered soot layer, or chemical change to the substrate.

The data collected on the binding energies for sulphur before and after irradiation are of interest. Sulphur's 164 eV binding energy corresponds to cystine's disulphide bond in keratin, while the 168 eV bond indicates an increased oxidation state [10, 11]. The structurally important disulphide bond is known to be affected by various agents including heat, UV and visible radiation and electric (plasma) discharge, resulting in changes in various physical characteristics, but is not usually associated with yellowing [8, 12]. Both of these binding energies are present in the untreated, sooted or unsooted samples, which is expected considering the pelican specimen's display history. Both binding energies remain as well in the case of the non-sooted sample irradiated at 355 nm. In the case of the sooted samples, however, the 164 eV peak disappeared after dry laser cleaning at all wavelengths. This change indicates that something is happening to, or onto, the feather substrate which contains the disulphide bond, when samples are irradiated. It cannot simply be that dirt is lifted off, since this would expose more of the disulphide bond, not less. Possible explanations are that the keratin surface is becoming masked by a residue that does not contain sulphur at 164 eV, and /or that chemical damage occurs to the disulphide bond. Since it was only possible to carry out one test in duplicate (VIS at 0.24 J/cm^2), further tests would be needed to confirm the reproducibility of these results.

4 Conclusions

While traditional methods cleaned soot-soiled feathers well without causing discoloration, Nd:YAG laser cleaning was more problematic. Under dry conditions (no added water), at 355 nm physical damage occurred as of 0.12 J/cm^2, and lower fluences did not give good results. At 1064 nm yellowing was pronounced at all fluences, even low. The best results were at 532 nm at the highest fluence tested (0.39 J/cm^2): L*, a*, b* values were similar to those of traditional methods. Laser cleaned unsoiled dusty feathers did not significantly yellow. The data collected on laser cleaning using water-assisted conditions was insufficient to draw conclusions. XPS showed that sulphur at

164 eV, corresponding to the disulphide bond, disappeared when soot-soiled samples were laser-cleaned at all wavelengths under dry conditions (no added water); only a peak at 168 eV remained. This may be due to chemical damage or to a residue masking the keratin surface.

Acknowledgements

The authors thank C. Bigras, K. Helwig, J. Powell, S. Tse and R.S. Williams of the Canadian Conservation Institute for their input; G. Pleizier, formerly of the National Research Council of Canada, for the XPS analysis; L. Bourbonnais for the XPS graph; and the National Center for Preservation Technology and Training, Natchitoches, USA for funding this work.

References

1. V. Vergès-Belmin and C. Dignard, J. of Cultural Heritage **4**, 238s, 2003
2. M. Strlic, J. Kolar, V.-S. Selih, and M. Marincek, Applied Surface Science **207**, 236, 2003
3. G. Pacaud and J. Lemaire, La Lettre de l'OCIM **67**, 21, 2000
4. M. R. Solajic, B. Pretzel, M. Cooper, J. H. Townsend, T. Seddon, J. Ruppel, J. Ostapkowicz, and T. Parker, in *Preprints of the 13th ICOM-CC Triennial Meeting*, Edited by R. Vontobel, Vol. 2, 701, 2002, James & James Ltd, London
5. M. R. Solajic, M. Cooper, T. Seddon, J. Ruppel, J. Ostapkowicz, and T. Parker, in *The Conservation of fur, feather and skin*, Edited by M. M. Wright, 69, 2002
6. S. Schaeuffelhut, H. Tello, and S. Schneider, in *The Conservation of fur, feather and skin*, Edited by M. M. Wright, 62, 2002
7. S. Spafford-Ricci and F. Graham, J.AIC **39**, 15, 2000
8. J. A. Maclaren and B. Milligan, *Wool Science: The Chemical Reactivity of the Wool Fibre*, Science Press, Marrickville (Australia), 1981
9. Canadian Centre for Occupational Health and Safety, *Carbon black*, CHEMINFO Database, 1997–2000 (http://www.ccohs.ca/oshanswers/chemicals/chem_profiles/carbonbl/basic_cb.html)
10. C. M. Carr, I. H. Leaver, and A. E. Hughes, Textile Research Journal **56**(7), 457, 1986
11. M. M. Millard, in *Contemporary Topics in Analytical and Clinical Chemistry*, Edited by D. M. Hercules, G. M. Hieftje, L. R. Snyder and M. A. Evenson,1, 1978
12. I. L.Weatherall, in *Historic Textiles, Papers, and Polymers in Museums*, Edited by J. M. Cardamone and M. T. Baker, ACS Symposium Series 779, 115, 2001

Surface Analysis of the Laser Cleaned Metal Threads

M. Sokhan[1], F. Hartog[2], and D. McPhail[1]

[1] Imperial College London, London, UK
marina.sokhan@imperial.ac.uk
[2] Victoria & Albert Museum, London, UK

Abstract. The laser cleaning of the tarnished silver threads was carried out using Nd:YAG laser radiation at IR (1064 nm) and visible wavelengths (532 nm). The preliminary tests were made on the piece of silk with the silver embroidery with the clean and tarnished areas. FIBS and SIMS analysis were used for analysing the condition of the surface before and after laser irradiation. It was found that irradiation below 0.4 J/cm^{-2} and higher than 1.0 J/cm^{-2} fluences aggravates the process of tarnishing and leads to the yellowing effect. The results of preliminary tests were used for finding the optimum cleaning regime for the laser cleaning of the real museum artefact: "Women Riding Jacket" dated to the beginning of 18th century.

1 Introduction

During the recent years the laser cleaning technique has proved to be one of the most successful methods in the cleaning of the different kinds of materials amongst them metals [1, 2]. The conventional methods of cleaning metals such as mechanical polishing or chemical removing of the corrosion from the surface are not applicable to the metal decorations on the fabrics such as wool, silk or cotton. One of the types of metal decorations on the textile is metal threads that could be woven in fabric itself or could be a part of the surface embroidery. As the metal thread consists of the metal foil of paper-like thickness spun around a core rod made of silk, cotton or linen, any metal cleaning will affect durability of rods. As it was shown by previous researchers the laser cleaning has number of advantages over the mechanical or chemical cleaning techniques for the metal threads [3, 4]. In this paper, we demonstrate the results of the laser cleaning of the tarnished silver thread using the surface analysis techniques. The Lynton Q-switch Nd:YAG laser was used for the radiation with wavelengths of 1064 nm (basic mode) and 532 nm (3rd harmonic) during the laser trials. The results were monitored with FEI 200 FIB equipped with SIMS attachment (focused ion beam workstation and secondary ion mass spectrometry). After detailed analysis of the silver and silk rods we applied the chosen regime to the cleaning of the 18th century riding jacket from the Victoria & Albert Museum Collection, London.

2 Experimental

The first initial cleaning tests were carried out on the silver thread embroidery (Fig. 1) on the piece of the woman silk dress dated approximately 18th century with Q-switch Nd:YAG laser emitting at 1064 nm and 532 nm with parameters: repetition rate 10 Hz, pulse duration 6 ns, fluences from 0.2 J/cm^{-2} to 2 J/cm^{-2}. The areas with the tarnished silver and with clean and shiny silver were submitted to the same cleaning regimes and the results were assessed with FIB-SIMS 200TEM from FEI Company.

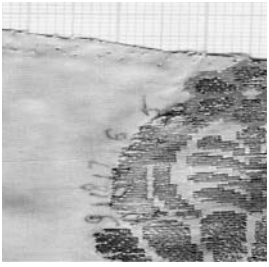

Fig. 1. The piece of the silk with silver thread embroidery

A focused ion beam workstation (FIB) operates similar to a scanning electron microscope as the images are formed by the spattered secondary electrons but the FIB uses gallium ions from a field emission liquid metal ion (FE-LMI) source.

The primary gallium ions beam has energy of 30 kV and could be controlled through a series of apertures that give beam current from 1 pA to 20000 pA. The incidence angle of the primary beam is 90°. The maximum current reached is 10^8 A/cm^{-2}. The vertical and lateral resolutions are 5 nm. The sensitivity is 1 ppt.

For imaging, we used 10 pA as a primary beam current so that the monolayer lifetime is long enough and that the surface is not damaged by bombardment. The mass spectra were obtained on the areas roughly $60 \times 60\,\mu m^2$ (magnification ×5000) with average five scanning. Static SIMS was used with a rather low beam current 300 pA and from areas not previously damaged so the surface monolayer lifetime is well above the time required for analysis. It offers the possibility of studying the elemental composition but also the chemical structure of the surface. The surface chosen allows us to have a high ion yield and a scanned surface big enough to be representative. The optimal regime was applied to the unique artefact (Riding Jacket) from the Victoria & Albert Museum Collection (Fig. 2). Two loose metal threads from the Riding Jacket were analysed prior and after laser treatment.

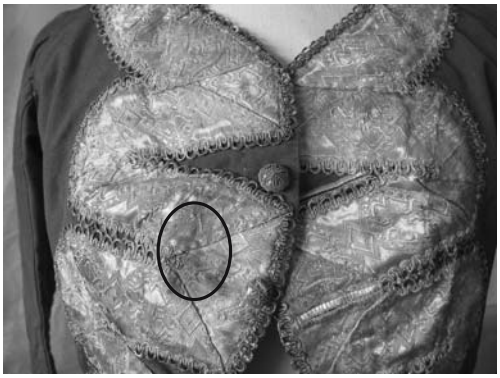

Fig. 2. The 18th century Riding Jacket

3 Results and Discussion

The final goal of this research was to find the optimal regime for the cleaning of the dark area on the silver thread embroidery on the woman wool riding jacket using surface analysis techniques for the assessment. It presented particular difficulties as the soiled spot on the front of the jacket appeared not as a result of the natural tarnishing of silver but as the result of the silver contamination from the unknown object that was attached to the area. The rest of the silver threads have natural tarnishing with touch of yellowish colour and the soiled spot after cleaning was expected to have the same appearance (Fig. 3).

Fig. 3. The area of the cleaned Riding Jacket

As it was shown by Svendsen et al. the ablation threshold for pure silver using laser radiation from Nd:YAG at 532 nm and pulse duration of 5 ns was about $0.6\,\mathrm{J/cm^{-2}}$ [4]. After extensive comparison between different areas

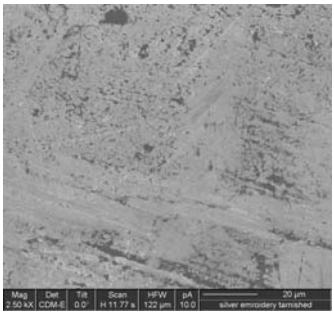

Fig. 4. The piece of the tarnished silver thread before laser irradiation

subjected to the fifteen laser cleaning regimes we found that damage threshold where we can observe the traces of melting on the surface of silver was about $0.85\,\mathrm{J/cm^{-2}}$ but the most appropriate regime at wavelength 532 nm was with fluence $0.61\,\mathrm{Jcm^{-2}}$ (Figs. 4, 5, 6). As we tested different parameters starting from $0.2\,\mathrm{J/cm^{-2}}$ up to $2\,\mathrm{J/cm^{-2}}$ we found that the side effects reported by C. Degrigny et al. could be observed for fluences below $0.4\,\mathrm{J/cm^{-2}}$ and higher than $1.0\,\mathrm{J/cm^{-2}}$ [1, 2]. The yellowing effect occurred for the fluences below $0.4\,\mathrm{J/cm^{-2}}$ at 532 nm and for fluences up to $1\,\mathrm{J/cm^{-2}}$ at 1064 nm. The white colour appeared on the surface for fluences higher than $1.0\,\mathrm{J/cm^{-2}}$ at 532 nm but at the same time we have found that the colour after laser cleaning depends to some extend on the nature of textile.

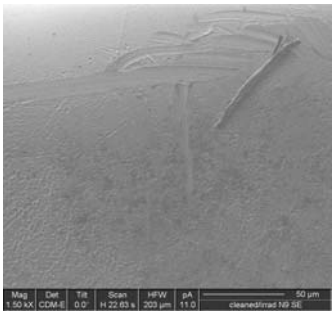

Fig. 5. Silver thread after laser irradiation

After analysing the FIB-micro images and mass spectra of affected areas we attributed these change of colour to the two mechanisms: the silver oxide are responsible for the light yellow colour while the dark yellow colour appeared as a result of the thin layer of silver sulphide (Fig. 7). The increase of the intensity peaks on the mass spectra for oxygen and sulphur on the surface of silver threads before and after laser cleaning could be partly due to these chemical reactions activated by the increase of the surface temperature.

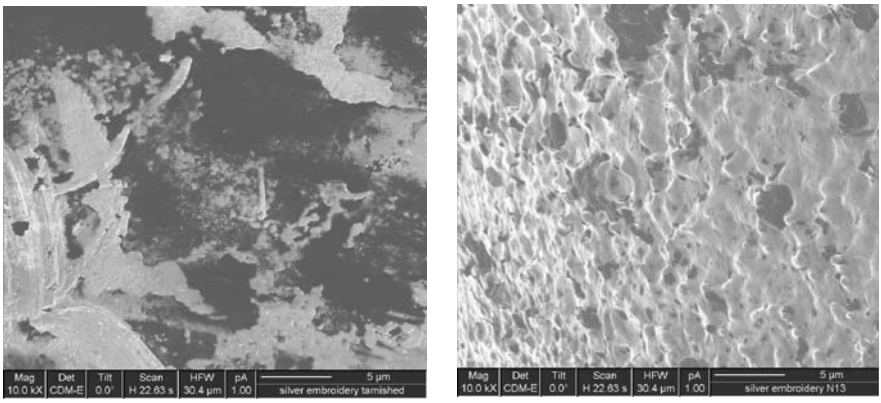

Fig. 6. The surface of silver thread before and after laser irradiation at 532 nm with fluence 0.6 J/cm^{-2}

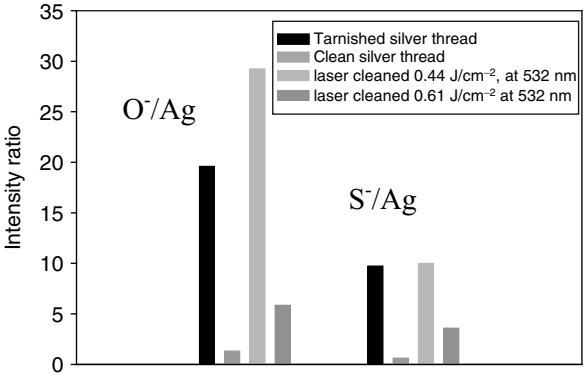

Fig. 7. Comparison between intensity for oxygen and sulphur normalised by silver

The depth profiling of the two pieces of the silver thread before and after laser cleaning have given ancillary information about distribution of the oxygen and sulphur on the surface of silver (Figs. 8,9). We have not found clear evidence of the melting on the surface but depth profiles show that with increase of beam fluences above of 0.6 J/cm^{-2} we can observe increase of sulphur signal over the oxygen. As the silver thread irradiated with 1.06 J/cm^{-2} had the more yellow appearance we assumed that the excess of sulphur is responsible for the colour and increase the fluence in order to match the colour of cleaned threads with the colour of the Riding Jacket.

Figure 10 represents the silver thread from the riding jacket before and after laser cleaning at 532 nm with 2 J/cm^{-2} and 3 pulses. The surface of the silver clearly shows that the contamination was removed but the effect of

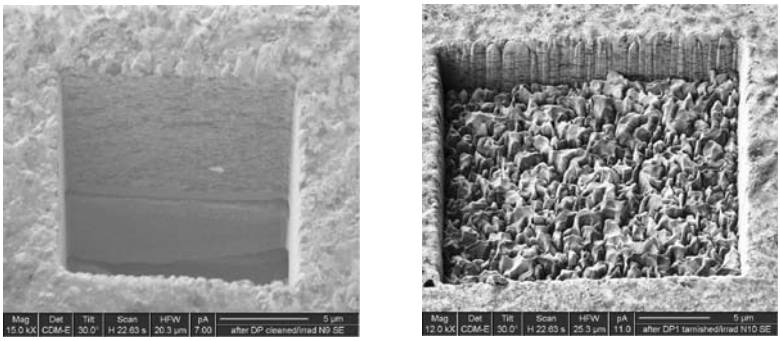

Fig. 8. FIB-micro images of the depth profile of the silver threads after laser cleaning at 532 nm with 1.03 J/cm^{-2} and 0.61 J/cm^{-2}

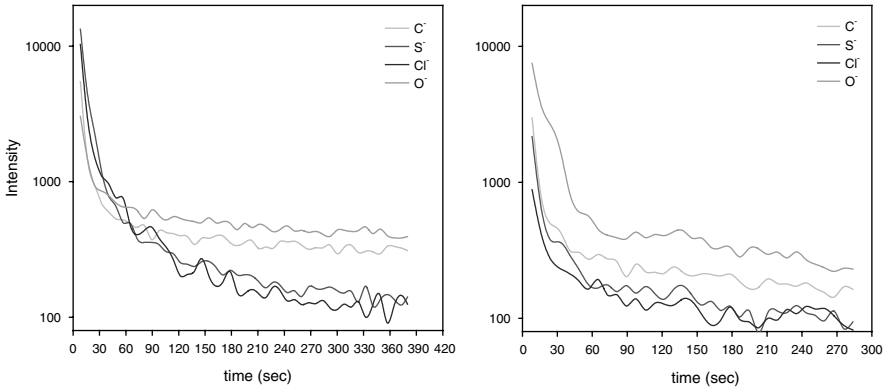

Fig. 9. Depth profiles for the silver threads laser cleaned at 532 nm with fluences 1.03 J/cm^{-2} (*left*) and 0.61 J/cm^{-2} (*right*)

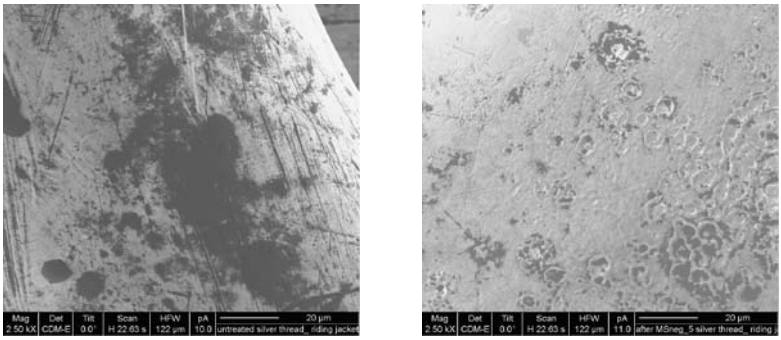

Fig. 10. The silver thread from the riding jacket before (*left*) and after (*right*) laser cleaning at 532 nm with 2 J/cm^{-2}

the cleaning was not uniform which could be attributed to the non-uniform density distribution of the laser beam.

The mass spectra on the Fig. 11 confirm our assumptions that during the laser irradiation some chemical reactions took place on the surface that depended on the cleaning environment. The increase of the chlorine peak shows that chlorine from the wool textile could be introduced to the surface during the laser irradiation.

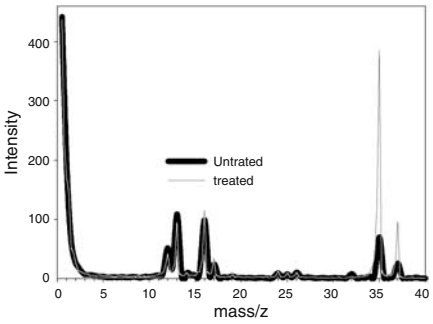

Fig. 11. The negative mass spectra for the silver threads from Riding Jacket

The comparison between intensities of different elements normalised by silver on the threads before and after cleaning (Fig. 12) shows that apart from chlorine the relative intensities of all contaminants decrease after the treatment.

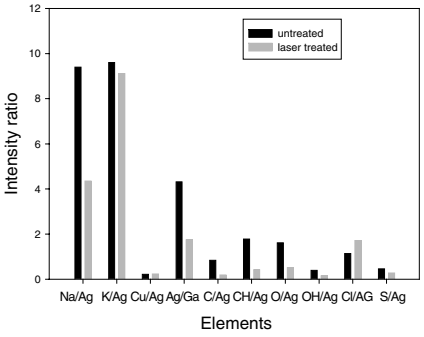

Fig. 12. Comparison between intensities of elements on the surface of silver threads before and after laser cleaning

4 Conclusions and Future Research

We have used the FIB-SIMS workstation to analyse the surface of the silver threads before and after laser cleaning. We have found that the FIB-micro technique lends itself perfectly to imaging these types of surfaces. Indeed, the images have relieved more intricate details than has been previously observed via more traditional imaging techniques such as SEM.

On the basis of FIB-SIMS analysis we have found that the laser cleaning of the silver thread by means of the Q-switch Nd:YAG laser with pulse duration – 6 ns at 1064 nm and 532 nm proved to be a powerful and effective tool for the treatment of silver incorporated into textiles. The FIB-micro images show that the laser irradiation with fluences below 1 J/cm^{-2} did not lead to the melting of silver or to the burning of silk and wool rods. At the same time mass spectra and depth profile analysis presented the evidence that the laser irradiation with intensity sufficient for the cleaning produced the alteration in the colour of the silver surface that could be attributed to the inducing of oxide and sulphide films during the irradiation. We have found the correlation between the fluences of irradiation and the colour of irradiated silver thread. The nature of these phenomena will be a subject of the future investigations. The practical application of our research was the laser cleaning of the soiled spot on the Woman Riding Jacket. The cleaning regime was a wavelength of 532 nm with fluence 2 J/cm^{-2}.

References

1. E. Degrigny, E. Tanduy, R. Le Gall, and V. Zafiropulos, Laser cleaning of tarnished silver and copper threads on museum textiles, LACONA IV, 2001, 89–92
2. J-M. Lee, J-E. Yu, and Y-S. Koh, Effect of wavelength in the laser conservation of silver textile, LACONA IV, 2001, 93–96
3. W. Svensen, J. Schou, B. Thestrup, and O. Ellegaard, Ablation from metals induced by visible and UV laser irradiation, Applied Surface Science **96–98**, 1996, 518–521
4. A. G. Nord, K. Tronner, A note on the analysis of gilded metal embroidery threads, Studies in Conservation **45**, 2000, 274–279

Part VI

Pigments, Conservation Layers

The Effects of Laser Radiation on Adhesives, Consolidants, and Varnishes

O. Madden[1], M. Abraham[1], S. Scheerer[2], and L. Werden[1]

[1] Laser Conservation Research Facility, Los Angeles County Museum of Art, 5905 Wilshire Blvd., Los Angeles, CA 90036, USA
OdileMadden@UCLAlumni.net

[2] Private Conservator, Stuttgart, Germany

Abstract. The Laser Conservation Research Facility at the Los Angeles County Museum of Art continues to research the effects of laser energy on adhesives, consolidants, and coatings that are commonly used in conservation or have been used in the past. This paper augments research that was presented at the LACONA IV conference under the title, "Possibilities for removing epoxy resins with lasers" [2]. That study focused on two epoxy resins commonly used in conservation. In this second stage of research, a selection of 35 conservation materials was exposed to several wavelengths of laser light (1064 nm, 532 nm, 355 nm, 351 nm, and 248 nm). The results demonstrate the importance of recognizing polymers and oligomers on artifacts and knowing the likely effects of laser exposure upon them. This preliminary research is intended to spur future research into these disparate materials by the LACONA community.

1 Introduction

The results of a systematic study of the effects of laser energy on a variety of polymers and oligomers that are commonly used in conservation or have been used in the past are presented here. While some existing research demonstrates the value of using lasers to remove varnish from paintings, the authors have observed that there has been little analysis of the effect of polymer/oligomer type on the removal process. This study attempts to address the fact that terms such as "varnish", "adhesive", or "consolidant" may be used to indicate a number of classes of chemicals, each of which may be expected to react differently to laser exposure as a result of its unique chemical structure.

The importance of this research is two-fold. First, there are instances where a conservator may want to remove a polymer/oligomer, such as discolored varnishes, other degraded coatings, and overpaint. Lasers can be considered among the tools to accomplish this. On the other hand, there are instances where polymeric/oligomeric material is present and unrecognized, or its removal is undesirable. In either case, advance knowledge of how a laser might affect the material can be critical to the success of laser treatment.

Materials tested in this study can be found in many forms on a wide variety of artworks and artifacts as a result of past conservation treatment.

Examples include binding media in paint and ink, coatings, varnishes, adhesives, consolidants, and fill materials. These and related materials can also make up the artwork itself as in the case of acrylic paintings and some modern sculpture.

2 Experimental Methods

A selection of 35 polymer and oligomer formulations (Table 1) was applied onto the following substrates: glass microscope slides, red/black granite slab, and white plaster. The polymers were chosen for their frequent use (past and present) and immediate availability during the sample preparation process. Some samples were artificially aged by exposure to ultraviolet light (700 hours) followed by exposure to elevated temperature (80°C, 65% relative humidity, 840 hours). All samples have been aging naturally for three years in normal laboratory conditions (approximately 21°C, 50% relative humidity).

The samples were exposed to pulsed laser light from two lasers: a Coherent Infinity Q-switched Nd:YAG laser with pulse duration of 3 nanoseconds (1064 nm, 532 nm, and 355 nm). With the Nd:YAG, exposure was determined empirically. That is, fluence was increased incrementally until a visible change was perceived in the sample.

Early in the experiment, the UV harmonic crystal for the Nd:YAG laser failed. It was decided to expose the samples to a XeF excimer laser operating at 351 nm to compensate. All samples were exposed to a KrF excimer laser operating at 248 nm. The excimer laser was a Lambda Physik pulsed laser with a pulse length of approximately 10 nanoseconds. In the interest of convenience and time, fixed exposure parameters were chosen for the excimer studies. All samples were exposed at 255 mJ/cm^2 at 10 Hz for 30 seconds.

Treated samples were evaluated visually and with the aid of a binocular microscope (1–40x magnification).

3 Results and Discussion

In looking for ways to describe the effect of laser radiation on the polymer/oligomer films, it was decided to avoid postulating mechanisms of damage and focus instead on describing visual observations. Observed phenomena were organized into five categories: no reaction, etching, structural breakdown, lifting/separation, and clean ablation. Results are summarized in Table 2.

In many cases, *no result* was seen after laser exposure. This was expected, especially when using visible laser light, as the polymers are often transparent to a broad band of wavelengths. However, these same materials might undergo reactions at fluences above those tested in this experiment.

Table 1. List of conservation materials tested classified with type of material, preparation notes, and source information

Name of Material	Preparation Notes (% = Weight/ Volume)	Material Type	Manufacturer or Distributor
Gelatin	15% in water	Protein	
Hide glue	15% in water	Protein	
Fish glue ®	As packaged, undiluted	Protein	Lee Valley Tools Ltd.
Wheat starch paste	Cooked and diluted in water	Polysaccharide	
Methocel MC 3000–5000 centipoise	3.5% in water	Polysaccharide	Fluka BioChemika, AG CH-9740 Buchs
Klucel GF	19% in water	Polysaccharide	Hercules Inc., Aqualon Division, USA
Gum Arabic	10% in water	Plant resin	Windsor & Newton
Shellac	10% in ethanol	Insect exudate	
Dammar	10% in turpentine	Plant resin	
Beeswax	Molten, no solvent	Wax, natural	
Carnauba wax	Molten, no solvent	Wax, natural	
Multiwax W-445	Molten, no solvent	Wax, microcrystalline	Conservation Support Systems, USA
Acryloid B-72	20% in ethanol	Acrylic resin	Rohm and Haas, USA
Acryloid B-44	20% in xylene	Acrylic resin	Rohm and Haas, USA
Acryloid B-48N	10% in toluene	Acrylic resin	Rohm and Haas, USA
Acryloid B-67	20% in benzine xylene	Acrylic resin	Rohm and Haas, USA
Plextol B500	As packaged, undiluted	Acrylic emulsion	Rohm GmbH, Postfach 4242, 61 Darmstadt, Germany
Lascaux 360HV	As packaged, undiluted	Acrylic emulsion	Alois K. Kiethelm AG CH-8306 Brüttisellen
Rhoplex AC33	As packaged, undiluted	Acrylic emulsion	Rohm and Haas, USA
Jade 403	As packaged, undiluted	Polyvinyl (PVA) acetate emulsion	Abbitt Adhesives, Inc.
AYAA	25% in ethanol	PVA resin	Union Carbide, USA
AYAF	25% in ethanol	PVA resin	Union Carbide, USA
BEVA 371	40% in toluene and n-heptane	Ethylene vinyl acetate copolymer (major component)	Conservation Support Systems, USA
Butvar B-79	45% in ethanol	Polyvinyl butyral	Monsanto
Butvar B-98	45% in ethanol	Polyvinyl butyral	Monsanto
Elmer's Glue All®	As packaged, undiluted	PVA emulsion	Borden, Inc., USA

(*continued*)

Table 1. (*Continued*)

Name of Material	Preparation Notes (% = Weight/ Volume)	Material Type	Manufacturer or Distributor
Hxtal NYL-1	2-part epoxy, per manufacturer's instructions	Epoxy resin	Conservation Support Systems, USA
Mastic	7% in turpentine	Plant resin	
Araldite AY103/HY991	2-part epoxy, per manufacturer's instructions	Epoxy resin	Ciba Geigy
Phillyseal R®	2-part epoxy, per manufacturer's instructions	Epoxy putty	ITW Philadelphia Resins, USA
Milliput® (superfine white)	2-part epoxy, per manufacturer's instructions	Epoxy putty	The Milliput Company
Calaton S	20% in ethanol	Soluble nylon	I.C.I., UK
GE 100% Silicone Rubber Sealant	As packaged, undiluted	Silicone	General Electric Co.
Hotmelt Glue	Molten, no solvent	PVA	H. B. Fuller Co.
Duco cement®	As packaged, undiluted	Cellulose nitrate	Devcon Consumer Products, USA

Some samples exhibited damage that originated at the top layer of the polymer/oligomer film and moved inward, through the film and down toward the substrate. This phenomenon is described here as *etching*. In other cases, the film was damaged from within. The type of damage varied. Sometimes, the sample softened and became tacky [2]. In other samples, the internal damage was more visible. Bubbles, pinpoint fractures, spots of dark coloration, crizzling (or shattering), and color shift were noted. In some samples, the damage originated at the join between the film and substrate resulting in lifting and separation of the two. Finally, some films were removed "cleanly" by certain wavelengths. The film was removed down to the substrate with little or no visible residue. This may have been a quick and effective removal by one or more of the other three mechanisms described above.

Though these tests are preliminary in nature, several trends are evident among the polymer types. These general trends are discussed below, and specific results of potential interest to the conservation field are highlighted.

Reference [2] discussed Hxtal-NYL and Araldite epoxy resins at the LACONA IV conference. In this round of experiments, two commercially prepared epoxy putties, Milliput® and Phillyseal R®, were tested. These materials reacted at all wavelengths tested. Most notably, the samples darkened with a gray-black halo forming around the treated area. This behavior

Table 2. Results of testing for samples mounted on glass slides. Damage threshold fluence is indicated, when possible, in subscript (J/cm^2)

		Nd:YAG			Excimer	
	Name of Material	1064 nm	532 nm	355 nm	351 nm	248 nm
1	Gelatin	N	N	$E_{0.2-0.3}$	N	A, S/o
2	Hide glue	N	N		N	S/o
3	Fish glue ®	N	E, S/$o_{0.4}$, $A_{0.5}$	$E_{0.2}$, $A_{0.25}$	L	A, L, S/b,o
4	Wheat starch paste	E_3	N	N	N	N
5	Methocel MC 3000–5000 cps	E_3	N	N	N	N
6	Klucel GF	N	N	-	N	N
7	Gum Arabic	N	N	-	N	N
8	Shellac	E_{1-3}	$E_{0.2-2}$	$E_{0.3}$, S/$s_{0.3}$	N	A, S/o
9	Dammar	N	E	$E_{0.05}$, $A_{0.3}$, S/$o_{0.3}$	E, S/c	A
10	Beeswax	S/$b_{2.5}$, A_3	$E_{0.7-1.5}$, L	-	L	A
11	Carnauba wax	?	$E_{0.4}$, S/b_1, $A_{1.5}$	$E_{0.13}$, $L_{0.13}$, $A_{0.34}$	N	A
12	Multiwax W-445	N	N	N	N	E, A
13	Acryloid B-72	N	N	N	N	S/b
14	Acryloid B-44	N	N	-	N	S/b,o
15	Acryloid B-48N	N	N	-	N	S/s,b
16	Acryloid B-67	N	N	N	N	S/s,b
17	Plextol B500	N	N	-	N	S/c,o
18	Lascaux 360HV	E_3, S/$bs_{0.3}$	N	-	S/s	S/s
19	Rhoplex AC33	N	N	-	S/c	S/c
20	Jade 403	N	N	N	N	A
21	AYAA	S/b_3, L_3	-	-	S/b	S/b, A
22	AYAF	N	N	S/$b_{0.3}$	N	S/b, A
23	BEVA 371	S/b, L	S/$b_{0.3}$, $L_{>1.7}$	$E_{0.06}$, S/$s_{0.2}$, $A_{0.2}$	N	S/b, L
24	Butvar B-79	N	N	-	N	N
25	Butvar B-98	N	N	-	N	N
26	Elmer's Glue All®	N	N	-	N	E
27	Hxtal NYL-1	N	N	-	N	S/o
28	Mastic	N	N	-	N	E
29	Araldite AY103/ HY991	$E_{2.5}$, S/s_3	N	-	N	S/b, L
30	Phillyseal R®	S/$o_{0.25}$, $A_{1.8-2.0}$	$E_{0.2}$, $A_{1.5}$	$E_{0.17-0.3}$, S/$o_{0.17-0.3}$	S/o	S/o
31	Milliput® (superfine white)	S/$o_{0.25}$, A_2	S/$o_{0.02-0.2}$, $A_{0.7}$	$E_{0.3}$, S/$o_{0.3}$	S/o	S/o, A
32	Calaton S	N	N	N	N	N
33	GE 100% Silicone Rubber Sealant	$E_{1.3-1.5}$, S/s_2	$L_{0.3}$	S/$s_{0.3}$, L	L	N

(*continued*)

Table 2. (*Continued*)

		Nd:YAG			Excimer	
	Name of Material	1064 nm	532 nm	355 nm	351 nm	248 nm
34	Hotmelt Glue	N	N	-	N	E, S/o
35	Duco cement®	N	$E_{0.3}$, $A_{0.5}$	$E_{0.1}$, $A_{0.3}$	L	A, S/o

N = No reaction E = Etching
L = Lifting/Separation A = Clean Ablation
S/s,b,f,d,c,o = Structural breakdown/softening, bubbles, fractures, dark spots, crizzling, or color shift/opacification)
\- = Not tested

was similar to samples in the previous study that had been mixed with titanium dioxide pigment, and it is suspected that titanium dioxide filler may be the cause of the discoloration in the two putties as well. It is a good example of how a polymer and filler react as a system, which is different from the reaction of the epoxy resin alone.

The acrylic resins tested were remarkably resilient to laser light, except when exposed to 248 nm radiation which made all four Acryloid resins soft and tacky. The interplay of film transparency and substrate was a factor for the samples exposed to Nd:YAG wavelengths. Whereas samples mounted on glass slides were unreactive, samples mounted on dark-colored stone separated from the substrate and the granite discolored to gray-black. With samples mounted on plaster, ablation was more successful than the glass slides, and the plaster beneath the film exhibited some surface ablation in the form of powdering.

Acrylic emulsions behaved equally well, with the only reactions occurring in the ultraviolet range (Table 2). The difference in the type of reactions that occurred with the two emulsions at 248 nm may be attributable to the fact that Rhoplex is a harder material with higher glass transition temperature.

Samples of polyvinyl acetate were moderately reactive to laser light, and the most common form of damage was bubbling. The reaction of BEVA 371 was of particular concern. Massive small bubbling followed by lifting occurred at all wavelengths except 351 nm. This has very important ramifications for the treatment of paintings that have been consolidated or lined with BEVA 371; massive bubbling and lifting would be particularly catastrophic in those cases.

With waxes, the natural beeswax and carnauba wax reacted at all wavelengths. On the other hand, the microcrystalline wax sample was only affected by the KrF excimer laser. These differences may be attributed to the presence of impurities in the natural waxes and/or the color of the natural materials. The protein glues were all cleanly ablated at 248 nm. The area surrounding the ablated spot turned a milky opaque color.

With the exception of cellulose nitrate, the polysaccharides tested did not react at any wavelength tested. Cellulose nitrate, a polymer known to be chemically unstable, reacted at all wavelengths except 1064 nm.

Silicone resin was reactive at all wavelengths tested except 248 nm. In most cases, the film separated from the substrate. At 1064 nm, small brown spots formed within the film. The spots appear to have resulted from higher power density focused into the film by lenses formed by an irregular topography of brush strokes on the film surface. Further experiments revealed that these lenses could also focus power density onto the reverse of the glass slide substrate, and onto a separate piece of glass placed at a distance from the film. In both cases, the *glass* beyond the silicone film was pitted by the laser.

Polyvinyl butyral, soluble nylon, and gum arabic did not react at any wavelength tested.

It is also interesting to note the reaction of several materials that have traditionally been used as varnishes and coatings. Dammar, shellac, the protein glues, and the natural waxes were cleanly ablated by the KrF excimer laser.

4 Conclusions

This research demonstrates that the reaction of polymers and oligomers to laser radiation is dependent upon their chemistry and the way in which they have been prepared (i.e., added fillers). A clear relationship exists between the type of polymer/oligomer and its reaction to laser light at specific wavelengths. For example, acrylic emulsions and resins underwent little or no change at 1064, 532, 355, and 351 nm. Natural waxes, epoxy putties, and epoxy resins exhibited changes in color, opacity, and texture at these same wavelengths. Variations in reactivity were also noted among different formulations of the same material class.

When treating transparent or translucent films, the laser can penetrate to the substrate, which can result in enhanced separation of the polymer film and/or changes in the substrate. Effects upon the substrate included color changes and etching. In these tests, color change appears to have resulted from laser light penetrating through the polymer/oligomer film to a substrate that is itself unstable to laser light. It has also been noted that a transparent film can act as a lens that focuses the laser beam onto an underlying point. There is good evidence that the surface topography and transparency of the film are the major predictors of this phenomenon. The "lensing effect" has resulted in breakdown of the polymer film itself, as well as etching and pitting of materials lying beyond the film.

The broad range of results reported here underscores the importance of testing specific adhesives, coatings, fill materials, paint layers, and other polymeric/oligomeric materials on artworks for their sensitivity to laser radiation.

Data obtained in this experiment is relevant only in the context of the materials tested, their preparation, and the laser parameters used. Different brands or formulations of these polymers/oligomers will probably produce results that deviate from those presented here. Laser parameters, such as higher fluence levels, may produce results in materials for which this experiment showed no reaction.

From the outset, this study was intended to draw attention to the wide range of polymeric and oligomeric materials used in conservation and the many areas in which they might be encountered. It is hoped that other groups in the LACONA community will incorporate studies of individual polymers and formulations into their research. Avenues for future research include the evaluation of individual products for reaction to laser radiation, the influence of preparation (i.e., presence of fillers) and substrate on the reaction, and the potential risks and applications of the "lensing effect".

Acknowledgements

The authors would like to thank the following institutions and individuals for their contributions to this research: National Center for Preservation Technology and Training, and in particular Dr. Mark Gilberg; the Samuel H. Kress Foundation; Dr. Dave Taylor of the Aerospace Corporation; Victoria Blyth Hill, Dr. Marco Leona, and Adam Avila of the Los Angeles County Museum of Art; and Maureen Russell of the Museums of New Mexico.

References

1. P. Bracco, G. Lanterna, M. Matteini, et al., "Er:YAG laser: an innovative tool for controlled cleaning of old paintings: testing and evaluation", in *Journal of Cultural Heritage*, Supplement 1, 202s–208s, 2003
2. S. Scheerer, M. Abraham, and O. Madden, "Study of the effects of laser radiation on epoxy resins and epoxy systems on stone, ceramic, and glass surfaces", Journal of Cultural Heritage, Supplement 1, 223s–229s, 2003
3. R. Teule, H. Scholten, O. F. van den Brink, et al., "Controlled UV laser cleaning of painted artworks: a systematic effect study on egg tempera paint samples", Journal of Cultural Heritage, Supplement 1, 209s–215s, 2003

A Study on the Oxidative Gradient of Aged Traditional Triterpenoid Resins Using "Optimum" Photoablation Parameters

C. Theodorakopoulos[1,2], V. Zafiropulos[2,3], C. Fotakis[2], J.J. Boon[4], J. v.d. Horst[4], K. Dickmann[5], and D. Knapp[5]

[1] RCA/V&A Conservation, Surface Studies Group, Victoria and Albert Museum, South Kensington, London SW7 2RL, UK
c.theodlos@vam.ac.uk
[2] Foundation for Research and Technology-Hellas (FORTH), Institute of Electronic Structure and Laser (IESL), P.O. Box 1527, Heraklion, Crete, 711 10 Greece
[3] Technical Educational Institute of Crete, Department of Human Nutrition & Dietetics, Ioannou Kondylaki 46, 723 00 Sitia, Crete, Greece
[4] Foundation for Fundamental Research on Matter (FOM), FOM Institute for Atomic and Molecular Physics, (AMOLF), Kruislaan 407, Amsterdam, Netherlands
[5] Lasercenter Fachhochschule Münster (LFM), University of Applied Sciences, Stegerwaldstraße 39, 48565 Steinfurt, Germany

Abstract. KrF excimer laser ablation of two artificially aged triterpenoid films was studied. Ablation rate variations across film thicknesses implied compositional change with depth. Deviations between calculated and measured depths-steps at deeper ablated layers verified previously determined gradients. The findings were confirmed with DTMS, which demonstrated that excimer laser ablation with optimum fluences does not induce oxidation.

1 Introduction

Ageing of painting varnishes results in their chemical and physical degradation due to oxidation and crosslinking, resulting in crazing, discoloration etc. which obscure the painted surface [1–6]. This degradation justifies studies on their removal with various means. Recently, excimer laser ablation was proposed for this purpose [7]. However, concerns have been expressed regarding the safety of the UV laser ablated artworks, given the vulnerability of common paint media upon UV absorption [8, 9] and the discoloration of pigments when irradiated with UV lasers [10].

Even the ablation of a resin film alone is not an easy task. In line with Beer's Law, suggestions are made regarding an exponential reduction of degradation across the depth profile of aged resins, resulting in a corresponding gradient in the obscurity effects as recently uncovered in [11]. These findings were consistent with other studies on polymers and varnishes [9, 12–14].

Upon degradation gradient, the effects of excimer laser ablation become uncertain. It could be suggested that while the top layers of an aged resin are ablated the excessive UV photons of the pulse may induce further oxidation to the less degraded deeper layers. Given the case-specific properties of excimer laser ablation [15], it is interesting to examine the effects of this depth-wise chemical change on the ablation process.

Here, the interaction of a KrF excimer laser with artificial aged triterpenoid resin films, commonly applied on paintings, is investigated. Laser ablation rate studies, cleaning studies and DTMS analysis are employed to elucidate the existence and the role of the oxidative gradient in the ablation process.

2 Experimental

Mastic and dammar in xylene 40% (w/v) were spin-coated to produce 55 μm thick films. After drying, ageing was accelerated in a Sunset CPS, Heraeous® xenon-arc fadeometer. With wavelengths longer than 295 nm, an outdoor exposure of full sunlight was imitated [9]. The films were irradiated for 500 hours at 60°C. The samples were then exposed to free oxygen conditions for 45 days and kept in the dark for 30 days.

Laser ablation was carried out with a Lamda Physic®, COMPex series, KrF excimer laser (248 nm, 25 ns) at a constant energy mode of approximately 380 mJ. Ablation rate studies were performed on both films twice. The etching depths were determined with a Perthometer® S5P.

The laser cleaning methodology was based upon scanning adjacent parts of the films with a pre-calculated number of laser pulses across the Gaussian profile of the laser beam, as described in [7]. Each scan was arranged to fire one pulse per single translation to obtain maximum control during the process. In this way zones of subsequent depths were laser-ablated identically to [11].

DTMS [16] was employed to analyze the laser-ablated zones. Scrapings of the ablated zones, were grated homogenously and brought in suspension with ethanol. Few μl of the suspended samples were applied to a Pt/Ph (9:1) filament (100 μm diameter) of a direct insertion probe to evaporate the ethanol *in vacuo*. With the filament insertion into the ionization chamber the temperature was gradually raised up to ∼ 800°C at a rate of 1A/min, while the MS (JEOL® SX-102 double focusing (B/E)) was monitoring the evolved compounds in the EI mode. Ionization took place at 16 eV and the readings were set at a mass range of 20–1000 Dalton at a cycle time of 1 s.

3 Results

3.1 Laser Ablation Rate Studies

The double laser ablation rate studies of both films are demonstrated in Fig. 1. White symbols represent ablation rates and efficiency trends at random depths across the film thicknesses, whereas black symbols represent the respective studies only at the surface layers of the films ($d \leq 10\,\mu m$).

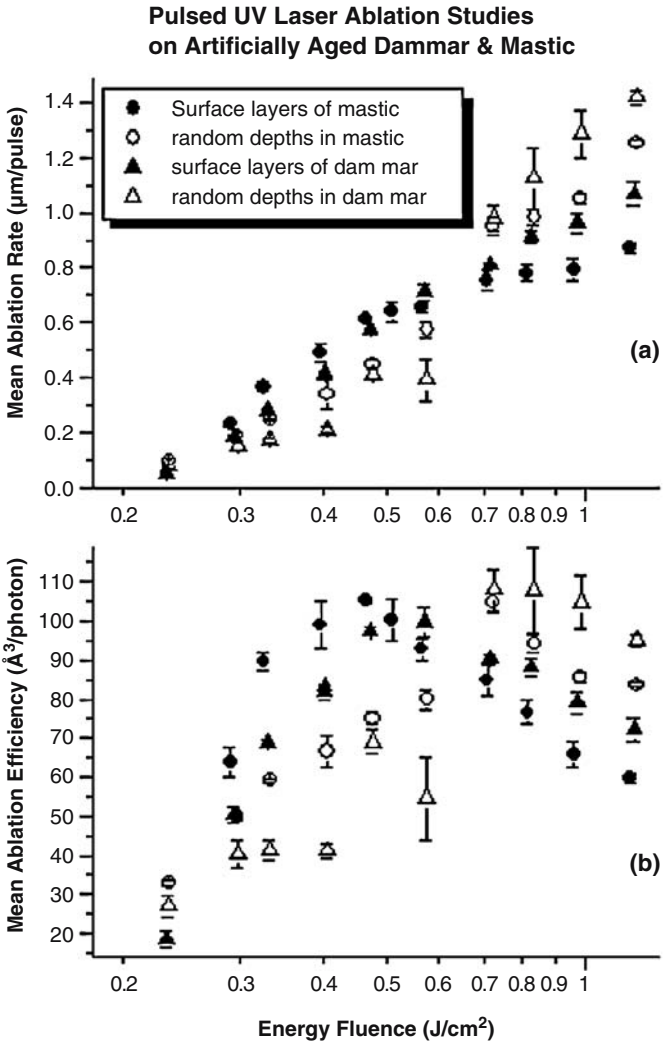

Fig. 1. Double laser ablation rate studies on whole thickness and surface layers of the artificially aged mastic and dammar resin films

Studies on the whole thickness of mastic demonstrate a linear increase of the ablation rate slope up to an energy fluence of $0.6\,\mathrm{J/cm^2}$ (Fig. 1a). From that point on the ablation rate increases abruptly. This behavior is also delineated in the corresponding efficiency slope (Fig. 1b). In contrast, the ablation rate slope on the surface layers is comparable with previous data for mastic [17]. The efficiency at the surface layers peaks at fluence $0.45\,\mathrm{J/cm^2}$.

Similarly, the laser ablation rate studies of whole thickness and surface layers in dammar are shown to have significant dissimilarities. In particular, the whole thickness ablation rate study obtains three different trends with increasing fluence, which along with the corresponding distorted efficiency curve, proves inappropriate for the choice of cleaning parameters. The study on the surface obtains the expected reliability. Here, the efficiency peaks at $0.6\,\mathrm{J/cm^2}$. Given the "normal" trends of the ablation rates at the surface layers for both films, fluences $0.45\,\mathrm{J/cm^2}$ for mastic and $0.6\,\mathrm{J/cm^2}$ for dammar were chosen as "optimum", for the following cleaning procedure.

3.2 Depth-Step Ablation

Arranging the lens-sample distance, the slit opening as well as the laser energy, the "optimum" fluences were set for the final scanning of the aged mastic and dammar. Owing to the essential 80% overlap across the Gaussian beam profile, there was an expected loss in the etching resolution by 5 times of that yielded in the ablation rate studies with the corresponding fluences [7]. Seven depth-step zones were laser ablated across mastic and six across dammar, in the same way with that described in [11]. Every additional pulse per scan obtained a depth-step that was about twice as deep as the previous scan. The results are demonstrated in Fig. 2.

In contrast to findings regarding excimer laser ablation of polymers [15], in this case the function of the final etched depths versus the number of laser pulses fired is not kept linear for none of the films examined here. The linear condition is maintained down to a layer of about $15\,\mu\mathrm{m}$ from the surface for both films. After this point the removal efficiency is significantly reduced.

3.3 Electron Ionization Total Ion Currents of Direct Temperature-Resolved MS Analysis

In Fig. 3 the EI DTMS TIC's of mastic are presented. The successive shifts of the volatilization peak (highest peak at the left) from the fresh towards the aged state of the film signify a significant oxidation increase [18]. In addition, the increase in the intensity of the pyrolysis peak (lower peak at the right) from the unaged to the aged state of mastic represents the crosslinking formation during ageing.

It is evident that both oxidation and crosslinking decrease gradually from the surface towards the deeper laser-ablated layers of the film. This trend,

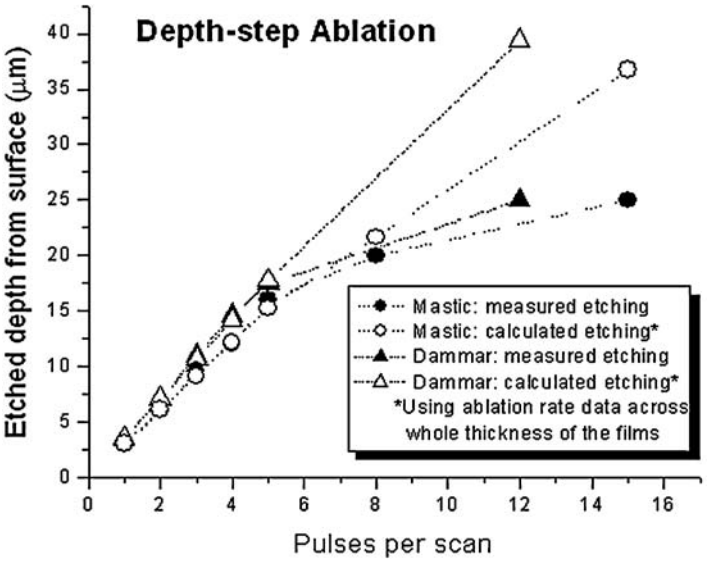

Fig. 2. Measured and calculated depth-steps versus the number of 248 nm pulses fired on the triterpenoid films

especially with regards to oxidation, is evident even from the first depth-step, which is 3 μm below the aged surface. The rate of oxidation decrease is such that at a depth of 15 μm from surface the film peaks its volatilization nearly in the half way between aged and unaged state. After this depth-step the rate of oxidation decrease is profoundly lower. The shifts between the laser-ablated depth-step at 25 μm and any layer below this point are considerably less than the volatilization shifts across the first 25 μm. The remaining 30 μm thick film therefore exhibits characteristics that are similar to the unaged state.

The relative intensity of the pyrolysis peak performs a similar trend, indicating a corresponding crosslinking gradient. The laser-ablated dammar film performed a similar gradient.

4 Discussion

Excimer laser ablation of discolorated varnishes applied on paintings has been a matter of controversy owing to possible damage of the substrate upon the absorption of the UV laser photons. Namely, most disputes argue the chances for potential oxidation of the residual laser ablated varnish and the discoloration of the underlying paint. Current findings demonstrate that at least surfaces coated with thick triterpenoid films run minor risks under a carefully planed and fully controlled laser cleaning process. Under these lines, the systematic inquiry for the optimum fluence per case is proved to be an essential

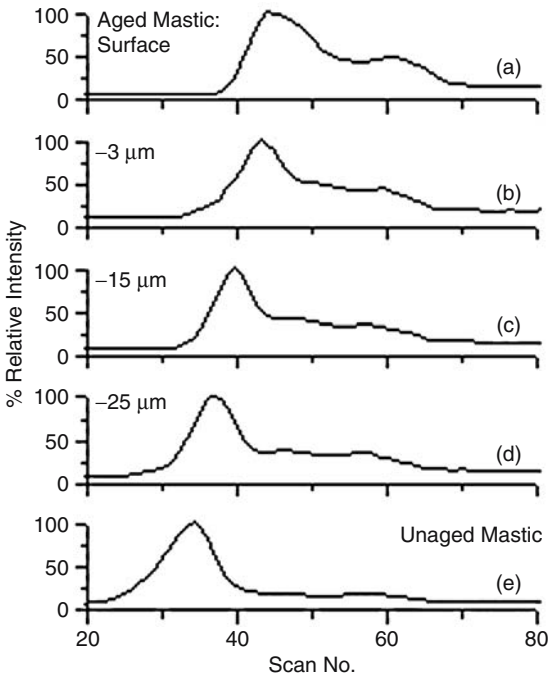

Fig. 3. Total ion currents of the DTMS analysis at electron ionisation mode of mastic from the surface (**a**) and laser ablated depth-steps at 3 μm (**b**), 15 μm (**c**) and 25 μm (**d**). TIC of the unaged film (**e**) is provided as a reference

condition. With this fluence the safety of the substrate is guaranteed. The findings described above are in principle valuable for the laser cleaning of paintings, where a thin layer of varnish should be left on the paint to prevent discoloration [7, 17]. To this end, the recently proposed integrated laser and chemical cleaning [11] would benefit painting conservation, by critically minimizing risks generated when laser or conventional cleaning are applied separately for the total removal of degraded varnishes.

MS analysis on the laser-ablated depth-steps highlighted the gradual decrease of oxidation and indicated a respective gradient in crosslinking. The diverse data emerged from the double laser ablation rate studies as well as the increasing deviations of the ablation steps below a 15 μm surface layer must be attributed to the crosslinking gradient. This is justified by findings regarding the interaction of UV lasers with polymers [15, 19, 20]. In these references the linear function of etching versus excimer laser pulses was determined as a consequence of the high degree of polymerization. Here, the linear etching-pulse function is not verified for the examined triterpenoid varnishes, suggesting a decreasing crosslinking degree with depth.

The change in the ablation step beyond the 15 μm depth-step did not influence the decreasing gradient in oxidation. It was determined here that oxidation is a self-limited phenomenon along the depth profile of both films examined. This trend could be suggested to have a versatile significance. In terms of ageing it could be suggested that oxygen consumption is content with the uppermost resin layers at the exposed film surface. This is in line with photochemical initiation reactions induced by the decreasing light penetration described by Beer's Law. The oxidation gradient of the aged triterpenoid varnishes justifies the protecting role of these coatings preventing oxidation to occur near the underlying layers. Here, the detection of the oxidation gradient across depth following excimer laser ablation determines the absence of oxidative contribution to the substrate, thus avoiding additional impairments to the already complex composition of the aged triterpenoid films. Thus, the free radicals yielded by the molecular bond-breakage upon UV laser absorption must be entrained into the plume preventing oxygen consumption within the substrate. In contrast, the UV laser photons seem to simply erase gradually the oxidized and crosslinked resin, exposing a different, less degraded resin in deeper layers.

5 Conclusions

The photo-ablation of two artificially aged triterpenoid varnish films, about 55 μm thick, was studied using a KrF excimer laser. Different laser ablation rate data emerged from etched spots down to deep depths and at the 10 μm surface layers. Laser scanning was carried out employing an 80% overlap across the Gaussian profile of the beam. The successive depth-steps had a decreasing resolution of the etching depth-pulse relation after the removal of a 15 μm thick layer from the surface. In effect, DTMS studies establish the existence of oxidative gradient across the depth profile of the aged triterpenoid films, confirming previous spin-off findings on this subject. This finding establishes also that there is no oxidative contribution of the excimer laser ablation to the substrate. Moreover, it is demonstrated that crosslinking undergoes a similar gradient. The ablation step appears to be stable at the uppermost surface layers of the aged films, as long the crosslinking degree is maintained somewhat high. However, more research is required to draw safe conclusions on the trend of crosslinking.

Acknowledgments

This research is performed partly at IESL/FORTH Ultraviolet Laser Facility, GR, by the Cluster of Large Scale Laser Installations (LIMANS) supported by the TMR Program of the European Community (5th Framework Program). DTMS analysis was provided by FOM-Institute AMOLF, NL, supported by FOM Program 49 (funded by FOM and NWO). Chemical Engineering

Department at Imperial College of Science, Technology and Medicine, UK, provided facilities for the fabrication of resin films. The Department of Conservation and Technology at the Courtauld Institute of Art, UK, provided accelerating ageing facilities. Foundation of State Scholarships, Hellas supports Theodorakopoulos PhD research project.

References

1. R. L. Feller, N. Stolow, and E. H. Jones (Editors) On picture varnishes and their solvents, Revised and enlarged edition. Washington DC: National Gallery of Art 1985
2. R. L. Feller, Studies in Conservation **3**, 162, 1958
3. G. Thomson, Studies in Conservation **3**, 64, 1957
4. E. R. De la Rie, Studies in Conservation **32**, 1, 1987
5. E. R. De la Rie, Studies in Conservation **33**, 53, 1988
6. L. Carlyle, N. Binnie., G. A. van der Doelen, J. J. Boon, B. McLean, and A. Ruggles, in *Firnis, Material Aesthetik Geschichte*, International Kolloquium, Braunschweig 110 1998
7. V. Zafiropulos and C. Fotakis, in *Laser in Conservation: an Introduction*, Edited by M. Cooper, Butterworth Heineman, Oxford. 79, 1998
8. R. L. Feller, Bulletin of the IIC-American Group **4**, 12, 1964
9. R. L. Feller, in *Accelerated Aging: Photochemical and Thermal Aspects*, Edited by D. Berland, The Getty Conservation Institute, Los Angeles, 1994
10. A. Athanassiou, A. E. Hill, T. Fourrier, L. Burgio, and R. J. H. Clark, Journal of Cultural Heritage **1** (Sup. 1), s209, 2000
11. C. Theodorakopoulos and V. Zafiropulos, Journal of Cultural Heritage **4** (Sup. 1), 216s, 2003
12. J. J. Boon and G. A. van der Doelen, in *Firnis, Material Aesthetik Geschichte*, International Kolloquium, Braunschweig 92, 1999
13. G. A. van der Doelen, and J. J. Boon, J. Photochemistry and Photobiology A: Chemistry **134**, 45, 2000
14. V. Zafiropulos, A. Manousaki, A. Kaminari, and S. Boyatzis, in ROMOPTO: *Sixth Conference on Optics*, Edited by V.I. Vlad, SPIE Vol. 4430, 181, 2001
15. R. Srinivasan and B. Braren, Chemical Reviews **89**, 1303, 1989
16. J. J. Boon, International Journal of Mass Spectrometry and Ion Processes **118/119**, 755, 1992
17. V. Zafiropulos, in *Optical Physics, Applied Physics and Material Science: Laser Cleaning*, Edited by B.S. Luk'yanchuk, World Scientific, 343, 2002
18. G. A.van der Doelen, Ph. D Thesis, University of Amsterdam 1999
19. R. Srinivasan, Applied Physics A **56**, 417, 1993
20. R. Srinivasan, in *Laser Ablation*, Edited by J.C. Miller, Springer, 107, 1994

Evaluation of the Effects of Laser Irradiation on Modern Organic Pigments

M. Abraham[1], O. Madden[1], T. Learner[2], and C. Havlik[3]

[1] Los Angeles County Museum of Art, Los Angeles, USA
m.abraham@lacma.org
[2] Tate London, UK
[3] State University College of NY at Buffalo, Conservation Program, USA

Abstract. The laser light threshold for color change in modern organic pigments is investigated. The 1064 nm and 248 nm wavelengths require significantly higher fluences to achieve a color change than the visible (532 nm) and the near UV (351 nm).

1 Introduction

Modern paints based on organic pigments in acrylic, alked and other medium can provide new challenges for conservators. Their stability when exposed to light and other effects of aging can vary. Laser cleaning may be one way to approach the treatment of works of art made with these materials. With this in mind, a careful examination of these pigments has been done to begin to evaluate the problems associated with laser-based treatment of these art materials.

We have noted that some pigments are prone to changes when exposed to lasers. In this study, the main classes of organic pigments are examined including some of the large class of azo pigments, as well as samples from the phthalocyanines, quinacridones, perinones, benzimidazolones and diketopyrrolo-pyrrole (DPP) pigments. These have been evaluated before and after laser irradiation. The pigments were exposed to the effects of Nd:YAG laser energy both as dry pigments and in the paint medium. Additionally, some of the acrylic media are evaluated before and after exposure to the Nd:YAG at several wavelengths.

Results are described using visual examination, colorimetry, and Raman spectroscopy, to characterize the effect of laser treatments on the materials. Generally, the IR and UV wavelengths caused change at fluences significantly higher then those required to alter the pigments when the laser was operating in the visible and near UV.

2 Experimental Methods

A series of over 50 samples of dry pigment were placed between glass slides. Four pockets of sample per slide were constructed. The first pocket was reserved as a control, while the other three were exposed to laser light. Two

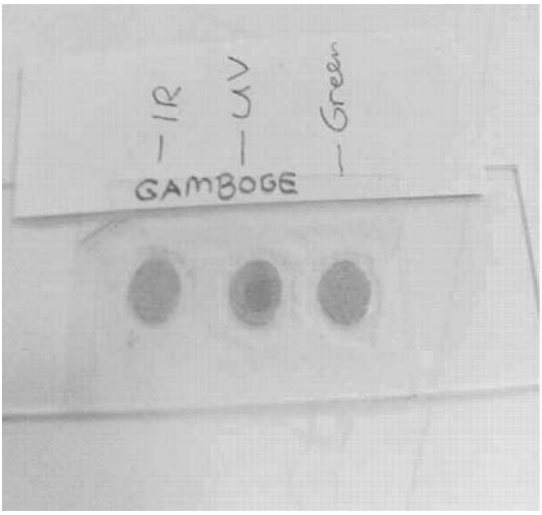

Fig. 1. Sample with UV exposure

were exposed to Nd:YAG at 1064 nm and 532 nm. The third was irradiated using an excimer laser operating at 351 nm (Xenon Fluoride). Additionally, some of the samples were placed between quartz slides and irradiated using an excimer laser operation at 248 nm (Krypton Fluoride).

A "Coherent" Q-switched Nd:YAG laser (top hat beam profile, 3 ns pulse length) was used, set at 3 Hz, 100 pulses. Edmond Scientific Plano-Concave lenses were used to diverge the beam. Only lenses used with 355 and 532 nm beams had an anti-reflective coating; the one for 1064 nm did not, producing small losses in fluence. A mask was placed in front of the sample and only a fraction of the light was used. This mask defined the spot size and was held at .5 cm. The energy was measured using a Coherent "LaserMate P" energy meter placed on the far side of the mask. An Ocean Optics spectrophotometer was used to measure reflectance and CIE L*, a* b* values.

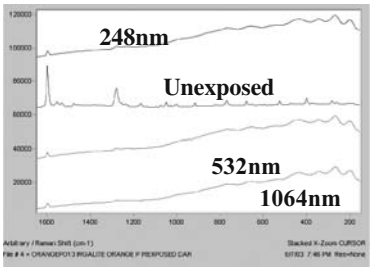

Fig. 2. Raman spectra of PO13 Irgalite Orange, color shifts seen at all wavelengths

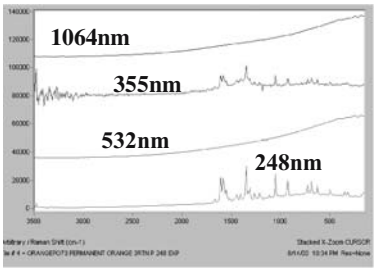

Fig. 3. PO73 Permanent Orange, all peaks lost in IR and Green

The excimer used was a Lambda Physik with a pulse length of 10 ns. In this case there was no lens used, but an iris was placed in front of the beam and only a fraction of the light was passed through to expose the sample. This iris defined the spot size and was held at .5 cm. The light through the iris was also measured using the energy meter as 50 mJ/.5 cm spot. The exposure time was limited to 5 seconds with the laser repetition rate set at 10 Hz. This resulted in a 50-pulse exposure for each sample. Again, an Ocean Optics spectrophotometer was used to measure reflectance and CIE L*, a* b* values.

3 Results and Discussion

Tables 1–4 give results of the tests for IR (1064 nm), visible (532 nm) and near UV (351 nm) laser exposure. The results are fairly straightforward. In most cases, the laser fluence required to cause a visible change in the pigment color was an order of magnitude higher for the 1064 nm then was required when using the visible and near IR (with the exception of some of the green and blue pigments). When the IR did change color the results were often more catastrophic with the color becoming much darker, while the changes were often less catastrophic when the changes were observed under green and near UV irradiation. These results were found through visible observation and confirmed using the colorimetry L*a*b* values. Raman spectroscopy (Chromex Senturion system operating at 785 nm) showed that when there was a large shift to darker colors, there was a loss of most of the Raman stretches. Further, the florescence under the Raman laser increased. This implies that most of the organic pigments bonds were broken by the laser irradiation. We surmise that the IR light is not absorbed as readily as the Visible and near UV but that when it does reach the threshold, the pigment is darkened due to excessive heating. In the case of the visible and near UV the color change begins at a lower fluence, but smaller color shifts are often seen. The Raman shifts are also more gradual and not all peaks are lost at the same rate. This may indicate that the light is coupling into some of the

bonds more readily. In a few cases (almost all of them with black or dark blue pigments) the L*a*b* values shifted lighter or the pigment bleached.

While the study was much less rigorous, a few of the pigments were exposed to 248 nm UV. The samples were less likely to darken catastrophically and generally required high fluences to change colors (60–80 Watts trough a 1.5 cm spot). At fluences above 100 Watts in the same spot the pigments fused in to a conglomerate. We found that in all cases the addition of medium (in this case acrylic) does inhibit the color change but should not be relied on to completely prevent surface changes to the pigments.

4 Conclusions

The conservation of paintings made using modern organic pigments is a new and often daunting challenge for conservators. The use of lasers may offer one solution to some of the problems faced when conserving these paintings. The laser may also be a good tool for removing over-paint that is based on modern organic pigments. In either case it is important to understand when color changes can be expected to occur and what type of changes to expect. It seems clear, that the use of IR or far UV wavelengths may inhibit color change, but that the IR is not forgiving if certain thresholds are crossed.

Acknowledgements

We would like to thank NCPTT, The Samuel H Kress Foundation, Los Angeles County Museum of Art and the Tate, as well as the following pigment suppliers Albion Colours, Avecia Ltd, Ciba Specialty Chemicals, Clariant, Golden Artist Colors Inc, Heubach, Lansco Colors, Royal Talens and Sun Chemical.

Table 1. Pigments tested with chemical type and manufacturer

CI #	Product	Manufacturer	Chemical Class	Before Exposure L*a*b*
Reds				
PR3	Hansa Scarlet RNC	Clariant	monoazo	40.76*51.53*40.73*
PR4	Hansa Red R	Clariant	monoazo	45.40*51.69*50.30*
PR5	Monolite Red CB	Avecia	monoazo	37.16*54.79*29.17*
PR23	1523 Naphthol Red	Lansco	monoazo	31.72*51.99*24.13*
PR49:1	Sunbrite Red 49:1	Sun	monoazo: Ba salt	33.75*52.79*34.72*
PR57:1	Sunbrite Rubine 4BK	Sun	monoazo: Ca salt	33.08*54.53*29.97*
PR83	Alizarine Crim son Dark	Kremer	anthraquinone	41.32*41.82*3.77*
PR112	Permanent Red FGR	Clariant	monoazo	42.95*60.15*44.54*
PR122	Sunfast Magenta 122	Sun	quinacridone	31.23*45.82*-6.88*
PR149	PV Fast Red B	Clariant	perylene	37.92*50.49*40.92*
PR170	Sunbrite Red 170	Sun	monoazo	32.01*50.36*29.57*
PR177	Cromophtal Red A2B	Ciba	anthraquinone	27.84*49.68*19.30*
PR178				38.39*50.99*25.09*
PR187	Novoperm Red HF4B	Clariant	monoazo	32.42*48.1*18.01*
PR188	Novoperm Red HF3S	Clariant	monoazo	49.90*61.17*50.98*
PR202	Cinquasia magenta RT-343-D	Ciba	quinacridone	25.10*42.11*-3.12*
PR206	Cinquasia Maroon RT-792-D	Ciba	quinacridone	23.61*20.09*-33.32*
PR209	Hostaperm Red EG transp	Clariant	quinacridone	40.35*54.23*31.48*
PR254	Irgazin DPP Red BO	Ciba	DPP (diketopyrrolopyrrole)	35.77*49.18*-6.47*
PR254	Irgazine red	Kremer 23180	diketo-pyrrolo-pyrrole	31.17*45.66*13.83*
PR255	Irgazin DPP Scarlet EK	Ciba	DPP	43.63*49.85*41.76*
PR255	Irgazine scarlet EK	Kremer 23179	diketo-pyrrolo-pyrrole	35.76*45.59*14.93*
PR264	Irgazin DPP Rubine TR	Ciba	DPP	24.49*49.06*25.17*
-	Irgazine ruby, opaque	Kremer 23182	diketo-pyrrolo-pyrrole	20.08*45.51*-41.84*
Oranges				
PO5	Monolite Red 2G	Avecia	monoazo	52.74*55.96*58.00*
PO13	Irgalite Orange P	Ciba	disazo	58.89*53.56*69.63*
PO36	Sunfast Orange 36	Sun	monoazo	51.27*43.84*48.39*
PO43	Hostaperm Orange GR	Clariant	perinone	55.07*56.03*63.46*

(*continued*)

Table 1. (*Continued*)

CI #	Product	Manufacturer	Chemical Class	Before Exposure L*a*b*
PO48	Cinquasia Gold YT-923-D	Ciba	quinacridone	30.54*28.5*27.24*
PO49	Cromophtal Orange 2G	Ciba	quinacridone	43.09*23.99*48.96*
PO62	Novoperm Orange H5G 70	Clariant	benzimidazolone	65.22*37.48*67.51*
PO73	Permanent Orange 3RTN p	Clariant	DPP	53.80*56.15*69.62*
-	Irgazine orange	Kremer 23178	diketo-pyrrolo-pyrrole	50.80*49.09*63.41*
Yellows				
PY1	Heuco Gelb 100100	Heubach	monoazo	76.69*4.07*85.99*
PY1:1	Monolite Yellow 2R	Avecia	monoazo	67.30*29.77*81.03*
PY3	Hansa-Gelb 10G	Clariant	monoazo	90.04*-9.49*93.98*
PY73	Hansa Brilliant Yellow 4GX	Clariant	monoazo	84.85*7.54*102.97*
PY74	Irgalite Yellow GO	Ciba	monoazo	81.12*4.68*91.77*
PY83	Sunbrite Yellow 83	Sun	disazo	73.26*31.58*99.19*
PY97	Novoperm Yellow FGL	Clariant	monoazo	83.94*6.67*95.35*
PY110	Irgazin Yellow 3RLTN	Ciba	isoindolinone	57.72*26.64*63.59*
PY128	Cromophtal Yellow 8GN	Ciba	disazo	84.10*2.76*93.33*
PY129	Irgazin Yellow 5GLT	Ciba	azomethine	48.23*-2.85*53.49*
PY154	Hostaperm Yellow H3G	Clariant	benzimidazolone	85.56*3.36*82.56*
Greens				
PG7	Monastral Green GNX-C	Avecia	phthalocyanine	30.55*-52.02*-0.783*
PG8	Bricofor Green L5837	Albion	nitroso (iron complex)	28.47*-21.86*10.39*
PG36	Monastral Green 6Y-C	Avecia	phthalocyanine	30.77*-51.39*11.15*
Blues				
PB15:0	Sunfast Blue	Lansco	phthalocyanine	18.58*11.96*-40.70*
PB60	Monolite Blue 3R	Avecia	indanthrone	10.14*-42.31*-1.06*
Violets				
PV19	Monolite Violet 4R	Avecia	quinacridone	14.50*30.64*1.15*
PV23	Cromophthal Violet	Golden	dioxazine	11.99*12.39*-7.25*
Blacks				
PBk1	PBk1	Royal Talens	azine	10.69*0.61*-1.01*
in media				
PR254	Irgazine red in acrylic (Lascaux 498)	Kremer 23180	diketo-pyrrolo-pyrrole	38.56*65.27*-8.88*

(*continued*)

Table 1. (*Continued*)

CI #	Product	Manufacturer	Chemical Class	Before Exposure L*a*b*
PR254	Irgazine red in oil (linseed)	Kremer 23180	diketo-pyrrolo-pyrrole	34.66*60.53*-8.49*
PR255	Irgazine scarlet EK in acrylic (Lascaux 498)	Kremer 23179	diketo-pyrrolo-pyrrole	40.67*54.77*55.52*
PR255	Irgazine scarlet in oil (linseed)	Kremer 23179	diketo-pyrrolo-pyrrole	41.67*61.75*-7.14*
-	Irgazine ruby, opaque in acrylic (Lascaux 498)	Kremer 23182	diketo-pyrrolo-pyrrole	22.18*42.66*-36.84*
-	Irgazine ruby, opaque in oil (linseed)	Kremer 23182	diketo-pyrrolo-pyrrole	17.57*37.43*-38.05*
-	Irgazine orange in acrylic (Lascaux 498)	Kremer 23178	diketo-pyrrolo-pyrrole	54.26*62.33*33.09*
-	Irgazine orange in oil (linseed)	Kremer 23178	diketo-pyrrolo-pyrrole	52.03*61.15*14.05*

Table 2. 1064 nm exposures with L*a*b* values and observations

CI #	Before Exposure L*a*b*	Nd:YAG 1064nm Visual Inspection	Laser Power (mJ) Where Change	L*a*b*
Reds			**observed**	
PR3	40.76*51.53*40.73*	shift to brn/black	.32 J/cm^2	16.67*16.26*12.45*
PR4	45.40*51.69*50.30*	shift to red/brn	.15 J/cm^2	13.88*8.07*-33.13*
PR5	37.16*54.79*29.17*	small shift darker	.37 J/cm^2	36.34*52.54*28.00*
PR23	31.72*51.99*24.13*	small shift darker	.32 J/cm^2	24.58*42.39*-1.58*
PR49:1	33.75*52.79*34.72*	shift lighter – yellow	.37 J/cm^2	35.89*54.86*37.48*
PR57:1	33.08*54.53*29.97*	shift to deep red/black	.37 J/cm^2	28.49*50.72*25.11*
PR83	41.32*41.82*3.77*	little or no shift	.37 J/cm^2	36.75*40.45*4.92*
PR112	42.95*60.15*44.54*	shift to black	.25 J/cm^2	12.54*23.97*-51.68*
PR122	31.23*45.82*-6.88*	shift to black	.37 J/cm^2	12.70*16.91*-3.69*
PR149	37.92*50.49*40.92*	shift to black	.17 J/cm^2	16.28*10.23*32.15*
PR170	32.01*50.36*29.57*	shift to darker	.45 J/cm^2	15.23*33.76*-45.23*
PR177	27.84*49.68*19.30*	shift pink/orange then black	.26 J/cm^2	11.54*12.67*-16.61*
PR178	38.39*50.99*25.09*	shift to black	.03 J/cm^2	32.14*40.83*20.54*
PR187	32.42*48.1*18.01*	shift lighter	.37 J/cm^2	32.61*43.91*15.49*
PR188	49.90*61.17*50.98*	small shift to brn	.37 J/cm^2	37.82*47.44*43.26*
PR202	25.10*42.11*-3.12*	shift to purple then black	.25 J/cm^2	15.67*19.94*-3.42*
PR206	23.61*20.09*-33.32*	shift lighter then dark red	.37 J/cm^2	10.99*7.51*-47.79*
PR209	40.35*54.23*31.48*	shift lighter then black	.25 J/cm^2	11.43*9.10*-44.82*
PR254	35.77*49.18*-6.47*	shift to dark red/brn	.25 J/cm^2	16.71*19.31*-35.67*
PR254	31.17*45.66*13.83*	shift to brn/black	.32 J/cm^2	12.12*11.46*-58/30
PR255	43.63*49.85*41.76*	small shift darker	.37 J/cm^2	38.64*48.36*37.88*
PR255	35.76*45.59*14.93*	shift darker	.25 J/cm^2	34.40*29.93*22.05*
PR264	24.49*49.06*25.17*	shift to darker/black	.32 J/cm^2	9.90*-45.01*-18.56*
-	20.08*45.51*-41.84*	shift to purple/black	.35 J/cm^2	6.79*-46.94*-16.26*
Oranges				
PO5	52.74*55.96*58.00*	small shift to brn	.25 J/cm^2	42.80*46.79*51.20*
PO13	58.89*53.56*69.63*	small shift to red/brn	.51 J/cm^2	40.19*43.57*32.20*
PO36	51.27*43.84*48.39*	shift lighter	.57 J/cm^2	44.91*36.78*47.25*
PO43	55.07*56.03*63.46*	black and disperse	.32 J/cm^2	11.38*5.59*-58.07*
PO48	30.54*28.5*27.24*	shift lighter	.19 J/cm^2	38.02*33.37*35.47*
PO49	43.09*23.99*48.96*	shift lighter – yellow	.05 J/cm^2	46.88*20.28*54.60*
PO62	65.22*37.48*67.51*	slightly tan @ center	.64 J/cm^2	56.72*32.68*62.92*
PO73	53.80*56.15*69.62*	black and disperse	.57 J/cm^2	21.51*26.26*-19.59*
-	50.80*49.09*63.41*	small shift to red	.76 J/cm^2	41.26*44.00*58.99*
Yellows				
PY1	76.69*4.07*85.99*	little or no shift	.28 J/cm^2	66.74*5.65*79.42*
PY1:1	67.30*29.77*81.03*	little or no shift	.28 J/cm^2	60.16*25.12*75.78*
PY3	90.04*-9.49*93.98*	small shift to brn	.28 J/cm^2	69.76*-2.09*76.23*
PY73	84.85*7.54*102.97*	little or no shift	.32 J/cm^2	74.21*5.87*87.86*
PY74	81.12*4.68*91.77*	little shift spot to brn	.32 J/cm^2	69.04*8.42*81.26*
PY83	73.26*31.58*99.19*	little or no shift	.37 J/cm^2	69.39*29.42*91.73*

(*continued*)

Table 2. *Continued*

CI #	Before Exposure L*a*b*	Nd:YAG 1064nm Visual Inspection	Laser Power (mJ) Where Change	L*a*b*
PY97	83.94*6.67*95.35*	slight shift to grey	.37 J/cm^2	67.71*3.61*78.44*
PY110	57.72*26.64*63.59*	black and disperse	.08 J/cm^2	15.54*2.15*7.96*
PY128	84.10*2.76*93.33*	black and disperse	.32 J/cm^2	29.65*3.70*29.29*
PY129	48.23*-2.85*53.49*	immediate shift darker	.03 J/cm^2	20.19*1.09*-4.54*
PY154	85.56*3.36*82.56*	slight shift to grey	.37 J/cm^2	66.70*0.477*59.56*
Greens				
PG7	30.55*-52.02*-0.783*	shift lighter center brown	.04 J/cm^2	19.28*-24.99*0.87*
PG8	28.47*-21.86*10.39*	immediate shift darker -yellow/brn	.02 J/cm^2	8.38*-8.46*-8.92*
PG36	30.77*-51.39*11.15*	immediate shift to black	.02 J/cm^2	16.97*-19.85*4.20*
Blues				
PB15:0	18.58*11.96*-40.70*	shift lighter purple outer black center	.05 J/cm^2	19.05*6.84*-37.03*
PB60	10.14*-42.31*-1.06*	shift lighter purple outer black center	.05 J/cm^2	8.56*-48.32*-1.97*
Violets				
PV19	14.50*30.64*1.15*	shift lighter	.37 J/cm^2	23.89*41.06*-8.81*
PV23	11.99*12.39*-7.25*	shift to red/purple black center	.05 J/cm^2	6.84*9.70*13.06*
Blacks				
PBk1	10.69*0.61*-1.01*	shift grey then center brn	.03 J/cm^2	20.00*0.38*0.40*

Table 3. 532 nm exposures with L*a*b* values and observation

CI #	Before Exposure L*a*b*	Nd:YAG 532nm Visual Inspection	Laser Power (mJ) Where Change	L*a*b*
Reds			**observed**	
PR3	40.76*51.53*40.73*	shift to brn/black	.015 J/cm^2	18.23*29.25*-45.40*
PR4	45.40*51.69*50.30*	shift to brn	.015 J/cm^2	34.13*42.66*40.58*
PR5	37.16*54.79*29.17*	immediate shift darker	.015 J/cm^2	28.86*44.08*20.70
PR23	31.72*51.99*24.13*	immediate small shift darker	.015 J/cm^2	27.07*48.11*24.46*
PR49:1	33.75*52.79*34.72*	shift duller - grey	.02 J/cm^2	30.64*34.03*22.47*
PR57:1	33.08*54.53*29.97*	shift darker also duller	.025 J/cm^2	28.12*24.69*11.91*
PR83	41.32*41.82*3.77*	little or no shift	.04 J/cm^2	35.06*35.67*5.64*
PR112	42.95*60.15*44.54*	small shift to brn/black	.015 J/cm^2	26.80*41.61*28.60*
PR122	31.23*45.82*-6.88*	shift darker black/red	.025 J/cm^2	21.39*34.93*-2.62
PR149	37.92*50.49*40.92*	immediate to brn	.015 J/cm^2	27.33*38.23*30.24*
PR170	32.01*50.36*29.57*	small shift to darker	.025 J/cm^2	30.93*47.29*25.04*
PR177	27.84*49.68*19.30*	immediate small shift darker	.015 J/cm^2	24.48*46.62*16.66*
PR178	38.39*50.99*25.09*	immediate shift to black	.015 J/cm^2	20.25*23..66*10.90*
PR187	32.42*48.1*18.01*	immediate small shift darker	.015 J/cm^2	29.45*48.63*17.20*
PR188	49.90*61.17*50.98*	shift to brn	.025 J/cm^2	32.70*43.65*12.57*
PR202	25.10*42.11*-3.12*	shift to deep purple/black	.015 J/cm^2	15.52*27.14*-2.41*
PR206	23.61*20.09*-33.32*	shift to purple/black	.02 J/cm^2	14.32*14.90*-43.37*
PR209	40.35*54.23*31.48*	shift to darker	.025 J/cm^2	26.46*35.82*22.58*
PR254	35.77*49.18*-6.47*	shift darker red	.015 J/cm^2	21.52*36.61*-27.04*
PR254	31.17*45.66*13.83*	shift to brn/black	.03 J/cm^2	17.69*20.61*-8.64*
PR255	43.63*49.85*41.76*	shift darker red	.03 J/cm^2	29.30*49.60*-5.53*
PR255	35.76*45.59*14.93*	shift darker/black	.04 J/cm^2	18.29*24.65*-26.72*
PR264	24.49*49.06*25.17*	immediate shift darker	.015 J/cm^2	21.66*32.09*10.56*
-	20.08*45.51*-41.84*	shift to brn/purple	.035 J/cm^2	12.11*11.92*-37.34*
Oranges				
PO5	52.74*55.96*58.00*	shift to brn/black	.015 J/cm^2	42.60*47.61*49.95*
PO13	58.89*53.56*69.63*	shift to brn/black	.025 J/cm^2	30.38*38.67*-20.55*
PO36	51.27*43.84*48.39*	shift to brn/black	.015 J/cm^2	36.59*31.45*26.45*
PO43	55.07*56.03*63.46*	immediate shift black	.015 J/cm^2	39.35*43.52*46.35*
PO48	30.54*28.5*27.24*	shift lighter & dispersion	.02 J/cm^2	33.53*27.32*30.07*
PO49	43.09*23.99*48.96*	shift lighter- yellow	.02 J/cm^2	41.36*14.80*48.03*
PO62	65.22*37.48*67.51*	shift to brn	.03 J/cm^2	45.51*26.94*16.34*
PO73	53.80*56.15*69.62*	shift red – some black	.03 J/cm^2	27.99*41.42*13.09*
-	50.80*49.09*63.41*	shift to red/brn	.04 J/cm^2	27.92*34.84*-10.06*
Yellows				
PY1	76.69*4.07*85.99*	shift to orange/brn	.05 J/cm^2	47.41*14.52*1.24*
PY1:1	67.30*29.77*81.03*	large shift to orange/brn	.05 J/cm^2	39.84*24.63*-3.70*
PY3	90.04*-9.49*93.98*	large shift to orange/brn	8 J/cm^2	37.78*7.74*1.30*
PY73	84.85*7.54*102.97*	shift to orange/brn	.12 J/cm^2	57.88*18.18*81.51*
PY74	81.12*4.68*91.77*	shift to brn/black	.04 J/cm^2	54.84*16.59*14.70*

(*continued*)

Table 3. (*Continued*)

CI #	Before Exposure L*a*b*	Nd:YAG 532nm Visual Inspection	Laser Power (mJ) Where Change	L*a*b*
PY83	73.26*31.58*99.19*	shift to brn/black	.04 J/cm^2	43.30*27.20*1.47*
PY97	83.94*6.67*95.35*	shift to brn	.06 J/cm^2	58.62*14.35*60.52*
PY110	57.72*26.64*63.59*	shift to brn/black(center)	.03 J/cm^2	34.73*11.37*40.57*
PY128	84.10*2.76*93.33*	shift to orange/brn	8 J/cm^2	58.56*5.20*68.46*
PY129	48.23*-2.85*53.49*	immediate shift darker	.015 J/cm^2	24.13*1.44*-0.22*
PY154	85.56*3.36*82.56*	shift to red/orange	7 J/cm^2	52.06*16.48*22.83*
Greens				
PG7	30.55*-52.02*-0.783*	shift lighter then brown	.03 J/cm^2	17.29*-21.29*-0.457*
PG8	28.47*-21.86*10.39*	immediate shift to brn	.015 J/cm^2	20.25*-11.41*15.08*
PG36	30.77*-51.39*11.15*	immediate shift to black	.015 J/cm^2	22.49*-36.52*7.94*
Blues				
PB15:0	18.58*11.96*-40.70*	shift deep blue then black	.025 J/cm^2	12.07*6.41*-36.42*
PB60	10.14*-42.31*-1.06*	immediate shift to black	.015 J/cm^2	8.26*-110.70*29.90*
Violets				
PV19	14.50*30.64*1.15*	some darkening dispersion	.03 J/cm^2	17.66*33.80*1.43*
PV23	11.99*12.39*-7.25*	shift to black – yellow haze	.015 J/cm^2	11.29*3.10*-1.81*
Blacks				
PBk1	10.69*0.61*-1.01*	immediate shift lighter – grey	.015 J/cm^2	19.38*-0.017*-2.22*
in media				
PR254	38.56*65.27*-8.88*	shift to dark red	.015 J/cm^2	35.28*53.22*37.58*
PR254	34.66*60.53*-8.49*	small shift dark ablation gloss loss	.015 J/cm^2	37.97*51.73*40.09*
PR255	40.67*54.77*55.52*	shift darker red	.015 J/cm^2	36.37*51.23*39.67*
PR255	41.67*61.75*-7.14*	shift darker red slight gloss loss	.015 J/cm^2	41.05*57.37*50.06*
-	22.18*42.66*-36.84*	shift darker	.015 J/cm^2	20.31*33.81*-24.55*
-	17.57*37.43*-38.05*	some gloss loss small shift dark	.015 J/cm^2	15.14*31.41*-43.33*
-	54.26*62.33*33.09*	gloss loss	.03 J/cm^2	44.82*56.28*57.14*
-	52.03*61.15*14.05*	little or no change	.015 J/cm^2	53.21*55.19*62.53*

Table 4. 351 nm exposed at .06 J/cm^2 with L*a*b* values and observations

CI #	**Before Exposure** L*a*b*	Excimer at 351nm Visual Inspection	After Expoxure L*a*b*
Reds			
PR3	40.76*51.53*40.73*	shift to brn	34.19*51.16*37.07*
PR4	45.40*51.69*50.30*	large shift to brn	28.42*31.29*27.95*
PR5	37.16*54.79*29.17*	small shift to darker	27.41*47.77*24.70*
PR23	31.72*51.99*24.13*	small shift to darker	25.30*43.73*24.52*
PR49:1	33.75*52.79*34.72*	small shift to darker	28.94*42.11*27.97*
PR57:1	33.08*54.53*29.97*	little or no shift	32.85*52.16*24.11*
PR83	41.32*41.82*3.77*	little or no shift	36.15*39.46*5.83*
PR112	42.95*60.15*44.54*	small shift to darker	34.53*58.15*40.83*
PR122	31.23*45.82*-6.88*	small shift to brn	21.55*48.17*-10.36*
PR149	37.92*50.49*40.92*	little or no shift	33.44*51.37*39.50*
PR170	32.01*50.36*29.57*	little or no shift	32.97*50.35*27.81*
PR177	27.84*49.68*19.30*	little or no shift	24.05*48.42*17.72*
PR178	38.39*50.99*25.09*	shift to red	24.34*27.63*15.62*
PR187	32.42*48.1*18.01*	small shift to purple	27.67*50.52*18.68*
PR188	49.90*61.17*50.98*	small shift to darker	40.42*60.56*49.10*
PR202	25.10*42.11*-3.12*	little or no shift	4.66*13.88*0.0933*
PR206	23.61*20.09*-33.32*	small shift to purple	13.62*19.43*-42.32*
PR209	40.35*54.23*31.48*	little or no shift	30.85*48.66*29.92*
PR254	35.77*49.18*-6.47*	shift darker	27.12*54.35*-17.36*
PR254	31.17*45.66*13.83*	shift darker	29.73*51.20*-7.95*
PR255	43.63*49.85*41.76*	small shift to darker	32.56*56.28*-22.22*
PR255	35.76*45.59*14.93*	shift darker	32.89*58.33*41.95*
PR264	24.49*49.06*25.17*	shift darker	19.35*36.56*13.68*
-	20.08*45.51*-41.84*	shift darker	16.04*23.32*-32.73*
Oranges			
PO5	52.74*55.96*58.00*	shift to brn	34.19*39.26*36.18*
PO13	58.89*53.56*69.63*	shift to brn	42.52*42.05*38.99*
PO36	51.27*43.84*48.39*	shift to brn	44.00*39.03*44.07*
PO43	55.07*56.03*63.46*	small shift to brn	46.21*61.83*62.70*
PO48	30.54*28.5*27.24*	small shift to brn	26.46*30.78*27.77*
PO49	43.09*23.99*48.96*	small shift to brn	33.77*22.37*37.82*
PO62	65.22*37.48*67.51*	shift to brn	38.08*35.96*57.01*
PO73	53.80*56.15*69.62*	little or no shift	51.91*61.77*8.64*
-	50.80*49.09*63.41*	shift to red/brn	38.21*44.51*40.87*
Yellows			
PY1	76.69*4.07*85.99*	shift to brn	62.75*19.26*73.08*
PY1:1	67.30*29.77*81.03*	shift to brn	64.37*33.71*82.09*
PY3	90.04*-9.49*93.98*	large shift to brn	63.89*6.55*67.47*
PY73	84.85*7.54*102.97*	shift to brn	69.50*14.79*87.26*
PY74	81.12*4.68*91.77*	shift to brn	69.64*19.90*60.08*
PY83	73.26*31.58*99.19*	large shift to brn	51.19*23.29*50.14*
PY97	83.94*6.67*95.35*	shift to brn	73.16*13.69*85.99*
PY110	57.72*26.64*63.59*	shift to brn	46.95*21.50*51.79*
PY128	84.10*2.76*93.33*	small shift to brn	73.41*5.03*81.96*
PY129	48.23*-2.85*53.49*	shift darker	30.41*0.56*26.15*
PY154	85.56*3.36*82.56*	shift darker	64.06*9.87*62.88*

(*continued*)

Table 4. (*Continued*)

CI #	**Before Exposure** L*a*b*	Excimer at 351nm Visual Inspection	After Expoxure L*a*b*
Greens			
PG7	30.55*-52.02*-0.783*	little or no shift	19.02*-27.57*0.243
PG8	28.47*-21.86*10.39*	small shift to darker	27.34*-13.33*11.54*
PG36	30.77*-51.39*11.15*	small shift to darker	13.54*84.44*-36.86*
Blues			
PB15:0	18.58*11.96*-40.70*	little or no shift	14.23*6.81*-30.77*
PB60	10.14*-42.31*-1.06*	little or no shift	6.45*-161.37*47.23*
Violets			
PV19	14.50*30.64*1.15*	little or no shift	13.95*37.60*-5.71*
PV23	11.99*12.39*-7.25*	little or no shift	4.27*2.96*3.25*
Blacks			
PBk1	10.69*0.61*-1.01*	little or no shift	14.42*-0.69*-0.60*
in media			
PR254	38.56*65.27*-8.88*	shift darker iridescent edge	33.89*63.35*-19.27*
PR254	34.66*60.53*-8.49*	gloss loss small shift dark	33.84*44.90*31.75*
PR255	40.67*54.77*55.52*	shift to darker red	40.04*63.94*49.76*
PR255	41.67*61.75*-7.14*	paint layer ablated	35.84*50.92*25.62*
-	22.18*42.66*-36.84*	no change	20.69*39.64*0.1133*
-	17.57*37.43*-38.05*	completely ablated	-
-	54.26*62.33*33.09*	slight shift darker	51.00*61.52*69.51*
-	52.03*61.15*14.05*	gloss loss slight shift dark	55.79*54.23*58.15*

Laser Paint Interactions Studied by Optical Emission Spectroscopy and Pump and Probe Analysis of the Ablation Plume

E. Rebollar, M. Oujja, M. Martín, and M. Castillejo

Institute of Physical Chemistry Rocasolano, CSIC, Serrano 119, 28006 Madrid, Spain
marta.castillejo@iqfr.csic.es

Abstract. The ablation plumes resulting from the laser irradiation of pigments in the form of pellets and as tempera paints were studied by optical spectroscopic methods including optical emission spectroscopy (OES) and laser induced fluorescence (LIF), using a probe laser, delayed with respect to the ablation laser. The differences observed between emissions from pellets and from tempera paints of a given pigment, and between organic and inorganic pigments, serve to discuss the mechanisms operating in the laser irradiation of the paint systems.

1 Introduction

Laser cleaning of artistic paintings aims at the removal of old polymerised varnish layers or to the elimination of superficial contaminants such as shoot, polymerised dirt, etc [1–3]. Safe laser cleaning of pictorial surfaces should incorporate in situ diagnostic techniques, such as LIBS (laser induced breakdown spectroscopy), to warn against the direct interaction of the laser beam with light-sensitive paint materials, including pigments and binders. Laser irradiation can cause discoloration, alterations in the molecular composition of pigments or degradation of the binding medium. Ongoing research [2, 4–9] points towards the elucidation of the physical and chemical alterations that result from these interactions and the underlying mechanisms. The latter should be dependent on the irradiation conditions (wavelength, pulse duration, fluence, etc) and on the nature of the paint materials. Pouli et al. [4, 8] have investigated the discoloration resulting from the 1064 nm irradiation of vermillion and several lead and copper based pigments and have suggested that the mechanism responsible for blackening is reduction. Cooper et al. [7] have analysed the laser-induced discoloration of lead white upon irradiation at 1064 nm and have given evidence for the formation of elemental lead, resulting from conversion of basic lead carbonate. Discoloration has been observed to be stronger in the presence of binding medium.

Analysis of the plasma plume by means of optical spectroscopic techniques is a widely used tool for the diagnosis of surface ablation processes [10, 11].

Starting with a preliminary study [12], and aiming at investigating the basic interactions of the laser with paint materials, we have undertaken a systematic spectroscopic characterisation of the plasma ablation plume created in vacuum by laser ablation of single and composite systems constituted by pigments in the form of pellets and in tempera mixtures. Systems under study, listed in Table 1, include traditional inorganic and organic pigments, such as azurite, lead white, lead chromate, zinc white and curcumin. Time resolved optical emission spectroscopy (OES) was employed to measure the spontaneous emission of electronically excited atomic and molecular species. A pump and probe scheme, with a probe dye laser temporally delayed with respect to the ablation laser, served to perform laser-induced fluorescence (LIF) measurements of non-emitting species present in the ablation plume.

Table 1. Selected emissions and velocity of flight measurements (by OES) for the pigments studied in this work. *T* and *P* stand for tempera and pellet respectively

Pigment	Composition	Selected Emissions in nm	Velocity of Flight $\times 10^3$ m/s [12]
Unpigmented		$C_2(d^3\pi_g)$, 516.5	7.7
Azurite	Basic copper carbonate, $2CuCO_3.Cu(OH)_2$	Cu I, 521.82;	10.4 (*T*), 10.8 (*P*)
Lead white	Basic lead carbonate, $2PbCO_3.Pb(OH)_2$	Pb I, 405.78; $C_2(d^3\pi_g)$, 516.5	9.1 (*T*), 8.2 (*P*) 7.6 (*T*)
Lead chromate	$PbCrO_4$	Cr I, 520.99; Pb I, 405.78	11.1 (*T*), 8.3 (*P*) 11.7 (*T*), 9.3 (*P*)
Zinc white	ZnO	Zn I, 481.05; Zn II, 491.1; O I, 777.3; ZnO, 383	10.5 (*T*), 7.4 (*P*) 11.5(*T*)
Curcumin	$C_{21}H_{20}O$	$C_2(d^3\pi_g)$, 516.5	8.0 (*T*), 8.0 and 3.0 (*P*)

2 Experimental Methods

Pigments were used as pellets and as paint tempera samples (of 500 µm and 200 µm thickness respectively). Tempera samples were prepared according to the procedure described in [13], by depositing a layer mixture of the pigment in powder with an egg-based binding medium (egg-yolk emulsion and mastic) on a sheet of Mellinex. Unpigmented tempera samples were also prepared for comparison. The films were allowed to dry in the dark for more than a year before measurements. Ablation, carried out in a cross-shaped glass vacuum cell (pressure 9 Pa), resulted in a visible plume that extends about 20 mm above the surface, allowing the spectroscopic characterisation of the plume with spatial resolution.

The samples were ablated with a pulsed KrF excimer laser (248 nm, 20 ns FWHM) or with the fourth harmonic of a Q-switched Nd:YAG laser (Quantel Brilliant B, 266 nm, 5 ns FWHM). LIB spectra were recorded with a 0.30 m spectrograph (TMc300 Bentham, 1200 grooves/mm, 500 nm blaze) coupled to a time gated ICCD camera (2151 Andor Technologies). The spectra were obtained at a suitable time delay, around 500 ns, and with a temporal observation window of typically 10 µs.

For OES, the spontaneous emission from selected regions of the emitting ablation plume, at various distances d from the sample surface, was viewed perpendicularly to the laser beam by a $f = 4$ cm quartz lens and imaged onto the entrance slit of a high intensity monochromator coupled to a photomultiplier (PMT, Hamamatsu R928, rise time 2.2 ns). To select emissions from regions of the plume at different distances from the surface, the assembly formed by the sample and the lens, that focuses the ablation laser onto the surface, were placed in a translational stage that could move perpendicularly to the fixed axis of detection. The signal from the PMT was fed into a 100 MHz digital oscilloscope interfaced with a PC for measurements of the time resolved emissions.

For LIF studies, the samples were ablated at 248 nm with the KrF laser and the plume probed by a tunable dye laser propagating at a given distance from the sample, around 8 mm, parallel to its surface and perpendicularly to the ablating laser. The ablation-probe delay, in the range of 0–10 µs, was controlled with a BNC555 delay generator, allowing the monitoring of products in the volume of the plume that was being probed at various times after the start of the ablating pulse. Time-resolved LIF, following the excitation of the selected transition, was observed with the PMT behind a combination of a cut off and a 10 nm bandwidth interference filters. LIF of C_2 in the $a^3\pi_u$ state, only 716.24 cm^{-1} above the ground state of the molecule, was carried out by excitation of the (0,0) band of the $C_2(d^3\pi_g \leftarrow a^3\pi_u)$ transition with Coumarin 522 dye at 516.5 nm. The fluorescence corresponding to the (0,1) band of the same electronic transition was observed at 560 nm. C_2 measurements were motivated by the fact that this molecule is considered to be a building stone for carbonisation or charring. Attempts were made to excite ZnO transients in the plume using as probe the second or the third harmonic of the Nd:YAG laser at 266 and 355 nm respectively. However, in the experimental conditions of this work, no laser induced signal was observed in the spectral range of 300 to 550 nm.

3 Results and Discussion

As reported previously [2, 6] the ablation plume of tempera samples, measured by LIBS, contains spontaneous emissions due to atomic species, present in the pigment composition, atomic calcium and molecular organic fragments

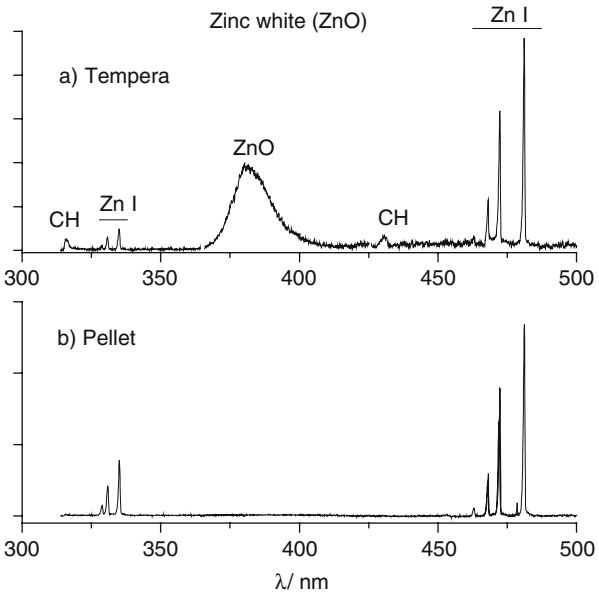

Fig. 1. LIB spectra of ZnO as tempera paint and pellet monitored at $d = 0$ from the surface. Samples were ablated at 266 nm at a fluence of $1.4\,\mathrm{J/cm^2}$

such as C_2, CN and CH. Comparison of the LIB spectra of pellets and of tempera paints reveals some differences. As an example, we show in Fig. 1 the LIB spectra of zinc white samples. The plume luminescence is due to excited Zn and O neutral atoms (Zn I and O I) and Zn^+ ions (Zn II), and, in the case of the tempera paint, it includes also the broad UV emission band of ZnO centred at 383 nm [12]. This emission, detected in regions of the plume close to the surface, could be due to fluorescence from the surface or to spontaneous photoluminiscence of ZnO nanoparticles formed by collisions between ablated particles or reactions with residual oxygen [15, 16]. As fluorecence from the surface should have been observed in the pellet as well, the second possibility is more likely. In fact, zinc oxide strongly absorbs at 248 nm as the photon energy exceeds the band-gap energy of the semiconductor (the optical absorption coefficient is $3.3 \times 10^5\,\mathrm{cm^{-1}}$ [10]). In the tempera mixture, the effective optical absorption should be reduced due to the presence of natural polymers in the binder with lower absorption coefficient at the laser wavelength. Consequently, for a given fluence above threshold, the thickness of layer ablated per pulse, expected to grow inversely with the effective absorption coefficient [2, 11], should be larger in the composite tempera than in the pellet. In the presence of the binder, the density of species in the plume is higher, increasing the number of collisions and the probability of reaction and recombination processes.

We measured the dependence of the more prominent atomic and molecular emissions on laser fluence, as listed in Table 1. The emission intensity was found to increase with increasing incident fluence as illustrated in Fig. 2 for the 266 nm ablation of zinc white. Up to $3\,J/cm^2$, emissions in the pellet of this pigment increase slowly with fluence, whereas a steeper increase is observed in the tempera sample in the same fluence range. The already mentioned higher density of species in the plume of the tempera sample, could explain the more sudden increase of emitters. For the pellet, the fraction of ions within the plasma plume is higher at increasing fluence (Fig. 2b). The similar fluence dependence found in this case for zinc neutrals and ions (Zn I and Zn II) suggests the participation of electron-ion recombination reactions [16] to give rise to the electronically excited neutrals.

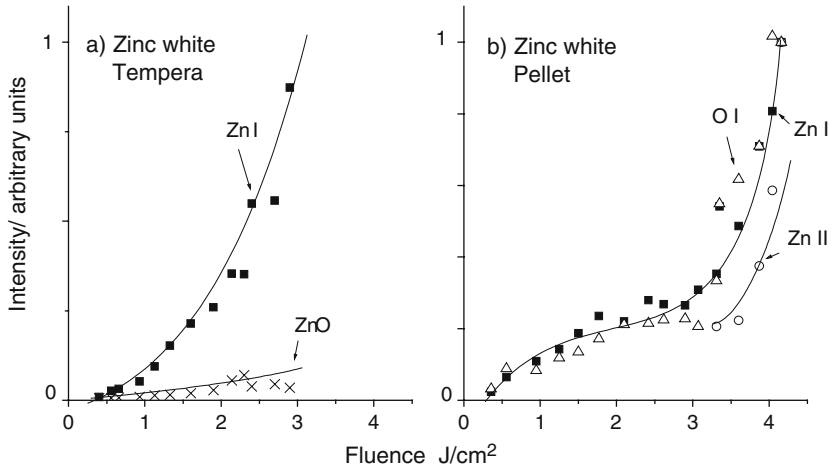

Fig. 2. Normalized time integrated emissions (measured with the ICCD detector) in the 266 nm ablation of a tempera sample (**a**) and of a pellet (**b**) of zinc white as a function of laser fluence, measured at $d = 6$ and 3 mm respectively from the surface. The lines are visual guides

The velocities of flight of the emitting transients were determined by OES through the correlation between the distance to the sample surface and the time of maximum signal intensity. Systematic measurements for the systems studied are summarized in Table 1. In Fig. 3 the distance-time correlation is displayed for the Zn I emission of zinc white and the $C_2(d^3\pi_g)$ emission of curcumin in the ablation at 248 nm. A linear correlation is observed in the case of zinc white, where the slope of the fit gives an estimation of the velocities of flight of the Zn I transient of 10.4×10^3 m/s for the tempera and slower, 7.2×10^3 m/s, for the pellet. As a general trend for the inorganic pigments (Table 1), the emitting transients from the tempera systems are ejected at higher velocities than from the pellets.

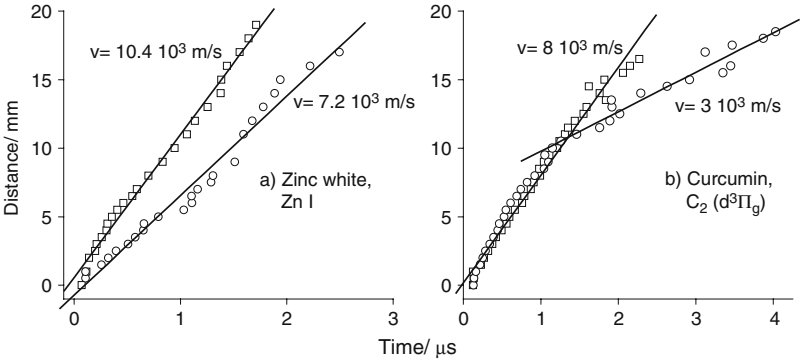

Fig. 3. Distance of observation *vs.* time of maximum intensity of emissions in the 248 nm ablation of pellets (*circles*) and tempera paints (*squares*) for: (**a**) neutral Zn at 481.05 nm from zinc white and (**b**) $C_2(d^3\pi_g)$ at 516.5 nm from curcumin. The slopes of the linear fits give the velocities of flight. Ablation fluence is 2.0 J/cm^2

In those systems, the thermal conductivity of the pure pigment is higher than in mixtures with the binder; henceforth, laser energy is easily dissipated into the substrate. On the contrary, in the presence of the binder, thermal build up in the ablation region should become important, explaining the higher translational energy of ejected species in the case of tempera mixtures.

For curcumin, the distance-time correlation was also found linear in the tempera system, with a transient velocity of flight of 8.0×103 m/s. However, in the pellet, a bimodal behaviour is observed with a slower velocity component of 3.0×10^3 m/s. This non-linear behaviour may reflect the different interaction of the laser with the pigment in absence of binding medium [11].

By means of LIF we measured the distribution of flight velocities of $C_2(a^3\pi_u)$ transients from the samples. Figure 4 shows the results for azurite. Fits to Maxwell-Boltzmann distributions [10] provided an estimation of the most probable translational velocities corresponding to 3.4×10^3 m/s (tempera) and 1.7×10^3 m/s (pellet) These results illustrate again, that transients produced in the ablation of inorganic systems fly at higher velocities in the plume of tempera paints than in the plume of pellets. These differences might reveal how the production of C_2 particles, through the interaction of the laser with the organic binding medium, is affected by the presence of the pigment in the paint.

4 Conclusions

The spectroscopical characterization of the UV laser ablation plumes of pigments as pellets and in mixtures with an egg-based binder allows observing substantial differences on the spectra, emission fluence dependence and velocity of flight of atomic and molecular species. These differences suggest

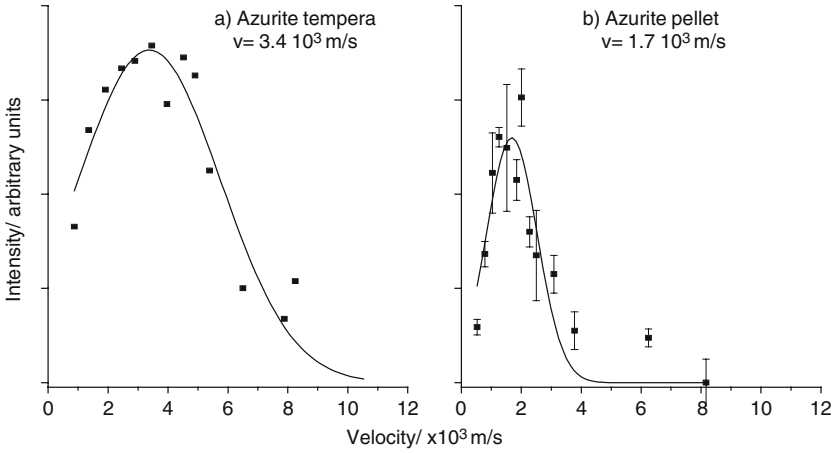

Fig. 4. LIF signal of C_2 ($a^3\pi_u$) as a function of flight velocity from samples of azurite: (**a**) as tempera paint, and (**b**) as pellet. The continuous lines represent fits to Maxwell–Boltzmann distributions with the indicated most probable velocity. Ablation is at 248 nm with a fluence of 2.0 J/cm^2

modifications of the laser interaction with the pigments in presence of the binding medium. For inorganic pigments with resonant absorption at the laser wavelength, the translational temperatures of the ejected species are higher in tempera than in pellets. Inorganic pigments feature higher thermal conductivity and heat diffusivity than the constituent polymeric materials of the binder or than the organic pigments. Therefore a higher thermal loading of the ablation region and a larger dimension of the heat-affected zone is expected when irradiating inorganic paints. This would explain the increasing discoloration in the presence of the binder as noticed by us and other authors [7]. In organic pigments, such as curcumin, although the laser will interact similarly with pigment and binder, mainly through photochemical interactions [2, 6, 12], the different spontaneous emission behaviour may reflect the enhanced photochemical activity attributed to the pigment.

Acknowledgements

Thanks to CORESAL, Spain, for sample preparation and to MCYT for funding (Project BQU2000-1163-C02-01). MO and ER thank CM and CSIC respectively for fellowships.

References

1. S. Georgiou, V. Zafiropulos, D. Anglos, C. Balas, V. Tornari, and C. Fotakis, *Appl. Surf. Sci.* **127–129**, 738, 1998

2. M. Castillejo, M. Martín, M. Oujja, D. Silva, R. Torres, V. Zafiropulos, O. F. van den Brink, R. M. A. Heeren, R. Teule, and A. Silva, *Anal. Chem.* **74**, 4662, 2002
3. M. Castillejo, M. Martín, M. Oujja, E. Rebollar, C. Domingo, J. V. García-Ramos, and S. Sánchez-Cortés, *J. Cult. Herit.* in press, 2003
4. P. Pouli, D. C. Emmony, C. E. Madden, and I. Sutherland, *Appl. Surf. Scien.* **173**, 252, 2001
5. V. Zafiropulos, T. Stratoudaki, A. Manousaki, K. Melesanaki, and G. Orial, *Surf. Eng.* **17**, 249, 2001
6. M. Castillejo, M. Martín, M. Oujja, J. Santamaría, D. Silva, R. Torres, A. Manousaki, V. Zafiropulos, O. F. van den Brink, R. M. A. Heeren, R. Teule, and A. Silva, *J. Cult. Herit.* **4**, 257s, 2003
7. M. I. Cooper, P. S. Fowles, and C. C. Tang, *Appl. Surf. Scien*, **201**, 75, 2002
8. P. Pouli, D. C. Emmony, C. E. Madden, and I. Sutherland, *J. Cult. Herit.* **4**, 271s, 2003
9. M. Chappé, J. Hildenhagen, K. Dickmann, and M. Bredol, *J. Cult. Herit.* **4**, 264s, (2003)
10. R. Srinivasan and B. Braren, *Chem. Rev.* **89**, 1303, 1989
11. D. Bäuerle, Laser processing and Chemistry, Springer, Berlin 2000, pp 527
12. M. Oujja, E. Rebollar, and M. Castillejo, *Appl. Surf. Sci.* **211**, 128, 2003
13. O. F Van den Brink, Molecular changes in egg tempera paint dosimeters as tools to monitor the museum environment, Ph.D. Thesis, University Amsterdam, 2001
14. V. Srikant, and D. R. Clarke, *J. Appl. Phys.* **83**, 5447, 1998
15. I. Ozerov, A. Bulgakov, D. Nelson, R. Castell, M. Sentis, and W. Marine, *J. Phys. IV* **108**, 37, 2003
16. F. Claeyssens, A. Cheesman, S. H. Henley, and M. N. R. Ashfold, *J. Appl. Phys.* **92**, 6886, 2002

Effects of Laser Irradiation on Artwork Pigments Studied by Laser Ablation and Time-of-Flight Mass Spectrometry

R. Torres, M. Jadraque, M. Castillejo, and M. Martín

Instituto de Química Física Rocasolano, C.S.I.C. Serrano 119, 28006-Madrid
mmm@iqfr.csic.es

Abstract. Laser ablation and time-of-flight mass spectrometric analysis of the ablation plume is used to study the different response of several inorganic pigments to laser irradiation. Lead white and lead chromate in pellets and in a binding media are studied. Lead white is compared to azurite, of similar stoichiometry. For lead white the plume composition is rather independent on laser ablation wavelength and does not show important changes after repeated laser beam exposure opposite to that observed for azurite. Ablation of lead white pellets leads to ionized and neutral Pb and $Pb_nO_mH_x$ clusters. Much less extent of aggregation in the plume is observed for lead chromate pellets and for the lead pigments in tempera. Similarities can be found between plume composition of ablated lead white and PbO, suggesting that laser/pigment interaction involves formation of PbO, therefore providing indications of the participation of a thermal decomposition mechanism.

1 Introduction

Understanding the mechanisms responsible for damage of pigments due to laser material interactions during laser cleaning is of relevance for an optimal design of laser cleaning procedures. For instance the presence of thermal effects can be revealed through investigation of the ablation processes as a function of wavelength and laser fluence, helping to a better choice of laser cleaning parameters.

Laser effects on pigments as a result of laser irradiation have been investigated by a variety of techniques [1]. Mass spectrometry is a highly sensitive technique that in combination with laser ablation or other techniques has been used in the characterization of inorganic materials.

This work aims at obtaining some insight into the mechanisms responsible for side effects on artwork pigments caused by radiation exposure during laser cleaning. The combination of laser ablation and time-of-flight mass spectrometric analysis of the plume is used to obtain information about the laser induced chemical changes on lead pigments, lead chromate ($PbCrO_4$) and lead white ($2Pb(CO_3{\cdot}Pb(OH)_2$). The response to laser interaction of lead white will be compared to some results obtained on azurite that has similar stoichiometry.

2 Experimental Methods

Pigments in the form of pressed pellets or dispersed in a tempera binding media were analysed. Laser irradiation was carried out at several excimer laser wavelengths (193, 248 and 308 nm). The experimental system has been described elsewhere [2] and only a brief description is given here. The samples were introduced in a vacuum chamber that houses the extraction/acceleration plates of a time-of-flight mass spectrometer. The sample was positioned with its surface perpendicular to the flight axis. The ablation laser entered the chamber with incidence along the surface normal and perpendicular to the flight axis. Laser fluences were kept to the minimum value to observe ion signal. This condition was achieved limiting the laser beam with apertures smaller than 5 mm in diameter. The laser energy entering the chamber was in the range of 0.5 to 2 mJ and the sample was placed between 0.5 to 2 cm away from the more focussed point of the laser beam. Ions produced in laser ablation/irradiation are deflected by the repeller plate, accelerated along the flight axis and detected by a dual 1.8 cm micro channel plate detector assembly. The drift region was 95 cm in length. Pulsed extraction voltages could be applied to the repeller at different time delays with respect to the ablating laser.

Neutral species formed in the laser ablation of the material were detected by post-ionisation with a second laser. The post-ionising laser (ArF at 193 nm) entered the chamber perpendicularly to both the ablation laser and the flight axis, intersecting the ablation plume in the region between the repeller/extracting plates of the TOF MS. The ion signal was detected by micro channel plates, recorded in a Tektronix TDS 3012 digital oscilloscope and transferred to a personal computer for storage and analysis.

3 Results and Discussion

Mass spectra of the ablation plume were recorded at laser wavelengths of 193, 248 and 308 nm and at different number of laser shots impinging on the same spot of the sample. Mass spectra obtained from lead white were rather independent on ablation wavelength. At the three wavelengths the spectrum of non previously irradiated samples showed broad features that can be assigned to Pb and clusters containing Pb. Successive laser irradiation led to narrower signal and improved spectral resolution.

Despite the similar chemical composition between lead white and azurite, the latter showed a rather different behaviour. The ablated species detected in the plume were strongly dependent on laser wavelength and number of laser shots. At the three studied wavelengths, the mass spectra from non irradiated samples showed only a broad feature assigned to K^+ impurity; successive beam irradiation, typically ten to twenty laser shots, was needed to make detectable other ejected species. Under ArF laser irradiation at 193 nm

the spectra showed signal from K^+ impurities and a single peak at m/z in the region of 207 amu that could not be unequivocally assigned. Under repeated laser ablation with a KrF laser at 248 nm Cu^+ is observed. At 308 nm a large abundance of species were detected in the plume, the main intensity corresponding to Cu^+, Cu_n, oxidised and mixed copper clusters.

In view of the higher number of ejected species that could be observed by ablation at 308 nm, plume composition was analysed at this wavelength. Species ionized in the ablation and neutral ejects, post-ionized with a second laser, could be detected. The effect of chemical composition and of a binding media was studied by comparing plume composition of pellets and tempera samples of lead white and lead chromate. The main neutral and ionised species produced in the ablation plume at 308 are listed in Table 1. Mass spectra of lead white in pellets are shown in Fig. 1. Pb^+ appears in all cases. Lead white pellets gave the most complex spectra consisting of series of $Pb_nO_{n-1}H_x^+$ and $Pb_nO_nH_x^+$ (n = 1–4; x = 1–3) clusters, decreasing in intensity with increasing n. Neutral ejected species are Pb and $Pb_nO_nH_x$ (n = 1,2; x = 1–3). The broad mass range (spanning 6 and 12 mass units for peaks containing one and two Pb atoms respectively makes uncertain the number of H atoms present. At long delays between ablation and post ionization the weak laser signal was readily assigned to pure Pb_n clusters (n = 3–10). Mass spectra of tempera samples showed several differences with respect to that of pellets. Pb_2^+ was the heaviest ionised cluster detected and several peaks in the m/z region between 57 to 158 amu were observed. The latter develop after a larger exposure to the laser than that required for Pb clusters detection. Mass peaks can be grouped in two series equally spaced by 16 amu. Features

Table 1. Plume composition of lead pigments after repeated XeCl laser beam exposure

Lead White (Pellets)	Lead White (Tempera)	Lead Chromate (Pellets)	Lead Chromate (Tempera)
Pb_n^+, Pb_n (n = 1, 2)	Pb_n^+ (n = 1, 2)	$Cr^{+(2)}$	Pb^+
$(PbO)_n$ Pb^+	Pb_n (n = 1–10)	Pb_n^+ (n = 1, 2)	$Pb_nO_m^+$ (n = 1,2)$^{(3)}$
(n = 1 − 4) $^{(1)}$	Pb_n O (ionized and	Pb	Two series m/z =
$(PbO)_nPbO^+$	neutral n = 1, (n = 2)$^{(1)}$	$Pb_nO_m^+$ (n = 1)$^{(3)}$	50–130
0 – 4)$^{(1)}$	Two series m/z =	Na^+, K^+	Na^+, K^+
Pb_nO (n = 1,2)$^{(1)}$	57-158 equally		
Na, K (ionized and	spaced by 16		
neutral	amu		
	Na, K (ionized and		
	neutral)		

[1]Could contain H atoms

[2]Only observed at ablation energies three times higher than the energy for Pb detection

[3]Uncertain assignment; some could correspond to KPb

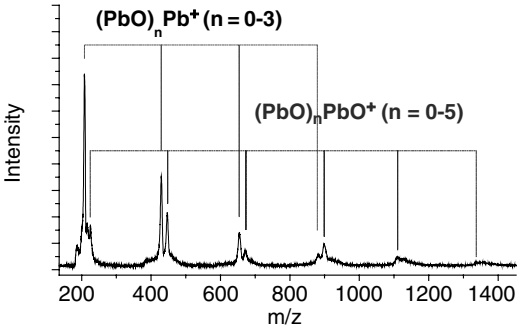

Fig. 1. Mass spectra of Lead white pellets obtained in the XeCl laser ablation

in the same m/z region can also be detected in the ablation of lead chromate in tempera but not in pellet samples, leading to the conclusion that they originate in the binding media ablation. Composition of the plume of lead chromate in pellets, did not show clusters heavier than two Pb atoms. Cr^+ was only detected at laser energies about three times higher than for Pb^+.

Positive lead oxide clusters observed in the plume composition of the ablated lead white are assumed to be formed by aggregation in the plume of PbO to PbO^+ and by successive additions of PbO to Pb^+ as it has been concluded in the ablation of other lead salts as PbO and Pb_3O_4 at 355 nm[3]; in ablation of the same lead oxides, carried out under higher mass resolution conditions, the presence of H is confirmed [4]. Incorporation of H atoms has been found to stabilize silicon oxide clusters [5, 6], and could induce a similar effect in the case of Pb_nO_m clusters.

We note that plume composition obtained in the 308 nm ablation of lead white has close similarity with that resulting from Pb_3O_4 targets ablated at 355 nm. Besides this, it has been pointed out that ablation of Pb_3O_4 in vacuum approaches that of PbO in an oxygen atmosphere [3]. The similar plume composition obtained for lead white suggests that PbO is formed in the laser ablation of the pigment. A relatively dense medium favouring aggregation within the plume would be provided by volatile species as H_2O formed in the pigment photo thermal decomposition. H_2O is not observed in the mass spectra although it should be mentioned that free water molecule is not observed either in the ablation of azurite but is positively detected forming ionized copper hydrated clusters [7]. The absence of volatile products of the ablation could explain the lack of heavy clusters in the case of lead chromate. The reasons for the lack of detection of clusters heavier than Pb_2 in the tempera samples are unclear. Different laser energy coupling might induce a different regime in the plume preventing aggregation. A better understanding of the role played by H atoms in the stabilization of lead clusters and on the possible mechanisms inhibiting H donation due to the binding media, might provide some indications about the mechanisms operating in tempera samples.

4 Conclusions

LAMS analysis of the plume obtained in the ablation of lead white shows that its composition is rather independent on laser photon energy at variance with azurite where different composition is obtained at longer (308 nm) and at shorter (248 and 193 nm) ablation wavelengths. This seems to indicate that, in the case of lead white, a photo thermal mechanism is involved in the ablation irrespective of the initial laser excitation.

Similarities between plume composition in the ablation of lead pigments and that of PbO targets can be interpreted as indicative of its formation in the decomposition of the pigments. This is compatible with the observations of PbO as the final product of the purely thermal decomposition of lead white [8] and is also in agreement with the results provided by different techniques based on the analysis of the ablated surface final composition [9].

Acknowledgements

Financial support has been provided by Spanish DGI, MCyT (BQU2000-1163-C02-01). Ricardo Torres and María Jadraque thank C.S.I.C. for student fellowships. Contribution from CORESAL (Madrid) to R.T. fellowship is also acknowledged.

References

1. M. Castillejo, M. Martín, M. Oujja D. Silva, R. Torres, A. Manousaki, V. Zafiropulos, O. van den Brink, R. M. A. Heeren, R. Teule, A. Silva, and H. Gouveia, *Anal. Chemistry*, Vol. 74, 4662, 2002
2. R. Torres and M. Martín, *Appl. Surf. Sci.* Vol.193, 149, 2002
3. N. Chaoui, E. Millon, and J. Muller, *Chem. Mater.* Vol. 10, 3888, 1998
4. F. Aubriet, N. Chaoui, R. Chety, B. Maunit, E. Millon, and J. F. Muller, *Appl. Surf. Sci.* Vol. 196, 282, 2002
5. T. Schenkel, T. Schlathölter, M. W. Newman, G. A. Machicoane, J. W. McDonald, and A. V. Hamza, *J. Chem. Phys.* Vol. 113, 2419, 2000
6. F. Zhou and J. D. Head, *J. Phys. Chem. B* Vol. 104, 9981, 2000
7. R. Torres, M. Jadraque, and M. Martin, submitted
8. D. A. Ciomartan, R. J. H. Clark, L. J. McDonald, and M. Odlyha, *J. Chem. Soc. Dalton Trans* 3639, 1996
9. M. I. Cooper, P. S. Fowles, and C. C. Tang, *Appl. Surf. Sci.* Vol. 201, 75, 2002

IR-Laser Effects on Pigments and Paint Layers

A. Schnell, L. Goretzki, and Ch. Kaps

Bauhaus-University, Chair of Building Chemistry, Coudraystr. 13c, 99423 Weimar, Germany
schnell@bauing.uni-weimar.de

Abstract. Laser cleaning of polychrome surfaces is currently problematic due to the fact, that laser irradiation can cause discoloration of pigments in paint layers. A test program was worked out to analyse the chemical and physical background of typical "blackening effects" for different pigments. The analytical methods ESEM, XRD, DTA, FTIR and NMR were used to describe the reactions of historically relevant inorganic pigments and organic binding media caused by laser irradiation at 1064 nm. The discoloration of pigments and paint layers was documented by colour measurement. Further the determination of discoloration thresholds of energy density of pigments and paint layers was a main part of the research.

1 Introduction

The use of laser technique for the cleaning of natural stone has been established for several years. Nd:YAG laser ablation is mainly based on thermal effects. The cleaning of polychrome surfaces is currently not suitable without problems due to the damage of many pigments in paint layers, that can be caused by laser irradiation. In most cases the colour of these pigments is changing to black or grey. Known reasons are phase changes and different decomposition reactions [1–5]. With some pigments these effects can be observed already at low energy densities. The objective of the research project is the cleaning of polychrome natural stone surfaces by laser ablation without causing damage to the contained pigments and binders.

2 Experimental Methods

Based on past investigations a test program was worked out to analyse the chemical and physical background of typical reactions for different pigments. Primarily historically relevant pigments and binders were chosen for the tests. Most of the 45 pigments were of inorganic origin. The binders used for the painting of sandstone samples were linseed oil, casein and gum arabic (resin of the acacia tree) as organic binders and lime as the only inorganic binder.

The laser effects were tested on pure pigments (pellets of 10 and 20 mm diameter; pressed under low pressure of 1.3 kN/cm^2) as well as on paint layers on sandstone samples. Within this study a Q-switched Nd:YAG laser at

1064 nm (Quanta System Palladio, customary in trade) at different energy densities was used for laser treatment of the samples. The beam delivery of the laser system is realised by a 7 mirror system integrated in an articulated arm. The diameter of the elliptical laser spot is approximately 7 mm.

For each sample the typical discoloration threshold of the energy density was defined. The colour measurement was done by a spectrophotometer (results: CIE-L*a*b* and specular reflectance). Various analysis techniques were further used to describe the reactions of pigments and organic binding media caused by laser irradiation. A general view of the applied techniques and instruments is given in Table 1.

Table 1. Analysis techniques and instruments

Analysis Technique	Type of Instrument
X-Ray Diffraction (XRD) analysis	Seifert XRD 3003 TT
Environmental Scanning Electron Microscope/Energy Dispersive X-ray analysis (ESEM/EDX)	Philips XL30 ESEM-FEG
Differential Thermal Analysis (DTA)	Setaram Setsys 16/18
Fourier Transform Infrared analysis (FTIR)	Biorad FTS 175 L
Nuclear Magnetic Resonance spectroscopy (NMR)	Bruker Avance 400
Colour measurement by spectrophotometer	Minolta CM 2600-d

3 Results and Discussion

The analysis of some laser treated inorganic pigments by Environmental Scanning Electron Microscope showed, that the small pigment particles are partially molten together at the surface of the pigment. These molten layers are thin, approximately 1 micron or less. The melting of pigment particles at the surface could be observed on almost all tested pigments including pigments with high melting points. Examples are given in Figs. 1 and 2 with the pigments titanium white (TiO_2; melting point at 1855°C) and zinc white (ZnO; melting point at 1975°C). The colour of zinc white was changing to brown/grey, titanium white turned to a blueish grey. The discoloration can be caused by the chemical decomposition of these metal oxides (example: $3\,TiO_2$ (*white*) $\rightarrow$ Ti_3O_5 (*blue, grey*) $+ (1/2)\ O_2$) or by physical effects (increasing particle size caused by the melting). The precise analysis of the discoloured material is difficult due to the thin modified layers on the surface of the pigment. EDX analysis of the melted surface of some metal oxide pigments is pointing at reduced oxygen contents. A phase change as reason for discoloration was detected by XRD (by grazing incidence diffraction GID) for the pigment cinnabar only.

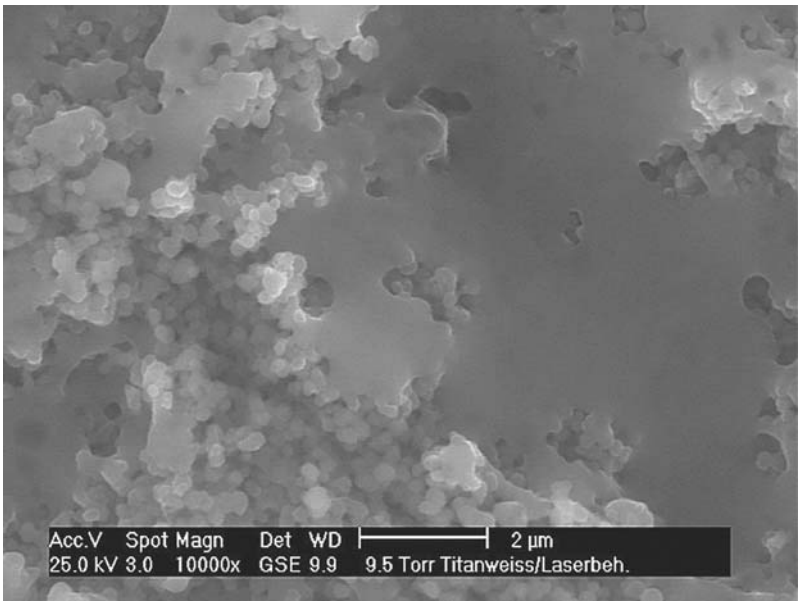

Fig. 1. Surface of titanium white pellet after laser irradiation at 600 mJ/cm^2 (magnification 10000x)

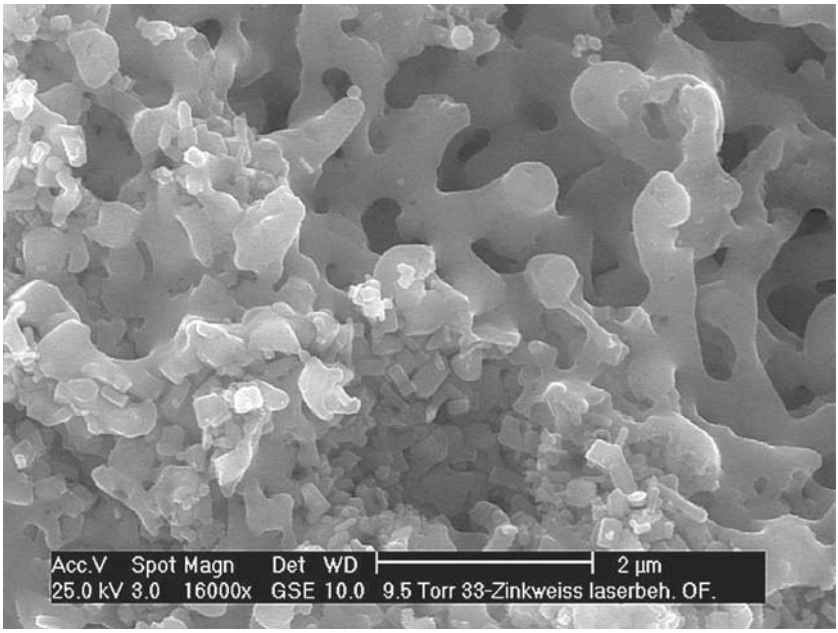

Fig. 2. Surface of zinc white pellet after laser irradiation at 600 mJ/cm^2 (magnification 16000x)

The gas phase developed during laser irradiation of different paint layers was analysed by NMR spectroscopy. For this tests, linseed oil paint layers containing pigments with low discoloration thresholds have been laser irradiated at high energy densities ($\sim 600\,\mathrm{mJ/cm^2}$) in an enclosed system. The reaction products were collected in a cooling trap, which was mounted to the system. Deuterized chloroform was used as solvent for H-NMR sample preparation. The proton spectra in Fig. 3 shows, that glycerin, alkenes, alkanes and some aldehydes were detected in the gas phase. The signal at 9,6 ppm is evidently originated from acrolein. This is confirmed by the crosspeak pattern in TOCSY spectra (total correlation spectroscopy, not shown here). Further many low-molecular reaction products are emitted, but have not been clearly detected yet. The presence of acrolein and other aldehydes points out to an incomplete "combustion" of the volatile compounds.

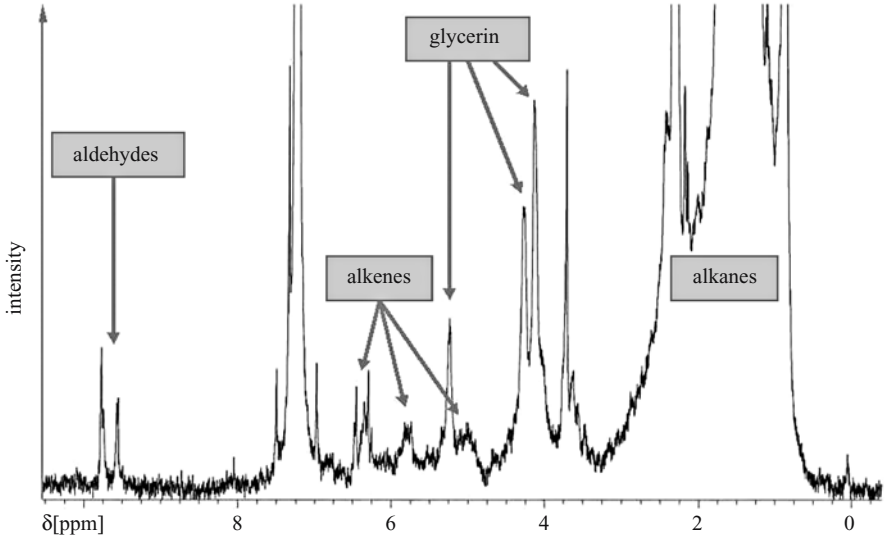

Fig. 3. H-NMR proton spectra (overview spectra) of solved gas phase emitted from paint layer containing linseed oil as binding media

A main part of the test program was the documentation of the discoloration by colour measurement and the determination of thresholds of energy density for the pure pigments and paint layers containing these pigments combined with different binders. A statistical evaluation of the thresholds of energy density of the tested pigments and paint layers is given in Fig. 4, where the "sensitivity" of the pigment or paint layer towards laser irradiation is structured in three groups.

A surface with a threshold of energy density of more then $200\,\mathrm{mJ/cm^2}$ is usually "easy to clean", which means that the most encrustations are

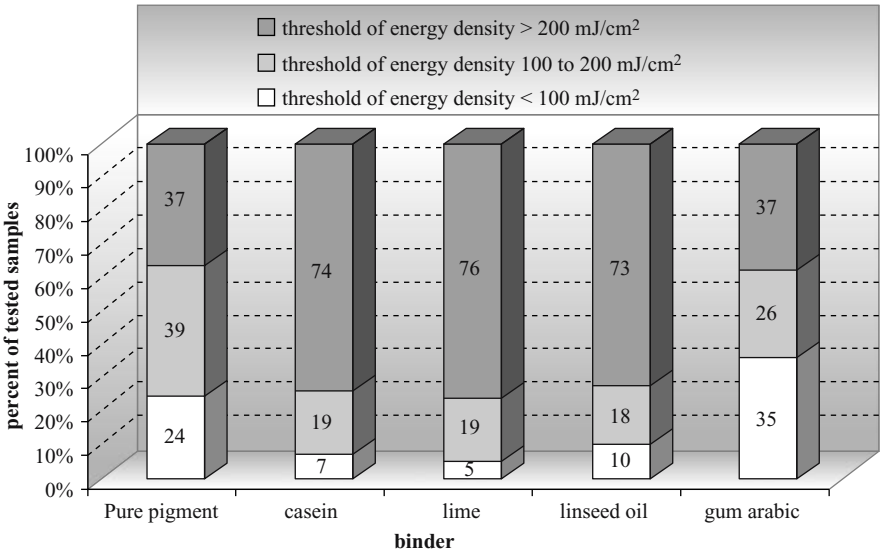

Fig. 4. Percentage distribution of discoloration thresholds of energy density (related to all tested pigments and paint layers)

removable by laser cleaning above this energy density. Thresholds below $100\,\mathrm{mJ/cm^2}$ are critical due to the fact, that laser ablation of dark crusts is usually not possible at this energy density. Laser ablation tests on samples with artificial black gypsum crusts on polychrome sandstone samples showed, that these crusts can be actually removed at energy densities $> 200\,\mathrm{mJ/cm^2}$. It was further possible to remove crusts at lower energy densities ($\sim 150\,\mathrm{mJ/cm^2}$) if water was sprayed on the crust right before laser cleaning.

4 Conclusions

Comprehensive tests showed, that laser cleaning using Q-switched Nd:YAG lasers at a wavelength of 1064 nm is suitable for the cleaning of polychrome surfaces. The main requirement for this is the limitation of energy density depending on the characteristics of the certain pigment. However there are a few pigments with very low discoloration thresholds. Polychrome surfaces containing these pigments could not be cleaned by laser ablation.

Reasons for discoloration of pigments are chemical decomposition reactions, phase changes or physical effects (melting of pigment particles). The binders contained in paint layers are less sensitive to laser irradiation. However the partially decomposition of linseed oil binders under laser irradiation has been detected by NMR. The emitted gases are cooled down very fast

due to adiabatic expansion caused by the short laser pulses. Oxidation is prevented by the reducing atmosphere.

Acknowledgements

The Thuringia Ministry for Science, Research and Art (TMWFK) is gratefully acknowledged for funding the research project "Entwicklung eines lasertechnischen Verfahrens zur Beseitigung von umweltbedingten Verschmutzungen an farblich gefassten Kunstgütern und Bauwerken" (B509-01013).

References

1. M. Chappé, J. Hildenhagen, and K. Dickmann, *Laser irradiation of medieval pigments at IR-, VIS- and UV-wavelengths*, in *Proceedings LACONA IV*, 143–146, Paris, 2001
2. A. Schnell, L. Goretzki, and Ch. Kaps, *Veränderungen von Farbpigmenten durch Laserlicht*, in GdCh-Monographie Bd. 25, 127–129, 2003
3. L. Shekede, *Lasers: a preliminary study of their potential for the cleaning and uncovering of wall paintings*, in *LACONA I*, Heraklion 1995
4. R. Sobott, u.a., *Anwendung des Lasergerätes bei der Beseitigung von Umweltschäden an national wertvollen Kulturgütern (Naturstein) unter Einbeziehung mittelständischer Unternehmen*, DBU-Project AZ 11473, 2001
5. M. Chappé, J. Hildenhagen, K. Dickmann, and M. Bedrol, Pigments historiques sous rayonnement laser (IR, VIS et UV), in L'actualité chimique, 2002

Reaction of Historical Colours and their Components Irradiated at Different Nd:YAG Laser Wavelengths (ω, 2ω, 3ω, 4ω)

J. Hildenhagen, M. Chappé, and K. Dickmann

Lasercenter Fachhochschule Münster (LFM), FB Physikalische Technik, University of Applied Sciences, Stegerwaldstr. 39, 48565 Steinfurt, Germany
hildenh@fh-muenster.de

Abstract. Cleaning of artworks with laser radiation may become a delicate situation in cases where a paint layer is directly underneath the undesired top layer. However, this is the situation in many applications of restoration, e.g. cleaning of paintings. It is known in general that historical colours may react very sensitive on illumination. Within an extensive study first we investigated separately the behaviour of 11 pigments and 3 binding materials under laser irradiation. Then in a next step we investigated the behaviour of 33 historical colours, consisting from a combination of pigments and bindings mentioned above. The experiments have been carried out using four different wavelengths from a Nd:YAG laser with optional frequency multiplier (1064 nm, 532 nm, 355 nm, 266 nm). At various laser fluences and wavelengths the corresponding colour change was analysed by CIE-L*a*b*-System. As a result of our study we have built up a data base containing threshold fluences for various historical pigments, bindings and their combinations.

1 Introduction

The behaviour of historical colours under laser irradiation has already been investigated earlier [1–6]. However, the results were mainly based on the fundamental Nd:YAG wavelength and/or did not include the separated investigations of pigments and bindings. During LACONA IV we introduced first attempts concerning solely various pigments [7].

For the present study we used a Q-switched Nd:YAG laser Type SAGA 220/10 ($t_d \approx 8$ ns, $f_{max} = 10$ Hz) with optional frequency multiplying (1064 nm, 533 nm, 355 nm, 266 nm). The maximum pulse energy was 1500 mJ@ 1064 nm, 800 mJ@532 nm, 450 mJ@355 nm and 260 mJ@266 nm, respectively. Beside CIE-L*a*b*-system we also used EDX, XRD and DTA in order to understand the fundamental reactions causing a colour change.

2 Irradiation of Separate Colour Components: Pigments

For our studies we used a selection of 11 different historical pigments as listed in Table 1 (left). The powdered pigments were pressed (7–15 tons)

Table 1. Employed historical pigments (left) and analysed reaction/interaction (right) after laser irradiation. This result is nearly independent for the wavelengths being used

Pigment	Chem. Composition	Kind of Reaction	Chem. Result	Interaction
Lead White	$Pb_3(CO_3/OH)_2$	thermic decomposition	Pb, PbO, PbO_2	thermic
Zinc Withe	ZnO	reduction	Zn	photochermic
Brown Ochre	Fe_2O_3, $Fe_2O_3{\cdot}nH_2O$	reduction	Fe_2O_3, Fe_3O_4, FeO	thermic
Naples Yellow	$BiVO_4$	-	-	-
Vermilion	$HgS_{Cinnabar}$	phase transforming	$HgS_{Metacinnaber}$	photochemic
Red Lead	Pb_3O_4	reduction	PbO	unknown
Madder Lake	Complex (Al, Ca) Alizarine	- -	- -	- -
Oxid of Chrom.	Cr_2O_3	-	-	-
Malachite	$Cu_2(Co_3{\cdot}(OH)_2)$	reduction	CuO, Cu_2O	thermic
Cobalt Blue	$CoO \cdot Al_2O_3$	oxidation	$Co_2O_3(Al_2O_3)$	photochemic
Ultramarine	$Na_8Al_6Si_6O_{24}S_4$	oxidation	$Na_8Al_6S_{i6}O_{24}(SO_4)$	thermic

to pellets (ø 13 mm). For each Nd:YAG wavelength the laser fluence was increased stepwise until a discolouration could be detected by CIE-L*a*b* (e.g. "lead white" in Fig. 1).

The corresponding fluence value was defined as "modification threshold" (e.g. 10 mJ/cm^2 for the pigment "lead white" @ 532 nm corresponding to Fig. 1). Modification thresholds for all pigments at various Nd:YAG wavelengths are included in the data base (Table 3). As can be seen there is a distinct decrease of the thresholds with decreasing wavelength for all pigments. Furthermore we found out that the analysed kind of reaction for each pigment (Table 2, right) was nearly independent of the four wavelengths being used for our investigations [8]. Table 2 also gives information about the basic interaction process. More details containing further information about chemical and physical reactions are published in [7].

3 Irradiation of Separate Colour Components: Bindings

In order to keep within limits of our data base we only used 3 different commonly used bindings (Table 2).

Test samples have been made to bulk material by a decelared drying process (several months). The investigation procedure was the same as

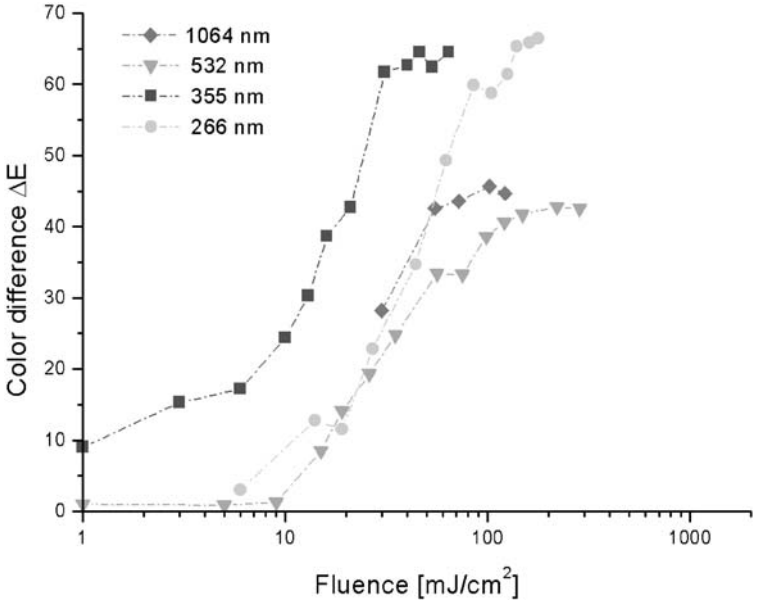

Fig. 1. Discoloration of pigment "lead white" versus fluence under irradiation by different Nd:YAG wavelengths

introduced for pigments (Chap. 2). The measured modification thresholds are depicted in Table 3. Again there is decrease of the threshold with decreasing wavelength. The obtained chemical/physical reactions and corresponding fundamental of the interaction process is also listed in Table 2.

Table 2. Employed binding materials and analysed reaction/interaction. Irradiated at different Nd:YAG wavelengths

Binding	Wavelength			
	1064 nm	532 nm	355 nm	266 nm
Caseine	spallation (physical reaction)		discolouration (thermal reaction)	
Linseed Oil	inner opacity (thermal hydration or lauric acid)		evaporation (photo chemical reaction or polymerisation)	
Sturgeon Glue	partial opacity of the surface (thermal reaction)		blister/burns (thermal reaction)	

Table 3. Modification thresholds of pigments, bindings and colours for various Nd:YAG laser wavelengths (exemplary extraction from a data base containing 33 different colours)

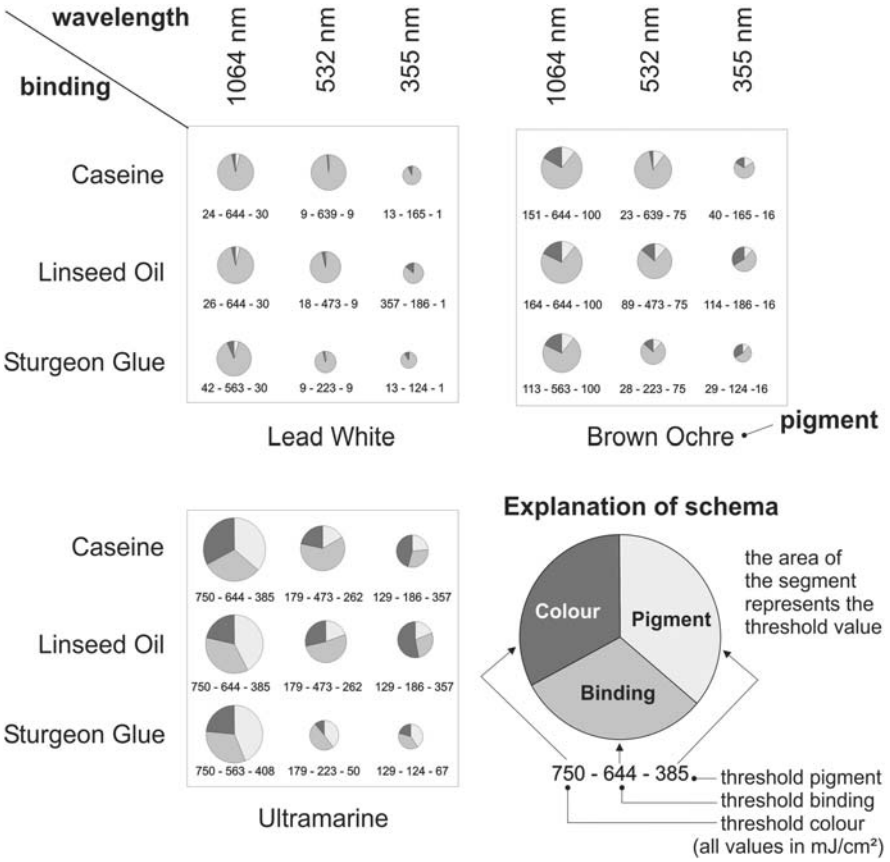

4 Irradiation of Colours

Colour samples were made by a commonly used ratio of mixture from the 11 pigments listed in Table 1 and 3 bindings listed in Table 2. Thus, our data base contains information about 33 different colours. An exemplary extract is given in Table 3. Here the thresholds for all the pigments, bindings and colours are summarized for the wavelengths 1064 nm, 532 nm and 355 nm, respectively (266 nm was not considered due to insufficient longterm stability of the laser output power at this wavelength). Furthermore Table 3 also illustrates threshold values by means of segment areas within a circle. (The area is proportional to the fluence value). Proceeding in accordance with data gained from the separated colour components (pigment, binding) obviously

there is no common principle allowing predictions for the threshold of the composed colour.

5 Outlook

Within our extensive study we investigated separately the reaction of several historical pigments as well as historical binding mixtures under laser irradiation. Based on these results we expected possible predictions for the compound "pigment/binding". However, as it has turned out, a general conclusion is not simple. In addition, in practice the situation becomes even more complex due to fluctuations of the individual pigment/binding–mixtures. Thus in the field of laser cleaning of artwork with paintings in any individual case the irradiation sensitivity of the paintings has to be identified. But with the results presented in this paper tendencies are pointed out and may be useful for laser restoration in practice.

Acknowledgements

This project is funded by the EUREGIO (INTERREG III Program) within the "EUREGIO CENTER for Art Restoration Technology" (ECEACT).

References

1. P. Pouli, D. C. Emmomy, C. E. Madden, and I. Sutherland, Analysis of the laser-induced reduction mechanisms of medieval pigments. App. Surf. Sci. 173 (2001) 252–261
2. J. Nimmrichter, Erfahrungen mit der Lasertechnik in der Konservierung von Steinskulpturen und Farbfassungen. Restauratorenblätter 18, pp 107–118
3. A. Sansonetti and M. Realini, Nd:YAG-Laser effects on inorganic pigments. Journal of Cultural Heritage 1 (2000) Supplement 1, pp 189–198
4. M. Chappé, Pigmente unter Laserbestrahlung, Restauro 1 (2003) 27–31
5. R. Sobott, Laser und Pigmente auf Naturstein, Restauro 2 (2003) 110–116
6. M. Chappé, Pigments historiques sous rayonnement (IR, VIS et UV), l'actualié chimique, Juillet (2002), 3–10
7. M. Chappé, J. Hildenhagen, K. Dickmann, and M. Bredol, Laser irradiation of medieval pigments at IR, VIS and UV wavelengths, LACONA 4, Journal of Cultural Heritage, Vol.4, Sup.1, 2003, pp 152–156
8. M. Chappé, J. Hildenhagen, K. Dickmann, and M. Bredol, Chemie in unserer Zeit, Vol.37, 2003, pp 348–356

Visual Effect of Laser Cleaning on Orissan Murals

A. Sah

INTACH Indian Conservation Institute, Orissa Art Conservation Centre,
State Museum Premises, Bhubaneswar-751014, Orissa, INDIA
icioacc@sancharnet.in

Abstract. Dispersed in villages of Orissa are a number of mural paintings most of which are covered with soot deposits. A preliminary cleaning test was effected on a representative sample of such paintings using a Nd:YAG Laser at the NMGM Conservation Centre in Liverpool. This article reports the visual observations of the laser cleaning test.

1 Introduction

In earlier times, the State of Orissa, on the East coast of India, was known as *Utkal*, the land of excellence in art. Amongst the various art forms that flourished here were the mural paintings, and the tradition of painting them is still alive. Following research and documentation by the author, with more than seventy mural sites having been brought to light, their conservation has become an issue in the State. Tests were conducted by the author at the Conservation Centre of National Museums and Galleries on Merseyside (NMGM), Liverpool in order to explore the efficacy of laser technology for cleaning the Orissan murals.

2 The Orissan Murals

The mural paintings in Orissa are executed on stone and brick walls over which first a coarse and then a fine lime plaster coat is applied, the latter burnished to a mild gloss. On the dry plaster, traditionally, a very limited palette of the pigments cinnabar, red ochre, lamp black, conch shell white and sometimes orpiment was applied using *kointho*, wood apple gum as the binding medium [1]. Within this palette, these pigments were mixed to form intermediary hues. The contemporary mural artisans, however, use a variety of natural and synthetic pigments adding plant gums and synthetic adhesives as binders. A large number of the extant Orissan murals are disfigured by thick soot deposits from the temple kitchen fires and ritual oil lamps. During the course of restoration of the murals, retouching is done using a variety of pigments and binders. At times, protective coats may also be applied on the murals.

3 The Test Sample

On a *patta*, a traditional Orissan canvas with a burnished lime base, a series of thumbnail sized spots were painted with a brush. The pigments, binders, paints and varnishes, bought in Chandanpur, a village near Puri in Orissa, were arranged in varying combinations so as to represent well the spectrum of extant polychromy of the Orissan murals as outlined in the preceding paragraph. This prepared test sample was then rubbed over with fine soot produced by an oil lamp of the type most commonly used in the region. At the same time a similar control sample was prepared for reference.

Table 1. Combination of pigments and binders on the test sample sheet

	A	B	C	D	E	F	G	H	I
1	Ge+K	Hi+K	Ha+K	LB+K	Dh+K	LB+ Ha+K	LB+ Dh+K	Hi+ Ha+K	Hi+ Ge+K
2+vc	Ge+K	Hi+K	Ha+K	LB+K	Dh+K	LB+ Ha+K	LB+ Dh+K	Hi+ Ha+K	Hi+ Ge+K
3+pc	Ge+K	Hi+K	Ha+K	LB+K	Dh+K	LB+ Ha+K	LB+ Dh+K	Hi+ Ha+K	Hi+ Ge+K
4	O+Fe	S+Fe	Y+Fe	Bp+ Fe	W+Fe	Gr+Fe	Bl+Fe	Pe+Fe	S+O+ Fe
5+pc	O+Fe	S+Fe	Y+Fe	Bp+ Fe	W+Fe	Gr+Fe	Bl+Fe	Pe+Fe	S+O+ Fe
6	Br	R	Ye	Blk	Mw	Dg	Sb	Gy	R+Br
7+jc	Ge+K	Hi+K	Ha+K	LB+K	Dh+K	LB+ Ha+K	LB+ Dh+K	Hi+ Ha+K	Hi+ Ge+K

Legend for Table 1

Ge - *geru*, naturally occurring red ochre, iron oxide
K - *kointho ottha,* wood apple gum as a binder
Hi - *hingul,o* naturally occurring cinnabar, mercuric sulphide
Ha - *haritala,* naturally occurring orpiment, arsenic sulphide
LB - *kolha,* lamp black
Dh - *sonkho dhaula,* conch shell white
vc - picture varnish coat, Camel trademark
pc - coat of 5% solution of Paraloid B-72 in toluene
O - red ochre from local hardware store
Fe - Polyvinylacetate emulsion as binder. Fevicol trademark
S - *german sindur,* a red pigment sold in the local market
Y - gamboge tint powder pigment. Camel trademark
Bp - black powder pigment from local market
W - conch shell powder from local market
Bl - *khandanila,* a locally available blue pigment mixed with white

Pe	-	*peorhi,* a yellow pigment from local market. (It is not the genuine Indian Yellow)
Br	-	brick red enamel paint. Asian Paints trademark
R	-	red enamel paint. Asian Paints trademark
Ye	-	yellow enamel paint. Asian Paints trademark
Blk	-	black enamel paint. Asian Paints trademark
Mw	-	milk white enamel paint. Asian Paints trademark
Dg	-	dark green enamel paint. Asian Paints trademark
Sb	-	sky blue enamel paint. Asian Paints trademark
Gy	-	golden yellow enamel paint. Asian Paints trademark
Gr	-	green (by mixing Bl and Y)
jc	-	*jhuna,* a natural resin melted and applied as a protective coat

4 Laser Cleaning

The soot deposits on the test sample sheet were cleaned using a Lynton Lasers 'Phoenix' system of the following specifications:

Laser	Q switched Nd:YAG laser
Output Wavelength	1064 nm
Max energy pulse	235 mJ
Repetition rates	1–20 Hz
Pulse duration	5–10 ns
Beam delivery	articulated arm
Average fluence	0.6 J/cm^2 – 0.8 J/cm^2 during the cleaning

The laser was operated by the author in the laser technology/sculpture conservation department of NMGM, Liverpool after training imparted by Dr. Martin Cooper. Only one half of each spot was irradiated while the other half was screened from the incident laser beam using "burn paper" [2]. The average fluence ranged from 0.6 J/cm^2 – 0.8 J/cm^2 during the cleaning.

5 Observations

Immediately following the laser cleaning, observations were recorded visually and repeat observations were taken six months after the laser cleaning. There were no variations in the observations after this time lapse of six months. On laser irradiation, the soot covered paint samples behaved in the following manner.

6 Concluding remarks

The soot deposits absorb strongly the Nd:YAG laser pulses of wavelength 1064 nm, and are easily removed. The cleaning of the soot can be effected

Soot layer	:	The soot layer was completely removed.
Lamp Black	:	The black paint layers in column D (1D, 2D, 3D, 4D, 5D, 7D) came away in patches off the test sheet especially when more than one pulse was incident on the same area.
Green	:	The green paint traditionally prepared by mixing orpiment and lamp black (1F, 2F, 3F, 7F) lightened in colour and suffered physical losses similar to those on the lamp black samples. Also visible were "laser impact rings", lighter coloured rings on the paint sample, demarcating the circumference of the laser impact spot. The synthetic greens (4F, 5F) were unaffected.
Grey	:	Interestingly, where lamp black and conch shell white were mixed to form a grey paint sample (1G, 2G, 3G, 7G), the grey sample turned to a whitish hue with no physical damage as suffered in other paints which had lamp black mixed in them.
Red	:	Of the red paints in column A, red ochre (1A, 2A, 3A, 4A, 5A, 7A) was hardly affected unless the pulse was incident repeatedly on the same spot. Pure cinnabar (1B, 2B, 3B, 7B) darkened considerably as did mixtures of pigments (1H, 2H, 3H, 7H, 1I, 2I, 3I, 7I) which had cinnabar added to them. However this darkening was of a purplish hue different from the black alteration reported in tests conducted by Pouli and Emmony [3]. The synthetic reds (4B, 5B) and mixtures (4I, 5I) seemed unaffected.
Yellow	:	The yellow orpiment spots (1C, 2C, 3C, 7C) were cleaned without visible damage while the powder art colour spots (4C, 5C) darkened. However, 5C which had a coat of Paraloid B-72 on it darkened less than 4C, the one without the coat. Similarly 5H, also with a Paraloid B-72 coat on it, seemed to darken less than 4H.
White	:	The whites (1E, 2E, 3E, 4E, 5E, 7E) turned very slightly off in hue after irradiation by the laser pulses.
Blue	:	The blues (4G, 5G) seemed unaffected after cleaning with the laser pulse.
Enamel paints	:	The enamel paints (6A, 6B, 6C, 6D, 6E, 6F, 6G, 6H, 6I) were not affected by the laser irradiation.
Resin coating	:	The entire row (7A, 7B, 7C, 7D, 7E, 7F, 7G, 7H, 7I) of paint samples was affected. The natural resin coats over the paint samples vapourised and the paints were affected even more strongly than when the resin coat was not present.

using a low fluence. In the six months between two sets of observations, there has been no visible "delayed amplification" [4]. The alterations that the pigments underwent are outlined in the preceding section titled "Observations". The presence of the plant gum and polyvinylacetate emulsion binders did not seem to make a difference to the effects of laser irradiation on the paint samples. The natural resin coat, however, accentuated the alteration effects on the paint samples. As with other conventional cleaning methods, test cleanings

apply for this tool too. Perhaps the observations on the enamel paints and paraloid coated paints provide hints on the preparation of barriers to effect selective laser cleaning on mural paintings.

The differences in the quality and nature of pigments and binders used by different artists and communities around the world will accordingly vary the results of laser cleaning the respective murals. Hence it would be practical to consider that results of laser cleaning mural paintings should not be generalized, and each individual painting must be individually tested. These tests evidence that more detailed, organized and encompassing studies need to be conducted to determine the effects as well as threshold values for the soiled paint layers. Laser, like any other conservation tool and material, needs to be properly handled and understood so that it can be utilized in a well informed conservation effort as a very effective cleaning medium for mural paintings, amongst other artistic and historic works.

Acknowledgements

I take this opportunity to thank John Larson, Martin Cooper and Sam Sportun of the NMGM, Liverpool who graciously supported my request to work at their laser technology section. This was also made possible due to support from the Charles Wallace (India) Trust, the British Council Division and Dr. O.P.Agrawal of the INTACH Indian Council of Conservation Institutes. The research and documentation of the Orissan Murals was undertaken thanks to support from the India Foundation for the Arts, and NORAD, Norway.

References

1. A. Sah, in *Secrets Orissan Murals*, Unpublished typescript 2002
2. M. Cooper, in *Operation of the Phoenix Laser System, Introduction to Laser Cleaning in Conservation*, Training Handout 1–5, 2002
3. P. Pouli and D. C. Emmony, in *The Effect of Nd: YAG Laser Radiation on Medieval Pigments,* Journal of Cultural Heritage, 1, S181–S188, 2000
4. A. Cruz, M. L. Wolbarsht, and S. A. Hauger, in *Laser Removal of Contaminants from Painted Surfaces*, Journal of Cultural Heritage, 1, S173–S180, 2000

Part VII

Fundamentals, Innovative Methods

Synchronous Use of IR and UV Laser Pulses in the Removal of Encrustation: Mechanistic Aspects, Discoloration Phenomena and Benefits

V. Zafiropulos[1], P. Pouli[1], V. Kylikoglou[2], P. Maravelaki-Kalaitzaki[3], B.S. Luk'yanchuk[4], and A. Dogariu[5]

[1] Foundation for Research and Technology Hellas (FORTH), Institute of Electronic Structures and Laser (IESL), Heraklion, Greece
zafir@iesl.forth.gr
Also, Department of Human Nutrition & Dietetics, Technical Educational Institute of Crete, Ioannou Kondylaki 46, 723 00 Sitia, Crete, Greece
[2] NCSR "Demokritos", Laboratory of Archaeometry, Athens, Greece
[3] Ministry of Culture, 25th Department of Prehistoric and Classical, Chania, Greece
[4] Data Storage Institute at National University of Singapore, Singapore
[5] University of Central Florida, School of Optics / CREOL, Orlando, Florida, USA

Abstract. The removal of encrustation from sculptures and monuments has been by far the most pronounced application of lasers in LACONA field. Considerable effort has been put in recognizing the operative ablation mechanisms when using different laser wavelengths and power levels, as well as in understanding the associated "yellowing" phenomenon. The deeper insight into the laser-matter interactions for different laser parameters as well as the understanding of side discoloration phenomena has led us in combining IR and UV laser pulses with excellent results. More specifically, the fundamental and the third harmonic of a Q-Switched Nd:YAG laser has been spatially and temporally combined to create a double pulse. The power levels must be fixed at a certain ratio for the two wavelengths in such a way, that the different operative removal mechanisms (mainly selective vaporization for IR- and spallation for UV-pulses) take action at the same depth from the surface of encrustation. The resulted surface after the final removal of encrustation lacks the yellowish hue, which is present when only IR pulses are used. A theoretical model has been applied to account for the different phenomena observed with the synchronous use of laser pulses as well as the absence of yellowing. This novel methodology has been applied to Parthenon West Frieze with success (see parallel *case study* contribution by Pouli et al.).

1 Background Knowledge

The removal of inorganic material by means of short laser pulses – in the order of a few ns – is achieved through two discrete mechanisms. These mechanisms depend on the wavelength of the laser radiation, on the applied fluence and

on the degree that this is absorbed from the layer to be removed and the substrate. In general terms, for stone-laser interaction two extreme cases are distinguished:

(a) In the case that the material to be removed absorbs the laser radiation of a certain wavelength more than the substrate or the binding material does, the energy density threshold for the removal of the superficial layer is usually less than the energy density required for the removal of the substrate material. In such a case, appropriate focusing of the laser beam can ensure the selective removal – mainly through selective explosive vaporization [1, 2] – of the unwanted layer or particles without the slightest damage to the substrate. Such a way to control the cleaning process is preferred owing to the "self-limiting" action of the laser beam and can be applied in certain substrate-encrustation combinations, mainly for cleaning stone surfaces (see original work by Amus [1]).

(b) In the case that the radiation-surface interaction results in significant shock wave generation material removal mainly proceeds through spallation [1, 2] and material removal occurs in discrete steps. For each "material"-"type of laser" combination the quantity of the removed material per single laser pulse can be determined as a function of the power or the energy density (when we refer to a certain pulse duration) of the applied laser radiation. Thus it is possible to precisely determine the energy density and the number of the laser pulses required in order to remove a layer of material of a certain thickness [3]. Although it has been found that "self-limiting" may still exist when using UV pulses [4], the exact thickness of the material and the fluctuation it may have across the surface is of major importance in order to achieve a homogeneous surface cleaning [5, 6].

So far, the removal of undesirable encrustation from sculpted stone surfaces of historic and artistic value is mainly performed by means of the fundamental wavelength radiation of a Nd:YAG laser, both in the normal and Q-Switched mode. The use of this specific radiation has been reserved, as in several cases the final surface appears to be slightly discolored towards yellow hue (*yellowing*) when the Q-Switched mode is used. These cases include among others, ancient marble sculptures covered with dark encrustation due to their exposure to the atmospheric pollution. In such cases it is not preferred to remove the whole encrustation as a certain part of the encrustation layer retains information of the authentic underlying surface.

2 Major Operative Mechanisms and Associated Optical Phenomena

In nanosecond laser divestment of inorganic encrustation using a Q-Switched Nd:YAG laser ($\lambda_L = 1064\,\text{nm}$) the prevailing processes are the selective explosive vaporization and the spallation induced by shock wave generation. A mathematical description of the former has been given by Asmus et al. [1],

and Watkins [2], while the results of shock wave action cannot be safely quantified. This is owing to the encountered lack of homogeneity, the random concentration of mixtures of minerals, and the irregular sequence of different encrustation layers that makes any modeling a difficult task. In the limited extent of this work we will not attempt any detailed analysis of the operation of the ablation mechanisms on these complex substrates. Rather, we will try to elucidate the problem by presenting evidence for the operation of these mechanisms, as well as the accompanying optical phenomena such as yellowing.

Divestment of black encrustation from marble/stone artifacts using the fundamental of a Q-Switched Nd:YAG laser has been fluently implemented in conservation during the last years [1, 7–11]. Other pulse durations [1, 12–14] and wavelengths [4–6, 15, 16] have been used as well. Actually, laser-assisted cleaning of sculptures and façades is by far the most frequently met application in the field of *Lasers in the Conservation of Artworks (LACONA)*. This is owing to the "self-limiting" divestment process that is described above. Therefore, by choosing proper laser fluence values between the two limiting thresholds one can remove the encrustation without affecting the substrate. Shock wave formation, however, may induce some structural damage (e.g. micro cracks) when working at fluence levels considerably above threshold [1]. Figure 1 shows ablation rate data from Pentelic marble and its thick dendritic-type encrustation [11]. The two sets of data clearly indicate the spallation thresholds of marble and crust (3.5 and 1.8 $\mathrm{J/cm^2}$ respectively) when using the fundamental of a Q-Switched Nd:YAG laser. The value 3.5 $\mathrm{J/cm^2}$ is the absolute maximum fluence for processing the particular marble/encrustation system. Using the third harmonic of a Q-Switched Nd:YAG laser ($\lambda_\mathrm{L} = 355\,\mathrm{nm}$) the corresponding fluence values for the same sample are 1.9 and 0.57 $\mathrm{J/cm^2}$, respectively.

The usual superposition of more than one encrustation layers prevents a more analytical approach to such laser divestment applications. At this point a generalization for the structure of the encrustation layer is very crucial. From previous studies [9, 17, 18], one can notice that in most cases there is always a layer that must be at least partially preserved located just on top of the marble/stone substrate. Although numerous types of encrustation – including biological, mixed or even multiple-layer encrustation – have been considered, the entencrustation removed using the fundamental of a Q-Switched Nd:YAG laser at fluences near vaporization threshold presents a couple of unique characteristics. The first characteristic is a yellowish hue of the resulted surface [15, 19] compared with the non-cleaned reference surface, or even with the same surface cleaned using other laser wavelengths or other techniques (e.g. micro sandblasting). The second characteristic of the substrates after the Q-Switched Nd:YAG laser action is the maintenance of the gypsum-rich layer, in which the dark particulates have been selectively vaporized [19]. Even in cases of multiple encrustation layers where the outer

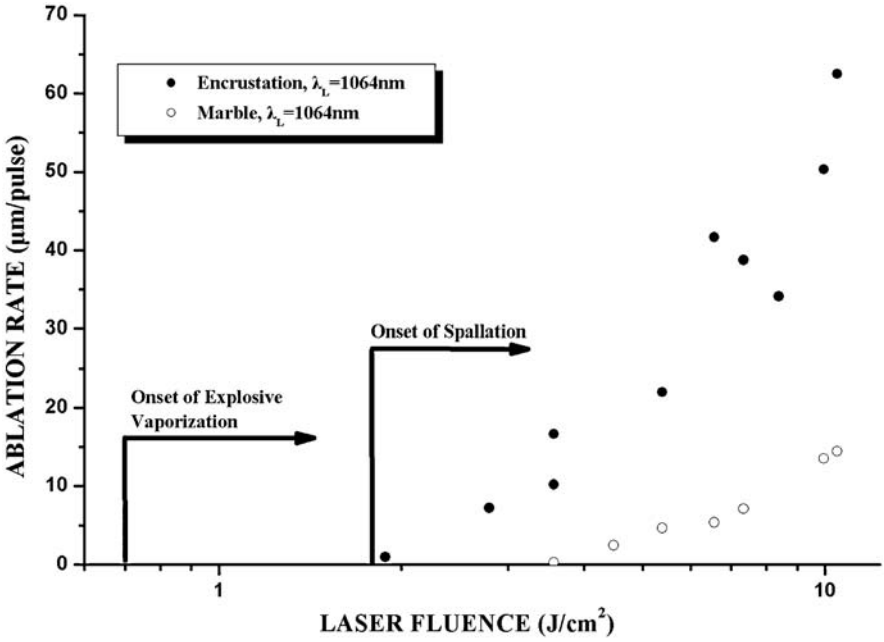

Fig. 1. Ablation rate data for Pentelic marble and a particular dendritic encrustation, a cross-section of which is shown in Ref. [19], obtained using the fundamental of a Q-Switched Nd: YAG. Arrows designate the various thresholds described in text

black layer (rich in carbon particles and other pollutants) is completely removed, the remaining gypsum-rich encrustation layer is left clean of black particles. Therefore, we could consider such a layer as being the most common encrustation encountered at the last stage of laser cleaning, below other existing layers. Typical cross-sections of single-layer encrustation on marble have been presented in previous communications [3, 19], a schematic representation of which is shown in Fig. 2a. Observing such a cross-section after laser processing using the fundamental of a Q-switched Nd:YAG laser at a fluence of $0.8\,\mathrm{J/cm^2}$ – just above the threshold of selective vaporization indicated in Fig. 1 at $0.7\,\mathrm{J/cm^2}$ – we see that the gypsum-based layer is preserved, while the dark carbon/iron/aluminum/silicate particles [11, 16, 18] are selectively vaporized [3, 19] (see Fig. 2b). This selectivity is due to the absorptivity of 1064 nm laser radiation, which is 3–4 times higher for the black particles than for the gypsum layer or the substrate [1]. The onset of this process occurs at much lower fluence values than the spallation threshold (see two threshold lines in Fig. 1). In a previous communication it has been suggested [19] that the voids resulting from the removal of the dark-colored particles, as well as the alteration of the absorption spectrum of the remaining encrustation (new ionic species from the vaporization of particles), may lead to the perception

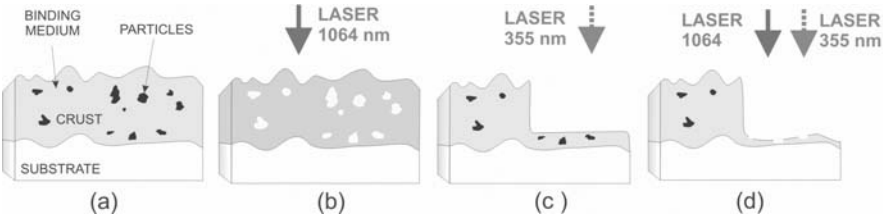

Fig. 2. Schematic representation of encrustation cross-section (**a**) and the two different ablative mechanisms: the selective vaporization using low fluence (0.7–1.0 J/cm^2) at $\lambda_L = 1064\,\text{nm}$ (**b**); and the spallation at higher fluence ($\sim$2 J/cm^2) or using $\lambda_L = 355\,\text{nm}$ (**c**). (**d**) represents the result when synchronously using both wavelengths at certain fluence values

that the final surface is discolored ("*yellowing*"). Figure 3 schematically represents the conception of this simple model as far as the scattering part concerns. Two collinear rays of different color enter into the remaining after laser cleaning encrustation layer. Using light scattering theory, it is easy to prove that the higher λ ray may finally escape while the lower λ ray may scatter back into the material suffering further absorption. The net effect is the higher absorption of blue wavelengths compared to higher λ colors. As a result the surface appears with a yellowish hue.

Asmus et al. have applied a one-dimensional surface-heating model [1] to predict the required laser fluence levels for selective vaporization. In this simplified model the temperature increase at the surface is found to depend on the surface absorbance, the incident laser flux, and the thermal parameters of the material. This model was mostly applied for a normal-pulse laser (pulse duration of the order of 10^{-3} s) and the results agreed very well with the experimental fluxes. In principle, it can be also applied to nanosecond pulses for fluxes below the spallation threshold of the surface layer, where selective vaporization of particles embedded in the gypsum-rich layer occurs. Finally, it can be corrected for non – planar laser/matter interaction, which is the

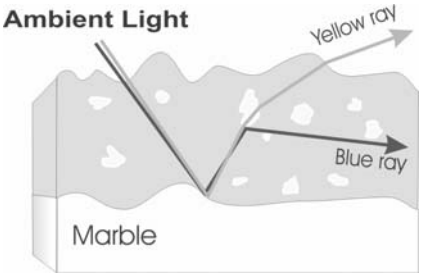

Fig. 3. Possible path of a blue and a yellow ray that have collinearly entered the encrustation layer

case of particle vaporization. For the highly variable, inhomogeneous and poorly characterized encrustations, the model is satisfactory in projecting laser effects and general fluence requirements. In our case the experimental onset of particle vaporization occurs at $0.7\,\mathrm{J/cm^2}$, which is surprisingly close to calculated values using different sets of parameters. For laser fluence values between $1.0\,\mathrm{J/cm^2}$ and $1.8\,\mathrm{J/cm^2}$, it was found that the generated shock wave had an additive effect on the delamination and finally the fragmentation of the encrustation when many pulses were used [3]. At fluences above $1.8\,\mathrm{J/cm^2}$ spallation starts and the amount of removed material per pulsed is fixed for a particular encrustation (see Fig. 1). In the latter case though, the very top layers of the remaining encrustation appear to be rather porous owing to an additional vaporization of embedded particles.

Using the third harmonic ($\lambda_\mathrm{L} = 355\,\mathrm{nm}$) of a Q-Switched Nd:YAG laser, the only observed process is spallation of the encrustation, each pulse removing a certain amount of the material as schematically shown in Fig. 2c. In this case, particles and bonding material of the encrustation equally absorb the ultraviolet laser radiation. Thus it is possible to remove material from the total mass of the crust without discriminating between dark particles and bonding material. After the release of each UV pulse, the remaining layers are unaffected by other processes such as selective vaporization. The main advantage of this mechanism is the absence of discoloration phenomena and voids or morphological alterations on the remaining surface. The disadvantage though, when an inhomogeneous encrustation is encountered, is the difficulty to control the removal process since the spallation threshold for the encrustation changes from point to point. As a result, over-cleaning phenomena can be easily observed locally [5] .

3 Combination of IR and UV Laser Pulses

The objective is the removal of superficial encrustation in a controlled way without discoloration or structural damage to the original surface. This objective has been achieved by the combined action of the two mechanisms of material removal mentioned above. This was accomplished by the simultaneous use of two laser beams of different wavelengths, whose pulses are temporally and spatially overlapped. For optimum results the energy densities of the two beams must be set to a certain ratio. The optimum energy densities of the two radiations as well as their ratio vary for each case of combination of superficial encrustation type and substrate. A theoretical model is under development to account for the quantitative findings as well as the optimum energy densities.

The temporal and spatial overlapping of the two laser beams can be achieved by either separating one part of the fundamental beam, before this enters the harmonic generator, by means of a beam splitter, or by using the

residual laser beam of the fundamental frequency after the harmonic generation procedure. In both arrangements it is possible to use any of the two wavelengths independently, in case it is required from the specific application. In this manner it is possible to exploit the action of the two material removal mechanisms either independently or in combination. Therefore, all problems associated with discoloring, or inhomogeneous and incomplete cleaning, e.g. in case where biological crust was also present on the surface, are prevented. The theoretical model for discoloration presented in the LACONA IV [19] has been extended to include the color of the resulted surface when combining IR and UV laser pulses. When the power densities of the two laser beams are such that the two ablation mechanisms operate in the same depth from the surface, the observed cross-section is represented in Fig. 2d corresponding to none or minimal color alteration [20].

The presented prototype comprises a functional solution for the complete control of the combination of the two laser beams of different wavelengths – here the fundamental and its third harmonic. The device allows the modification of both the total energy of the system as well as the ratio of the energies of the two combined laser beams. The device has been successfully used in the restoration of the Parthenon West Freeze [see accompanying contribution by Pouli et al., 20].

4 Conclusions

The presented work illustrates – for the first time – the emerging advantages of using spatially and temporarily overlapping UV and IR nanosecond laser pulses for removing certain types of encrustation without surface discoloration. This is owing to the controlled action of the two different operative mechanisms in laser-encrustation interaction, i.e. (i) the explosive vaporization of dark colored particles embedded in gypsum-based encrustation and (ii) the spallation. Theoretical work is currently in progress for supporting the experimental findings and we hope to present these theoretical results in LACONA VI.

Acknowledgements

This work was fully supported by the E.U. large Installations Plan DGXII (HCM) program ERBCHGECT920007 at the Ultraviolet Laser Facility operating at *FO.R.T.H.* – *IESL*, Heraklion, Greece. We would like to thank Prof. Th. Skoulikidis and Mrs. P., Papakonstantinou for their moral support and helpful advice. Finally, we acknowledge the financial support by the Acropolis Restoration Service (YSMA) of the Ministry of Culture under the advice of the Committee for the Preservation of Acropolis Monuments.

References

1. J. F.Asmus, M. Seracini, and M. J. Zetler, Lithoclastia **1**, 23 ,1976
2. K. G. Watkins, in *Restauratorenblätter, Sonderband – Lacona I*, Edited by E. K**o**nig and W. Kautek, Verlag Mayer & Comp., Vienna, 7, 1997
3. V. Zafiropulos, Chap. 8 in *Laser Cleaning*, Edited by B. Luk'yanchuk, World Scientific, Singapore, New Jersey, London, Hong Kong, 2002
4. S. Klein, T. Stratoudaki, Y. Marakis, V. Zafiropulos, and K. Dickmann, Applied Surface Science **157**, 1, 2000
5. G. Marakis, Diploma thesis, Technical Educational Institute of Athens & FORTH-IESL, Greece, 2000
6. G. Marakis, P. Pouli, V. Zafiropoulos, and P. Maravelaki-Kalaitzaki, Journal of Cultural Heritage **4**, 83s, 2003
7. J. F. Asmus, in *IEEE Circuits and Devices Magazine*, 6, 1986 (March)
8. J. F. Asmus, Interdisciplinary Science Reviews **12**, 171, 1987
9. M. Cooper, *Cleaning in Conservation: an Introduction*, Butterworth Heinemann, Oxford, 1998
10. V. Vergès-Belmin, in *Restauratorenblätter, Sonderband – Lacona I*, Edited by E. K**o**nig and W. Kautek, Verlag Mayer & Comp., Vienna, 17, 1997
11. P. V. Maravelaki, V. Zafiropulos, V. Kylikoglou, M. Kalaitzaki, and C. Fotakis, Spectrochimica Acta B **52**, 41, 1997
12. S. Siano, F. Margheri, P. Mazzinghi, R. Pini, and R. Salimbeni, Applied Optics **36**, 7073, 1997
13. S. Siano, R. Pini, and R. Salimbeni, Applied Physics Letters **74**, 1233, 1999
14. S. Siano, F. Fabiani, R. Pini, R. Salimbeni, M. Giamello, and G. Sabatini, Journal of Cultural Heritage **1**, S47, 2000
15. Th. Skoulikidis, P. Vassiliou, P. Papakonstantinou, A. Moraitou, V. Zafiropulos, M. Kalaitzaki, I. Spetsidou, V. Perdikatsis, and P. Maravelaki, in *Workshop on "Lasers in the Conservation of Artworks"*, Heraklion, Book of Abstracts, 1995
16. P. Maravelaki-Kalaitzaki, V. Zafiropulos, and C. Fotakis, Applied Surface Science **148**, 92, 1999
17. Th. Skoulikidis and P. Papakonstantinou-Ziotis, Br. Corrosion Journal **16**, 63, 1981
18. P. Maravelaki-Kalaitzaki, D. Anglos, V. Kilikoglou, and V. Zafiropulos, Spectrochimica Acta B **56**, 887, 2001
19. V. Zafiropulos, C. Balas, A. Manousaki, G. Marakis, P. Maravelaki-Kalaitzaki, K. Melesanaki, P. Pouli, T. Stratoudaki, S. Klein, J. Hildenhagen, K. Dickmann, B. S. Luk'yanchuk, C. Mujat, and A. Dogariu, Journal of Cultural Heritage **4**, 249, 2003
20. P. Pouli, K. Frantzikinaki, E. Papakonstantinou, V. Zafiropulos, and C. Fotakis, in *current volume*

Numerical Modelling of Laser Cleaning and Conservation of Artworks

J. Marczak, K. Jach, and A. Sarzyński

Institute of Optoelectronics, Military University of Technology, 2 Kaliski Str., 00-908, Warsaw, Poland
jmarczak@wat.edu.pl, kjach@wat.edu.pl, asarzynski@wat.edu.pl

Abstract. Laser radiation is often used in cleaning and conservation of artworks. Interaction of laser radiation with matter is so sophisticated process that analytical solutions rarely bring the valuable formulas. Even numerical methods seldom give quantitative insight into the physics of processes. Chemical and physical properties of surface impurity layers may change from point to point within the same sample. In spite of this, theoretical description of laser cleaning is necessary, as it allows to explain some characteristic features of processes under investigation. In this work we present a model for laser pulse interaction with graphite layer placed on aluminium substrate. The model is limited to one dimensional hydrodynamic equation. Numerical calculations and experimental results give a qualitative agreement.

1 Introduction

Laser interaction with matter is a field of science intensively developed for dozen or so years. It accompanied the works on design of new laser devices. During short time it has been evident that it is one of the most complicated fields of contemporary physics both having in view its experimental and theoretical problems.

The interaction of laser radiation with matter becomes more complex with increasing intensity of laser pulses. For relatively low densities of the pulses power ($q \leq 10^3 \div 10^6$ [W/cm^2]), only radiation absorption and medium heating without melting and evaporation are observed. At the higher densities of pulse power ($q \approx 10^6 \div 10^7$ [W/cm^2]), body surface starts to melt and evaporate. More and more higher densities of the pulses power ($q > 10^9$ [W/cm^2]), usually cause formation of a cloud of the evaporated layer that can interact with incident radiation and partially absorb it. Due to the pressure of the ablation cloud, shock waves can be generated inside the target. Further increase of pulse power densities ($q > 10^{11}$ [W/cm^2]) causes creation hot plasma that can achieve in some extreme cases the parameters characteristic for controlled thermonuclear fusion.

Modelling behaviour of bodies influenced by laser pulses of various power density (energy), the equations of continuous media mechanics (hydrodynamics equation and mechanics equation of solid bodies) will be used supplemented with equations describing typical plasma effects, e.g. ionisation or radiation transport.

Systems of differential equations forming the model are difficult to solve analytically because of their nonlinearity and multidimensionality. Only the solutions obtained with computer physics methods are discussed, because analytical solutions can be obtained for very simplified models which do not express complexity of all simultaneously proceeding phenomena and physical effects coupled between each other.

Moreover, too much troublesome is to find (or experimentally determine) empirical functions and coefficients describing behaviour of real centres within wide range of changes in thermodynamic parameters. Particularly difficult is to determine such parameters as thermal conductivity or absorption coefficient as a function of temperature, density, and ionisation degree. We are interested exclusively in qualitative analysis of processes under investigation. So we use in our calculations graphite instead of the impurity and aluminium instead of the real substrate. Mechanical, optical and thermodynamical characteristics of graphite and aluminium are much better known than characteristics of real impurities and substrates.

2 Theoretical One-Dimensional Model

The system of partial differential equations describing the considered problem results from the laws of conservation of mass, momentum, and energy. For one-dimensional case the system is of the form (plane symmetry) [1–5]

$$\frac{d\rho}{dt} + \rho\frac{\partial \upsilon}{\partial z} = 0 \tag{1}$$

$$\rho\frac{d\upsilon}{dt} = -\frac{\partial p}{\partial z} \tag{2}$$

$$\rho\frac{d\varepsilon}{dt} = -p\frac{\partial \upsilon}{\partial z} + \frac{\partial}{\partial z}\left(\chi\frac{\partial T}{\partial z}\right) - \frac{\partial q^+}{\partial z} + \frac{\partial q^-}{\partial z} - \rho K_{re} - Q_S \tag{3}$$

In (1–3), ρ is the density, υ – mass velocity, p – pressure, ε – specific internal energy, t – time, z – spatial variable, T – temperature, χ – thermal conductivity, Q_S – energy losses in ionisation, q^+,q^- – beams of laser radiation propagating in a medium; q^+ – incident beam and q^-– beam reflected from critical surface and returning to the surface, K_{re} – term describing average interaction of matter with its thermal radiation. Position of the critical surface results from the relation $n_e = n_e^{kr}$, where n_e is the electrons concentration, n_e^{kr} is the critical concentration of electrons related to wavelength of the laser radiation [5]:

$$n_e^{kr} = \frac{m_e}{4\pi \cdot e^2}\left(\frac{2\pi \cdot c}{\lambda}\right)^2 \tag{0.5}$$

where m_e – electron mass, e – electron charge, c – the light velocity, λ-wavelength of laser radiation (for $\lambda = 1,06\,\mu\text{m}$, $n_e^{kr} = 10^{21}$ [cm^{-3}]).

If $K(z,t)$ is the absorption coefficient of laser light, variable in time and space, the beams q^+ and q^- can be expressed as:

$$q^+ = q_0\,(t) \exp\left[- \int\limits_{z_0(t)}^{z} K(z',t)dz' \right] \tag{0.6}$$

$$q^- = q_k\,(t) \exp\left[- \int\limits_{z}^{z_k(t)} K(z',t)dz' \right] \tag{0.7}$$

where $q_0(t)$ – incident beam, $q_k(t)$ – beam reflected at the critical surface, $z_0(t)$ – position of the sample surface, and $z_k(t)$ – position of the critical surface.

The equation of radiation transport and ionisation are described elsewhere [12]. Relation between the internal energy ε – and the temperature T of the medium is defined as [3, 10, 11]:

$$T = \frac{\varepsilon}{c_V} + 300 \tag{0.17}$$

where c_V – specific heat for a constant volume. Taking into account medium ionisation it can be presented as follows:

$$c_V = c_{V0}(T)(1 + Z) \tag{0.18}$$

The above system of equations should be supplemented with the equation of state of the investigated media. In the literature, we can find many various forms of these dependencies: $p = p\,(\rho, \varepsilon)$ or $p = p\,(\rho, T)$ [3, 10, 11].

3 Selected Results of Numerical Calculations

We present here only several typical calculation results to illustrate the possibilities of the 1D code. One-dimensional codes are well described in the literature [1].

Examples of typical distributions of temperatures and pressures for different time interval from the beginning of a laser pulse, different parameters of laser pulses and irradiated medium: i.e. energy density, pulse duration, thickness, type of material, and so on, obtained using 1D code are shown in Figs. 1–4.

It should be pointed out that the pressure peak appears in a gas layer adjoining a solid graphite. The pressure peak, i.e. tensile stresses peak (also temperature) appears in the area of high absorption of laser radiation, what occurs near the critical concentration (spatial coordinate equals to 0).

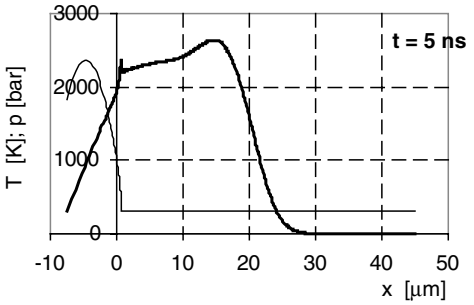

Fig. 1. Temperature (*thin line*) and pressure (*thick line*) diagrams after the time t = 5 ns from the start of the laser pulse (at pulse power peak). The triangle laser pulse, half-time of pulse duration 5 ns, fluence of 1 J/cm^2

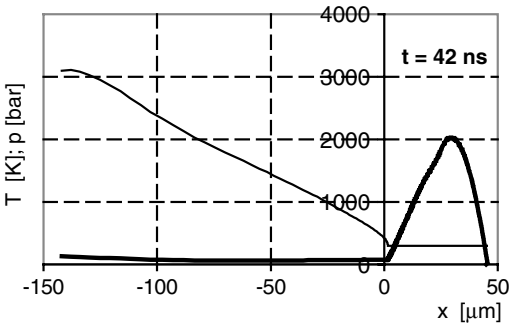

Fig. 2. Temperature (*thin line*) and pressure (*thick line*) diagrams after t = 42 ns from the laser pulse start. Maximum of the compressive stresses. The triangle laser pulse, half-time of pulse duration t = 5 ns, fluence of 1 J/cm^2

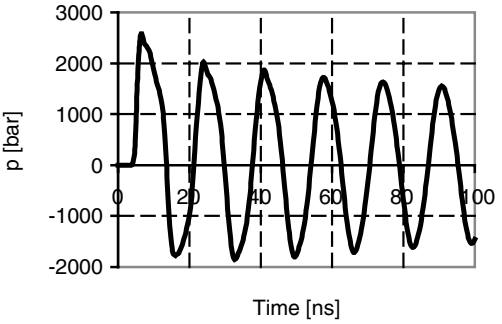

Fig. 3. Pressure diagram in the centre of aluminium layer vs. time. The triangle laser pulse, half-time of pulse duration 5 ns, fluence of 1 J/cm^2

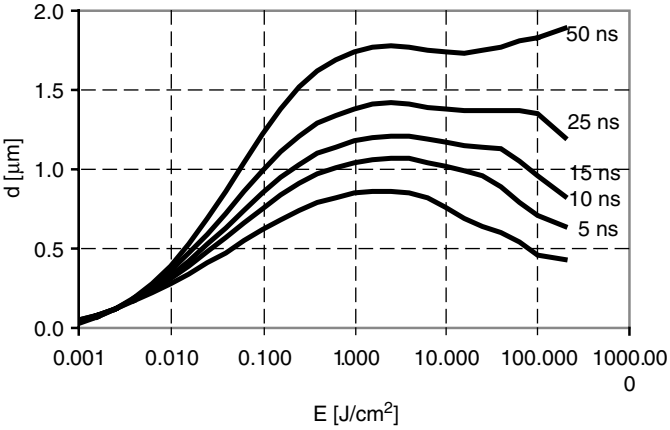

Fig. 4. Thickness of a graphite layer evaporated from aluminium substrate by a laser pulse: the numbers denote pulsewidth of a laser pulse. It was assumed that the pulse is of triangular shape and graphite layer is homogeneous

These results are of qualitative nature. They can insignificantly vary, first of all in dependence on the applied model of radiation absorption. However, some optimal density of laser pulse exists for which a thickness of removed graphite layer is maximal. The summary diagram is presented in Fig. 4.

The power of laser radiation and also the pulse energy can vary in a very wide range depending on a mode of laser operation [6–8]. Here, we do not deal with the changes of radiation power generated by the real laser. We assume that laser generates 1, 2 or 4 identical pulses during one microsecond.

Using the model of 1D type, it is also possible estimation of the ablation phenomenon for replacement of monopulse with pulse train of the same total energy.

For each case, the calculations were carried out for up to 1000 ns, value limited by a calculation power of our computers. Figure 5 presents the diagram of a thickness of evaporated layer vs. time for 1, 2 and 4 pulses. The initial thickness of graphite layer was 3 μm for all cases.

Figure 5 shows that delivery of the same energy in several portions, not in one portion, enables the more effective cleaning of a sample surface.

Interesting are also the temporal characteristics of stresses (Fig. 6, 7). The pressure grows up to specific maximum value at the end of a laser pulse and then exponentially decays. It is connected with the attenuation of stresses by thermoelastic effects.

Fast decay of stresses oscillation shown in Fig. 7 is caused by the "crack" of aluminium substrate into several separate layers in which the stresses are strongly attenuated.

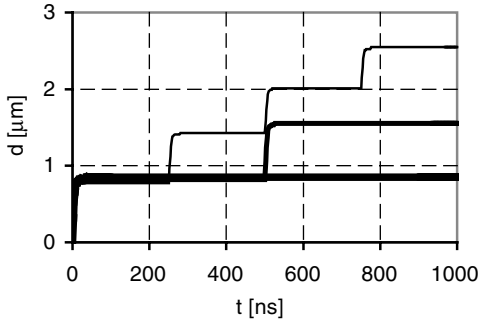

Fig. 5. Diagram of a thickness of evaporated layer vs. time. Total fluence of $1\,\mathrm{J/cm^2}$

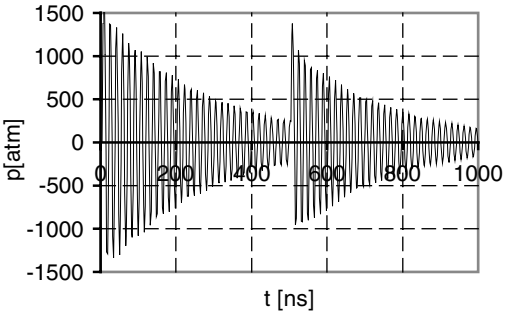

Fig. 6. Diagram of stresses occurred in a half thickness of aluminium substrate vs. time. Two laser pulses, total fluence of $1\,\mathrm{J/cm^2}$

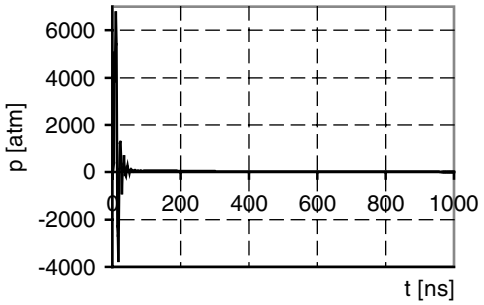

Fig. 7. Diagram of stresses occurred in a half thickness of aluminium substrate vs. time. One laser pulse, total fluence of $10\,\mathrm{J/cm^2}$

4 Conclusions

The results of numerical calculations appear to be consistent with experimental observations. First of all, a thickness of evaporated contaminant layer does not vary significantly in the broad range of laser energy densities (Fig. 4). This effect agrees well with the experiment. Decrease of laser pulse power at the same level of energy density enlarges thickness of evaporated layer (Fig. 4). Evaporation occurs only above a certain threshold value of laser pulse power. In the presented model, however, we cannot describe this threshold phenomenon because we disregarded phase transitions (melting and vaporization).

Thickness of evaporated layer increases also if energy is delivered to the sample being worked out in a few separated in time portions instead of one. During the period between constituent pulses, created plasma expands and its density decreases. This leads to a drop of plasma screening of laser radiation. A subsequent pulse can thus more deeply penetrate the irradiated medium and cause ablation of non-distorted layers.

Laser pulse generates the high amplitude stress waves in elastic media (Fig. 6), sufficient to cause mechanical crushing of majority of materials. These stress pulses can shell contaminants from the substrate due to mechanical disruption, without melting or vaporization.

References

1. D. Potter, *Computational Physics*, John Wiley & Sons, London, New York, Sydney, Toronto, (1973)
2. J. J. Duderstadt and G. A. Moses, *Inertial confinement fusion*, Wiley and Sons, New York, 1982
3. K. Jach, A. Morka, M. Mroczkowski, R. Panowicz, A. Sarzynski, W. Stepniewski, R. Swierczynski, and J. Tyl, *Komputerowe modelowanie dynamicznych oddzialywan cial metoda punktów swobodnych*, PWN, Warszawa (2000)
4. K. Jach, Modelowanie komputerowe zjawisk kumulacyjnych, WAT, Warszawa (1990)
5. M. Martin and A. Blatter, *Laser-Beam Interactions with Materials*, Springer series in Materials Sciences, 2nd Edition, Springer, 1994
6. S. Siano, F. Margheri, R. Pini, P. Mazzinghi, and R. Salimbeni, *Cleaning processes of encrustated marbles by Nd:YAG lasers operating in free-running, and Q-switching regimes*, Applied Optics, Vol. 36, No. 27, pp 7073–7079, (1997)
7. R. B. Cheslar, M. A. Karr, and J. E. Geusic, Proc. IEEE, vol. 58, pp 1899–1914, (1970)
8. J. Marczak, *Wykorzystanie promieniowania laserowego w renowacji dziel sztuki i obiektów zabytkowych w architekturze*, Zeszyty Naukowe Instytutu Maszyn Przeplywowych PAN w Gdañsku, "Lasery i nowe techniki w konserwacji obiektów zabytkowych '2002", Vol. 524/1483/2002, str. 23–46 (2002)
9. C. L. Mantell, *Carbon and Graphite Handbook*, Interscience Publishers, Willey and Sons (1968)

10. S. Eliezer, A. Ghatak, H. Hora, and E. Teller, *An introduction to equations of state – Theory and applications*, Cambridge University Press, Cambridge, 1986
11. G. L. Kerley and L. Chhabildas, *Multicomponent-Multiphase Equation of State for Carbon*, Sandia Report, SAND2001–2619, Sandia National Laboratories, September, 2001
12. J. Marczak, A. Sarzynski, and K. Jach, *Numerical Modelling of Laser-Matter Interaction*, SPIE 2003

Laser Signal Dependence on Artworks Surface Characteristics: A Study of Frescoes and Icons Samples

E. Esposito, P. Castellini, N. Paone, and E.P. Tomasini

Dipartimento di Meccanica – Università Po litecnica delle Marche, via Brecce Bianche, 60131, Ancona, Italy
e.esposito@mm.univpm.it

Abstract. Use of laser-based instrumentation is gaining a wider diffusion during the conservation process of artworks, being employed in many different applications ranging from cleaning of surfaces, to chemical analysis and physical diagnostics. In this last respect, scanning laser Doppler vibrometry (SLDV) is a powerful tool to diagnose the presence of delaminations, voids and cracks in multi-layered artworks such has frescoes and icons. SLDV offers many advantages over other diagnostics techniques but, for effective operation of the instrument, a certain amount of laser light must be reflected towards the laser head. This fact poses operative limits to vibrometers due to increasing measurement distances, surface roughness and type of finishing, angle of view and reflection dependence on surface pigments. In this work we will investigate maximum distances and angles of view that still allow a clear detection of defected areas in artworks by SLDV, using frescoes and Byzantine icons prepared by professional restorers. Our results will be used in future measurement sessions to evaluate the feasibility of the diagnostics process by SLDV. Moreover we will also study the noise properties of the laser signal to determine its Power Spectral Density (PSD) and Signal to Noise Ratio (SNR) when aimed at areas with different pigments.

1 Introduction

The SLDV is an instrument with an extremely high sensitivity but, to correctly acquire vibration velocities of a structure, a minimum amount of laser light must be back scattered towards the laser head by the structure's surface [1]. Being this condition satisfied, the modulation/demodulation section of the SLDV will be able to extract from the Doppler signal an analog voltage proportional to surface velocity. If this threshold is not reached, usually about 5% of instrument full scale, we will have the output signal to "drop-out". A series of remedies have been implemented to avoid this situation, and in particular companies producing SLDVs recommend optimal measurement distances and the application of special paints.

Moreover, drop-outs depend on the realization scheme of the SLDV; for example, Ometron vibrometers always present the behaviour reported in Fig. 1, where drop-outs are represented by downward oriented spikes.

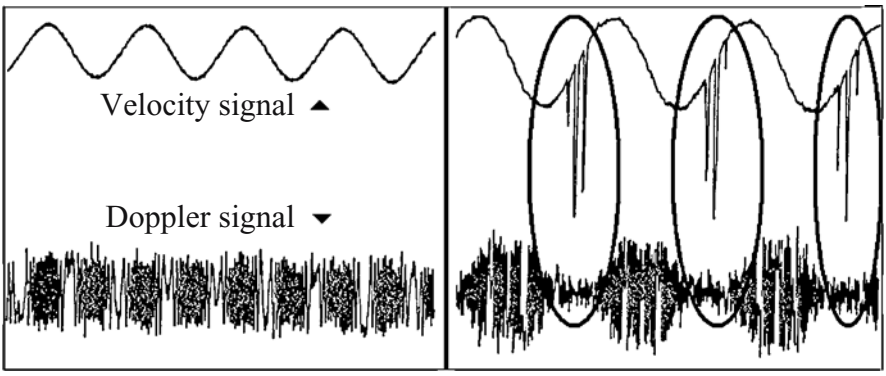

Fig. 1. Velocity and Doppler signals for optimal diffusive surface (*left*) and bad surface (*right*)

Unfortunately, not all if any of proposed countermeasures for drop-outs are applicable to artworks and so we have investigated the applicability of SLDV to artworks diagnostics in terms of:

1. maximum distance and maximum angle of view for defect detection and determination of correspondent Doppler signal level;
2. Signal to Noise Ratio (SNR) of the SLDV output signal;
3. Power Spectral Density (PSD) of noise in the output signal.

Four fresco samples, supplied by the Laboratoire de Recherche des Monuments Historiques – LRMH, Paris, have been examined: Plate VII and VIII are identical but for the surface finish, which is smoother in the first case, while Las6ES and Las1ES differ only for the number and disposition of the defects. Benaki Museum, Athens, prepared a single icon painted with different colors and with a wide gold area at the bottom; see Fig. 2 for geometrical details of all the samples.

2 Experimental Methods

Samples have been mounted on a steel heavy support positioned one meter in front of the laser and they have been put into vibration by a loudspeaker system fed with white noise. A SLDV scan has been conducted and defects (delaminations, cracks) identified; after this first acquisition, the sample has been rotated and the defects identification procedure repeated. This procedure has been iterated for distances of 3, 5, 8 and 10 meters, at angles of 0°, 30°, 45°, and 60° degrees. At the same time, detailed maps of Doppler signal amplitude have been recorded, using a small piece of retro-reflective 3M tape as the reference spot.

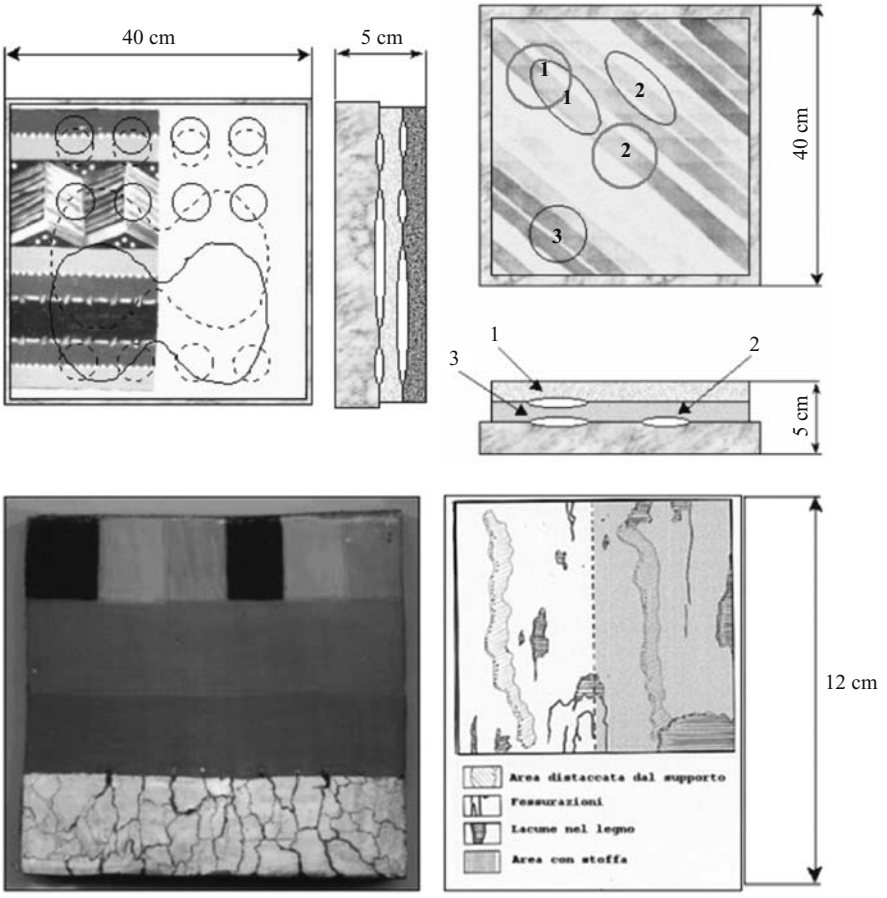

Fig. 2. Employed samples with dimensions and positions and types of defects. *Above left*, scheme of fresco Plate VII and VIII, *above right* Las6ES and Las1ES (defects of these plates are identified by an asterisk). Below, icon sample

To evaluate signal SNR and PSD a different procedure has been implemented, based on a sinusoidal excitation at the resonance frequencies of the identified defected areas. Single point measurements have been conducted in areas of different pigments, where a defect is present or where there are not any. An ONO SOKKI CF5200 spectrum analyzer has been employed to acquire the SLDV signal and to calculate its noise PSD, expressed as an average level with units of $\mu V/(Hz)^{1/2}$ or $(\mu m/s)/(Hz)^{1/2}$. The SNR has been calculated only for a fresco sample, using the amplitude of the spectral line at the excitation frequency as the reference signal. All measurements have been conducted using an Ometron VPI4000 system, being the UK Company

a partner of the Polytechnic University in the research project that has led to these investigations.

3 Results and Discussion

In Fig. 3 we report the graphs summarizing the results of the measurements of Doppler level, while in Table 1 we show the results obtained for the definition of the maximum operative limits of the SLDV. Table 2 is an example of the measurements of the PSD and SNR on fresco sample VIII excited acoustically at 1038 Hz. A series of observation may be done:

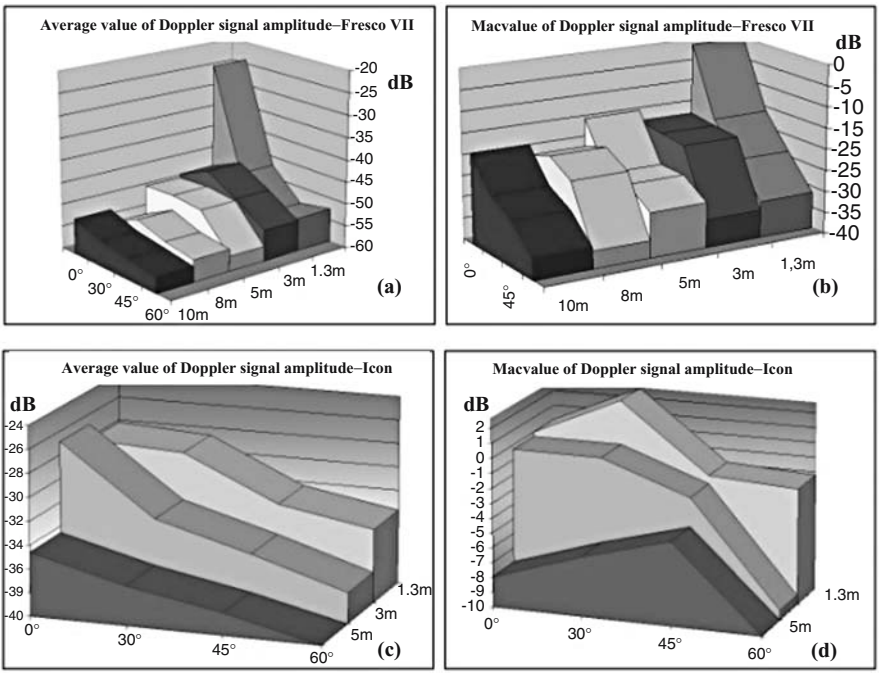

Fig. 3. Graphs of Doppler level on samples fresco, above, and icon, below, samples

1. Defects are detected up to ten meters for the frescoes and up to five meters for the icons, with a maximum rotation angle of 45° and 30° respectively. The dimensions of the lab room limited the possibility of exploring longer distances, and we think twelve meters is a more realistic maximum distance.
2. For frescoes, Doppler level depends a lot on color, with higher values for yellow, white and red, while the worst response is from black pigment. On

the contrary, the influence of surface roughness seems to be negligible, at least on our samples.

3. Doppler level for the icons greatly depends on the surface shiny finish, and in this situation the icon shape will determine the amount of backscattered laser light. As a confirmation from Fig. 3 we observe that the range of the Doppler signal is limited to 15 dB for the icon and raises to 40 dB for frescoes (sample VII).
4. SNR and PSD have been measured only on fresco samples. We have obtained a PSD average values of $0.99\,\mu m/s/Hz^{1/2}$ and $0.46\,\mu m/s/\,Hz^{1/2}$ for non defected and defected areas respectively, with a best value of $0.4\,\mu m/s/Hz^{1/2}$on yellow and red pigments. SNR best result has been of 23.4 dB, as measured on a yellow painted defected area.

Table 1. Maximum distances and rotation angles for defects identification in frescoes (■) and icons (♦)

Distance from SLDV(m)	Rotation angle			
	0°	30°	45°	60°
1,3	■		♦	
3		■	♦	
5		♦	■	
8		■		
10		■		

Table 2. PSD and SNR values for fresco sample VIII at excitation freq. of 1038 Hz (dBV)

Color	PSD No defect	PSD Defect	SNR No defect	SNR Defect
Red		−66,1		19,5
White	−62,0	−60,3	10,2	10.7
Black	−45,1	−63,0	−3,53	20,1
Yellow		−68,4		23,4
3M	−73,2	−65,3	22,7	27,8

Finally we observe that defects presence lowers noise contribution, as can be seen in Fig. 4, where the PSD for two different measures on the same black area is reported. This behaviour may be explained by the electro/optical technology employed for the construction of the Ometron SLDV employed in our experiments, that will give a lower performance for quasi-static objects in favour of moving targets, such as a detached region.

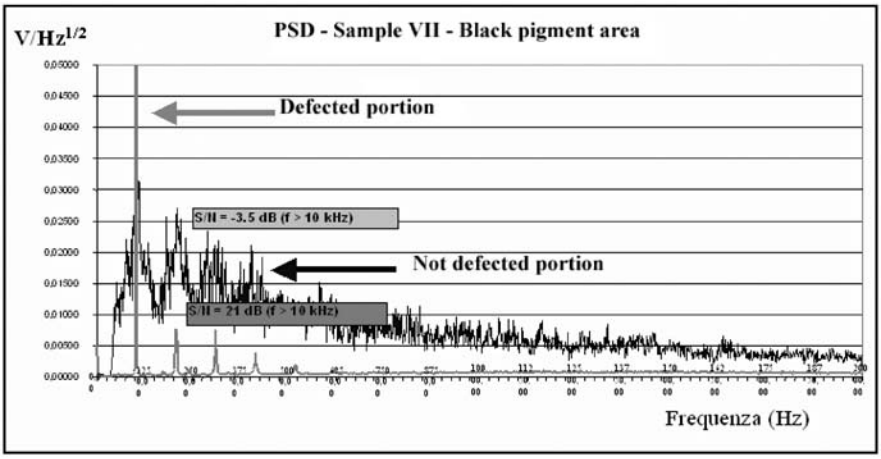

Fig. 4. Velocity spectra of defected and not-defected areas of fresco sample

4 Conclusions

In this paper we have presented a study of the operative limits of SLDV instrumentation when applied to artworks diagnostics, in order to establish maximum measuring distance and maximum angle of view. We have also found typical values of SLDV signal PSD and SNR, and, although our findings are strictly related to SLDV, we think they contribute to a better understanding of the interaction of laser light with artworks surfaces and could be useful also for other lased based diagnostic instrumentation.

Acknowledgements

We wish to acknowledge the EU financing, which by the LASERART contract – SMT4962062 has made this work possible.

Reference

1. R. F Strean, L. D. Mitchell, and A. J. Barker in *Proceedings of 15th International Modal Analysis Conference – IMAC XV*, Kissimmee, USA, 1229, 1997

Pollution Encrustation Removal by Means of Combined Ultraviolet and Infrared Laser Radiation: The Application of this Innovative Methodology on the Surface of the Parthenon West Frieze

P. Pouli[1], K. Frantzikinaki[2], E. Papakonstantinou[2], V. Zafiropulos[1], and C. Fotakis[1]

[1] Institute of Electronic Structure and Laser (IESL), Foundation for Research and Technology-Hellas (FORTH), Heraklion, PO Box 1527, 71110, Crete, GREECE
ppouli@iesl.forth.gr

[2] The Acropolis Restoration Service (YSMA), Ministry of Culture, 10 Polygnotou St., 10555, Athens, GREECE
epapak@yahoo.com

Abstract. This study refers to the innovative laser cleaning methodology developed at FORTH IESL on the combination of ultraviolet and infrared laser radiation emitted from a Q-switched Nd:YAG laser for the successful removal of pollution encrustation from marble substrates. The above-mentioned methodology is presented as regards its successful application on the fragile and demanding surface of the Parthenon West Frieze in collaboration with the Committee for the Preservation of the Acropolis Monuments. The aim of this intervention was to remove encrustation, accumulated on the stone due to the atmospheric pollution, without any discoloration or structural alteration to the original surface. The preliminary experiments on all the possible substrates and encrustations present on the surface of the Acropolis monuments and the laser cleaning parameters are presented in detail.

1 Introduction

The Pheidian Frieze of the Parthenon is without doubt the most precious and fragile monument of the Acropolis. Severe weathering and damage as well as the accumulation of thick pollution encrustation on its surface can be attributed to the microclimate and the microstructure of the marble, its exposure to atmospheric conditions, various incidents such as an ancient fire, many earthquakes, a destructive explosion in 1687 etc. combined with the intense atmospheric pollution of the modern city of Athens. Since the removal of the West Frieze from the Parthenon in 1992–93, significant multidisciplinary research efforts have focused on the assessment of various conservation methodologies in order to prevent further deterioration and preserve its authentic surface.

The application of lasers for the removal of pollution encrustation from its surface had been until recently prohibited, as the existing laser cleaning

methodologies were found insufficient to meet the criteria set by the Committee for the Preservation of the Acropolis Monuments. According to the Committee any cleaning intervention on the surface of the Parthenon West Frieze should not cause any discoloration, chemical or structural alteration to the original marble surface.

2 The Condition of Preservation

The various types of pollution encrustation encountered on the Acropolis sculpture and monuments can be distinguished as follows [1]:

- Thin layers of *loose deposits* (up to 100 μm thick) consisting of airborn carbon particles, gypsum, traces of minerals and metals, earth, organic compounds etc.
- *Homogeneous compact crust* with good adhesion to the surface. Practically this crust comprises loose deposits of significant thickness, which obscure significantly the original surface.
- *Dendritic black crust*, which appear on surfaces directly exposed to rain and consist of re-crystallized and re-precipitated calcium carbonate in dendritic formation.

The above-mentioned types of encrustation may be encountered either on deteriorated marble substrate or on "monochromatic surface layers" forming thus six distinctive cases of cleaning problems. The monochromatic surface layers (an orange-brown skin rich in calcium oxalates and a beige coating rich in calcium carbonate) cover almost the 33% of the sculpted surface of the West Frieze blocks and they are considered important historical documents as they indicate the original surface while preserving original tool-marks [2, 3].

It is therefore very important to ensure that the cleaning methodology will respect the surface including all its particularities (tooling traces, monochromatic surface layers, deterioration etc.) while leading to a pleasing aesthetic result.

3 The Methodology and the Innovation

Infrared radiation at 1064 nm emitted from Q-switched Nd:YAG laser systems is a well established cleaning methodology with numerous applications worldwide [4]. However, the preliminary tests performed on representative samples from the surface of the Acropolis monuments were found to be inappropriate, as the cleaned surface appeared to be discoloured giving the impression of a yellow hue [5, 6]. Removal of unwanted encrustation by means of infrared radiation is mainly achieved through *photothermal* mechanisms. In this case the dark particles, which are embedded in the encrustation's matrix, absorb the infrared laser radiation several times more intensively [7]

than does the calcitic stone substrate and/or intermediate gypsum layer and therefore the energy threshold for the removal of the superficial layer is significantly lower than that required to remove the substrate material (in most cases the sulphated outer surface). Appropriate laser focusing, to adjust the energy density of the laser within a specific range, ensures the selective and *self-limiting* removal of the encrustation without the slightest alteration to the stone.

When the applied laser energy density is lower than the energy density threshold necessary for the removal of the encrustation material (mainly gypsum), s*elective vaporisation* of the embedded dark-coloured airborne particles occurs, which slightly affects the main crust body. The gaps resulting from the removal of the dark-coloured particles, as well as the change of the absorption spectra of the remaining encrustation, leads to the impression that the final surface is discoloured ("*yellowing*") [5].

Such discoloration impression may be avoided if ultraviolet radiation is used (3^{rd} harmonic of a Nd:YAG laser at 355 nm) [8], where *photomechanical* phenomena predominate. Material removal takes place in discrete steps while it was found that ultraviolet radiation is absorbed by the dark particles/encrustation to the same extent as by the gypsum layer or underlying stone. In such case, the thickness of the encrustation and the fluctuation that this may have throughout the surface is very important for a homogeneous surface cleaning. This drawback gets noteworthy in the case of thick dendritic crusts. Moreover, discoloration of the final surface towards grey hues was observed.

To avoid discoloration and structural alteration problems the IESL-FORTH research-team suggested the combining action of the two discrete laser ablation mechanisms [9]. This was accomplished by temporally and spatially overlapping of two laser beams of different wavelengths, namely the fundamental and the third harmonic of a Q-switched Nd:YAG laser. The energy densities of the two beams are set to a specific ratio.

Following preliminary laboratory tests, a research program has been established between IESL-FORTH and the Acropolis Restoration Service (YSMA) to assess this innovative cleaning methodology on site. This involved the development of a prototype laser system and preliminary trials on all the possible substrates and encrustations present on the surface of the Acropolis monuments in order to determine the optimum laser cleaning parameters [1].

4 Experimental Methods

The prototype laser system transferred on the Acropolis site is a commercial Q-switched Nd:YAG system (BMI series 5022 DNS 10) specially modified in order to deliver spatially and temporally overlapping pulses of 1064 and 355 nm. The relative ratio of the energies of the two beams is adjusted externally by means of a homemade set-up, which includes variable attenuators.

Experiments have been initially performed on "newer corner additions" of the Parthenon West frieze blocks. The newer corner additions have been adjoined onto the frieze in the early sixties during reconstruction and preservation works and bare the same encrustation problems as the rest of the frieze, while their substrate is newer Pentelic marble without weathering. The advantage of using these samples for preliminary studies is that it is possible to perform a large number of cleaning tests as well as to destructively analyse them in order to evaluate the result (for example prepare cross sections for microscope viewing).

The starting point was the ablation threshold fluences for each radiation and encrustation as determined in previous studies [8] while wavelength blending tests were ranging between various infrared ($F_{IR} = 0.5 - 3.0\,J/cm^2$) and ultraviolet ($F_{UV} = 0.15 - 0.5\,J/cm^2$) energy densities as well as various "ultraviolet to infrared" energy density ratios ($F_{UV}/F_{IR} = 0.25$ up to 0.8) and variable number of pulses (2 up to 200). In individual cases the application of a very thin layer of water (saturated with $CaCO_3$) has been considered [1].

The evaluation of the cleaning trials included stereomicroscopic observation of the surfaces, colorimetric measurements following the L*a*b* system, polarizing microscope observation of ultra-thin and cross-sections, XRD, FTIR and SEM-EDAX analyses of the surfaces before and after cleaning as well as artificial ageing tests on cleaned samples [1]. The colorimetric instrument used is a portable Micromatch Plus, which measures totally flat areas (of 2 cm in diameter) illuminated by reference sources at 65° angles while the observation angle is 10°.

Once the analytical assessment of the preliminary experiments on "newer corner additions" was satisfactory and the method was proven, the Central Archaeological Council of the Greek Ministry of Culture inquired a large-scale cleaning plan on selected architectural pieces form the Parthenon in order to optimise the suggested methodology prior its application on the Parthenon West Frieze. The architectural pieces selected for this purpose either show the same weathering and encrustation problems as the actual frieze (i.e. a cornice block, "*geisson*", from the North side) or *monochromatic layers* are still preserved on their *surface* (i.e. a frieze crown block, "*thranos*", and part of a capital from the opisthodomos of the Parthenon).

5 Results and Discussion

A series of laser cleaning tests on a fragment from the corner addition of the West Frieze's block (ref. number 11, ΔZ XI) with thin compact crust are shown in Fig. 1. The starting point was the ablation threshold fluences for infrared, area 1, and ultraviolet radiation, area 2, as determined in previous studies [8]. Both areas were not favourable as discoloration towards yellow and grey hues was observed. The areas 3 to 6 have been irradiated with different

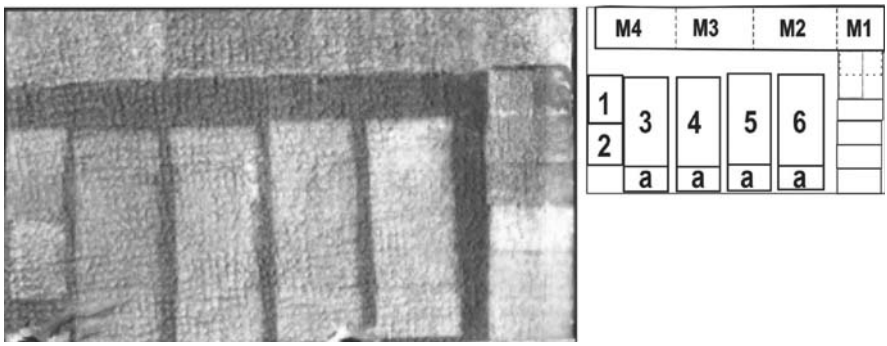

Fig. 1. Preliminary laser cleaning trials on a newer corner addition from the West Frieze Block number 11 (ΔZ XI)

energy densities and ultraviolet to infrared ratios. The detailed information on the laser parameters, the applied number of pulses and the L*a*b* colour co-ordinates (mean values of three measurements on adjacent areas) are shown in the Table 1.

The remarkable difference in the colour of the surfaces irradiated with infrared (area 1) and ultraviolet (area 2) radiation is also confirmed by the L*a*b* coordinates shown in Table 1. A significant shift of the yellow-blue coordinate b* is observed between area 1 (b* = 20, yellow hue) and area 2 (b* = 11.2, grey hue), while areas irradiated with the combination of the two wavelengths lay between these two values. The resulting colour depends on two factors; the energy density of each individual radiation (F_{UV}, F_{IR}) as

Table 1. Laser parameters and the corresponding colour co-ordinates of the preliminary cleaning tests on a fragment from the newer corner addition of the Parthenon West Frieze block no 11 (ΔZ XI)

Area no	F_{IR} (J/cm^2)	F_{UV} (J/cm^2)	F_{UV}/F_{IR}	Number of pulses	Colour Co-ordinates L*	a*	b*
1	0.84	-	-	50	64.3	5.1	20.0
2	-	0.36	-	50	61.7	2.5	11.2
3	0.64	0.15	0.23	50	61.6	4.3	16.8
3a	0.64	0.15	0.23	200	67.8	2.7	15.9
4	0.76	0.2	0.26	50	68.8	2.9	16.2
4a	0.76	0.2	0.26	200	70.2	2.3	15.5
5	0.68	0.28	0.43	50	64.0	3.3	14.0
5a	0.68	0.28	0.43	200	67.4	2.2	13.2
6	0.84	0.36	0.42	50	66.5	2.8	13.8
6a	0.84	0.36	0.42	200	71.1	2.4	14.0
	Suggested optimum L*a*b* coordinates [1] :				60–70	2.8–5	13–16

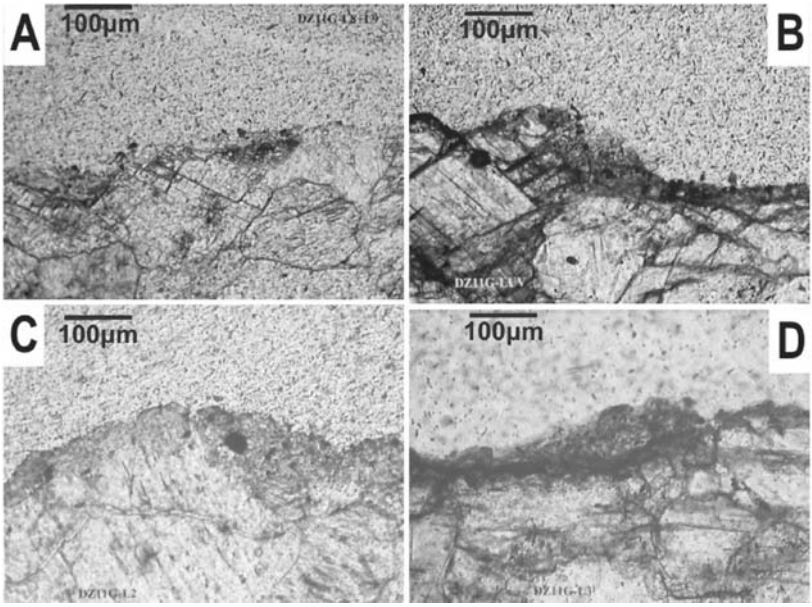

Fig. 2. Polarizing microscope photos of cross sections of areas irradiated with 1064 nm (**a**) 355 nm (**b**) and their combination in various ratios (**c**) and (**d**) (reference bar = 100 μm)

well as the percentage of each radiation to the combined beam (F_{UV}/F_{IR}). Thus areas irradiated with different ultraviolet percentage, i.e. areas 4 and 5 appear less yellow as the ultraviolet component increases, i.e. area 5. In the same way areas irradiated with similar ultraviolet to infrared ratio component (i.e. areas 5 and 6) result into different cleaning levels according to the applied energy fluences.

The most favourable cleaning result was chosen after comparison of all the three coordinates to the L*a*b* values of reference areas [1]. As reference there were considered areas where no pollution crust has been accumulated e.g. on the South Parthenon Frieze (L*a*b* = 76.5/ 3.60/ 15.6), wash-out areas on the West Frieze blocks (L*a*b* = 70.4/ 2.8/ 13.3), over-cleaned areas on the North Frieze blocks kept in the British Museum in London (L*a*b* = 77.2/ 1.3/ 9.8), new Pentelic marble (L*a*b* = 80.8/ 1.1/ 4.9) etc. Thus, it was suggested [1] that the L*a*b* values of the cleaned areas should lay between L = 60 and 70, a* = 2.8 to 5 and b* = 13 to 16 in order to avoid unpleasant discolorations.

Microscopic observation of cross sections of the above areas confirms the selective vaporization mechanism at relatively low infrared energy densities ($F_{IR} = 0.85\,J/cm^2$). This results into a semi-transparent layer of remaining crust in which the majority of the dark inclusions have been removed (Fig. 2a). On the opposite close examination of areas irradiated with

ultraviolet radiation only, verify the photomechanical material removal mechanism, which eliminates the encrustation bulk in discrete steps and therefore results into thinner layers of the same encrustation material (Fig. 2b). An intermediate situation is observed in areas irradiated with the combined beam (Fig. 2c and 2d) where it is shown that the higher the ultraviolet percentage in the combined beam (Fig. 2d) the more dense and thin the remaining encrustation appears.

Similar experiments on all the types of encrustation and substrates present on the Acropolis sculptures resulted into the following remarks:

- the combination of the infrared and ultraviolet radiation at relatively low energy fluence values ($F_{IR} = 0.6 - 0.8\,J/cm^2$ and $F_{UV} = 0.15 - 0.3\,J/cm^2$ in the case of loose deposits and $F_{IR} = 0.8 - 1.2\,J/cm^2$ and $F_{UV} = 0.2 - 0.4\,J/cm^2$ in the case of homogeneous compact crust) as well as a moderate number of pulses (10–50) resulted to a very successful cleaning with no discoloration problems to the underlying marble surface. On the other hand dendritic black crusts on marble could only be removed with infrared laser pulses, with energy fluence values that lay beyond the $1.8\,J/cm^2$, which ensure that the "whole body" of the crust (the gypsum matrix including the embedded dark airborne particles) is effectively removed without selective vaporisation of the embedded particles. As a result there is no remaining crust on the final surface, which would give the impression of yellowing. The number of pulses is closely related to the thickness of the crust while in several cases the application of a thin layer of water was found to enhance the cleaning process.
- The use of ultraviolet radiation or any combination of ultraviolet and infrared radiation was found to significantly discolour the "monochromatic surface layers". 2 to 10 pulses of infrared laser radiation at energy fluence values of 0.5 to $0.8\,J/cm^2$ resulted into satisfactory removal of loose deposits and homogeneous compact crust while dendritic black crust required significantly higher energy fluence values and the application of a thin layer of water.

6 Conclusions

Following the preliminary studies a prototype laser system has been developed and is now used for the cleaning of the Parthenon West Frieze. The simultaneous action of the two wavelengths (1064 and 355 nm) was proved to be able to remove the deposits in a controllable way, with no discoloration or surface alteration phenomena to the original marble surface, as proved by the physicochemical analyses performed by the Acropolis Conservation team [1]. It was shown that for every encrustation and substrate there is a unique set of parameters ("ultraviolet to infrared radiation" ratio, applied energy fluence values and number of pulses) that may result to acceptable results [1].

Acknowledgements

The authors would like to thank the Greek Institute of Geology and Mineral exploration (IGME), the 1st Ephorate of Pre-historical and Classical Antiquities and the Committee for the Preservation of the Acropolis Monuments.

References

1. E. Papakonstantinou, K. Frantzikinaki, P. Pouli, and V. Zafiropulos, in *Study on the cleaning of the West Frieze, Study on the Restoration of the Parthenon* **7**, edited by the Greek Ministry of Culture and the Committee for the Preservation of the Acropolis Monuments, Athens, 2002 (in Greek with English summaries)
2. K. Kouzeli, N. Beloyannis, Ch. Tolias, and G. Dogani in *Proceedings of the International Symposium "Le pellicole ad ossalati: origine e significato nella conservazione delle opere d' arte",* Milano, 327, 1989
3. A . Galanou and G. Dogani in *The West Parthenon Frieze- Conservation Study, Study on the Restoration of the Parthenon* **3c**, edited by the Greek Ministry of Culture and the Committee for the Preservation of the Acropolis Monuments, Athens, 1994 (in Greek)
4. M. Cooper, in *Laser cleaning in conservation: an introduction*, Edited by Butterworth Heinemann, Oxford, 1998 and *LACONA I Proceedings, Restauratorenblaetter (Special Issue),* Edited by W. Kautek and E. Koenig, Mayer & Comp., Wien, 1997
5. V. Zafiropulos, C. Balas, A. Manousaki, G. Marakis, P. Maravelaki-Kalaitzaki, K. Melesanaki, P. Pouli, T. Stratoudaki, S. Klein, J. Hildenhagen, K. Dickmann, B. S. Luk'yanchuk, C. Mujat, and A. Dogariu, in *Journal of Cultural Heritage* **4**, S249, 2003
6. Th. Skoulikidis, P. Vassiliou, P. Papakonstantinou, A. Moraitou, V. Zafiropulos, M. Kalaitzaki, I. Spetsidou, V. Perdikatsis, and P. Maravelaki, Some remarks on the Nd:YAG and Excimer UV lasers for cleaning soiled sulfated surfaces, LACONA I Conference, Book of Abstracts, 7, 1995
7. J. F. Asmus, M. Seracini, and M. Zetler in *Lithoclastia* **I**, 23, 1976
8. G. Marakis, P. Pouli, V. Zafiropoulos, and P. Maravelaki-Kalaitzaki, *in Journal of Cultural Heritage* **4**, S83, 2003
9. V. Zafiropulos, P. Pouli, V. Kylikoglou, P. Maravelaki-Kalaitzaki, B. S. Luk'yanchuk, and A. Dogariu in *current issue*

Mössbauer and XRD Study of the Effect of Nd:YAG-1064 nm Laser Irradiation on Hematite Present in Model Samples

M. Gracia[1], M. Gaviño[2], V. Vergès-Belmin[3], B. Hermosin[2], W. Nowik[3], and C. Sáiz-Jiménez[2]

[1] Instituto de Química Física "Rocasolano", CSIC, Madrid, Spain
rocgracia@iqfr.csis.es
[2] Instituto de Recursos Naturales y Agrobiología, CSIC, Sevilla, Spain
mgavino@irnase.csic.es
[3] Laboratoire de Recherche des Monuments Historiques, Champs-sur-Marne, France
veronique.verges-belmin@culture.gouv.fr

Abstract. Modification induced by a common (Nd:YAG-1064 nm) laser cleaning treatment on model samples was studied using Mössbauer spectroscopy and XRD. Model samples were prepared mixing graphite and/or gypsum with hematite. Reduction of hematite into magnetite, formation of ferric species which are paramagnetic at RT, and dehydration of gypsum to give bassanite were the physicochemical changes induced by the employed laser treatment.

1 Introduction

It has been observed that laser cleaning sometimes induces changes in surface coloration of the lithic materials especially when a Qswitched Nd:YAG laser ($\lambda = 1064$ nm) is employed [1–5]. The study of physicochemical processes occurring after laser irradiation can help to understand the changes that take place when these treatments are applied for cleaning artistic materials. In this context, discoloration of marble during laser removal of surface deposits has been related to the presence of iron compounds in surface encrustations [2, 3]. Thus, the aim of this work was to determine possible changes in iron species induced by laser cleaning treatments. As the sulphation of calcium carbonate leads to the formation of gypsum crusts on limestone materials exposed to urban atmospheres [6], we focused the study to follow the hematite evolution after a laser treatment in model samples prepared by mixing different amounts of gypsum, carbon and hematite. Laser irradiation parameters of a typical cleaning treatment [1, 3, 5], and Mössbauer spectroscopy and X-ray diffraction (XRD), as analytical tools, were selected for this exploratory study.

2 Experimental Methods

Model samples were prepared by grinding and mixing gypsum and hematite (GH samples) and gypsum, graphitic carbon and hematite (GCH samples). Compositions of the prepared samples are shown in Table 1. The powdered specimens were placed in a Petri dish and irradiated through its glass cover using a Nd:YAG laser (λ =1064 nm) exposure at 695 mJ cm^{-2} and 30 pulses s^{-1} during 16 min. The irradiation homogeneity was assured by performing eight separated exposures (3×2.5 min, 2×2 min, 3×1.5 min) and mixing specimen grains between exposures. Glass-cover prevents sample spillage at the cost of absorbing a part of the laser energy but without wavelength change. Powdered hematite was also laser irradiated as reference sample. ^{57}Fe-Mössbauer spectra were recorded at RT and 20 K with a constant-acceleration spectrometer using a ^{57}Co/Rh source and a helium closed-cycle cryogenerator. Fe-thickness of the absorbers was 4.5 $\pm$ 0.5 mg cm^{-2} except for the GCH-2 absorber which was prepared with about 1 mg cm^{-2} of Fe. The spectra were computer-fitted to a sum of Lorentzian lines by applying adequate constraints. The relative concentration of the different species was calculated from the spectral area ratio assuming equal f factor (probability of Mössbauer effect) for all implicated species. X-ray powder diffraction patterns were recorded with a Philips X'Pert diffractometer using Cu$K\alpha$ radiation.

Table 1. Composition ($wt\%$) of model samples (as prepared)

	Gypsum	Graphite	Hematite
GH-9	91	-	9
GH-17	83	-	17
GCH-2	91	7	2
GCH-8	79	13	8

3 Results and Discussion

As expected, Mössbauer spectra of all untreated samples exhibit the typical hyperfine magnetic sextet of the hematite (Fig. 1-a, S_H). After laser exposure, the colour of the samples changed from red to grey or to a more light grey hue in the case of greyish-coloured carbon-containing samples. The spectra recorded at RT from the four model samples after irradiation showed a similar pattern (Fig. 1-c-d) constituted by the sextet of the hematite (S_H), a central doublet (D) and a small magnetic component, which seems to be constituted by two sextets (S_{M1} and S_{M2}). The RT spectra were best fitted by considering three hyperfine magnetic sextets (S_H, S_{M1} and S_{M2}) and a paramagnetic doublet (D). Some representative spectra are depicted in Fig. 1 and

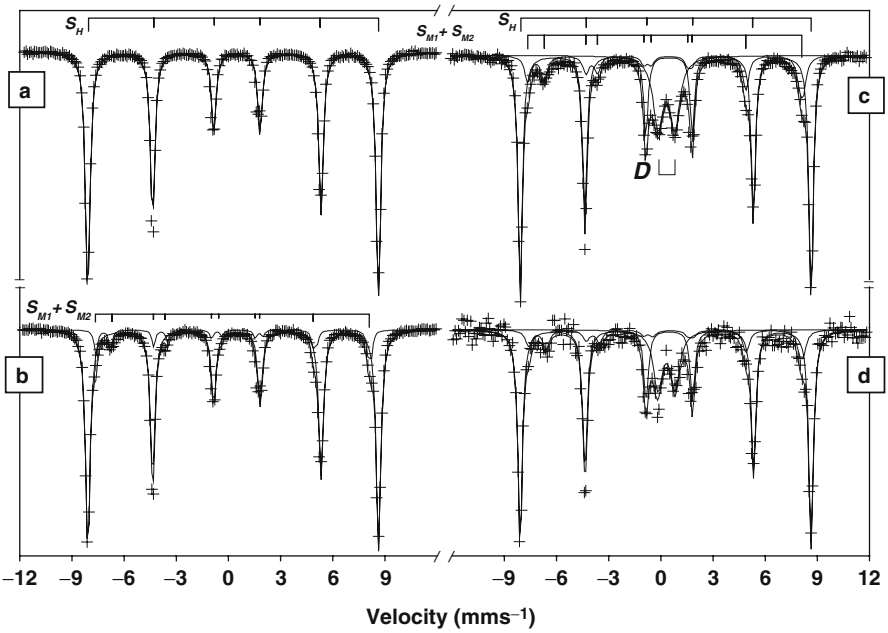

Fig. 1. Mössbauer spectra recorded at RT from (**a**) untreated hematite; (**b**) laser-irradiated hematite sample;(**c**) laser-irradiated GH-17 sample; (**d**) laser-irradiated GCH-2 sample. The fits are shown as solid lines

the relative concentrations of the species calculated from their corresponding spectral areas are shown in Table 2.

Table 2. Relative concentrations (%) of the Fe species found in the laser irradiated samples (calculated from the corresponding spectral areas)

	GH-9	GH-17	GCH-2	GCH-8	Hematite (ref.)
S_H (hematite)	70 ± 2	62 ± 2	67 ± 3	76 ± 2	85 ± 4
$S_{M1} + S_{M2}$ (magnetite)	17 ± 2	18 ± 1	15 ± 2	13 ± 1	15 ± 3
D (octahedral Fe^{3+})	13 ± 1	20 ± 1	18 ± 2	11 ± 2	-

The parameters obtained from the fits for S_H ($\delta_{(\alpha-\mathrm{Fe})} = 0.39\,\mathrm{mm\ s^{-1}}$; $2\varepsilon = -0.19\,\mathrm{mm\ s^{-1}}$; H = 52.1 T) and for the two small sextets, S_{M1} (Fe^{3+} tetrahedral sites: $\delta_{(\alpha-\mathrm{Fe})} = 0.29\,\mathrm{mm\ s^{-1}}$; $2\varepsilon = -0.12\,\mathrm{mm\ s^{-1}}$; H = 49.2 T) and S_{M2} (Fe^{3+}/Fe^{2+} octahedral sites: $\delta_{(\alpha-\mathrm{Fe})} = 0.72\,\mathrm{mm\ s^{-1}}$; $2\varepsilon = 0.03\,\mathrm{mm\ s^{-1}}$; H = 46.5 T), allow their assignment to hematite (S_H) and magnetite (S_{M1} and S_{M2}) [7]. Parameters of D ($\delta_{(\alpha-\mathrm{Fe})} = 0.31\,\mathrm{mm\ s^{-1}}$; $\Delta = 0.95\,\mathrm{mm\ s^{-1}}$) are characteristic of a Fe^{3+} species in octahedral

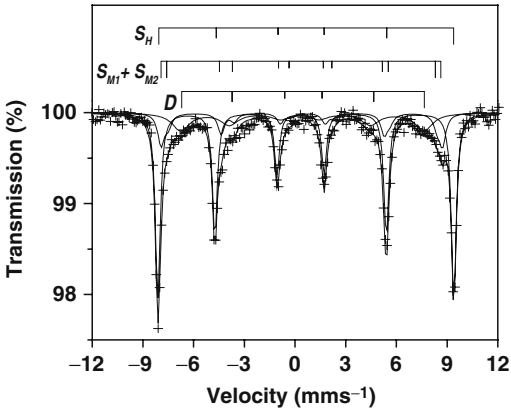

Fig. 2. Mössbauer spectrum recorded at 20 K from GH-17 sample after laser exposure

coordination. Superparamagnetic or amorphous Fe-oxides and even some ternary Ca-Fe oxides give RT doublet patterns compatible with D. The high linewidth ($\Gamma = 1\,\mathrm{mm\,s^{-1}}$) of D can be also indicative of the simultaneous presence of different ferric species. The characteristic pattern of magnetite is also present in the spectrum of the irradiated hematite (Fig. 1-b). Doublet D is not present in this reference spectrum. Therefore, the formation of the ferric species contributing to D seems to be related with the presence of gypsum in the sample. In order to gain insight on the origin of D, a Mössbauer spectrum was taken at 20 K from the sample GH-17 (Fig. 2). Figure 2 shows that D magnetically splits in a broad sextet, whereas S_H, S_{M1} and S_{M2} follow the expected trend, yielding 20 K Mössbauer parameters attributable to hematite (S_H) and magnetite (S_{M1} and S_{M2}). The uncertainty in the obtained Mössbauer parameters of D, due to the strong overlap of D with the hematite and magnetite sextets, precludes an unequivocal assignment of D-species from the 20 K spectrum. Summarizing, the Mössbauer study proves that the laser treatment induces the formation of magnetite. Besides magnetite, other ferric species form in gypsum containing samples. These species are paramagnetic at RT being their parameters compatible with low-crystallinity or small particle Fe^{3+} oxides [7] and also with ternary Fe-Ca oxides.

X-ray powder diffractograms recorded from GH and GCH samples showed gypsum, bassanite and hematite lines (Fig. 3). A considerably increase of the ratio bassanite/gypsum is noticed for laser-treated samples. This indicates that laser exposure induces a dehydration of gypsum to give the calcium sulphate hemihydrate, bassanite. Incipient presence of magnetite was also detected in the diffractograms recorded from the irradiated samples (Fig. 3).

Reduction of hematite into magnetite was observed after pulsed excimer laser ablation of the surface of hematite pellets [8] and when powder particles

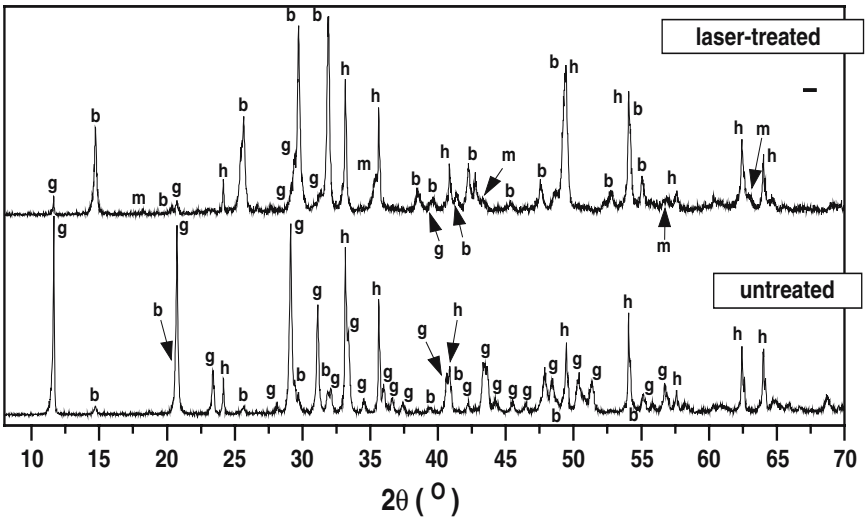

Fig. 3. XRD patterns of the GH-17 sample before (*bottom*) and after (*top*) laser exposure (*g*, gypsum; *b*, bassanite; *h*, hematitie; *m*, magnetite)

of iron oxides were irradiated with a Nd:YAG laser operating at 1064 nm [9]. In our case, no significant differences in the extent of hematite reduction were observed among the samples (see Fig. 1 and Table 2). Thus, gypsum and graphite contents seem to have no influence in the transformation of hematite into magnetite. Further experiments varying laser parameters appear to be necessary to explain mechanisms of laser interaction with the different constituents of the sample. Contrary to the fact generally accepted that the high temperatures reached in laser treatments cause oxidative reactions, Pouli et al. [10] proved that some pigments underwent a laser-induced reduction. According to [10] a shortage of oxygen in the dense plasma generated by laser irradiation could favour the decomposition of irradiated material into their constitutive elements. Thus, oxygen, sulphur and carbon can be released to the atmosphere whereas iron in metallic state would remain on the surface. During the quick cooling down, if there is a lack of sufficient oxygen, this metallic iron could be oxidized giving magnetite instead of hematite, which is the final product of the iron oxidation.

Iron oxide nanoparticles have been prepared by means of laser treatments [11, 12] because the high heating-cooling rates reached in the process favour the precipitation of particles with nanoscale dimensions. In the present case, a more detailed XRD study using standards could be useful to prove that a fraction of the hematite was transformed into finely divided or amorphous iron oxides.

Finally, it is evident that the observed dehydration of gypsum is attributable to the heating conditions of the laser treatment.

4 Conclusions

Nd:YAG (1064 nm, 695 mJ cm^{-2}, 30 pulses s^{-1}) laser irradiation of hematite containing samples induces (i) partial reduction of hematite into magnetite and (ii) formation of ferric species different to the hematite initially present in the samples. Bassanite formed in the irradiated samples at the expense of gypsum proves that laser treatment dehydrates the gypsum contained in model samples.

Acknowledgements

The authors thank Dr. M. T. García González (CCMA, CSIC) for XRD facilities. This work was supported by the EC (project EVK4-CT2000-00029) and the French Ministry of Culture (subvention de recherche chapitre 6698 20, exercise 2001).

References

1. D. Eichert, V. Vergès-Belmin, and O. Khan, J. Cult. Heritage **1**, S37, 2000
2. S. Klein, F. Fekrsanati, J. Hildenhhagen, K. Dickmann, H. Uphoff, Y. Marakis, and V. Zafiropoulos, Appl. Surf. Sci. **171**, 242, 2001
3. A. Aldrovandi, C. Lalli, G. Lanterna, and M. Matteini, J. Cult. Heritage **1**, S55, 2000
4. P. Bromblet, M. Labouré, and G. Orial, J. Cult. Heritage **4**, 17s, 2003
5. V. Vergès-Belmin, and C. Dignard, J. Cult. Heritage **4**, 238s, 2003
6. V. Vergès-Belmin, Atmos. Environ. **28**, 295, 1994
7. E. Murad, and J. H. Johnston, in *Mössbauer Spectroscopy Applied to Inorganic Chemistry*, Edited by G. J. Long, Plenum Press, New York, Vol 2, 507, 1987
8. S. Joshi, and S. B. Ogale, in *Surface Modification Technologies V*, Edited by T. S. Sudarshan and J. F. Braza, The Institute of Materials, London, 423, 1992
9. A. R. da Costa, Scripta Materialia **47**, 327, 2002
10. P. Pouli, D. C. Emmony, C. E. Madden, and I. Sutherland, Appl. Surf. Sci. **173**, 252, 2001
11. L. Xinyong, L. Enhui, Z. Changyan and L. Shuben, J. Mater. Chem. **5**, 1953, 1995
12. S. Martelli, A. Mancini, R. Giorgi, R. Alexandrescu, S. Cojocaru, A. Crunteanu, I. Voicu, M. Balu, and I. Morjan, Appl. Surf. Sci. **154–155**, 353, 2000

Can Laser Microprobe Mass Analysis do any Work in Artwork Conservation?

R. Wurster

Institut für Physik und Meteorologie, Universität Hohenheim, Garbenstr. 30, 70599 Stuttgart, Germany
wurstero@uni-hohenheim.de

Abstract. The benefit of laser microprobe mass analysis as applied both to individual microparticles and extensive particle collections mainly is due to its high sensitivity, speed of analysis and the elemental/chemical information the time-of-flight mass spectra are providing. Though the poor reproducibility of the results is a major drawback in achieving quantitative analyses the method is a proven tool for the characterization and identification of particulate matter usually entailed with the atmospheric environment.

1 Introduction

More than 20 years ago laser microprobe mass analysis (LAMMA) was introduced as an innovative and promising microanalytical technique firstly being applied to thin sections in biological and medical research [1]. Investigation of individual atmospheric airborne particles quickly became another important research area profiting by the unique features of this sensitive and fast analytical tool [2].

As artwork conservation by laser also includes monitoring of environmental pollution future applications of LAMMA will be meaningful.

2 Experimental Methods

LAMMA is based on the laser-induced vaporization/ionisation of a tiny fraction of the specimen. The LAMMA 500 instrument (Leybold-Heraeus, Cologne) and its basic principle of operation are explained in Fig. 1 Typically an amount of 10^{-12} g is consumed when the focussed laser beam (frequency quadrupled Nd:YAG, Q-switched, 10 ns) interacts with the specimen.

The specimen is mounted on a metallic grid (Cu, Ni) that must be covered by a thin supporting foil (pioloform 20 nm) for particle analysis. The grid is fitted to the sample stage that can be x-y-adjusted for aiming at a region of interest. Both imaging of the sample and focussing of the laser to a nearly diffraction limited spot is done by a light microscope objective (Ultrafluar 100, immersion type). The cover glass also works as interface between the evacuated sample chamber and the microprobe forming microscope.

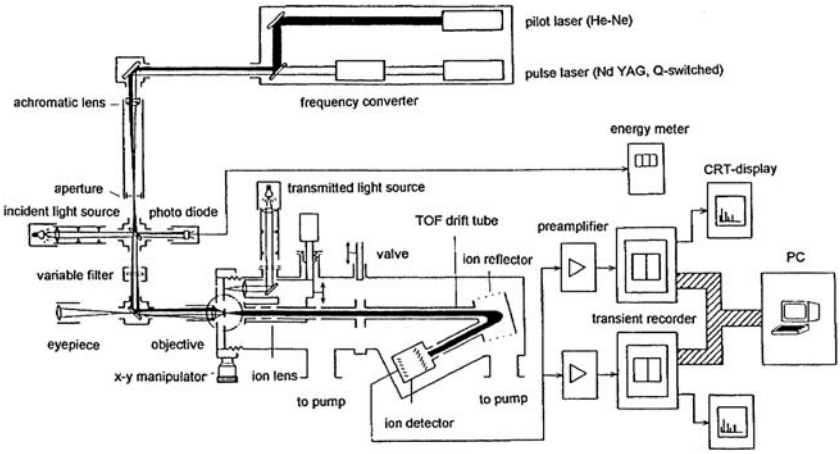

Fig. 1. The LAMMA instrument consists of 3 main parts: A light microscope objective focusses the beam of a frequency-quadrupled pulse of a Nd:YAG laser. The laser-induced ions are analyzed by means of a time-of-flight mass spectrometer

Laser irradiance can be varied between $10^8\,\mathrm{W/cm^2}$ and $10^{12}\,\mathrm{W/cm^2}$ by means of a set of filters and/or defocusing the beam, thus strongly influencing the pattern and information content of the mass spectra and the damage to the sample as well.

Figure 2 shows a few scanning electron micrographs of laser-induced craters and perforations. This reveals related processes as e.g. heating, melting and traces of micro-explosions.

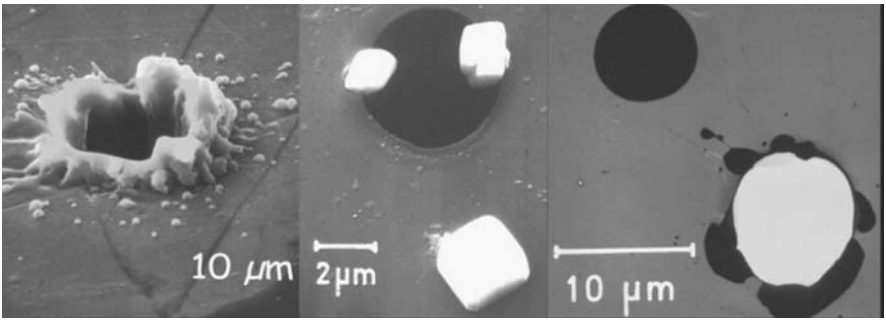

Fig. 2. Laser–target interaction produces craters and perforations at the surface of a bulky sample and in the substrate foil of the particles, respectively. Scanning electron micrographs of these intrinsic damages can help to understand the involved processes

The laser induced and transient microplasma contains neutral and charged elemental and molecular species as shown schematically in Fig. 3 Ions of either positive or negative polarity are accelerated, separated along the tube of a time-of-flight mass spectrometer and eventually detected by means of an open secondary electron multiplier at a moderate mass resolution of $m/\Delta m = 700$.

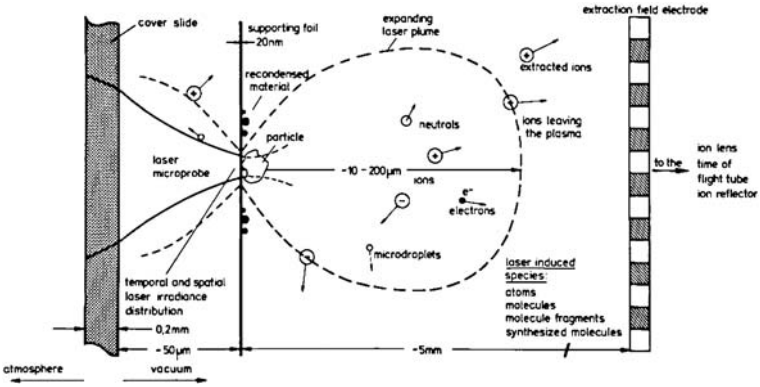

Fig. 3. Laser matter interaction produces elemental and molecular positive and negative ions that are accelerated by an extraction electrode to the entrance aperture of the TOF

In order to reduce particle size effects that may complicate the interpretation of the mass spectra aerodynamically separated size categories of particles usually will be collected and deposited onto copper grids by means of a 5-stage minicascade impactor [3]. A few examples of typical mass spectra are shown in the following section. They illustrate that this methodology is suited to characterize particle sources in terms of elemental/chemical composition.

3 Results and Discussion

Though the interpretation of the mass spectra is difficult LAMMA has been successively used in aerosol research for analyzing both single particles and particle collections. As an example, Fig. 4 shows the TOF mass spectrum of negative ions obtained from an individual aerosol particle. The elemental peaks of F, Cl, Br and J clearly indicate the particle's anthropogenic origin. More representative measurements of particle collections taken near a motorway include the analysis of some thousand particles. In applying multivariate statistical methods to the data set, TOF spectra of both positive and negative ions can be discriminated in terms of similar elemental and molecular mass line patterns that may eventually be assigned to a specific particle source (Fig. 5). All these spectra are showing a more or less prominent peak of Pb^+

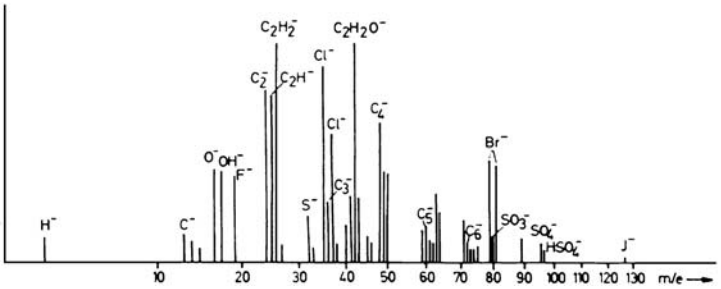

Fig. 4. TOF spectrum of negative ions obtained from a single atmospheric aerosol particle of about 1.4 µm diameter. The elemental peaks of F, Cl, Br and J clearly indicate the particle's anthropogenic origin

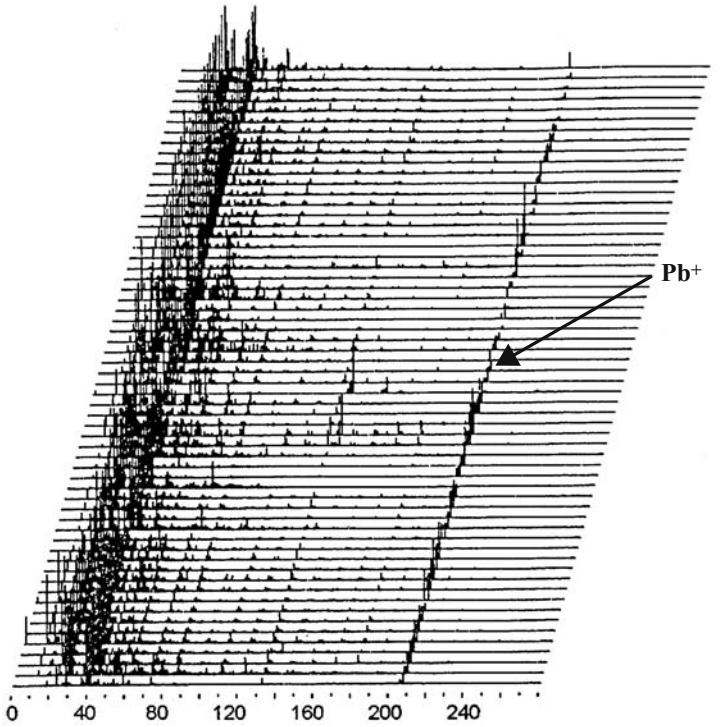

Fig. 5. Calibrated set of TOF spectra of positive ions obtained from particles collected in a distance of 15 m from a motorway. Aerodynamic particle diameter .5 µm, vertical axis: ion signal, arbitrary units. The spectra are showing a more or less prominent peak of Pb+ at mass number 208 (*arrow*) that originates from leaded gasoline

that originates from leaded gasoline. In considering TOF spectra sets of both polarities the chemical interpretation of mass spectra may even become more straightforward.

Soft ionization by laser desorption of nonvolatile and thermally labile substances is among others a useful method in organic mass spectrometry. Figure 6 shows mass spectra obtained from artificial organic microparticles with the cationized parent molecule of sucrose and one of its fragment ions.

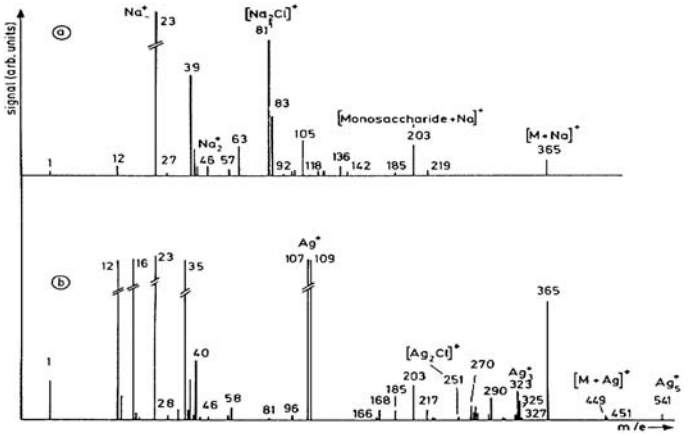

Fig. 6. TOF mass spectra of positive ions obtained from NaCl doped sucrose particles showing the cationized parent molecule peak $[M+Na]^+$. Substrate: pioloform (**a**), Ag (**b**)

4 Conclusions

LAMMA has proven to be a powerful tool in aerosol research. This methodology may also be successfully applied to particulate matter contained in artworks. Artworks are often exposed to rough environment that can cause surface erosion and deposition of extraneous particles. On the other hand cleaning or removal of corrosion layers will always be accompanied by the production of microparticles which can than be analysed with LAMMA.

References

1. R. Wechsung, F. Hillenkamp, R. Kaufmann, R. Nitsche, E. Unsöld, and H. Vogt, LAMMA – A new laser-microprobe-mass-analyzer, Microscopica Acta (Suppl.) 2 (1978) 281–296

2. P. Wieser, R. Wurster, and H. Seiler, Identification of airborne particles by laser induced mass spectroscopy, Atmospheric Environment 14 (1980) 485–494
3. P. Wieser and R. Wurster, Application of laser-microprobe mass analysis to particle collections, in: Physical and chemical characterization of individual airborne particles (K. R. Spurny, ed.), Ellis Horwood Ltd. (1986) 251–270
4. P. Wieser and R. Wurster, Some experiments on laser induced cationization of sucrose, in: Ion Formation from Organic Solids (A. Benninghoven, ed.), Springer Verlag (1983) 235–239

An X-Ray Microprobe for In-Situ Stone and Wood Characterization

P. Lovoi[1] and J.F. Asmus[2]

[1] XOFT Microtube, Inc, 49000 Milmont Dr, Fremont CA 94538 USA
[2] University of California, San Diego, 9500 Gilman Dr., La Jolla, CA 92093-0360, USA
jfasmus@ucsd.edu

Abstract. NonDestructive Testing (NDT) has become an essential ingredient in the conservation of artworks and in the preservation of historic buildings. In many instances it is necessary to characterize the underlying strata of an artistic or historic object in order to plan technical conservation measures, to understand its history, to authenticate it, or to search for hidden features. X-ray and gamma-ray radiography as well as infrared imaging have been ubiquitous in conservation practice for generations. Recent decades have also seen the introduction of ultrasonic imaging, thermovision, x-ray fluorescence, neutron activation analyses, holographic interferometry, isotopic and trace element analyses, the electron microprobe, the laser microprobe, microwave impulse radar, eddy current imaging, and fiber-optic imaging. Unfortunately, for mainstream conservation and preservation some of these technologies are too costly or difficult to be implemented in any general way. In other instances penetration is too superficial or signals from the depth of interest are masked by interferences. Nevertheless, sufficiently important problems have arisen to warrant the utilization of each of the above NDT technologies as well as still others. A new diagnostic device has been introduced into the conservation field. Stone characterization analyses are reported using miniature x-ray devices that can be inserted into cracks and holes in specimens of interest. The family of x-ray tubes employed in these studies range in diameter from 1 to 6 mm. Operating voltages up to 50 kV are available. Electrical power and cooling are delivered through a flexible cable that has a bend diameter of less than 3 cm. Thus, it was possible to insert the x-ray tube into small holes and cracks in marble stones. In this manner radiographs of the outer strata of stones (and embedded metal pins) have been produced without having to transmit through the entire thickness of large blocks. It should also be possible to perform XRF microanalyses within stone in order to monitor changes in composition with depth.

1 Introduction

A family of miniature x-ray sources has been developed that offer novel solutions for a variety of diagnostic needs. These small x-ray sources operate with peak voltages up to 50 kV and anode power dissipations up to 5 Watts. This power dissipation is sufficiently low so as to be able to avoid damage to almost all materials when inserted into small cavities or cracks. The family of miniature x-ray sources ranges in diameter from 1 to 6 mm and length from

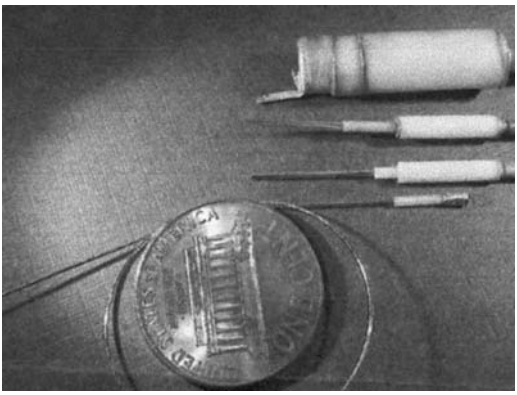

Fig. 1. Fiber-mounted miniature x-ray tubes shown in relation to a small coin

7 to 25 mm. The smallest devices do require cooling when operating at higher power levels.

These devices are mounted on glass fibers and can be configured for specific applications. Figure 1 shows the size of a number of these miniature x-ray sources in relationship to a small coin. This family of x-ray tubes is generally configured to emit radiation uniformly in all directions (Fig. 2). However, one version is also manufactured with a restricted aperture so that diagnostic information is acquired in one direction, only (Fig. 3).

2 Conservation Applications of Miniature X-ray Sources

The Energetic radiation is utilised in numerous ways in conservation of stone and wooden objects. Miniature sources (as described above) open new ways of implementing both diagnostics and treatment.

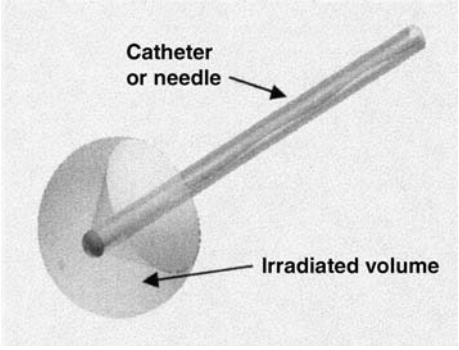

Fig. 2. Isotropic radiation pattern that is produced by a bare x-ray tube

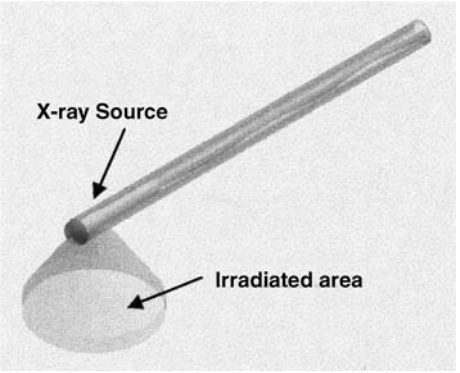

Fig. 3. Miniature source with a restricted radiation field for spatially-resolved diagnostics

Both fungi and insects attack wood [1]. These sources are small enough to be threaded down wormholes and cracks in order to irradiate (and kill) both fungi and insects. Further, local radiation imaging is also possible in order to characterize the deterioration and monitor its progress.

Stone is subject to biological attack as well [2]. As in the case of wooden objects, the insertion of a radiation device into small cracks or holes may afford a means of either treatment or analysis. Stone damage induced by the corrosion of interior metal pins is also a hazard to conservation and preservation. Imaging and detection of hidden pins may be accomplished with a miniature source inserted into cracks without having to perform radiography through the entire thickness of large stones. Both imaging and in-situ XRF are possibilities.

3 Stone Imaging Results

Initial experimental trials were performed by inserting a miniature x-ray tube into a hole in limestone and imaging a nearby iron pin. The hole for the X-ray microtube was parallel to the stone surface and 1cm beneath that surface. X-ray film was placed in contact with the limestone face. A 5 mm steel pin was inserted into another hole (between the microtube and the stone surface). Figure 4 presents a typical radiographic shadow cast by the steel pin. (The low resolution is a consequence of the internal scattering of the very low energy X-ray photons.)

Fig. 4. Radiographic shadow of a steel pin in limestone generated by a miniature X-ray source located in a nearby hole

4 Wormholes in Wood

In preparation for in-situ irradiation of insects in wood it was found empirically that a 1 mm microtube could be threaded successfully into wormholes in a panel painting's wooden support ("Our Lady of Tikvin", 17th C. Serbian). It was determined that the 1mm glass fiber was sufficiently flexible and the wormholes were sufficiently straight so that the microtube could be inserted to a depth of several centimeters. Further, neither the microtube nor the panel overheated during protracted operation.

The next phase or this research effort will involve the development of a real-time diagnostic system to monitor the biological viability of insects as a function of radiation dose. It is anticipated that fMRI will fulfill this function.

5 Conclusions

A new miniature X-ray source (fiber microtube) has been considered for use in art conservation. Initial applications of in-situ radiography, XRF, and sterilization have been proposed and considered. As radiographic detection of foreign objects embedded in stone has been successful, the other applications are promising.

References

1. A. Stamm, Wood deterioration and its prevention, Conservation of Stone and Wooden Objects 2 (1970) 1–12
2. S. Richardson, Biological deterioration of ancient buildings, Conservation of Stone and Wooden Objects 2 (1970) 63–68

Non-Invasive Monitoring of Water Intake in Limestones

P. Prado[1] and J.F. Asmus[2]

[1] Quantum Magnetics, 7740 Kenmar Court, San Diego, CA 92121, USA
pprado@qm.com
[2] University of California, San Diego, 9500 Gilman Dr., La Jolla, CA 92093-0360, USA
jfasmus@ucsd.edu

Abstract. Water content profiles were rendered non-invasively in two limestone samples from the US Capitol Building. The measurements were performed with a recently developed portable magnetic resonance instrument producing depth resolution automatically. Two tests were performed, i.e. water intake monitoring with a one minute time resolution and depth profiling of water content with sub-millimeter spatial resolution. For these porous stones, it was shown that the water intake close to the surface of the stone progresses three times faster than 5 mm deeper. The effect of porous media waterproofing was observed and quantified monitoring non-invasively the water content behind treated and clear areas of the limestone cornice.

1 Introduction

Dedicated mobile magnetic resonance (MR) sensors are used to measure material properties non-invasively from a near surface region [1–4]. The magnet and radio-frequency technology is based on the so-called inside-out MR [5], where material inspection is non-contact and has no restriction on the size of the sampled specimen. The MR protocol is similar to stray field imaging [6] in that the measurement is performed outside the magnet, in the presence of moderate to large magnetic field inhomogeneities.

MR is a powerful tool to determine the moisture content in porous media. Several non-destructive applications such as moisture content of wall masonry, plaster, woods and frescos require depth resolution during the sensing procedure. The main issue to achieve spatial resolution using a single-sided MR sensor is to configure properly the magnet array in order to produce tailored magnetic fields away from the probe head. This challenge originates in the inherent field inhomogeneities resulting from generating static magnetic fields outside the sensor. The present instrument accomplished spatial resolution automatically. Layers parallel to the sensor head are selected to render depth profile of MR signals.

2 Experimental Setup

The current device utilizes automatic frequency shifting capabilities in order to render depth profiles of MR signal (1D MRI). The tailored static field distribution is produced by an array of high-grade permanent magnet blocks. A range of 0–20 mm is automatically switched.

3 Water Intake Results

The water intake was followed using the single-sided MR sensor. A limestone sample oven dried at 60 °C for 24 hours and then placed above the sensor head as shown in Fig. 1. A flat face of the stone was exposed to a water bath with a level kept at about 2 mm. Two spacers lifted the sample 1 mm from the bottom of the tray, in order to have continuous water supply. The MR signal was collected with a 1-min period from 5 and 10 mm above the stone surface. The signal was collected from 5 and 10 mm alternatively, with a 1-min signal averaging per scan (Fig. 2). No signal was observed from the water bath bellow the sensitive volume. About 30 ml of water was gradually added to the bath in order to maintain a constant water level.

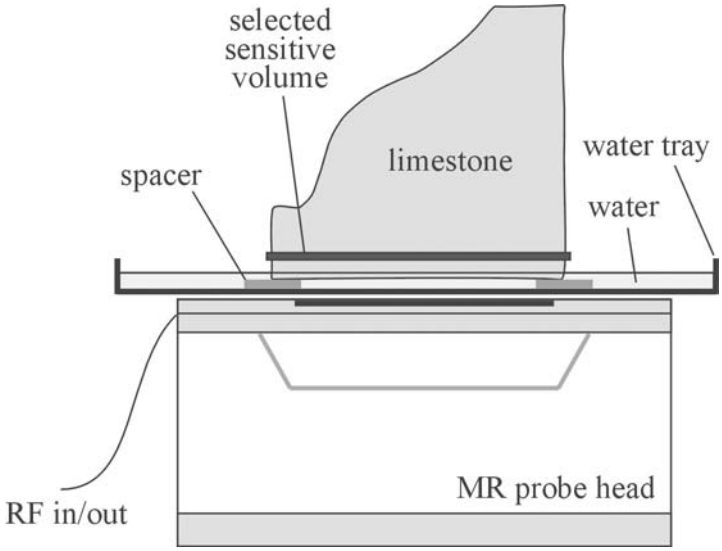

Fig. 1. Sketch for the setup of the water intake experiment. The limestone was placed over the sensor head with a small gap to allow for water intake. The MR signal was collected from 5 and 10 mm above the sensor. The probe head base is 13 cm × 13 cm

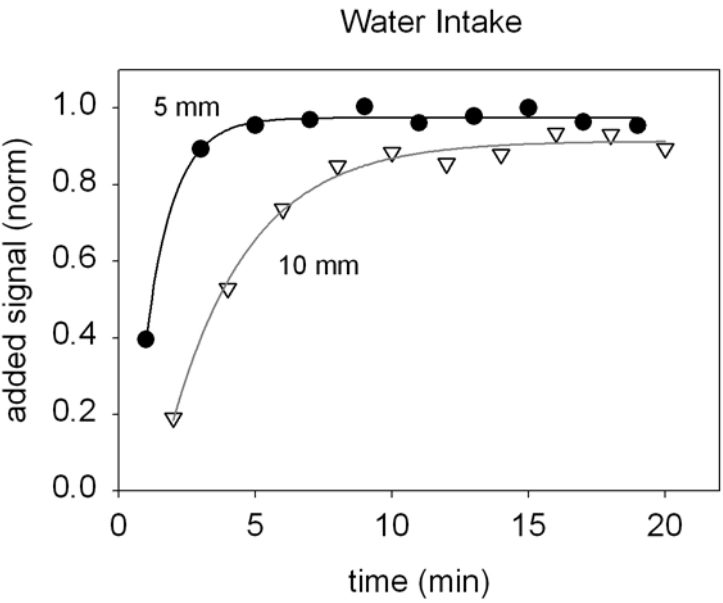

Fig. 2. MR signal amplitude for 5 mm and 10 mm above the probe head

The water intake is quantified in Fig. 2. The solid lines are single exponential fits to the data (Equation 1) where t is the elapsed time

$$S = S_o + a(1 - e^{-bt}) \tag{1}$$

and S is the signal intensity. The parameters from the fit are used to compute the values presented in Table 1. The onset time is calculated by the initial time of the curve.

Table 1. Water intake parameters obtained from a least square fit to the coefficients for data presented in Fig. 2

Parameter	5 mm depth	10 mm depth
Onset time	1.0 min	1.4 min
Intake time	0.3	1.0
Maximum level	100%	94%

4 Water Content Profile

A larger limestone sample was used to compare the water intake through a non-treated surface and a small area treated with water proofing. Figure 3

shows the area where the sealant was applied. The treated face was immersed in water for 5 min (Fig. 3A) and then the limestone was placed above the MR sensor (Fig. 3B). The thin epoxy layer stopped lateral adsorption of water. The excess water was removed with a dry cloth before starting data collection.

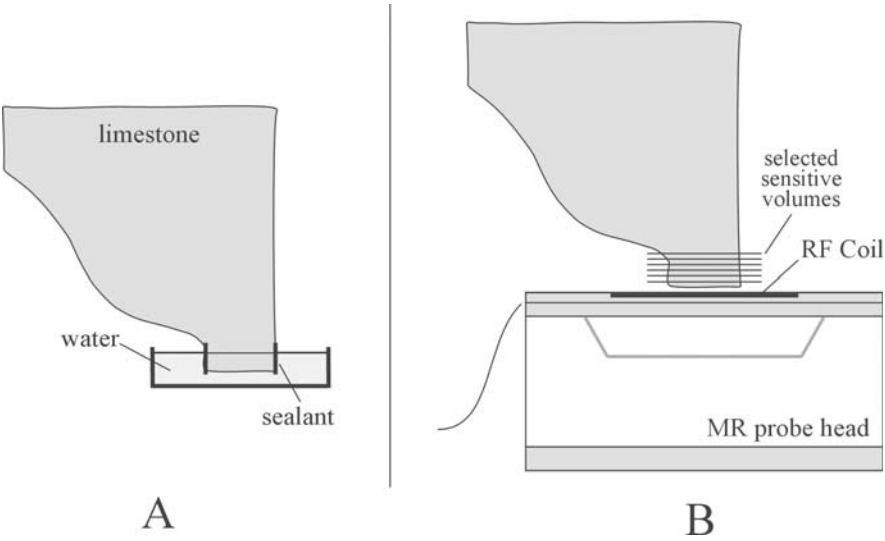

Fig. 3. Total experimental setup for the water profile measurement. The limestone was immerse in water for 5 min (*left*) and then the treated face was positioned flat over the MR sensor head (*right*)

The data acquisition started about 5 min after the sample was taken out of the bath. As seeing in Fig. 2, the water is effectively uniformly distributed after that period. The data was rendered for the area without treatment and then the stone was repositioned to the water proofing area. The profiles were collected with a total time of 7 min per position. The signal amplitude was normalized by the profile of a uniform sample and the results are plotted in. The signal intensity from the first millimeter is low due to surface irregularities and therefore was discarded. The effect of water proofing is clearly quantified by the results presented in Fig. 4. The low water content over the treated area can be assigned to the equilibrium moisture content (this sample was not oven dried prior to the test). The uniformity of the profile is due to the elapsed time from immersing the stone in water to data acquisition.

5 Conclusions

A new magnetic resonance sensor was used to follow the water intake in porous stone. The water content is measured at different depths within the

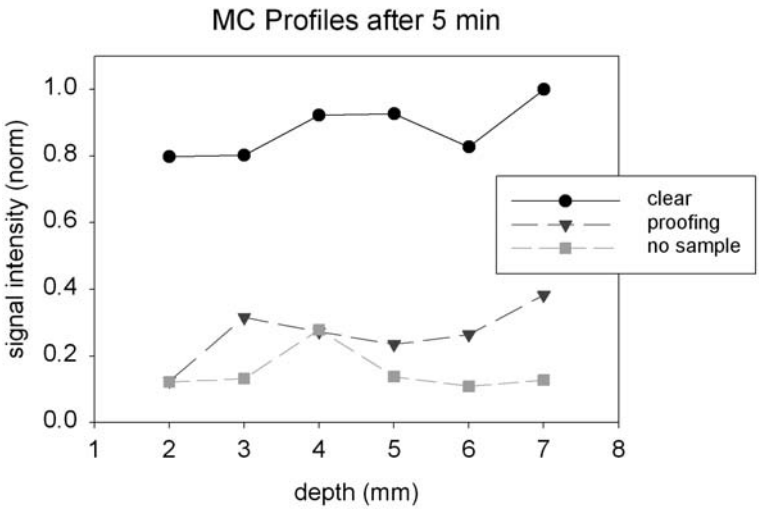

Fig. 4. Intensity of the signal for the first 7 mm in depth from the open surface. The circles represent high water content from the non-treated area, the triangles represent the water content above the water proofing area, and the squares are the signal intensities for the empty coil

stone in a non-invasive manner. Two limestone specimens from a cornice of the U.S. Capitol Building were used for the measurements. For these particular stones, the water intake close (5 mm) to the surface exposed to water, proceeds three times faster than the water intake after conventional water proofing. By monitoring the water content at various depths inside the stone, it was shown that variations in water intake can be monitored effectively with this new technology.

References

1. G. A. Matzkanin in *Nondestructive Characterization of Materials* Edited by P. Höller, G. Dobmann, C.O. Ruud, and R. E. Green, Springer, Berlin, 1989
2. W. L. Rollwitz in *Using Radio-frequency Spectroscopy in Agricultural Appl.*, Agricultural Engineering **66**, 12–14, 1985
3. B. Blümich, P. Blümler, G. Eidmann, A. Guthausen, R. Haken, U. Schmitz, K. Saito, and G. Zimmer in *The NMR-mouse: Construction, Excitation, and Applications*. Magnetic Resonance Imaging, **16**, 479, 1998
4. P. J. Prado in *NMR Hand-Held Moisture Sensor*. Magn. Reson. Imaging **19**, 506–8, 2001
5. R. L. Kleinberg in *Well Logging*, Edited by D. M. Grant and R. K. Harris, Encyclopedia of NMR, Wiley, New York, 4960–9, 1996
6. P. J. MacDonald in *Stray Field Magnetic Resonance Imaging*, Progress in NMR **30**, 69–99, 1997

Nd, Er and Excimer Laser Sources: Laboratory Evaluation of Cleaning Efficacy and of Interaction with Substrate

A. Sansonetti[1], M. Realini[1], L. Toniolo[1], and G. Valentini[2]

[1] ICVBC CNR Sezione "Gino Bozza", piazza Leonardo da Vinci 32, 20133 Milan, Italy
antonio.sansonetti@polimi.it
[2] Dipartimento di Fisica, Politecnico di Milano, piazza Leonardo da Vinci 32, 20133 Milan, Italy
gianluca.valentini@polimi.it

Abstract. Three different laser sources (Nd:YAG, Er:YAG and XeCl Excimer) have been tested on two different stone materials important as concern historical use and diffusion as Carrara marble and Verona red limestone. Damage threshold and soiling removal efficacy have been evaluated using mycroscopical observations, chromatic measurements and weight loss. The obtained results encourage the research of alternative sources for stone cleaning with respect to the most used at the moment, namely Nd:YAG. In fact both Nd:YAG and Er:YAG lasers have provided good results even if delicate materials such as Verona red limestone must be cleaned with caution. As a matter of fact, Er:YAG source in particular represents an innovative cleaning method, even if needing further experimentation.

1 Introduction

Different laser sources were studied in order to define the harmfulness threshold with respect to the substrate and the fluence values useful for safe cleaning. The laboratory experimental set up allowed a very precise control of each laser parameter (fluence [J/cm^2], repetition rate [pulses/sec]). Moreover, the laser beam was focused in spots having a precise size and delivered to the sample in a regular pattern through a X-Y galvanometric scanner. Adiacent spots had a partial superposition. In such a way, the fluence onto the sample was almost constant, since beam inhomogeneities averaged out. In some cases the scanning of the laser beam over the sample was repeated twice or more times. The repetition density was defined as the number of full scans delivered to the sample. The precise control of fluence and repetition density is a very significant feature, because it is not available in field.

The research was carried out on two litho types largely employed in cultural Heritage: Carrara marble and Verona red limestone. Carrara marble was chosen because of its white colour: literature and site experience refer about a possible yellowing occurring on white surfaces treated with Nd:YAG source. Verona red limestone was chosen because it contains iron compounds which seem to be very sensible to laser radiation.

Laser harmfulness was evaluated on unsoiled specimen (Table 1) by optical microscope observations, by measurement of surface colour changes (CIE Lab system) and by weight loss.

Table 1. Used fluences and repetition densities on specimen of Carrara marble and Verona red limestone

Carrara	Unsoiled Fluence (repetitions density)				Soiled Fluence (repetitions density)			
Nd:YAG	2.5 (1–2)	4.0 (1–2)	5.5 (1–2)	7.0 (1–2)	2.5 (5)	2.0 (5)	2.5 (5)	5.5 (2)
Er:YAG	2.0 (1)		3.0 (1)		2.0 (6)		3.0 (3)	
XeCl	0.8 (1)		1.2 (1–2)		1.2 (20)			

Verona	Unsoiled Fluence (repetitions density)				Soiled Fluence (repetitions density)			
Nd:YAG	1.0 (1–2)	1.2 (1–2)	1.5 (1–2)	2.0 (1–2)	1.25 (10)	1.50 (10)	1.75 (10)	2.0 (10)
Er:YAG	2.0 (1)		3.0 (1)		2.0 (7)		3.0 (5)	
XeCl	0.20 (1)	0.40 (1)	0.80 (1)	1.20 (1)	1.20 (20)			

Laser cleaning efficacy was evaluated on artificially soiled specimen (Table 1) with the aid of optical microscope observations. The artificial soiling layer was realised with a mixture of lime, water, crushed black crusts and bone black pigment. The artificial soiling was deposited on to specimen surfaces by a brush. A compositional similarity with real "black crusts" and a good adhesion between soiling layer and stone were achieved.

2 Results and Discussion

2.1 Nd:YAG Source

For what concerns threshold values on Carrara Marble, the results indicate that no morphological variations of some significance are detectable below $4\,J/cm^2$ fluence. At a fluence of $5.5\,J/cm^2$ some detachments of micro fragments are observed (Figs. 1 and 2) and the weight variation is in good agreement with these results. As regarding chromatic variation (Fig. 5) an increase in lightness is recorded, due to the formation of micro cavities responsible for a light scattering. Verona Red limestone is characterised by a less homogeneous structure, so the laser interaction is locally different. However a diffuse damage is produced at $1.5\,J/cm^2$ fluence with micro abrasions especially located on the nodules borders which are darker in colour. Chromatic variations confirms a damage threshold between 1.5 and $2\,J/cm^2$ (Fig. 6).

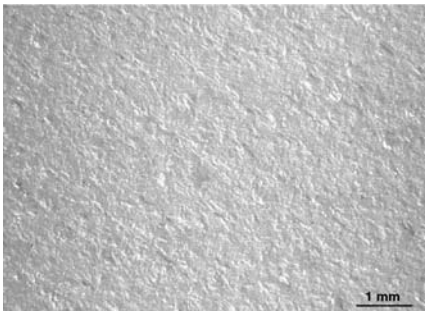

Fig. 1. Carrara Marble before laser Interaction

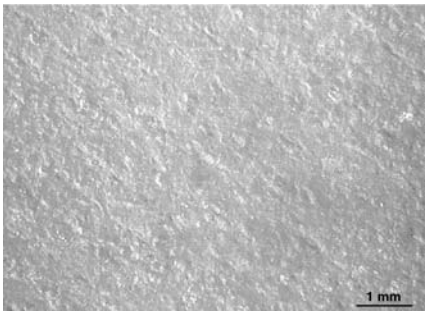

Fig. 2. Laser Nd:YAG Interaction 5.5 J/cm^2

Cleaning tests with the Nd:YAG source have shown good efficacy at fluences of 1.5 J/cm^2. This value is lower with respect to the damage threshold set for Carrara marble but it coincides with the threshold set for red Verona Limestone. This implies that a complete removal of soiling by this material could produce damage to the substrate.

2.2 Er:YAG Source

With fluences below 3 J/cm^2 no damage has been detected on Carrara Marble. As to Verona limestone, a strong difference is evident between dark and light red areas: the former are abraded at fluences of 2 J/cm^2, while the latter seem to remain undamaged at 3 J/cm^2 (Figs. 3 and 4). Chromatic variations, are of lesser importance with respect to what observed for the Nd:YAG source. Erbium laser is successful in removing soiling at 2 J/cm^2, but this latter is the damage threshold of darker areas.

2.3 Excimer Source

Carrara Marble is damaged at fluences over 1.2 J/cm^2; in correspondence to this fluence a loss of brightness is recorded.

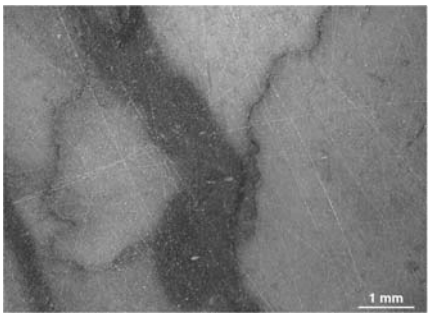

Fig. 3. Red Verona Limestone before laser Interaction

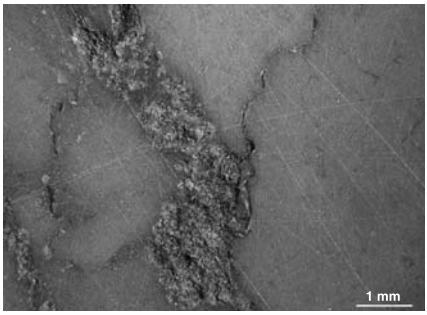

Fig. 4. Laser Er:YAG Interaction 3 J/cm^2

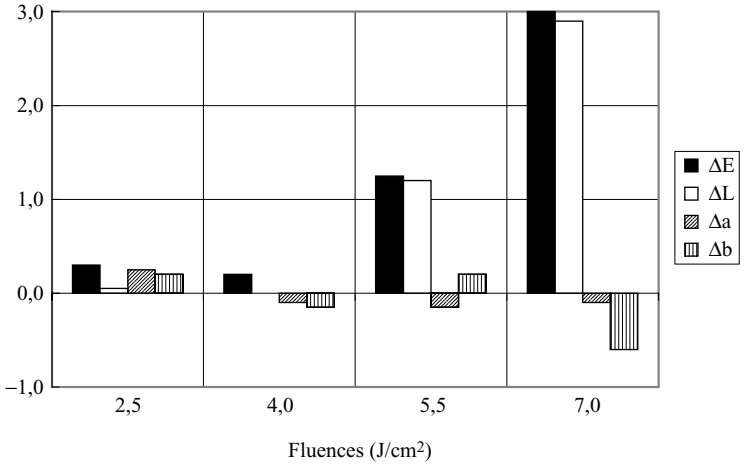

Fig. 5. Nd:YAG. Colour change on Carrara marble

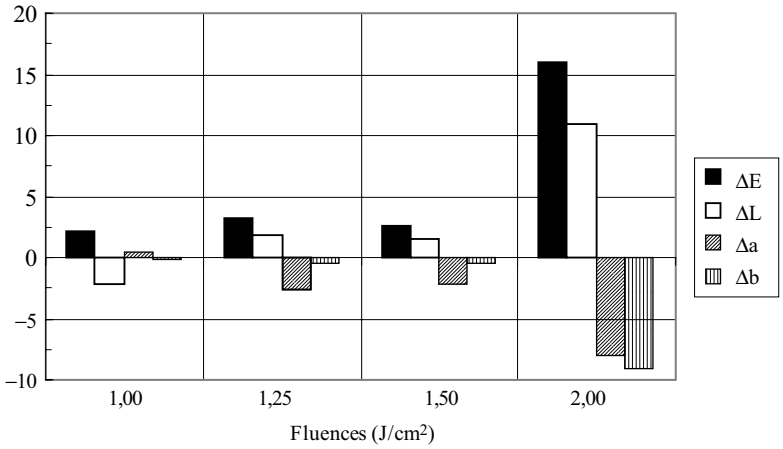

Fig. 6. Nd:YAG. Colour change on Verona red limestone

As to Verona red limestone, fluences higher than $0.4\,J/cm^2$ produced uniformly distributed damages, which are confirmed also by chromatic characterisation and by measurements of weight loss. Moreover this kind of source has showed a complete lack of efficacy with respect to removal of thick soiling.

3 Conclusions

Interaction laser/Stone/soiling is extremely complex: it involves a high number of parameters as characteristics of the system soiling/stone, laser pulse duration, used wavelenghts and repetition frequency. Anyway it is possible to carry out useful surveys to define potentialities of laser sources to remove soiling from stones.

Nd:YAG

Damage threshold: As regard Carrara Marble all the obtained results agree to individuate the fluence of $4\,J/cm^2$ the threshold under which there are not neither morphological nor color variations. For fluences higher then $5.5\,J/cm^2$ microscopical detachment can be achieved.

Verona red limestone is less homogeneous hence laser intaraction is different area by area. A damage diffused over all the surface is produced at $1.5\,J/cm^2$. Below this value light abrasions have been evidenced in correspondance to the dark borders of calcareous nodules.

Cleaning tests: Nd source has shown a good cleaning efficacy for fluences of $1.5\,J/cm^2$. This value is below the damage threshold of Carrara marble but it corresponds with the one of Red Verona Limestone, this situation implies that soiling could be removed only producing a substrate attack.

Er:YAG

Damage threshold: analysis agree in remarking that no damages are evidenced till fluences of $3\,J/cm^2$on Carrara Marble. On Verona limestone the laser interaction is strongly interactive with darker areas where morphological analysis evidences an etching on the dark nodules borders. On the contrary lighter areas do not suffer either morphological or colour variations till $3\,J/cm^2$.

Cleaning tests: Erbium laser shows a good cleaning efficacy at $2\,J/cm^2$, but at this fluence the laser interact with the dark areas.

Excimer Laser

Damage threshold: Carrara Marble shows a damage threshold higher than $1.2\,J/cm^2$ .In correspondence of this fluence only a light decrease of brightness is revealed. As regards Verona limestone a general alteration evenly sprayed all over the surface is revealed at fluences higher than $0.4\,J/cm^2$. Colorimetric analysis confirm these results.

Cleaning tests: Excimer source has shown no efficacy in thick soiling removing. May be that the removing of thinner soiling layer could be more effective.

References

1. G. Alessandrini, A. Sansonetti, A. Pasetti, "The cleaning of stone surfaces: comparison between laser and traditional methods. Evaluation of the harmfulness" in *Proceedings of 4*th *International Symposium on the Conservation of Monuments in the Mediterranean*, vol. 3, 19–30, 1997
2. A. Sansonetti and A. Pasetti, "Comparison between cleaning procedures with laser and other methods. Some applications on monuments in Italy" in *Proceedings of 4*th *International Symposium on the Conservation of Monuments in the Mediterranean*, vol. 3, 345–354, 1997
3. S. Siano, F. Fabiani, R. Pini, R. Salimbeni, M. Giamello, G. Sabatini, "Determination of damage threshold to prevent side effects in laser cleaning of pliocene sandstone of Siena" in *Journal of Cultural Heritage* 1, 47–53, 2000
4. M. Labouré, P. Bromblet, G. Orial, G. Wiedemann, C. Simon-Boisson, "Assessment of laser cleaning rate on limestones and sandstones" in *Journal of Cultural Heritage* 1, 21–27, 2000
5. A. Aldrovandi, C. Lalli, G. Lanterna, M. Matteini, "Laser Cleaning: a study on greyish alteration induced on non-patinated marbles" in *Journal of Cultural Heritage* 1, 55–60, 2000

Part VIII

Working Groups and Networks

Euregio-Center of Expertise for Art Conservation Technology

G. von Bally[1], K. Dickmann[2], and D. Schipper[3]

[1] Laboratory of Biophysics (LfB), University of Münster, Germany
lbiophys@uni-muenster.de
[2] Lasercenter FH Münster (LFM), University of Applied Sciences Münster, Germany
[3] Art Innovation, Hengelo, The Netherlands

Abstract. The Euregio-Center of Expertise for Art Conservation Technology (ECE:ACT) is introduced. The participating partners as well as the scientific methods and technologies they offer in the field of laser cleaning and related diagnostic tasks are presented.

1 Introduction

The Euregio-Center of Expertise for Art Conservation Technology (ECE: ACT) funded by the European Community within the frame of the EUREGIOprogram INTERREG III is a network of scientific and commercial institutions which aims to deploy innovative technologies for the use of art analysis, presentation and restoration. This will be achieved by knowledge transfer to restorers and by allocation of new techniques in art preservation. In this contribution the present project partners, the Laboratory of Biophysics of the University of Münster, Germany, the Lasercenter (LFM) of the University of Applied Sciences Münster, Germany and the company Art Innovation from Hengelo, the Netherlands, as well as the technologies which they offer for restorers and other groups working in the field of cultural heritage will be introduced.

2 3-D Documentation and Analysis Methods at the Laboratory of Biophysics of the University of Muenster

One of the scientific methods offered by the Laboratory of Biophysics of the University of Münster, Germany, is the recording of high resolution holograms for analysis and archiving of art and cultural objects [1]. This technology allows to achieve high resolution three dimensional information of very rare or fragile originals in situ. Another focus of interest of this group is optical profilometry for three dimensional digital acquisition and analysis of objects [2, 3]. Here, a pattern of bright and dark fringes is projected onto the object

of interest. This pattern is distorted according to the structure of the object's surface and is observed by a camera. At a given geometry of the camera and the illumination every point of the surface can be calculated as a distinct value. These values contain the 3-dimensional information of the observed object which can be virtually reconstructed with a computer.

The basis of the system for 3D coordinate measurements is a topometric sensor head consisting of two CCD cameras and a fringe projector fixed on an adjustable rail (Fig. 4). During the measuring process a sequence of four phase shifted quasi-sinusoidal fringe patterns is projected onto the object and registered as stereo images by the CCD cameras. After calculating the phase distribution, the stereoscopic images are evaluated by photogrammetric techniques and a 3D coordinate is calculated for each valid pixel. The achievable measurement accuracy depends on the triangulation angle (angle between the cameras), the image field size, as well as on the number of camera pixels. With a triangulation angle of 40 degrees and an image diagonal of approximately 20 cm, for example, the height resolution is situated at $<50\,\mu$m, the lateral at approx. $200\,\mu$m.

With this computer controlled setup, data from different viewpoints can be acquired, integrated and processed automatically. Using the obtained coordinate points (*point cloud*) the object surface is reconstructed by triangulation, i.e. by covering it with a grid of triangles. As the investigated objects are quite complex, an approach is used which does not make special assumptions about the surface structure and iteratively connects neighbouring points, only controlled by preset angular and distance constraints. It allows automatic processing - including the computation of range images - of large numbers of samples. As examples the rendered point clouds of a cuneiform tablet (Fig. 1–3) and of a madonna head from the workshop of the handcraft academy "Schloß Raesfeld", Germany, (Fig. 5) are displayed.

3 Laser Cleaning with Nd:YAG Lasers at the Laser Center FH Münster

As a co-operation partner of the ECE:ACT project, the Lasercenter (LFM) of the University of Applied Sciences Münster, Germany, is responsible for laser cleaning of various artworks with Nd:YAG-lasers.

For research work as well as service for restorers and museums located in the cross boarder region of Muenster (D) and Twente (NL) a novel Nd:YAG-Q-switch laser with frequency multiplying $(\omega, 2\omega, 3\omega, 4\omega)$ is available. It is the purpose of LFM within this project to demonstrate the potential of laser cleaning to interested restorers. The service is addressed to conservators from restoration shops and museums and also covers consulting of industrial companies dealing with laser cleaning equipment. As an example of our co-operation Fig. 6 shows a result of cleaning investigations on a painting with aged varnish.

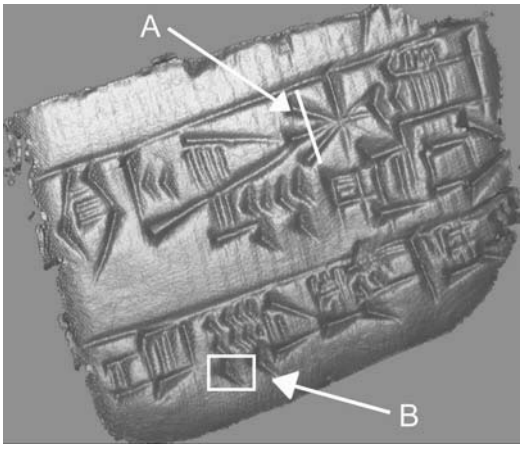

Fig. 1. Virtually reconstructed 3-dimensional surface of a cuneiform writing obtained by optical profilometry (resolution: 0.1 mm)

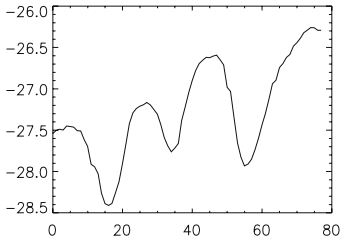

Fig. 2. Surface profile at position A

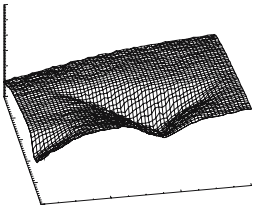

Fig. 3. Surface detail at position B

The painting "Rheinische Landschaft" (Germany, appr. 1870) was covered by brownish varnish and was partially cleaned at 532 nm wavelength of a Nd:YAG Laser (E_p = 400 mJ). The processing time for the exposed area (s. Fig. 6) was 5 min. Further applications cover the range of artworks from stone via textiles to iron. Figure 7 shows a part of stucco (appr. 1890) being cleaned with Nd:YAG laser by order of a local restorer.

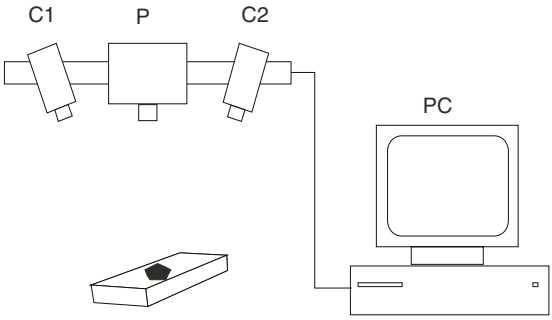

Fig. 4. Experimental setup for 360 degree 3D data acpuisition P: fringe projector, C1, C2: CCD-cameras, Ob: Object, PC: personal computer

Fig. 5. Point cloud of a head of a madonna sculpture

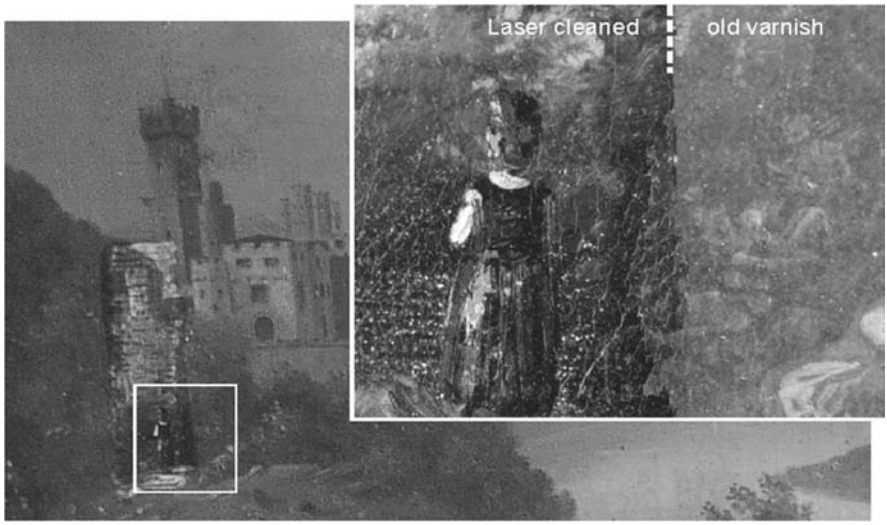

Fig. 6. Painting "Rheinische Landschaft" (Germany, appr. 1870) with brownish varnish layer due to aging. Test arrays show the suitability of 2ω-Nd:YAG laser radiation (532 nm)

Fig. 7. Stucco from a chimney (appr. 1890) cleaned at 1064 nm (*left part*)

Beside pure service LFM also develops new laser cleaning procedures for specific artwork objects (e.g. in combination with conventional cleaning methods).

Furthermore scientists at LFM pay special attention on possible side effects on the original artwork surface affected by laser irradiation. As one example, our investigations concerning the colour change of sensitive historical pigments under laser irradiation (see Fig. 8) shall be mentioned [4].

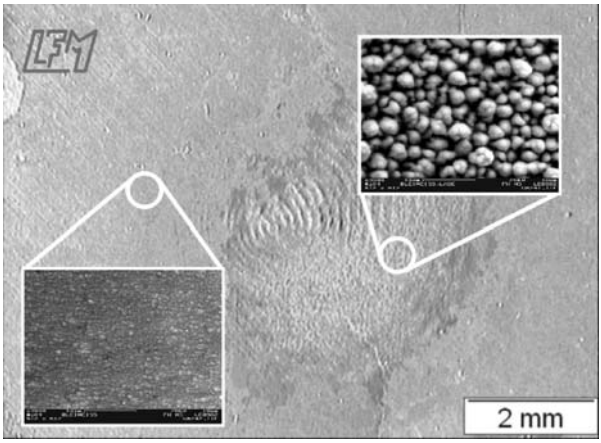

Fig. 8. Laser irradiation(1064 nm; 145 mJ/cm^2) of historical pigment area "lead white". *Left*: unaffected pigment area *Right*: laser irradiated pigment area [$2PbCO_3 \cdot Pb(OH)_2 \overset{\text{Laser}}{\rightarrow} Pb + Pb0 + Pb0_2 + H_2O + 2CO_2$]

During an extensive study based on more than 15 historical pigments it has turned out that most of the pigments are very sensitive to laser radiation within the investigated wavelength range 266 nm – 1064 nm. Remaining colour changes have been observed at low fluence <100 mJ/cm^2 [5].

In order to investigate the behaviour of various artwork surfaces during laser cleaning, at LFM there is a versatile analysis technique available (e.g. SEM, AFM, STM, EDX, XRD, DTA). For example, we have used high speed camera technique in order to study the ablation mechanism on various artworks. Fig. 9 reveals the removal process during laser irradiation of encrusted marble. As can be seen due to laser induced shock waves the encrustation is powdered into micro particles followed by an ejection supported by the plasma. This kind of investigation is useful in order to match optimal processing parameters with lowest side effects onto the artwork.

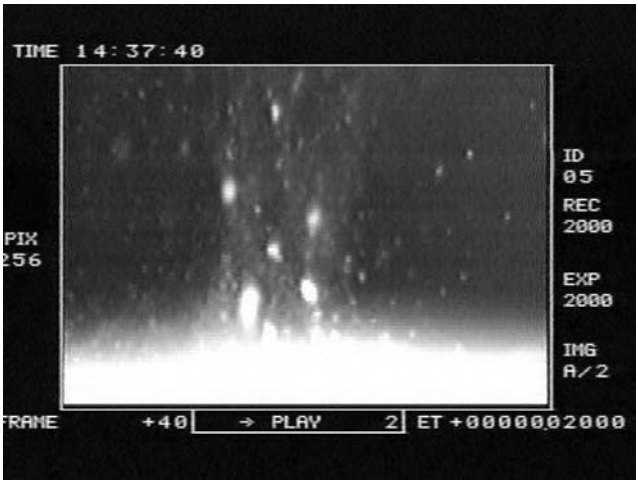

Fig. 9. Plasma formation and ejected micro particles during laser irradiation of encrusted marble (the sample is laser irradiated from the top)

A common problem of laser cleaning of artworks in many cases is the effect of "overcleaning". To avoid this, several techniques, mainly spectroscopy (LIBS), have shown their capability [6]. Within the ECE:ACT project LFM is also responsible for further development of online monitoring technique with specific regard to practical application in restoration [7].

4 UV Laser Cleaning Tools for Paintings at Art Innovation

A further co-operation partner of ECE:ACT, Art Innovation from Hengelo, the Netherlands, develops laser cleaning tools for art restoration. Evaluation of laser cleaning during the past three years has shown that it can be an indispensable and innovative tool for the treatment of complex, delicate and

time-consuming conservation cases. Fundamental research has helped to define optimal laser cleaning parameters for common conservation problems, which cover a wide range of artwork materials including paper, paintings, metals and stone. Art Innovation has developed a UV laser workstation for cleaning of painted surfaces (Fig. 10). This workstation consists of a KrF excimer laser and a motorized "optical arm' to direct the laser beam accurately to the painting surface.

In Fig. 11 the portrait of Van Hogendorp by J. H. Neuman (oil painting on canvas, 1864, $111 \times 95.5\,\mathrm{cm}^2$) covered with yellowed varnish is shown. An old cut in the canvas near the right hand was fixed from the backside with linen and wax during a previous restoration. In front, the cut was amply filled and retouched. The paint in the retouch (near the cut) was superficially burnt due to excessive heating of the wax.

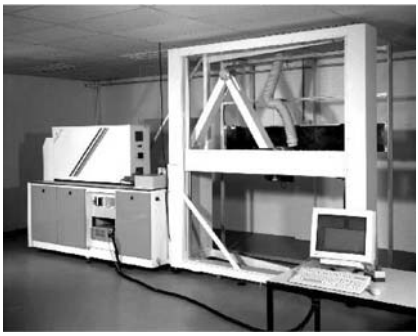

Fig. 10. Laser cleaning workstation at Art Innovation

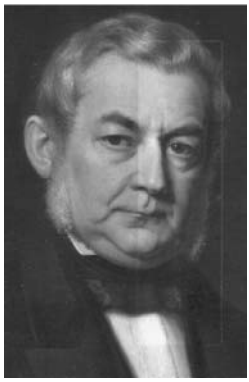

Fig. 11. Portrait of Van Hogendorp

The use of solvents for the removal of the yellowed varnish or retouches was undesirable, since the chemicals would penetrate deeply into the dried up paint layers. Prior to relining of the painting, the thick fillings and burnt paint needed to be removed. Using the laser workstation with a narrowly focused beam (reduced to a $1.3 \times 5\,\mathrm{mm}^2$ spot), the top layers of the burnt retouch and filling were gradually removed. The laser beam was scanned over the surface, following the shape of the cut, with an energy fluence of $0.43\,\mathrm{J/cm}^2$, using a total of 8 pulses with 80% overlap over the whole length of the cut.

After 8 pulses, the remaining paint in the retouch was easily removed with a brush. With a total of 30 laser pulses, 80% overlap, all the paint from the retouch was removed. The charred top layer of the burnt paint is removed, uncovering undamaged pigments, which could be secured in the relining process. Although in removing the burnt paint, the paint layers were irradiated directly by the laser light, no discoloration or alteration was visible in the original flesh tones and black parts. The lead white used in the retouch of the sleeve turned grey, but this was easily be regenerated.

The process of cleaning can be evaluated by fluorescence images of cross-sections of the painting (Fig. 12). In fluorescence mode, it is clearly visible that the varnish layer, appearing light grey on the image of the untreated sample (top), has been thinned in the treated sample, while a very thin layer of varnish remains.

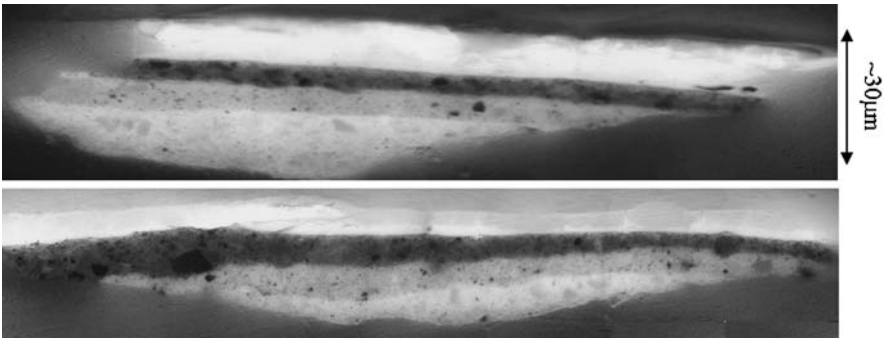

Fig. 12. Control of the thinning of a varnish on fluorescence images of cross-sections before and after laser cleaning of a painting

In conclusion, it can be stated that the Euregio-Center of Expertise for Art Conservation Technology (ECE:ACT) offers a broad range of innovative technologies for the use of art analysis and restoration. The most important task in future will be to transfer this knowledge to restorers to the benefit of preservation of our cultural heritage.

References

1. F. Dreesen, H. Delere, and G. von Bally, in *Optics Within Life Sciences (OWLS V): Optical Technologies in the Humanities*, Edited by C. Fotakis, T. Papazoglou, and C. Kalpouzos, 349, 2000
2. D. Dirksen, Y. Kozlov, and G. von Bally, in Optics Within Life Sciences (OWLS IV): Optical Technologies in the Humanities, Edited by D. Dirksen, and G. von Bally, 257, 1997
3. D. Dirksen, G. von Bally, and F. Bollmann, in Optics Within Life Sciences (OWLS V): Biomedicine and Culture in the Era of Modern Optics and Lasers, Edited by C. Fotakis, T. Papazoglou, and C. Kalpouzos, 147, 2000
4. M. Chappé, J. Hildenhagen, K. Dickmann, and M. Bredol, in Restauro 1, 27, 2003
5. M. Chappé, J. Hildenhagen, K. Dickmann, and M. Bredol, in Journal of Cultural Heritage 4, 264, 2003
6. S. Klein, J. Hildenhagen, K. Dickmann, T. Stratoudaki, and V. Zafiropulos, in Journal of Cultural Heritage 1, 287, 2000
7. J. Hildenhagen, and K. Dickmann, in Journal of Cultural Heritage 4 , 343, 2003

COST G7 Action Creates a Durable Instrument for Advanced Research Implementation in Artwork Conservation by Laser

R. Radvan

National Institute of Research and Development for Optoelectronics – Centre for Restoration by Optoelectronical Techniques, Bucharest – Romania, 1 Atomistilor Str., Magurele-Bucharest, Romania MG 5,
rradvan@inoe.inoe.ro

Abstract. The paper presents the new designed instrument for advanced research implementation in artwork conservation mainly by laser. The idea of this instrument is an output of the COST G7 activity during the previous three years as a result of the acute demonstrated necessity. It will dress the form of a European institute (ISAAC) with a permanent operative activity as an *e*-institution, involved in partnership formation for concrete projects with European value, with the attributes of a co-ordination action into a multi annual project in CULTURE 2000 Program. It has to be more than specialists' forum, and more than dissemination frame, but a pragmatic context for an efficient transfer of know-how and technology from research towards restoration/conservation, respectively SME's. ISAAC is very suitable to entirely or partly sustain activities of large interest but often too expensive for separate groups – partner mediation events, consulting, demonstrations, workshops, editing & publication, audits etc.

1 Introduction

The presentation will focus first on the positive results of COST Action G7 "Artwork Conservation by Laser". The action was initiated by INOE in 1999 and it is the first action in COST frame that is approved for a five-years duration owing to the unanimous interests expressed by twenty eligible countries. The dedicated website of this action is hosted at http://alpha1.infim.ro/cost. The activity was developed by the delegates of participating countries as well as by the invited experts and it has resulted into an informational database and an editorial plan.

Accumulated experience and observations regarding the acute necessity of harmonization of the activities between scientists and restorers, as well as the deep conscience that the process of integration of advanced techniques in conservation applications is a long process lead G7 members to create a frame of work.

2 COST G7 Outputs

The activity of COST G7 has a structured activity in three main working groups with a well defined working packaging, that stimulate the efficient collaboration between scientists by fundamental research presentation and applied research results dissemination.

WG1 – "Laser systems for cleaning applications" is composed of representatives of 41 institutions in 20 COST countries. The members have several backgrounds: (i) Physicists, Chemists, Biologists and Engineers performing fundamental and applied research on laser cleaning systems and laser-matter interactions on diverse substrates: paper, parchment, stone, canvas and mural paintings, glass, ceramics and metals; (ii) Conservation scientist & Conservators specialized in the pre-quated materials; (iii) Laser Manufacture & Equipment companies.

Leaders of this working group are two personalities of the laser cleaning field: Dr. Véronique Verges-Belmin, responsable de la Section "Pierre"-Laboratoire de Reserche des Monuments Historiques from Paris, France, and Dr. Wolfgang Kautek from Laboratory of Thin Film Technology Federal Institute for Materials Research & Testing, Berlin, Germany.

WG2 – "Laser and optical systems in analysis and diagnostics" brings together 33 institutions in 19 COST countries, performs both fundamental and applied research on laser and optical techniques, systems and protocols for analysis and diagnostics of works of art and related activities (conservation, display, cataloguing). Fundamental research is largely devoted to the investigation of the potential of laser spectroscopic techniques (laser-induced fluorescence, LIF; laser-induced-breakdown spectroscopy, LIBS; Raman and Infrared spectroscopy) as tools for the characterisation of materials (e.g. LIF for pigments, binding media, varnishes; LIBS for pigments, stratigraphic analysis, on-line monitoring). Other laser-based techniques (3-D scanning, holography, holographic interferometry, Doppler vibrometry, fluorescence imaging either spectrum- or time-resolved or both), non-laser related optical techniques (diffuse-reflectance spectroscopy, colorimetry), and techniques borrowed from other fields, such as nuclear physics, are the subject of basic research investigating their potential for the characterisation of processes (ageing, restoration, ablation, weathering, structural alteration etc.). The most developed applied research activities are related to the monitoring of various conservation procedures including laser-assisted and traditional cleaning applications. These applications already concern real artefacts and valuable objects.

Working group leaders are Dr. Alessandra Andreoni from Department of Chimistry and Mathematics University Insubria from Como, Italy, and Dr. Gerard Sliwinski from Polish Academy of Sciences ‚Institute of Fluid-Flow Machinery' – Gdansk.

WG3 – "Real-time equipment for environmental aspects and the response of artworks" – The remit of this working group includes the evaluation of current measurement techniques available for the monitoring/characterization of

an artwork and its environment. Such techniques have many applications including: (i) characterization of the state of an artwork prior to intervention (thereby allowing choice of the most appropriate form of treatment), (ii) characterization of the response of an artwork to its environment under different weathering conditions and (iii) on-line process (cleaning) control. The main focus of WG3 is exploitation of advances in laser and electro-optic technologies for development of cost-effective and non-invasive in situ environmental monitoring instruments.

These will allow fast, accurate monitoring of the local environment to which an artwork is exposed, thereby enabling detailed study of the effect of various environmental parameters on the artwork and the causes of deterioration. Research and technological innovations are needed to address this issue as the detection sensitivities required for artwork environmental monitoring are orders of magnitude lower than those required for outdoor pollution monitoring.

Working group leaders are Dr. Marta Castillejo from Instituto de Química Física – Rocasolano, CSIC, Madrid, Spain, and Dr. Rafi Ahmad from Cranfield University, UK.

The first elected chair of COST G7 was Dr. Vassilis Zafiropulos from FO.R.T.H, Greece and the recent elected chair is Dr. Renzo Salimbeni from IFAC-Florence, Italy.

Their contributions and contacts are available on action's web site.

Almost all management committee meetings were accompanied by dedicated workshops with invited scientists, restorers, conservators, and decision makers or representatives of local authorities for cultural heritage administration in different countries. We remind here last two workshops: "Conservators and the use of laser techniques in conservation" – organized on October 18, 2002, at EVTEK Institute of Art and Design from Vantaa, Finland by an active member – Prof. Christian Degrigny; and "Safety Aspects in Laser Conservation" organized on April 27, 2002, at Federal Institute for Materials Research and Testing from Berlin, Germany, by a personality in this field – Prof. Wolfgang Kautek. The summaries of main part of several presentations are available on website.

Action's web site presents the aim of the partnership, the calendar of the action, national representatives, invited personalities from Europe and USA, and announces related important events.

COST facilities are permanently exploited and rigorous managed through periodical meetings and thematic debates of idea and by STSM's (short-term scientific missions).

General interest of the national representatives and invited specialists focused to create a synthetic picture of the first dispersed researches and multinational activities. In this context a comprehensive database was design. It is permanently updated in several main directions:

(i) A bibliographic database containing information on publications in the field with detailed technical information – which has now over 150 records;
(ii) Laser and optical methods in monitoring, analysis and diagnostics demands for new research projects – which has now over 40 records;
(iii) Laser cleaning systems for conservation – This contains information on all conservation laser cleaning systems manufactured in Europe. This includes commercially available systems, prototype systems and systems in institutions where access and expertise can be made available through collaborative projects – which has now over 50 records;
(iv) Current and future demands for research in the field of COST Action G7 – which has now over 15 records;
(v) A new collection of data created for a complete demonstration of the end-users interest in concrete applications. It contains validation cases.

Fig. 1. COST G7 national representatives and invited specialists during the 4th Management Committee Meeting at Heraklion, Crete

3 Advanced On-Site Laboratory for European Antique Heritage Restoration

A proof of the domain maturity and scientists – representatives of COST G7 and other interested groups and specialists – determination for good practice demonstration is concreted by an on going project in CULTURE 2000

Program [1]. The project envisages creation of a temporary multinational and multidisciplinary partnership for a functional advanced laboratory for restoration/conservation. The *Laboratory* will be organized in Constanta in April 2004. It is an innovative form of representation of the synergy and the European contributions to the preservation of Ancient Cultural Heritage – a demonstrative most advanced laboratory created for a precious and relative new discovered ancient site (1957–1988) in Dobrogea region.

This *Laboratory* is the first one in the world that will benefit by such a number of advanced techniques and modern methods of restoration. Presented techniques – remote sensing control of environment quality, light dosimeters, laser cleaning systems with various characteristics, portable holographic interferometer, portable laser induced breakdown spectrometer, and multispectral analyser – never been integrated in the same restoration studio or yard.

Co-organizers are National Museum of History and Archaeology from Constanta, Romania, CERTO – Bucharest, Romania, FO.R.T.H – Heraklion, Greece, IFAC – Florence, Italy, NMGM–Liverpool, UK. This important event will benefit by a large number of experts from Romania, Greece, Italy, Malta, Germany, Austria, Portugal, Spain, The Netherlands, Sweden and UK.

Projects description and the main casuistries are presented to http://inoe.inoe.ro/constanta.

This *Laboratory* focuses its activity on the four concrete aspects:

- Introductory course on objective history and cultural significance and on applied advanced techniques for restoration/conservation; Creation of a dialogue frame for historians-art historians-restorers-scientists;
- Complex analysis on site and risk factor evaluation; Elaboration of a scientific schedule for analysis and investigations;
- Museum's knowledge on restoration-conservation – putted in value by a significant quantity of restorations records – are activated to be used in further cultural heritage restoration.

This *Laboratory* serves the following purposes:

- To take out in light a less known European treasure – part of the European cultural heritage;
- To stimulate the co-operation of an interdisciplinary and multinational team formed by valuable experts and by groups with international significant results for the rescue of the European heritage and, especially, for the demonstration of the compatibility teams and of a modern working mode.
- To put in value accumulated modern knowledge in restoration technique/methodology, adding value to the European research results due to an innovative for of collaboration and practice on a certain objective;

□ To increase the visibility over a cultural rich but less known European region bringing in first line ancient sites that must be rescued, conserved and cultural "exploited".

4 ISAAC – Innovative Science Application for Cultural Heritage

Developments regarding laser application in restoration/conservation/preservation are without doubts a European privilege in this moment. Several scientists and restorers representing important research groups and conservation education departments considered necessary to well establish a coherent frame of cooperation between scientists – endusers/restorers – economical agents/SME's in order to stimulate technology transfers and activity harmonization concerning two aspects:

– research offers and conservation practice;
– National legislation regarding restoration/conservation/preservation.

A special attention is spent to use all communication media in view to diffuse national legislation, know-how and research works on science application for cultural heritage.

Several remarks and conclusions of various recent conferences and seminars pointed discrepancies between the technique development and their popularity in restoration practice.

ISAAC uses the CULTURE 2000 opportunity because is the most suitable available instrument for the detected needs to European level. All national representatives and invited partners have experiences in international collaborations. Eureka Program sustains only applied research by multinational consortium, COST Program consists of basic and recompetitive research as well as activities of public utility, IP's sustain certain researches and technological developments, and NoI's are just for co-ordination research and information exchange.

Multi-annual projects in Cultural Heritage Area of CULTURE 2000 covers a gap for the superior development and rational exploitation of the accumulated knowledge by national and European projects.

ISAAC will cover activities such as:

- the organization of conferences
- meetings
- the performance of studies
- exchange of personnel
- the exchange and dissemination of good practices
- publications
- setting up common information systems and expert groups.

ISAAC – Innovative Science Application for Cultural Heritage – is a pan-European cyber-instrument that will support the dialogue between restorers/conservators and scientists. It will act as an innovative network in applied scientific and technical aspects focused to support concrete restoration projects, to promote "good practice" based on modern techniques and sustains dialogues for the harmonisation of educational process in respect with. Project aims to create a frame of work and continuing the cooperation in the field sustaining the access to advanced scientific and technical means.

Fundamentally, ISAAC will be an ***open*** **network** for the promotion and support of innovation activities, coordination of research and dissemination of good practice, setting up common information systems and expert groups. *Open* network means that it will be guarantee by the leader, co-organizers and partners, but it will be used by any other institution or specialist that can be informed through ISAAC activities and/or can inform the specialist's community about new projects, results and demands. This aspect assures the pan-European feature of ISAAC. Further, the number of beneficiary countries being exceeded the number of initiator countries that are from various European regions and with different socio-economical development (EU and candidate country).

This instrument comes to cover an important gap in the European cultural landscape- mainly organised till now by professional associations of conservators and restorers, or institutions with educational programmes, but rarely in oriented actions for cultural heritage rescue and good practice promotion. ISAAC is not designed to be restrictive within this spirit, but will bring together into a thematic partnership research institutes, centres and groups, museums, art studios etc. that carry out research or implement and disseminate results.

Acknowledgements

I would like to express my gratitude to all national representatives and invited specialists that contributed to COST G7 activity and, especially, to Prof. Vassilis Zafiropulos for his attentions and dedication for the action development.

Also, I would like to thank Prof. Zafiropulos, who helped me in order to prepare ISAAC application and documentation. A substantial support I have received for ISAAC project from Dr. Renzo Salimbeni and Dr. Salvatore Siano, involved partners in on site restoration laboratory, too.

References

1. "Culture 2000" Programme adopted on 14 February 2000 by the European Parliament and the Council, Decision No 508/2000/EC published in OJ L 63, 10.3.2000, p.1
2. CULTURE 2000: CALL FOR PROPOSALS FOR 2004 (2003/C 195/14)

The Project OPTOCANTIERI: A Synergy between Laser Techniques and Information Science for Arts Conservation

R. Salimbeni, R. Pini, and S. Siano

Institute of Applied Physics "N. Carrara", Via Madonna del Piano, Sesto Fiorentino (FI) 50019, Italy
r.salimbeni@ifac.cnr.it

Abstract. The general acceptance of innovation in the techniques employed everyday in conservation is increasing, due to the importance of the contributions coming from laser, optoelectronic and information technologies. The project OPTOCANTIERI is linking in Tuscany conservation institutions, restoration centres, research centres, technology producers and professional end-users to exploit in several restoration yards the potential of various techniques: laser cleaning, 3D scanning, radar investigations, information systems. This activity will take place in prestigious sites of Florence, Pisa and Siena. In this frame the conservator will be acquainted with innovative diagnostic and intervention systems, and will take advantage of informative systems capable to handle the increasing amount of data collected with these techniques.

1 Introduction

In Tuscany a series of special research projects, devoted to exploit the potential of these technologies in arts conservation, has clarified that innovation in this field requires an appropriate approach and needs a prolonged period of time. In facts only a strong and long lasting cooperation between the many categories of specific skills contributing to this objective will have chance to establish a real technology transfer.

The aim of this paper is to present the project Optocantieri (an Italian short form for optoelectronic techniques brought in the restoration yard), the aims and the preliminary results.

2 The Project Structure

Under the initiative of the Tuscany Region, a series of projects were put in sequence in the period 1997–2003, specifically devoted to promote innovative technologies in cultural heritage conservation, which is considered a strategic sector for culture and economy in Tuscany.

The Optocantieri project is consolidating in a network of public institutions and private companies, all located in the Tuscany Region, the task of

technology transfer from research centres to end-users. The core of the scientific background lies in optoelectronic and information technologies, which in Tuscany have a high concentration of activities in CNR institutes and in industrial initiatives. The sources of conservation expertise are located in prestigious public conservation centres of Tuscany, such as the *Opificio delle Pietre Dure*, the *Centro di Restauro della Soprintendenza Archeologica della Toscana,* the *Soprintendenze*, government organisations devoted to the preservation of the artistic, architectural and archaeological heritage, and in organisations linked to the patrimony of cities of art such as Florence, Pisa and Siena among many other important historical centres. In 2003–2004 Optocantieri is carrying out demonstrative and dissemination actions, will contribute to projects of advanced research, will propose, through associated companies, services for the conservation of artworks, monuments and historical buildings, will organise courses with a high professional profile. The proposed technologies are: laser applications for the cleaning of stone [1] and metals [2], reflectographic investigations of paintings [3], 3D digital documentation using optical and laser scanning [4], environmental monitoring in museums [5], investigation of archaeological sites using radar techniques, diagnostics of masonry and wood structures, informative systems [6].

The contributors to the project are 4 research centres (Institute of Applied Physics "N.Carrara", Institute of Applied Optics, Institute for Conservation and Valorisation of Cultural Heritage, Institute for Information Science and Technology), 1 university dept. (Univ. of Siena), 1 museum (*Musei Comunali* of Florence), 4 conservation institutions (*Soprintendenza ai Beni Architettonici di Pisa*, *Opera Primaziale Pisana*, *Opera di S.Maria del Fiore*, *Opera Metropolitana di Siena*), 2 restoration centres (*Opificio delle Pietre Dure*, *Soprintendenza Archeologica della Toscana*), 4 technology producer companies (EL.EN.Spa, IDS Spa, Falcon Instruments Srl, Sistemi Informativi Srl), 8 professional restoration companies (General Engineering Srl, RestauroItalia Srl, Meridiana Restauri Srl, MIDA Srl, Legnodoc Srl, Stefano Landi, Daniela Manna, Katryn Potthoff).

3 The Innovative Aspect

The main task of the project strategy has been to increase the acceptance of the conservation community for these technologies by means of a synergy between them, an evolution of prototypes toward products and a widening of the number of professional restorers with a validated experience in the use of these products.

The increasing number of applications of laser cleaning of stone in monuments and historical buildings is the leading edge of this strategy, because it involves conservation institutions and professional restorers in a crucial way: the conservation institution has to be perfectly conscious about the importance of the benefits using laser instead of less precise techniques; on the

other hand professional restorers have to be able to respond with trained personnel to the demand for a laser approach, when it is actually needed.

With these premises, laser cleaning is a sort of icebreaker technology, which allows a wider acceptance for the other technologies promoted in the project. The opening of a demonstrative activity in several restoration yards in Florence, Pisa and Siena gives a real opportunity for such synergy. The restoration yards are set at:

- "*Porta della Mandorla*", a side door by Nanni di Banco of the cathedral of *S. Maria del Fiore* in Florence. At this site the cleaning of Carrara marble and other types of stones (red ammonitic, green serpentine) will be carried out; 3D laser scanning will give a digital file of the Madonna before and after cleaning; radar will investigate the presence of a wall fracture;
- "*Porta del Paradiso*" a gilded bronze by Lorenzo Ghiberti, and main door of the Baptistery in Florence. The ability of a special laser suitably constructed to avoid any risk to the gold film is employed for the cleaning of 48 decorations of the door.
- "*Minerva di Arezzo*", a Hellenistic bronze, found in an archaeological Roman site. After a partial cleaning with laser, the use of 3D digital file will help for the dismantling and remounting of the bronze, needed to correct for damages and for an improper previous restoration.
- "The Earth globe" by Ignazio Danti, in *Palazzo Vecchio*. Not invasive diagnostics and 3D digital representation will provide information about the globe structure, which is crucial for a further step of restoration, while museum light effects on the pigments will be monitored by a suitable system.
- the door of the Cathedral of Pisa, where laser cleaning will be employed also in view of the general plan of preservation of *Piazza dei Miracoli*.
- the façade of the church of *S. Pietro in Vinculis*, which will be cleaned by laser.
- the "*Fonte Gaia*" by Jacopo della Quercia, in Siena. The many fragments of the monuments will be cleaned, their shape will be recorded by 3D digital files, to provide a virtual remounting of the pieces, and radar investigations will explore the original foundations of the *Fonte* in *Piazza del Campo*.
- the floor of the cathedral of Siena, where photogrammetric recording of the indoor floor, 3D digital documentation, will be extended outside the building for investigations of the underground voids.

All these efforts will produce an extensive amount of data, images and texts, which will be presented on the project web site (http://optocantieri.ifac.cnr.it), along with an experimental 3D digital documentation. Because of this experience the use of information tools and the exchange of images and other digital files through mobile communication is certainly fostered in the conservation community by the evident utility in the restoration yard.

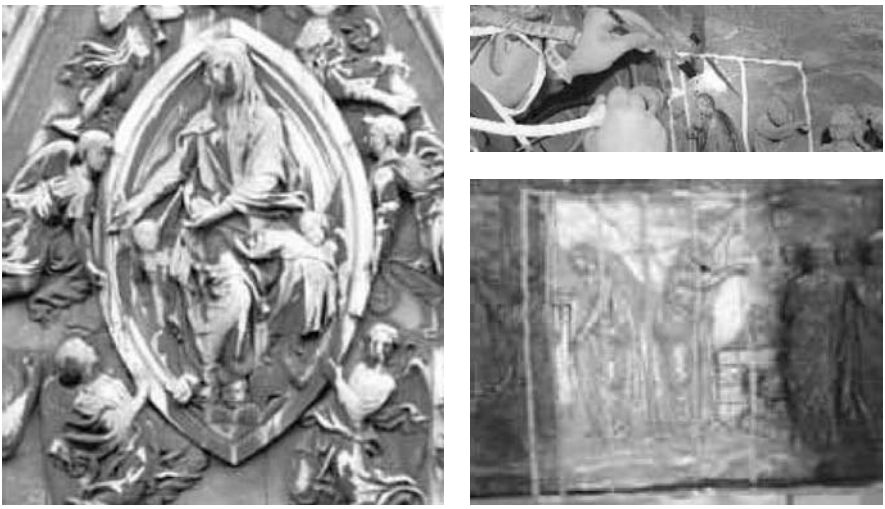

Fig. 1. *On the left*: Detail of the Madonna in an almond (*mandorla*); *on the right*: Detail of the gilded bronze of the *Porta del Paradiso*

Fig. 2. *On the left*: Fragment of the *Fonte Gaia* (Siena), with a partial laser cleaning; *on the right*: Typical black encrustations on the façade of *S. Pietro in Vinculis* (Pisa)

4 Conclusions

In conclusion the application of optoelectronic techniques and information science are likely to be better accepted by the conservation community, if they are presented all together as an important contribution coming from physics to the innovation needed in the field. The project Optocantieri is on his way, promoting the use of laser, radar, IR scanners, 3D digital documentation by institutions and professional end-users. The laser cleaning employs the well-known intermediate pulse duration regime, with microseconds pulse duration. This approach has solved the problems previously shown by Q-switch lasers,

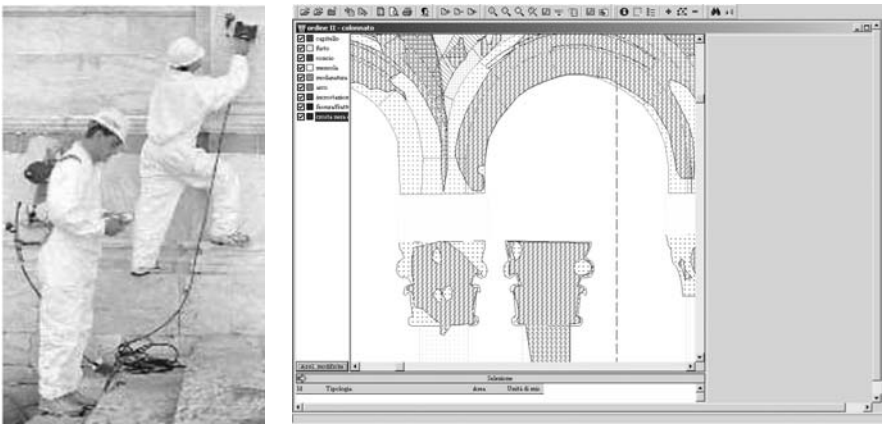

Fig. 3. On the left: Radar at work in *Piazza dei Miracoli* (Pisa); on the right: Mapping of the deterioration state of the 2nd order columns of the Tower of Pisa, with the Akira GIS by Sistemi Informativi Srl

and represents a successful result, which has been validated in many case studies. Besides laser cleaning, the other diagnostic techniques will certainly help in modelling the conservation state and in predicting the behaviour after the restoration intervention. This could be a very important task to be pursued in the next future, and the integration of various science & technology fields is a crucial step in view of this objective.

Acknowledgements

The authors wish to acknowledge the specific support given to Optocantieri by the Regione Toscana, Dept. for Productive Activity, PRAI Program and the entire partnership of Optocantieri for their contribution.

References

1. S. Siano, et al., Applied Optics **36,** 70–73, 1997
2. S. Siano and R. Salimbeni, Studies in Conservation **46**, 269–281, 2001
3. L. Marras, M. Materazzi, L. Pezzati, and P. Poggi, Insight **45–4**, 276, 2003
4. Fontana et al., Journ. of Cultural Heritage **3**, 325, 2002
5. A. G. Mignani, et al., in IEEE Sensors Journal **3–1**, 108–114, 2003
6. G. Capponi, S. Bonannini, P. Lanari, U. Parrini, M. Sartor, and A. Vecchi, Rapporto Interno, Comitato Int. Salvaguardia Torre di Pisa“, 1999

Spanish Thematic Network on Cultural Heritage

M. Castillejo[1], M.-T. Blanco[2], and C. Sáiz-Jiménez[3]

[1] Institute of Physical Chemistry Rocasolano, CSIC, Serrano 119, 28006 Madrid, Spain
marta.castillejo@iqfr.csic.es
[2] Institute of Building Science, CSIC, Serrano Galvache s/n, 19002 Madrid, Spain
[3] Institute of Natural Resources CSIC, Avenida de Reina Mercedes, 10, 41012 Seville, Spain

Abstract. A Thematic Network on Cultural Heritage has been recently launched to coordinate the activities related to Cultural Heritage (CH) of several groups working in the Spanish Scientific Research Council (CSIC), the largest public research organisation in Spain. The Network involves 21 leading research groups from 16 institutes. Different aspects of CH are approached including Archaeology and Architectonic Heritage, Biology, Physics, Geology and Materials Science.

1 Introduction

A Thematic Network on Cultural Heritage (TNCH) was created in October 2001 to include Spanish scientists from the Scientific Research Council (CSIC) working on CH. This Network is supported by CSIC and the Spanish Ministry of Science and Technology. The initiative was launched as part of the CSIC programme for coordinating selected innovative or social-interesting areas. It was set out to provide co-ordination between CSIC research institutes working separately on CH in many different topics, from Archaeology to industrially relevant research and technological development (laser techniques, new materials, etc).

2 Composition of the Network and Objectives

The TNCH involves 21 leading research groups from 16 Institutes with more than 65 scientists as listed in Table 1. Its main objective is to support research on CH and to promote cooperation between European research centres, professional associations and technological companies. This new organisation aims to participate in relevant areas of the 6th Framework Programme of the European Commission, National Research and Technological programmes, and to promote exchanges, common discussions and co-operations in the field of CH.

Advanced and comprehensive instrumentation and knowledge exist within this consortium for the different involved fields. The TNCH is a platform

Table 1. Research institutes included in the Thematic Network on Cultural Heritage

Centre	City
Institute of Archaeology (IA)	Mérida
Institute of Building Science (IBS)	Madrid
Centre of Environmental Sciences (CES)	Madrid
Institute of Ceramic and Glass (ICG)	Madrid
Institute of Economical Geology (IEG)	Madrid
Institute of History (IH)	Madrid
Institute of Material Science (IMSS)	Seville
Institute of Material Structure (IMSM)	Madrid
Institute of Natural Resources (INRSA)	Salamanca
Institute of Natural Resources (INRSE)	Seville
Institute of Physical Chemistry Rocasolano (IPCR)	Madrid
Institute Padre Sarmiento (IPS)	Santiago de Compostela
National Centre for Metallurgical Research (NCMR)	Madrid
National Centre of Accelerators (CAN)	Seville
National Museum of Natural Sciences (NMNS)	Madrid
School of Arabic Studies (SAS)	Granada

of access to these resources that can more easily be approached by other researchers. The necessary mechanisms of exchange and collaboration are being created to ensure the critical mass needed for multidisciplinary research projects on CH and the good use of investments. Additionally the TNCH contributes to dissemination of its activities and capabilities to the end users, including local and national culture administrations, Foundations, enterprises, etc.

3 Research Activity

The TNCH includes five areas of research activity that are briefly described below. Table 2 lists specific activities included in each area.

3.1 Archaeology and Architectonic Heritage

Activities in this area aim at the knowledge of CH (origin, transformations across time and meaning) as a basis for its adequate conservation. Techniques used fall within the scope of architecture, archaeology, and art history. Photogrammetry and historical analysis of the buildings are two of the possible approaches.

Table 2. Research activity at the TNCH

Area	Research activity
Archaeology and Architectonic Heritage	Architectural Archaeology. Landscape Archaeology. Architectonic photogrametry. Research and restoration of architectonic and archaeological heritage.
Biology	Molecular biology applied to biodeterioration of CH. Characterization, ecology y physiology of living organisms involved in biodeterioration. Electron Microscopies.
Physics	Physical techniques applied to the study of CH. Laser techniques applied to the restoration and conservation of CH.
Geology	Rock Art: geochemistry, hydrochemistry and micro-climatology karstic environments. Characterization of stone building materials. Diagnosis of the state of conservation of architectonic heritage: pathologies and origins. Geoarchaeology and geochronology. Building and ornamental stone: characterization, durability and localization of quarries. Conservation and restoration treatments for the architectonic heritage.
Materials Science	Conservation of mortars and concrete. Conservation of historic glass heritage. New materials for surface treatments. Design of new mortars for restoration. Study of ceramics, stone materials and painting techniques.

3.2 Biology

Organisms contribute to the deterioration of materials in buildings and monuments, as well as art objects made of paper, wood, glass, ceramic, etc. A wide variety of organisms from bacteria to higher plants and animals are involved in biodeterioration processes. The use of modern electron microscopy techniques, molecular methods and *in situ* observations allow the diagnosis of the type of organism involved in biodeterioration and the proposal of control measures for their eradication.

3.3 Physics

This area deals with the study at molecular level of ageing and damage of constituent materials of artistic objects, the application of non-destructive or micro destructive techniques based in optical and vibrational spectroscopies for analysis and identification of materials and assessment of their state of conservation. The activity includes the development of advanced

laser techniques for cleaning and diagnosis of surfaces of artistic interest and the use of nuclear techniques from the National Centre of Accelerators.

3.4 Geology

This area contributes with petrographycal, chemical and petrophysical characterisation of the stone materials (building stones, bricks, mortars, etc) used in CH. The use of the corresponding techniques allows to evaluate the state of conservation, the analysis of degradation processes on materials and eventually to design the adequate corrective strategies, including control of environmental conditions (microclimate, hydrochemistry, atmospheric pollution, etc) and elaboration of consolidants and protective treatments.

3.5 Materials Science

The main objective in this area is to achieve the knowledge about the origin and mechanisms of the processes of damage of the objects or buildings of CH. Based in this knowledge, novel materials with improved properties and new control and intervention technologies will be developed. Preventive actions or conservation measures can also be designed.

4 Activities within the Scope of LACONA

The activities of several groups belonging to the TNCH are related with the use of lasers for the conservation of artworks. At IPCR laser ablation is used for treatments removal or cleaning of artwork surfaces (stone, polychromes on wood, etc), and for micro chemical analysis using laser-induced breakdown spectroscopy (LIBS) and time of flight mass spectrometry (ToFMS) [1]. The fundamentals, diagnosis and modelling of the laser materials interactions are also studied at this node [2]. The group at IMSM uses advanced vibrational spectroscopies for analysis and identification of artwork materials and assessment of modifications induced on artwork surfaces by laser cleaning, environmental pollution, etc. [3]. At INRSE, gas chromatography-mass spectrometry and pyrolysis techniques have been used for assessing the nature of stone yellowing produced after laser cleaning [4].

References

1. M. Castillejo, C Domingo, J. V. García-Ramos, M. Martín, M. Oujja, S. Sánchez, D. Silva, and R. Torres, *Appl. Spectros.* **55** , 992, 2001
2. M. Oujja, E. Rebollar, and M. Castillejo, *Appl. Surf. Sci.* **211**, 128, 2003

3. M. Castillejo, M. Martín, M. Oujja, D. Silva, R. Torres, A. Manousaki, V. Zafiropulos, O. F. van den Brink, R.M.A. Heeren, R. Teule, A. Silva, and H. Gouveia, Analytical study of the chemical and physical changes induced by KrF laser cleaning of tempera paints, *Anal. Chem.* **74,** 4662, 2002
4. M. Gaviño, B. Hermosin, V. Vergès-Belmin, W. Nowik, and C. Saiz-Jimenez, The use of gas chromatography-mass spectrometry and pyrolysis techniques for assessing the nature of stone yellowing produced after laser cleaning, Proceedings 7th International Conference on Non-Destructive Testing and Microanalysis for the Diagnostics and Conservation of the Cultural and Environmental Heritage, Antwerp, Belgium, R. Van Grieken, K. Janssens, L. Vant't dack and G. Meersman (eds.), University of Antwerp, (2002) pp 1–8

Part IX

Cleaning Stations and Process Control for Practise

Laser Cleaning System for Automated Paper and Parchment Cleaning

W. Kautek and S. Pentzien

Federal Institute for Materials Research and Testing
Laboratory for Thin Film Technology, Unter den Eichen 87,
12205 Berlin, Germany
wolfgang.kautek@bam.de

Abstract. A prototype of a computerized laser cleaning system suitable for high-precision cleaning of flat large area substrates, e.g. paper and parchment objects, has been developed. It is based on a compact high pulse energy diode pumped Q-switched Nd:YAG laser operating at 1064 nm and 532 nm, and a pulse duration of 8 ns. It can function under Laser Class I conditions, so that the operator does not require safety goggles. Objects can be scanned supported by a remote computer control system. The operator can follow the process on the computer screen through a camera system. The scanning can be controlled manually or programmed in the computer, defining the pulse energy, number of pulses, laser spot overlap and shape of the area to be treated. As an alternative, an optical fibre with an ergonomic hand piece can be used for manual cleaning of objects under Laser Class IV conditions requiring eye protection. The workstation features on-line visible, ultraviolet and fluorescence imaging for the identification and documentation of visible and chemical changes of the irradiated substrate areas. Examples of applications in paper and parchment conservation are presented in order to illustrate how complex pigment and ink structures can be preserved on paper and parchment by automated high-precision laser beam scanning.

1 Introduction

Pulsed lasers are becoming new tools in the hands of restorers [1–3]. Most activities, however, were concerned with the laser cleaning of stone artefacts, wall paintings, and facades. There also exist fundamental knowledge and experience on the cleaning of technical surfaces relevant e.g. in the electronic industry [4, 5] or the high-precision removal of inorganic and organic films e.g. in biosensoric technology [6]. The contactless laser cleaning of biogenetic surfaces such as parchment, on the other hand, has been approached only in recent years [7–12]. By now, laser beam delivery has been realized either via an optical fibre or an articulated optical arm to a hand-held output optics common in facade laser cleaning, or it is immobile relying on the movement of a scanning mounting supporting the work piece.

The cleaning objects paper and parchment belong to the chemically most fragile substrates exposed to high-power laser radiation. The main constituent of paper is cellulose (Fig. 1). It is a linear polymer of β-(1 $\rightarrow$ 4)-D-

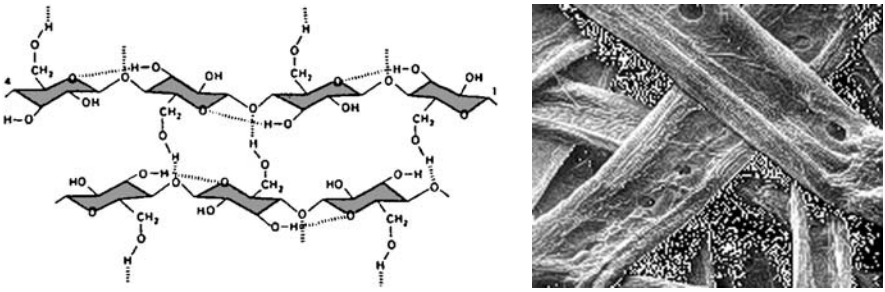

Fig. 1. Cellulose – constituent of paper. *Left*: cellulose structure with important hydrogen bond cross-links. *Right*: paper fibrils (SEM by J. Jameel, NC State University)

glucopyranose units in $^4C_1$ conformation with two coexisting phases, cellulose I_α (triclinic) and cellulose I_β(monoclinic). It forms crystals where intramolecular (O3-H→O5' and O6→H-O2') and intra-strand (O6-H→O3') hydrogen bonds hold the network flat allowing the more hydrophobic ribbon faces to stack. The tendency to form crystals utilizing extensive intra- and intermolecular hydrogen bonding makes it completely insoluble in normal aqueous solutions. The overall structure is of aggregated fibrils with extensive pores capable of holding relatively large amounts of water by capillarity.

Collagen forms long ropes and tough sheets (Fig. 2). All contain a long stretch of triple helix connected to different types of ends. The simplest is merely a long triple helix, with blunt ends. These "type I" collagen molecules associate side-by-side, like fibres in a rope, to form tough fibrils (Fig. 2, right). (Fig. 2), left, depicts a basement membrane, which forms a tough surface that supports e.g. skin or parchment. A different collagen–"type IV"–forms an X-shaped complex supporting extended networks. Two other molecules - cross-shaped laminin and long, snaky proteoglycans - fill in the spaces, forming a dense sheet.

2 Laser Cleaning System

A laser cleaning system for high-precision cleaning of flat large area substrates under Laser Class I conditions (with no safety goggle requirement) has been developed. It allows the restoration of artefacts of organic materials, such as paper, parchment, leather, textiles, wood, but also inorganic materials, such as metals, alloys, and ceramics.

The laser spot is scanned over the objects through a remote computer control system (Fig. 3). The operator can follow the process on the computer screen through a camera system (Fig. 4). The cleaning process is controlled manually through keyboard, mouse and/or foot pedal operation or can be programmed for automatic laser beam scanning operation. A high

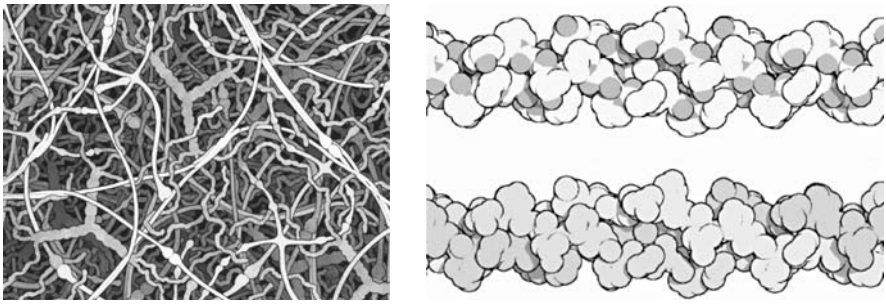

Fig. 2. Collagen – constituent of parchment. *Left*: Simulation of base membrane consisting of various collagen helix types. *Right*: collagen triple helix with glycine, proline, hydroxyproline. (D. S. Goodsell, Scripps Research Institute, La Jolla)

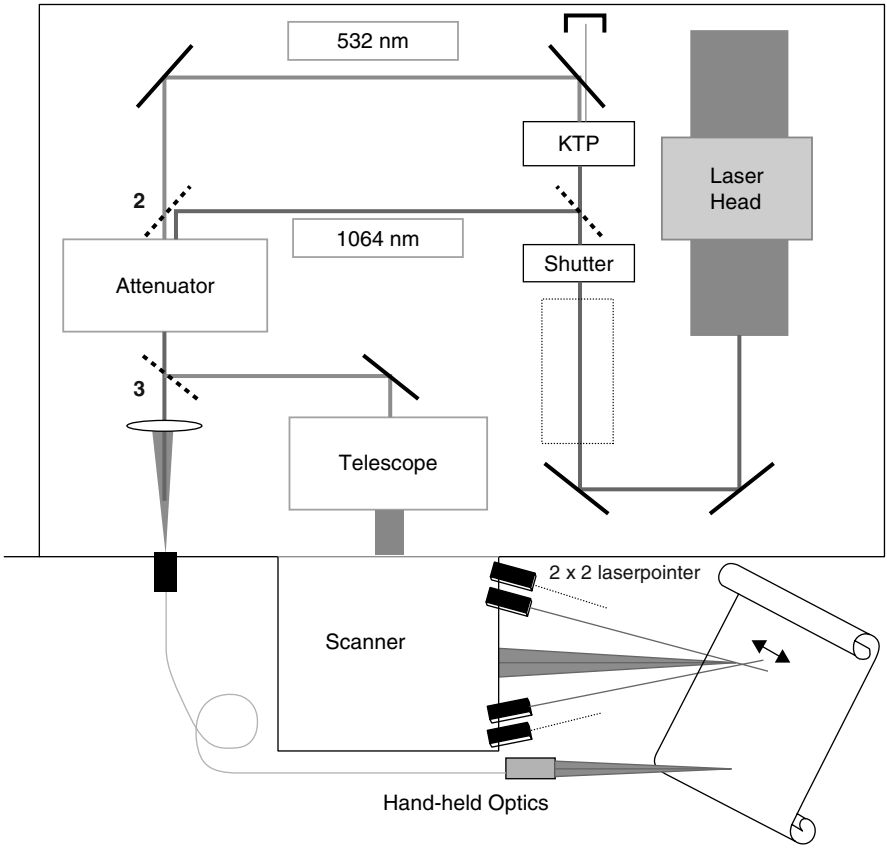

Fig. 3. Scheme of cleaning laser system (BAM Prototype; IB Laser AG; Berlin)

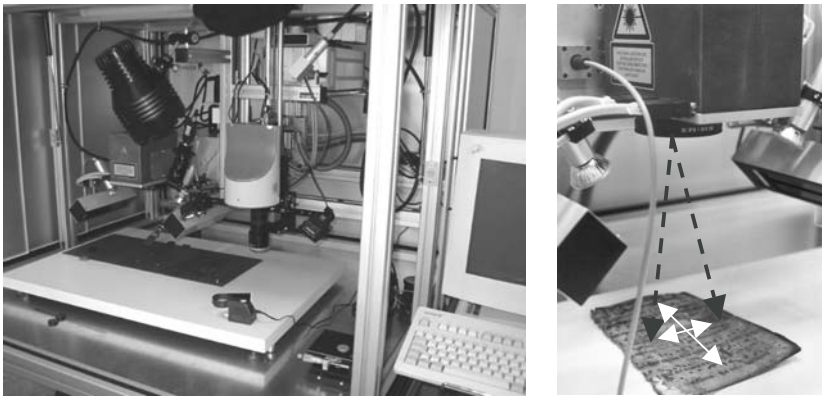

Fig. 4. Cleaning laser system (BAM Prototype). Remote control scanning principle

pulse energy diode pumped Q-switched Nd:YAG laser operating at 1064 nm and 532 nm was integrated in a laser-processing compartment with an integrated exhaust system. The set-up consisted of a scanning optical system (254 mm focal length) which delivered a spot size of approximately 100 µm and maximum energy densities (fluences) in the range of up to $F(532\,\mathrm{nm}) = 10\,\mathrm{Jcm}^{-2}$. The pulse duration is 8 ns and the repetition rate can be chosen up to 1000 Hz. As an alternative, an optical fibre with an ergonomic hand piece can be used for manual cleaning of 3D objects with a laser spot of c. 300 µm (Fig. 3).

The workstation features on-line diagnostic tools such as visible, ultraviolet and fluorescence imaging for the identification and documentation of visible and chemical changes of the irradiated substrate areas.

The multi-spectral imaging system (MuSIS 2007, Art Innovation, Hengelo, The Netherlands) operated in a spectral range from 320 nm up to 1550 nm]. Several imaging modes are possible: visible reflection, infrared reflection, visible fluorescence, and ultraviolet reflection.

Semiquantitative colour measurements (spectral reflectance) can be carried out with the same system. The illumination conditions are the same as in the imaging mode (qualitatively similar spectral characteristics as standard illuminant D_{65} with UV and VIS components). CIE-$L^*a^*b^*$ colour coordinates may therefore formally be used for the evaluation. The data allow relative, not absolute, comparisons in respect to both lightness changes ΔL and saturation and hue changes given by the chromaticity coordinates Δa^* and Δb^*. The vector between two data sets in the colour sphere is the colour difference ΔE. It is very useful for semiquantitative assessments of colour changes:

$$\Delta E = \sqrt{L^{*2} + a^{*2} + b^{*2}} \tag{1}$$

Lightness changes ΔL quantified by this relative technique can be correlated with the cleaning status. The overall colour difference ΔE includes also the colour changes for which the human eye is particularly sensitive.

3 Applications

Based on experiences of laser cleaning with various conventional research laser systems [7–12] examples of recent studies with the new prototype system are presented to demonstrate its potential for high-precision cleaning and automated industrial or restoration applications.

Preliminary tests showed that any polygons drawn on the computer screen with the hand-held mouse could be transferred by means of the scanned laser beam. The black toner print on photocopy paper could be removed with high precision (Fig. 5). The extent of this cleaning action was controlled by the preset laser beam energy, the scan rate, and the number of scans as can be seen on the left sample of Fig. 5.

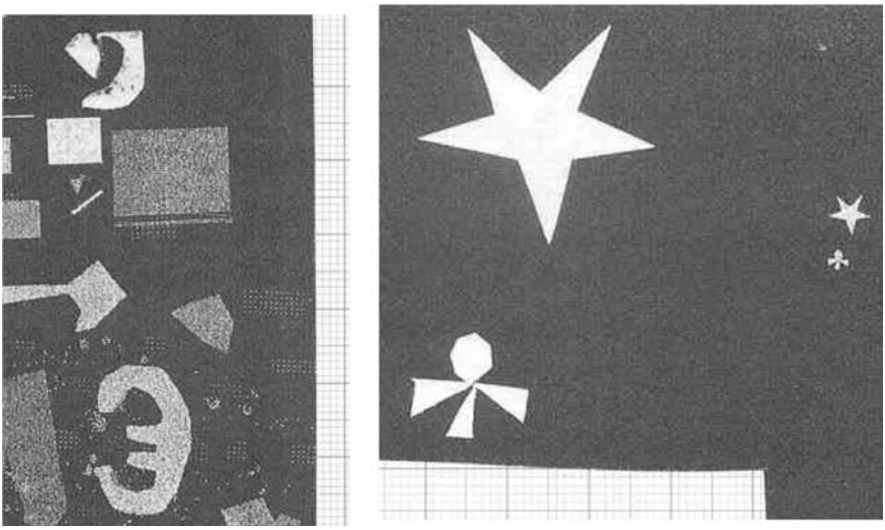

Fig. 5. Precision laser cleaning on test samples (black photocopies)

One of the major challenges of precision cleaning is to avoid areas of ink, printed letters or pigments. A section of an old office document on rag paper was contaminated with pencil scratching almost to unreadability (Fig. 6). The area to be laser-cleaned was drawn on the computer screen by the mouse movement as a customized lithographic mask. Then, the system automatically scanned the intended area.

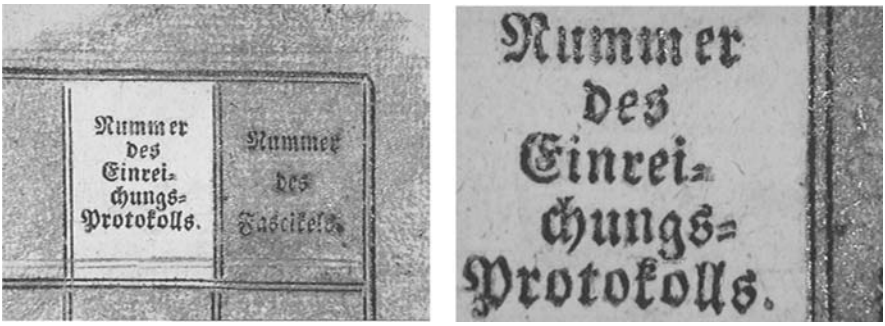

Fig. 6. Precision laser-cleaned printed paper (c. 1900)

The cleaning system also proved successful on original, such as a sheet of music of a psaltery from 15th century, which was heavily soiled during a bombing attack at very end of Second WorldWar (Fig. 7). There, handwritten ink letters, notes, and lines of the staff often have to be preserved from the converting action of the laser beam. Again, the cleaning result demonstrates the feasibility of this ultra-precise "contactless rubber".

Fig. 7. Precision-cleaned ancient parchment (15th century, Southern Germany; private W. Kautek)

On-line diagnostics in the form of multispectral imaging is integrated into the laser-cleaning prototype. Cotton paper e.g. was treated with increasing fluence on the patches numbered with 1, 2 and 3 (Fig. 8). The visible image shows no alteration below the ablation threshold fluence above 1.4 Jcm^{-2}. At a drastically higher value, at 5.0 Jcm^{-2}, the visible image only indicates a faint darkening.

Invisible diagnostic tools, however, allow a more sensitive judgment on the degradation status. The reduction of the IR and UV reflectivity indicate an increased absorption in IR and UV due to chemical changes. This UV absorption increase is accompanied by a drastic fluorescence increase.

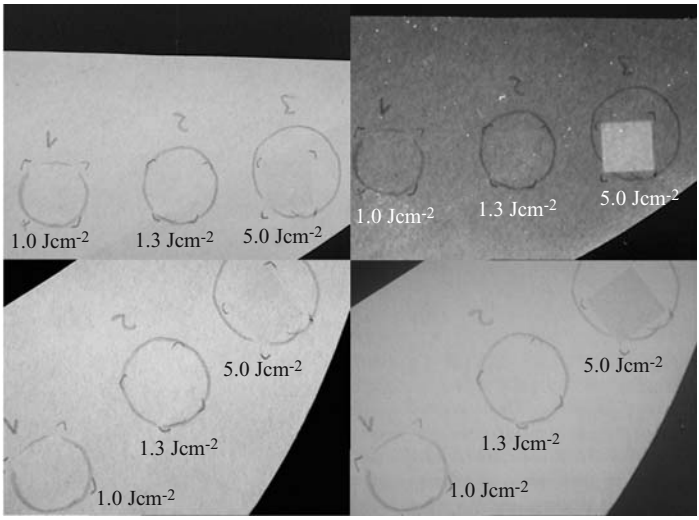

Fig. 8. Multispectral imaging diagnostics of laser-treated cotton paper (Whatman filter paper). (**a**) VIS reflectivity, (**b**) fluorescence, (**c**) IR reflectivity, (**d**) UV reflectivity. Fluence [Jcm^{-2}]: (1) 1.0, (2) 1.3, (3) 5.0

Currently, special efforts are undertaken to develop process modes to speed up the scanning of larger areas. It has to be remarked that an efficient exhaust system is not only vital for the operator's safety but also to avoid redeposition of already vaporized contaminants. Further research on the molecular understanding of the influence of laser radiations with various photon energies is under way.

Acknowledgements

The EUREKA project "Laser Cleaning of Paper and Parchment (LACLEPA)" $\Sigma!$ 1681 served as an umbrella for this research. One of the authors (W. K.) acknowledges partial financial support by the EU TMR project "Modelling and Diagnostic of Pulsed Laser-Solid Interaction: Applications to Laser Cleaning", No. FMRX-CT98-0188. We thank particularly B. Smandek, IB Laser AG, Berlin, for stimulating discussions during the development phase.

References

1. W. Kautek and E. König (Eds.), *Lasers in the Conservation of Artworks I*, Restauratorenblätter (Special Issue), Verlag Mayer & Comp., Wien, 1997
2. *Lasertechnik in der Restaurierung*, Restauro, Vol. 104/6, 1998
3. M. Cooper, *Laser Cleaning in Conservation*, Butterworth-Heinemann, 1998

4. D. Bäuerle, *Laser Processing and Chemistry*, Third Edition, Springer–Verlag, Berlin, Heidelberg, New York 2000
5. R. Oltra, E. Arenholz, P. Leiderer, W. Kautek, C. Fotakis, M. Autric, C. Afonso, and P. Wazen, Proc. SPIE, Vol. 3885, 499, 2000
6. J. Bonse, S. Baudach, J. Krüger, and W. Kautek, Proc. SPIE, Vol. 4065, 161–172, 2000
7. W. Kautek, S. Pentzien, P. Rudolph, J. Krüger, and E. König, Appl. Surf. Sci., Vol. 127–129, 746–754, 1998
8. P. Rudolph, S. Pentzien, J. Krüger, W. Kautek, and E. König, Restauro, Vol 104(6), 396–402, 1998
9. W. Kautek, S. Pentzien, J. Krüger, and E. König, in *Lasers in the Conservation of Artworks I*, Restauratorenblätter (Special Issue), Edited by W. Kautek and E. König, Mayer & Comp., Wien, 69, 1997
10. W. Kautek, S. Pentzien, P. Rudolph, J. Krüger, C. Maywald-Pitellos, H. Bansa, H. Grösswang, and E. König, in *Optics and Lasers in Biomedicine and Culture*, Edited by C. Fotakis, T. Papazoglou, and C. Kalpouzos, Optics within Life Science Series, Springer–Verlag, Heidelberg, 100–107, 2000
11. W. Kautek, S. Pentzien, P. Rudolph, J. Krüger, C. Maywald-Pitellos, H. Bansa, H. Grösswang, and E. König, J. Cultural Heritage, Vol. 1, S233–S240, 2000
12. W. Kautek, S. Pentzien, D. Müller-Hess, K. Troschke, and R. Teule, SPIE, Vol. 4402, 130–138, 2001
13. M. Chaplin, Food Research Centre, London South Bank University, London, UK
14. A. A. Baker, W. Helbert, J. Sugiyama, and M. J. Miles, Biophys. J., Vol. 79, 1139–1145, 2000

Laser Cleaning Monitored by a Spectroscopic Technique – Experimental Data on The Gotlandic Sandstone Case

M. Jankowska, K. Ochocińska, and G. Śliwiński

Polish Academy of Sciences, IF-FM, Dept. of Photophysics and Laser Technique
Fiszera 14, 80-231 Gdansk, Poland
marja@imp.gda.pl

Abstract. The LIPS spectra obtained for the historical samples of Gotlandic sandstone (XVI c) under pulsed laser irradiation at 355 and 1064 nm are analysed and applied for monitoring of the surface cleaning process. The spectra are recorded in the range 370 – 760 nm upon successive cleaning pulses and depend strongly on the laser wavelength and dose applied. Peaks assigned to Ca I, Ca II, Al I, Ba I, Li I and Mg I (crust) and to Si I, Si II and Al II (stone) are observed. An exponential decay of the Ca I, Ca II and Al I peak intensities accompanies the cleaning progress. The short term colour changes of the sandstone surface due to laser irradiation are not revealed by colorimetric measurements.

1 Introduction

Sandstone differs from other stones like marble or limestone in the chemical composition and structure as well as in the way of creation of the patina and encrustation layers due to prolonged environmental influence [1]. The Gotlandic sandstone represents a material widely used in the past in Northern Europe. It is composed of quartz grains joined by limestone binder and characterized by a green-greyish hue [2]. In the case of historical sandstone objects the following layers are most frequently observed: the dirt layer under the crust coverage, the degraded stone layer, and the unchanged stone below it [3].

Problems related to sandstone restoration have been extensively described in the literature. Numerous works are devoted to the surface cleaning of the historical objects. There are well established conventional methods of the encrustation removal, such as washing, washing with the use of chemicals, mechanical abrasion, ultrasound cleaning, and sand blasting. Among them, only the microabrasive cleaning and the use of hydrofluoric acid solutions assure a relatively low destruction of the original material [3]. However, in both cases the process of encrustation removal is difficult to control and could result in an irreversible surface damage of the original material. For one decade or so the laser cleaning has been applied more frequently to stone conservation, too [4–7]. This technique represents an interesting alternative to conventional ones and proves to be quite efficient when applied to objects

of well developed surfaces with complicated curvatures. Moreover, the process of laser ablation can be easily controlled.

In the case of sandstone cleaning by laser only a few published data are known regarding application of the LIPS (Laser Induced Plasma Spectroscopy) technique for the process diagnostics. The LIPS spectra for this material in the 250–320 nm region are known from recent works [8, 9]. However, the spectral features in the visible region have not been considered in the literature yet.

In this work the LIPS spectra of the Gotlandic sandstone in the range of 370 – 780 nm obtained during laser cleaning of the historical samples are considered. The elemental composition of the crust and the underlying material is identified and analysed. The investigation focuses on spectra observed under pulsed excitation by means of the Nd:YAG laser at 1064 nm and 355 nm. Moreover, the results of colorimetric measurements are discussed.

2 Experimental

For experiments the samples of historical elevation (XVI c.) made of Gotlandic sandstone were used. Samples originated from a collection of sculptures and architecture details in the St. John's church in Gdansk, and were originally covered with black encrustation of thickness of about 100 μm, resulting from the long term environmental interaction. Below the crust a layer of patina was present, but it could not be marked out as clearly as in the case of other stones, e.g. marble, for which stratigraphic observation of the visible thin layer of the Ca-oxalate film was reported in the literature [10].

For sample irradiation the Nd:YAG laser (Quantel) operating in a Q-switched, single pulse mode and characterized by the pulse duration of 6 ns (FWHM) was used. The laser beam was delivered to the sample surface via an optical train of variable geometry, which assured controlling of the beam position and focusing. During the experiments a constant pulse energy of 330 mJ and 10 mJ were applied at the infrared (1064 nm) and ultraviolet (355 nm) wavelengths, respectively. The laser beam was directed perpendicularly to the surface and the selected area of the surface was treated until the crust was completely removed. The beam was focused on the sample surface only for the LIPS measurements executed under excitation at 355 nm. For irradiation at 1064 nm, the fluence on the sandstone surface was equal to 1.3 J/cm^2. During laser ablation the LIPS spectra were recorded. The visible region was selected for detection of the plasma emission because of the complex spectral structure observed and due to the fact that such results were not discussed in the literature yet. The emitted light was collected by collimating optics and transmitted by an optical fibre to the entrance slit of the 0,5 m spectrograph (Acton), equipped with a grating of 300 grooves/mm (blaze at 500 nm) and 150 grooves/mm (blaze at 500 nm) for the UV and VIS regions. The dispersed light was registered by a Peltier-cooled CCD camera

(CVI) and the respective synchronization of the excitation pulse, light detection and recording of the spectra was ensured by use of the delayed pulse generator DGD 535 (Stanford Res.).

The colorimetric measurements were performed in conformance with the LAB colour space, using the unique Display Measurement System constructed on the basis of DMS of Autronic-Melchers GmbH. The diameter of the detected spot was 1.25 mm, and a layer of the magnesium oxide was used as a reference. Four types of samples were studied:

– covered with thin black crust, non-cleaned by the laser,
– covered, laser cleaned,
– without encrustation, non-irradiated,
– without encrustation, laser irradiated.

For surface cleaning by the 1064 nm laser the energy density of 0.5 J/cm^2 was set below the ablation threshold of the sandstone. The laser was operated at the pulse frequency of 2 Hz and the number of pulses applied to each surface location did not exceed 50.

3 Results

The LIPS spectra averaged over several measurements and recorded for a number of successive cleaning pulses are shown for the 1st and 50th pulse in Figs. 1a and 1b for the plasma excitation at 355 nm and 1064 nm, respectively. The dotted lines represent spectra of the superficial encrustation and the solid ones those of the sandstone substrate. The assignment of spectral lines was based on the literature and the line positions are additionally listed in Fig. 2 [11, 12]. Comparison of the results indicates that spectra of the UV-excited plasma are more complex, thus containing more information.

The preferred conditions of LIPS measurements are concluded from the above and changes in intensities of selected peaks observed during the cleaning process are shown in Fig. 2. In graphs a, b, c and d the irradiation-dependent intensities of the spectral lines belong to Si, Ca, Al, Mg, Ba and Li elements in the removed layer.

Most of the lines are characterized by the intensity peaks decreasing markedly under prolonged irradiation, i.e. with the pulse number, and for some of them the decrease proceeds to the reference level after several pulses. This is clearly observed for the lines of Ca I, Ca II and A1 I. This is in agreement with the previous studies, where the rate of encrustation removal was investigated in dependence on the acoustic signal amplitude under various process conditions [13]. However, for Si I and Si II lines a different course of changes is observed. A decrease of these peak intensities is preceded by an initial growth. This difference is most probably caused by the fact that Si lines originate from the components of sandstone and the other lines – from

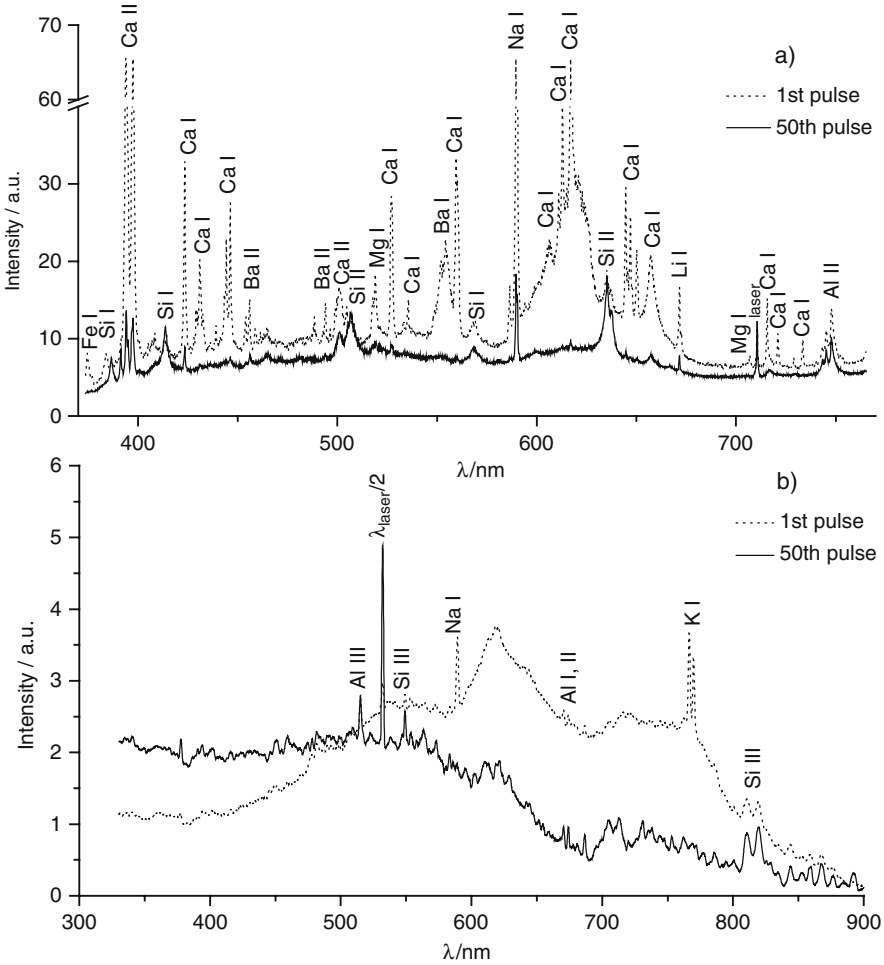

Fig. 1. The LIPS spectra corresponding to the 1st and 50th pulse: (**a**) of 355 nm laser radiation; (**b**) of 1064 nm laser radiation; intensities in Fig. (**a**) and (**b**) are comparable

the dirt coverage. The presence of other elements in the crust and also in the bulk of the stone was recorded, too. The respective lines appear in the spectrum just after the first excitation pulse. For instance, the presence of Ca at the surface and also in the sandstone bulk is due to the fact that it belongs to the binder, and under the influence of water and SO_2 it changes into gypsum which accumulates at the surface. These results are confirmed by a SEM study, too [14].

A series of colorimetric measurements was performed both for the crust-covered samples and non-covered ones. In addition, the crust-free samples

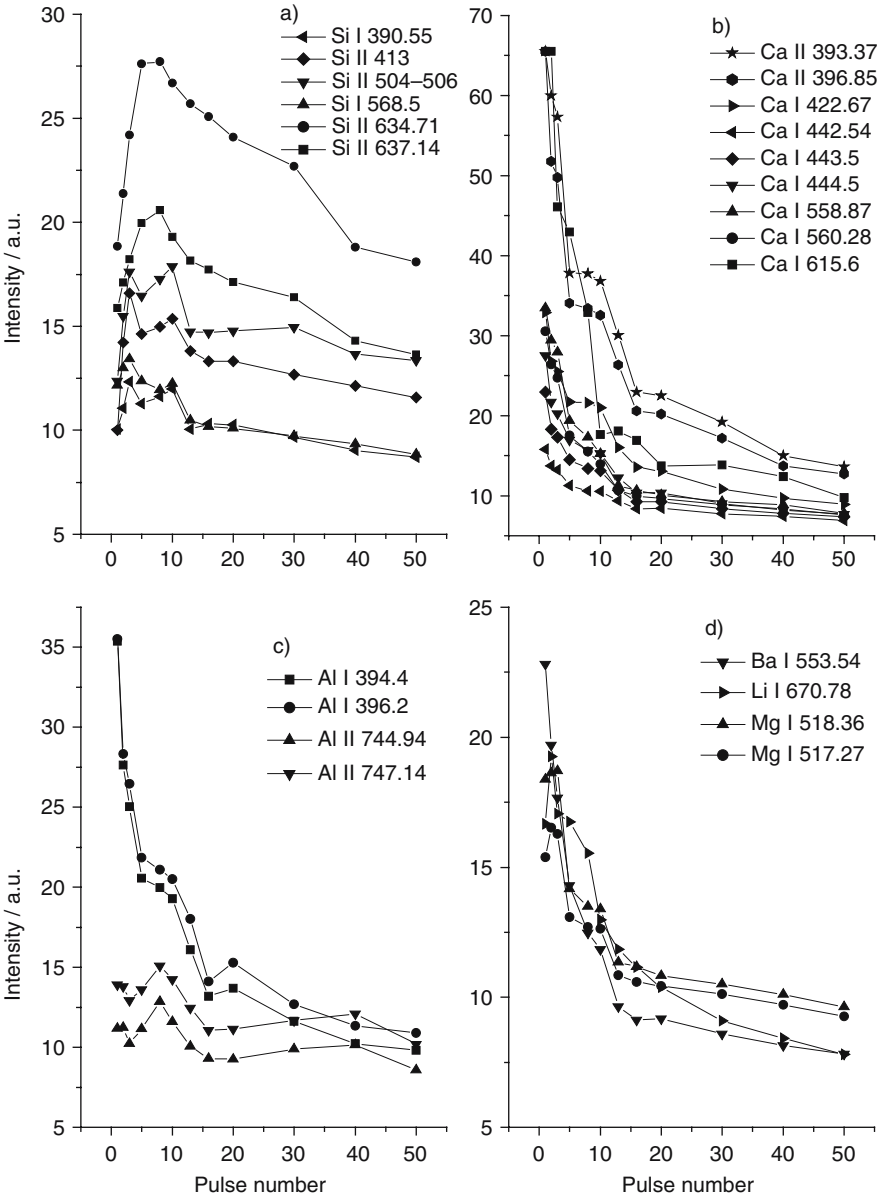

Fig. 2. Dependence of the line intensities of the LIPS spectra recorded under 355 nm excitation on the laser pulse number for selected elements: (**a**) Si I and Si II, (**b**) Ca I and Ca II, (**c**) Al I and Al II and (**d**) Ba I, Li I and Mg I

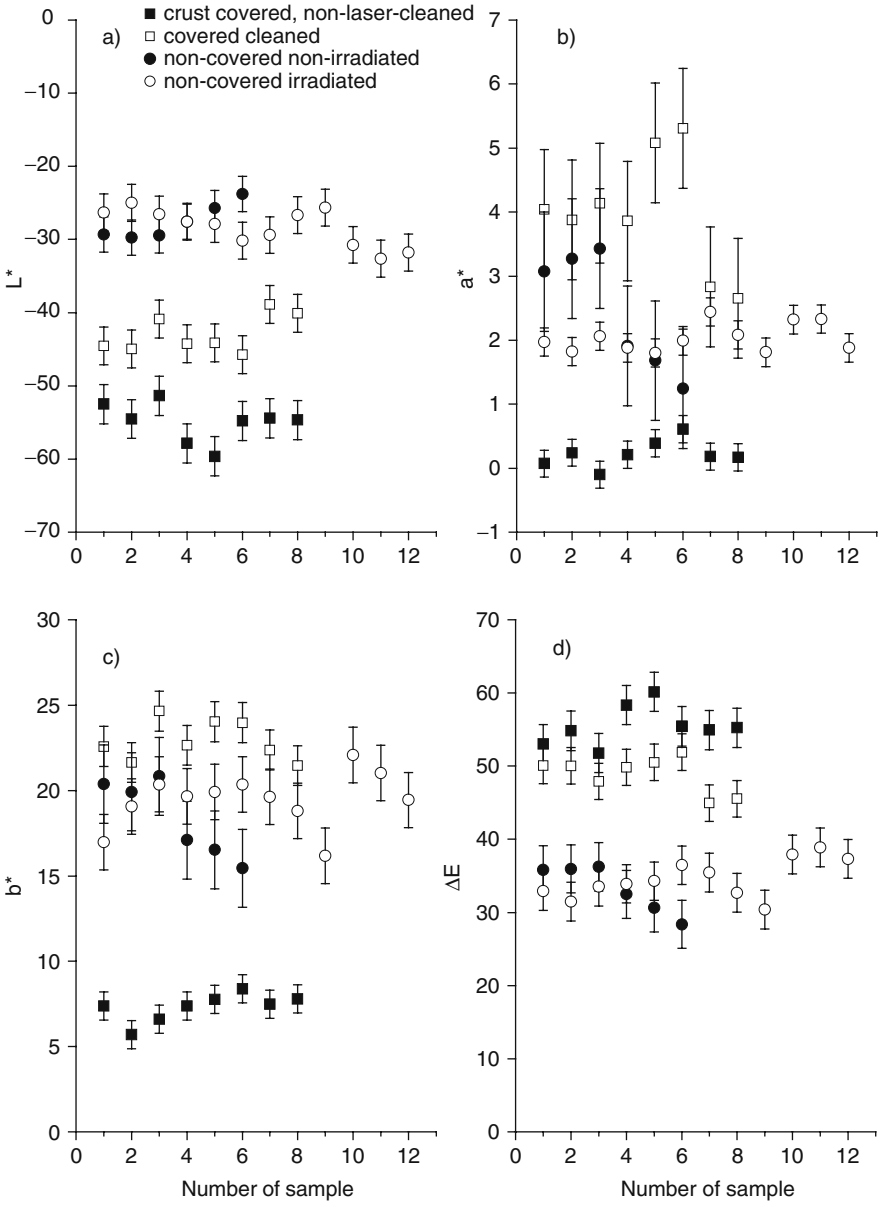

Fig. 3. The changes in colorimetric parameters: **dL** – (**a**), **da** – (**b**), **db** – (**c**) and **dE** – (**d**); bars correspond to standard deviation of individual data; the cleaning and irradiation were performed with the 1064 nm laser

were irradiated at the same laser wavelengths as used for the crust removal of the historical ones. This made possible for comparison of the results and answering the question if the colour differences or yellowing due to laser irradiation can be observed for the Gotlandic sandstone. The numerical data corresponding to the changes in lightness **L***, the colour changes **a*** and **b*** related to the MgO reference, and also the resulting changes **ΔE** all given as averages of data series together with error bars are shown in Fig. 3. Results obtained for the historical, crust-covered samples (squares) indicate that after cleaning the sample becomes more bright ($\Delta_{L^*} = 12 \pm 4$), more red ($\Delta_{a^*} = 4 \pm 1$) and more yellow ($\Delta_{b^*} = 16 \pm 2$). The slight increase of the colorimetric parameters results from the surface cleaning and is due to the better exposition of the original material and its natural hue being set apart.

For the sandstone not covered by the crust (circles) the differences between colorimetric parameters for the laser irradiated and non-irradiated samples were lower than the experimental error. The error was relatively large because of the variation in the natural hue of the samples. It has been concluded that the applied laser radiation did not influence the colorimetric parameters of the historical, non-contaminated Gotlandic sandstone.

4 Conclusions

The laser surface cleaning process of the Gotlandic sandstone was monitored by means of the LIPS spectroscopic technique. The components of the crust layer such as Ca, Al, Mg, Ba and Li and of the top stone layer, Si, were identified. The exponential decay of the line intensities assigned to the crust was in agreement with data obtained from the acoustic process monitoring and with the literature.

The colorimetric measurements did not reveal systematic changes in colour of the Gotlandic sandstone irradiated by the 1064 nm laser and the natural hue of the original material remained unchanged when observed on the short time scale. The long term effects require further investigation.

The results indicate that the on-line LIPS diagnostics of the laser cleaning of Gotlandic sandstone can be effective when using UV excitation (355 nm). The practical application is of particular interest in the case of stone covered with specific crust and cleaned by means of the 355 nm laser.

Acknowledgements

This work was supported by the Polish State Committee for Scientific Research via project SPUB-M/DZ220. The authors are grateful to Dr. A. Mazikowski for technical assistance.

References

1. Jarmontowicz, R. Krzywoblocka-Laurow, and J. Lehmann, Sandstone in historical architecture and sculpture (in Polish), *TOZ*, Warsaw, 1994
2. Majdzinska, in *Students about conservation, Proceedings of the 3rd Polish Scientific Conference of Students of Art Conservation* (in Polish), 105–118, 2001
3. W. Domaslowski et al., Prophylactic conservation of the stone historical objects (in Polish), *Nicholas Copernicus University Press*, Torun, 1993
4. M. Cooper, Laser cleaning in conservation, *Butterworth Heinemann*, 1997
5. G. Marakis et al., in *Journal of Cultural Heritage*, Vol. 1, Suppl. 1, 61–64, 2000
6. S. Klein et al., in *Appl. Surf. Sci.* 171, 242–251, 2001
7. K. Beadman and J. Scarrow, in *Journal of Architectural Conservation* No 2, 39–53 July 1998
8. S. Klein, T. Stratoudaki, V. Zafiropulos, J. Hildenhagen, K. Dickmann, and Th. Lehmkuhl, in *Applied Physics A* 69, 441–444, 1999
9. S. Klein, J. Hildenhagen, K. Dickmann, T. Stratoudaki, V. Zafiropulos, in *Journal of Cultural Heritage* Vol. 1, Suppl. 1, 287–292, 2000
10. G. Sabatini, M. Giamello, R. Pini, S. Siano, and R. Salimbeni, in *Journal of Cultural Heritage*, Vol. 1, Suppl. 1, 9–19, 2000
11. N. Zajdel, W. K. Prokofiew, C. M. Rajskij, W. A. Slawnyj, and J. J. Szrejder, Tablicy spektralnych linij, *Izdatelstwo "Nauka", Glawnaja Redakcija Fiziko-matematiczeskoj literatury,* Moscow, 1977
12. NIST Atomic Spectra Database, http://physics.nist.gov/cgi-bin/AtData/main_asd
13. M. Jankowska and G. Sliwinski, in *Journal of Cultural Heritage*, Vol. 4, Suppl. 1, 65–71, 2003
14. M. Jankowska and G. Sliwinski, in *Radiation Physics and Chemistry*, Vol./Issue 68/1–2, 147–152, 2003

From the Research Lab to the Restoration Yard: Practical Procedures to Evaluate *in situ* the Use of Laser Cleaning on Façades

R. Pini[1] and C. Baracchini[2]

[1] Istituto di Fisica Applicata, Consiglio Nazionale delle Ricerche, Firenze, Italy
R.Pini@ifac.cnr.it
[2] Soprintendenza Beni Ambientali, Architettonici, Artistici e Storici, Pisa,

Abstract. We present three examples of simplified tests and measurements which can be performed *in situ* to evaluate laser cleaning in real application cases: reflectance analysis, identification of ablation and damage thresholds, and evaluation of laser cleaning productivity. Such tests have been applied in the restoration yards of two churches in Pisa.

1 Introduction

Laser cleaning applications to façades of historical buildings have been widely reported in the past ten years. Nevertheless, in most of the cases, tests were performed on surfaces of limited size in order to obtain scientific information, rather than to perform and complete large-scale conservation interventions, and in most of the cases the laser was operated by scientists instead of restorers.

In Italy, and in particular in Tuscany, this picture is changing, thanks to the interest of local *Soprintendenze* (public conservation boards, responsible of the safeguard of Cultural Heritage) and to the support of specific Regional Programs which have stimulated the transfer of new technologies, including lasers, from research groups to conservation enterprises and services.

This step toward the practical use of laser cleaning in the restoration yard is evidencing some important issues, that will need further development:

- Training of expert laser operators,
- Definition and standardization of performances of commercial laser devices,
- Definition and standardization of protocols for the correct application of laser leaning and for the assessment of this technique,
- Evaluation of times and costs of the laser intervention.

Moreover, beside scientific analyses and tests, typically performed in the preliminary phase to determine the state of conservation of the materials to be treated, our experiences in real operative cases of laser cleaning on large surfaces of façades suggested that restorers and operators in charge of the work would take advantage of some simplified procedures and tests

to be used *in situ* in order to evaluate and control safety, effectiveness and productivity of laser operations during the intervention.

In the following we present some examples of these simplified tests that have been employed in two pilot restoration yards in Pisa. They represent to some extent a first approach toward the definition of laser application protocols. They were designed to be easily applicable *in situ* and to be used by restorers which do not have a university level scientific background.

2 Reflectance Analysis

As is well known, laser ablation offers gradual and controlled removal of alteration layers, allowing precise cleaning up to a pre-determined level. In this respect, the use of colorimetric and reflectance analysis *in situ* during laser operations can be useful to provide objective and quantitative reference of the cleaning degree to be reached, resulting in a more homogeneous aspect of the cleaned surface. Fig. 1 shows an example of spectral reflectance measurements which have been routinely performed in the restoration yards of Pisa, by means of a portable spectrometer in order to evaluate the cleaning level on different sites of the façade. Such measurements were typically associated to mineralogical and petrographic analyses on samples collected from the same sites in order to identify surface materials.

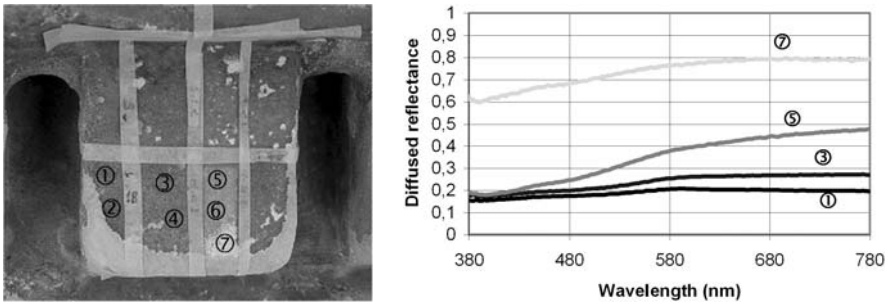

Fig. 1. Spectral reflectance measurements on different levels of laser cleaning performed with a Nd:YAG laser on polluted marble. *Left*: sampling site; *right*: results

Moreover, another parameter which is important to know is the integrated reflectance R of the materials to be cleaned, as measured at the laser emission wavelength, since it determines the absorbance $A = 1 - R$, corresponding to the fraction of laser light effectively absorbed by the material. In fact, when laser absorption of the alteration is higher than that of the stone substrate, the self-limiting cleaning effect can be accomplished, which is characteristic of laser ablation and greatly simplifies cleaning operations. Worth noting is that this value can be substantially different from the one in the visible,

depending on the laser wavelength. Table 1 reports a comparison among values measured on the sites of Fig. 1, for R in the visible and at 1064 nm. Of course, measurements of R at the laser wavelength have to be executed in the exact operative conditions of laser cleaning, for example on wet surfaces, whenever sprayed water will be used in association with laser ablation (see values in brackets of Table 1).

Table 1. Integrated reflectance of the sites of Fig. 1. Material types were determined by petrographic analysis. Italic numbers in brackets indicate reflectance values of wet surfaces

Site	Surface material	Integrated reflectance in the visible [%]	Reflectance @ 1064 nm [%]
1	black crust	20	21, (*14*)
2	black crust	20	–
3	partially cleaned black crust	24	30, (*14*)
4	partially cleaned black crust	25	30, (*14*)
5	Ca-oxalate film	36	66, (*59*)
6	Ca-oxalate film	38	68, (*61*)
7	sulphated marble	75	–

In our applications, considering that the Nd:YAG emission wavelength is usually out of the sampling range of portable spectrometers, we devised a simple and portable device to perform such a measurement, composed of an integrating sphere, an energy meter and the hand piece of the laser itself, used as the light source in condition of low pulse energy. Fig. 2 shows the scheme of this device and its use in the restoration yard by the restorer.

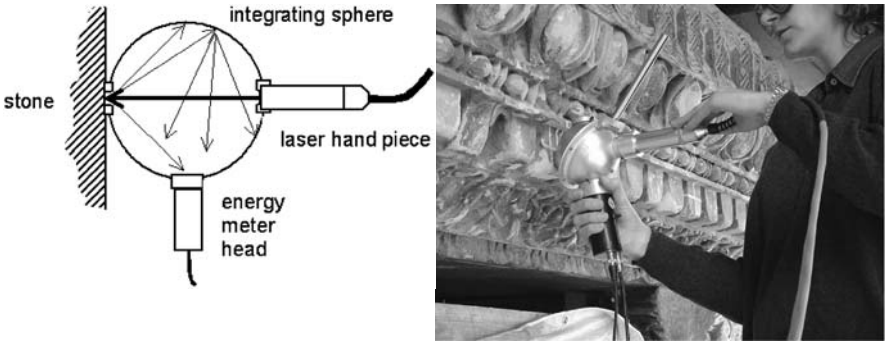

Fig. 2. Integrating sphere for reflectance measurements at the laser emission wavelength

3 Identification of Ablation and Damage Thresholds

The determination of laser ablation thresholds and ablation rate curves of stones and stone alterations as a function of the laser fluence is typically accomplished by means of laboratory measurements on collected samples. Also, identification of laser damage thresholds is done by careful microscopic analysis on the treated surfaces. Such measurements are not easy to be performed and require instruments that cannot be used *in situ* (such as precision scale, microscope, SEM, profilometer, etc.). On the other hand, in many practical cases what the laser operator actually needs is the identification of the more suitable operative range of laser fluences to be employed on a specific site to be cleaned. Such an operative range can be defined in a simplified way, by assuming, as the lower limit, the ablation threshold of the material to be removed, whilst the upper limit is represented by the damage threshold of the underlying material to be preserved, such as the patina. This last value corresponds in general to the ablation threshold of the patina. In case of evidence of bleaching, yellowing and other colour change effects on the patina occurring at a lower fluence than the one of ablation, the damage threshold must be assessed also by reflectance measurements on larger areas of ∼10-50 cm^2 cleaned by the laser.An example of a simple application protocol to achieve such a result is the following:

Test Conditions:

Let us consider the very frequent case of laser cleaning of a calcareous stone where previously performed petrographic analysis has revealed a stratigraphy composed of a calcium oxalate film and an overlying thick layer of black crusts.

Principle:

The aim of the test is to evaluate the operative range of laser fluences, which is in this case delimited between the ablation threshold of the black crust and the damage threshold of the calcium oxalate film.

Method:

Laser ablation tests are performed on small size areas for increasing laser fluences and the result is observed by a portable microscope (e.g. 30 ×).

In detail:

- The laser hand piece is locked in a fixed position to keep constant both the irradiated area and the distance from stone surface (Fig. 3, left).
- The laser spot diameter is measured in order to calculate the laser fluence
- Contiguous ablation spots (Fig. 3, right) are produced, each one at the same laser repetition rate and with the same number of pulses.

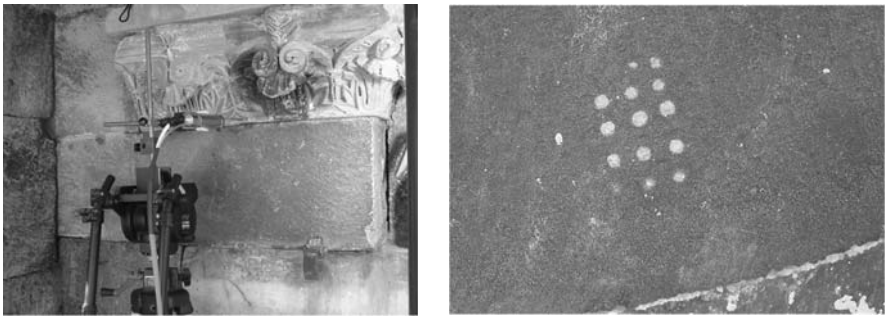

Fig. 3. Ablation test on marble and detail of laser ablation spots

Test Report:

Laser parameters and observations are recorded as in Table 1. Finally, results are summarized in a diagram that can be easily interpreted by laser operators, as shown in Fig. 4.

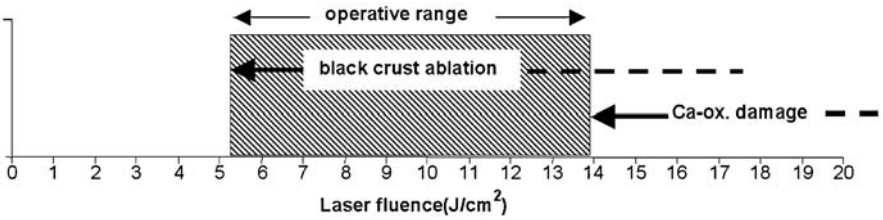

Fig. 4. Operative range: the dashed area indicates the interval allowing safe cleaning of black crust with preservation of the patina. The higher values in this range provide the higher productivity

Note:

The test has to be repeated in all the sites where the stratigraphy of the alteration varies, as previously verified by petrographic analysis.

The results of Table 2 can be synthesized in the schematic diagram shown in Fig. 4, which permits ready visualization of the operative range for safe laser cleaning on polluted marble.

4 Evaluation of Laser Cleaning Productivity

Restorers and conservation enterprises are usually familiar with methods to provide preliminary estimation of times and costs of conventional cleaning

Table 2. Example of a test report for the evaluation of ablation thresholds

Site XX: Marble with black crusts overlying a Ca-oxalate film
Laser type: Nd:YAG Mod.XX – 50 microseconds pulse duration
Spot diam.: 2.70 mm, Spot area: 0.0573 cm^2
Exposure time:10 sec, Rep. rate: 5 Hz
Note: distilled water sprayed on surface during laser cleaning

Laser Energy (mJ)	Fluence (J/cm^2)	Observations
100	1,75	no effect
200	3,49	weak ablation of black crust
300	5,24	ablation of black crust, no effect on Ca-ox. film
400	6,99	ablation of black crust, no effect on Ca-ox. film
500	8,73	ablation of black crust, no effect on Ca-ox. film
600	10,48	ablation of black crust, no effect on Ca-ox. film
700	12,23	ablation of black crust, no effect on Ca-ox. film
800	13,97	ablation of black crust, bleaching of Ca-ox. film
900	15,72	ablation of Ca-ox. film
1000	17,47	ablation of Ca-ox. film

techniques, but can find some trouble to manage laser parameters in order to optimise working productivity when laser cleaning is concerned. As previously described, laser fluence is one of the main emission parameters that has to be considered to compare different working conditions.

To simplify this we asked the laser manufacturer to improve the devices to be used in the restoration yard by providing the operator with direct read out of the laser fluence on the display, after the laser spot diameter has been entered by digitising its value on the keyboard. Considering that such lasers are equipped with a hand piece including a variable focusing system, it was necessary to pre-calibrate the achievable spot sizes by fixing and numbering the variation steps corresponding to different distances between the fibre and the focusing optics. Such a calibration table is presently included in the laser manual. In our opinion the easy readability of the laser fluence should become a standard requirement for all laser manufacturers. In this condition, the restorer can simply carry out *in situ* the necessary tests to evaluate laser cleaning times, without further measuring equipment.

A possible protocol for such tests may be the following:

– The "operative range" of laser cleaning is measured, as described earlier.
– The restorer chooses three values of laser fluence included in this range corresponding, respectively, to a value just above the ablation threshold, a value in the middle of the range and a value close to the upper limit of the damage threshold.

Fig. 5. Laser cleaning tests performed on flat and decorated surface of a façade with a Nd:YAG laser

- The laser spot diameter to perform the tests is set according to the following principle:
  a) Working on flat surfaces, the spot diameter has to be maximized (and consequently the pulse energy will be increased to maintain the fixed fluence) in order to maximize cleaning productivity
  b) On decorated surfaces, the maximum usable spot diameter is determined by the minimum size of the details of the decoration
- Cleaning tests are executed on sampling areas of 50–100 cm^2.

An example of the results of such a test is described in Fig. 5 and Table 3. In details, this is the case of a façade made of white carbonatic stone (marble from San Giuliano) where the alteration is composed of two distinct calcium oxalate patinas. The aim of laser cleaning was to remove the upper dark patina, and to preserve the lower clearer one. Optimum fluence values we found, as reported in Table 3, are about 50% greater than those at the ablation threshold. In this case, it was not convenient to increase the fluence in order to increase the cleaning productivity, since just one laser shot was sufficient to remove the upper dark patina.

Table 3. Optimised values of laser cleaning productivity on the surfaces of Fig. 5

Sites A, B, C: San Giuliano marble with two superimposed Ca-oxalate films
Laser type: Nd:YAG Mod.XY, 100 microseconds pulse duration, Rep. rate: 15 Hz
Note: distilled H2O sprayed on surfaces during laser cleaning

Site	Laser spot diam. [mm]	Laser fluence [J/cm^2]	Surface (plane) [cm^2]	Equivalent surface [cm^2]	Cleaning time [seconds]	Clean. time per m^2 [hours/m^2]
A	6	4.2	57.2	57.2(×1)[1]	143	6.9
B	6	4.2	135.8	271.6(×2)[1]	813	16.7(8.3)[2]
C	5	6.1	33.3	99.9(×3)[1]	328	27.2(9.1)[2]

[1] Surface correction factor [2] Values in brackets referred to corrected surfaces

5 Conclusions

In our opinion, beside scientific demonstrations on the effectiveness and safety of laser cleaning in conservation, other practical aspects have to be investigated to favour the diffusion of this technique. Here we described three examples of tests that we designed to facilitate laser operation in real application cases. They can represent a first step toward the definition of recommendations and standardized protocols to be used in the restoration yard to assess the correct application of laser cleaning.

Acknowledgements

This study has been carried out in the frame of the "OPTOCANTIERI" Project, supported by the Program of Innovative Actions of Tuscany Region.

Sensor Concept for Controlled Laser Cleaning via Photodiode

M. Lentjes, D. Klomp, and K. Dickmann

Lasercenter Fachhochschule Münster (LFM), FB Physikalische Technik,
University of Applied Sciences, Stegerwaldstr. 39, 48565 Steinfurt, Germany
m_lentjes@fh-muenster.de

Abstract. In the field of laser cleaning of artworks the effect of "over-cleaning" is a commonly well known problem. The detection of laser induced plasma is one possibility in order to identify the kind of material just being irradiated by the laser beam. LIBS is a powerful method for the extraction of spectral information. Instead the detection of the plasma intensity contains much less information. However, this can be realised by using a fast photodiode. It has turned out that for several applications in laser cleaning of artworks a reliable identification of layers during the cleaning process is possible. In cooperation with restorers we proved that this low-cost method may be used for online monitoring as well as automated closed loop cleaning.

1 Introduction

In general laser removal of various layers from artworks takes place at high intensities of some 10 MW/cm^2 accompanied by a plasma plume above the irradiated area. The properties of the plasma mainly depend on the laser intensity, laser wavelength and chemical composition of the ablated matter. The plasma signal is characterized by the duration, spectrum and amplitude.

Utilisation of the plasma signal for online process control in order to avoid over-cleaning is well known for laser cleaning of artworks [1–3]. Therefore mainly Laser Induced Breakdown Spectroscopy (LIBS) is used and has been proved in several application cases [4–6]. In contrast to the spectrum of the plasma its integral value contains much less information about the removed matter. However, it may be sufficient for selected applications as has been reported in [7]. In our experimental setup we use a fast photodiode for the plasma detection. Furthermore in combination with separate optical filters even limited spectral information may be extracted from the plasma signal.

2 Experimental Setup

The schematic of the detection principle is shown in Fig. 1 For irradiation of various artwork samples we used a KrF-excimer laser (Lambda, LPX 305i) with maximum pulse energy of 1200 mJ, repetition rate 1 – 50 Hz, pulse duration 20 – 40 ns (@ $\lambda = 248$ nm). A part of the laser induced plasma radiation

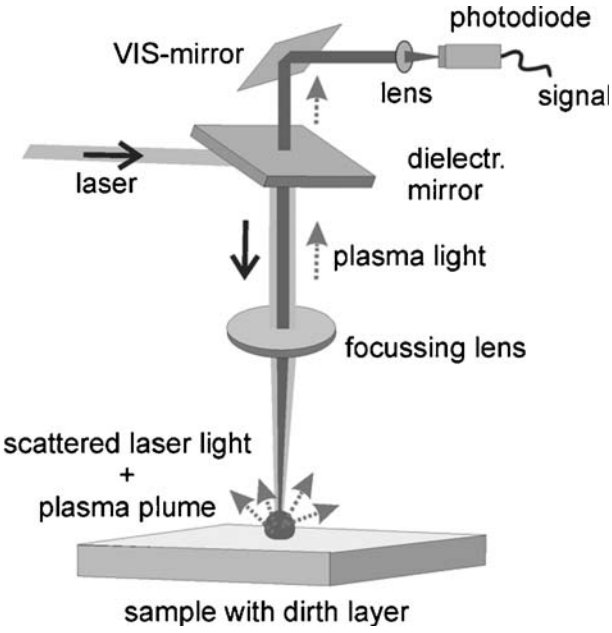

Fig. 1. Schematic diagram of the optical setup

is collimated by the focussing lens and is directed through the dielectric mirror (HR@248 nm) onto a fast silicon PIN photodiode ($T_{rise} < 1$ ns). In the present case a separation of the scattered laser radiation from plasma radiation was ensured by the absorption of optical elements (@ 248 nm) in front of the photodiode as well as low sensitivity of the photodiode @ 248 nm.

The output signal of the photodiode may be used either for monitoring the cleaning process by the restorer or for automated closed loop cleaning. The corresponding setup is shown in Fig. 2. The oscilloscope, laser and xy-stage controller are linked up by a PC, which controls the data transfer and communication between these modules by a LabView written program.

3 Control Process

A reference value of the plasma signal ("compare level") being necessary for comparison of the required and actual signal has to be defined by the operator. This can be found either based on restorers experience or by a teaching procedure on test samples. During the laser removal process, the plasma signal of each laser pulse is compared with the reference signal. Laser removal will continue until the reference signal is reached. In a next step, corresponding to the spot size, the xy-control moves the sample to a new position directly beside it. The flow diagram is given in Fig. 3.

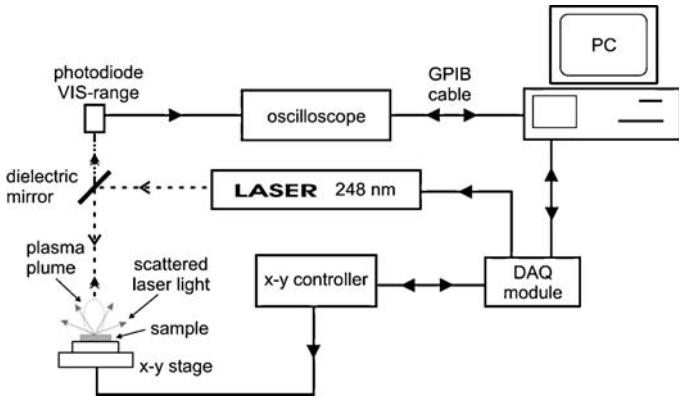

Fig. 2. Schematic of electronic setup for controlled laser cleaning via photodiode

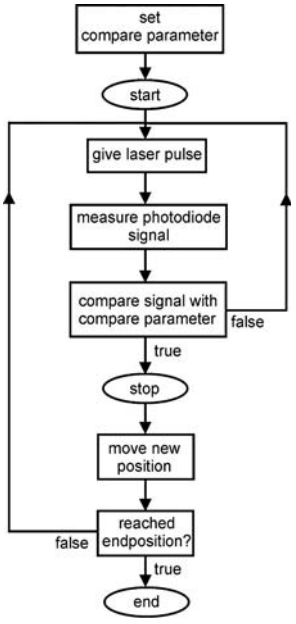

Fig. 3. Flow-diagram of closed loop cleaning operation

4 Results

On various layers/substrate-arrangements we observed a distinct alteration of the plasma signal going along with the removal process. Using this signal, not only different types of layers could be detected, but also gradients of compositions within the same layer. Figures 4a–4d shows the recorded diode signals versus pulse numbers and the corresponding samples with cleaned areas.

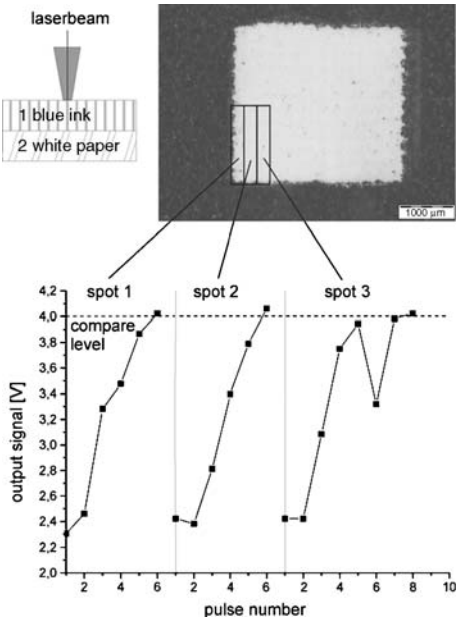

Fig. 4a. Blue ink removed from paper by controlled laser cleaning. Monitored photodiode signal (*peak*) vs number of laser pulses for the first three spots

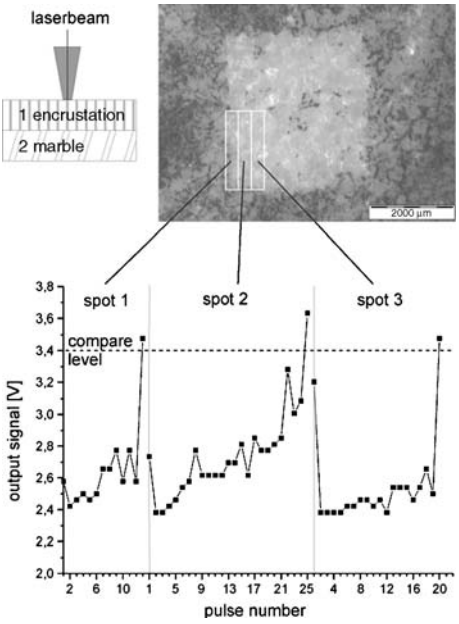

Fig. 4b. Encrustation removed from marble by controlled laser cleaning. Monitored photodiode signal (*peak*) vs number of laser pulses for the first three spots

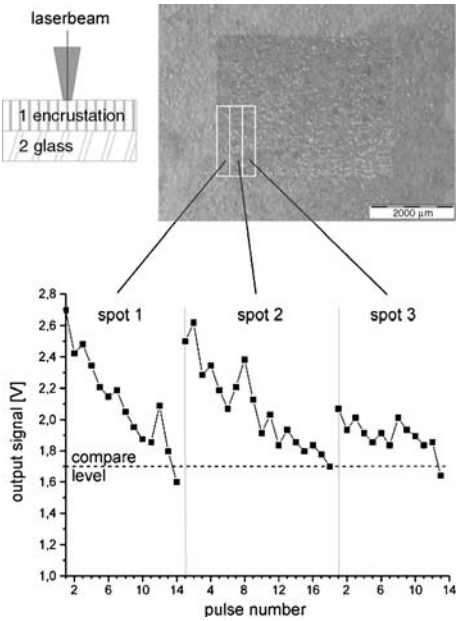

Fig. 4c. Encrustation removed from glass by controlled laser cleaning. Monitored photodiode signal (*peak*) vs number of laser pulses for the first three spots

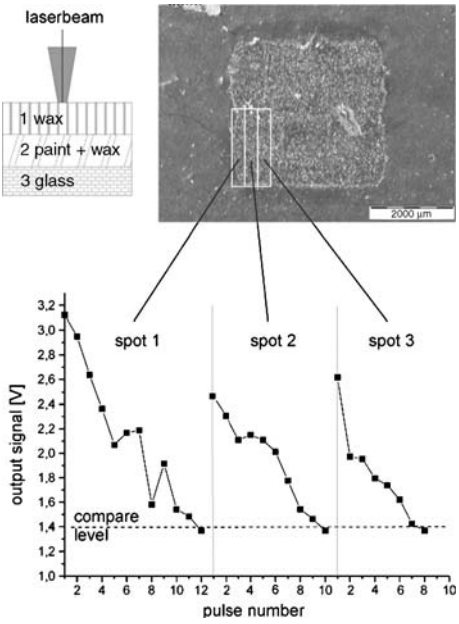

Fig. 4d. Wax-layer removed from paint by controlled laser cleaning. Monitored photodiode signal (*peak*) vs number of laser pulses for the first three spots

In Figs. 4a and 4b there is a rise of the photodiode signal with increasing pulse number. In this case the plasma intensity is increasing when approaching to the original surface. The fast increasing graph in Fig. 4a shows that the composition within the same layer (here blue ink) differs, while penetrating deeper into this layer. In contrast, Fig. 4b reveals a more homogeneous composition of the layer to be removed. Fig. 4c and 4d display a decreasing plasma intensity during the cleaning process. In these cases the distinct downward tendency of the detected plasma signals enables a reliable identification of various layers during the ablation process. Concluding, deduced from the Figs. 4a, 4b, 4c, 4d it is obvious that each individual spot on the surface needs a specific number of pulses for complete cleaning. With increasing inhomogeneity of the surface layer (e.g. artworks) this fact gains of importance. In first attempts we have used this detector principle for successful closed-loop laser cleaning.

Acknowledgements

This project is funded by the EUREGIO (INTERREG III Program) within the "EUREGIO CENTER for Art Restoration Technology" (ECEACT).

References

1. Gobernado-Mitre, A. C. Prieto, V. Zafiropulos, Y. Spetsidou, and C. Fotakis, On-Line Monitoring of Laser Cleaning of Limestone by Laser-Induced Breakdown Spectroscopy and Laser-Induced Fluorescence, in *Appl. Spectroscopy*, Vol 51, No 8, 1997, pp 1125–1129
2. P. V. Maravelaki, V. Zafiropulos, V. Kilikoglou, M. Kalaitzaki, and C. Fotakis, Laser-induced breakdown spectroscopy as a diagnostic technique for the laser cleaning of marble, in *Spectrochimica Acta*, Part B, 52, 1997, pp 41–53
3. D. Anglos, S. Couris, A. Mavromanolakis, I. Zergioti, M. Solomidou, W. Q. Liu, T. G. Papazoglou, V. Zafiropulos, C. Fotakis, M. Doulgeridis, and A. Fostiridou, Laser Induced Breakdown Spectroscopy (LIBS) and Laser Induced Fluorescence (LIF) Spectroscopy, LACONA 1, in *Restauratorenblätter*, Wien 1997, pp 113–118
4. S. Klein, T. Stratoudaki, V. Zafiropulos, J. Hildenhagen, K. Dickmann, and Th. Lehmkuhl, Laser-induced breakdown spectroscopy for on-line control of laser cleaning of sandstone and stained glass, in *Appl. Physics A*, 69, 1999, pp 441–444
5. J. H. Scholten, J. M. Teule, V. Zafiropulos, and R. M. A. Heeren, Controlled laser cleaning of painted artworks using accurate beam manipulation and on-line LIBS-detection, LACONA 3, in *Journal of Cultural Heritage*, Vol.1, Sup.1, 2000, pp 215–220
6. R. Teule, H. Scholten, O. F. v/d Brink, R. M. A. Heeren, V. Zafiropulos, R. Hesterman, M. Castillejo, M. Martín, U. Ullenius, I. Larsson, F. Guerra-Librero, A. Silva, H. Gouveia, and M. B. Albuquerque, Controlled UV laser cleaning of

painted artworks: a systematic effect study on egg tempera paint samples, LACONA 4, in *Journal of Cultural Heritage*, Vol.4, Sup.1, 2003, pp 209–215
7. J. Hildenhagen and K. Dickmann, Low-cost sensor system for online monitoring during laser cleaning, LACONA 4, in *Journal of Cultural Heritage*, Vol.4, Sup.1, 2003, pp 343–346

Ultra-Stable, New Generation Q-Switched Monolithic Laser Cleaners for Fine Art Conservation

F. Brioschi and P. Salvadeo

Quanta System s.p.a., via IV Novembre 116, 21058 Solbiate Olona (VA), Italy
rd@quantasystem.com

Abstract. The increasing use of laser cleaners in fine art conservation boosts the demand on improvements of the laser performances. More power and more wavelengths are required by the current applications, while laser should be more reliable, rugged and compact. The characteristics and performances of a new generation of laser cleaners are presented as a result of a dedicated research and development program.

1 Introduction

One of the main modern goals in art conservation, particularly while focusing on masterpieces located in urban areas, is the fast and effective removal of the so called "black crust", deposits and deterioration layers, caused by pollution, using high intensity laser beams, while preserving the original surfaces texture.

The advantages of laser cleaning are represented by an immediate feedback and almost non-invasive processes, with absolutely no mechanical contact. With lasers, selective treatments vs. wavelength and energy – with full respect of valuable patinas – are now possible.

The laser interaction process is absolutely ecological.

The objective of the study presented here was to develop a new generation of laser cleaners, which are able to deliver more pulse energy, more wavelengths at higher repetition rate.

2 The Laser Cleaning Process

The cleaning techniques consist of different steps. In Q-switched mode, the laser active medium stores the energy in the excited state, releasing it on command ("optical switch") forming a macro pulse, lasting a few nanoseconds. The pulse peak power typically reaches some tens millions of Watts. The emitted power is then absorbed by the solid body under cleaning and furtherly a localised photoablation of the superficial material layer occurs.

This consists in the expansion of a plasma plume with further material tensioning. The subsequent creation of shock waves leads to the final material espulsion.

The cleaning process depends on some different parameters which characterize the laser source. Among these it is worth to mention:

- the pulse energy and duration;
- the beam cross-section over the target;
- the output average power;
- the output wavelength.

The pulse energy, its duration and the beam cross-section determine the intensity of the laser radiation on the surface to be cleaned. The intensity in turn has a strong influence on the cleaning process: higher intensity is in general attractive but could have some unwanted effects to the cleaned surface. To avoid this a laser cleaning system should give the possibility to finely adjust the output intensity in a realiable way, while leaving to the user's experience and sensibility the choice for the optimum cleaning parameters.

On the other hand, new opportunities are offered by the possibility to choose the laser wavelength, which means a better selectivity in the cleaning process. In fact, the absorbed amount of laser energy will depend on the *"color"* of both the laser beam and the treated material, making possible to selectively remove the dirty layer, while leaving unaffected any polychromatic surface below. The new generation of laser cleaners must provide for multiple wavelength emission.

Finally, the speed of the cleaning process will depend on the average output power, which means high repetition rate of the laser pulses.

3 The New Generation Laser Cleaner

Taking into account the extensive studies on the interaction between laser radiation and matter and the recent evolution in the restoration technique, the research and development have been addressed with the aim to make available in selectable way 1064, 532, 355 and 266 nm output wavelengths, with output power up to more than 20 W (depending on wavelength). Therefore, an efficient harmonic generation scheme has been studied, based on both the careful selection of non-linear crystals type and geometry and the design of a high energy, low divergence Q-switched Nd:YAG laser.

The laser source configuration depends on the required specifications which are set by the application. In the basic version the laser is made by a single Positive Branch Unstable Resonator (PBUR), equipped with a Variable Reflectivity Mirror (VRM). The resonator was designed, taking into account the thermal lensing effect in the laser rod, to provide a large mode volume inside the Nd:YAG active medium, which in turn results in high energy output pulse. By choosing suitable values for output coupler reflectivity profile,

resonator magnification and mirror curvature, the resonator can be optimized for low divergence at the desired pump power. While a good far-field beam quality, which means low divergence, is very important for a high conversion efficiency into harmonics, a smooth near-field beam profile is required in the cleaning process where the intensity distribution should be ideally flat over the beam crosssection. This can be achieved not only by a proper design of the resonator, but, depending on the application, also by manipulating the beam with suitable homogenizing optics and focusing lenses.

A single oscillator laser can deliver more than 500 mJ per pulse at 1064 nm, with a pulse duration of about 8 ns and a PRF of 20 Hz. The output beam diameter can be customized, but usually ranges from 7 to 10 mm. This laser configuration can be optionally followed by an amplifier and/or by a second harmonic generation module.

With the amplifier the laser source reaches the maximum output power: more than 900 mJ per pulse at 25 Hz in the infrared and up to 450 mJ in the green can be achieved.

Figure 1 shows a photograph of the laser configuration with oscillator and amplifier followed by the second harmonic generation system. The laser wavelength can be selected between 1064 and 532 nm, by alternatively di-

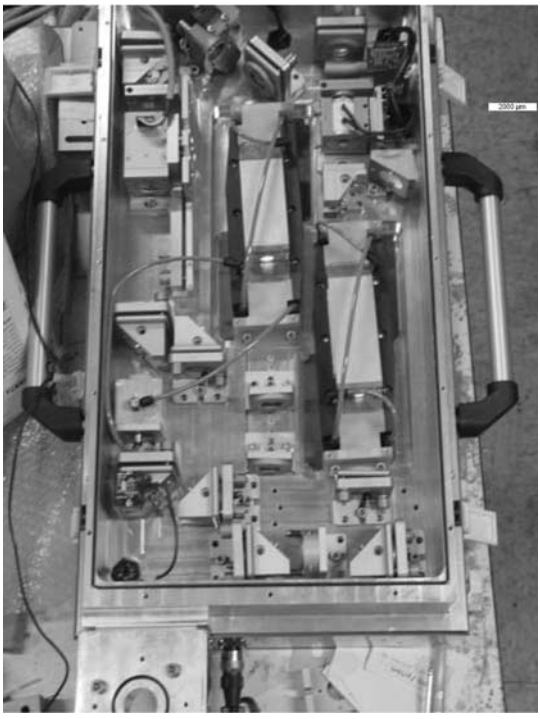

Fig. 1. Layout of the laser with amplifier and 2nd harmonic generation

recting the fundamental beam inside or outside the second harmonic crystal, by means of an automatic movable mirror.

The mechanical structure of the laser is a monolithic box, machined from a single aluminum block. This choice comes from the need to have a rugged, stiff and shock resistant laser head, which is also completely sealed and waterproof. Moreover the optical section is completely separated from any electronic circuit and the laser head is filled with nitrogen. This avoids any contamination of the optical components by dust, water or de-gasing of composite materials.

The laser beam is delivered with an articulated arm with seven mirrors which was designed to preserve the alignment with a very small tolerance. Moreover it is also sealed against dust and water.

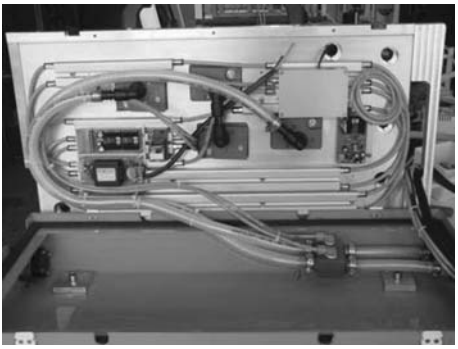

Fig. 2. Thermal stabilization of the laser structure

The thermal and mechanical stability is very important in a system which has to guarantee a very precise alignment of the beam inside the articulated arm. Moreover the laser should be able to operate in bad environmental conditions. Therefore the laser box is kept at constant temperature by the cooling system which includes a chiller. Figure 2 shows the lower side of the laser box with the heat exchanging pipes in which the stabilized water flows. The geometry and the layout of these pipes assure the uniformity of the temperature distribution over the laser structure, preventing any distorption due to thermal gradients.

In order to make easy the utilization of the system, the laser head is separated from the power supply and the cooling system. In this way the laser can be very easily handled over scaffolding, leaving at the ground level the chiller and the electronics. Hence, cables and pipes linking the two parts are 15 m long and the chiller can pump the cooling water to the laser head for a maximum elevation difference of 15 m. In Figs. 3 and 4 the laser head and the power supply-cooling system are shown respectively.

Fig. 3. Power supply and cooling system

Fig. 4. Laser head

The system is controlled by a microprocessor which checks the correct operation according to an auto-diagnostic routine. The laser head is equipped with a console which displays in real-time the most important operating parameters which can be set by the operator by means of the console keyboard.

When UV wavelengths are required by the application, an additional harmonic module is added to the basic structure given in Fig. 1. In Fig. 5 a laser head for the emission at 1064, 532 and 355 nm is shown. The UV harmonic module can house the 3rd and 4th crystals and includes all the automatic mirrors for the selection of the output wavelength.

The module is equipped with two articulated arms, one for IR and green, the other one for 355 and 266 nm laser beam.

As in the case of the basic laser head, the structure of the UV module is all the same machined from a single aluminium block, is sealed and filled with nitrogen.

4 Conclusions

The increasing application of the laser cleaning techniques in fine art restoration has boosted the development of new generation laser cleaners. The results of the research effort can be summarized as follows:

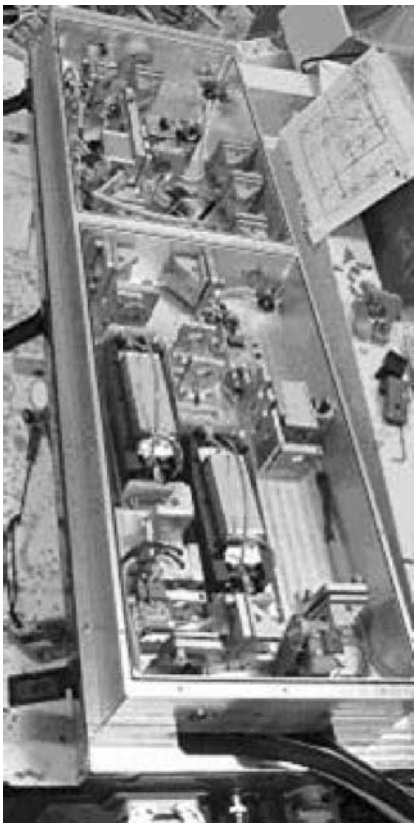

Fig. 5. Laser head for IR, green and UV emission

– more laser wavelengths available for the most advanced applications;
– more pulse energy and more average power for an improved cleaning speed (up to 5 m^2 per hour);
– compact and rugged design for improved reliability and operation in hostile environment.

Future developments will probably lead to new output wavelengths and furtherly reduced size and weight.

Part X

Spectroscopy for Monitoring and Identification

Analysis of Archaeological Objects with LMntI, a New Transportable LIBS Instrument

K. Melessanaki[1], A. Mastrogiannidou[1], S. Chlouveraki[2], S.C. Ferrence[3], P.P. Betancourt[3], and D. Anglos[1]

[1] Institute of Electronic Structure and Laser, Foundation for Research and Technology-Hellas (IESL-FORTH), 71110 Heraklion, Crete, Greece
alina@iesl.forth.gr, anglos@iesl.forth.gr
[2] Institute for Aegean Prehistory - Study Center for East Crete (INSTAP-SCEC), Pacheia Ammos, 72220 Ierapetra, Crete, Greece
[3] Department of Art History, Temple University, Philadelphia PA 19122, USA

Abstract. The analysis of archaeological objects was carried out using LMntI (el-em-ent-one), a new Laser-Induced Breakdown Spectroscopy (LIBS) instrument. The main components and layout of the instrument are briefly described. Indicative results from the analysis of a wide variety of archaeological findings are presented.

1 Introduction

The growing need for scientific analysis of archaeological objects/samples has created an interest for compact, portable instrumentation, which can be used in the conservation laboratory, the museum or even at the excavation site in order to provide in a rapid way, in-situ, analytical information about the qualitative, semi-quantitative or quantitative elemental composition of a wide variety of materials. Research efforts over the last decade [1–11] have shown that Laser-Induced Breakdown Spectroscopy (LIBS) features several analytical advantages and as such, can be a potential alternative to other spectroscopic, mass spectrometric, or X-ray techniques used in art conservation and archaeology [12–19]. LIBS is a practically non-destructive as well as rapid elemental analysis technique with the critical advantage of being applicable in situ, thereby avoiding sampling and sample preparation. Indeed, it has been used for the analysis of pigments in easel paintings, icons, polychromes, pottery, glass and metal objects and the results clearly demonstrate the prospects of the technique to become a useful analytical tool in art and archaeology.

Along these lines, IESL-FORTH in collaboration with INSTAP worked on the development of a compact instrument, designed to suit the demand of the archaeology laboratory for the analysis of materials used in antiquity, aiding the characterization of archaeological objects and/or samples. The outcome of this project is LMntI (el-em-ent-one), a new transportable LIBS instrument (Fig. 1a), for the fast characterization of the elemental content of objects. This paper presents in brief the main components and layout of

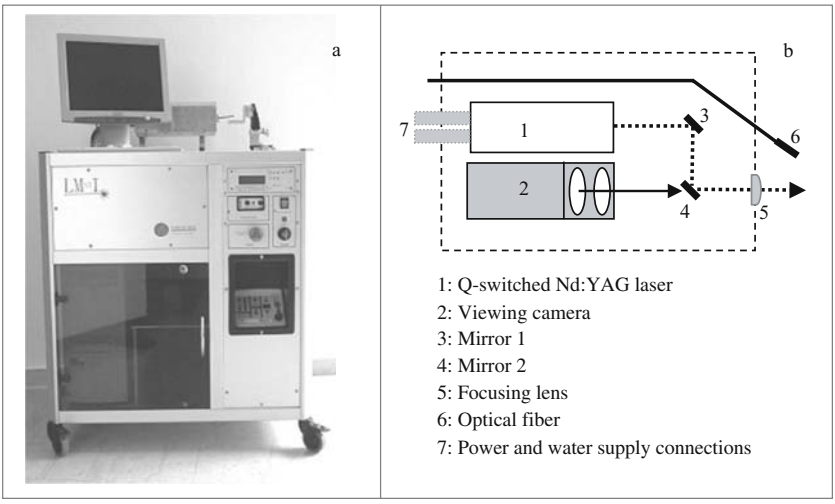

Fig. 1. (**a**) Front view of LMNTI; (**b**) layout of the laser, viewing camera and beam guiding/focusing components

the instrument and provides representative results from the use of LMNTI in the compositional analysis of materials in a wide variety of archaeological findings. All measurements were carried out at the conservation laboratory of INSTAP-SCEC.

2 Experimental Methods

The instrument is a bench-type, independent unit (H: 90 cm, W: 80 cm, D: 65 cm), which is easily transported from site to site on a van while it can be conveniently moved within a laboratory/building on wheels (Fig. 1a). The main components of LMNTI are quite standard and include the following:

- compact Q-switched Nd:YAG laser (with power supply), producing 10 ns pulses at 1064 nm with energy up to 50 mJ;
- 0.19 m imaging spectrograph with two diffraction gratings offering spectral resolution of 0.5 nm and 1 nm respectively;
- quartz optical fiber (0.6 mm) for collecting the plume emission into the spectrograph;
- intensified CCD detector and a pulse generating unit to provide proper gating;
- platform on a XYZ translation stage for mounting and positioning objects and samples;
- small color CCD camera for accurate sample viewing and aiming;
- personal computer for instrument control and data analysis.

The laser, beam guiding optics and viewing camera, are housed in a subunit (Fig. 1b), mounted on the top surface of the instrument along with the sample platform stage. The PC monitor and keyboard are also placed on the top surface. The rest of the components are housed in the main body of the instrument. All components and measurements are controlled through a unified user-friendly software environment, which, in addition, provides the user the ability to perform data analysis.

In typical analysis the sample/object is placed on the translation stage and the area to be analyzed (ca. 100–200 μm diameter) is positioned at the focal point of the focusing lens with the aid of the viewing camera. Emission spectra are recorded following irradiation of the sample with a single laser pulse. When a depth profiling study is carried out, spectra are acquired separately for each one of several successive laser pulses. Elements are identified through the analysis routine of the instrument's software on the basis of the characteristic wavelength values of the emission lines from various elements while the option of overlaying acquired spectra with reference ones for a variety of materials is also available.

3 Results and Discussion

Within the scope of archaeological analysis, the analytical questions facing the conservation scientist or archaeologist range from simple identification of materials to quantitative compositional analysis and aim to the determination of major, minor or even trace elements. Plain qualitative analysis provides valuable information about the identity of materials that can be used to characterize objects as they come out of an excavation or to guide proper conservation actions. Quantitative analysis, on the other hand, can lead to detailed characterization of objects revealing production procedures (pottery making, metallurgy) or even origin of materials. In our test studies with LMNTI, a broad variety of archaeological findings were examined, including painted and glazed pottery, vitreous materials (glass, faience), different types of metal objects, and jewelry. Both qualitative and quantitative analyses were performed addressing different types of problems.

For example, a small bead recently excavated in a Minoan burial site in Crete was examined (Fig 2a). On the basis of its appearance it was initially thought that the bead was made of faience, a form of glass used in antiquity, composed mainly of silica (SiO_2). To our surprise, the LIBS spectrum (Fig. 3a) showed clearly that the bead was made of lead. Evidently extended corrosion had transformed lead into a compact mass of salts/oxides preserving the initial shape but giving the bead the appearance of a faience-like object. It is pointed out that the analysis required a single laser pulse, which instantly revealed the identity of the bead. In a similar case a glass bead (Fig. 2b) was examined in order to identify the pigment used on its surface.

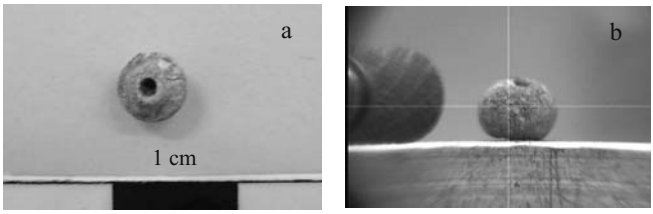

Fig. 2. (**a**) Lead bead from Late-Minoan excavation (**b**) Silver coated glass bead shown on the sample stage with the optical fiber holder on the left; the cross-hair indicates the spot probed by the laser

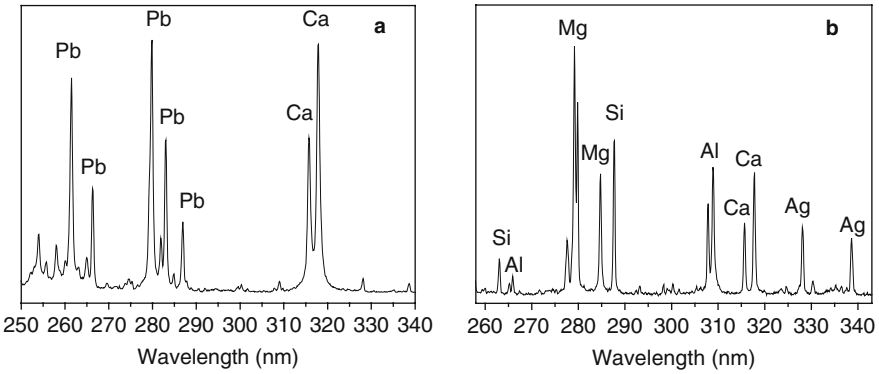

Fig. 3. LIBS spectra from (**a**) lead bead and (**b**) silver coated glass bead

The emission recorded (Fig. 3b) indicates the presence of silver on the surface proving that the corroded grey material covering the bead was actually the remainder of a silver coating. The speed of analysis, as demonstrated in these two cases, is indeed a critical advantage of the LIBS technique, permitting the examination of potentially large numbers of objects, which is often a common situation in archaeological analysis.

Several pottery sherds were also examined focusing particularly on the analysis of paint on their surface. As an example the bright yellow glaze used to decorate the interior and exterior rim of a ceramic bowl (dated from the Ottoman period) was analysed. On the basis of the LIBS spectrum, the glaze was found to contain Pb, Ca, and Cr (Fig. 4a). The combined presence of lead and chromium suggests that chromium yellow (lead chromate, $PbCrO_4$) has been used. Chromium yellow, a synthetic pigment, was introduced as a colouring agent in ca. 1818. This implies that the pottery dates not before the early 19th century, which is in agreement with the excavation data as the sherd was found close to the surface of the area excavated. This type of information suggests that LIBS can be employed, in certain cases, to determine/confirm the date of certain types of pottery.

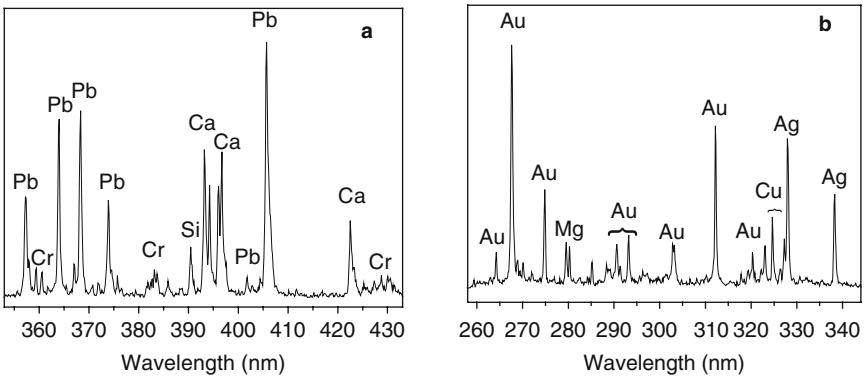

Fig. 4. LIBS spectra from (**a**) yellow paint on glazed pottery and (**b**) golden bead from Minoan necklace

In the analysis of metal objects, several pieces of jewelry (golden beads, ear rings, rings etc.) from the Late Minoan IIIA period (ca. 14th C. BC) were analyzed showing different relative intensities of emission lines of Au, Ag and Cu suggesting variable proportions in the composition of these main components in the alloys used (Fig. 4b). These results indicate that LIBS analysis can quickly provide information on the qualitative and semi-quantitative elemental content of different metal objects and aid their characterization and classification. Quantitative analysis by LIBS is also possible using proper reference samples or alternative calibration-free approaches, such as the one recently used for the quantitative analysis of precious metal alloys [20, 21].

Our tests regarding quantitative analysis were centered on the determination of the amount of tin (Sn) in bronze objects. Copper and bronze were common materials in the Bronze Age for making all types of metal artefacts ranging from tools and weapons to home utensils and jewelry. Bronze is a binary alloy composed of copper and tin. Addition of tin to copper at the level of 5–10% by weight was found to produce a slightly harder alloy, which was easier to cast. Measuring the level of tin in bronze objects can help the archaeologist to classify the object and possibly to determine its origin or extract information on the metallurgical capabilities at the particular site of origin. In addition, proper selection of conservation procedure and materials can be determined on the basis of the type of alloy identified. A reliable methodology to quickly assess the content of tin in bronze objects is of significance for the archaeological conservation laboratory. To this end we have analyzed by LIBS a series of reference bronze samples with tin concentration in the range of 0.5–13% by weight to construct a calibration curve, which is used for the quantitative analysis of bronze objects. The ratio of emission intensity from tin (=286.33 nm) versus that from copper (=282.44 nm) is plotted against the corresponding concentration ratio producing a calibration curve, linear over the range of tin concentrations explored (Fig. 5).

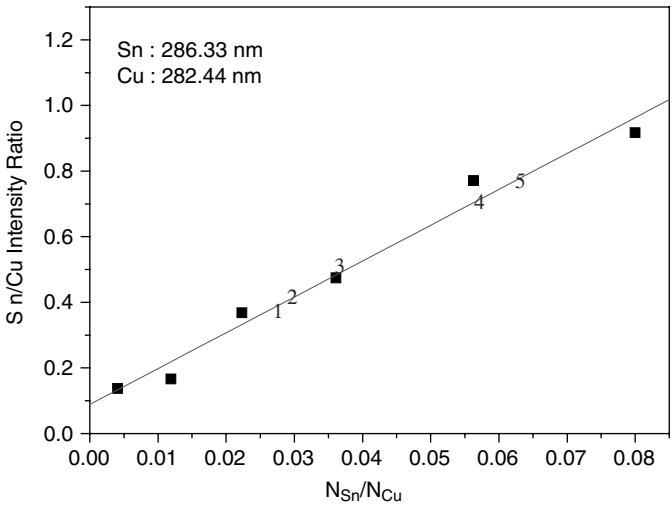

Fig. 5. Calibration curve (Sn/Cu emission intensity ratio vs atomic concentration ratio) employed for bronze analysis. Squares indicate measurements from the reference samples while numbers 1 to 5 indicate data from the ancient bronze objects analyzed

On the basis of this calibration curve a few Minoan bronze objects were analysed and found to contain tin in the range of 5–11% by weight. More work is currently in progress to compare LIBS analysis results in archaeological bronze objects against the actual alloy composition obtained with a standard technique and in addition to assess the reliability of the Cu-Sn reference samples used as models of the ancient bronze alloys. An additional factor of concern that might affect the reliability of the analysis is the extended corrosion of bronze, which leads to material alteration and possible loss of certain metals in the form of soluble salts [22]. To minimize this effect we carefully identified areas on the bronze objects analyzed, where corrosion was minimal and used the first 5 pulses from the laser to remove any superficial corrosion layers.

4 Conclusions

The results presented in this paper demonstrate the advantages of LIBS in obtaining elemental analysis information about the materials used for making and decorating ancient pottery or metal artefacts. The compact instrumentation and user-friendly interface provided by LMNTI makes the instrument a powerful tool for performing routine, rapid, on site sample analysis and/or screening of a large variety of materials leading to quick characterization and classification of archaeological findings.

Acknowledgements

The authors wish to thank INSTAP and IESL-FORTH for funding and collaboration on this project. They are also grateful to T. Brogan of INSTAP-SCEC for the providing access to the metal objects analysed, to M. Panagiotaki and E. Hatzaki for collaboration on the glass and faience analysis and to L. Robbiola for providing the bronze reference samples and valuable input on the analysis of archaeological bronze. The contribution of A. Hatziapostolou, A. Petrakis, K. Hatzigiannakis and S. Kotoulas in construction of LMntI is gratefully acknowledged.

References

1. E. Tognoni, V. Palleschi, M. Corsi, and G. Cristoforetti, Spectrochim. Acta **B57**, 1115, 2002
2. D. Anglos, Appl. Spectrosc., **55**, 186A, 2001
3. D. Anglos, S. Couris, and C. Fotakis, Appl. Spectrosc., **51**, 1025, 1997
4. L. Burgio, R. J. H. Clark, T. Stratoudaki, M. Doulgeridis, and D. Anglos, Appl. Spectrosc. **54**, 463, 2000
5. P. Maravelaki-Kalaitzaki, D. Anglos, V. Kilikoglou, and V. Zafiropulos, Spectrochim. Acta **B56**, 887, 2001
6. K. Melessanaki, M. Mateo, S. C. Ferrence, P. P. Betancourt, and D. Anglos, Appl. Surface Sci. **197–198**, 156, 2002
7. I. Borgia, R. Fantoni, C. Flamini, T. M. Di Palma, A. Giardini Guidoni, and A. Mele, Appl. Surface Sci. **127–29**, 95, 1998
8. I. Borgia, L. M. F. Burgio, M. Corsi, R. Fantoni, V. Palleschi, A. Salvetti, M. C. Scuarcialupi, and E. Tognoni, J. Cult. Heritage **1**, S281, 2000
9. F. Colao, R. Fantoni, V. Lazic, and V. Spizzichino, Spectrochim. Acta **B57**, 1219, 2002
10. Y. Yoon, T. Kim, M. Yang, K. Lee, and G. Lee, Microchemical Journal **68**, 251, 2001
11. K. Müller and H. Stege, Archaeometry **45**, 421, 2003
12. P. Mirti, Ann. Chim. **79**, 455, 1989
13. A. Casoli and P. Mirti, Fresenius' J. Anal. Chem. **334**, 104, 1992
14. R. J. H. Clark, L. Curri, G. S. Henshaw, and C. Laganara, J. Raman Spectrosc. **28**, 105, 1997
15. B. Gratuze, J. Archaeol. Sci. **26**, 869, 1999
16. P. Mirti, X-Ray Spectrometry **29**, 63–72 (2000)
17. M. Mantler and M. Schreiner, X-Ray Spectrometry **29**, 3, 2000
18. K. Janssens, G. Vittiglio, I. Deraedt, A. Aerts, B. Vekemans, L. Vincze, F. Wei, I. De Ryck, O. Schalm, F. Adams, A. Rindby, A. Knöchel, A. Simionovici, and A. Snigirev, X-Ray Spectrom. **29**, 73, 2000
19. C. P. Swann, S. Ferrence, and P. P. Betancourt, Nucl. Instr. And Meth. In Phys. Res. B **161–163**, 714, 2000
20. Ciucci, M. Corsi, V. Palleschi, S. Rastelli, A. Salveti, and E. Tognoni, Appl. Spectrosc. **53**, 960, 1999
21. M. Corsi, G. Crisoforetti, V. Palleschi, A. Salvetti, and E. Tognoni, Eur. Phys. J. *D* **13**, 373, 2001
22. L. Robbiola, J. Blengino, and C. Fiaud, Corrosion Science **39**, 2083, 1988

Spectroscopic Monitoring of the Laser Cleaning Applied to Ancient Marbles from Mediterranean Areas

V. Lazic[1], F. Colao[1], R. Fantoni[1], L. Fiorani[1], A. Palucci[1], J. Striber[2], A. Santagata[3], A. Morone[3], and V. Spizzicchino[4]

[1] ENEA, FIS-LAS, Frascati (RM), Italy
lazic@frascati.enea.it
[2] ENEA guest with a fellowship – Permanent address: INOE, Bucharest, Romania
[3] CNR, IMIP, Tito Scalo (PZ), Italy
[4] El-En, V. Baldanzese 17 – Calenzano (FI), Italy

Abstract. Laser Induced Breakdown Spectroscopy (LIBS) analysis by Nd:YAG laser emitting at 355 nm were performed on different clean and dirty surfaces of marble fragments collected from ancient quarries in Greece, Turkey and Italy, in order to determine semi-quantitavely the atomic composition of the bulk material and encrustation. The method here developed for element concentrations retrieval could be applied during laser cleaning process to supply the information about the effective crust composition at different depths and the point where the process should be interrupted. The knowledge of the crust composition along successive layers is also important for determining the restoration procedures. The elements measured in the encrustations, such as Si, Al, Ca, C, Ti, Mn, Mg, Na, Ba, Sr and Cu are also present in the bulk, but at different concentrations whose determination allows for the process monitoring. The only element here observed in the crusts and not detected in the bulk materials is Chromium, whose progressive disappearance from LIBS spectra could be used as another indicator of the laser cleaning effectiveness. On a sample from Turkey also Vanadium was detected in the encrustation. The present LIBS measuring method was validated by SEM-EDX and ICP analyses. The clean marble surface and encrustations were further analysed by Laser Induced Fluorescence (LIF), which could be used as an alternative technique for the on-line control of the cleaning effectiveness. Better discrimination between dirty and clean marble surface was obtained when 266 nm excitation was applied instead of 355 nm. Characteristic LIF spectral signatures allows for the discrimination between different type of the natural stones, even under the water.

1 Introduction

The laser cleaning is nowadays a widely used technique in the preservation of stone artworks exposed to environmental stresses. In particular, problems related to the laser treatment of marble surfaces in monuments have been already studied in detail, leading to phenomenological models of the process for samples exposed to different aging factors, including chemical pollution [1]. However, it is of interest to characterize the sample surface before and during

the laser ablation in order to implement an automatic control of the cleaning process. One of the most promising techniques for the on-line control of the laser cleaning is LIBS spectroscopy, where the emission spectra of the laser ablated layer gives indications about the layer composition, different for crust and bulk marble. These information are also very useful for deciding the restoration procedure. The proposed controlling parameter is the ratio of different element emission intensities to Ca emission [2]. However Ca, the major marble constituent, generally shows strongly saturated lines, so the normalization on its intensity could lead to a poor process control. Other LIBS quantitative measuring methods [3, 4], applicable for multi-layered samples such as encrusted marble, are based on the knowledge of the concentrations of the all major elements and, in the case of marble, suffer from the uncertainty of O and S by LIBS.

In the present work a LIBS method for the element concentration measurements during laser cleaning of marble, was developed and validated for the on-line process control.

2 Results

Four sets of significantly different marble samples, distinguishable by slightly different colorations either in the bulk or on the encrustations, have been selected for the present work. The examined samples were collected in four different quarries utilised in ancient times, located in: Carrara (Italy), Proconnesos (Turkey), Paros isle (Greece), Naxos isle (Greece). The samples were covered with a dark dendritic crust, with typical thickness of about 100 μm, as observed by SEM. The sample surfaces are generally irregular, particularly in the case of marble from Paros where the black deposit penetrates into the bulk.

LIBS measurements were done with our standard experimental set-up [3] by applying the laser energy of 20 mJ on a spot size of about 150 m diameter. The measurements were firstly performed on five calibration samples prepared by mixing a certified reference soil sample (NIST 2710) with a $CaCO_3$ standard powder (Carlo Erba), by acquiring the full spectra (240–750 nm). Calibration was obtained through the intensity normalisation on the nearby background emission for the chosen element transition [6], followed by the correction for the plasma temperature measured previously on Fe I lines [3, 6], and for the electron density calculated from Stark broadening of Si I line at 250.7 nm. This method allows for the LIBS quantitative analyses regarding a single element of interest and by data acquisition in a limited spectral range. The influence of the variable ablation rate and sample properties on the final results was strongly reduced through the applied signal normalization. The correction for the plasma parameters was necessary due to significant differences between reference samples and marbles. In the latter case plasma temperature was 1500–2000 K lower and the electron density was an order of

magnitude lower, so the ratio of the atomic and ionic concentration in the plasma was different and the final calibration includes both species, assuming Local Thermal Equilibrium and the validity of Saha equation.

LIBS measurements on the samples were then performed by acquiring the full spectra mediated over 20 laser shots, moving the sample holder between the laser pulses. The ablation rate per pulse is typically 1–1.5 μm, measured by SEM. The composition of sample bulks and encrustations were also measured by SEM-EDX, and for two samples also by ICP. These two techniques generally gave the results comparable with LIBS in the case of bulk materials (Table 1). However, the sample irregularities and strong inhomogeneities also observed from the random scattering among the results of LIBS-EDX-ICP analyses obtained for different sampling areas and volumes, reduce the three analytical techniques to the semi-quantitative level. Results obtained on

Table 1. Concentrations of the most characteristic elements measured by LIBS, EDX and ICP; the values are given in ppm if not specified

Sample		Proconnesos		Carrara		Naxos		Paros	
		Bulk	crust	Bulk	Crust	Bulk	Crust	bulk	crust
Ca	LIBS	40.8%	27.0%	30.1%	27.6%	29.9%	14.8%	34.2%	25.8%
	EDX	40.4%	27.6%	36.2%	28.4%	41.1%	19.7%	42.7%	21.9%
	ICP	39.8%	19.8%	–	–	–	–	46.9%	52.7%
C	LIBS	12.2%	–	11.1%	–	11.9%	–	12.2%	11.2%
	EDX	9.08%	23.6%	8.69%	25.8%	12.2%	41.7%	8.61%	21.4%
Si	LIBS	0.72%	12.1%	0.076%	3.71%	0.603%	5.70%	0.127%	2.34%
	EDX	–	3.16%	0.100%	0.270%	0.62%	1.98%	–	3.63%
	ICP	0.644%	0.734%	–	–	–	–	0.705%	1.11%
Al	LIBS	1.20%	6.40%	0.0309%	4.23%	1.64%	5.22%	0.0428%	2.45%
	EDX	1.16%	3.5%	0.43%	0.800%	0.54%	2.06%	0.780%	6.96%
	ICP	0.0466%	6.14%	–	–	–	–	0.0299%	1.96%
Fe	LIBS	486	13600	733	7720	238	1020	–	4630
	EDX	–	8400	–	–	–	5900	–	11100
	ICP	972	50900	–	–	–	–	411	1980
Mg	LIBS	6940	2110	344	1530	1420	1320	1410	1520
	EDX	3300	2300	2400	–	1600–	–	–	3400
	ICP	2340	1330	–	–	–	–	2340	9290
Mn	LIBS	165	1670	212	527	158	1380	–	666
	ICP	111	115	–	–	–	–	120	1020
Ti	LIBS	366	7102	137	4650	98	3270	–	1880
	ICP	248	1904	–	–	–	–	405	325
Ba	LIBS	98	847	185	719	–	600	–	172
	ICP	88	189	–	–	–	–	30	48
Cu	LIBS	250	437	191	756	118	1200	–	–
	ICP	240	128	–	–	–	–	75	128

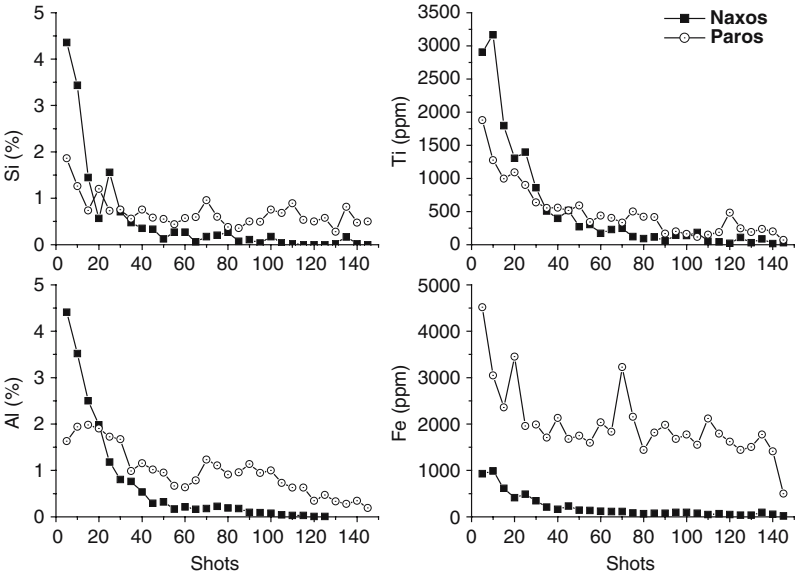

Fig. 1. Concentration change of Si, Al, Ti and Mn during the encrustation removal

encrustations by the different techniques often differ for the rapid changing of the element distribution with depth (Fig. 1).

The LIBS analysis of clean surfaces of marble samples confirmed their main composition as Calcium and Magnesium Carbonates, with a minor extent of Manganese, as bulk constituents. Minor presence of Aluminium, Iron, Silicon and Titanium was detected on the clean surfaces, whereas on the dirty layers their concentrations were found to be up to two orders of magnitude higher. In all the samples Strontium and Copper were detected in traces, both in the bulk and deposited material. On the samples extracted in Greece, Lithium was also detected in the encrustation, which together with high level of Manganese and Titanium is characteristic for marine sediments. An interesting feature is the presence of Chromium only in the encrustation: its progressive vanishing from LIBS spectra below the detection threshold could be also used as a simply control parameter during the laser cleaning of the examined marbles. On a sample from Turkey also Vanadium was detected in the encrustation.

The depth profile analysis of sample crusts were also performed in order to monitor the laser cleaning effectiveness and to determine the right point when the process must be interrupted. The element distributions inside the crust were measured at limited number of the central monochromator wavelengths, by averaging the acquisitions over 5 laser shots. Quantitative data are obtained for most elements detected in encrustations either as major components or traces. All the crusts here analysed show a relative abundance of

Si, Al, Ti, Mn and Fe that decrease rapidly with the depth down to the levels present in the bulk (Fig. 1). Basing on the depth distribution of these elements, the crust could be considered removed with less than 50 laser shots, after which the surface composition remains practically constant thus indicating that the bulk material has been already reached. In spite the inability of the present LIBS method to detect Sulphur, the data here obtained give indirect information on the sulphation process related to the presence of transition metals at the surface (Fe, Ti, Mn, Cu, V). These elements may act as catalysts for the transformation from marble to gypsum [2], once detected at the concentrations reported in Table 1 which are compatible with this role [7].

LIF spectra on clean and encrusted sample areas were measured by defocusing the same laser beam onto the surface and using a gated OMA coupled to a low-resolution monochromator. The spectra of bulk material differ from one sample to another and these differences could be used also for the remote mapping of extended objects [5]. The characteristic spectral features maintain if the sample is immersed into water. The detectable variation of LIF spectra between clean and encrusted marble surface here observed (Fig. 2) could be also used as an indicator of the cleaning effectiveness. After performing the same measurements but with the laser operating at 266 nm, the LIF spectral difference between clean and encrusted surface results more pronounced than in the previous case, thus allowing for a better control of the laser cleaning process.

3 Conclusions

In the present work, for the first time it was demonstrated that quantitative analyses by LIBS could be also performed on marbles and their encrustations. The method here developed for the absolute concentration retrieval on calcareous stones was validated by comparative EDX and ICP measurements. The importance of such LIBS characterization regards not only the analyses

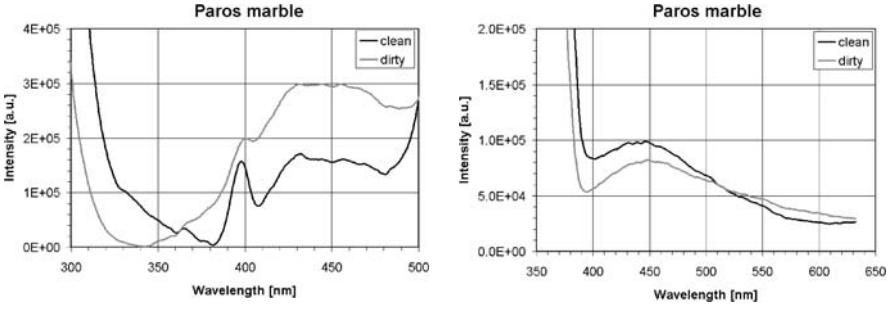

Fig. 2. LIF spectra of Paros marble clean and encrusted surface: laser exc. at 266 nm (*left*) and 355 nm (*right*)

of the artworks before deciding the best restoration procedure, but also the possibility to implement a reliable automatic control during the laser cleaning, basing on the elemental composition changes inside the encrustation until reaching the bulk marble. Further developments of the present LIBS analyses should regard extension of the quantitative analyses to other elements important for stone and crust characterization and increasing of the calibration range for some elements already analyzed.

With LIF technique it was shown that different stones and presence of their encrustations could be recognized also under water, which is important in deciding if to recover from the sea bottom ancient artifacts.

Acknowledgments

The present work supported by the Italian MIUR PON-FESR Project TECSIS (Diagnostic Technologies and Intelligent Systems for Developing Archaeological Parks in Southern Italy).

References

1. R. Salimbeni, R. Pini, and S. Siano "Controlled Laser ablation for the restoration of artworks: principles and applications", in *ALT'99 Int. Conf. on Advanced Laser Technologies*, V. I. Pustovoy and V. I. Konov, eds., SPIE Proceed. Vol. 4070, 18–26 (SPIE, Bellingham 2000)
2. P. Maravelaki-Kalaitzaki, D. Anglos, V. Kilikoglou, and V. Zafiropulos, "Composition characterization of encrustation on marble with laser induced breakdown spectroscopy", Spectrochim Acta B 56 (2001) 887–903
3. F. Colao, R. Fantoni, V. Lazic, and V. Spizzichino, Laser Induced Breakdown Spectroscopy for semi-quantitative and quantitative analyses of artworks – application on multi-layered ceramics and copper based alloys, Spectrochim Acta B 57 (2002) 1219–1234
4. A. Ciucci, V. Palleschi, S. Rastelli, A. Salvetti, and E. Rognoni, "A new procedure for quantitative elemental analyses by laser induced plasma spectroscopy", Appl. Spectrosc. 53 (1999) 960–964
5. D. Lognoli, G. Cecchi, I. Mochi, L. Pantani, V. Raimondi, R. Chiari, T. Johansson, P. Weibring, H. Edner, and S. Svanberg, "Fluorescence lidar imaging of the cathedral and baptistery of Parma", Appl. Phys. B 76 (2003) 457–465
6. R. Barbini, F. Colao, V. Lazic*, R. Fantoni, A. Palucci, and M. Angelone, On board LIBS analysis of marine sediments Collected during the XVI Italian campaign in Antarctica, Spectrochim Acta B 57 (2002) 1203–1218
7. P. Elfving, I. Panas, and O. Lidqvist, "Model study of the first steps in the deterioration of calcareous stones III – Manganese and Iron mediated sulphation of natural stone" Appl. Surf. Sci. 78 (1994) 373–384

Part XI

Laser Diagnostics

Artwork Monitoring by Digital Image Correlation

K.D. Hinsch[1], G. Gülker[1], H. Hinrichs[2], and H. Joost[1]

[1] Applied Optics, Institute of Physics, University of Oldenburg, D-26111 Oldenburg, Germany;
klaus.hinsch@uni-oldenburg.de
[2] Rebhuhnweg 10, D-26316 Varel;
heiko.hinrichs@surfeu.de

Abstract. The mechanical response of artwork to external loads from varying climate is monitored by time-records of displacement maps. These are obtained by digital correlation of series of images from either ordinary photographs in white-light illumination or speckle images in laser light. Special features and the advantages of either version are discussed. Both methods are applied in the study of degradation in historical leather tapestry – right at the site (some representative halls of Jever castle in Northern Germany) as well as for basic model investigations on leather behavior in artificial climate. Ideas are presented to derive the stress situation in the material from the original displacement data.

1 Introduction

During their long life historical artwork is exposed to varying external loads that stress the materials involved. Damage occurs when the forces exceed a threshold strength. Thus, a device to monitor stresses would be an ideal instrument to provide an early warning that such a critical situation is approaching. Unfortunately, in most cases a direct measurement of stresses is not possible without harming the integrity of the object – a priority requirement in all artwork. However, it is possible to determine instead the strain field from a position-resolved measurement of the displacement. The stress distribution may then be estimated by utilizing elastic constants and border conditions of the experiment. Thus, it is generally agreed that devices to monitor displacement fields in artwork can provide a wealth of information on the state of the object. Often, deformation monitoring under everyday conditions of varying climate can provide valuable conservational hints. In addition, data are obtained from the response of the object to some standard load which may be introduced thermally or mechanically.

In this paper techniques are presented to derive displacements from a comparison of subsequently obtained images of the object surface. Local displacement data are obtained from the digital correlation of sub-images in the records. Two methods of digital image correlation are discussed and applied that each have specific features: the one uses images produced in white light,

the other speckle patterns in laser illumination – Digital Speckle Photography (DSP). In either case, the setups are relatively simple (as compared to interferometric methods like electronic speckle pattern interferometry – ESPI) and the evaluation is fairly straightforward. The techniques are used in the study of degradation in historical leather tapestry – both at the historical site and during model experiments on leather specimen under artificial climate. The derivation of the stress situation in the object from strain data is considered for this case.

2 Experimental Method

Generally, the method of choice for displacement mapping depends on the type and scale of displacement values. Interferometric techniques like ESPI offer sub-wavelength sensitivity and can be designed to provide even three-dimensional displacement data. In-plane ESPI has been used successfully in the investigation of paintings on canvas with problems quite similar to those in leather [1]. When the problem is two-dimensional with predominantly in-plane deformations and the expected displacement is above a micrometer a non-interferometric technique suffices. A straightforward approach is to compare details in a series of digital images of the surface obtained while loading the object. A basic requirement is that the object image is covered by details small enough that they can be used as markers to follow the motion. When the displacement assumes values of more than a micrometer and the object surface provides sufficient image details a simple setup utilizing white-light illumination is appropriate. Resolution depends on the size of the markers on the object in combination with pixel size and magnification. In many on-the-site applications the necessary surface details are provided by object texture, patterns of micro-cracks, features in the design of the painting or surface profiles that can even be enhanced by oblique illumination.

A complete deformation record of the object is obtained by tracking the motion of small sub-areas in the images versus time. Since the patterns usually encountered are irregular or even random the evaluation is done by a computer-based cross-correlation of sub-area images. Such a correlation function displays a pronounced peak. Its shift with regard to the origin yields the relative displacement between the sub-areas, the peak height of the normalized function gives the cross-correlation coefficient that indicates the degree of similarity between the images [2]

In the absence of sufficiently small-sized features laser illumination has been used to produce speckle patterns by scattering from the rough-surface profile. The laser speckles thus move with the object and can be tracked just like the surface features before – a well-established method known as digital speckle photography (DSP) that allows to produce image details down to a micron in size [3, 4]. Since laser speckle patterns are produced by the coherent superposition of light scattered randomly from surface irregularities, the

use of such patterns is extremely sensitive to minute changes by surface processes. Here, the amount of decorrelation (the change in similarity) observed between subsequent images and indicated by the magnitude of the correlation coefficient, i.e., the peak height in the correlation output, can serve as a measure for microscopic changes in the surface that are below direct resolution. Thus, in addition to the displacement map position-resolved data about such effects can be recorded – typical examples are corrosion or growth of crack systems. Often already the condensation of water may cause effects large enough to rule out this version – a reason to try for the more robust white-light setup whenever possible.

For each practical situation a decision has to be made whether to use ordinary illumination or laser light. The robustness and simplicity of the former has been mentioned. The later works even in the absence of the required object image details and provides higher sensitivity due to the small size of the speckles. Yet, it is more easily impaired by background motions and side effects that change the surface structure. We have investigated the application potential of the direct correlation of white-light object images right at the site of the historical object. For model laboratory studies on the basic behavior of leather in artificial climate we have used the speckle method. During earlier involvement in the expansion of speckle technologies we have developed a powerful software to handle these type of data for fast and efficient production of displacement and correlation fields [2].

3 On-The-Site Measurements of Historical Leather Tapestry

Deformation mapping by digital image correlation has been applied in the investigation of motions in 18^{th} century leather tapestry lining several representative halls in Jever castle of northern Germany. The wall coverage consists of leather patches stitched together and mounted on wooden frames. The visible side of the leather is covered by a thin silver layer that carries the painted ornaments. Our study was to reveal motions in the tapestry due to varying room climate to guide in identifying weak regions in the leather and in planning considerate air conditioning, optimum mounting and acceptable public access to the cultural heritage.

The experimental setup consisted of a powerful white-light lamp and a CCD-camera (Hamamatsu C4742-95; 1280 × 1024 pixel, 10 bit; pixel size $6.7 \times 6.7\ \mu m^2$) connected to a PC. The illumination was directed such that the images showed maximum contrast features. CCD-data (pixel size and number) as well as the size of the smallest details to be detected in the displacement field determine the required magnification and thus the size of the field of view. In the example presented here the $25 \times 20\,cm^2$-area section studied contained parts of four leather patches connected by horizontal and

vertical stitches. An essential issue in the study was to relate object motions to the ambient climate and to focus on relative displacements between patches that could stress the seams. With self-operating equipment it has been possible to obtain records over many days. The original data provide locally resolved displacement maps versus time – usually represented by fields of small arrows anchored to the reference points and indicating magnitude and direction of displacement.

For an example, let us show the motion within a 27-hour period in a section at the lower end of a 2.18 × 0,90 m^2 leather sheet in the Edzard hall of Jever Castle. During the measuring time the relative humidity in the room increased by about 10%. The sheet is fastened at top and bottom to the wooden frame construction. Figure 1 (left) gives the 25×20 cm^2 measurement area as it appears in the video camera showing the ornamental pattern as well as one horizontal and two vertical seams connecting individual leather patches, No. 1 being labeled for later identification. At the bottom of the figure the wooden panel that lines the lower part of the wall is just visible. The right side figure shows the according field of displacement arrows. The

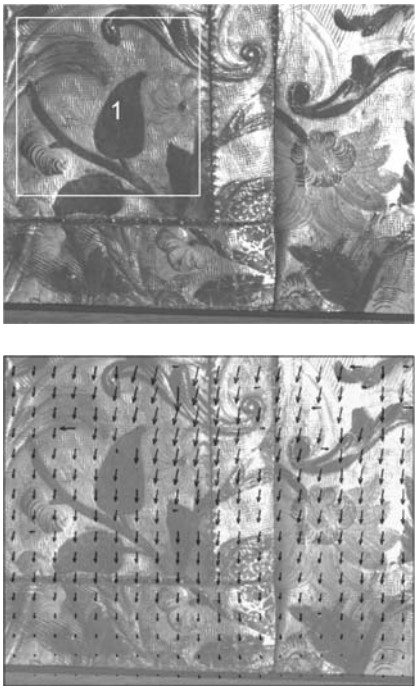

Fig. 1. *Left*: Leather tapestry at Jever castle: 25 × 20 cm^2 area at the bottom of a sheet of 2.18 m in length fastened at upper and lower end; patch No. 1 marked in figure for identification. *Right*: Humidity-induced motion, longest arrow: 2.7 mm displacement

longest arrows correspond to about 2.7 mm in displacement. Obviously, there is a gross downward motion due to an expansion of the leather. Displacement gets zero, of course, when approaching the bottom region where the leather is fastened to the supporting frame structure.

The motion could be related to the ambient climate by simultaneous registration of temperature and humidity. It was found that the strain in the leather is predominantly induced by changes in the ambient relative humidity. For an illustration we plot in Fig. 2 the mean vertical and horizontal displacement value in patch No. 1 together with the relative humidity versus time over a period of some twelve days. All displacements are relative to a starting situation indicated by "reference image". The measurements prior to this moment show a few interruptions due to communication breakdowns. Due to the integrating effect over the whole length of the sheet the vertical displacement exceeds the small horizontal motions by an order of magnitude. The situation shown in Fig. 1 was recorded at the overall maximum of the vertical displacement on May 9. It is quite obvious that the data reveal a pronounced correlation of the daily period of relative humidity and leather motion over several days. Thus, the main motor for motion is the swelling of the leather with increasing humidity. As a matter of fact, an average value for the humidity-induced strain ε in this historical material can be derived by comparing, for example, the reference state with the situation at maximum where some 10% change in relative humidity has produced about 2 mm increase in length at the top of Fig. 1 yielding $\varepsilon = 0.1 \cdot 10^{-3}$ per % of relative humidity.

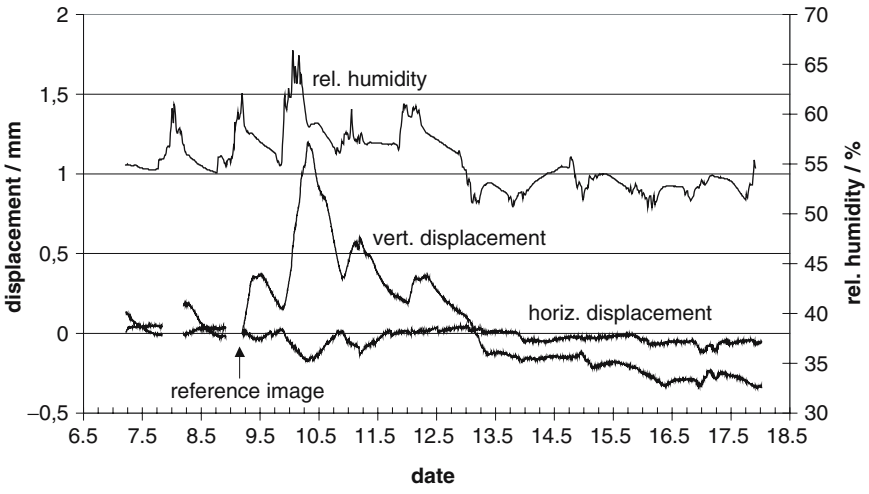

Fig. 2. Humidity-induced average displacement of a leather patch close to the bottom of a 2.18 m long sheet (patch No. 1 in Fig. 1). Positive vertical displacement means lengthening of the material – due to swelling by incorporated moisture

The seams where the patches in leather tapestry have been stitched together are critical locations. When the patches move away from each other the thread, for example, may pull out and harm the leather. Such a situation can be characterized by calculating the relative average displacement between patches. In the present case the situation was relaxed because the long sheet was loosely suspended and could easily respond to the shrinking and swelling. The horizontal seem responds by an out-of-plane motion to intercept the leather expansion.

4 From Displacement to Stress – Modeling the Behavior of Leather

The primary data from the experiments are a map of local two-dimensional displacement vectors. To estimate possible hazards of these motions for the object it is necessary to turn them into stresses. However, this can only be achieved by input of characteristic elastic quantities of the material involved. Furthermore, constraints from the geometric mounting of the specimen govern the situation. When a sample piece of leather, for example, is free to respond to the material-inherent shrinkage due to drying out (desiccation) we expect little harm to the leather by external mechanical stress. When, on the other side, the specimen is tightly mounted in a frame, stress will build up that could cause irreversible damage once it exceeds a threshold value.

In finding a decisive parameter characterizing the load on the material let us illustrate the local situation in a very small region of interest during desiccation. We assume that the area A of this piece located at coordinates (x, y) shrinks by an amount δA. This is due to the relative change in length (strain) ε_{xx} and ε_{yy} which in turn can be calculated from the derivatives with respect to position of the displacement vector $\boldsymbol{s}(x, y)$

$$\varepsilon_{xx} = \frac{\partial s_x}{\partial x}; \varepsilon_{yy} = \frac{\partial s_y}{\partial y} \tag{1}$$

because the length of the region changes by the difference in displacements at its two sides. Quite generally, the material may be non-isotropic so we have to take into account the direction which is taken care of by the combination of indices in ε. We thus arrive at a relation for the relative change in area

$$\alpha = \frac{\delta A}{A} = \frac{\partial s_x}{\partial x} + \frac{\partial s_y}{\partial y} \tag{2}$$

where the sum of the partial derivatives is sometimes referred to as "normal strain". These derivatives are available from the displacement map.

Now let us consider the relaxed condition where an elementary region is free of any constraints and can yield to shrinkage due to reduced humidity.

This will result in a certain value α_0 for the relative change in area. In realistic situations, there will be various kinds of restrictions – like the mounting of the leather sheets – so any experiment will result in a different value for the locally determined values of α. As an extreme case, rigidly fixed edges will not allow any change in area at all and thus $\alpha = 0$. Thus, the amount of stress on the area element can be estimated from the difference value $\Delta\alpha = \alpha - \alpha_0$.

The determination of reliable values for α_0 is not easy because of the great variety, inhomogeneity and anisotropy of a naturally grown material like leather. A first estimate can be obtained from the strain value $\varepsilon = 0.1 \cdot 10^{-3}$ per % of relative humidity measured earlier in the long leather sheet in the castle. Assuming isotropy and zero constraints equation (2) yields $\alpha_0 = 0.2 \cdot 10^{-3}$ per % of change. Mind that this value is rather problematic and need to be checked in any actual situation – preferably by systematic investigations of samples as similar in properties to the material under study as possible.

It should be noted that there are additional processes of degradation that are not determined in this way. Externally applied mechanical pre-stretching, for example, which is used during mounting to stretch the tapestry produces a strain field that can be directly related to the stress field. This interpretation has been used in testing stretchers in canvas paintings [3]. Even without external mechanical stress compound leather tapestry will age from the repeated shrinking and swelling of the materials involved. The arguments outlined here should at least help in locating weak areas that suffer from fluctuations in the ambient climate.

5 Speckle Correlation in Laboratory Environment

We apply the geometric approach outlined above to data obtained from measurements on historical and virgin leather samples of size $10 \times 10\,\mathrm{cm}^2$ in the artificial climate of a climatic chamber. Since these displacements were expected to be in the micrometer range, the laboratory environment guaranteed mechanically stable conditions, and the virgin leather lacked sufficient surface features the investigations were done by DSP on speckle patterns in the green light of a Nd:YAG laser. In this case, images were recorded by a Pulnix TM1010 CCD camera of a 1018×1016 pixel array. The map of displacement vectors was evaluated for a grid of locations spaced 3 mm in each direction and processed to yield strain data. For this purpose estimates for the derivatives were obtained by analyzing a small neighborhood of each location in the displacement field. We then calculated fields of "normal strain", i.e., the relative change in area α to be compared to the reference value α_0. Besides the displacement maps we also evaluated maps of the correlation coefficient that indicate surface changes provoked by the action of humidity. These were quite pronounced in the soft virgin leather – less in the historical

samples covered by silver and paint. Quite probably, water condenses in the rough-surface virgin leather much more easily.

Figure 3a presents a map from this study including displacement vectors and correlation coefficients – the originally color-encoded values show not quite as well in the gray scale representation. The specimen consists of two pieces of original material from the leather wall-cover that have been stitched together along a seam running horizontally through the field of view. At the top the leather was fixed by nails, at the bottom it was held in a mobile metal clamp that was loaded with a 1 kg weight in the dry state at 40% relative humidity and then locked. Now, changes were measured while the humidity in the chamber was gradually increased. The example in the figure gives the difference at 60% humidity. The vector field shows that the leather which was pre-stressed in the dry state expands into the free side regions as it takes up moisture at higher humidity. The longest arrows shown indicate about 150 µm displacement. With a few exceptions the correlation coefficient is high at about 0.8; on the rigid metal surface of the clamp, of course, it is close to 1.0 – which means that there are no surface changes.

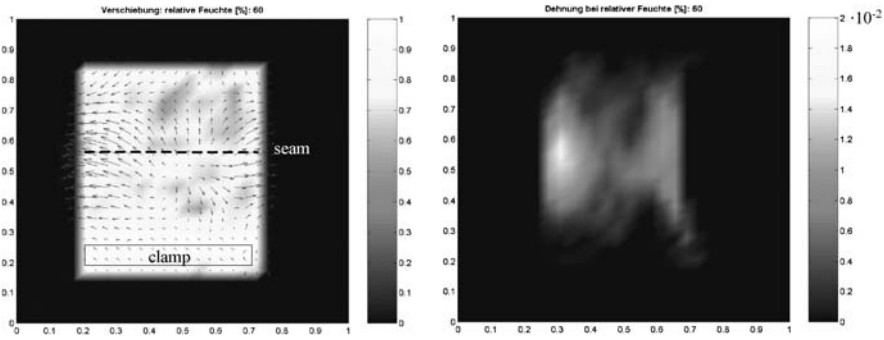

Fig. 3. Response of a historical leather specimen (size $10 \times 10\,\mathrm{cm}^2$) to a change in relative humidity from 40% to 60%. (**a**) (*left*): Displacement arrows and correlation coefficient (*gray scale*); longest arrows: about 150 µm displacement. (**b**) (*right*): Local change in relative area (*normal strain*)

In Fig. 3b this displacement field has been evaluated for the normal strain α, i.e., the relative change in area, here encoded in gray values – again there is a loss in quality as compared to the original color plots. These values were each calculated from displacement data in a neighborhood of 3×3 sub-areas after smoothing by a low-pass filter. Now these typical data need to be compared with α_0. Assume that the value from the free-field measurements in the castle applies here, too; for a 20% change in humidity this yields $\alpha_0 = 0.4 \cdot 10^{-2}$. The mechanical stress on the material at a certain location should then increase with the difference between its α-value and the reference α_0 – for larger values the area element has expanded more than natural, for

lower values it has not expanded enough. Back to the figure: bright regions are obviously more stressed than the dark values around $0.4{\cdot}10^{-2}$. Recall, however, that we are not quite sure whether this value applies here.

6 Conclusions

The application of digital image correlation to white light cords from art objects under real-world conditions promises to be a powerful – yet simple and robust – technique to obtain displacement fields. It yields pure in-plane motions that are well-suited in two-dimensional objects like leather, canvas or paper. For objects with insufficient surface features or in situations of smaller displacements the setup is just as well suited for digital speckle photography in laser light. After the successful implementation of the instrument in the present study of historical leather tapestry it is expected that there will be numerous similar problems benefiting from this technique. Moisture impact on wooden paneling or in church altars, for example, are problems well-suited for such a device.

Acknowledgements

The studies were sponsored by Deutsche Bundesstiftung Umwelt DBU (Osnabrück) through a grant to ZMK Hannover.

We dedicate this paper to Dr. Peter Königfeld, Niedersächsisches Landesamt für Denkmalpflege, Hannover, on occasion of his retirement. For almost two decades he has counseled, encouraged and promoted our work from the restorer's point of view. We gratefully acknowledge this assistance and thank for all we learned about artwork and its conservation.

References

1. C. R. T. Young: Optics and Lasers in Engineering **31**, 163–170, 1999
2. K. D. Hinsch, T. Fricke-Begemann, G. Gülker, and K. Wolff: Optics and Lasers in Engineering **33**, 87–105, 2000
3. K. D. Hinsch and G. Gülker: Lasers in art conservation. Physics World **14**, 37–42, 2001
4. M. Sjödahl: Digital speckle photography. In: *Digital Speckle Pattern Interferometry and Related Techniques*, edited by P. K. Rastogy, John Wiley & Sons, Chichester, 289–336, 2001

A 3D Scanning Device for Architectural Relieves Based on Time-Of-Flight Technology

M.C. Gambino[1], R. Fontana[1], G. Gianfrate[2], M. Greco[1], L. Marras[1], M. Materazzi[1], E. Pampaloni[1], and L. Pezzati[1]

[1] Istituto Nazionale di Ottica Applicata (INOA), largo E. Fermi 6, 50125, Florence, Italy
mchiara@ino.it

[2] Università degli Studi di Lecce, Dip. Ingegneria dell'Innovazione, via per Arnesano, 73100 Lecce, Italy
gabriella.gianfrate@unile.it

Abstract. In this work we present the results of some architectural and archaeological relieves realized by means of a Time-Of-Flight (TOF) laser scanner developed by the Art Diagnostic Group of Istituto Nazionale di Ottica Applicata – INOA (the National Institute of Applied Optics). The instrument is composed of a commercial distance meter mounted on a high precision scanning system, and is equipped with a tripod for total-stations. The device was projected in order to have the following characteristics: reliability, good accuracy and compatibility to other systems. For Cultural Heritage applications it is important to integrate the data acquired with different instruments, but a problem met with many commercial systems is the lack of compatibility with classic survey methodologies. Moreover, superimposition of results from different techniques is possible only if the output is metrically correct. Up to now, the realization of accurate 3D models of buildings was a prerogative of the photogrammetric devices, but the recent progress in opto-electronic technology and 3D software of analysis made possible the production of accurate 3D models. Laser scanning has the main advantage of allowing the acquisition of dense data sampling with high accuracy and high speed.

1 Introduction

The 3D survey has always held an important place in architectural and topographic studies for the analysis and the structural investigation of a piece of architecture [1, 2], thus representing both a measurement and an artwork overall evaluation providing information on the construction technique [3]. In any case, and for any application, the 3D survey is the starting point to base any kind of research or investigation on the studied piece of architecture.

This is the reason why enormous technological efforts [4, 5] have always been done in order to find efficient, accurate and user-friendly methods and techniques for the 3D survey. The latter should give complete information on the investigated object in order to provide the analysis with all the

geometrical parameters that make the survey a useful application for architects, restorers and conservators.

The traditional technique for the architectural survey is photogrammetry, but the introduction on the market of laser scanning devices spurs a new era in the three-dimensional relief measurement. As a matter of fact, laser scanning enables extremely dense data sampling of the object at a high acquisition rate, with high accuracy and resolution. The relative ease of acquisition of millions points in a three-dimensional array is a step further of the technology, but, on the other hand, it arises the problem of dealing with such a big amount of acquired data, and their organization in a 3D digital model [6, 7]. The growing technological progress of the laser-based instrumentation for three-dimensional survey fostered the study of the problems related to the representation and to the use of the digital models [8, 9].

The possible scenarios involved in the utilization of digital models [10] range from the monitoring of the deterioration due to pollutant, to the realization of digital archives easy to access and long-lasting; from reverse-engineering to fast-prototyping [11]; from the analysis of the conservation condition to the monitoring of the restoration interventions. Besides, the digital model, realized starting from the 3D data, can be used for virtual reality [12] applications.

For the three-dimensional survey in the architectural field, the Time-Of-Flight (TOF) laser scanner is the proper device to measure huge structures such as buildings, archaeological sites, courts. In practice, it consists of a radar system that employs a pulsed light source.

In this work we present a TOF laser scanner, developed at INOA, specifically devoted to Cultural Heritage applications.

2 The Time of Flight Working Principle

The basic principle of an optical TOF instrument can be summarized as follow: a source emits a light pulse and starts a highly accurate stopwatch. The light pulse travels to the target and back. Reception of the light pulse by the detector halts the stopwatch, which now shows the time of flight of the light pulse. The light pulse travels the distance twice, back and forth from the distance meter to the target. An essential property of this set-up is the fact that the emitter and detector are synchronous. The light source and the receiver are located very close to each other: this facilitates a compact set-up that is essential for *in situ* measurements.

When measuring distances over wide areas, the TOF distance-meter is integrated to a scanning device that spans the light spot over the investigated area and serially acquired the elevation data points assembling them in the so-called range map.

Instead of the scanning technique, the entire scene can be illuminated to perform the 3D survey and the signals from some hundred or thousand

of points detected in parallel with a multi-channel plate detector. If, on one hand, this position-sensitive detection method is time-saving, on the other hand it lacks in accuracy and resolution. Thus its output has only a qualitative meaning.

3 The Instrument

The TOF instrument developed at INOA is composed by a commercial distance meter mounted on a scanning system, made up of two motorized rotational stages (see Fig. 1). In order to have a proper correspondence between measurements obtained with our instrument and with instruments traditionally employed for the topographic survey, our scanner is mounted on tripod for total-stations equipped with a base onto which a spherical level is set. In such a way, the instrument is interchangeable, when set at the measure points, with the instruments traditionally employed for the topographic survey, as for example total stations are. All the measurement campaigns described in this paper were done in collaboration with the IUAV of Venice, in order to compare the measurements obtained with their theodolite and the data acquired with our instrument: the measurement analysis is still in progress.

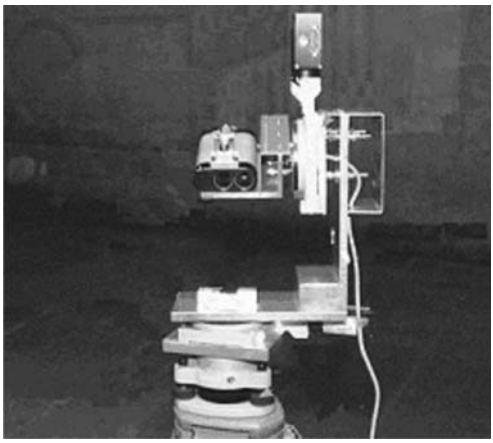

Fig. 1. Image of the TOF laser scanner prototype developed at INOA

Among the commercial distance meter, the CM-30 by Noptel was chosen because it is cost-effective and because it combines good accuracy and resolution with fast acquisition rate. The rotational stages are two micro-positioning devices characterized by high precision and resolution and continuous rotary motion. A mechanical interface, for assembling the rotational stages and the optical head, was specifically designed to allow the alignment of the mutual orientation of the three rotational axis.

After a calibration procedure, the laser scanner characteristics are the following: at a stand-off distance that ranges from 2 m to 30 m, the instrument has a quota resolution of 1 cm on 4 averages, an accuracy higher than 2 cm and a maximum acquisition rate of 1.2 kHz. At maximum working distance the laser spot diameter is 5 cm. The number of averages sets the device resolution: in measurement campaigns presented herein, we made four acquisitions for each measured point in order to reach a good compromise between quota resolution and acquisition time, due to the huge dimensions of the surveyed objects (an archaeological site and a cloister). Tests were carried out in Florence on smaller object with an increasing number of averages, to verify the instrument performance in the detection of architectural details. A laser pointer was placed on the distance-meter top in order to visualize the target shot point. The scanner is entirely computer controlled: before starting the measure, the angular range is set, along with the number of points that fixes the measurement transversal resolution, and the acquisition rate. The result of a single range map measurement can be displayed in an image format where the depth information is expressed in color or gray scale. The acquisition software can also display the quota (z) profiles in the x and y directions.

4 Applications

Preliminary measurements were carried out at our laboratory in the Opificio delle Pietre Dure in Florence, where usually the instrument is kept. These 3D restitutions allowed us to verify the good performance of the instrument, before *in situ* measurements.

The first 3D survey of an architectural building was held at the "Chiostro degli Olivetani" (see Fig. 2) in Lecce, where the History and Art Department is presently located. It is a two floor building with a cloister having double based column arches belonging to the XVI century. In the middle of the court there is a well enriched with four curved columns and a Baroque canopy. Some range maps of both the cloister and the well where acquired from different points of view, in ordr to eliminate the shaded areas (see Fig. 3 and 4).

The spanned volume for the acquisition of the well was in the range 46° in the vertical direction and 69° in the horizontal one, and for the cloister in the range of 84° in the vertical direction and 50° in the horizontal one, due to its bigger dimensions. The angular resolution in vertical and horizontal directions was 1.56 and 1.32 mrad, respectively. The corresponding range maps consist of more than 600000 points: a snapshot obtained with the program we use for the 3D-model visualization (by ISTI-CNR Pisa) is shown in Fig. 4. Data processing for the realization of the complete 3D digital model is in progress.

Some measurement campaigns were realized even in hostile environmental conditions: for instance, the survey of the dig in the archaeological site "Roca Vecchia" nearby the "grotta della Poesia" at Roca (Lecce, Italy). This area

Fig. 2. Picture of the Chiostro degli Olivetani" during the TOF laser scanner measurement campaign

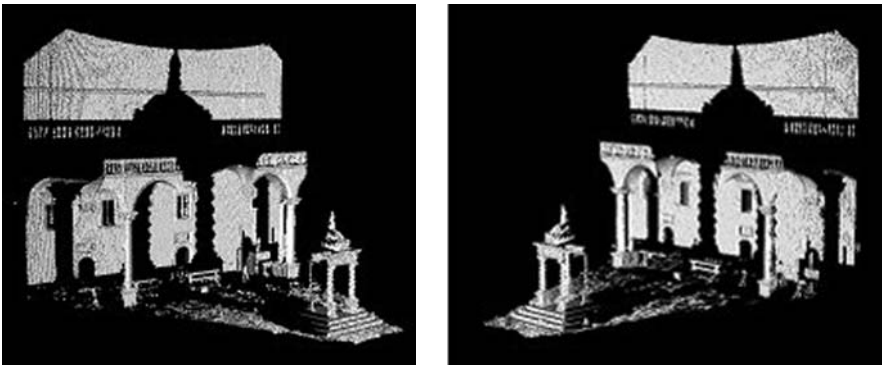

Fig. 3. Snapshot of two different range map orientations of the well in the middle of the "Chiostro degli Olivetani"

was discovered in 1983 and since then it has been extensively studied by archaeologists. It is a big Karst hollow presently invaded by the sea. The cave was a cult site for a Messapic divinity: the religious ceremonial envisaged text and figure inscriptions on the cave walls. So the surface is actually covered by the epigraphic activity is more than 600 square meters, and its documentation is difficult to carry out by means of traditional techniques. A 3D survey of the cave with our TOF instrument is planned: this will be used as a box for referencing the results from other analysis.

The documentation of the cave conservation state and its digital reproduction is particularly important due to the danger posed by infiltration by sea water that could either irreversibly damage it or make the hollow inaccessible.

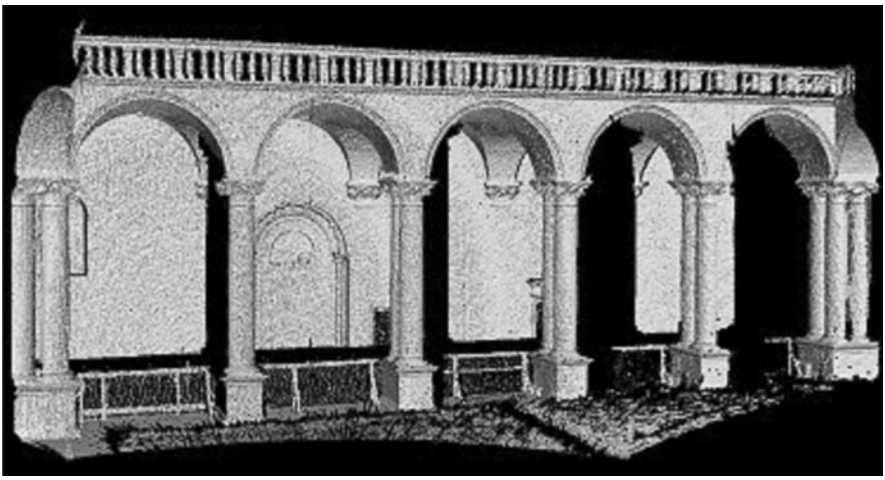

Fig. 4. Snapshot of a range map of the cloister

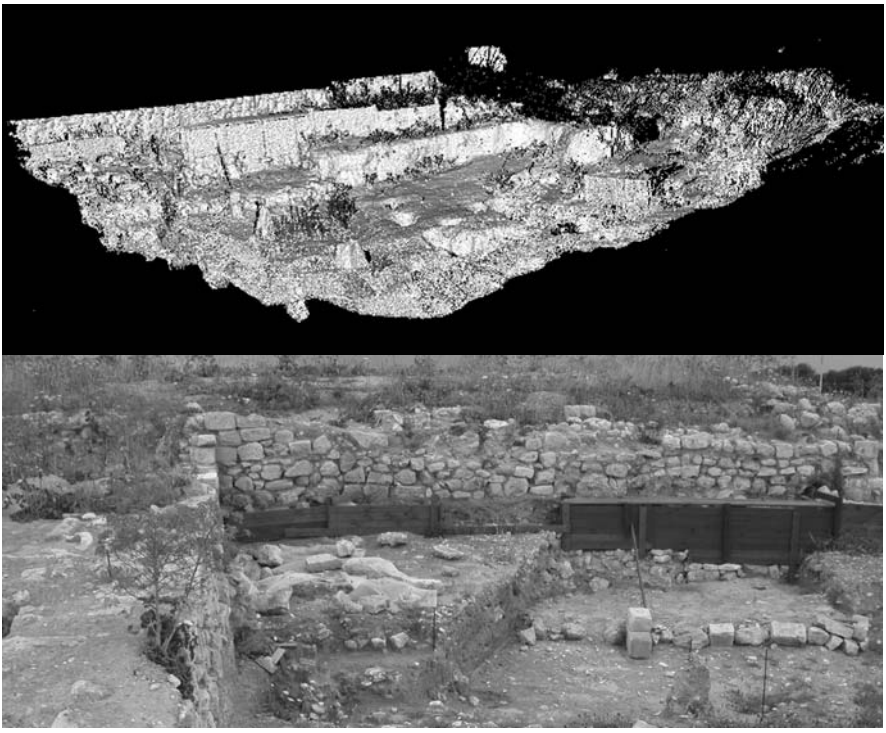

Fig. 5. Snapshot of a single range map of the archaeological dig outside the "Grotta della Poesia" (*top*) and corresponding picture image (*bottom*). The range map was acquired with a scanning range of 95° (951 points) in the vertical direction and 50° (660 points) in the horizontal direction

The conservation and monitoring intervention, that involves many public institutions among which the Archaeological Department of the University of Lecce, IUAV of Venice, ISTI of Pisa, and INOA, entails also the 3D survey of the archaeological dig (excavation) outside the cave. Range maps of different areas were acquired by varying the vertical scanning range. A preliminary result of the 3D survey is shown in Fig. 5.

5 Conclusions

In this work a 3D scanning device based on the Time-Of-Flight technology is presented. The instrument, devoted to architectural applications in the Cultural Heritage field, was set up in order to provide good resolution and accuracy in a limited range of working distance. It is composed by a high precision scanning system equipped with a commercial low-cost distance-meter. The TOF laser scanner is accurate and fast, allowing, thus, a more dense data sampling with respect to the traditional techniques.

In order to compare and integrate the data acquired with the instrument usually employed for the topographic survey, the scanner is mounted on a standard tripod.

The results of a few architectural and archaeological measurement campaigns are presented. The realization of a complete digital model of the measured objects is in progress.

References

1. C. Monti, *Per una conoscenza metrica dell'architettura,* Tema n. 34, FAE, Milano, 1996
2. R. A. Genovese, *Il rilevamento per il restauro architettonico e ambientale*, Quaderni di restauro – Tecniche di rilevamento nuove frontiere della tecnologia, ed. E.S.I, Napoli, 157/2001
3. C. Achille and C. Monti, *Nuove metodologie di rilievo rappresentazione e visualizzazione*, Quaderni di restauro – Tecniche di rilevamento nuove frontiere della tecnologia, ed. E.S.I, Napoli, 2001
4. A. Cabrucci, *La scansione laser nel rilevamento architettonico*, Quaderni di restauro – Tecniche di rilevamento nuove frontiere della tecnologia, ed. E.S.I, Napoli, 157/2001
5. M. Pieraccini, G. Guidi, and C. Atzeni, "3D digitizing of cultural heritage", *Journal of Cultural Heritage* Vol. 2, N 1, 2001, 63–70
6. C. Rocchini, P. Cignoni, C. Montani, P. Pingi, and R. Scopigno, "A Suite of Tools for the Management of 3D scanned Data", *Proceedings of the 2001 Workshop of Italy-Canada on 3D Digital Imaging and Modelling Applications of Heritage*, Industry, Medicine & Land, Padua, Italy, 3–4 April 2001
7. P. Cignoni, C. Montani, C. Rocchini, and R. Scopigno, "External Memory Management and Simplification of Huge Meshes", *IEI-CNR Tech. Rep., submitted paper*, Jan. 2001, pp 10

8. B. Curless and M. Levoy, "A volumetric method for building complex models from range images", *In SIGGRAPH '96 Proceedings*, ACM SIGGRAPH, 1996, pp 303–312
9. M. Garland and P. S. Heckbert, "Surface simplification using quadric error metrics", *In SIGGRAPH 97 Conference Proceedings*, ACM SIGGRAPH, 1997, pp 209–216
10. J.-A. Beraldin, F. Blais, P. Boulanger, L. Cournoyer, J. Domey, S. F. El-Hakim, G. Godin, M. Rioux, and J. Taylor, "Real world modelling through high resolution digital 3D imaging of objects and structures", ISPRS Journal of Photogrammetry & Remote Sensing 55: 230–250; 2000
11. M. Levoy, S. Rusinkiewicz, M. Ginzton, J. Ginsberg, K. Pulli, D. Koller, S. Anderson, J. Shade, B. Curless, L. Pereira, J. Davis, and D. Fulk, "The Digital Michelangelo Project: 3D Scanning of Large Statue", Proceedings of SIGGRAPH 2000, New Orleans, Luisiana, USA, 23–38 July 2000
12. R. Lange, P. Seitz, A. Biber, and R. Schwarte, "Time-of-flight range imaging with a custom solid-state image sensor", Laser Metrology and Inspection, Proc. SPIE, Vol. 3823, 1999

Surface Roughness Relief

L. Marras, R. Fontana, M.C. Gambino, M. Greco, M. Materazzi,
E. Pampaloni, L. Pezzati, and P. Poggi

INOA – Istituto Nazionale di Ottica Applicata, Largo E. Fermi 6, 50125
Firenze, Italia
beniculturali@ino.it

Abstract. The knowledge of the shape of an artwork is an important element for its study and conservation. When dealing with a stone statue, roughness measurement is a very useful contribution to document its surface conditions, to assess either changes due to restoration intervention or surface decays due to weathering agents, and to monitor its time-evolution in terms of shape variations. In this work we present the preliminary results of the statistical analysis carried out on acquired data relative to six areas of the Michelangelo's David marble statue, representative of differently degraded surfaces. Determination of the roughness and its relative characteristic wavelength is shown.

1 Introduction

Many non-invasive optical techniques for shape measurements derived from industrial metrology, but the peculiarity of each artwork does not allow for a straightforward application. Roughness measurement deriving from an optical shape survey is thus a new application in the Cultural Heritage field, where scarce attention was paid to this kind of diagnostic. Roughness measurement of an artwork is important to document the surface condition, to assess both the changes due to possible restoration intervention and the surface decay due to wearing agents; moreover the data acquired can monitor the evolution in time in terms of shape variations.

There are several problems in measuring the roughness of a marble statue; the lack of standards defining it for this specific case, the need of a high accurate measurement of the surface, with a high resolution in the microscopic range; moreover this type of measure is often very difficult to perform, because it must be executed *in situ*, specially for large statues.

Generally speaking [1], the surface of an object can be described using three parameters, according to the spatial frequencies considered: *shape* (low frequencies), *waviness* (mid frequencies) and *roughness* (high frequencies). The three frequency ranges depend on the object dimensions: in general, shape is related to the overall geometric form, waviness is related to the deviation between projected and manufactured form, and roughness represents the surface irregularity due to the material intrinsic morphology or to the mechanical features of the instruments used to the manufacture.

In this work we present the preliminary results concerning statistical analysis carried out on data relative to roughness measurements on six $4 \times 5\,\mathrm{cm}^2$ areas, representative of the differently degraded surface of the Michelangelo's David marble statue. A three-dimensional survey was carried out by means of a laser scanning micro-profilometer. Measurements were realized before restoration had started and they will be repeated after the restoration intervention.

2 Measuring the Roughness

When describing the surface integrity of an artwork, an important parameter to deal with is roughness, arising both from the working process and from an intrinsic amount of microscopic irregularity, even if only at a molecular level. The features which contribute to it may be either random or regular (periodic).

The commonly used techniques for *in situ* roughness measurements are contact techniques, and they make use of stylus profilometers. The sample surface is investigated by means of a stylus or needle that is moved along the surface; its profile is then recorded. The system is usually calibrated with a known, flat surface: depth information is obtained by calculating the difference between sample and reference measurement. These profilometers have a very good quota resolution (nanometers), whereas lateral resolution depends on stylus diameter.

Alternatively, for *in situ* roughness measurements optical instruments based on light scattering can be used. RMS roughness is then calculated on the illuminated area with a depth resolution up to 10 nm.

A variety of high resolution microscopes can also be employed for accurate roughness measurements, but only for laboratory applications.

A novel non-contact optical technique, the so-called conoscopic holography, has been recently developed. A laser beam, coupled to an optical microscope system, is split and then focused onto the test surface. Surface height is computed from intensity and phase information on the interference pattern: quota differences result in optical path differences that are seen as light and dark fringes on a video camera or diode array detection system. The whole surface shape is then obtainable by mechanical scanning. In the diagnostics of artworks the non-contact characteristic is a mandatory step: this requirement makes optical techniques particularly suitable for this purpose, and conoscopic holography is probably the best compromise between good resolution and high data sampling.

3 The Instrument Set-Up

Roughness measurements on the Michelangelo's David, were realized by means of a conoscopic micro-profilometer system realized at INOA (National Institute for Applied Optics, Florence, Fig. 1). The instrument is composed of a commercial Conoprobe mounted on two motorized high-precision linear stages. The probe (Conoprobe 1000 by Optimet) working principle is as follows: A light beam projected by a diode laser on the sample is both reflected and back scattered, and it impinges on a uniaxial birefrangent crystal placed between two circular polarizers (Fig. 2). The ordinary and the extraordinary beams are then generated inside the crystal and produce an interference pattern [2, 3]. The probe we used is equipped with a 50 mm lens which sets a quota resolution of nearly 1 µm and a dynamic range of 8 mm at a stand-off distance about 40 mm. The overall accuracy is better than 6 µm. The scanning device is composed of two motorized high-precision (0.1 µm)

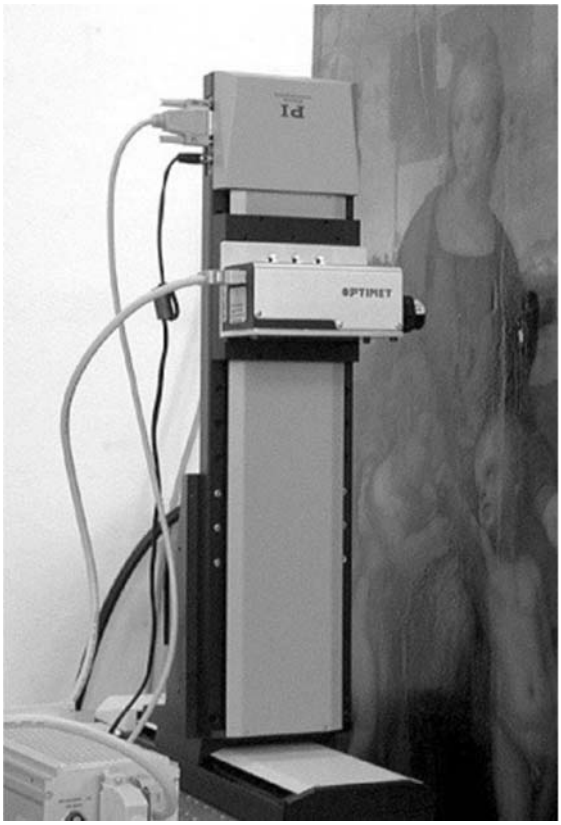

Fig. 1. The laser scanner micro-profilometer during a measurement on the panel painting "Madonna del Cardellino" by Raffaello

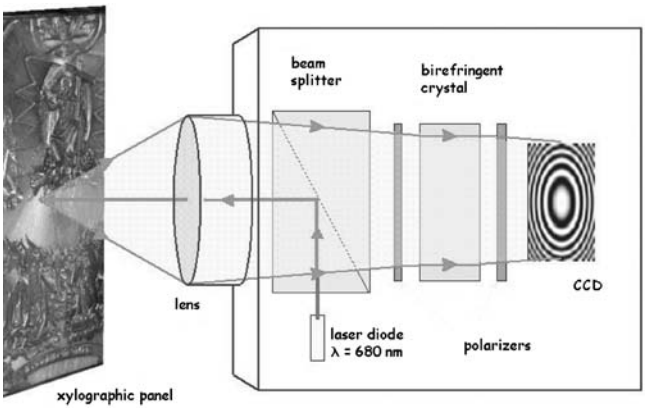

Fig. 2. The working principle of the conoscopic system

linear stages, perpendicularly assembled. The system allows measurement on a maximum area of about $280 \times 280\,\mathrm{mm}^2$. The instrument has a maximum transversal resolution of $20\,\mu\mathrm{m}$ with an acquisition speed ranging from 100 to 400 point/s, depending on the set spatial sampling frequency.

The micro-profilometer enables measurements on surfaces with almost any reflectivity, with an incident angle up to 85° , very close to grazing incidence. Very small details can even be detected, as for example holes smaller than 1 mm diameter and 25:1 ratio between quota and diameter [4, 5]. Moreover the instrument, not sensitive to colour gradients, is suitable for surveys of very detailed surfaces characterized by high chromatic contrast [6]. These characteristics, combined with co-linearity, allow the measuring of thin grooves and deep holes.

During the diagnostic measurements, the David statue has been embedded on a scaffold more then 7 meters high, and a special mechanical arm was realized to survey parts otherwise difficult to detect. Due to its very fine resolution, the micro-profilometer body was tightened to the statue so as to minimize vibrations and possible connected measurements errors, unavoidable when working on the scaffold above described. In order not to damage the statue, contact points were protected with felt.

4 Measurement and Data Analysis

The micro-profilometer scanning technique was applied on various panel paintings and statues, where the instrument configurations have been purposely studied in order to put in evidence details which are not visible at sight and often not detectable with other techniques. The measurement results allow to reveal painting detachments, deformations of the materials and also the roughness of the surface.

We report here the study of roughness of a huge marble statue: the Michelangelo's David. The statue, presently exposed at the *Museo dell'Accademia* of Florence, is currently under restoration. The restoration project has two objectives: first of all studying and then monitoring the "health" of the sculpture and doing the whole cleaning that the statue, darkened and stained by the dirt accumulation. The history of the statue is very tormented: its surface was seriously damaged in a first incident occurred in 1512, when the base of the statue was struck; later in 1527 the left arm was broken into pieces during an uprising in *Piazza della Signoria*.

Between 1808 and 1815 an "encausto" patina (wax coating) was applied to David statue in order to protect it from pollutant. In 1843 the statue surface was cleaned with a solution containing 50% chloric acid, and finally in 1873, when David statue was moved from *Piazza della Signoria* to the *Galleria dell'Accademia*, the statue suffered from instability and numerous cracks occurred. The analysis of the roughness certainly allows to understand how much those previous interventions of restoration or the various accidents affected the statue had compromised the marble surface.

To damp possible vibrations induced both by the instrument motion and by the environment, during the measurement it is necessary to secure the instrument to the statue. This has been a tough point in the measurement, since it is clearly not possible to fix something directly onto David statue: the contact with the statue has been realized with suitable materials preventing any damage to the artwork itself, like felts and a synthetic tape, thus avoiding surface scratches (Fig. 3).

Fig. 3. The probe-statue fixing system

Since the scanning procedure takes a long time, we decided to acquire only very small areas; it has been necessary to accurately select the areas being investigated, in order to obtain a meaningful sampling of the whole surface.

We proceeded in this choice according to the indications by the scientific committee for the David Project; six areas $4 \times 5\,\mathrm{cm}^2$ large were investigated, each with a high space frequency sampling ($50\,\mu\mathrm{m}$) so that the number of acquired points is 801×1001. The acquisition software (developed at INOA) allows to register the z profile of the surface, as well as the x and y profiles. Roughness can be defined in terms of deviations from a mean surface level and can be described by means of the RMS (Root Mean Square) value around it (R_q) and the related wavelength (λ_q).

Assuming a horizontal surface ($\overline{z}$), roughness is then given by

$$R_q = \sqrt{\frac{1}{N}\sum_{i=1}^{N}(z_i - \overline{z})^2} \tag{1}$$

where z_i is the measured quota for the i point and N the number of points. Defining Δq as

$$\Delta q = \sqrt{\frac{1}{N}\sum_{i=1}^{N}\left(\frac{\Delta z_i}{\Delta y_i}\right)^2} \tag{2}$$

where Δy_i the spacing between adjacent points, the wavelength λ_q is

$$\lambda_q = 2\pi\frac{R_q}{\Delta q} \tag{3}$$

Therefore R_q is a measure of the roughness amplitude, λ_q is a measure of its characteristic length.

We selected $1 \times 1\,\mathrm{cm}^2$ "nearly flat" areas, i.e. we chose areas where there was not abrupt shape variation within them, representative of the whole sampled area. Moreover, in order to correct any minor shape variation (waviness) within the sample area, for each acquired line a parabolic fitting curve was computed and subtracted from the data. The RMS roughness value was computed on each acquired line, and the mean value and the standard deviation were then calculated for each sample area. The results are shown in Fig. 4, together with the error bars representing the measurement variability range.

A more detailed study of the roughness will be carried out by varying the dimensions of the sub-area under investigation, and by varying the investigated area itself, since roughness measurements of marble statues is quite an unexplored field, due to the absence of rules or case studies.

By applying suitable filters (*embossing*) to the acquired 3D maps of the surface, a raking light illumination is simulated. This qualitative approach shows the corrosion of the investigated areas: working signs, scratches, chisel marks and also the possible signs left during the restoration (Fig. 5).

Area	Roughness RMS (microns)
Head	38.61
Shoulder	44.64
Sling	79.89
Chest	22.61
Right foot	30.89
Left foot finger	62.74

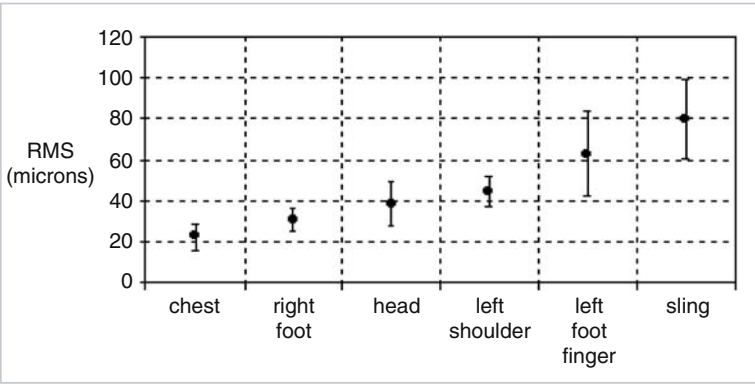

Fig. 4. The table and the roughness RMS graph for the six investigated areas

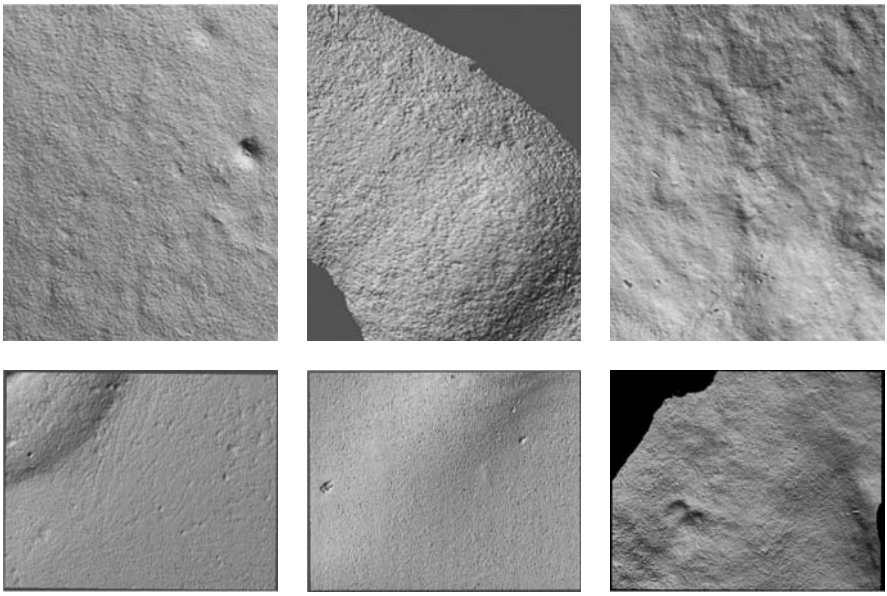

Fig. 5. The investigated areas: from *top left*, clockwise, the left shoulder, the left foot, the sling, the head, the right foot and the chest

5 Conclusions

In this paper we reported the roughness measurement of the Michelangelo's David, carried out by a system assembled by the Artwork Diagnostic Group of INOA. This preliminary measurement underlines the complex situation of the marble surface due to previous restoration interventions and to pollutant. At the end of the present restoration the measurements will be repeated and the two situations will be compared. These measurements will be used to analyze how the cleaning process has affected the surface of the statue, in the selected areas.

References

1. D J Whitehouse, *Handbook of Surface Metrology,* Institute of Physics Publishing Bristol and Philadelphia
2. Spragg R Cand Whitehouse DJ, 1970/1 *A new unified approch to surface metrology* Proc. ImechE 185 47–71
3. D. Charlot, *Holographie conoscopique – reconstructions numeriques,* Annales des Telecommunications 9:23–26, 1988
4. G. Y. Sirat and D. Psaltis, *Conoscopic holograms,* Opt. Comm., 9(65):243–245, 1988
5. G. Y. Sirat and D. Psaltis, *Conoscopic holography,* Optics Letters, 10(1): 4–6, 1985
6. M. Levoy, K. Pulli, B. Curless, and S. Rusinkiewicz, "The Digital Michelangelo Project: 3D scanning of large statues", In Comp. *Graph. Proc., Annual Conf. Series* (Siggraph' 00), Addison Wesley, July 24–28 2000, pp 131–144

Integration of Imaging Analysis and 3D Laser Relief of Artworks: A Powerful Diagnostic Tool

L. Marras, R. Fontana, M.C. Gambino, M. Greco, M. Materazzi,
E. Pampaloni, A. Pelagotti, L. Pezzati, and P. Poggi

INOA – Istituto Nazionale di Ottica Applicata, Largo E. Fermi 6, 50125 Firenze, Italia
benículturali@ino.it

Abstract. When analysing a work of art, imaging data from multiple sources can be effectively integrated and added to a 3D digital model, in order to form an improved multi-dimensional dataset. Herein we present the IR-colour reflectography, the UV fluorescence and the 3D microprofilometry diagnostic devices, developed at INOA, and we discuss the integration of 2D and 3D datasets, the former giving information of the surface (or nearly sub-surface) properties of a painting, the latter giving shape information of the surface itself.

1 Introduction

Any imaging digital diagnostic technique produces as a result a 2D map of points. The data are generally acquired by remotely sampling the object on a spatially dense grid (image), either point by point (scanning), or acquiring the whole map at once. A certain grey level is then associated to each picture element (pixel), according to the measured value. The tonal dynamics depends on the number of dedicated bits. Imaging techniques are well suited for the analysis of nearly flat objects like panel and canvas paintings or frescoes.

The state of the art diagnostic tools for paintings are mainly based on a 2D representation, and they are focussed on providing information on the history, the nature and the state of conservation of the object.

In the last few years, also 3D techniques have been applied to the analysis of artworks. However, they have been mainly applied to statues, architectures, and archaeological objects, and only rarely to paintings, often considered as flat objects. With the evolution of highly accurate systems, the 3D measurement of painting surfaces has revealed many and interesting aspects, especially when the 3D data are related to the 2D ones, and it is possible to analyse the two sets together.

2 The Diagnostic Techniques

The aim of the optical research at INOA is to develop innovating imaging and 3D devices and techniques that could improve the classical diagnostic

methods. Moreover we aim at combining and comparing the data acquired with the various techniques to obtain a more complete database. Hereafter we present the developed devices. In following paragraph, their integration will be discussed.

Infrared (IR) reflectography [1, 2] is one of the most suitable optical techniques traditionally employed in non destructive diagnostics of ancient paintings. Thanks to partial transparency to NIR radiation ($\lambda = 0{,}8$–$2\,\mu$m) of the materials which compose the pictorial layers, it allows to reveal features underlying the external layers of panels, canvas and wall paintings.

Therefore reflectography allows the revelation of pictorial layers hidden by superimposed ones, as well as the visualization of the under-drawing, executed by the artist on the preparation. The reflectogram can be obtained by acquiring the image of the back-scattered NIR radiation from a reflecting preparation; the visibility of the underlying features depends on thickness and chemical composition of the paint layers, on the contrast between the radiation reflected by the preparation and the underdrawing, and on the materials which compose them. The paints transparency generally increases with the radiation wavelength. For $\lambda = 1.6 - 1.7\,\mu$m nearly all the pigmented compounds are at least partially transparent.

The high resolution INOA scanning device (Fig. 1) has a spatial sampling of 4 points/mm (16 points/mm^2) and a tonal dynamics of thousands of gray level. The quality of the IR images acquired with this device is still not achieved with any other traditional system. Images are obtained by scanning the paintings surface with an optical head mounted on an X–Y motorized translation stage; the optical head, holding the lighting and the detection

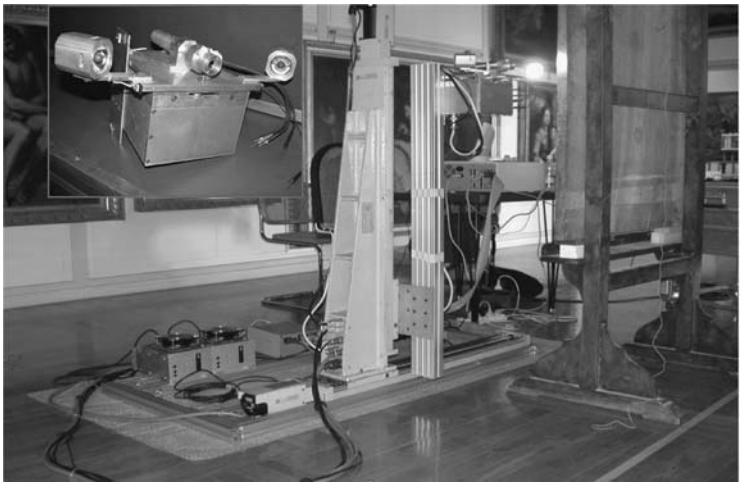

Fig. 1. The IR-Colour scanner in the Borghese Gallery (Rome) and the Optical Head

systems, moves jointly with the vertical stage. Since the lighting and detection systems move together, the surface warming is minimized and a uniform illumination is ensured.

The detection system is composed by an IR InGaAs photodiode, having spectral response between 0.9 and 1.7 μm, and 3 photodiodes sensitive in the visible region of the spectrum. This allows the simultaneous acquisition of the reflectogram and of the colour image with the same spatial resolution, thus allowing a perfect superimposition. A point by point comparison between the colour image and the IR reflectogram greatly improves the interpretation of this last one. The use of a single element instead of spatially – extended sensors, removes both the non-uniform lighting problem, the geometric distortions typical of objectives and large sensors, and the trouble of finding aberration-free lenses for NIR spectral region.

Inside the optical head, an achromatic doublet with f = 73 mm conjugates four adjacent points of the painting surface on the terminations of four optical fibers, each coupled with a photodetector corresponding to the IR or a RGB colour channel. These terminations are mounted to keep the core-to-core spacing at a proper distance, equal to the sampling step of 250 μm. The detector output signals are processed by 12 bit A/D converters, resulting in a tonal dynamics of thousands of gray levels each channel. The colour image and the reflectogram are then reconstructed in a standard image format by a purpose-developed software.

The *ultraviolet (UV) fluorescence* is another very useful non destructive technique for painting diagnostics. When a paint surface is lightened by UV radiation, this is partially reflected and partially absorbed by the external layers; a fraction of the absorbed radiation is then re-emitted in the visible spectrum (400–750 nm) as fluorescence radiation, depending on the contribution of the external transparent varnishes, the binders and the pigments used.

Binders and pigments are mixed together to obtain different compounds, each with a characteristic fluorescence spectrum. This distinctive characteristic allows to distinguish and locate each material on the painting surface. Varnishes, if laid uniformly over the painting surface, give a diffuse and uniform contribution, which can partially hide the radiation emitted from the underlying layers; however, their fluorescence changes in time, and this can help to locate damaged, retouched or restored areas.

The device developed at the INOA (Fig. 2) [3] has a cooled CCD camera, with a high sensitivity, 14 bit, and a silicon matrix of 1024 × 1024 effective pixels, which is very sensitive until nearly 1100 nm, coupled by a Rodenstock 50 mm objective to a 2" filter wheel, as acquisition tool. To acquire a multispectral fluorescence image a filter wheel with 7 interferential filters, with a bandwidth of 50 nm each, able to cover nearly all the visible spectrum (400 – 700 nm) has been set up.

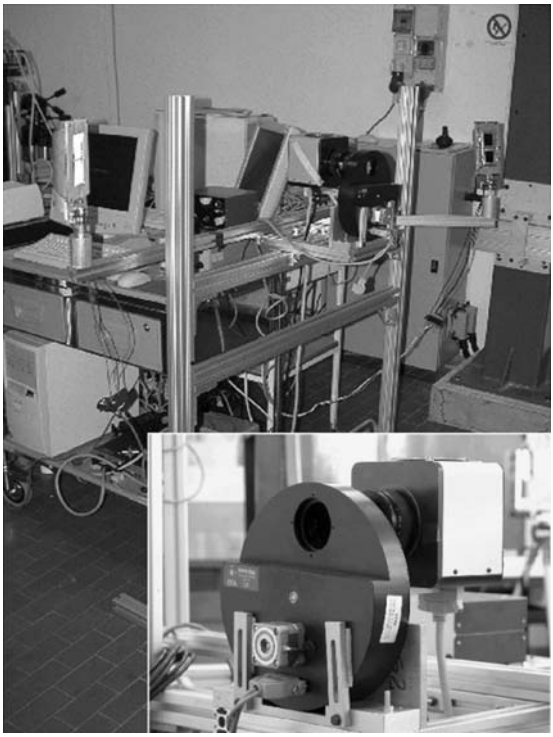

Fig. 2. The UV fluorescence device, with a detail of the CCD camera and the filter wheel

The lighting system is a visible-filtered flash Xenon lamp that leads to some advantage respect to the traditional photographic technique: the flash can be synchronized to the exposure time of the camera, allowing to work in a not fully darkened environment, and reducing the radiating time of the painting surface. This is important, since the UV radiation produces artificial ageing on pigments.

The developed multispectral acquisition technique makes a spectral and colorimetric characterization possible, and the digital format easily allows to manipulate the acquired data in order to highlight the different features of the painting. For example, in the multi-spectral recomposed images, the contrast factor between areas of different fluorescence can be greatly emphasized with respect to the RGB photographic image in order to better locate otherwise difficult to detect non-homogeneities.

The *conoscopic micro-profilometry* [4, 5] is an optical technique that allows the measurement of the shape of an artwork. This represents an important element for the study of the artwork and the determination of its conservation state; moreover, measurements realized at different times can provide data on the deformations induced by mechanical stresses, (due for

example to variations of the microclimate), the degradation of the surfaces subjected to atmospheric agents or the shape altering due to restorations.

The 3D digital model can be used for the measurement of colour raisings, detachments and engravings, or the detection of support deformation; moreover, via software, it is possible to apply to the 3D model various kinds of rendering or some digital filter, e.g. simulating the shading of raking light photography.

The INOA prototype (Fig. 3) makes use of a distance-meter device based on conoscopic holography; this interferometric technique combines the capability to work on surface of different materials, highly contrasted or reflecting, with a very high resolution at angles very close to grazing incidence (up to $\pm$ 85°). The conoscopic probe is a video camera coupled with a conoscopic module, consisting in an uniaxial birefringent crystal sandwiched between two circular polarizers. A laser diode with $\lambda = 680\,\text{nm}$ lighten a spot area on the surface; the module then splits the light beam coming back from the investigated point in the ordinary and the extraordinary beam, that interfere after having run different optical paths. By measuring the fringe spacing was be obtained the distance of the investigated point from the conoscopic probe.

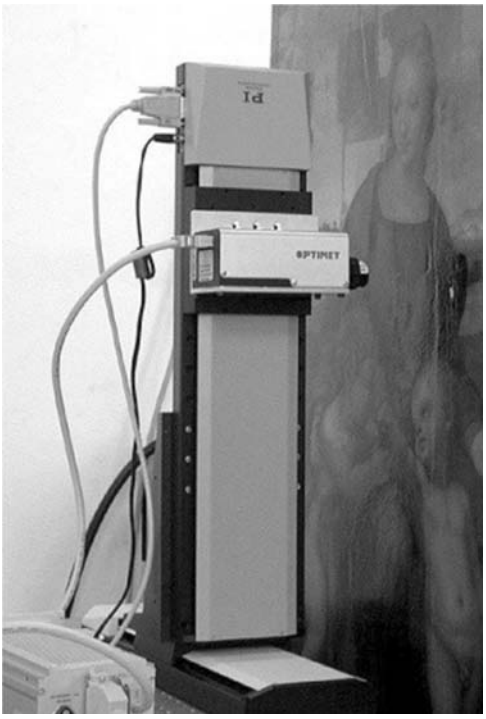

Fig. 3. The conoscopic probe during a measure on the Madonna del Cardellion of Raffello

The conoscopic micro-profilometer used in the prototype, produced by Optimet, has a quota resolution of about 1 µm, an accuracy better than 6 µm, and a transverse resolution of about 20 µm (the laser beam diameter). The probe is mounted on two motorized linear stages, allowing a maximum scanning area of 280 × 280 mm^2. The typical acquisition rates ranges from 100 to 400 Hz.

3 Data Integration Strategies

A reliable integration of data from various sources can be obtained with a consistent spatial referencing and then with a good superimposition of different datasets. The 2D data are usually sampled on evenly spaced XY grids, so that 2D datasets are projections on a flat surface of some measured quantity. In this plane, the spacing between adjacent samplings can be related to a physical distance, with criteria depending on the set-up of the different instruments: as the spatial position of the measured pixels can change, the superimposition between sampling grids could require a data interpolation process.

Hardware integration is the best way to obtain spatial correspondence: when acquiring simultaneously the data of interest, the spatial sampling of the object is identical and the results are directly comparable. When the hardware integration is not physically possible, software integration must be used, because images acquired with different techniques cannot be merely superimposed. Corrections for geometrical distortions, as well as spatial referencing, have often to be taken into account. In case of the spatial sampling step kept constant, or congruent, and negligible geometrical distortion, the integration can be done almost exactly. The quasi-flat surfaces of paintings greatly help to ease an exact superimposition.

The same considerations are applicable when merging a 2D dataset with a 3D one. Hardware integration has identical rules, with the introduction of the third coordinate (the quota). For a software integration, the projection made at the measurement stage to obtain the 2D dataset is to be "reversed" on the 3D digital model of the object shape. The IR-Colour scanner is a case of hardware integration: the superimposition of IR and colour image leads to a strong impact on the reflectographic diagnostic technique, because greatly improves the readability of the underdrawings and can contribute to the diagnostics, the knowledge of the realization techniques, the historical framing and the attribution of the painting. On the contrary, adding 3D datasets to IR-Colour image needs a software integration.

4 Applications

We show here the application on the "Madonna dei Fusi" attributed to Leonardo da Vinci (private collection), a $38 \times 50\,\mathrm{cm}^2$painted panel; it was scanned by means of the micro-profilometer with a $125\,\mu\mathrm{m}$ sampling step, thus gathering more than 12 million points. The 3D model revealed the presence of the imprinting of a canvas used for the transfer during restoration, with a warp yarn step of about $100\,\mu\mathrm{m}$ and a relief amplitude of about $25\,\mu\mathrm{m}$.

Moreover, the 3D relief permitted to identify a few specific critical areas that were investigated with a higher sampling density ($50\,\mu\mathrm{m}$ spacing), like the Child's head (Fig. 4).

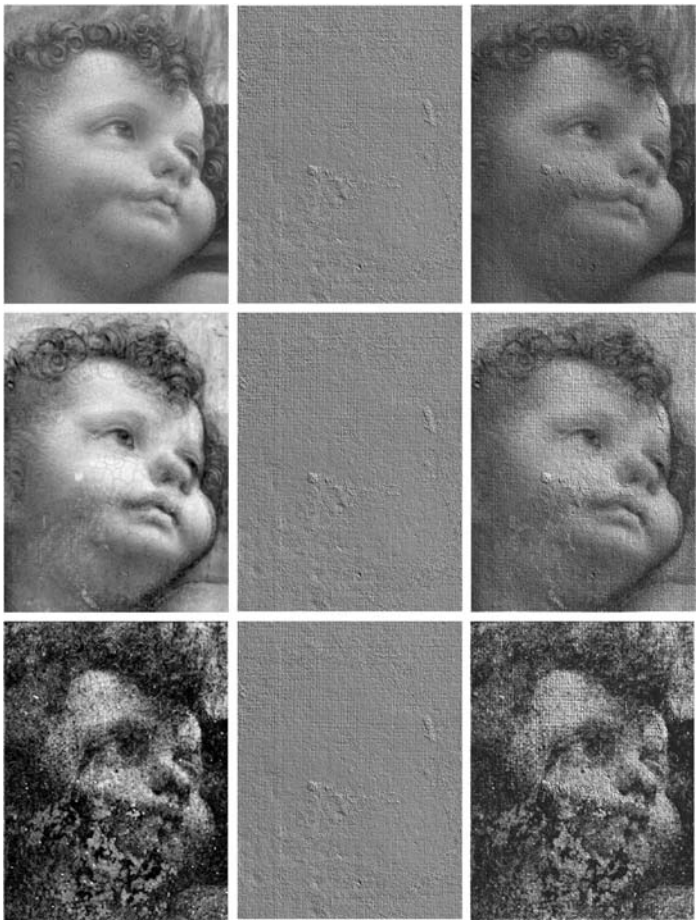

Fig. 4. Attributed to Leonardo da Vinci, Madonna dei Fusi; detail of the Child's face with the colour, IR and UV fluorescence images (*left*), the 3D shape relief (*middle*) and the superimpositions 2D-3D (*right*)

The retouch on the Child's forehead is not visible in the colour image whereas is clearly distinguishable in the 3D model, but any reference with the painting is there lost. The superimposition of colour image and simulated raking light image of the 3D model, spatially locates the protruding retouch (60 to 90 μm over its extension area). This retouch is clearly visible in the IR reflectogram and in the fluorescence UV image but it can be exactly quantified only by means of the superposition to the three-dimensional model.

A wide retouch is well visible also in the Child's cheek and neck, where the colour image is able to show tonal non-homogeneities. Only the 3D model together with the UV fluorescence, however, can reveal several details on the shape and the extension of this retouched area, which appears to be very complex.

5 Conclusions

In this paper, we presented the integration of IR and colour images with UV fluorescence and a high-resolution 3D measurement.

We discuss how data integration represents a new, significant upgrade in the analysis of artworks, particularly for paintings. New results and better understandings of an object can be obtained by simply adding together and comparing datasets gathered with various techniques. The integration can be achieved both at software and at hardware level, depending on if data have been acquired separately, and then merged, or if they have been acquired simultaneously. The optimal data merging can be obtained when the spatial step of the acquisition is the same for all the datasets.

As an example, we showed how integrating IR, UV and 3D data, provides a new powerful means to reveal retouches in a panel painting.

References

1. D. Bertani et al., "A Scanning Device for Infrared Reflectography", *Studies in Conservation*, Vol. 35, p. 113, 1990
2. R. Fontana, M. C. Gambino, M. Greco, L. Marras, M. Materazzi, E. Pampaloni, L. Pezzati, and P. Poggi, "New high resolution IR-colour reflectography scanner for painting diagnosis", *SPIE International Symposium on Optical Metrology*, Munich, June 2003
3. F. Fabbri, P. Mazzinghi, and A. Aldrovandi, "Tecnica di identificazione di materiali pittorici attraverso l'acquisizione di immagini digitali multispettrali in fluorescenza UV", *Quaderni di Ottica e Fotonica*, n. 6, pp 94–104, 2000
4. J. F. Asmus, "Holograph interferometry of painted surfaces",Conservation of wood in Painting and the Decorative Arts, Oxford Congress 1978, IIC 141–144
5. D. Charlot, ≫Holographie conoscopique – reconstructions numeriques≪, *Annales des Telecommunications* pp 23–26, 1988

Parallel Acquisition of 3-D Surface Coordinates and Deformations by Combining Electronic Speckle Pattern Interferometry and Optical Topometry

D. Dirksen[1], B. Kemper[2], A. Guttzeit[2], G. Bischoff[3], and G. von Bally[2]

[1] Department of Prosthodontics, University of Muenster, Waldeyerstrasse 30, D-48129 Muenster, Germany
dirksdi@uni-muenster.de
[2] Laboratory of Biophysics, University of Muenster, Robert-Koch-Str. 45, D-48129 Muenster, Germany
LBiophys@uni-muenster.de
[3] Lasercentre, University of Applied Sciences Muenster, Stegerwaldstr. 39, D-48565 Steinfurt, Germany
laserlab@fh-muenster.de

Abstract. Electronic Speckle Pattern Interferometry (ESPI) is a well-established tool for non-destructive testing which allows the detection of surface deformations and micro-movements on a sub-micrometer scale. The interpretation and evaluation of the resulting correlation fringe patterns, however, can be complicated by perspective image distortions as well as by an image scale varying with depth if the object under investigation is extended in depth. In this paper a method is presented which combines ESPI with a stereoscopic 3-D coordinate measurement using photogrammetry. With this approach every image detail including the fringe patterns can be precisely oriented in space.

1 Introduction

Electronic Speckle Pattern Interferometry (ESPI) is a highly sensitive technique for monitoring surface alterations such as deformations and micro-movements on a sub-micrometer scale [1] as they may occur e.g. during a laser cleaning process. In the case of objects which are extended in depth, however, a precise evaluation of the interferometric data is complicated by perspective image distortions as well as by an image scale varying with depth. These problems can also lead to errors in the calculation of the interferometric sensitivity vector [2] and thus in the resulting displacements. Moreover, in the case of complex three-dimensional object strutures, the exact allocation of the observed processes can be difficult. Photogrammetry, on the other hand, is a well established technique for the optical acquisition of 3-D coordinates from at least two camera images taken from different viewpoints [3]. It offers the tools for a calibrated quantitative investigation of image geometries. A combination of these methods, therefore, has an interesting potential

for the digital documentation and analysis of cultural heritage; e.g. during a laser cleaning process, for which then various types of diagnostic tools may be employed for numerical evaluation and comparison.

2 Experimental Methods

The setup for combined ESPI and photogrammetry (topometric ESPI) is illustrated in Fig. 1. The coherent light source is an argon ion laser with etalon ($\lambda = 514.5\,\text{nm}$). With an acousto-optic modulator (AOM) the light intensity can be regulated by using the first diffraction order. Behind the AOM the laser light is divided into object illumination (O) and reference waves (R). For the object wave as well as for reference wave the light is coupled into mono mode optical fibers. For object illumination, a micro lens system is fixed at the end of the fiber of the object wave for beam expansion. The adjustment of the mean intensity ratio of the of R and O can be adjusted by neutral density filters and polarizers. The interference patterns are recorded by a progressive-scan (full frame) digital camera (c-mount objective, focal length $f = 50\,\text{mm}$) with a CCD-Sensor (Sony XCD 700, resolution: 1024×768). The camera is

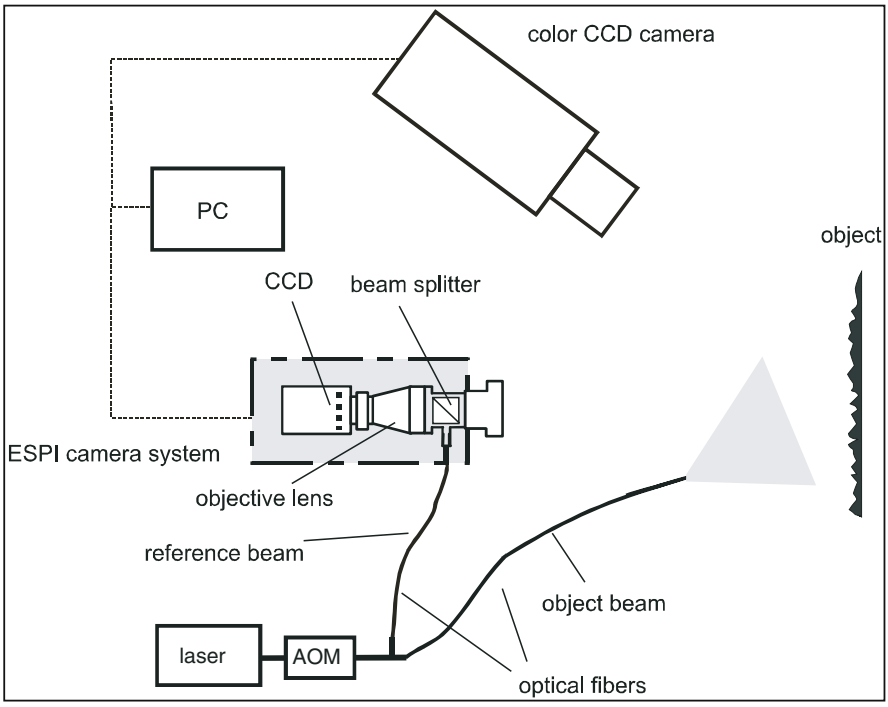

Fig. 1. Topometric ESPI camera system. PC: personal computer, AOM: acousto-optic modulator

connected to the image processing system (PC, Pentium IV CPU, 2.4 GHz) via a digital interface (IEEE1394), thus no extra image processing board is necessary. This system allows one to record the intensity patterns with 15 Hz with variable exposure times. Simultaneously, the related correlation paterns can be visualized with a rate of 7.5 Hz by. (For details see [4, 5]).

For photogrammetric calculation of 3-D coordinates within the measurement volume, an additional color CCD camera (Sony DFW X700, resolution 1024×768, IEEE 1394 interface, c-mount objective, $f = 50$ mm) is used. After calibrating both cameras, i.e. determining the imaging parameters via a least square matching algorithm [6, 7] the orientation of each camera is calculated using a target field behind the object under investigation (Fig. 2). After the marking of a number of identical (homologous) object points in both images, the 3-D coordinates can be calculated using the collinearity equations [2]. By grouping coordinate triples, a triangulated surface is generated to which the corresponding image sectors from either camera can be mapped as textures. Both the white light and the ESPI images can be observed from arbitrary viewing angels with a 3-D viewer developed in the Java programming language.

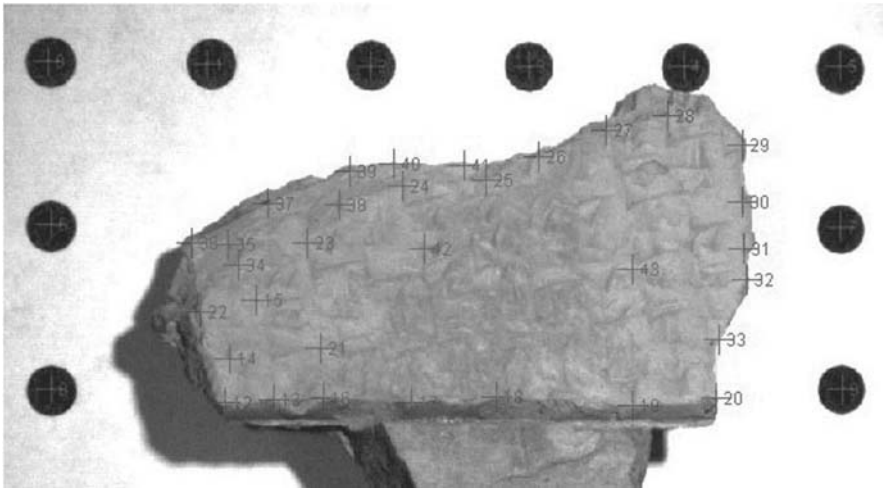

Fig. 2. Image (ESPI camera) of a fragment of a cuneiform tablet with photogrammetric targets (*circles*) for external orientation and measuring marks (*crosses*)

3 Results and Discussion

To demonstrate the method, a fragment of a cuneiform tablet (Fig. 2) is investigated with the topometric ESPI system. Surface deformations are induced

by heating the sample for a few seconds. During the cooling process, ESPI correlation fringes are observed (Fig. 3, subtraction method, exposure time 1/128 s). Before or after the ESPI measurement, white light images both with the ESPI camera and the additional color CCD camera are recorded. After calculating a number of 3-D coordinates, the white light image is projected onto the reconstructed surface (Fig. 4).

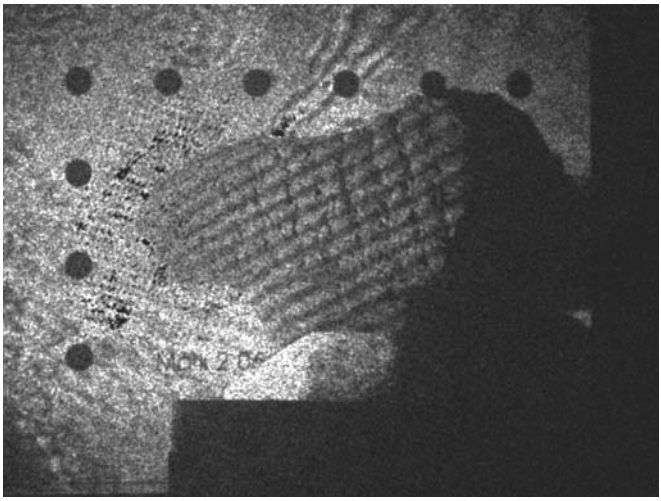

Fig. 3. Correlation fringes on the cuneiform tablet as observed with the ESPI camera system after heating the fragment

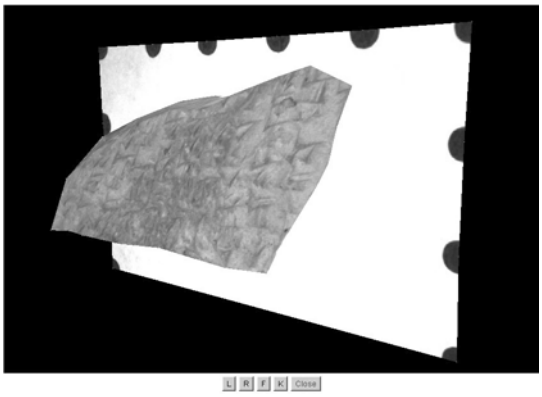

Fig. 4. White light camera image of the cuneiform tablet projected to a triangulated surface acquired by photogrammetric coordinate measurement

As the camera orientations are the same as during the ESPI measurement – it has to be kept in mind that the displacements during an interferometric measurement take place on a microscopic scale, whereas the photogrammetric orientation only changes in consequence of macroscopic displacements – the ESPI fringe images correspond to the same 3-D geometry. They may thus be projected onto the same triangulated surface (Fig. 5).

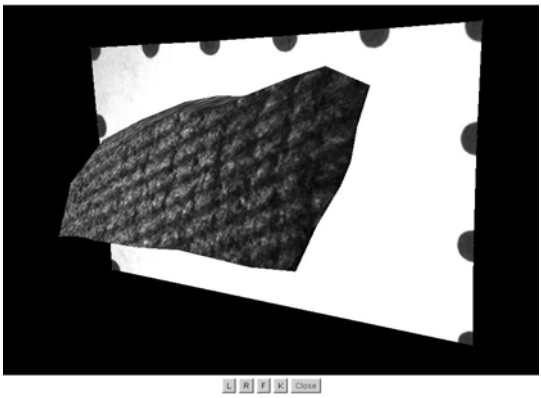

Fig. 5. ESPI correlation fringe image of the cuneiform tablet projected to a triangulated surface acquired by photogrammetric coordinate measurement

4 Conclusions

The presented method combines ESPI correlation fringe images, which indicate object deformations or movements on a sub-micrometer scale, with topometric information on the object geometry. Especially in the case of non-planar objects, this method allows a noticeably better spatial allocation of object behavior as can be seen by comparing Fig. 3 and 5. In addition, image distortions caused by deficiencies of the objectives used can be reduced numerically by employing the imaging parameters obtained during the calibration process. As the developed photogrammetric system does not require additional information on the used sensor or imaging device, it is applicable to a wide range of imaging systems which include even endoscopes, which, in turn, are of special interest if ESPI measurements inside cavities are regarded (see also [4]).

Acknowledgements

Financial support of the European Union within the frame of the Interreg IIIa program (project ECE:ACT) is gratefully acknowledged.

References

1. R. Jones and C. Wykes, *Holographic and Speckle Interferometry - A Discussion of the Theory, Practice and Application of the Techniques*, Cambridge University Press, 1983
2. T. Kreis, Holographic Interferometry: *Principles and Methods*, Akademie-Verlag, 1996
3. K. Kraus, Photogrammetry Vol. 1, Dümmler Verlag, 1993
4. B. Kemper, D. Dirksen, W. Avenhaus, A. Merker, and G. von Bally, *Endoscopic Double-Pulse Electronic-Speckle-Pattern Interferometer (ESPI) for Technical and Medical Intra Cavity Inspection,* Applied Optics, 39 (22), 3899–3905, 2000
5. B. Kemper, D. Dirksen, J. Kandulla, and G. von Bally, *Quantitative determination of out-of-plane displacements by endoscopic electronic-speckle-pattern interferometry,* Optics Communications 194, 75–82, 2001
6. A. A. R. Cooper and S. Robinson, *Theory of close range photogrammetry*, in: K. B. Atkinson, *Close range photogrammetry*, Whittles publishing, 9–51, 1996
7. Z. Zhang, *A versatile camera calibration technique for high-accuracy 3D machine vision metrology using off-the shelf tv cameras and lenses*, IEEE Journal of Robotics and Automation, 3(4), 323–344, 1987

Scanning Laser Doppler Vibrometry Application to Artworks: New Acoustic and Mechanical Exciters for Structural Diagnostics

A. Agnani and E. Esposito

Dipartimento di Meccanica – Università Politecnica delle Marche, via Brecce Bianche, 60131, Ancona, Italy
alexia@mm.univpm.it

Abstract. After first attempts some years ago, the scanning laser Doppler vibrometer has become an effective way of diagnosing different types of artworks; successful applications regard frescoes, icons, mosaics, ceramic artefacts and wood inlays. Also application to historical bridges has been successfully developed and a recently approved European Commission project will see the employment of scanning laser Doppler Vibrometry (SLDV) for the dynamical characterization of ancient buildings. However, a critical issue consists in the adequate excitation of the structure under test. Moreover different types of defects and different kinds of artworks require different types of excitation, so this topic needs a deep consideration. In this work we will present two new types of exciters developed at our Department, namely an acoustic exciter and a mechanical one. Acoustic exciters allow remote non-invasive loading but are limited in the lower frequency range and in the amount of vibrational energy input into the structure. The proposed automatic tapping device based on a commercial impact hammer overcomes these problems. Also another acoustic exciter, a HyperSonic Sound (HSS) source has been evaluated, showing interesting features as regards sound radiation.

1 Introduction

One of the most important problems in every kind of mechanical measurement is to provide an adequate excitation of the object under study. In the case of artworks the biggest issue is to limit as much as possible the exciter intrusivity; for this reason, a number of acoustic sources have been developed and tested at our department. The basic requirements of an acoustic source employed in this way are briefly summarised as:

1. high efficiency/sound pressure level;
2. well controlled radiation region;
3. uniform frequency response;
4. limited annoyance to operators and nearby persons.

Efficiency and annoyance are typically contrasting features, as in the case of uniform directivity horns; a solution employing a highly focused source has

been found using an elliptic mirror [1], but in that case the active region on the examined surface is limited to a disc with a radius of a dimension comparable to the wavelength of sound in air. Our new proposals still regards sources with a limited radiation lobe, but with a plane wave behaviour, thus ensuring a long throw but again a small angular aperture. Two different solutions have been tested:

1. a parabolic mirror with a midrange loudspeaker in its focus,
2. the HyperSonic^{TM}Sound (HSS^{TM}) source.

Due to its geometric shape, the first device will provide a sound plane wave if the speaker is uniformly illuminating the mirror, while the second one employs a mixed acoustic/ultrasound approach to directly produce a sound wave with a lobe aperture of approximately seven degrees. HSS is a proprietary, ultrasonic-to-audio, parametric sound generator, developed and refined in the labs of American Technology Corporation. The HSS audible sound is created by the ultrasonic interaction with the air which causes the audio information to be demodulated from the ultrasonic beam into audible sound; at some distance, usually greater than about six meters, the ultrasonic beam will be at a lower level than the audio, no longer contributing significantly to the production of audible sound [2, 3].

To verify systems performance our work has thus been divided into three steps:

1. construction/acquisition of acoustic sources and full characterization in the Department semi-anechoic chamber;
2. validation as diagnostic support tools using a fresco sample;
3. comparison with a well-established acoustic exciter, the horn loudspeaker.

As regards mechanical contact devices, they become necessary when acoustic energy is not providing a sufficient excitation of studied objects, in terms of amplitude and/or frequency content; the latter case has been fully solved by the use of small piezo exciters [1], while to ease the first issue we have designed a tapping device employing a small impact hammer driven by an electromagnetic actuator. In Fig. 1 we present photos of proposed devices.

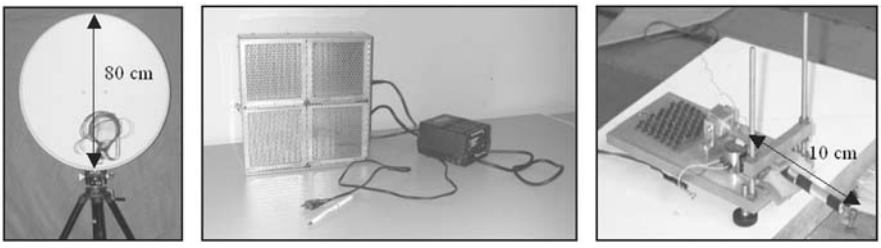

Fig. 1. Parabolic mirror exciter, HSS Mod. R220A, automated impact hammer

2 Experimental Results

The parabolic mirror has been evaluated using both an Ometron VPI4000 scanning laser Doppler vibrometer (SLDV) and a Bruel & Kjaer acoustic intensity measurement system. First test has allowed determining the absence of spurious vibrations in the frequency range of interest (> 500 Hz) with a maximum sound pressure on the dish of 104 dB, while the second one has been employed to describe the emission lobe of the system, defined by the angle where the pressure value is –3 dB with respect to the on axis maximum. Table 1 summarises our findings for this exciter.

Table 1. Parabolic mirror radiation characteristics

Frequency (Hz)	1000	1250	3150	5000	8000	10000	80–10000**
Emission lobe (degrees)	12*	12*	10	8.5	6	6	5

* pressure amplitude decreases just 1 dB at grid edge. Grid appears to be too small to measure actual radiation lobe that is underestimated

** pressure amplitude calculated as RMS value in the 80–10000 Hz band

Acoustic intensity has been also applied to the HSS and results are reported in Table 2. In this case it has been possible to correctly measure the emission lobe even at lower frequencies, where it is limited at just 14 degrees. At higher frequencies the HSS and the parabolic dish show a similar behaviour, so the former exhibits a more consistent performance altogether. Finally we characterized the hammer in terms of its Frequency Response Function (FRF) and time response, using it to hit a sample of beech wood: a peak force of 17 N and a useful frequency range of almost 5 kHz will allow using this device in many different situations. The force developed by a human being when knocking on such a surface is about 30 N, while the pressure of acoustic sources driven at 100 dB SPL is limited to values of 2 N/square meter [1].

Table 2. HSS radiation characteristics

Frequency (Hz)	1250	3150	5000	000	10000	80–10000
Emission lobe (degrees)	14	14	10	6	6	8.2

As examples of the use of presented devices as companions of the SLDV in the diagnostic process, we show in Fig. 2 the identification of a delamination in a fresco sample (a) done by exciting it with parabolic dish (b),

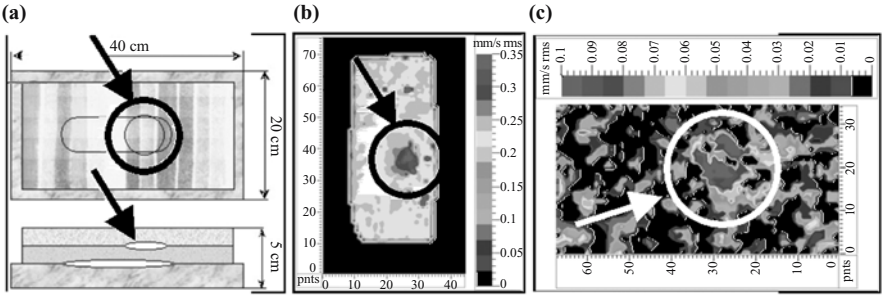

Fig. 2. Delamination identification in fresco sample (**a**) by parabolic dish (**b**) and HSS (**c**)

and by the HSS (c) at two and six meters respectively. Figures shows map of measured surface velocity, which will show greater values where a delamination occur due to greater vibration activity (see [4] for more details on the SLDV technique applied to artworks diagnostics). Both devices are able to lead to the identification of the upper defect, while the inner one is not detected; we must point out that this defect has not been identified by the horn either, Fig. 3, so there remain some doubts about its actual presence, although it has been included in the drawing submitted by the restorer that prepared the sample. Finally we present in Table 3a the comparison of the sound levels measured during our tests for defect detection; as we see, using focused sources not only gives good results for diagnostics but also greatly reduces the SPL far from the measurement site, thus reducing the annoyance for technicians and for other people being around as well (see Fig. 4 for identification of measurement positions). The sound level has been kept constant at the sample position (A) when comparing different exciters; the dish and the HSS could not deliver more than the indicated levels and the horn has been regulated consequently.

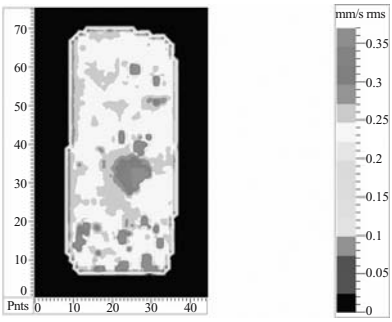

Fig. 3. Delamination identification in fresco sample by horn loudspeaker

Table 3a. Sound levels (dB) of parabolic dish and horn sources during diagnostic process on fresco sample (distance between source and sample is 2 m, input signal white noise)

Parabolic dish	Horn	Position
102.8	102.8	A (sample)
91.2	99	B (SLDV)
77	81.4	C (far field)

Table 3b. Sound levels (dB) of horn and HSS sources during diagnostic process on fresco sample (distance between source and sample is 6 m, input signal white noise)

HSS	Horn	Position
77.7	77.7	A (sample)
68	90.5	B (SLDV)
65.5	74	C (far field)

Finally, the hammer has been employed on a simple wood structure, a standard pallet, Fig. 5(a), that has been examined by SLDV before (b) and after (c) a board had been broken. The free edges of the damaged area vibrate much more than the rest of the structure, so the crack is clearly identified by the higher values of vibration velocity as shown in Fig. 5(c).

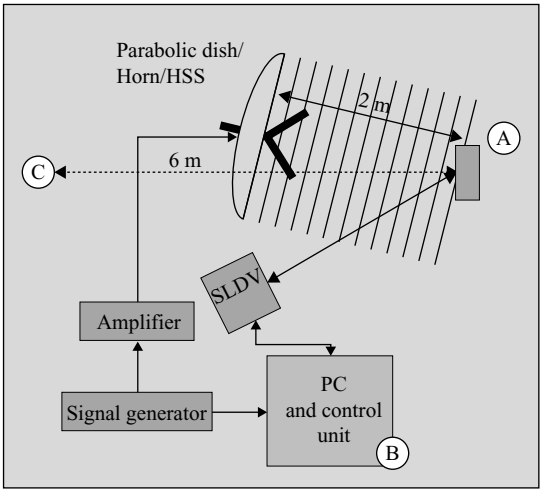

Fig. 4. Measurement positions as referred in Tables 3a + b

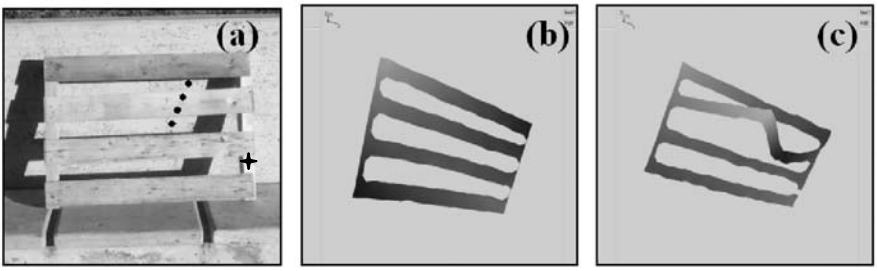

Fig. 5. SLDV measurement of a wood structure (**a**) 3D map of vibration velocity at 18.75 Hz before cracking (**b**) and after cracking a board (**c**). Black star identifies point of impact of the hammer

3 Conclusions

In this paper we have presented three new excitation sources for artworks diagnostics and verified their performance in terms of capability of exciting defects, respect of performance assumptions, low annoyance for the public. They showed great promises and are currently employed not only on frescoes and wood but also for other types of artworks, such as mosaics and ceramics.

References

1. P. Castellini, E. Esposito, N. Paone, and E. P. Tomasini, in *Proceedings of V International Conference on Optics Within Life Sciences - OWLS V*, Heraklion, Crete, 174, 13–16 October 1998.
2. American Technology Corporation "Theory, History, and the Advancement of Parametric Loudspeakers. A Technology Overview - Abridged Edition!", Part #98–10006–1100 Rev. C, 2001
3. American Technology Corporation "Frequently Asked Questions And Answers", Part #98–10050–AFAQ Rev. E
4. P. Castellini, E. Esposito, B. Marchetti, N. Paone, and E. P. Tomasini, in *Journal of Cultural Heritage*, Vol. 4/S1, 321, 2003

Supporting the Restoration of the Minerva of Arezzo

M.C. Gambino[1], R. Fontana[1], M. Greco[1], E. Pampaloni[1], L. Pezzati[1], P. Pingi[2], P. Cignoni[2], and R. Scopigno[2]

[1] Istituto Nazionale di Ottica Applicata (INOA), largo E. Fermi 6, 50125, Florence, Italy
mchiara@ino.it

[2] Istituto Scienza e Tecnologie dell'Informazione (ISTI), via G. Moruzzi 1, 56124, Pisa, Italy
pingi@isti.cnr.it

Abstract. The aim of this work has been to show how 3D scanning techniques can provide new, useful and powerful tools to the restorers. In fact, 3D models are able both to monitor the restoration process: e.g. variations of the shape of a statue, due for example to the removal of plaster and wooden parts, and to keep trace of the modifications that take place during the conservation operations: e.g. the polishing of a corroded bronze surface. The focus of this project was to acquire 3D data with different resolutions, with specially designed acquisition means, and to integrate and merge them with specially designed software tools. The first set of 3D data was obtained with a laser scanner, the other with a micro-profilometer. The whole statue known as the Minerva of Arezzo was investigated. The laser scanning was performed twice, before and during the restoration process, to monitor the variations of shape on the whole statue. The high-resolution survey with the micro-profilometer was carried out on selected areas, to monitor the corrosion of the bronze surface.

1 Introduction

The knowledge of the shape of an artistic object is an important element for both historical and artistic studies and for conservation; in particular, for an analysis of the artwork conditions and for supporting the restoration interventions. Three-dimensional models can be used to assemble 3D catalogues and archives, to realize virtual musea, to acquire information about the artwork history, to make moulds by fast prototyping and also to support the restoration process. For example, 3D models allow to locate mechanical stresses, to quantify the effects of the microclimatic variations (temperature and/or humidity), to measure the wear of the surface exposed to atmospheric agents or to monitor the shape variations of the statue introduced by the restoration process.

The shape complexity of the most part of artworks, such as sculptures, often makes inadequate the modeling by means of classic 3D tools, whereas 3D scanning [1–3] and modern graphic techniques are sufficiently accurate to provide a high fidelity reproduction of the shape of an object.

This work is aimed at the integration of different data in the 3D digital model of the Minerva of Arezzo. In fact, shape measurements were carried out by means of a laser scanner specifically devised to meet the needs and constraints found in restoration-oriented applications. The monitoring of the surface corrosion was achieved by means of a high-resolution microprofilometer [4]. A suite of software tools was developed for the integration of the two data set.

2 Surveying the Minerva

The Minerva is a bronze statue (see Fig. 1), presumably dated III century B.C., discovered in Arezzo in 1541. Normally located at the Archaeological Museum in Florence, it is currently under repair at the Restoration Centre of the Soprintendenza Archeologica of the Tuscany Region. The lower part of the statue was entirely restored with wood and plaster, while the right arm, from the shoulder, was integrated in 1785 and is bronze made. The artwork is about 155 cm high and its weight is about 150 Kg. The body is inscribable in a cylindrical volume having a diameter of about 50 cm, except for the protruding right arm, that extends outward for about 40 cm.

Fig. 1. The Minerva of Arezzo: images taken with a Nikon digital camera of the whole statue (*left*) and a detail of the head (*right*)

The planned restoration intervention foresees the removal of the non-original parts as well as the polishing of the aging corroded surface.

The 3D survey was carried out by means of a laser scanner realized by the *Art Diagnostic Group* of INOA. The laser scanner working principle, like that of most 3D profilometers, is based on the optical triangulation, which is obtained by projecting a collimated laser beam onto a target, and by acquiring the profile shape with an imaging device (a CCD). In details, as the object is passed through the sheet of light emitted by a laser, a CCD camera, located at a known position, sees the profile defined onto the object by the laser light. The spatial positions of sampled points in the profile are obtained by triangulation, provided that the relative position of laser, CCD camera and object are known, which it is previously obtained by measuring them when calibrating the instruments. The complete 3D acquisition is attained by scanning the object and by acquiring closely-spaced parallel profiles.

The instrument developed at INOA is composed by an optical head mounted on a motorized stage to allow the scanning of statues, high-relieves and architectural mouldings. The source employed is a diode-laser line projector ($\lambda = 670\,\text{nm}$, $P = 30\,\text{mW}$, fan angle 60°); the detector is a HRES CCD camera (1300×1030 pixel, $6.7\,\mu\text{m}$ wide, S/N$> 56\,\text{dB}$) equipped with a lens ($f = 16\,\text{mm}$) and a band-pass filter, chosen to match the wavelength of the laser light. Since the filter stops ambient light, but for a small window of wavelengths centered around the one emitted by the laser, this configuration allows the system to operate without the need for darkening the measurement environment.

The experimental set-up is shown in Fig. 2: in its typical configuration, the laser blade is horizontal, but to facilitate the scanning of hidden parts, the system can be oriented anyhow rather freely. The gantry consists of two vertical aluminum profiles on which the frame containing the motorized stage can be translated and rotated. The scanner has a quota resolution of $50\,\mu\text{m}$, an accuracy better than $0.3\,\text{mm}$ and a scanning area of about $30 \times 30\,\text{cm}^2$ with a stand-off distance of $50\,\text{cm}$. The acquisition time is about 4 minutes for 1 million points.

The surface corrosion measurement was carried out by means of a micro-profilometer composed by a commercial distance meter (Conoprobe 1000, Optimet see Fig. 3) mounted on a scanning device realized with two perpendicularly assembled motorized linear stages. The probe is equipped with a $50\,\text{mm}$ lens which sets a quota resolution of nearly $1\,\mu\text{m}$ and a dynamic range of $8\,\text{mm}$ at a stand-off distance about $40\,\text{mm}$. The overall accuracy is better then $6\,\mu\text{m}$. The scanning device is composed by two motorized high-precision ($0.1\,\mu\text{m}$) linear stages perpendicularly assembled. The system allows measurement on a maximum area of about $280 \times 280\,\text{mm}^2$. The instrument has a maximum transversal resolution of $20\,\mu\text{m}$ with an acquisition speed ranging from 100 to $400\,\text{point/s}$, depending on the set spatial sampling frequency. The whole system is computer controlled.

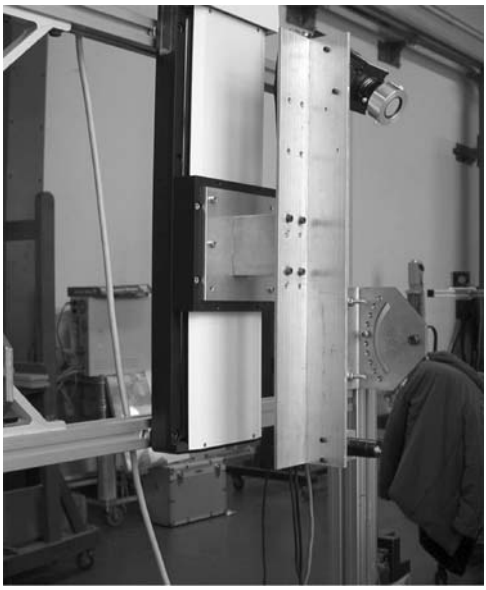

Fig. 2. Experimental set-up of the laser scanner realized at INOA: detail of the optical head

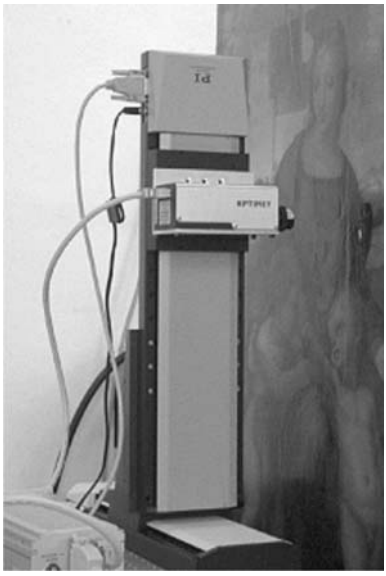

Fig. 3. The laser scanner micro-profilometer during a measurement on the panel painting "Madonna del Cardellino" by Raffaello

The probe working principle [5] is as follows: a light beam projected by a laser diode on the sample is both reflected and back scattered, and it impinges in an uniaxial birefrangent crystal placed between two circular polarizers. The ordinary and the extraordinary beams are then generated inside the crystal and produce an interference pattern.

3 Results

The complete digital model of the Minerva before its repair is shown in Fig. 4. For a complete acquisition of the whole statue surface, we took 119 range maps with different shooting area depending on the scanned part, with a spatial sampling frequency of 0.25 mm. The range maps acquired to scan the Minerva of Arezzo were registered and merged in a single [6], rather big, triangulated mesh of 26 millions of faces. To improve usability, the triangulated mesh was simplified by using an external memory simplifier [7]. The results presented are, thus, simplified models representing the whole statue, with about 1 M faces and a detail of the head with about 1.1 M faces (see Fig. 4).

Fig. 4. The Minerva of Arezzo: snapshot sampled from the complete digital model of (*left*) the full body and (*right*) the head of the statue

Other 3D surveys were realized during the various restoration phases in order to monitor the whole process. Six areas (the spur, the helmet, the shoulder, the hair and two areas of the waist) were investigated with the micro-profilometer. Each investigated area is $4 \times 5\,\mathrm{cm}^2$ and was sampled with a $50\,\mu\mathrm{m}$ step, corresponding to a range map of 801×1001 points. These acquired data were then processed, by specially designed software tools, in order to reveal very small details such as signs of working or corrosion. An example of the acquisition of the hair area is shown in Fig. 5.

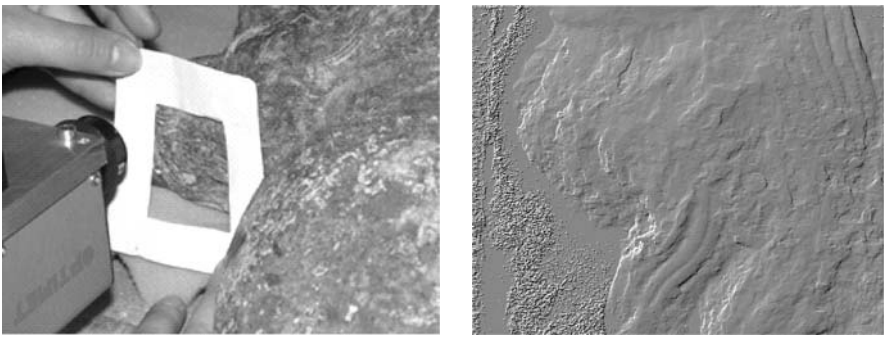

Fig. 5. The photo (*left*) and the elaborated acquisition (*right*) of the hear

The merging of the two 3D datasets [8, 9], the large one with the worst resolution and the small one with the highest resolution, presents some technical difficulties that made impossible to use the standard mesh reconstruction tools. For this reason a set of innovative software tools was designed in order to merge these two 3D data set that are very different in terms of scale (see Fig. 6).

4 Conclusions

A laser scanning device along with a number of software tools for high-quality 3D digital modeling of objects have been realized. This device was used for recording the shape of the Minerva of Arezzo before and during its restoration. The survey of small areas by means of micro-profilometry was carried out to measure the bronze surface corrosion of the statue.

The 3D model of the Minerva stands as the only description of the statue's shape, before the restoration process irreversibly changed it. During the statue's repair, the wooden inferior part as well as the right are have been removed. The 3D model can be used either to reproduce and place exactly the missing parts, or to keep trace of possible further form alterations.

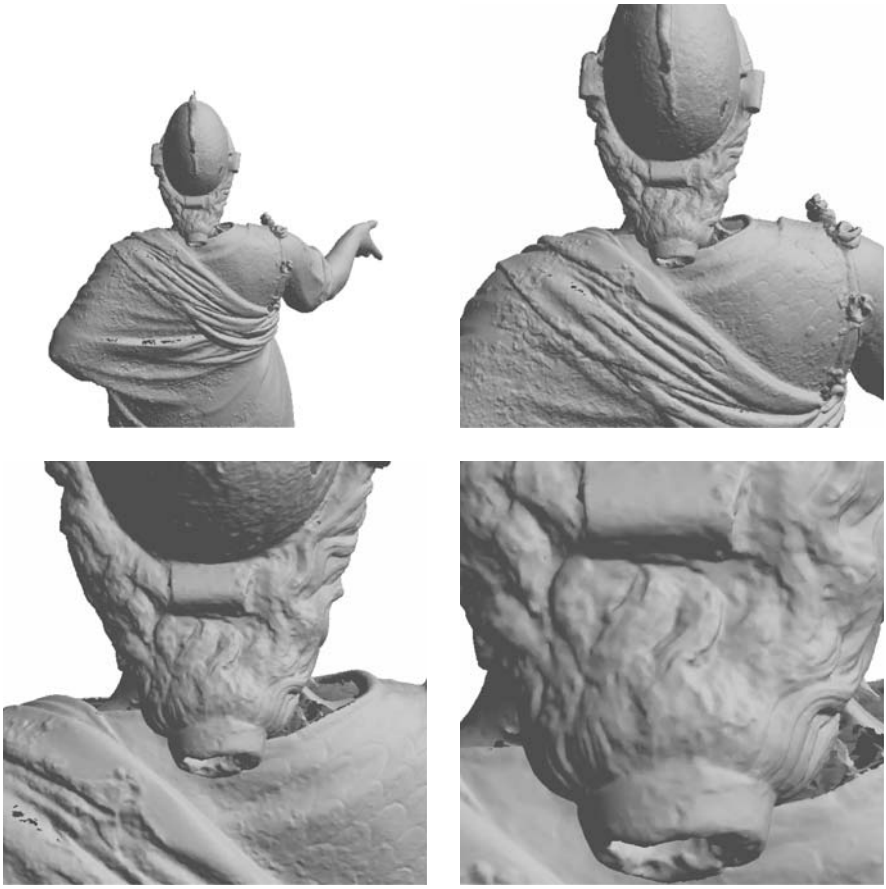

Fig. 6. Four images with different levels of detail of the hear of the Minerva, in which there were integrated the results obtained with the laser scanner and the micro-profilometer

References

1. M. Levoy, K. Pulli, B. Curless, and S. Rusinkiewicz, The Digital Michelangelo Project: 3D scanning of large statues, Comp. Graph. Proc., Annual Conf. Series (Siggraph'00), Addison Wesley (2000) 131–144
2. H. Rushmeier, F. Bernardini, J. Mittleman, and G. Taubin, Acquiring input for rendering at appropriate levels of detail: digitizing a Pieta, Eurographics Rendering Workshop 1998, G. Drettakis and N. Max (ed.), Springer Wien (1998)
3. M. Gaiani, M. Balzani, and F. Uccelli, Reshaping the Coliseum in Rome, Computer Graphics Forum 19(3) (2000) 369–378
4. D J Whitehouse, *Handbook of Surface Metrology,* Institute of Physics Publishing Bristol and Philadelphia

5. G. Y. Sirat, and D. Psaltis, *Conoscopic holograms,* Opt. Comm., 9(65):243–245, 1988
6. C. Rocchini, P. Cignoni, C. Montani, and R. Scopigno, The Marching Intersections Algorithm for merging range images, IEI-CNR Tech. Rep. July 2000.
7. B. Curless and M. Levoy, A volumetric method for building complex models from images, SIGGRAPH '96 Proceedings, ACM SIGGRAPH (1996) 303–312
8. P. Cignoni , C. Montani, C. Rocchini, and R. Scopigno, Out Of Core Management and Simplification of Huge Meshes, IEEE Transactions on Visualization and Computer Graphics, IEEE Press, 2002 (in press)
9. P. Cignoni, C. Montani, C. Rocchini, and R. Scopigno, External Memory Management and Simplification of Huge Meshes, IEI-CNR Tech. Rep., submitted paper, Jan. 2001, p. 10

Comparative Holography in the Conservation Structural Diagnosis: An El Greco Exemplary Exploitation

V. Tornari[1], A. Bonarou[1], V. Zafiropulos[1], C. Fotakis[1], N. Smyrnakis[2], and S. Stassinopoulos[2]

[1] Foundation for Research and Technology-Hellas/Institute of Electronic Structure and Laser, Voutes, 7110 Heraklion, Crete, Greece
vivitor@iesl.forth.gr
[2] Benaki Museum, Koumparh 1, 106 74 Athens, Greece

1 Introduction

1.1 Conservation Aims and Laser Based Structural Diagnostics

The aim of this paper is to examine and introduce the applicability of holographic interferometry and holography related techniques to the comparative measurements often required in conservation structural diagnostic procedures. The paper is divided in two parts: the first signifies the suitability and requirements for techniques to be qualified as appropriate for comparative measurements and the second an exploratory example of the methodology on an early El Greco painting.

In art conservation in general for a technique to be applied on artworks and mainly for a laser-based one there should be satisfied certain suitability characteristics. Most prior of them being the non destructive character of the applied technique, ideally the surface preparation or sample removal to be avoided, an important aspect being the laser wavelength to be safe for the artwork and the operator and uniquely suited if the technique can be performed independently of shape complexity, surface roughness and texture. All of the above mentioned prior requirements to define the suitability of a technique for application on artworks' structural diagnostics are satisfied in holographic interferometry related measurements [1, 2].

Additionally, the range of applicability in structural diagnosis varies from the detection of internal hidden defects the information on their propagation or interconnection and the degree of deterioration under stressing conditions, the definition of mechanical stability and structural integrity, the monitoring of environmental effects and of intervention processes, to the mapping of responses in induced alteration. All the above being common identifiable and usual everyday diagnostic challenges. Since the described applications can be fulfilled by means of the holography techniques the latter can be qualified as an important method of broad applicability in a number of crucial investigation demands.

1.2 Specific Aims and Comparative Studies

The broad aim to map the responses of the artwork itself due to any known or unknown induced alteration has a lot of significance since highlights specific problems of augmented importance in modern conservation such as the effects due to transportation, handling and microclimate changes.

A neglected but significant problem in nowadays is the increased demand of transportation and its effects. By transportation is defined any reallocation action, starting from the removal from one gallery of a museum to the other or from storage to display or either transportation from exterior to interior or loans for traveling exhibitions. The implications of transportation can signify drastic interventive or accidental changes to the integrity or structural condition of an art object.

In this context the suitability characteristics of a technique to serve for the specified demand of comparative application is primarily the accurate comparison of small changes, additionally the complementary production of visual images for direct assessment of drastic changes and the processing through optoelectronic and image correlation platforms for further elaboration requirements, therefore technical features uniquely satisfied from holographic interferometry techniques [3–6]. Another important characteristic is the flexibility of the technique to be used either under laboratory strict boundary conditions or to specifically developed investigating methodologies, both possible by means of holography. Nevertheless for demanding highly sophisticated conservation research an issue of major importance becomes the information content of the applied technique.

Holography is an interference record on highly resolved photosensitive medium. Despite the broad range of these mediums varying from various photorefractive crystals to CCDs of variable number of pixels and pixel size the most effective medium to record high spatial frequencies remains the silver halide material usually in the form of film layered emulsions. The latter can resolve up to 5000 lines/mm producing simultaneously a three dimensional image of the artwork and temporal information of the induced alteration through sequentially recorded holographic interference fringes [7]; while detecting changes in the artwork responses as small as the half wavelength of the operating laser providing an ideal scale for unknown comparative measurements [6–8]. The record is an encoded form of reactions as bright and dark fringes in which the hidden defects located under the surface are visualised on the surface by their distinct reaction and are recognised by spotting the difference they produce compared to the neighboring areas. The straightforward decoding however obeying the ambiguities of the inverse identification problem has been the subject of intense research for many years in which the verification was primarily achieved by mechanical models and computer simulation [9–11]. The fringe patterns experimentally produced from samples simulating construction of real artworks with intentionally induced defects is proved through correlation of known to real defect experiments to share

common topological characteristics describing specific causes from which are generated [12, 13].

Nowadays the issue of loan for travelling exhibitions is of critical importance since the interest of visitors is steadily increasing with the demand for organising safe for loaned objects travelling exhibitions. A loaned object undergoes cycles of environmental changes and is endangered by handling and transportation non monitored actions which accumulate stresses on the structure, generate defects and deteriorate the objects' integrity. Despite the fact that these changes are invisible in their growth the effect can be deleterious in longer terms since the alterations are not reversible. It is thus becoming of major importance the condition assessment of the object between far different states during its travel.

2 Experimental Methodology

In this context an early El Greco painting the "Adoration of magi" dated back to 1456 was requested from Benaki Museum in Athens to get loaned for an exhibition around few major cities in Europe raising many concerns on the possible effects of such an attempt on the painting. The investigation demand was to acquire the highest possible information content in a whole field recorded image in order to enable the conservator to study both the response of the painting as a whole structure and also the localised irregularities due to specific defects. The photograph of the front painting surface and the back wood support are shown in Fig. 1. Due to the multilayered construction of a painting the deep cracks crossing the wood and the surface cracks can individually influence the structural responses provoking complex dimensional changes.

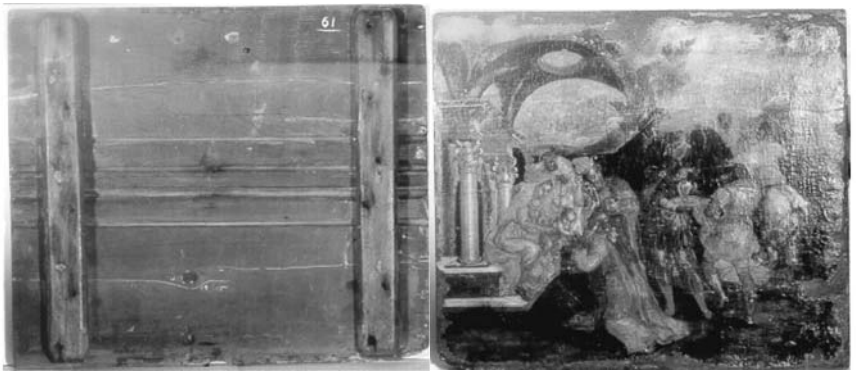

Fig. 1. Photographs of rear and front surface of EI Greco painting "The adoration of Magi"

Accordingly to serve the above investigation demand has been employed the double exposure holographic interferometric technique with an investigation methodology to allow for the non-destructive comparison, dominated by an extended time lapse due to the loan of the painting. Therefore the painting was twice after a separation of a year holographically investigated with an extended beam diameter of 30 cm from laser output energy 2 W getting in recording plane an average intensity of $125\,\mu W/cm^2$. The recording medium was of silver halide material with sensitivity of $150\,\mu J/cm^2$ and exposure times of $t_{exp} = I_{sens}/I_{rec}$ of the order of 60-max 80 sec. Chemical solution of triethalonamine was used for emulsion swelling to allow for recording of more fringe planes for film presensitisation allowed to cut the exposure time in half or quorter, thus each exposure was of the order of 15–40 sec. The high information content was provided by the off axis geometry with reference to object beams angle separation of $\theta = \min 30^\circ - \max 45^\circ$, a parameter partly depending on the reflective properties of the painting surface which in this case due to the varnish layer limited a maximum offset angle. A TEM00 laser provided a highly coherent beam at 532 nm and since $f_y = \sin\theta/\lambda$, the holographic interferograms were acquired with dense spatial frequencies such as of the order of $3 - 5 \times 10^3$ lines/mm depending in turn on angle θ. All settings were computer stored for identical reproduction of each hologram next year. Each recorded holographic interferogram could thereafter observed in whole field viewing of the hologram window or deliberately zoomed-in parts of interest by a 10× NAVITAR zoom lens retaining a resolution of 28×10^3 pixels/cm and get compared with corresponding areas of the second set a year later after the return of the loaned painting and the repetition of the investigated procedure.

The experimental methodology envisages prior classification of painting responses under controlled thermal alteration at specific time intervals between exposures on which is based the investigation procedure for the generation of the reference and comparison holographic interferograms. As can be seen in graphs of Fig. 2 the excitation produced by thermal load is transient of the order of maximum 120 secs on which depends on the duration and direction of application. Also defining among these times the limits of the interval between two exposures in specific recording times providing simultaneously the ΔT information of each.

It is expected a visible interference pattern to be produced by the induced transient load. The most effective fringe pattern in terms of structural displacement and defect detection dominates the selection of the applied load. In this way series of consequent holographic interferograms were acquired and stored for comparison at a later stage under the pre-specified experimental methodology.

In Table 1 is summarised the dependence of interval time from the duration and direction of thermal load.

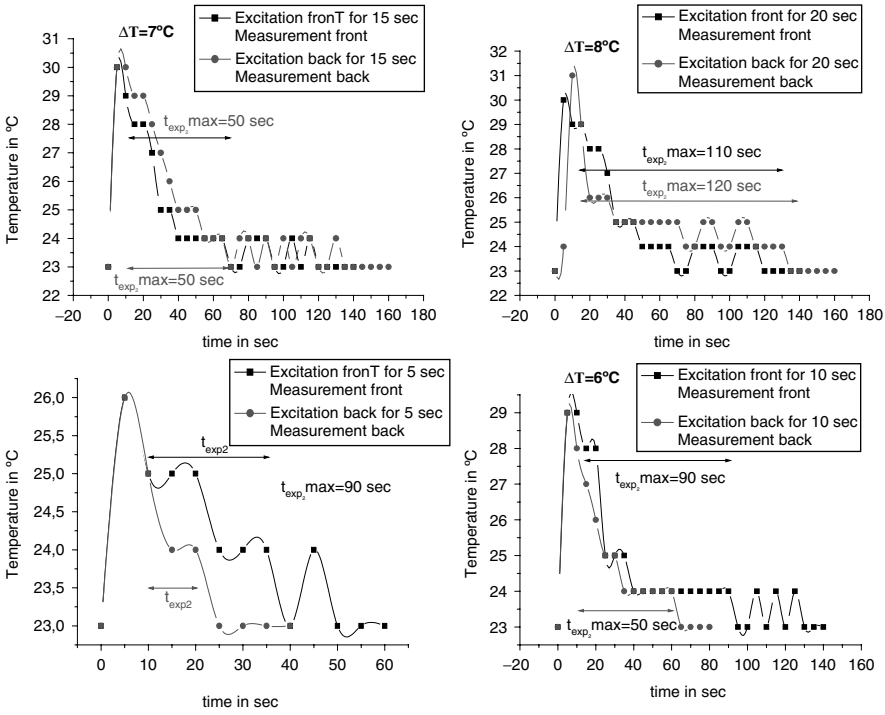

Fig. 2. Thermal alteration monitored through probe reading for different duration and direction of induced alteration

Table 1. Painting Definition Between Exposures

Initial Temperature °C	Duration of thermal load (sec)	Direction of thermal load	Final temperature °C	ΔT °C	Transient Time (sec)
23	5	front	26	3	**25**
23	5	back	26	3	**10**
23	10	front	29	6	**90**
23	10	back	29	6	**50**
23	15	front	30	7	**50**
23	15	back	30	7	**50**
23	20	front	31	8	**110**
23	20	back	31	8	**120**

3 Experimental Results

According to the graphs and the Table 1 holographic interferograms were recorded with the predominated settings chosen as follows:

The acquired data was indicative of low cohesion between front and rear side of the painting visualised by the absence of influence between the two sides. The finding was revealed by straightforward qualitative estimation of the holographic interferograms. As can be seen in Fig. 3a excitation from the rear side of the painting while recording is performed from the front surface, there is not any visible interference fringe generation. When the excitation direction is from the same direction with the recording, as in Fig. 3b, the generated interference fringe system correlates to rigid front surface displacement and does not visualise local irregularities.

Table 2. Experimental Settings

1^{st} exposure	Thermal excitation	Time interval	2^{nd} exposure	Total experimental time
15 sec	10 sec	10 sec	15 sec	50 sec
15 sec	15 sec	15 sec	15 sec	60 sec

However due to known presence of defects in the upper layers the result was questioned since there should be visualised. Therefore the above results were accompanied with thermal probe readings from opposite sides with settings as in Table 1, the result seen in Fig. 4 where a flat line is produced from integer measurements of Celsius degrees. Additional computer simulated mechanical model according to the front side experiment produced similar fringe system indicating the displacement as of thin membrane-like border-constrained surfaces as shown in Fig. 5a.

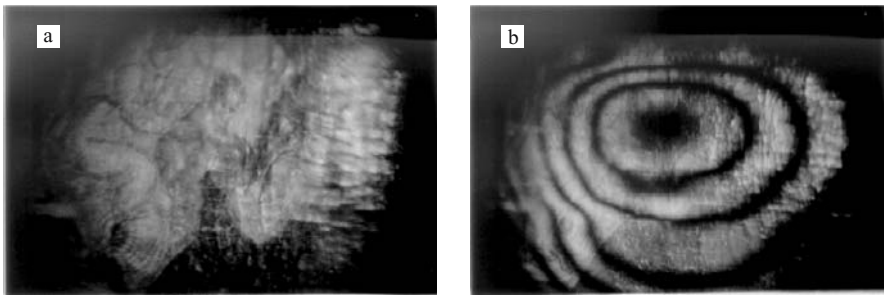

Fig. 3. In (**a**) excitation from the rear side of the painting while recording is performed from the front surface proved without influence, in (**b**) the excitation direction is from the same direction with the recording with fringe system formed from whole front surface displacement.

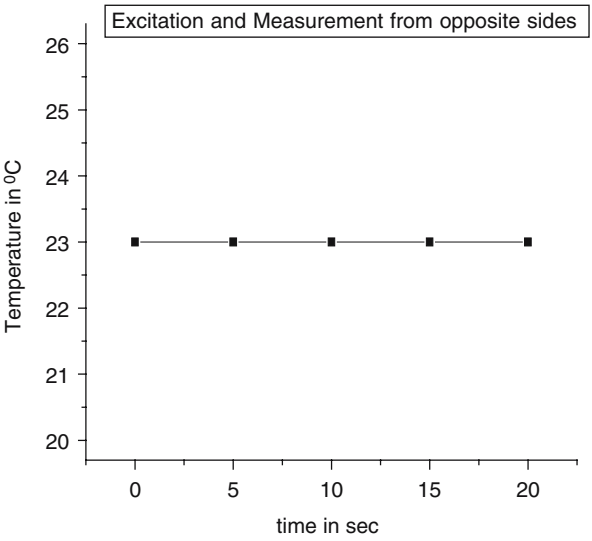

Fig. 4. Thermal probe readings from opposite sides produces no evidence of influence between the two sides (measured in integer degress)

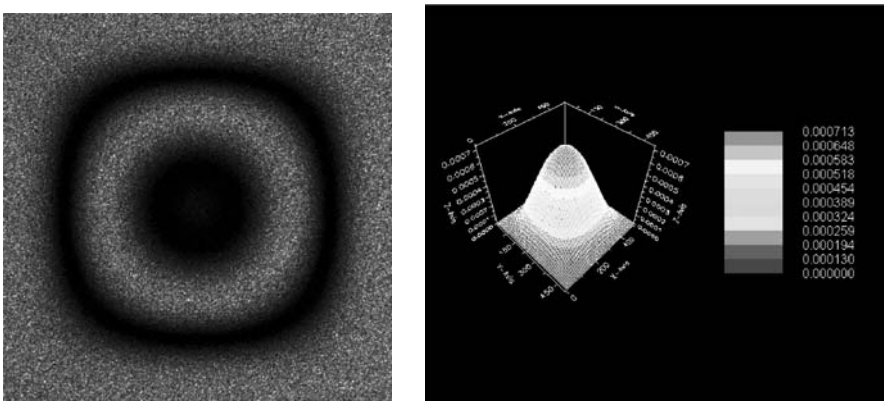

Fig. 5. Computer simulated mechanical model of the front side experiment produced fringe system as in the case of thin membrane-like edge-constrained surfaces

Dividing the thermal excitation half in back and half in front surface produced the dense fringe systems, an example shown in Fig. 6. Thus it was succeeded the interacting fractions of the transmitted to the other surface thermal gradients to bring in evidence the smaller effects and their influence. Among the dense and complex fringe systems can be recognized and traced plethora of small cracks and detachments in painting surface overlaying on fringe systems produced from the effect of the cracks of the wood support. The strong effect of local irregularities in the front surface of the painting

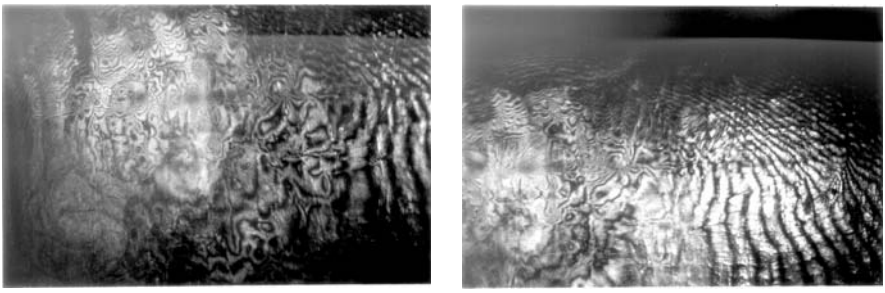

Fig. 6. Photographs of holographic interferograms zoomed from different viewpoints . The dense fringe system produced by influence between front and rear side of the painting becomes uniform towards the stable influence of frame at the edges

highlights the importance of the restoration and significance of consolidation in order to integrate back again the front and rear side of the structure. Towards the edges the fringe systems become more uniform due to stable effect of frame while is getting interrupted by the back surface cracks. The influence thus of each surface is identifiable and separately stored.

When a year later, after drying out of consolidation and restoration processes and by the return of the painting from the loan, the investigation was repeated the configuration of the acquired fringe systems showed effective changes. There were studied according to the previous settings and findings. Thus in terms of the interaction between the two sides of the painting was now existed and visualised. As can be seen in Fig. 7b the back surface affects front producing two main fringe systems visualising the influence of the central crack of the wood surface. In case of front surface, Fig. 7a can be seen in comparison with Fig. 3b, the reaction in the induced displacement witnesses an increased sensitivity and the excitation time and intervals had to be de-

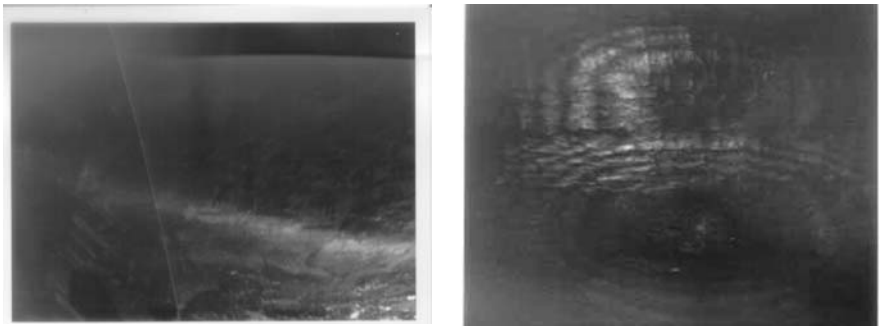

Fig. 7. In (a) previous settings were not capable to produce distinguishable front surface fringe system revealing permanent structural alteration, in (b) previous setting now successfully visualized back surface influence

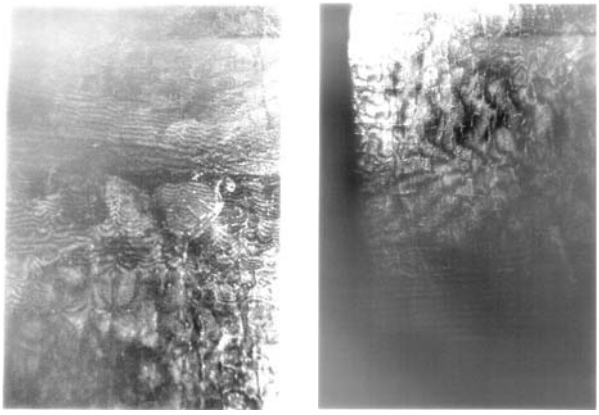

Fig. 8. Photographs from holographic interferograms second series. In **(a)** restorable defects are not causing now the previously observed dense fringe systems whereas permanent defects are getting better visualized, **(b)** towards the edges the stability is dectreased due to permanent structural deterioration

creased substantially. The changes in the initial settings indicate however a permanent alteration of irreversible influence on structural condition. Can be compared to the results seen in Fig. 8a where only the influence of the non restored wood back surface is visualized in the fringes and not the previous front surface irregularities that have been consolidated for travel.

Thus the effects of loan are not studied through changes in the restorable defects but through the influence on permanent structure and the alteration of experimental settings. Indeed all the holographic interferograms acquired in the repeated investigation revealed a uniform front painting surface with minimized local irregularities and a better visualization of the permanent effects of wood support. Nevertheless should be noted the alteration of structural condition as is also witnessed by complexity of the fringe systems towards the framed edges of the painting previously more uniform, compare Fig. 6b to 8b. Classification of the observed changes through comparison of the complete series of holographic interferograms indicated from one hand a significant structural deterioration of the painting state and from the other, the absence of the high number of local irregularities witnessed the successful intervention of restoring the front surface defects.

4 Conclusions

Holographic interferometry provides the technical requirements for demanding research in conservation structural diagnostics. Experimental methodologies can be flexibly adjusted to serve answering specific investigation demands. An irreplaceable painting was studied and compared before and

after interventive actions such as restoration and transportation in different countries. By classifying the responses of the painting in the predefined experimental settings into which later were compared it became possible a long term comparison despite the absence of fringe systems similarities. Although indirect the results indicate suitability of the technique and can be precious for developing new methods and strategies to serve for standardization in loan requirements and insurance rules.

Acknowledgements

From this position we wish to thank Benaki Museum of Athens for providing and cooperate in the investigation of the El Greco painting. The study carried out under the R&D EC funded project LASERART in the premises of FORTH/IESL.

References

1. V. Tornari, A. Bonarou, V. Zafiropulos, C. Fotakis, FORTH/IESL, and M. Doulgeridis NGA, "Holographic Applications in evaluation of Defect and Cleaning Procedures", LACONA III, 3rd *International Conference on Lasers in Art Conservation-April 1999,* Elsevier, Journal of Cultural Heritage 1 (0) (2000) pp S325–S329
2. V. Tornari, V. Zafiropulos, A. Bonarou, N. A. Vainos, and C. Fotakis, " Modern technology in artwork conservation: A laser based approach for process control and evaluation", Journal of Optics and Lasers in Engineering, vol. 34, (2000), pp 309–326
3. Charles M. Vest, Holographic Interferometry, John Wiley & Sons, NY, 1979
4. Robert J. Collier, Optical Holography, Academic Press, NY, 1971
5. R. Jones & C. Wykes, Holographic and Speckle Interferometry, Cambridge University Press, 1989
6. V. Tornari, A. Bonarou, E. Esposito, W. Osten, M. Kalms, N. Smyrnakis, and S. Stasinopulos, "Laser based systems for the structural diagnostic of artworks: an application to XVII century Byzantine icons", SPIE 2001, Munich Conference, June 18–22, 2001, vol. 4402
7. V. Tornari, A. Bonarou, and L. Antonucci, "Sequential holographic interferometric recording: a key to monitor dynamic displacements in long-term effects", 4th International workshop on automatic processing of fringe patterns, Bremen 17–19 September 2001, *Elsevier* FRINGE 2001, pp 680–685
8. V. Tornari, A. Bonarou, V. Zafiropulos, C. Fotakis, N. Smyrnakis, and S. Stassinopulos, ≪Structural evaluation of restoration processes with holographic diagnostic inspection≫, LACONA IV Paris 10–14 September 2001, Journal of cultural Heritage, Suppl 1, Vol. 3, 2002
9. Z. Fuzessy, Simulation and Experiment in laser metrology, Academie Verlag, pp 209–216, 1996
10. W. Osten et al., J. Mod. Optics, V35, 1717–1725, 1998
11. U. Mieth et al, Fringe 01, Elsevier, pp 163–172, 2001

12. V. Tornari and W. Osten, Electr.Imag., V5, pp 2–9, 1998
13. V. Tornari, Applications of Holographic Interferometry in Preventive Conservation and the Diagnosis of Works of Art", MPhil Thesis, V&A/RCA & British Libraries, (UK), 1996

A Case Study of Frescoes Diagnostics by Scanning Laser Doppler Vibrometry (SLDV): The Brumidi Corridors and The President's Room at The United States Capitol

G. Adams[1], J. Bucaro[2], E. Esposito[3], A.J. Kurdila[4], B. Marchetti[3], E.P. Tomasini[3], and J.F. Vignola

[1] Cunningham-Adams, Fine Arts Paintings Conservation, Cambridge, USA
GeoWAdams@att.net
[2] Acoustics Division – Physical Acoustics Branch, Naval Research Laboratory, Washington, USA
vignola@code7136.nrl.navy.mil
[3] Dept. of Mechanics, Polytechnic University of Marche, Ancona, Italy
e.esposito@mm.univpm.it
[4] Dept. of Mechanical & Aerospace Engineering, University of Florida, Gainesville, USA
ajk@mae.ufl.edu

Abstract. The United States Capitol contains large expanses of important fine art and decorative paintings, including buon frescos, executed directly on the original lime plaster. Of particular concern is assessing the presence of deteriorated plaster, a condition known to exist in various parts of the building, but that has not been comprehensively surveyed. The authors report here on tests to assess the effectiveness of SLDV for detecting and characterizing deficiencies in the plaster support behind fine arts and decorative paintings in the United States Capitol. In particular our analysis will be focused in two of the Capitol's important artworks: the Brumidi Corridors and the President's Room. The Brumidi Corridors are the richly painted hall-ways on the first floor of the Senate Wing. As in the President's Room, the wall paintings were designed by the famous Italian artist Costantino Brumidi. The conservator's aim is to find a proper technique to carefully diagnose and monitor structural defects like that they discovered in the above mentioned places: loss of cohesion within a layer, delamination from the brick substrate, and interlayer delamination between layers. This project has just started and in this work we will present some preliminary results obtained from sample panels in the Corridors and in a small room of the Capitol.

1 Introduction

The structure underlying the art work in the already mentioned areas of the Capitol is in general terms a multi-layered panel structure. The art is painted on three layers of plaster totalling approximately 2 cm thick. The uppermost layer is about 0.3 cm, the middle layer is about 0.7 cm, and the deepest layer is about one cm, but is to have substantial thickness variations.

This multi-layered plaster structure is attached to a thick supporting masonry foundation.

A successful non-destructive evaluation technique should be able to detect and locate defects anywhere throughout this structure. This would include problems within the paint layer itself, faults within the plaster, and delaminations between the layers and at the attachment of the mortar layer to the wall supporting structure.

This article reports the demonstration of the applicability of the SLDV to this specific diagnostic application, employing two different excitation techniques, namely acoustic excitation and shaker excitation. How to properly excite the structure under test and the optical characteristics of its surface in terms of laser light diffusivity are two major issues when using Doppler vibrometers, and have been dealt with in different papers [1], with two more examples in this conference [2, 3]. For these reasons, we tested the two excitation sources mentioned above and also had to check the Doppler level when aiming the laser beam at the painted surfaces. Details of the application of Doppler vibrometers to artworks diagnostics may be found elsewhere [4, 5] and also references to other optical technicques for frescoes diagnostics are in [6] and [7], so these topics will not be dealt with here, but we would point out that shaker based laser Doppler vibrometry offers an effective approach to the art conservation community for detecting defects in the supporting layered structure of frescoes, an approach that has never been used before to the knowledge of the authors. Shaker based laser Doppler vibrometry is attractive because it takes less time, provides a more well-defined wall forcing function, and is quieter than speaker excitation. This last advantage means that work around the measured area may continue while the experiment is in progress. Fig. 1 shows the SLDV system while operating in the President's Room and Brumidi Corridors, and also in a smaller room that has been used as the first test site.

Fig. 1. SLDV in the President's Room, in the Brumidi Corridors, and in room S-0311

2 Experimental Results

In Fig. 2 we show the result of a SLDV scan on the east quadrant of Room S-0311 ceiling using the acoustic excitation.

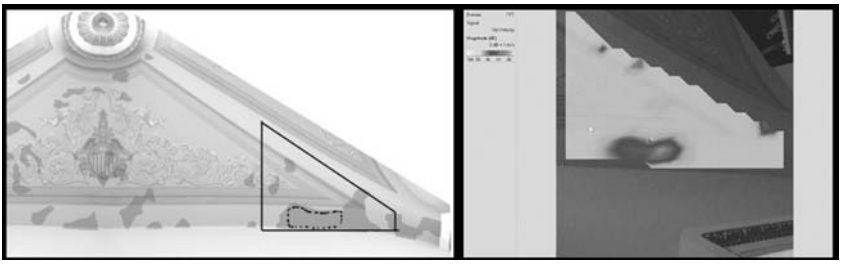

Fig. 2. SLDV scan on East vault of room S-0311; restorer defects map and SLDV map at 376 Hz

On the left part of the figure we present a map of delaminated areas prepared by a conservator with a black trapezoidal shape identifying the area examined by the SLDV. On the right part of the picture the amplitude of the velocity of vibration at 376 Hz is reported, and we may observe a good correlation between the two maps. As explained in [4, 5], higher velocity areas identify delaminated ones, and we trace the dark irregular one in the SLDV map as the dotted line shape in the restorer's descripton. Identification of only a portion of the detachment is due to single frequency examination and may be completed by considering other resonance frequencies of the defect.

In the following picture, Fig. 3, we have an example of the investigations conducted in the Brumidi Corridors by shaker excitation, this device located in the lower left part of the examined panel. Again the SLDV map reports values of vibration velocity, although with a different code.

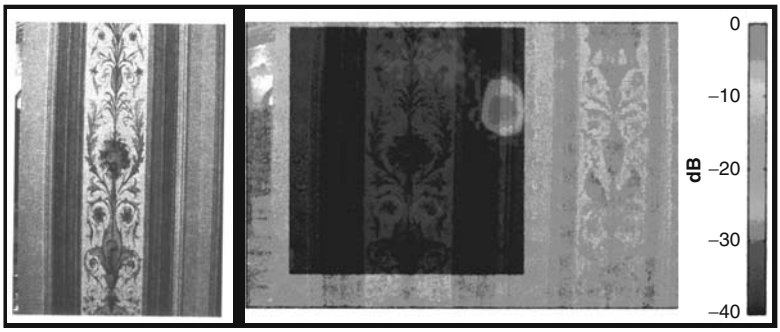

Fig. 3. SLDV scan on Brumidi Corridor panel; photo of the panel and SLDV map in the 460 Hz band

In the case of Fig. 3 individual narrow-band results were summed to form broadband maps. An example of such a resulting map is shown for the band 435 to 465 Hz and a mobile area can be seen in the upper right side of the scan. Both the extent and location of this mobile patch coincides with a defect area discovered earlier in the tap test data by the conservator.

3 Conclusions

As already noted in the quoted articles, laser Doppler vibrometry offers an effective tool to the art conservation community for detecting defects in the supporting structures of artwork. This tool will allow a conservator to quickly and non-intrusively determine defect areas in the structure supporting a work of art. Digital maps can be easily made clearly showing defects. After the restoration process, another measurement will allow the conservator to evaluate the restoration. This process provides a higher resolution map than the current tapping technique, and includes more information, such as the resonance frequency of the defected area, that is both useful to the conservator and correlates very well with the conservator's post hoc judgment of panel condition. This work at the United States Capitol is another demonstration that this technique is reaching a good degree of maturity and field applicability. There still remain some questions open, for example how to exactly locate the delamination in the layered structure. At present qualitative assessment may be done by looking at the resonances of defects, but a more effective approach based on mathematical modelization of frescoes structures will help give more detailed information.

References

1. R. F Strean, L. D. Mitchell, and A. J. Barker, in *Proceedings of 15th International Modal Analysis Conference – IMAC XV*, Kissimmee, USA, 1229, 1997
2. A. Agnani and E. Esposito, in *Proceedings of Lasers in the Conservation of Artworks – LACONA V*, Osnabrueck, Germany, September 15–18, 2003, to be published
3. E. Esposito, P. Castellini, N. Paone, and E. P. Tomasini, in *Proceedings of Lasers in the Conservation of Artworks – LACONA V*, Osnabrueck, Germany, September 15–18, 2003, to be published
4. P. Castellini, E. Esposito, N. Paone, and E. P. Tomasini, in *Measurement*, Vol. 28, 33, 2000
5. P. Castellini, E. Esposito, B. Marchetti, N. Paone, and E. P. Tomasini, in *Journal of Cultural Heritage*, Vol.4/S1, 321, 2003
6. V. Tornari, A. Bonarou, P. Castellini, E. Esposito, W. Osten, M. K. Kalms, N. Smyrnakis, and S. Stasinopulos, in *Proceedings of Laser Techniques and Systems in Art Conservation*, Munich, Germany, 172, June 18–19, 2001
7. G. Guelker, K. D. Hinsch, and H. Joost, in *Proceedings of Laser Techniques and Systems in Art Conservation*, Munich, Germany, 184, June 18–19, 2001

SPRINGER PROCEEDINGS IN PHYSICS

50 **Magnetic Properties of Low-Dimensional Systems II**
New Developments
Editors: L.M. Falicov, F. Mejía-Lira, and J.L. Morán-López

51 **The Physics and Chemistry of Organic Superconductors**
Editors: G. Saito and S. Kagoshima

52 **Dynamics and Patterns in Complex Fluids**
New Aspects of the Physics–Chemistry Interface
Editors: A. Onuki and K. Kawasaki

53 **Computer Simulation Studies in Condensed-Matter Physics III**
Editors: D.P. Landau, K.K. Mon, and H.-B. Schüttler

54 **Polycrystalline Semiconducturs II**
Editors: J.H. Werner and H.P. Strunk

55 **Nonlinear Dynamics and Quantum Phenomena in Optical Systems**
Editors: R. Vilaseca and R. Corbalán

56 **Amorphous and Crystalline Silicon Carbide III, and Other Group IV–IV Materials**
Editors: G.L. Harris, M.G. Spencer, and C.Y. Yang

57 **Evolutionaly Trends in the Physical Sciences**
Editors: M. Suzuki and R. Kubo

58 **New Trends in Nuclear Collective Dynamics**
Editors: Y. Abe, H. Horiuchi, and K. Matsuyanagi

59 **Exotic Atoms in Condensed Matter**
Editors: G. Benedek and H. Schneuwly

60 **The Physics and Chemistry of Oxide Superconductors**
Editors: Y. Iye and H. Yasuoka

61 **Surface X-Ray and Neutron Scattering**
Editors: H. Zabel and I.K. Robinson

62 **Surface Science**
Lectures on Basic Concepts and Applications
Editors: F.A. Ponce and M. Cardona

63 **Coherent Raman Spectroscopy**
Recent Advances
Editors: G. Marowsky and V.V. Smirnov

64 **Superconducting Devices and Their Applications**
Editors: H. Koch and H. Lübbing

65 **Present and Future of High-Energy Physics**
Editors: K.-I. Aoki and M. Kobayashi

66 **The Structure and Conformation of Amphiphilic Membranes**
Editors: R. Lipowsky, D. Richter, and K. Kremer

67 **Nonlinearity with Disorder**
Editors: F. Abdullaev, A.R. Bishop, and S. Pnevmatikos

68 **Time-Resolved Vibrational Spectroscopy V**
Editor: H. Takahashi

69 **Evolution of Dynamical Structures in Complex Systems**
Editors: R. Friedrich and A. Wunderlin

70 **Computational Approaches in Condensed-Matter Physics**
Editors: S. Miyashita, M. Imada, and H. Takayama

71 **Amorphous and Crystalline Silicon Carbide IV**
Editors: C.Y. Yang, M.M. Rahman, and G.L. Harris

72 **Computer Simulation Studies in Condensed-Matter Physics IV**
Editors: D.P. Landau, K.K. Mon, and H.-B. Schüttler

73 **Surface Science**
Principles and Applications
Editors: R.F. Howe, R.N: Lamb, and K. Wandelt

74 **Time-Resolved Vibrational Spectroscopy VI**
Editors: A. Lau, F. Siebert, and W. Werncke

75 **Computer Simulation Studies in Condensed-Matter Physics V**
Editors: D.P. Landau, K.K. Mon, and H.-B. Schüttler

76 **Computer Simulation Studies in Condensed-Matter Physics VI**
Editors: D.P. Landau, K.K. Mon, and H.-B. Schüttler

77 **Quantum Optics VI**
Editors: D.F. Walls and J.D. Harvey

78 **Computer Simulation Studies in Condensed-Matter Physics VII**
Editors: D.P. Landau, K.K. Mon, and H.-B. Schüttler